foods

Special Issue Reprint

Sensory Detection and Analysis in Food Industry

Edited by
Dongrui Zhao and Jianan Zhang

mdpi.com/journal/foods

MDPI

Sensory Detection and Analysis in Food Industry

Sensory Detection and Analysis in Food Industry

Guest Editors

Dongrui Zhao
Jianan Zhang

MDPI

Basel • Beijing • Wuhan • Barcelona • Belgrade • Novi Sad • Cluj • Manchester

Guest Editors

Dongrui Zhao
School of Light Industry
Beijing Technology and
Business University
Beijing
China

Jianan Zhang
School of Food Science and
Engineering
Central South University of
Forestry and Technology
Changsha
China

Editorial Office
MDPI AG
Grosspeteranlage 5
4052 Basel, Switzerland

This is a reprint of the Special Issue, published open access by the journal *Foods* (ISSN 2304-8158), freely accessible at: https://www.mdpi.com/journal/foods/special_issues/38N8NL336Z.

For citation purposes, cite each article independently as indicated on the article page online and as indicated below:

Lastname, A.A.; Lastname, B.B. Article Title. *Journal Name* **Year**, *Volume Number*, Page Range.

ISBN 978-3-7258-9051-4 (Hbk)
ISBN 978-3-7258-9052-1 (PDF)
https://doi.org/10.3390/books978-3-7258-9052-1

© 2026 by the authors. Articles in this reprint are Open Access and distributed under the Creative Commons Attribution (CC BY) license. The reprint as a whole is distributed by MDPI under the terms and conditions of the Creative Commons Attribution-NonCommercial-NoDerivs (CC BY-NC-ND) license (https://creativecommons.org/licenses/by-nc-nd/4.0/).

Contents

About the Editors . . . . . **vii**

Preface . . . . . **ix**

Dongrui Zhao and Jianan Zhang
From Molecular Flavor Signatures to Mechanism-Oriented Food Quality: Advances in Flavoromics, Fermentation Ecology, Functionality, and Safety
Reprinted from: *Foods* **2026**, *15*, 2337, https://doi.org/10.3390/foods15132337 . . . . . **1**

Jianxin Wu, Xiaotong Ma, Zongyi Wang, Ying Wei, Yuting Liu, Jiaqian Men and Wenyu Ma
Rapid Determination of Several Biogenic Amines in Cold-Chain Fish Samples by Portable Ion Trap Mass Spectrometry with Nano-Electrospray Ionization
Reprinted from: *Foods* **2026**, *15*, 1802, https://doi.org/10.3390/foods15101802 . . . . . **6**

Lijuan Fu, Wenjing Liu, Lihua Ren, Xiangxin Lin, Jia Guo, Hao Chen, et al.
Systematic Characterization of Flavor Profiles and Screening of Potential Key Aroma-Active Components in *Prunus salicina* var. *cordata* cv. 'Younai'
Reprinted from: *Foods* **2026**, *15*, 1787, https://doi.org/10.3390/foods15101787 . . . . . **17**

Junzhe Hua, Kemin Mao, Wenlong Yu, Zongyang Li, Runhan Wen, Lingyu Li, et al.
Multi-Omics Integration to Investigate the Effects of Variety and Origin on Volatile and Non-Volatile Metabolites in Melons
Reprinted from: *Foods* **2026**, *15*, 1746, https://doi.org/10.3390/foods15101746 . . . . . **37**

Jinxiao Liu, Jia Zheng, Jihong Wu, Ying Sun, Mingquan Huang, Jian Su, et al.
Identification of Potential Bioactive Compounds in Strong-Flavor-Type Baijiu via Integration of Widely Targeted Metabolomics and Network Pharmacology
Reprinted from: *Foods* **2026**, *15*, 1509, https://doi.org/10.3390/foods15091509 . . . . . **64**

Tianyu Dong, Panpan Wu, Jie Sun, Haitao Chen and Shuqi Wang
Decoding the Flavor Code of Fresh and Dried *Tengjiao* (*Zanthoxylum armatum* DC.) for Preparing Fried *Tengjiao* Oil Through Molecular Sensory Science
Reprinted from: *Foods* **2026**, *15*, 1326, https://doi.org/10.3390/foods15081326 . . . . . **85**

Jun Zhang, Yehui Han, Xiaolong You, Xiaochun Zhu, Youlan Sun, Feng Hu, et al.
Characterization of Retronasal Aroma Differences in High- and Low-Alcohol Jiangxiangxing Baijiu Using Temporal Sensory Evaluation, Retronasal Olfactory Thresholds, and Dose-over-Threshold Analysis
Reprinted from: *Foods* **2026**, *15*, 1156, https://doi.org/10.3390/foods15071156 . . . . . **106**

Aygul Alim, Chengfei Huang, Xin Zhao, Saren Gaowa, Runrong Zhang, Junrong Zhang, et al.
Investigating the Impact of Different Drying Methods on the Aroma of Citri Reticulatae Pericarpium Using GC–MS/GC–IMS and E-Nose Technology
Reprinted from: *Foods* **2026**, *15*, 1117, https://doi.org/10.3390/foods15071117 . . . . . **131**

Dandan Song, Lulu Song, Xian Zhong, Yashuai Wu, Yuchao Zhang and Liang Yang
Integrated Molecular Informatics and Sensory-Omics Study of Core Trace Components and Microbial Communities in Sauce-Aroma High-Temperature Daqu from Chishui River Basin
Reprinted from: *Foods* **2026**, *15*, 599, https://doi.org/10.3390/foods15030599 . . . . . **146**

Panling Lu, Chunfang Wang, Yongxue Zhang, Haijun Jin, Shaofang Wu, Xiaotao Ding and Hongmei Zhang
Diversity of Volatile Profiles and Nutritional Traits Among 29 Cucumber Cultivars
Reprinted from: *Foods* **2025**, *14*, 3878, https://doi.org/10.3390/foods14223878 . . . . . **183**

Xinxin Zhang, Changfeng Zhang, Menglian Gong, Pao Li, Hui Tang, Liwen Jiang and Yang Liu
Dynamics of Lactic Acid Bacteria Dominance in Sour Bamboo Shoot Fermentation: Roles of Interspecies Interactions and Organic Acid Stress
Reprinted from: *Foods* **2025**, *14*, 3481, https://doi.org/10.3390/foods14203481 . . . . . **199**

Yiyuan Chen, He Huang, Ruiyang Yin, Xiuli He, Liyun Guo, Yumei Song, et al.
Multi- Technique Flavoromics for Identifying Key Differential Volatile Compounds Underlying Sensory Profiles in Lager Beers
Reprinted from: *Foods* **2025**, *14*, 3428, https://doi.org/10.3390/foods14193428 . . . . . **214**

Dandan Song, Chunlin Zhang, Yashuai Wu and Liang Yang
Ecological Risks in Daqu Storage and Their Impact on Baijiu Flavor: Precision Process Strategies for Damage Mitigation While Preserving Aroma
Reprinted from: *Foods* **2026**, *15*, 1195, https://doi.org/10.3390/foods15071195 . . . . . **257**

Dandan Song, Xian Zhong, Yashuai Wu, Jiaqi Guo, Lulu Song and Liang Yang
From Artisan Experience to Scientific Elucidation: Preparation Processes, Microbial Diversity, and Food Applications of Chinese Traditional Fermentation Starters (Qu)
Reprinted from: *Foods* **2025**, *14*, 3814, https://doi.org/10.3390/foods14223814 . . . . . **293**

About the Editors

Dongrui Zhao

Dongrui Zhao is affiliated with the School of Food and Health, Beijing Technology and Business University. His research interests focus on food flavor analysis, evaluation of functional ingredients, quality factor discovery in fermented foods, and product development related to Baijiu, beer, and food and medicine homologous resources. He has led research projects supported by the National Natural Science Foundation of China and industry collaborations, with work covering molecular flavor characterization, sensory evaluation, fermentation quality regulation, and functional component assessment. He has published extensively on food flavor and fermentation science and has received several science and technology awards for his contributions to food quality research and industrial applications.

Jianan Zhang

Jianan Zhang is affiliated with the School of Food Science and Engineering, Central South University of Forestry and Technology. Her research interests include food flavor chemistry, sensory mechanisms, fermentation science, taste active compounds, and the molecular basis of food perception. Her work has involved the discovery and characterization of umami peptides, flavor-related compounds, and fermentation-derived quality factors, using approaches such as sensory evaluation, molecular docking, molecular dynamics simulation, and foodomics analysis. She has contributed to studies on fermented food flavor, taste enhancement, and sensory-guided quality evaluation, providing useful insights into the relationship between food composition, processing, and consumer perception.

Preface

This Reprint brings together recent studies that reflect the continuing transformation of food quality research from descriptive evaluation toward mechanism-based understanding and practical applications. Food flavor, fermentation, functionality, and safety are no longer isolated topics. They are closely connected through molecular composition, microbial ecology, processing conditions, sensory perception, nutritional value, and quality control. The works collected in this Reprint cover fermented foods and beverages, traditional fermentation starters, fruits and vegetables, botanical seasonings, functional food components, and rapid safety detection. Together, they show how instrumental analysis, sensory science, multi omics, chemometrics, artificial intelligence, and process engineering can be used to explain flavor formation, microbial succession, quality differentiation, and safety risks in complex food systems.

The motivation for preparing this Reprint is to provide readers with an integrated view of current progress in food flavor and quality science. The contributions included here move beyond the simple identification of compounds or microorganisms and place greater emphasis on sensory relevance, biological function, process regulation, and industrial translation. We hope that this Reprint will serve as a useful reference for researchers, graduate students, food scientists, sensory analysts, fermentation technologists, quality control specialists, and industry professionals who are interested in understanding how modern analytical and data-driven approaches can support the design of foods that are flavorful, safe, stable, nutritious, culturally distinctive, and acceptable to consumers.

Dongrui Zhao and Jianan Zhang
Guest Editors

foods

MDPI

Editorial

From Molecular Flavor Signatures to Mechanism-Oriented Food Quality: Advances in Flavoromics, Fermentation Ecology, Functionality, and Safety

Dongrui Zhao [1,2,3,4,*] and Jianan Zhang [5]

[1] Key Laboratory of Geriatric Nutrition and Health, Ministry of Education, Beijing Technology and Business University, Beijing 100048, China
[2] Key Laboratory of Brewing Molecular Engineering of China Light Industry, Beijing Technology and Business University, Beijing 100048, China
[3] National Baijiu and Huangjiu Research Institute, Beijing Technology and Business University, Beijing 100048, China
[4] China Food Flavor and Nutrition Health Innovation Center, Beijing Technology and Business University, Beijing 100048, China
[5] National Engineering Research Center for Rice and By-Product Deep Processing, School of Food Science and Engineering, Central South University of Forestry and Technology, Changsha 410004, China; fez.jianan@foxmail.com
* Correspondence: zdr@btbu.edu.cn; Tel.: +86-10-68984044; Fax: +86-10-68984890

Food quality is now understood less as a single attribute than as an integrated system of flavor perception, nutritional value, microbial ecology, processing history, and safety assurance. This shift is especially visible in fermented foods, brewed beverages, fresh fruits and vegetables, botanical seasonings, and rapidly perishable animal products, where volatile and non-volatile metabolites interact with microbial succession, matrix composition, and consumer perception. The papers collected in this Special Issue reflect this transformation. Together, they move from descriptive quality evaluation toward mechanism-oriented food science, in which instrumental analysis, sensory science, multi-omics, chemometrics, and process control are combined to explain why foods taste, smell, age, ferment, and deteriorate as they do. Recent advances in sensomics and flavoromics emphasize that meaningful flavor research should connect molecular identification with sensory prediction, while machine-learning-assisted flavoromics is becoming an important strategy for defining characteristic food flavor signatures [1,2].

Fermented and brewed matrices form one of the major threads of this collection. The study on lager beers demonstrates the value of combining GC-MS, GCxGC-TOF-MS, GC-O-MS, sensory evaluation, odor and taste activity analysis, multivariate statistics, and flavor addition experiments to distinguish brand-specific aroma profiles at the molecular level. Rather than treating beer flavor as a simple sum of abundant volatiles, this work highlights the importance of sensory-active trace compounds and their combined effects. A parallel focus appears in the contributions on Baijiu. The study of sauce-aroma high-temperature Daqu from the Chishui River Basin links trace volatile fingerprints, sensory scoring, molecular docking, and bacterial and fungal community structures, thereby providing a more integrated explanation of Daqu quality. The work on high- and low-alcohol Jiangxiangxing Baijiu further shifts attention from orthonasal aroma alone to retronasal perception, showing that differences in olfactory thresholds and dose-over-threshold distributions can explain why low-alcohol products may lose aroma richness even when compound concentrations appear similar. These studies echo the broader consensus that

the Baijiu ecosystem is driven by complex microbial communities, enzymatic functions, and metabolite interactions [3–5].

Microbial succession and starter ecology are another central theme. The research on sour bamboo shoot fermentation clarifies how organic acids, especially lactic and acetic acids, help drive the transition from Enterobacteriaceae-dominated early communities to lactic-acid-bacteria-dominated fermentation systems. This finding is important not only for traditional vegetable fermentation, but also for the broader question of how microbial stress tolerance, interspecies interactions, and acidification jointly shape safety and flavor. The review on Chinese traditional fermentation starters (Qu) provides a wider technological context by organizing preparation parameters, microbial diversity, and food applications across Daqu, Xiaoqu, Hongqu, wheat bran or Jiangqu, Douchi Qu, and Furu-related starters. The companion review on ecological risks during Daqu storage extends this perspective from starter preparation to post-production stability, emphasizing that environmental disturbances can alter microecological balance, enzyme activity, and aroma formation. These contributions align with recent multi-omics research showing that precise characterization of microorganisms and their functional pathways is essential for understanding fermented food quality and for designing controlled microbial processes [6,7].

The Special Issue also broadens flavor science beyond fermented systems into fresh and processed plant-derived foods. Studies on cucumber, melon, Younai plum, Citri Reticulatae Pericarpium, and fried Tengjiao oil demonstrate how cultivar, origin, drying or storage conditions, and raw-material state can reshape volatile profiles, nutritional traits, and sensory attributes. In cucumbers, HS-SPME-GC-MS and chemometrics reveal cultivar-dependent volatile signatures and nutritional variation. In melons, multi-omics integration connects saline-alkali cultivation with changes in volatile and non-volatile metabolites, especially pathways related to flavonoid biosynthesis. The Younai plum study builds a baseline for linking sugar-acid composition, aroma-active compounds, and untargeted metabolomics. The work on Citri Reticulatae Pericarpium combines GC-MS, GC-IMS, electronic nose, sensory evaluation, and microstructure analysis to show how controlled drying and storage support volatile retention and aroma complexity. Meanwhile, the Tengjiao oil study uses molecular sensory science, AEDA, OAV analysis, recombination and omission tests, and chiral analysis to decode the flavor differences between oils prepared from fresh and dried raw materials. These examples show why modern food flavor analysis increasingly depends on complementary techniques such as GC-O-MS and GC-IMS, which can connect chemical fingerprints with sensory relevance more effectively than single-platform profiling [8,9].

Functionality and safety provide the final axis of the collection. The study on strong-flavor-type Baijiu uses widely targeted metabolomics and network pharmacology to screen potential bioactive compounds and predicted biological targets, thereby expanding Baijiu research from volatile aroma chemistry into possible functional components. Although such computational predictions require further biological validation, they provide useful hypotheses for future work on the relationship between complex food matrices and health-relevant small molecules. The contribution on cold-chain fish samples addresses a different but equally important problem: rapid safety screening. By developing a portable ion trap mass spectrometry method with nano-electrospray ionization for biogenic amines, the study responds to a long-standing need for fast, field-adaptable quality control in perishable aquatic products. This is particularly relevant because histamine and other biogenic amines are widely recognized as important food safety and freshness indicators, and their determination has remained an active analytical challenge [10].

Taken together, the articles in this Special Issue suggest several priorities for the next stage of food flavor, fermentation, and safety research. First, sensory validation should

https://doi.org/10.3390/foods15132337

remain central. Compound annotation, even at high resolution, becomes most useful when linked to orthonasal and retronasal perception, temporal sensory dynamics, thresholds, recombination, and omission experiments. Second, multi-omics datasets should be connected more directly to process variables, microbial functions, and industrial decision points. This will allow researchers to move from correlation toward controllable mechanisms. Third, standardized data structures, shared reference materials, and transparent chemometric or machine-learning workflows will be needed if flavoromics is to support reliable prediction across varieties, origins, production batches, and storage conditions. Finally, practical translation should be kept in view. The ultimate value of these approaches lies in helping producers design foods that are flavorful, safe, nutritionally meaningful, culturally distinctive, and technologically reproducible. By bringing together work on brewed beverages, traditional starters, fermented vegetables, fruits, botanical seasonings, functional components, and rapid safety detection, this Special Issue provides a timely snapshot of a field that is becoming more integrated, more quantitative, and more capable of linking food chemistry with real eating experience.

Frontier Perspectives

Looking forward, food flavor, fermentation, functionality, and safety research is expected to move further toward predictive, causal, and application-oriented science. One important frontier is the construction of sensory-guided flavoromics systems that can link molecular fingerprints with real human perception. Future studies should not only identify volatile and non-volatile compounds, but also clarify how these compounds contribute to orthonasal aroma, retronasal aroma, taste, mouthfeel, aftertaste, and temporal sensory changes. Threshold determination, recombination and omission experiments, time-intensity analysis, and consumer-oriented sensory validation will remain essential for distinguishing chemically detectable compounds from truly sensory-relevant quality markers.

A second frontier lies in the deeper integration of multi-omics data with microbial ecology and process engineering. In fermented foods and brewed beverages, microbial communities do not simply coexist with flavor compounds; they actively drive substrate transformation, enzyme production, metabolite accumulation, and quality differentiation. Therefore, future research should connect metagenomics, metatranscriptomics, metabolomics, proteomics, and sensory data with fermentation parameters such as temperature, oxygen exposure, raw-material composition, starter preparation, storage environment, and process duration. Such integration will help researchers move beyond correlation-based interpretation and toward controllable mechanisms that can guide industrial production.

Artificial intelligence and machine learning will also become increasingly important in food quality prediction. Data-driven models can help screen key flavor markers, classify origins and varieties, predict sensory attributes, optimize fermentation conditions, and detect quality deterioration at an early stage. However, the reliability of these models will depend on standardized datasets, transparent feature selection, external validation, and interpretable algorithms. Future work should avoid treating machine learning as a purely statistical tool and instead use it as a bridge between chemical composition, biological function, sensory perception, and process control.

Another promising direction is the development of portable, rapid, and on-site analytical technologies. For highly perishable foods such as aquatic products, meat, fresh produce, and fermented products under storage, laboratory-based analysis alone may not meet the needs of real-time quality management. Portable mass spectrometry, electronic nose systems, electronic tongue systems, biosensors, spectral imaging, and intelligent detection platforms may provide faster tools for monitoring freshness, safety risks, microbial spoilage, and flavor deterioration. When combined with chemometrics and cloud-based databases,

https://doi.org/10.3390/foods15132337

these technologies could support more efficient quality control across production, storage, transportation, and consumption.

Finally, future food quality research should pay more attention to translation from scientific discovery to practical food design. The ultimate goal is not only to explain why foods differ in flavor, safety, or functionality, but also to help producers design products that are stable, safe, flavorful, nutritionally meaningful, culturally recognizable, and acceptable to consumers. This requires closer collaboration among food chemists, microbiologists, sensory scientists, data scientists, process engineers, nutrition researchers, and industry practitioners. Through this interdisciplinary framework, food quality science can evolve from post hoc evaluation toward intelligent prediction, precision regulation, and consumer-centered innovation.

Author Contributions: Conceptualization, D.Z. and J.Z.; writing—original draft preparation, D.Z. and J.Z.; review and editing, D.Z. and J.Z. All authors have read and agreed to the published version of the manuscript.

Funding: This research was supported by the National Natural Science was Foundation of China (No. 32572737), Beijing Elite Scientist Sponsorship Program of BAST (No. BYESA.2023055), Research Foundation for Youth Scholars of Beijing Technology and Business University (RFYS2025), the National Key Research and Development Program of China (No. 2022YFD2101205), and the National Natural Science Foundation of China (No. 32322068).

Data Availability Statement: Not applicable.

Acknowledgments: As the Guest Editors, we would first like to express our sincere gratitude to Yashuai Wu, for his substantial assistance, active cooperation, and dedicated support throughout the preparation, organization, and development of this Special Issue. We sincerely thank all authors who contributed their high-quality work to this Special Issue, as well as all anonymous reviewers for their careful evaluations, constructive comments, and important efforts in helping improve the submitted manuscripts. Their collective contributions have been essential to the successful completion of this Special Issue and to the advancement of research in this field.

Conflicts of Interest: The authors declare no conflict of interest.

List of Contributions:

1. Chen, Y.; Huang, H.; Yin, R.; He, X.; Guo, L.; Song, Y.; Zhao, D.; Sun, J.; Li, J.; Huang, M.; et al. Multi-Technique Flavoromics for Identifying Key Differential Volatile Compounds Underlying Sensory Profiles in Lager Beers. *Foods* **2025**, *14*, 3428. https://doi.org/10.3390/foods14193428.
2. Zhang, X.; Zhang, C.; Gong, M.; Li, P.; Tang, H.; Jiang, L.; Liu, Y. Dynamics of Lactic Acid Bacteria Dominance in Sour Bamboo Shoot Fermentation: Roles of Interspecies Interactions and Organic Acid Stress. *Foods* **2025**, *14*, 3481. https://doi.org/10.3390/foods14203481.
3. Song, D.; Zhong, X.; Wu, Y.; Guo, J.; Song, L.; Yang, L. From Artisan Experience to Scientific Elucidation: Preparation Processes, Microbial Diversity, and Food Applications of Chinese Traditional Fermentation Starters (Qu). *Foods* **2025**, *14*, 3814. https://doi.org/10.3390/foods14223814.
4. Lu, P.; Wang, C.; Zhang, Y.; Jin, H.; Wu, S.; Ding, X.; Zhang, H. Diversity of Volatile Profiles and Nutritional Traits Among 29 Cucumber Cultivars. *Foods* **2025**, *14*, 3878. https://doi.org/10.3390/foods14223878.
5. Song, D.; Song, L.; Zhong, X.; Wu, Y.; Zhang, Y.; Yang, L. Integrated Molecular Informatics and Sensory-Omics Study of Core Trace Components and Microbial Communities in Sauce-Aroma High-Temperature Daqu from Chishui River Basin. *Foods* **2026**, *15*, 599. https://doi.org/10.3390/foods15030599.
6. Alim, A.; Huang, C.; Zhao, X.; Gaowa, S.; Zhang, R.; Zhang, J.; Zhang, X.; Jin, Y.; Hu, W. Investigating the Impact of Different Drying Methods on the Aroma of Citri Reticulatae Pericarpium Using GC-MS/GC-IMS and E-Nose Technology. *Foods* **2026**, *15*, 1117. https://doi.org/10.3390/foods15071117.

7. Zhang, J.; Han, Y.; You, X.; Zhu, X.; Sun, Y.; Hu, F.; Yu, X.; Chen, S.; Xu, Y. Characterization of Retronasal Aroma Differences in High- and Low-Alcohol Jiangxiangxing Baijiu Using Temporal Sensory Evaluation, Retronasal Olfactory Thresholds, and Dose-over-Threshold Analysis. *Foods* **2026**, *15*, 1156. https://doi.org/10.3390/foods15071156.
8. Song, D.; Zhang, C.; Wu, Y.; Yang, L. Ecological Risks in Daqu Storage and Their Impact on Baijiu Flavor: Precision Process Strategies for Damage Mitigation While Preserving Aroma. *Foods* **2026**, *15*, 1195. https://doi.org/10.3390/foods15071195.
9. Dong, T.; Wu, P.; Sun, J.; Chen, H.; Wang, S. Decoding the Flavor Code of Fresh and Dried Tengjiao (*Zanthoxylum armatum* DC.) for Preparing Fried Tengjiao Oil Through Molecular Sensory Science. *Foods* **2026**, *15*, 1326. https://doi.org/10.3390/foods15081326.
10. Liu, J.; Zheng, J.; Wu, J.; Sun, Y.; Huang, M.; Su, J.; Zheng, F.; Zhao, D. Identification of Potential Bioactive Compounds in Strong-Flavor-Type Baijiu via Integration of Widely Targeted Metabolomics and Network Pharmacology. *Foods* **2026**, *15*, 1509. https://doi.org/10.3390/foods15091509.
11. Hua, J.; Mao, K.; Yu, W.; Li, Z.; Wen, R.; Li, L.; Song, L.; Sang, Y.; Wang, X. Multi-Omics Integration to Investigate the Effects of Variety and Origin on Volatile and Non-Volatile Metabolites in Melons. *Foods* **2026**, *15*, 1746. https://doi.org/10.3390/foods15101746.
12. Fu, L.; Liu, W.; Ren, L.; Lin, X.; Guo, J.; Chen, H.; Chen, F.; Yan, S. Systematic Characterization of Flavor Profiles and Screening of Potential Key Aroma-Active Components in Prunus salicina var. cordata cv. 'Younai'. *Foods* **2026**, *15*, 1787. https://doi.org/10.3390/foods15101787.
13. Wu, J.; Ma, X.; Wang, Z.; Wei, Y.; Liu, Y.; Men, J.; Ma, W. Rapid Determination of Several Biogenic Amines in Cold-Chain Fish Samples by Portable Ion Trap Mass Spectrometry with Nano-Electrospray Ionization. *Foods* **2026**, *15*, 1802. https://doi.org/10.3390/foods15101802.

References

1. Han, H.; Blank, I.; Duan, Y.; Xu, K.; Guo, Z.; Liu, S.; Ding, S.; Lucini, L.; Zhong, F.; Wang, B. From Molecule Identification to Sensory Prediction: Approaches, Applications, and Perspectives of Sensomics and Flavoromics in Volatile Flavor Compound Research. *J. Agric. Food Chem.* **2026**, *74*, 3316–3331. [CrossRef] [PubMed]
2. Cai, D.; Li, X.; Liu, H.; Wen, L.; Qu, D. Machine learning and flavoromics-based research strategies for determining the characteristic flavor of food: A review. *Trends Food Sci. Technol.* **2024**, *154*, 104794. [CrossRef]
3. Cai, W.; Wang, Y.; Ni, H.; Liu, Z.; Liu, J.; Zhong, J.; Hou, Q.; Shan, C.; Yang, X.; Guo, Z. Diversity of microbiota, microbial functions, and flavor in different types of low-temperature Daqu. *Food Res. Int.* **2021**, *150*, 110734. [CrossRef] [PubMed]
4. Huang, Y.; Li, D.; Mu, Y.; Zhu, Z.; Wu, Y.; Qi, Q.; Mu, Y.; Su, W. Exploring the heterogeneity of community and function and correspondence of "species-enzymes" among three types of Daqu with different fermentation peak-temperature via high-throughput sequencing and metagenomics. *Food Res. Int.* **2024**, *176*, 113805. [CrossRef] [PubMed]
5. Zou, W.; Zhao, C.; Luo, H. Diversity and Function of Microbial Community in Chinese Strong-Flavor Baijiu Ecosystem: A Review. *Front. Microbiol.* **2018**, *9*, 671. [CrossRef] [PubMed]
6. Yuan, J.; Ma, D.; Yang, Y.; Zhao, Y.; Ren, H.; Liu, X.; Tan, M.; Li, K. A review and prospects: Multi-omics and artificial intelligence-based approaches to understanding the effects of lactic acid bacteria and yeast interactions on fermented foods. *Innov. Food Sci. Emerg. Technol.* **2025**, *99*, 103874. [CrossRef]
7. Shi, H.; An, F.; Lin, H.; Li, M.; Wu, J.; Wu, R. Advances in fermented foods revealed by multi-omics: A new direction toward precisely clarifying the roles of microorganisms. *Front. Microbiol.* **2022**, *13*, 1044820. [CrossRef] [PubMed]
8. Song, H.; Liu, J. GC-O-MS technique and its applications in food flavor analysis. *Food Res. Int.* **2018**, *114*, 187–198. [CrossRef] [PubMed]
9. Wang, S.; Chen, H.; Sun, B. Recent progress in food flavor analysis using gas chromatography-ion mobility spectrometry (GC-IMS). *Food Chem.* **2020**, *315*, 126158. [CrossRef] [PubMed]
10. Sentellas, S.; Nunez, O.; Saurina, J. Recent Advances in the Determination of Biogenic Amines in Food Samples by (U)HPLC. *J. Agric. Food Chem.* **2016**, *64*, 7667–7678. [CrossRef] [PubMed]

Disclaimer/Publisher's Note: The statements, opinions and data contained in all publications are solely those of the individual author(s) and contributor(s) and not of MDPI and/or the editor(s). MDPI and/or the editor(s) disclaim responsibility for any injury to people or property resulting from any ideas, methods, instructions or products referred to in the content.

foods

MDPI

Article

Rapid Determination of Several Biogenic Amines in Cold-Chain Fish Samples by Portable Ion Trap Mass Spectrometry with Nano-Electrospray Ionization

Jianxin Wu, Xiaotong Ma, Zongyi Wang *, Ying Wei, Yuting Liu, Jiaqian Men and Wenyu Ma

Beijing Key Laboratory of Agricultural Product Detection and Control for Spoilage Organisms and Pesticides, College of Food Science and Engineering, Beijing University of Agriculture, Beijing 102206, China; 15011216964@163.com (J.W.); m13095157604@163.com (X.M.); proudwy@126.com (Y.W.); 13020087674@163.com (Y.L.); 15383291685@163.com (J.M.); mawy2872@163.com (W.M.)

* Correspondence: 20107001@bua.edu.cn; Tel.: +86-10-80799174

Abstract

A novel method was developed for the rapid determination of five biogenic amines (BAs)—histamine (HIS), tyramine (TYR), cadaverine (CAD), spermidine (SPD), and spermine (SPM) in cold-chain fish by portable ion trap mass spectrometry with nano-electrospray(nESI) ionization. Samples were homogenized and extracted with aqueous solution containing 1% (v/v) formic acid and 80% (v/v) acetonitrile. With HIS-d4 as an internal standard, the sample solutions were directly injected with the nESI injection device and detected by a portable ion trap mass spectrometer at MS/MS detection mode. The results showed good linearity in the invested range of 0.2 (or 0.5)–10 μg mL^{-1} with $R^2 > 0.992$, The limit of detection (LODs) and limits of quantification (LOQs) for HIS were less than 1.5 mg/kg and 4.0 mg/kg, respectively; the LOD and LOQ for other four BAs were less than 4.0 mg/kg and 12.5 mg/kg, respectively. Recoveries at three fortified levels ranged from 84.26% to 106.6% with relative standard deviations between 4.56% and 13.84%. With the safety limits of HIS as the concentrations of concern, this method demonstrated excellent performance when applied to the eligibility fast screening of HIS in cold-chain fish. The study provided a valuable methodological reference for the rapid detection of BAs in food.

Keywords: biogenic amine; nano-electrospray ionization (nESI); portable ion trap mass spectrometry; cold-chain fish; eligibility fast screening

1. Introduction

Biogenic amine (BA) is a class of basic nitrogenous compounds of low molecular mass in foods produced mainly by decarboxylation of free amino acids or aldoketo amination reactions [1,2]. Low levels of BAs in the body have important physiological functions such as growth regulation, neurotransmission, and inflammatory mediators [3,4], but consumption of foods with high levels of BA can lead to toxic reactions such as respiratory distress, elevated blood pressure, vomiting, and headache [5,6]. In addition, BA in foods can react with nitrites to convert them into carcinogenic nitrosamines [7,8]. Usually, fresh aquatic products contain low levels of BAs, but due to improper storage and transportation, these protein- and amino acid-rich aquatic products are prone to producing large amounts of BAs [9,10], which affects the quality of the products. As a result, BA has also become one of the key indicators for assessing food safety and freshness in many countries. There

is no uniform international limit standard for BA in food, and the existing regulatory limits mainly focus on fish and their products, and the BAs involved are mainly histamine (HIS) and tyramine (TYR), which have the most toxic effects [11,12]. For example, the U.S. Food and Drug Administration (FDA) stipulates a limit level of 50 mg/kg for HIS and no more than 100 mg/kg for TYR, while in China, only a limit for HIS in aquatic products has been set, which stipulates a limit level of 400 mg/kg in high-histamine fishes, such as mackerel, tuna and skipjack tuna, and 200 mg/kg in other seawater fishes.

Currently, the analytical methods reported for BAs mainly include high-performance liquid chromatography (HPLC) using different kinds of detectors [13,14], gas chromatography-mass spectrometry (GC-MS) [15], high-performance liquid chromatography-tandem mass spectrometry (HPLC-MS/MS) or ultra performance liquid chromatography-tandem mass spectrometry (UPLC-MS/MS) [16,17], capillary electrophoresis (CE) [18] and ion mobility spectrometry[IMS] [19]. Among them, CE and IMS are less used in routine food analysis; HPLC and GC-MS both require pre-column or post-column derivatization, which is inconvenient; the advantages of HPLC-MS/MS or UPLC-MS/MS in solving the tasks of qualitative and quantitative analysis of micro- and trace multicomponent targets in complex matrices are very prominent, in terms of BAs, derivatization-free detection could be achieved, so it has been more widely used in the detection of BAs in food, but there are problems such as relying on large-scale equipment, high detection cost and inability to realize on-site detection.

Ambient ionization mass spectrometry (MS) is a rapidly developing ionization technique from the 2000s, which can complete the analysis of samples without or only with simple sample pretreatment and has the advantages of fast analysis speed, simplicity and high efficiency [20–22]. A large number of ambient ionization techniques have been reported and applied in the field of food and drugs to date [23,24]. In recent years, with the rapid development of mass spectrometry technology, the combination of ambient ionization technology and portable mass spectrometry has realized the miniaturization of the instrument, while still retaining the advantages of qualitative and reliable mass spectrometry, and also enabling rapid detection. The paper capillary spray (PCS) [25–27] and nanoelectrospray (nESI) technique [28] are two of the better-developed ambient ionization techniques used in portable mass spectrometers. The PCS technology combines a metal capillary with a paper substrate by loading solid or liquid samples onto the surface of the paper substrate, eluting them with a suitable solvent, and entering the capillary for electrospraying them, which improves spraying stability and sensitivity compared to paper spraying technology. The nESI technique loads a liquid sample into a glass capillary (lined with a metal wire) for electrospraying; Compared with PCS, nESI provides higher sensitivity, better reproducibility and larger sample loading capacity, which is more conducive to quantitative analysis. Both techniques are characterized by easy operation, high detection efficiency, and on-site real-time determination in conjunction with portable mass spectrometry, but few studies have been reported on analyzing BAs in cold-chain fish products. Therefore, it is of great value to apply this technique to the quality evaluation and monitoring of cold chain fish products.

In this study, it is proposed to nESI ionization combined with a small portable ion trap mass spectrometer to establish and validate a novel method for the rapid detection of five types of BAs, namely, HIS, TYR, cadaverine (CAD), spermine (SPM) and spermidine (SPD), in cold-chained fish products, which could provide a valuable technology reference for the rapid screening and on-site detection of BAs content in cold-chained fish products.

https://doi.org/10.3390/foods15101802

2. Materials and Methods

2.1. Chemicals and Reagents

The standards of HIS, CAD, TYR, SPM and SPD were purchased from Sigma Aldrich Shanghai Co. (Shanghai, China). Histamine-d4 (HIS-d4) was purchased from Tianjin Alta Technology Co. (Tianjin, China). HPLC-grade acetonitrile, methanol, formic acid and n-hexane were purchased from Beijing Myriad Technology Co. (Beijing, China).

2.2. Standard Solution Preparation

Stock solutions of each BA at 1.0 mg mL^{-1} and HIS-d4 at 0.1 mg mL^{-1} were prepared in methanol and were stored frozen between −12 °C and −18 °C. Intermediate standard solutions of the mixture of five BAs at 100 μg mL^{-1} and the HIS-d4 internal standard working solution at 10 μg mL^{-1} were prepared by diluting the stock solutions with methanol, respectively. The calibration standard solutions of the mixture of the five analytes (0.2, 0.5, 1, 2, 5 and 10 μg mL^{-1}) were prepared by diluting the intermediate standard solutions with an aqueous solution containing 1% (v/v) formic acid and 80% (v/v) acetonitrile.

2.3. Sample Preparation

About 200 g of the edible portion of the was taken from each fish sample after deboning and was fully crushed in a sample pulverizer (Midea MJ-WBL2531H, Guangdong Midea Living Electrical Appliances Manufacturing Co., Ltd., Foshan, China). The sample extraction was performed following the method described by WU et al. [29] with appropriate modifications and briefly summarized as follows: 2.0 g (accurate to 0.0001 g) of the sample was crushed and weighed into a 50 mL centrifuge tube, and 10 mL of aqueous solution containing 1% (v/v) formic acid and 80% (v/v) acetonitrile was added. Then, the sample in the tube was homogenized using a homogenizer (FSH-2 Adjustable High-speed Homogenizer, Changzhou Guohua Electric Co., Ltd., Changzhou, China) at a speed between 9500 and 10,500 r/min for 30 s. After that, the tube was put into the centrifuge (Eppendorf Centrifuge 5180 R, Eppendorf AG, 2231 Hamburg, Germany) and centrifuged at 8000 rpm for 5 min. The supernatant was transferred to a 25 mL volumetric flask. The blade head of the homogenizer was rinsed for 30 s at same rotational speed with another 50 mL centrifuge tube containing 10 mL of the aqueous solution containing 1% (v/v) formic acid and 80% (v/v) acetonitrile, and the rinsate was then poured into the original tube containing the sample residue for a second extraction by vortexing the mixture for 30 s and centrifuging again at 8000 rpm for 5 min; the supernatant from the second extraction was also combined into the same volumetric flask and was diluted to the volume with the aqueous solution containing 1% (v/v) formic acid and 80% (v/v) acetonitrile. Then, 2 mL of the sample extraction solution was transferred into a 10 mL centrifuge tube, and 3 mL of n-hexane was added. The tube was vortexed for 30 s, then left to stand until fully stratified, and the upper layer of n-hexane solution was discarded. The lower layer sample extraction solution was filtered through a 0.22 μm syringe filter and collected into a 2 mL vial, ready for analysis.

2.4. Portable Ion Trap Mass Spectrometry Analysis

2.4.1. Instrumentation and Analysis Conditions

The rapid determination was carried out using a CELL portable ion trap mass spectrometry system on the MS/MS detection mode with PMS Client Pro analytical software and the simple, small nESI injection device containing an injection base and a nano-spray needle (Beijing Qingpu Analytical Instrument Co., Ltd., Beijing, China). The analytical parameters of each analyte are shown in Table 1.

https://doi.org/10.3390/foods15101802

Table 1. Analytical parameters of five BAs and the internal compound HIS-d4.

Item	HIS	HIS-d4	CAD	TYR	SPD	SPM
Ionization mode	ESI+	ESI+	ESI+	ESI+	ESI+	ESI+
Ionization Voltage (V)	2500	2500	2000	2500	2000	2500
Injection time (s)	60	60	40	60	60	60
Scan range (m/z)	20–250	20–250	20–250	20–250	20–250	20–250
Collision gas	Air	Air	Air	Air	Air	Air
Precursor ion (m/z) and Collision energy (eV)	112; 0	116; 0	103; 0	138; 0	146; 0	203; 0
Product ions (m/z) and Collision energy (eV)	95; 2	99; 2	86; 1.5	121; 2	129; 2	129; 2.5

2.4.2. Operating Procedures

A volume of 100 μL of the final sample extraction solution and 20 μL of internal standard working solution were accurately pipetted into a 2 mL centrifugal tube and mixed by vortexing, then not less than 20 μL of the mixing sample solution was pipetted into the nano-spray needle of the nESI injection device. Next, the nESI injection device was inserted into the injection port of the small mass spectrometer and MS detection was performed. For the series of mixture calibration standard solutions, the detection was carried out with the same procedures.

2.5. Method Validation

2.5.1. Linearity, Limit of Detection (LOD), Limit of Quantification (LOQ), Accuracy and Precision

Linearity was evaluated by injection of the calibration standard solutions and least-square regression between the concentration ratios of analytes to the internal standard HIS-d4 and the ratios of their response. The LOD and LOQ were estimated based on the quantitative results of the actual samples or the samples fortified with analyte at the low level, with a signal-to-noise ratio of $\geq$3 and $\geq$10 as criteria, respectively. The accuracy and precision were evaluated through analyzing the samples fortified with each analyte at three concentrations (near LOQ, medium, and high) and calculating the recoveries and relative standard deviations (RSDs).

2.5.2. Threshold and Positive Detection Rate

Threshold is the value that determines whether the detection result exceeds the concentration of concern when a quantitative analytical method is used for the purpose of an eligibility screen. It was calculated according to the determining results of multiple replicate samples spiked with the analyte at the same level of concentration of concern. The calculation equation was as Formula (1).

$$\text{Threshold} = \overline{x} - t_{\alpha}(f) \cdot \frac{S}{\sqrt{n}} \quad (1)$$

where $\overline{x}$ is the average result of the multiple independent determinations; $t_{\alpha}(f)$ is the value of the t-distribution when the significance level is α (here, α = 0.05) and the degree of freedom is f (here, $f = n - 1$); S and n are the standard deviation and number of independent repeated determinations, respectively.

For a concentration of concern, if the determining result of the analyte was above the threshold, the sample was recorded as a positive sample for the analyte, and if that was below the threshold, the sample was recorded as a negative sample for the analyte. Series gradient spiked samples with analyte concentrations close to (below, above, and equal to) the concentration of concern were prepared with 20 replicate samples for each gradient level. The analyte was determined in those samples, and positive detection rates

were calculated at each fortified level. The positive detection rate, calculated according to Formula (2).

$$\text{positive detection rate} = \frac{n}{N} \times 100\% \quad (2)$$

where n is the number of positive samples at a level; N is the total number of samples at the level.

The concentration level at which the positive detection rate is at least 95% is defined as the minimum reliable detection level for positive samples; the concentration level at which the positive detection rate is at most 5% is defined as the maximum reliable detection level for negative samples.

3. Results and Discussion

3.1. Mass Spectrometry Detection

Firstly, single standard solutions of each analyte at an injection concentration of 10 μg/mL were injected for analysis. The $[M + H]^+$ ions of each target compound were selected as precursor ions for full-scan MS acquisition with a collision energy of 0 eV. Taking the maximum response intensity as the evaluation index, the ionization voltage and injection time were optimized to determine their optimal values. Subsequently, MS/MS scanning was performed at different collision energies to screen the optimal fragment ions and their corresponding collision energies. The optimized mass spectrometry parameters are summarized in Table 1. The mass spectra of the five target BAs and the internal standard HIS-d4 under the optimized conditions are shown in Figure 1. The sample solvent is another factor that affects the performance. Although multi-stage ion trap mass spectrometry can provide better selectivity, the detection sensitivity decreases accordingly. For the BAs compounds with small molecular masses ranging from 103 to 203 Daltons, here, the experiments showed that MS/MS detection not only ensured good selectivity but also maintained high sensitivity. Therefore, MS/MS detection was used.

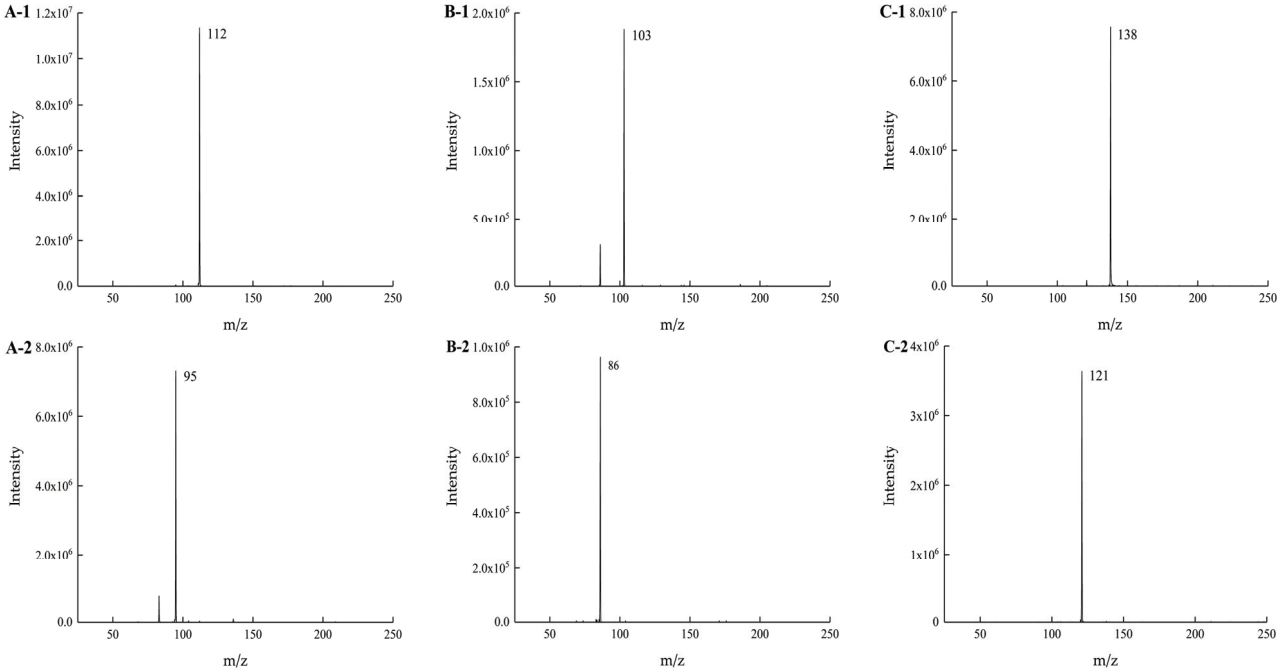


Figure 1. *Cont.*

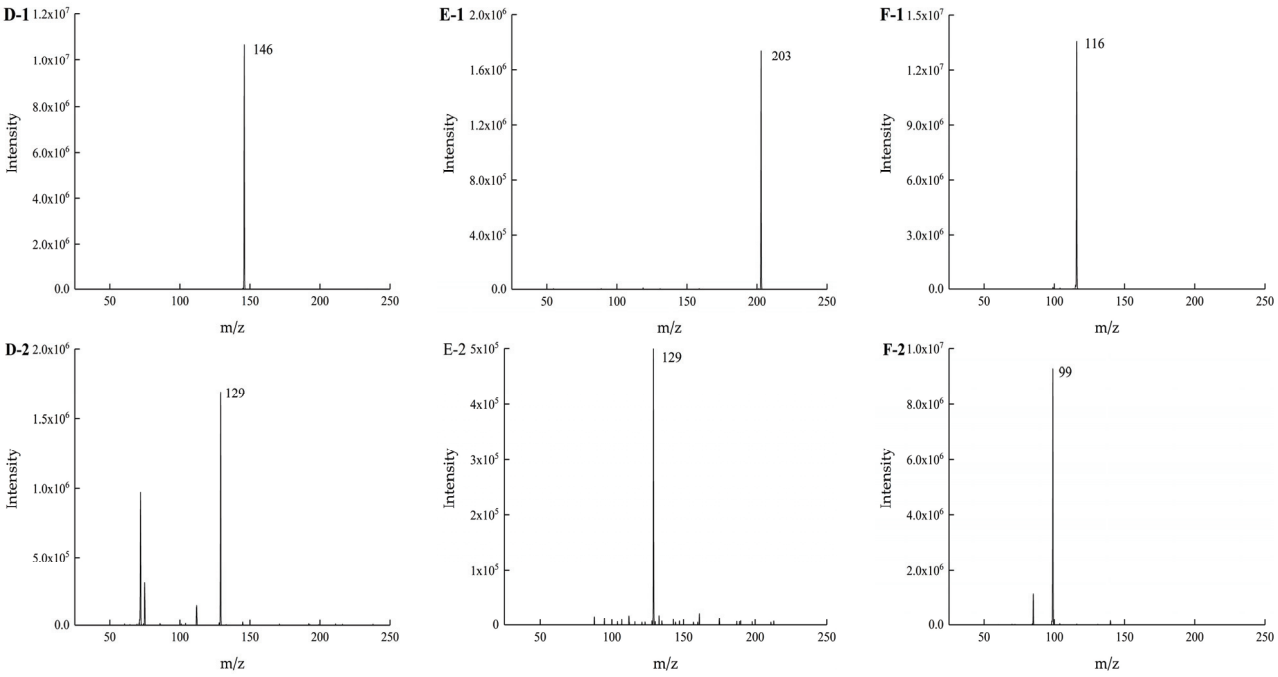


Figure 1. The primary mass spectra ((**A-1**) HIS, (**B-1**) CAD, (**C-1**) TYR, (**D-1**) SPD, (**E-1**) SPM and (**F-1**) HIS-d4) and secondary ((**A-2**) HIS, (**B-2**) CAD, (**C-2**) TYR, (**D-2**) SPD, (**E-2**) SPM and (**F-2**) HIS-d4) mass spectra.

Sample solvent is another factor that affects the sensitivity of mass spectrometry detection. To better align the MS detection with the sample pretreatment process, in addition to adding 1% (v/v) formic acid to the solvent [29], the experiment further investigated the effect of different acetonitrile-water ratios. The results showed that when the acetonitrile ratio was between 70% (v/v) and 90% (v/v), the ion signals of the target compounds were relatively stronger; outside this range, the signal decreased significantly (see Figure 2). This is primarily because acetonitrile, as an aprotic solvent, is not conducive to the ionization of target compounds when its ratio is too high. Conversely, when the ratio is too low, the volatility of the solvent decreases, leading to poor nebulization efficiency. Therefore, the acetonitrile ratio in the final sample solution was controlled within this range. In this study, the aqueous solution containing 1% (v/v) formic acid and 80% (v/v) acetonitrile was used as both extraction solvent and diluent, and its combination with hexane in a partitioning step effectively removes proteins and fatty materials, meeting the requirements for detection by mass spectrometry.

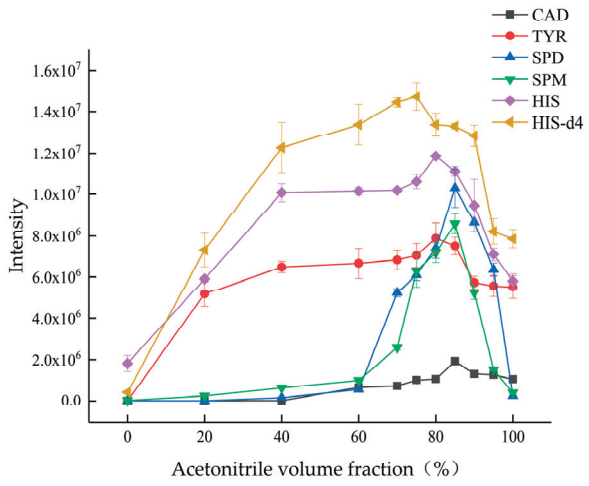


Figure 2. Effect of different acetonitrile volume fractions on the response values of analytes.

https://doi.org/10.3390/foods15101802

3.2. Method Validation

Under the optimized mass spectrometry conditions and sample pretreatment methods, the LOD and LOQ for the five BAs are presented in Table 2. Among these, HIS exhibited the lowest LOD and LOQ, reaching 1.5 mg kg^{-1} and 4.0 mg kg^{-1}, respectively, which are significantly below the allowable lowest limits of 50 mg kg^{-1} (FDA) for HIS in aquatic products. This satisfies the requirements for HIS eligibility fast screening and quantification analysis for quality evaluation using BAs as markers.

Table 2. Linearity, Limit of detection (LOD) and Limit of quantification (LOQ).

BA	LOD (mg/kg)	LOQ (mg/kg)	Linear Equation	Range (μg/mL)	R^2
HIS	≤1.5	≤5.0	$y = 0.4370x + 0.0224$	0.2~10	0.9961
CAD	≤4.0	≤12.5	$y = 0.0659x + 0.0053$	0.5~10	0.9936
TYR	≤4.0	≤12.5	$y = 0.5616x + 0.0425$	0.5~10	0.9923
SPD	≤4.0	≤12.5	$y = 0.2063x + 0.0332$	0.5~10	0.9959
SPM	≤4.0	≤12.5	$y = 0.3691x + 0.0769$	0.5~10	0.9932

y is the peak area ratio of each BA to HIS-d4; x is the content ratio of each BA to HIS-d4.

The linearity of the method was further investigated across concentrations ranging from 0.2 or 0.5 μg mL^{-1} (equivalent to LOQ in samples) to a maximum of 10 μg mL^{-1} for each analyte. The results demonstrated good linearity, with R^2 values ranging from 0.9923 to 0.9961 (See also Table 2).

The accuracy and precision were further evaluated via a spike recovery experiment with three fortified levels and six replicates at each level. Because the background contents of SPD and SPM in the samples are relatively high and mostly above the LOQ, it is difficult to prepare spiked samples near the LOQ level; So, the lowest fortification level of SPD and SPM was set at 50 mg/kg in the experiment. The results are shown in Table 3. The recoveries ranged from 84.26% to 106.6%, with relative standard deviations (RSDs), the intra-day repeatability, between 4.56% and 13.84%, indicating that the method exhibits good accuracy and precision. Since BAs are stable, the instrument was recalibrated before each batch of sample analysis, and in addition, the stable isotope-labeled BA (HIS-d4) was adopted as the internal standard for overcoming matrix effects and operational errors. Accordingly, the evaluation of precision using only intra-day replicates is sufficient for method validation, and inter-day precision was therefore not conducted in this study.

Table 3. The results of the spiked recovery experiment (n = 6).

BA	Add Level (mg kg^{-1})	Recovery (%)	RSD (%)
CAD	12.5, 100, 200	85.36, 96.85, 92.41	12.53, 6.78, 5.68
HIS	5, 100, 200	85.44, 99.10, 94.28	9.62, 4.56, 4.74
TYR	12.5, 100, 200	97.47, 88.41, 103.6	11.26, 8.30, 6.69
SPD	50, 100, 200	84.26, 98.64, 97.49	12.86, 9.42, 8.87
SPM	50, 100, 200	104.8, 106.6, 88.75	13.84, 5.76, 8.02

Regarding fish products, HIS is currently the only BA with established safety limits; however, these limits vary across countries. The U.S. FDA sets a limit of 50 mg kg^{-1}, while China differentiates between low-histamine and high-histamine fish, with limits of 200 mg kg^{-1} and 400 mg kg^{-1}, respectively. Therefore, the primary application of this method is rapid eligibility screening for histamine. For evaluating the performance of this eligibility screening method, three decision thresholds were calculated with the typical three safety limit concentrations of HIS mentioned above as the concentrations of concern, and the threshold values calculated were 49.35, 195.8, and 396.9 mg kg^{-1},

respectively. With threshold values, the positive detection rate curves were constructed, and the minimum reliable detection concentration for positive samples (with a detection rate ≥95%) and the maximum reliable detection concentration for negative samples (with a positive detection rate ≤ 5%) were determined. The results, as shown in Figure 3, indicate that unreliable determinations are confined to a narrow concentration range from the maximum reliable detection concentration for negative samples to the minimum reliable detection concentration for positive samples, which were 40–50 mg kg^{-1}, 180–200 mg kg^{-1} and 380–400 mg kg^{-1}, respectively; the results demonstrated that this method is well-suited for the eligibility fast screening needs.

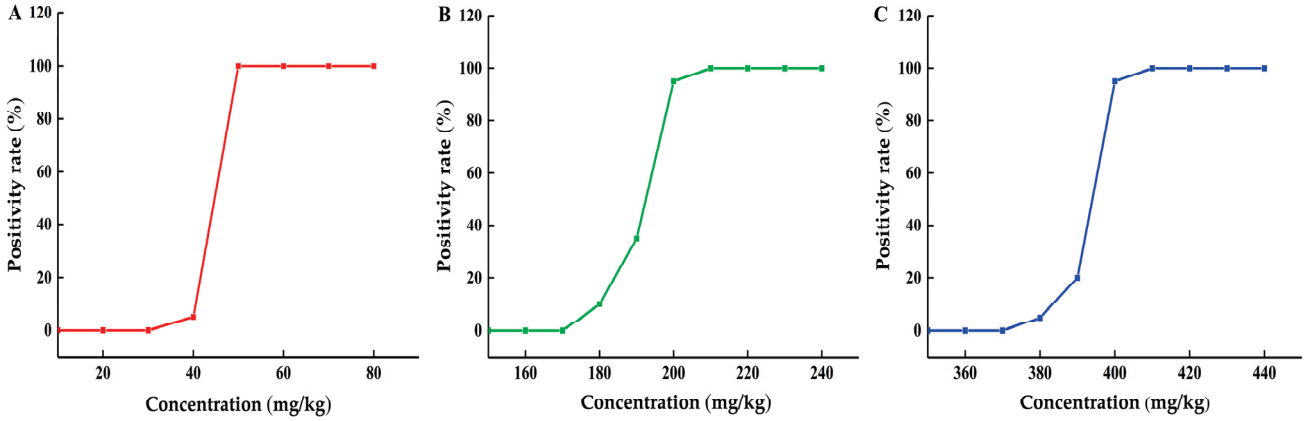


Figure 3. Positive rate detection curves of HIS in the fish matrix at three concentrations of concern. (**A**) Concentration of concern at 50 mg kg^{-1}; (**B**) Concentration of concern at 200 mg kg^{-1}; (**C**) Concentration of concern at 400 mg kg^{-1}.

3.3. Practical Applications

With the method developed, BAs were detected in nine actual commercially available cold-chain fish products, and the detection results were re-verified using HPLC-MS/MS [29], as shown in Table 4. The results indicated that all nine samples tested negative (with a concern concentration of 50 mg/kg) for histamine, and the correctness of the determination results could be confirmed by HPLC-MS/MS. Only a few samples showed SPD and SPM levels exceeding the method's LOQ, and these results were not significantly different from those obtained by the HPLC-MS/MS method ($p \geq 0.05$). All the above indicate that the established method is feasible.

Table 4. Determination results of 5BAs in actual cold-chain fish products with the portable ion trap mass spectrometry and HPLC-MS/MS.

Sample	Content (mg kg^{-1})				
	HIS	**CAD**	**TYR**	**SPD**	**SPM**
Salmon	ND [a] 0.96 ± 0.04 [b]	<LOQ 6.12 ± 0.02	ND 1.31 ± 0.10	<LOQ 10.80 ± 0.76	18.87 ± 3.03 21.63 ± 1.77
Mackerel	ND 0.97 ± 0.08	<LOQ 5.96 ± 0.05	ND 1.18 ± 0.09	12.79 ± 1.48 10.75 ± 0.50	ND 9.36 ± 0.82
Yellow Croaker	ND 1.01 ± 0.04	<LOQ 6.38 ± 0.01	ND 1.20 ± 0.01	ND 7.76 ± 0.54	17.57 ± 0.87 19.43 ± 3.06
White pomfret	ND 1.41 ± 0.07	44.64 ± 3.27 47.69 ± 0.26	<LOQ 7.90 ± 0.19	ND 13.23 ± 0.24	ND 16.96 ± 1.11
Chilled sea bass	ND 1.41 ± 0.57	<LOQ 6.35 ± 0.30	ND 1.38 ± 0.03	14.04 ± 1.85 16.49 ± 1.29	26.85 ± 2.73 31.78 ± 1.63

Table 4. *Cont.*

Sample	Content (mg kg^{-1})				
	HIS	**CAD**	**TYR**	**SPD**	**SPM**
Codfish	ND 0.96 ± 0.01	<LOQ 6.42 ± 0.25	ND 0.99 ± 0.01	<LOQ 6.95 ± 0.56	<LOQ 8.78 ± 0.63
Balsa	ND 0.99 ± 0.03	<LOQ 5.69 ± 0.10	ND 1.06 ± 0.01	<LOQ 5.76 ± 0.57	ND 3.31 ± 0.45
Pacific saury	ND 1.23 ± 0.18	<LOQ 6.97 ± 0.34	ND 1.14 ± 0.04	16.03 ± 1.16 18.10 ± 0.58	20.31 ± 3.09 22.09 ± 0.96
Spanish mackerel	ND 1.26 ± 0.04	<LOQ 11.45 ± 0.16	ND 2.04 ± 0.07	16.68 ± 2.82 17.70 ± 0.27	17.88 ± 1.68 16.78 ± 0.60

ND means not detected. [a] Portable ion trap mass spectrometry analysis results. [b] HPLC-MS/MS analysis results.

4. Conclusions

This study established a novel method for the rapid detection of five BAs, including HIS, TYR, CAD, SPD, and SPM, in cold-chain fish products with portable ion trap mass spectrometry with nano-electrospray ionization. The developed method features simple sample preparation, requires no derivatization or chromatographic separation, low cost and offers easy operation and rapid analysis with satisfactory accuracy and precision; It meets the requirements for BA safety detection and quality evaluation using BAs as markers in the cold-chain fish products. For HIS, which has safety limits in fish, the method could be successfully applied for the eligibility fast screening. The study provided a valuable methodological reference for the rapid detection of BAs in food.

Author Contributions: Conceptualization, Z.W.; methodology, Z.W., J.W. and X.M.; validation, J.W., X.M., Y.L., J.M. and W.M.; data curation, J.W. and X.M.; writing—original draft preparation, J.W.; writing—review and editing, Z.W.; supervision, Y.W.; project administration, Z.W.; funding acquisition, Z.W. All authors have read and agreed to the published version of the manuscript.

Funding: This work was supported by the Science and Technology Deputy General Manager Program of Changping District of Beijing [grant numbers: 2064115223], Capital Science and Technology Innovation Voucher Program [grant numbers: 2064115284], and Key Educational Reform Project of Beijing University of Agriculture [grant numbers: 5046516650/204].

Institutional Review Board Statement: Not applicable.

Informed Consent Statement: Not applicable.

Data Availability Statement: The data that support the findings of this study are available from the corresponding author upon request.

Acknowledgments: We gratefully acknowledge Miao Yu and Hongfen Zuo for the technical support and instrument operation training from Beijing Qingpu Analytical Instrument Co., Ltd.

Conflicts of Interest: The authors declare no conflicts of interest.

References

1. Dabadé, D.S.; Jacxsens, L.; Miclotte, L.; Abatihet, E.; Devlieghere, F.; Bruno De Meulenaer, B. Survey of multiple biogenic amines and correlation to microbiological quality and free amino acids in foods. *Food Control* **2021**, *120*, 107497. [CrossRef]
2. Wang, Y.; Yan, B.; Xu, H.; Huang, Y.; Sheng, Q.; Wang, L.-H. Biogenic amines in fermented foods: A comprehensive review from formation pathways, risk analysis, detection technologies to control measures. *Food Res. Int.* **2026**, *223*, 117832. [CrossRef]
3. Rane, R.S.; Prashant Anil Pawase, P.A.; Shams, R.; Darshan, G.; Bashir, O.; Roy, S. A critical review on biogenic amines in dairy: Formation pathways, toxicity, and regulatory standards. *J. Food Compos. Anal.* **2025**, *142*, 107496. [CrossRef]

4. Ahmad, W.; Mohammed, G.I.; Al-Eryani, D.A.; Saigl, Z.M.; Alyoubi, A.O.; Alwael, H.; Bashammakh, A.S.; O'Sullivan, C.K.; El-Shahawi, M.S. Biogenic amines formation mechanism and determination strategies: Future challenges and limitations. *Crit. Rev. Anal. Chem.* **2020**, *50*, 485–500. [CrossRef] [PubMed]
5. Feddern, V.; Mazzuco, H.; Fonseca, F.N.; de Lima, G.J.M.M. A review on biogenic amines in food and feed: Toxicological aspects, impact on health and control measures. *Anim. Prod. Sci.* **2019**, *59*, 608–618. [CrossRef]
6. Wójcik, W.; Łukasiewicz, M.; Puppel, K. Biogenic amines—Formation, action and toxicity-review. *J. Sci. Food Agric.* **2020**, *101*, 2634–2640. [CrossRef]
7. Zhou, Q.; Jiang, L.; Zhu, J.; Lu, Y.; He, Q. The metabolic regulation mechanism of gallic acid on biogenic amines and nitrosamines in reduced-nitrite Chinese fermented sausages: A perspective of metabolomics and metagenomics. *Food Chem.* **2024**, *456*, 139900. [CrossRef] [PubMed]
8. Chen, C.; Wang, Z.; Wu, J.; He, S.; Wang, Y.; Dong, Z.; Ma, X. Analytical Method Development and Accumulation Factors Analysis for Volatile Nitrosamines in Cured Fish with Gas Chromatography-Tandem Mass Spectrometry. *Food Sci. Technol.* **2025**, *50*, 303–311. (In Chinese with English Abstract) [CrossRef]
9. Visciano, P.; Schirone, M.; Paparella, A. An Overview of Histamine and Other Biogenic Amines in Fish and Fish Products. *Foods* **2020**, *9*, 1795. [CrossRef]
10. Ding, T.; Li, Y. Biogenic amines are important indices for characterizing the freshness and hygienic quality of aquatic products: A review. *LWT* **2024**, *194*, 115793. [CrossRef]
11. Abdullah, O.; Mohammed, R.R.; Ameen, P.S.M.; Abas, Z.A.; Ekici, K. Presence of biogenic amines in food and their public health concerns. *J. Food Prot.* **2021**, *84*, 1539–1548. [CrossRef]
12. Ruiz-Capillas, C.; Herrero, A.M. Impact of Biogenic Amines on Food Quality and Safety. *Foods* **2019**, *8*, 62. [CrossRef]
13. Yue, C.S.; Selvi, C.; Tang, A.N.; Chee, K.N.; Ng, H.Y. Determination of biogenic amines in malaysian traditional wine by high performance liquid chromatography. *Anal. Lett.* **2021**, *54*, 1968–1994. [CrossRef]
14. Eirini, K.; Apostolia, T.; Constantinos, K.Z.; Paraskevas, D.T. Specific determination of histamine in cheese and cured meat products by ion chromatography coupled to fluorimetric detection. *Microchem. J.* **2021**, *168*, 106513. [CrossRef]
15. Papageorgiou, M.; Lambropoulou, D.; Morrison, C.; Namieśnik, J.; Płotka-Wasylka, J. Direct solid phase microextraction combined with gas chromatography—Mass spectrometry for the determination of biogenic amines in wine. *Talanta* **2018**, *183*, 276–282. [CrossRef] [PubMed]
16. Zhang, X.; Fang, C.; Huang, D.; Yang, G.; Tang, Y.; Shi, Y.; Kong, C.; Cao, P.; Cai, Y. Determination of 8 biogenic amines in aquatic products and their derived products by high-performance liquid chromatography-tandem mass spectrometry without derivatization. *Food Chem.* **2021**, *361*, 130044. [CrossRef] [PubMed]
17. Xia, H.; Zhang, H.; Zhu, Z.; Tong, K.; Chang, Q.; Zhang, H.; Fan, C.; Chen, H. Rapid determination of eight biogenic amines in air-dried yak meat by QuEChERS combined with ultra-performance liquid chromatography-mass spectrometry. *J. Food Compos. Anal.* **2024**, *133*, 106466. [CrossRef]
18. Seyfinejad, B.; Jouyban, K.; Dehpour, A.R.; Razieh Mohammad Jafari, R.M.; Charkhpour, M.; Mogaddam, M.R.A. Ion-pair hollow fiber liquid-phase microextraction combined with capillary electrophoresis for the determination of biogenic amines in rat tissues. *J. Pharm. Biomed. Anal.* **2022**, *219*, 35803014. [CrossRef]
19. Parchami, R.; Kamalabadi, M.; Alizadeh, N. Determination of biogenic amines in canned fish samples using head-space solid phase microextraction based on nanostructured polypyrrole fiber coupled to modified ionization region ion mobility spectrometry. *J. Chromatogr. A* **2017**, *1481*, 37–43. [CrossRef]
20. Takáts, Z.; Wiseman, J.M.; Gologan, B.; Cooks, R.G. Mass spectrometry sampling under ambient conditions with desorption electrospray ionization. *Science* **2004**, *306*, 471–473. [CrossRef]
21. Cody, R.B.; Laramée, J.A.; Durst, H.D. Versatile new ion source for the analysis of materials in open air under ambient conditions. *Anal. Chem.* **2005**, *77*, 2297–2302. [CrossRef] [PubMed]
22. Feider, C.L.; Krieger, A.; DeHoog, R.J.; Livia, S.E. Ambient ionization mass spectrometry: Recent developments and applications. *Anal. Chem.* **2019**, *91*, 4266–4290. [CrossRef]
23. Liu, C.; Pan, Y. Principle and applications of ambient photo ionization mass spectrometry. *Chin. Mass Spectrom. Soc.* **2021**, *42*, 514–531. [CrossRef]
24. Yuan, Y.; Lian, J.; Shao, Z.; Zeng, D.; Wang, H.; Li, M. Ambient mass spectrometry and ambient ionization mass spectrometry imaging in rapid food safety detection. *Food Sci.* **2025**, *46*, 290–298. (In Chinese with English Abstract) [CrossRef]
25. Xie, Y.; Huang, S.; Zhang, Q.; Zhang, S.; Han, Z.; Yu, J.; Wang, X.; Chen, K.; Wang, Z.; Li, L.; et al. On-site analysis and rapid authentication of valuable agarwood samples by paper capillary spray miniature mass spectrometry. *J. Anal. Test.* **2025**, *9*, 61–67. [CrossRef]
26. Ma, X.; Wu, J.; Wang, Z.; Yu, M.; Zuo, H. Rapid detection of histamine in wine by portable ion trap mass spectrometry. *J. Beijing Agric.* **2025**, *40*, 113–117. (In Chinese with English Abstract)

27. Zhang, S.; Li, L.; Xie, Y.; Fan, L.; Wang, Y.; Wang, N.; Han, Z.; Wang, Z.; Chen, K.; Yang, L. Rapid identification and on-site analysis by miniature mass spectrometry of chemical markers for fragrant rosewood authentication. *J. Pharm. Biomed. Anal.* **2025**, *252*, 116490. [CrossRef] [PubMed]
28. Lv, Y.; Shang, Y.; Li, L.; Zhang, Y.; Ma, Q. Online hyphenation of in-capillary aptamer-functionalized solid-phase microextraction and extraction nanoelectrospray ionization for miniature mass spectrometry analysis. *Analyst* **2023**, *148*, 1815–1823. [CrossRef] [PubMed]
29. Wu, J.X.; Wang, Z.Y.; Yu, M.; Bi, G.B.; Zhang, W.Q.; Dong, Z.Q.; Ma, X.T. Determination of 16 biogenic amines in cold-chain fish and shrimp by volatile ion-pair reversed-phase liquid chromatography-tandem mass spectrometry. *Food Sci.* **2025**, *46*, 282–289. (In Chinese with English Abstract) [CrossRef]

Disclaimer/Publisher's Note: The statements, opinions and data contained in all publications are solely those of the individual author(s) and contributor(s) and not of MDPI and/or the editor(s). MDPI and/or the editor(s) disclaim responsibility for any injury to people or property resulting from any ideas, methods, instructions or products referred to in the content.

foods

MDPI

Article

Systematic Characterization of Flavor Profiles and Screening of Potential Key Aroma-Active Components in *Prunus salicina* var. *cordata* cv. 'Younai'

Lijuan Fu [1,2,†], Wenjing Liu [1,†], Lihua Ren [1], Xiangxin Lin [1], Jia Guo [1], Hao Chen [3], Faxing Chen [2,*] and Sun'an Yan [1,*]

[1] Institute of Quality Standards & Testing Technology for Agro-Products, Fujian Academy of Agricultural Sciences/Fujian Key Laboratory of Agro-Products Quality and Safety, Fuzhou 350003, China; fulijuan_f@163.com (L.F.); liuwj163163@163.com (W.L.); rlhlyx123@163.com (L.R.); linxiangxin2008@163.com (X.L.); 15960102868@163.com (J.G.)
[2] College of Horticulture, Fujian Agriculture and Forestry University, Fuzhou 350002, China
[3] Fujian Green Food Development Center, Fuzhou 350003, China; chenhao007321@sina.com
* Correspondence: cfaxing@126.com (F.C.); yansunan1982@163.com (S.Y.)
† These authors contributed equally to this research.

Abstract

Prunus salicina var. *cordata* cv. 'Younai' is a characteristic stone fruit germplasm resource of Fujian Province, yet its core flavor components remain unclear. This study aimed to comprehensively characterize the flavor chemistry of Younai by determining the contents of sugar–acid components and volatile compounds, combined with untargeted metabolomics analysis. Results showed that fructose was the predominant sweet component, while malic acid was the dominant organic acid in Younai. (Z)-3-Hexen-1-ol, 1-Hexanol and (Z)-3-Hexen-1-yl acetate were screened as potential key aroma-active compounds based on odor activity values, and γ-Decalactone plus Linalool further enriched the fruit aroma hierarchy. Untargeted metabolomics identified 26 saccharides and 21 organic acids in the fruits. Additionally, Younai fruit metabolites were dominated by polyphenols, with flavonols and phenolic acids as the core polyphenol subclasses. This study provides a chemically grounded baseline characterization of Younai flavor. The screened potential aroma-active compounds and metabolite profiles provide a foundation for future sensory validation studies and the development of quality evaluation criteria.

Keywords: *Prunus salicina* var. *cordata* cv. 'Younai'; flavor profiles; sugar–acid components; aroma-active compounds; metabolites

1. Introduction

Prunus salicina var. *cordata* cv. 'Younai' is a unique cultivated variety of Chinese plum endemic to Fujian Province, China, mainly distributed in core producing areas such as eastern and northern Fujian. It is a distinctive fruit tree with both fresh-eating and processing value, featuring crisp tender flesh, a well-balanced sweet–sour taste and fresh fruit aroma [1]. According to the Fujian Provincial Bureau of Statistics, the planting area of Younai has reached 300,000 mu (1 mu ≈ 666.7 m^2). As a core producing area, Gutian County has a planting area of 62,000 mu for Younai, with an annual output of approximately 30,000 tons and an annual output value exceeding 140 million RMB. Furthermore, "Gutian Younai" has been awarded the National Geographical Indication Certification Trademark. Its products are sold to Hong Kong, Macao and Southeast Asian markets, and an integrated

industrial chain covering production, supply, sales and processing has been formed, making it one of the pillar industries for rural revitalization in the region.

Flavor quality is the core factor determining the commercial competitiveness and market potential of Younai [2,3]. Fruit flavor is mainly determined by the combined action of water-soluble sugar–acid taste-active compounds and volatile aroma compounds [3]. Among these, the composition and ratio of soluble sugars and organic acids form the core material basis of sweet–sour flavor [4]. Meanwhile, metabolites provide crucial support for the synthesis and accumulation of flavor compounds, and in-depth analysis of the flavor metabolic mechanisms of Younai fruits offers a theoretical basis for the quality improvement of *Prunus* fruit tree germplasm resources.

Flavor research on stone fruits such as plum, peach and apricot has developed a well-established research system [5–7]. In terms of soluble sugar and organic acid components, systematic qualitative and quantitative methods have been established for major sweet compounds (i.e., fructose, glucose, sucrose) and key acidic components (i.e., malic acid, citric acid) [6,8]. For volatile aroma compounds, various aroma components including esters, lactones, alcohols and aldehydes have been identified [5,9], and signature key aroma-active compounds such as hexyl acetate, γ-decalactone and linalool have been screened out via the odor activity value, thus fully constructing the characteristic aroma profiles of stone fruits [5,10]. In addition, combined with metabolomics techniques, core metabolic pathways closely related to flavor compound synthesis have been excavated, such as starch–sucrose metabolism, the tricarboxylic acid cycle and phenylpropane–flavonoid metabolism [11].

Despite the broad understanding of stone-fruit flavor chemistry accumulated for species such as peach, apricot, and plum, systematic flavor characterization of Younai remains notably limited. First, no systematic quantitative analysis has been conducted on core sugar–acid components such as fructose, glucose and malic acid, making it impossible to identify the key factors driving its sweet–sour flavor. Second, there exists a notable gap in flavor research, with no potential aroma-active compounds that actually contribute to its aroma screened out. Third, the metabolic background underlying flavor compound formation remains unclear, which fails to support the demands for cultivar breeding and quality standardization evaluation. To date, no comprehensive study has simultaneously profiled the sugars, organic acids, volatile compounds, and metabolites of Younai fruit across multiple cultivars and production sites. This gap limits both scientific understanding of Younai flavor and the development of quality evaluation criteria for this cultivar.

This study aimed to characterize the flavor profiles of Younai fruits. We used fruits at commercial ripening stage of three main cultivated Younai cultivars as experimental materials. These fruits were sampled from six representative orchards in five core producing areas of Fujian Province. High-performance liquid chromatography (HPLC), headspace solid-phase microextraction–gas chromatography–mass spectrometry (HS-SPME-GC-MS) and ultra-performance liquid chromatography–quadrupole time-of-flight mass spectrometry (UPLC-QTOF-MS) were employed to determine the taste-active components (soluble sugars and organic acids), volatile compounds and metabolic profiles of Younai fruits. These analyses screened the potential key aroma-active compounds and their preliminary associations with metabolite classes, filling the research gap in Younai flavor studies and providing theoretical support for the quality standardization evaluation of Younai.

2. Materials and Methods

2.1. Experimental Materials and Reagents

2.1.1. Plant Materials

The tested Younai cultivars were Shiban Wannai (SB), Cuiping Younai (CP) and Wanhuangjin (WHJ), with two sampling sites set for each cultivar. The sampling information

https://doi.org/10.3390/foods15101787

and corresponding sample codes are listed as follows: SB with two samples, collected from Jianyang Germplasm Resource Bank in Jianyang District, Nanping City, China, (SB-JY, geographic coordinates 27.35° N, 118.02° E) and Jiushan Family Farm in Gutian County, Ningde City, China, (SB-GT, geographic coordinates 26.63° N, 118.71° E). CP with two samples, collected from Caiheli Family Farm in Youxi County, Sanming City, China, (CP-YX, geographic coordinates 26.29° N, 117.72° E) and Zhengzhonghai Family Farm in Gutian County, Ningde City, China, (CP-GT, geographic coordinates 26.68° N, 118.77° E). WHJ with two samples, collected from Yinglian Family Farm in Liancheng County, Longyan City, China, (WHJ-LC, geographic coordinates 25.88° N, 116.72° E) and Liaochunsheng Family Farm in Jian'ou District, Nanping City, China, (WHJ-JO, geographic coordinates 26.82° N, 118.33° E). The quantified data of producing areas, production units and basic fruit traits for each sampling site are detailed in Supplementary Table S1.

All samples were mature fruits with stable commercial properties, and the sampling time of each cultivar was based on the full bloom stage. SB was sampled at 150 d after full bloom (DAFB), CP at 135 DAFB, and WHJ at 165 DAFB. The sampling orchards were under standardized management. For each orchard, three independent trees were selected as biological replicates. From each selected tree, 20 fruits at commercial maturity were randomly collected and pooled to prepare one homogenized sample per tree. Consequently, each orchard yielded three biological replicates (n = 3), with each replicate representing an independent pooled fruit batch from a single tree. These three biological replicate samples were analyzed independently for all subsequent chemical analyses. After harvesting, the fruits were immediately placed in a 4 °C constant temperature incubator to eliminate field heat, and then transported to the laboratory rapidly. Upon arrival at the laboratory, the peel and stone were manually removed. The mesocarp was collected, cut into small pieces, snap-frozen in liquid nitrogen, and stored in an ultra-low temperature refrigerator at −80 °C for subsequent index determination.

2.1.2. Reagents

Hydrochloric acid, sodium hydroxide, Folin–Ciocalteu reagent and other reagents were of analytical grade and purchased from China National Pharmaceutical Group Chemical Reagent Co., Ltd., Shanghai, China. Chromatographic grade standard substances (purity $\geq$ 98.0%), including fructose, sucrose, glucose, sorbitol, malic acid, citric acid, tartaric acid and 3-octanol, were obtained from Sigma-Aldrich (St. Louis, MI, USA). Chromatographic grade solvents such as methanol, acetonitrile and formic acid were purchased from Merck (Darmstadt, Germany) and Fisher Scientific (Waltham, MA, USA), respectively.

2.2. Determination of Total Soluble Solids

A PAL-1 handheld refractometer (ATAGO Co., Ltd., Tokyo, Japan) was used to determine the total soluble solids (TSS) content of fruits. Six fruits with uniform maturity and size were selected for each sample, rinsed with distilled water and air-dried. The fruits were pitted, chopped, homogenized and juiced, and the juice was collected for TSS determination after filtration through four layers of gauze.

2.3. Determination of Titratable Acid

The stoned plum flesh was homogenized, diluted with water to a constant volume, and then stood still prior to filtration. The obtained supernatant was subjected to neutralization titration with 0.1 mol/L standard sodium hydroxide solution using phenolphthalein as the indicator. The titration end point was recorded when the solution turned pale red and remained unchanged for 30 s. A blank test was conducted simultaneously, and each sample was determined in triplicate. The titratable acid (TA) content was calculated with malic acid (conversion coefficient of 0.067) as the conversion standard.

2.4. Determination of Fruit Firmness

A TA.XT Plus texture analyzer (Stable Micro Systems, Godalming, Surrey, UK) was used to determine the firmness of whole Younai fruits in the Texture profile analysis (TPA) mode, with a 36 mm diameter cylindrical probe (P/36) adopted. The test parameters were set as follows: pre-test, test and post-test speeds all at 1.0 mm/s, target deformation at 10%, trigger force at 6 g, and probe interval time at 5 s.

2.5. Determination of Sugar Component Contents

The method was adapted from Xiao et al. [6] with minor modifications: Accurately weigh 1.00 g of frozen powder sample, add 10 mL of ultrapure water, vortex-mix thoroughly, and perform ultrasonic extraction for 30 min (200 W, 30 °C), followed by centrifugation at 12,000 r/min for 10 min. The supernatant was collected, the extraction was repeated twice, and all supernatants were combined. The combined supernatant was filtered through a 0.22 μm aqueous filter membrane, and the filtrate was collected for subsequent use.

The Waters E2695 HPLC system (Waters, Milford, MA, USA) equipped with a refractive index detector (RID) and an amino chromatographic column (4.6 mm × 250 mm, 5 μm) was employed. The mobile phase was acetonitrile–ultrapure water (75:25, v/v) with a flow rate of 1.0 mL/min, column temperature of 30 °C, and injection volume of 20 μL. Qualitative analysis was conducted by comparing the retention times with those of fructose, sorbitol, glucose and other standard substances. Quantitative analysis was performed via the external standard method: standard curves were plotted, and the contents of sugar components were calculated based on peak areas.

2.6. Determination of Organic Acid Contents

The method was adapted from Xiao et al. [6] with minor modifications. The sample pretreatment was performed according to the procedure described for sugar component analysis. High-performance liquid chromatography (HPLC, Waters E2695, Waters Corporation, Milford, MA, USA) was employed, equipped with an ultraviolet (UV) detector (detection wavelength: 210 nm) and a C18 chromatographic column (4.6 mm × 250 mm, 5 μm). The mobile phase was 0.05 mol/L potassium dihydrogen phosphate solution (pH 2.5), with a flow rate of 0.8 mL/min, a column temperature of 25 °C and an injection volume of 20 μL. Qualitative analysis was conducted by comparing the retention times with those of standard substances including malic acid, citric acid, tartaric acid and quinic acid. Quantitative analysis was performed via the external standard method: standard curves were plotted, and the organic acid contents were calculated based on peak areas.

2.7. Volatile Compounds Analysis

2.7.1. GC-MS/MS Determination

The determination of volatile substances was conducted according to the method described by Zhang et al. [12] with partial modifications: Accurately weigh 1.00 g of Younai fruit sample, grind it in liquid nitrogen, transfer it to a sample vial, add 1 mL of saturated NaCl solution and 10 μL of internal standard (3-octanol, final concentration 11.36 μg/g), and vortex-mix thoroughly. A SPME system (Cat. No.: 5610-5861, Switzerland) was used for volatile aroma extraction, with a 1.1 mm diameter three-phase coated fiber (DVB/CarbonWR/PDMS) paired with a CTC PAL auto-sampler. The SPME fiber was preconditioned as recommended by the manufacturer before the first extraction. The extraction conditions were set as follows: equilibrium at 40 °C for 30 min, followed by SPME fiber extraction for 30 min, then injected into a gas chromatography–tandem mass spectrometry (GC-MS/MS) system.

A Shimadzu GCMS-TQ8050 system (Shimadzu Corporation, Kyoto, Japan) was employed for the determination of volatile compounds, equipped with a DB-5MS capillary column (30 m × 0.25 mm × 0.25 μm). The inlet temperature was set at 250 °C, with splitless injection. High-purity helium (purity ≥ 99.999%) was used as the carrier gas at a flow rate of 1.0 mL/min. The temperature program was as follows: initial temperature 40 °C, held for 3 min; increased to 150 °C at 5 °C/min; and then increased to 250 °C at 10 °C/min, held for 5 min. The ion source was electron impact ionization with an ionization energy of 70 eV, ion source temperature of 230 °C, interface temperature of 280 °C, and solvent delay of 3 min.

2.7.2. Semi-Quantification and Relative Odor Activity Value (rOAV) Calculation

Volatile compounds were tentatively identified via mass spectral matching against the NIST 17.0 database with a similarity index (SI) of no less than 80. For quantification, 3-octanol was added as internal standard at 11.36 ug/g, and all volatile compounds were semi-quantified relative to this internal standard. All contents were quantified as μg/g FW. These data represent relative abundances instead of accurate absolute concentrations.

The relative odor activity value (rOAV) is a well-established method for identifying key flavor compounds in food matrices, which integrates the quantified concentration of each volatile compound with its odor threshold to assess its contribution to the overall aroma profile of the sample. This approach has gained widespread application in recent years to characterize aroma-active compounds across diverse food systems. In general, a compound is considered to make a direct contribution to the characteristic flavor of the sample if its calculated rOAV is ≥1. In this study, rOAV values were determined following previously described protocols [13–15] using the formula

$$\mathrm{rOAV_i} = \frac{\mathrm{C_i}}{\mathrm{T_i}}$$

where $rOAV_i$ is the relative odor activity value of compound i, C_i is the concentration of compound i (μg/g FW), and T_i is its corresponding odor threshold (μg/g). The odor threshold data were cited from Ref. [16]. A compound is generally considered to make a direct contribution to the characteristic aroma of the sample if its rOAV is ≥1.

It should be noted that this study employed chemical quantification and rOAV screening as a foundational approach to identify potential aroma-active compounds. While an rOAV above 1 is conventionally interpreted as indicating potential aroma relevance, definitive confirmation of flavor-driving components would require complementary sensory validation methods such as gas chromatography–olfactometry (GC-O), descriptive sensory analysis, or aroma recombination studies, which were not performed in the present work.

2.8. Determination of Metabolites

The determination of metabolites in Younai was performed using the method established in our laboratory. Sample Pretreatment: Younai samples were lyophilized and ground into powder. Then, we accurately weighed 0.100 g of powder into a 15 mL centrifuge tube, added 10 mL of 80% methanol–water, shook for extraction for 15 min, and centrifuged at 10,000 rpm at 4 °C. Finally, the supernatant was filtered through a 0.22 μm organic filter membrane and transferred to a sample vial.

Instrumental analysis was conducted on a SCIEX X500R UPLC-QTOF-MS system (SCIEX, Marlborough, MA, USA). The liquid chromatography conditions were as follows: HSS T3 chromatographic column (1.8 μm, 2.1 × 100 mm). Mobile phase A: 0.01% formic acid water; mobile phase B: acetonitrile. Flow rate: 0.4 mL/min. Column temperature: 40 °C. Injection volume: 1 μL. Gradient elution program: 1.00 min 95%A/5%B, 1.10 min

60%A/40%B, 16.00 min 50%A/50%B, 24.00 min 10%A/90%B, 28.00 min hold 10%A/90%B, 28.10 min return to 95%A/5%B, 30.00 min end.

The mass spectrometry conditions were: ESI ion source (positive/negative ion mode). Acquisition mode: TOF MS-MS/MS. TOF MS mass-to-charge ratio range: 100–1300 Da. TOF MS/MS mass-to-charge ratio range: 50–1300 Da. CDS and DBS were enabled. Ion source parameters included: ESI voltage 5500 V (positive)/−4500 V (negative), curtain gas 30 psi, nebulizer gas GAS2 55 psi, GAS1 50 psi, source temperature 550 °C, declustering potential 60 V (positive)/−60 V (negative), collision energy 35 ± 15 V (positive)/−35 ± 15 V (negative).

Quality control (QC) was ensured by preparing a pooled QC sample from equal aliquots of all biological samples. This QC sample was injected every 10 samples throughout the run sequence. QC clustering was assessed by principal component analysis (PCA). QC samples clustered tightly together and distinctly from biological samples, confirming analytical stability. Only metabolites with a relative standard deviation (RSD) < 30% across QC injections were retained for downstream analysis. Data normalization was performed using total ion current (TIC) normalization. Missing values (occurring when a metabolite was detected below the limit of detection in some samples) were handled as follows: metabolites with missing values in >50% of samples within any group were excluded. Remaining missing values were imputed with half the minimum positive value in the dataset. Substance identification was conducted through the SCIEX OS database and the One-Map platform cloud database (using MExplorer Ultimate software, me.5omics.com, format: accessed on 1 August 2025), with a primary mass deviation <5 ppm. QC samples exhibited tight clustering in the PCA score plot (Supplementary Figure S1), verifying the stability and reproducibility of the metabolomics analysis.

2.9. Data Analysis Methods

A total of six fruit samples of Younai were harvested at the commercial full-ripening stage in this study, with three biological replicates set for each sample. All samples were unique cultivar-orchard combinations, specifically coded as SB-JY, SB-GT, CP-YX, CP-GT, WHJ-JO, and WHJ-LC, covering three major cultivated cultivars and five core production orchards of Younai. Statistical analysis was performed using SPSS 25.0 software (IBM Corp., Armonk, NY, USA). Data were analyzed by one-way ANOVA, with independent Younai sample type set as the single factor (six levels). Post hoc multiple comparisons were conducted using Tukey's honestly significant difference (HSD) test to analyze the differences in the contents of sugars, organic acids and other flavor-related compounds among different samples. $p < 0.05$ was considered statistically significant. Result charts were drawn using OriginPro 2021, MetWare Cloud Platform (https://cloud.metware.cn, format: accessed on 1 December 2025) and Omicshare (https://www.omicshare.com/, format: accessed on 1 December 2025).

3. Results

3.1. Analysis of Morphological Characteristics and Basic Sugar, Acid and Texture Indicators of Younai Fruits

As shown in Figure 1A, the sampling sites were Jianyang District, Gutian County, Youxi County, Liancheng County and Jian'ou City in Fujian Province. According to the data from Fujian Provincial Bureau of Statistics, these areas are all core producing areas of Younai, accounting for more than 80% of the total planting area of Younai in the province. Figure 1B shows the fruiting morphology of three main Younai cultivars. All three cultivars exhibited a cluster-bearing fruiting habit, with peach-shaped fruits and a thin waxy bloom on the surface. Figure 1C shows the cross-sectional morphology of Younai fruits from different

producing areas. Among them, CP was light green, while SB and WHJ were light yellowish-green. Combined with the data in Supplementary Table S1, the longitudinal diameter of CP fruits (61.00~62.01 mm) was significantly larger than that of SB (55.48~55.75 mm) and WHJ (55.61~55.64 mm). The single fruit weight of CP was 118.52~124.22 g, while those of SB and WHJ were both between 96~103 g. Although there were differences in fruit size and peel color among the three cultivars, they all maintained the core morphological characteristics of Younai, reflecting the stable germplasm characteristics of the main cultivated Younai cultivars in Fujian Province.

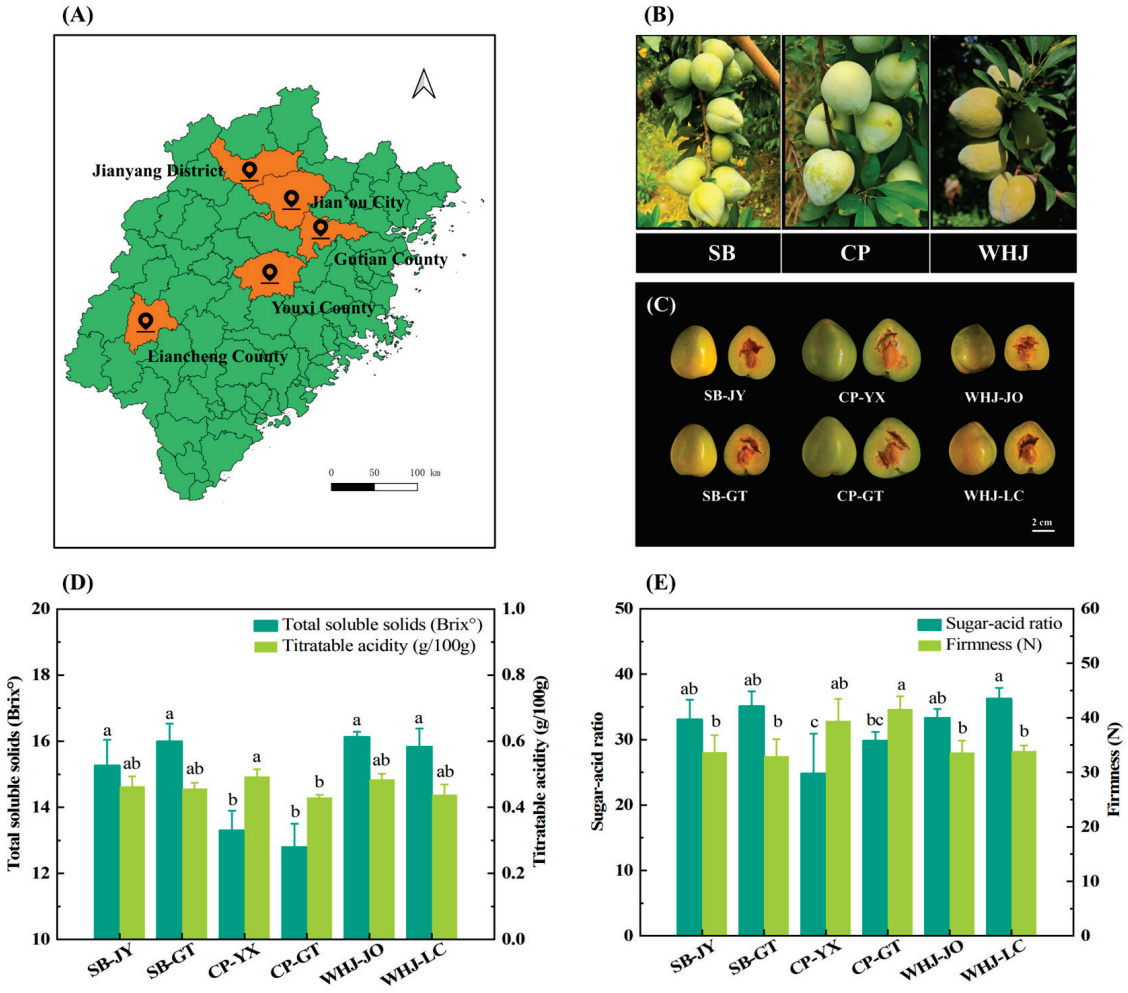


Figure 1. Analysis of morphological characteristics and basic sugar, acid and firmness indicators of Younai fruits. (**A**) Sampling sites of five major core producing areas in Fujian Province; (**B**) fruiting morphology of three main cultivated Younai cultivars; (**C**) cross-sectional morphology of Younai fruits from different producing areas (scale bar = 2 cm); (**D**) contents of total soluble solids (TSS, °Brix) and titratable acid (TA, calculated as malic acid, g/100 g); (**E**) sugar–acid ratio and fruit firmness (N). Data are presented as mean values ± standard deviation (n = 3). Different letters indicate significant differences ($p < 0.05$). SB means Shiban Wannai, CP means Cuiping Younai, WHJ means Wanhuangjin. SB-JY: Shiban Wannai from Jianyang District; SB-GT: Shiban Wannai from Gutian County; CP-YX: Cuiping Younai from Youxi County; CP-GT: Cuiping Younai from Gutian County; WHJ-JO: Wanhuangjin from Jian'ou City; WHJ-LC: Wanhuangjin from Liancheng County. Other figure annotations are the same as above.

The sweet and sour flavor of Younai fruits is their core edible quality characteristic. Figure 1D shows the TSS and TA contents of Younai samples. The results showed that the TSS content ranged from 12.80 to 16.13 °Brix overall. Among them, the TSS contents of SB and WHJ (15.27~16.13 °Brix) were significantly higher than that of CP (12.80~13.30 °Brix).

The TA content fluctuated slightly overall, stably ranging from 0.43 to 0.49 g/100 g. Figure 1E shows the sugar–acid ratio and firmness characteristics of Younai fruits. The sugar–acid ratio is a core indicator reflecting the sweet and sour palatability of fruits. The sugar–acid ratio of Younai samples ranged from 24.80 to 36.25. Among them, the sugar–acid ratios of SB and WHJ samples were relatively high (33.08~36.25), while that of CP was relatively low (24.80~29.82). These differences among cultivars enrich the flavor types of Younai and meet different consumer demands. In terms of fruit firmness, the firmness of CP-GT (38.89~43.21 N) was significantly higher than that of SB (32.90~33.89 N) and WHJ (33.12~33.57 N), and there was no significant difference among different producing areas of the same cultivar.

3.2. Analysis of Sugar and Acid Components in Younai Fruits

To clarify the material basis of core flavor, the identification and content analysis of soluble sugars and organic acids were further carried out. As shown in Figure 2A, the contents of soluble sugar components showed a stable order of fructose > glucose and sorbitol > sucrose in all samples. Fructose was the most dominant soluble sugar, with a content ranging from 2.73 to 3.81 g/100 g. Glucose (1.84~2.63 g/100 g) and sorbitol (1.45~3.49 g/100 g) followed, while sucrose content (0.78~1.92 g/100 g) was relatively low. From the perspective of flavor chemistry, the sweetness coefficient of fructose (1.73) was significantly higher than that of sucrose (1.0), glucose (0.74) and sorbitol (0.6) [6]. As a characteristic polyol of *Prunus* fruits [17], sorbitol not only provides a mild sweet contribution, but also improves the moist taste of fruits and effectively relieves the sweetness cloying caused by high fructose content. This flavor modulation characteristic mediated by characteristic polyols is also an important flavor feature that distinguishes Younai from other stone fruits such as peaches and pome fruits such as apples [18].

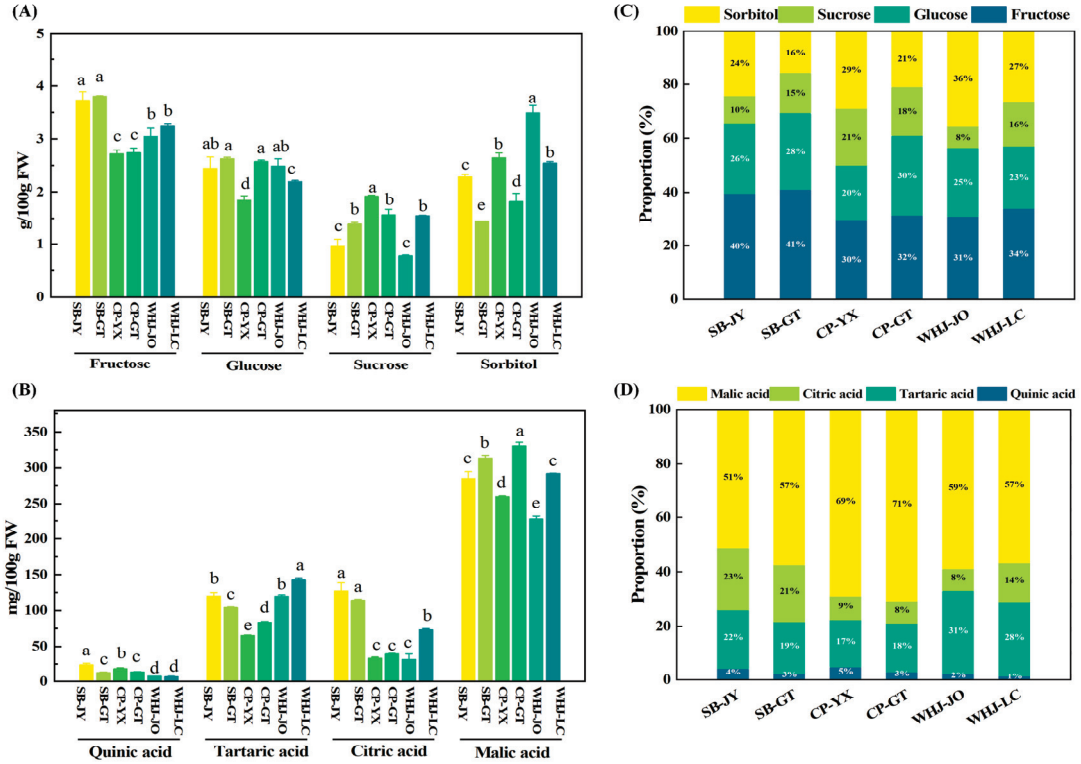


Figure 2. Analysis of sugar and acid components in Younai fruits. (**A**) Contents of major sugar components (fructose, glucose, sucrose, sorbitol) (g/100 g); (**B**) contents of major organic acid components (quinic acid, tartaric acid, citric acid, malic acid) (mg/100 g); (**C**) proportions of major sugar components; (**D**) proportions of major organic acid components. Data are presented as mean values ± standard deviation (n = 3); Different letters indicate significant differences ($p < 0.05$).

Figure 2B presents the contents of core organic acid components in Younai fruits. The average contents of organic acids in the samples showed a stable order of malic acid > tartaric acid and citric acid > quinic acid. Malic acid was the predominant organic acid, with a content ranging from 227.35 to 330.59 mg/100 g, followed by tartaric acid (65.40~142.68 mg/100 g). Citric acid and quinic acid were present at relatively low levels, with contents of 31.22~127.63 mg/100 g and 6.68~24.10 mg/100 g, respectively. As a characteristic organic acid of stone fruits, malic acid has a mild, persistent and non-irritating sour taste [19], and it could generate a flavor synergy with the fresh sweet taste of fructose, which serves as the core material basis for the coordinated sweet–sour taste. Tartaric acid enriches the sour taste layers and effectively compensates for the monotony of sour taste induced by malic acid alone [20]. Citric acid and quinic acid further modulate the sour taste balance of the fruits [21].

3.3. Analysis of the Proportion of Sugar and Acid Components in Younai Fruits

Figure 2C shows the proportion characteristics of main sugar components in Younai fruits. Fructose accounted for the highest proportion (more than 30%), being the primary contributor to the sweetness of Younai. Sorbitol and glucose followed in proportion, while sucrose had the lowest proportion. Even though there were cultivar differences in the absolute content of sugar components among different samples, their proportion pattern remained stable, which suggested the high stability of Younai's sweet flavor at the component structure level. In this study, the sugar composition pattern, with fructose as the main component, glucose and sorbitol as supplements, and sucrose as a minor component, is the core characteristic of Younai germplasm and not significantly affected by the producing area environment.

Figure 2D shows the proportion characteristics of major organic acid components in Younai fruits. The results indicated that malic acid was absolutely dominant in all samples, accounting for more than 50% of the total organic acids. Tartaric acid (17~31%) and citric acid (8~23%) were the next most abundant in proportion, while quinic acid accounted for less than 5%. In this study, consistent with the proportion pattern of sugars, the proportion pattern of organic acids in Younai was conserved across different cultivars and producing areas. This indicated that the organic acid composition pattern dominated by malic acid and supplemented by tartaric acid was the core determinant of the sour flavor of Younai fruits, supporting the germplasm dominance of the sweet–sour flavor in Younai.

Based on the above findings, Younai fruits have established a stable material basis for the sweet–sour flavor that is centered on fructose-malic acid and co-regulated by other soluble sugars and organic acids. This pattern exhibited conservation across the six sample groups (SB-JY, SB-GT, CP-YX, CP-GT, WHJ-JO, and WHJ-LC) from five producing areas selected in this experiment. These results characterize the sugar and organic acid composition of Younai fruit. The perceived balance of sweetness and sourness would require sensory validation. Although environmental factors of producing areas (such as climate, soil and cultivation management practices) exerted a significant effect on the absolute contents of sugar and acid components in Younai fruits, these factors did not alter its core sugar–acid composition pattern.

https://doi.org/10.3390/foods15101787

3.4. Composition and Content Distribution of Volatile Compounds in Younai Fruits

Volatile compounds are key components of Younai fruit flavor, which, together with sweet and sour tastes, determine the edible quality. After analysis by headspace solid-phase microextraction coupled with HS-SPME-GC-MS, a total of 28 volatile organic compounds (VOCs) were identified by excluding noise components with a detection rate lower than 30% (Table 1). The principal component analysis (PCA) score plot for volatile compounds is provided in Supplementary Figure S1.

Table 1. Categories and contents of 28 volatile compounds in various Younai fruit samples.

Compound Name	SB-JY	SB-GT	CP-YX	CP-GT	WHJ-JO	WHJ-LC
	μg/g, FW					
(Z)-3-Hexen-1-ol	23.34 ± 3.19	15.39 ± 7.26	—	23.50 ± 8.24	26.71 ± 3.36	32.55 ± 1.99
1-Hexanol	33.78 ± 5.70	17.75 ± 7.49	39.07 ± 19.99	24.61 ± 7.25	37.52 ± 5.77	43.25 ± 0.70
Hexanal	—	—	1.67 ± 0.92	5.59 ± 6.53	3.00 ± 1.03	—
Nonanal	—	—	—	0.24 ± 0.09	0.19 ± 0.02	—
Eicosane	0.70 ± 0.67	—	—	—	0.05 ± 0.03	—
Heneicosane	—	—	—	0.35 ± 0.23	0.05 ± 0.02	0.21 ± 0.05
Heptadecane	0.17 ± 0.08	0.05 ± 0.03	—	0.05 ± 0.01	0.15 ± 0.12	0.08 ± 0.03
Hexadecane	0.15 ± 0.03	0.06 ± 0.02	—	0.06 ± 0.02	0.06 ± 0.02	0.10 ± 0.03
Pentadecane	0.07 ± 0.02	—	—	—	0.04 ± 0.00	0.06 ± 0.01
Tetradecane	0.07 ± 0.01	—	—	—	0.03 ± 0.00	—
(Z)-3-Hexen-1-yl acetate	22.37 ± 9.53	15.42 ± 8.35	10.71 ± 4.57	7.33 ± 3.85	4.83 ± 1.34	7.71 ± 2.14
(Z)-3-Hexenyl butanoate	2.25 ± 1.65	—	—	0.75 ± 0.68	—	0.73 ± 0.29
(Z)-3-Hexenyl hexanoate	—	—	—	0.74 ± 0.70	—	0.39 ± 0.15
4-Hexen-1-yl hexanoate	3.31 ± 2.91	—	0.74 ± 0.37	—	—	—
Butyl acetate	—	7.94 ± 5.71	1.18 ± 1.46	—	—	—
Butyl butyrate	2.74 ± 0.82	0.17 ± 0.01	1.32 ± 0.73	0.35 ± 0.35	—	0.49 ± 0.16
Ethyl (Z)-7-octenoate	0.62 ± 0.35	—	—	—	—	0.30 ± 0.02
Ethyl acetate	15.78 ± 7.08	21.66 ± 7.36	5.62 ± 3.00	3.84 ± 3.23	2.29 ± 0.62	5.07 ± 1.73
Ethyl octanoate	2.26 ± 1.42	—	0.92 ± 0.24	0.23 ± 0.11	—	0.13 ± 0.02
Ethyl palmitate	0.14 ± 0.07	0.13 ± 0.06	—	0.04 ± 0.01	0.07 ± 0.03	0.14 ± 0.02
Hexyl hexanoate	2.56 ± 2.43	—	1.01 ± 1.00	0.43 ± 0.47	—	0.20 ± 0.08
Octyl acetate	—	1.15 ± 0.98	0.31 ± 0.15	—	—	—
6,10,14-Trimethyl-2-pentadecanone	—	—	0.13 ± 0.07	0.11 ± 0.07	0.07 ± 0.03	0.05 ± 0.00
γ-Decalactone	—	7.60 ± 2.99	5.95 ± 1.91	—	—	—
δ-Decalactone	—	0.70 ± 0.35	0.53 ± 0.16	—	—	—
Cedrol	0.09 ± 0.01	—	0.67 ± 0.56	0.28 ± 0.18	0.12 ± 0.01	0.10 ± 0.01
Linalool	—	0.60 ± 0.20	0.80 ± 0.10	—	—	—
β-Dihydroionone	—	—	—	—	0.20 ± 0.07	0.08 ± 0.01

Note: Volatile concentrations represent semi-quantitative estimates relative to an internal standard (3-octanol, 11.36 ug/g) and are expressed as ug/g fresh weight.

These VOCs were classified into seven categories (alcohols, aldehydes, alkanes, esters, ketones, lactones, terpenes) based on their chemical structures. In terms of the number of compounds (Figure 3A), esters were the most abundant with 12 types, accounting for 42.86%; alkanes followed with six types (21.43%). There were three types of alcohols and terpenes each, two types of aldehydes and lactones each, and only one type of ketones. In terms of content proportion (Figure 3B), alcohols were the dominant volatile category with the highest total content, ranging from 33.14 to 75.80 μg/g with an average of 51.25 μg/g.

Esters ranked second, with a total content of 7.20–52.02 μg/g and an average of 25.90 μg/g. The contents of alkanes, aldehydes, terpenes, lactones and ketones decreased in turn, with ketones having the lowest content and only being detected in some samples.

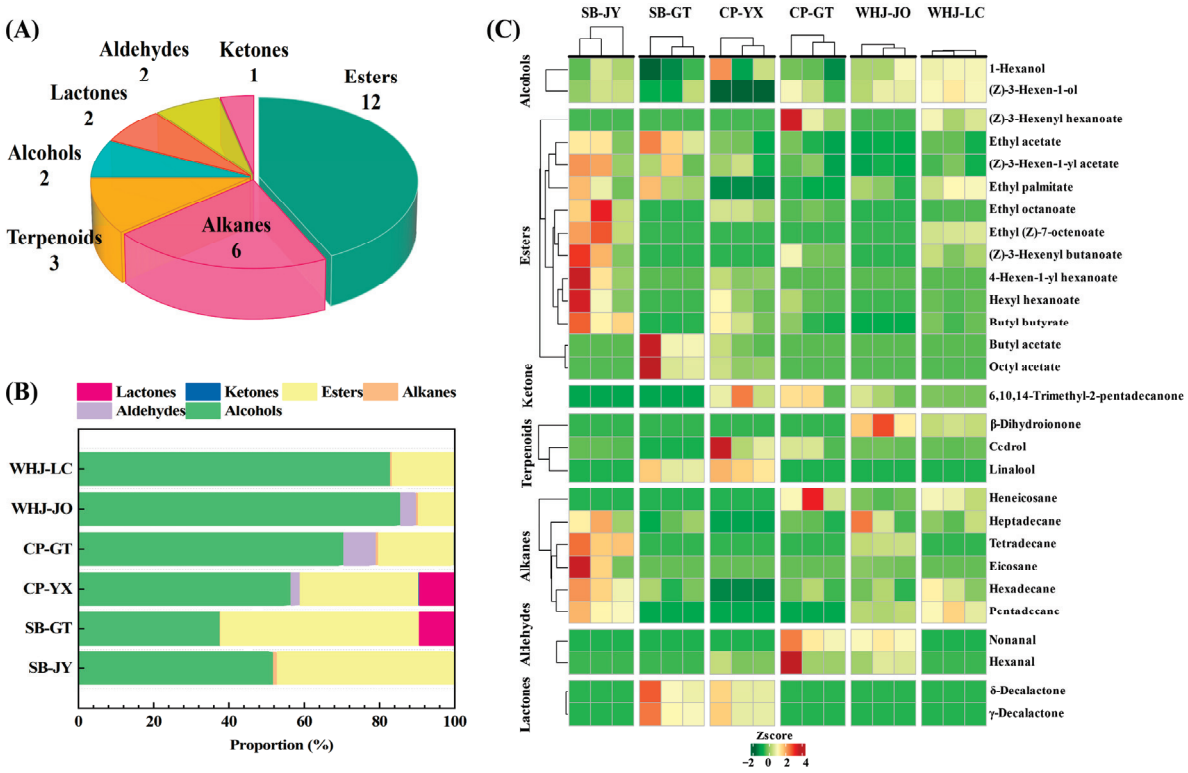


Figure 3. Composition, content distribution and cluster analysis of volatile compounds. (**A**) Pie chart showing the classification of 28 volatile compounds; (**B**) stacked bar chart of volatile compound contents in different groups; (**C**) heatmap of cluster analysis based on volatile compound contents.

Figure 3C presents the differences in the contents of volatile compounds among samples. Ester monomers (ethyl acetate, (Z)-3-hexen-1-yl acetate, ethyl palmitate) were highly accumulated in SB-JY and SB-GT, consistent with the overall trend of prominent ester contents in SB samples shown in Figure 3B. Alcohol monomers (1-hexanol, (Z)-3-hexen-1-ol) were highly accumulated in WHJ-JO and WHJ-LC, matching the high alcohol content trend of WHJ samples in Figure 3B. Alcohols and esters in the highly accumulated volatile compound clusters are the main potential contributors to Younai flavor, and can be regarded as key targets for preliminary screening.

The Sankey diagram (Figure 4) of volatile compounds intuitively reflects the corresponding relationship between aroma categories and their contents through the distribution of material flow intensity. The results showed that alcohols had a strong material flow correlation with all sample groups, being the only aroma category with high content detected in all samples and wide correlation, further confirming that alcohols are the common core aroma category of Younai fruits. The correlation between esters and SB-JY and SB-GT was significantly higher than that with CP and WHJ. Aldehydes formed weak correlations with CP-YX, CP-GT and WHJ-JO. Lactones had a trace material flow correlation with SB-GT and CP-YX. Terpenes showed weak and uniform material flow distribution with all sample groups, while alkanes and ketones had the lowest correlation with samples, with scattered material flow and no obvious regularity.

https://doi.org/10.3390/foods15101787

From the perspective of material distribution, the correlation characteristics of the Sankey diagram further explain the rich layers of Younai aroma with "common basis + specific expression". The broad-spectrum and strong correlation of alcohols makes them the basic aroma background of all Younai samples, while esters, aldehydes and lactones add more flavor layers.

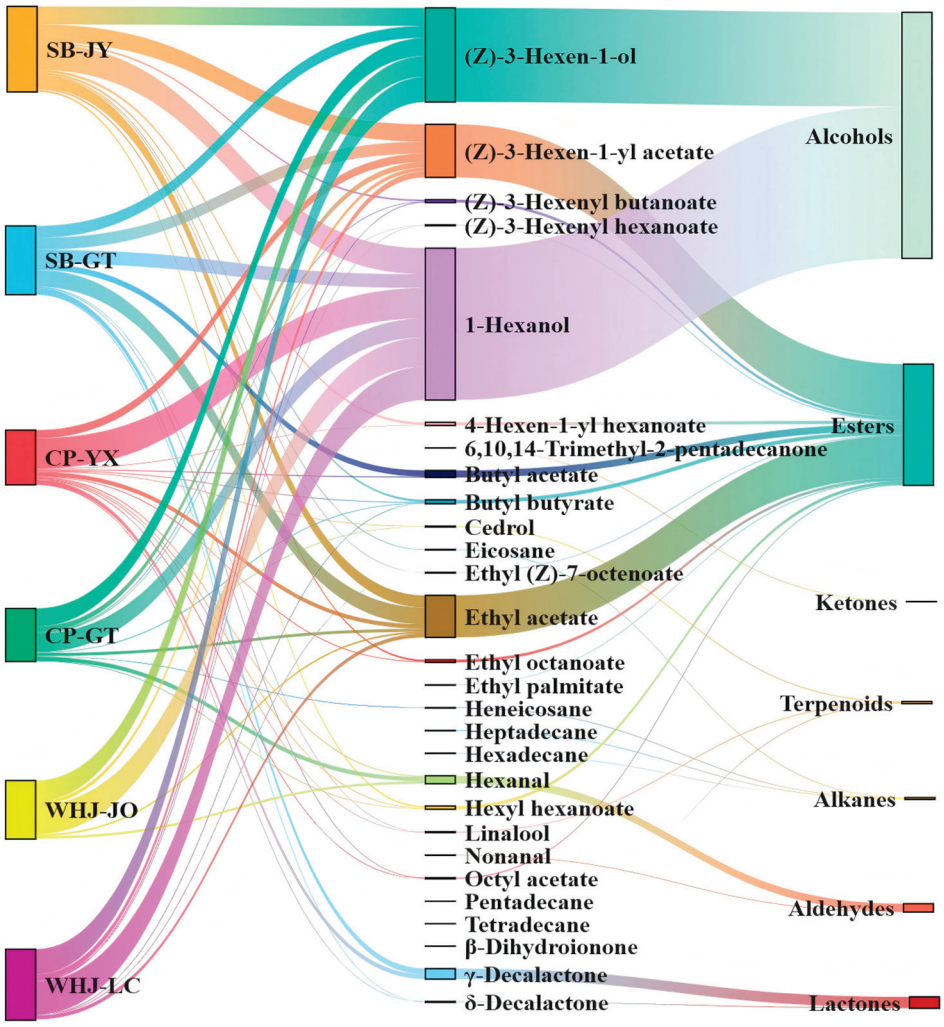


Figure 4. Sankey diagram of flux correlation between volatile aroma compound categories and sample groups in Younai fruit.

3.5. Preliminary Screening of Potential Odor-Active Compounds in Younai Fruits

Studies have shown that the aroma is closely related to the threshold concentration of volatile compounds, which is usually evaluated by relative OAVs [16]. In this study, OAV > 1 was used as the standard to screen the key potential odor-active compounds in Younai fruits. The results are shown in Table 2.

In terms of categories, alcohols and esters were the core categories of potential odor-active compounds, with rOAVs > 1 in all samples, making them the main potential contributors to Younai aroma. Among alcohols, (Z)-3-hexen-1-ol and 1-hexanol were the main content contributors, and their grassy and green leafy flavor characteristics made them the core potential active compounds of the basic aroma of Younai. Among esters, (Z)-3-hexen-1-yl acetate, (Z)-3-hexenyl butanoate, (Z)-3-hexenyl hexanoate and other ester compounds had rOAVs > 1 in all detected samples; most of these compounds had fruity and sweet flavor characteristics, serving as the core potential active compounds of the fruity flavor of Younai. Aldehydes, lactones and terpenes were potential odor-active com-

pounds, which were only detected in some samples with rOAVs > 1. Among aldehydes, hexanal and nonanal added fatty and green leafy flavor layers to Younai. Among lactones, γ-decalactone and δ-decalactone mainly exhibited peach and creamy flavors. Terpenes including linalool and β-dihydroionone exhibit floral and sweet fruity characteristics, and these compounds, based on their rOAV values, potentially contributed to Younai aroma as important regulatory compounds for its aroma layers. Ketones and alkanes had high thresholds, with rOAVs ≤ 1 in all samples, so they could be excluded from the candidates for core odor-active compounds of Younai.

Table 2. Relative odor aroma activity values (rOAV) of volatile compounds in Younai fruits.

Volatile Compounds	Aroma Thresholds (μg/g)	SB-JY	SB-GT	CP-YX	CP-GT	WHJ-JO	WHJ-LC
		Relative Odor Activity Values (rOAV)					
(Z)-3-Hexen-1-ol	0.05	466.75	307.83	—	470.01	534.29	650.99
1-Hexanol	0.25	135.11	71	156.3	98.43	150.09	172.98
Hexanal	0.011	—	—	151.55	508.37	273.03	—
Nonanal	0.01	—	—	—	23.9	19.13	—
(Z)-3-Hexen-1-yl acetate	0.02	1118.29	770.93	535.54	366.32	241.64	385.68
(Z)-3-Hexenyl butanoate	0.005	449.28	—	—	149.28	—	146.69
(Z)-3-Hexenyl hexanoate	0.007	—	—	—	105.83	—	55.02
4-Hexen-1-yl hexanoate	0.012	275.53	—	61.29	—	—	—
Butyl acetate	0.066	—	120.27	17.93	—	—	—
Butyl butyrate	0.01	274.22	17.47	132.12	35.01	—	49.29
Ethyl (Z)-7-octenoate	0.003	208.23	—	—	—	—	100.5
Ethyl acetate	5	3.16	4.33	1.12	0.77	0.46	1.01
Ethyl octanoate	0.005	451.69	—	183.24	46.75	—	26.71
Hexyl hexanoate	0.02	127.97	—	50.49	21.6	—	10.12
Octyl acetate	0.012	—	95.9	25.94	—	—	—
γ-Decalactone	0.011	—	691.01	541.2	—	—	—
δ-Decalactone	0.05	—	13.96	10.63	—	—	—
Cedrol	120	—	—	0.01	—	—	—
Linalool	0.006	—	99.34	132.71	—	—	—
β-Dihydroionone	0.004	—	—	—	—	50.13	18.99

Note: Relative odor activity values were calculated using odor detection thresholds from the published literature, not measured directly in Younai. The odor threshold data were cited from Refs. [13–16].

From the perspective of flavor chemistry, the composition of aroma compounds in Younai is consistent with the aroma commonalities of *Prunus* stone fruits [22,23]. As two core aroma components, alcohols and esters together form the main framework of the basic aroma profile of Younai. Alcohols, typical characteristic substances with grassy and green leafy aromas, are the signature aroma during the ripening process of stone fruits [24]. Esters exhibit fruity and sweet aromas [25]. Meanwhile, aldehydes, alcohols, terpenes and lactones add richer layers to the aroma characteristics [24]. The above results define the core target range for the subsequent screening of potential odor-active compounds.

3.6. Analysis of the Core Metabolic Basis of Younai Fruit Flavor

The untargeted metabolomics analysis identified 293 metabolites across six major classes, providing a preliminary chemical fingerprint of Younai fruit. The PCA results for metabolites, including QC sample clustering verification, are displayed in Supplementary Figure S2. The 293 metabolites could be divided into 13 major categories based on their chemical structures and functions, clarifying the overall composition characteristics of metabolites in Younai fruits (Figure 5A). Among them, 135 were polyphenols, accounting for 46.06% of the total identified metabolites, making them the largest metabolite category in Younai fruits, followed by sugars (26 species), amino acids (25 species) and organic acids

(21 species). These three categories accounted for 25.60% of the total metabolites, and the proportions of other categories were all less than 10%.

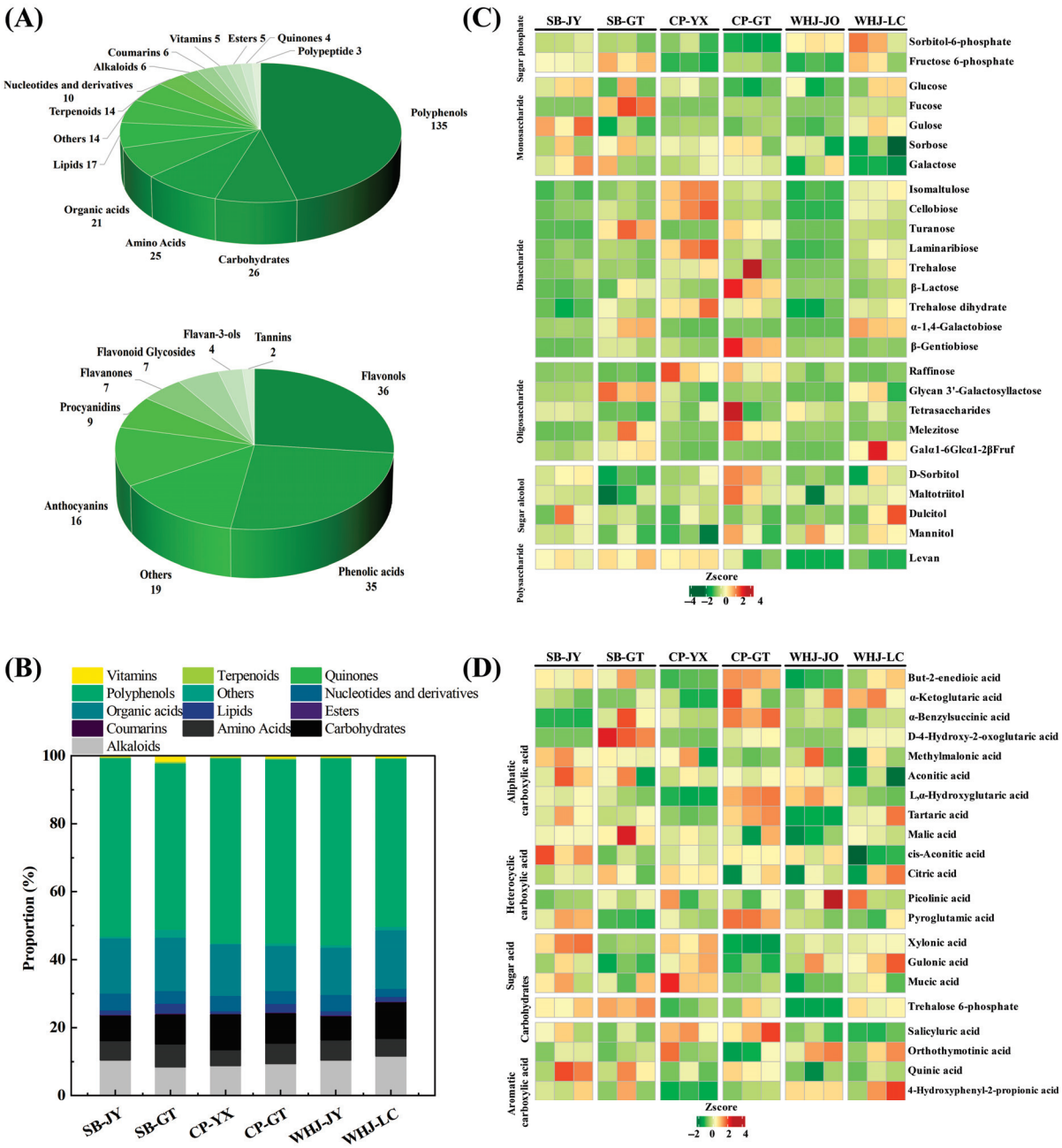


Figure 5. Analysis of metabolite category composition and soluble sugar, organic acid metabolites in Younai fruits. (**A**) Overall category composition of metabolites and composition of polyphenol subcategories in Younai fruits; (**B**) stacked chart of relative peak area proportions of different metabolite categories; (**C**) hierarchical cluster heatmap of soluble sugar metabolite subcategories; (**D**) hierarchical cluster heatmap of organic acid metabolite subcategories in Younai fruits.

https://doi.org/10.3390/foods15101787

Polyphenols could be divided into nine subcategories, among which flavonols (36 species) and phenolic acids (35 species) were the two most abundant subcategories, accounting for 52.59% of the total polyphenols. Followed by anthocyanins (16 species) and proanthocyanidins (nine species), the number of other polyphenol subcategories was small, accounting for less than 20% in total. Flavonols, phenolic acids and proanthocyanidins are the three major polyphenol subcategories closely related to Younai flavor. Studies have shown that flavonols and phenolic acids are not only the main regulatory substances for the astringency of fruits [26], but also can serve as aroma precursors to generate volatile aroma compounds such as aldehydes and alcohols through degradation reactions, participating in the formation of Younai's fruity and grassy aromas [24]. Proanthocyanidins mainly contribute to the slight astringency of Younai and enhance the flavor layering [27].

Focusing on the core flavor components, further analysis of the 26 soluble sugars and 21 organic acids was performed, with the results shown in Figure 5B. The soluble sugar components encompassed disaccharides, monosaccharides, oligosaccharides, sugar alcohols, sugar phosphates, and polysaccharides, and the contents of monosaccharides varied among different samples. Isomaltulose, raffinose, etc., could impart a mellow flavor to the fruits, while characteristic *Prunus* sugar alcohols such as sorbitol and mannitol were consistently present in all samples. Previous studies have confirmed that these sugar alcohols are characteristic flavor-contributing components of *Prunus* fruits, endowing them with a cool and sweet aftertaste [17].

The organic acid components, as shown in Figure 5C, were identified to belong to categories such as aliphatic carboxylic acids, heterocyclic carboxylic acids, sugar acids, and aromatic carboxylic acids. Among them, aliphatic carboxylic acids such as malic acid, citric acid, and tartaric acid served as the core source of acidity in stone fruits [6], as well as the primary contributor to the acidity of Younai fruits. Other organic acid components, including sugar acids and aromatic carboxylic acids, further modulated the fruit flavor and enhanced the flavor layers, and, in synergy with antioxidant substances, improved the nutritional quality of the fruits [28].

3.7. Correlation Analysis of Fruit Quality, Flavor and Volatile Compound Contents in Younai Fruits

To clarify the synergistic/antagonistic regulatory relationships between core quality indicators, flavor components and volatile compounds in the formation of Younai fruit quality, Pearson correlation analysis was performed on 13 key indicators, with the results shown in Figure 6 (Supplementary Tables S3 and S4). Fruit firmness was extremely significantly negatively correlated with TSS ($r = -0.98$, $p = 0.0007$), which is consistent with the common ripening rule of stone fruits [29]. Specifically, during fruit ripening and softening, cell wall structure degrades, while photosynthetic products are continuously transported to fruits and converted into soluble sugars, promoting TSS accumulation. TA was significantly positively correlated with malic acid ($r = 0.84$, $p = 0.04$), confirming that malic acid is the main contributor to the total acidity of Younai fruits.

https://doi.org/10.3390/foods15101787

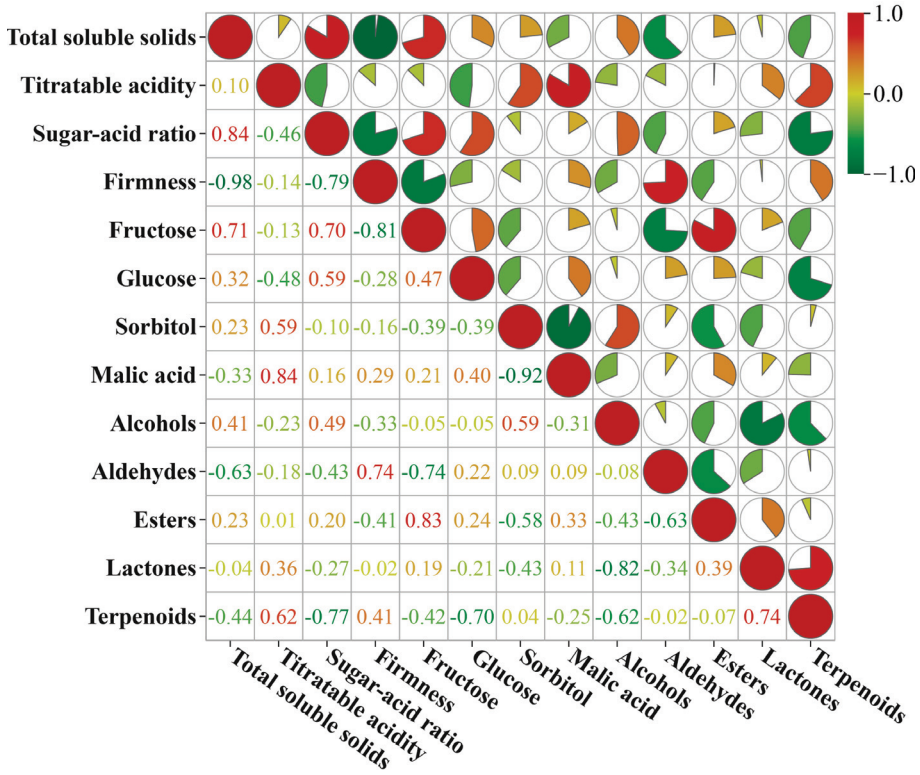


Figure 6. Heatmap of correlation analysis of core flavor compounds in Younai fruits. The color depth in the heatmap represents the magnitude of the correlation coefficient. Red indicates a positive correlation, while green indicates a negative correlation, and the numbers represent the specific correlation coefficient values. Pearson correlation coefficients and raw (uncorrected) *p*-values are reported. The analysis was performed using the MetWare Cloud Platform, which does not apply built-in multiple testing correction. Readers are advised to interpret correlations with *p*-values near the threshold with appropriate caution.

4. Discussion

The above results suggest that Younai has established a basic flavor framework centered on fructose and malic acid taste and combined with characteristic volatile compounds, with the basic skeleton characterized by "fructose-sorbitol-glucose-malic acid-(Z)-3-hexen-1-ol-(Z)-3-hexen-1-yl acetate", and polyphenols (flavonols and phenolic acids) serving as the core polyphenol metabolites. In the 293 metabolites detected in this study, polyphenol metabolites accounted for a dominant proportion. These polyphenol substances provide Younai with astringent, bitter and antioxidant characteristics, while their degradation products also serve as precursors of aromatic compounds [29]. For example, phenolic acids such as chlorogenic acid and gallic acid can generate aromatic aldehydes through oxidative degradation, while flavonols such as quercetin can release aromatic components during the Maillard reaction [30,31]. This metabolic link between polyphenols and volatile compounds further enriches the flavor diversity and complexity of Younai.

To comprehensively elucidate the flavor formation characteristics of Younai, this study systematically compared its sugar–acid components and volatile aroma profiles with published data from other *Prunus* cultivars and related stone fruit species. For organic acids, malic acid was the absolutely dominant component in Younai, highly consistent with major Japanese plum cultivars including 'Angeleno' and 'Black Amber' [32]. This aligns with the core organic acid metabolic pattern of *Prunus* fruits, further validating the reliability of our results. Significant cultivar-specific differences were observed in soluble sugars. Fructose was the predominant sugar in Younai, whereas Xiao et al. (2024) [6] reported glucose as the dominant sugar across 86 plum cultivars. This discrepancy may mainly stem from the

unique genotype of Younai, combined with effects of harvest maturity, local climate and soil conditions. For volatiles, C6 alcohols and esters were the basal aroma components of Younai, matching the common "fresh fruity" trait of *Prunus* fruits. γ-decalactone and linalool were identified as potential core contributors to Younai's unique volatile profile, distinguishing it from other plums [32,33]. This trait may be closely related to abundant carotenoids (key precursors for terpenoid and lactone aroma biosynthesis) in Younai's yellow flesh [23,34], as well as cultivar-specific expression of key aroma biosynthesis genes.

In this study, core polyphenol metabolites, flavonols and phenolic acids, accounted for a dominant proportion of the 293 metabolites. It has been reported in other plant systems that certain phenolic compounds may serve as potential precursors for volatile aldehydes and alcohols through enzymatic and non-enzymatic degradation reactions during fruit ripening and processing [35]. However, it is important to emphasize that the present study did not perform direct precursor-product analysis or pathway-level investigation to establish such links in Younai specifically. The relationship between polyphenol composition and volatile formation in this cultivar therefore remains a hypothesis. Further studies could combine metabolomics with transcriptomics to trace the origin and transformation of polyphenol metabolites in Younai, providing a more comprehensive theoretical basis for its flavor formation mechanism.

It is important to acknowledge several limitations of the present study. First, although we employed rOAV calculations to prioritize potential aroma-active compounds, direct sensory validation—such as descriptive sensory panel evaluation, GC-O, or aroma recombination and omission tests—was not performed. Therefore, the identification of key flavor-driving components in this study represents a chemically grounded screening rather than a sensory-confirmed determination. Second, the metabolomics analysis was primarily descriptive. Pathway enrichment analysis, metabolite–metabolite network analysis, and transcriptomic integration were beyond the scope of this work but would be necessary to establish mechanistic links between metabolite classes and flavor chemistry. Third, the volatile quantification method was semi-quantitative relative to an internal standard rather than fully validated absolute quantification using authentic standard curves for all compounds. Additionally, systematic climate, irrigation and soil matrix data were not collected in this study, which precludes the quantitative analysis of environmental effects on Younai flavor. Meanwhile, our nested sampling design (SB-JY, SB-GT, CP-YX, CP-GT, WHJ-JO, WHJ-LC) prevents clear disentanglement of cultivar and production site effects, further hindering the determination of each factor's specific contribution to Younai flavor. We also acknowledge differential harvest dates among cultivars as a potential confounding factor, and we plan to conduct sampling with multiple harvest dates per cultivar in future research to clarify temporal effects on flavor chemistry.

In summary, this study provides a useful baseline dataset for the chemical composition of Younai fruit flavor. These data contribute to the understanding of this regionally important cultivar and may serve as a foundation for future studies incorporating sensory validation, transcriptomic analysis, and expanded sampling. The development of a quality standardization evaluation system for Younai will require integration of the present chemical data with direct sensory measurements and broader cultivar–site–season coverage.

5. Conclusions

This study provides a comprehensive chemical characterization of flavor-related components in *Prunus salicina* var. cordata cv. 'Younai'. The results indicate that fructose and malic acid are the predominant sugar and organic acid, respectively, and that C6 alcohols and esters—notably (Z)-3-hexen-1-ol, 1-hexanol, and (Z)-3-hexen-1-yl acetate—are the major volatile compounds. Based on odor activity values, γ-decalactone and linalool

https://doi.org/10.3390/foods15101787

were additionally screened as potential contributors to the characteristic aroma of Younai. Untargeted metabolomics identified 293 metabolites, with flavonols and phenolic acids representing the most abundant classes, providing a preliminary chemical fingerprint of this cultivar. This study provided a theoretical basis for the construction of a quality standardization evaluation system.

Supplementary Materials: The following supporting information can be downloaded at https://www.mdpi.com/article/10.3390/foods15101787/s1, Table S1: Sampling sites and basic fruit traits of test samples; Table S2: The 293 metabolites in Younai fruits; Table S3: The correlation coefficients of core flavor compounds in Younai fruits; Table S4: The *p* values of the correlation analysis of core flavor compounds in Younai fruits. Figure S1: Principal component analysis (PCA) score plot of volatile compounds across different sample groups. SB-GT: Shiban Wannai from Gutian County; CP-YX: Cuiping Younai from Youxi County; CP-GT: Cuiping Younai from Gutian County; WHJ-JO: Wanhuangjin from Jian'ou City; WHJ-LC: Wanhuangjin from Liancheng County. Other figure annotations are the same as above, Figure S2: Principal component analysis (PCA) score plot of metabolomic profiles across different sample groups and quality control (QC) samples.

Author Contributions: Conceptualization, S.Y.; methodology, L.F. and W.L.; formal analysis, L.F. and W.L.; investigation, L.F., W.L. and H.C.; resources, F.C.; data curation, L.F., W.L. and S.Y.; writing—original draft preparation, L.F.; writing—review and editing, W.L., L.R. and S.Y.; visualization, L.F.; supervision, X.L., J.G. and H.C.; project administration, X.L., J.G. and H.C.; funding acquisition, S.Y. All authors have read and agreed to the published version of the manuscript.

Funding: This research was funded by the Public Welfare Scientific Research Institute Special Project of Fujian Province (Grant No. 2024R1021002) and the Innovation Team Project of Fujian Academy of Agricultural Sciences (Grant No. CXTD2021011-1).

Institutional Review Board Statement: Not applicable.

Informed Consent Statement: Not applicable.

Data Availability Statement: The data presented in this study are available on request from the corresponding author due to the fact that the data contain unprocessed original detection data and related experimental parameters.

Acknowledgments: The cluster analysis heatmap was performed using the Metware Cloud. (https://cloud.metware.cn, format: accessed on 1 December 2025).

Conflicts of Interest: The authors declare no conflicts of interest.

Abbreviations

The following abbreviations are used in this manuscript:

rOAV	Relative Odor Activity Value
HPLC	High Performance Liquid Chromatography
HS-SPME-GC-MS	HeadSpace Solid Phase Microextraction–Gas Chromatography Mass Spectrometry
UPLC-QTOF-MS	Ultra Performance Liquid Chromatography Quadrupole Time of Flight Mass Spectrometry
SB	Shiban Wannai
CP	Cuiping Younai
WHJ	Wanhuangjin
JY	Jianyang District
GT	Gutian County
YX	Youxi County
JO	Jian'ou District
LC	Liancheng County

DAFB	Day After Full Bloom
TSS	Total Soluble Solids
TA	Titratable Acid
GC-O	Gas Chromatography–Olfactometry

References

1. Liao, R.; Zhao, M.; Lan, Q.; Peng, S.; Lin, F.; Li, Z. Comprehensive assembly and comparative analysis of chloroplast genome and mitogenome of *Prunus salicina* var. *cordata*. *Genes* **2025**, *16*, 660. [CrossRef]
2. Berta Gonçalves, I.O.E.B.; Maria Cristina Morais, A.A.; Fernanda Cosme, J.V.; Pinto, R.A.A.T. *Generation of Aromas and Flavours*; IntechOpen: London, UK, 2018. [CrossRef]
3. Jiang, Y.; Song, J. Fruits and Fruit Flavor: Classification and biological characterization. In *Handbook of Fruit and Vegetable Flavors*; John Wiley & Sons, Inc.: Hoboken, NJ, USA, 2010; pp. 1–23, ISBN 9780470622834. [CrossRef]
4. Chen, B.; Lin, X.; Liang, Z.; Chang, X.; Wang, Z.; Huang, M.; Zeng, X. Advances in food flavor analysis and sensory evaluation techniques and applications: Traditional vs emerging. *Food Chem.* **2025**, *494*, 146235. [CrossRef] [PubMed]
5. Liu, H.; Zhang, M.; Su, M.; Zeng, W.; Wang, S.; Du, J.; Zhou, H.; Yang, X.; Zhang, X.; Li, X.; et al. Multidimensional analysis of the flavor characteristics of yellow peach at different ripening stages: Chemical composition profiling and sensory evaluation. *Food Chem.* **2025**, *471*, 142772. [CrossRef]
6. Xiao, Q.; Ye, S.; Wang, H.; Xing, S.; Zhu, W.; Zhang, H.; Zhu, J.; Pu, C.; Zhao, D.; Zhou, Q.; et al. Soluble sugar, organic acid and phenolic composition and flavor evaluation of plum fruits. *Food Chem. X* **2024**, *24*, 101790. [CrossRef]
7. Zeng, X.; Zhang, S.; Zhang, Z.; Chen, Y.; Wang, S.; Tang, Z.; Zhou, W.; Geng, W. Integration of transcriptomics and metabolomics reveals the mechanism of aroma formation during apricot fruit development. *Sci. Hortic.* **2025**, *350*, 114351. [CrossRef]
8. Magwaza, L.S.; Opara, U.L. Analytical methods for determination of sugars and sweetness of horticultural products—A review. *Sci. Hortic.* **2015**, *184*, 179–192. [CrossRef]
9. Liu, G.; Bi, J.; Chen, Q. Recent advances on peach aroma: Key aroma-active compounds and their metabolic pathways, analysis strategies, and innovative processing tools. *Trends Food Sci. Technol.* **2025**, *159*, 104992. [CrossRef]
10. Cao, X.; Su, Y.; Zhao, T.; Zhang, Y.; Cheng, B.; Xie, K.; Yu, M.; Allan, A.; Klee, H.; Chen, K.; et al. Multi-omics analysis unravels chemical roadmap and genetic basis for peach fruit aroma improvement. *Cell Rep.* **2024**, *43*, 114623. [CrossRef] [PubMed]
11. Wang, R.; Shu, P.; Zhang, C.; Zhang, J.; Chen, Y.; Zhang, Y.; Du, K.; Xie, Y.; Li, M.; Ma, T.; et al. Integrative analyses of metabolome and genome-wide transcriptome reveal the regulatory network governing flavor formation in kiwifruit (*Actinidia chinensis*). *New Phytol.* **2022**, *233*, 373–389. [CrossRef]
12. Zhang, Y.; Liu, W.; Zhang, B.; Zhang, Y.; Cai, Z.; Song, H.; Ma, R.; Yu, M. Analysis of volatile compounds and their potential regulators in four high-quality peach (*Prunus persica* L.) cultivars with unique aromas. *LWT* **2022**, *160*, 113195. [CrossRef]
13. Xue, J.; Liu, P.; Yin, J.; Wang, W.; Zhang, J.; Wang, W.; Le, T.; Ni, D.; Jiang, H. Dynamic changes in volatile compounds of shaken black tea during Its manufacture by GC × GC–TOFMS and multivariate data analysis. *Foods* **2022**, *11*, 1228. [CrossRef]
14. Huang, W.; Fang, S.; Wang, J.; Zhuo, C.; Luo, Y.; Yu, Y.; Li, L.; Wang, Y.; Deng, W.; Ning, J. Sensomics analysis of the effect of the withering method on the aroma components of Keemun black tea. *Food Chem.* **2022**, *395*, 133549. [CrossRef]
15. Fang, X.; Xu, W.; Jiang, G.; Sui, M.; Xiao, J.; Ning, Y.; Niaz, R.; Wu, D.; Feng, X.; Chen, J.; et al. Monitoring the dynamic changes in aroma during the whole processing of Qingzhuan tea at an industrial scale: From fresh leaves to finished tea. *Food Chem.* **2024**, *439*, 137810. [CrossRef] [PubMed]
16. Burdock, G.A. *Fenaroli's Handbook of Flavor*, 6th ed.; CRC Press/Taylor & Francis: Boca Raton, FL, USA, 2010; p. 2159. [CrossRef]
17. Niu, X.; Deng, L.; Wang, H.; Wang, Q.; Xu, M.; Li, S.; Okaiyeto, S.A.; Xiao, H. Transformation of cell wall pectin profile during postharvest ripening process alters drying behavior and regulates the sugar content of dried plums. *Food Chem.* **2024**, *458*, 140093. [CrossRef] [PubMed]
18. Stacewicz-Sapuntzakis, M.; Bowen, P.E.; Hussain, E.A.; Damayanti-Wood, B.I.; Farnsworth, N.R. Chemical composition and potential health effects of Prunes: A functional food? *Crit. Rev. Food. Sci. Nutr.* **2001**, *41*, 251–286. [CrossRef] [PubMed]
19. Zhang, L.; Zhang, A.; Xu, Y.; Zhu, L.; Ma, B.; Li, M. Accumulation and regulation of malate in fruit cells. *Fruit Res.* **2024**, *4*, e031. [CrossRef]
20. Junge, J.Y.; Bertelsen, A.S.; Mielby, L.A.; Zeng, Y.; Sun, Y.; Byrne, D.V.; Kidmose, U. Taste interactions between sweetness of sucrose and sourness of citric and tartaric acid among Chinese and Danish consumers. *Foods* **2020**, *9*, 1425. [CrossRef]
21. Kader, A.A. Flavor quality of fruits and vegetables. *J. Sci. Food. Agric.* **2008**, *88*, 1863–1868. [CrossRef]
22. Ba, L.; Wang, X.; Luo, C.; Cao, S.; Chen, J.; Luo, D. Transcriptomics combined with HS-SPME-GC/MS and IMS was used to investigate aroma compound formation in 'Fengtang' plum at different maturity stages. *Food Chem.* **2026**, *506*, 148096. [CrossRef]
23. Long, Y.; Wu, Z.; Liu, D.; Fang, B.; Zhao, X. Color and aroma of plums: Biosynthesis, regulation, and interrelationships. *J. Agric. Food. Chem.* **2025**, *73*, 31742–31759. [CrossRef]

24. Gonçalves, B.; Oliveira, I.; Bacelar, E.; Morais, M.C.; Aires, A.; Cosme, F.; Ventura-Cardoso, J.; Anjos, R.; Pinto, T. *Aromas and Flavours of Fruits*; IntechOpen: London, UK, 2018. [CrossRef]
25. Li, X.; Liu, C.; Wu, J.; Su, K.; Xiao, X.; Zhang, L.; Eberhart, B.L.; Chen, C.; Song, F. Comprehensive investigation on the dynamic changes of volatile organic compounds in three peach cultivars during fruit development. *Food Res. Int.* **2025**, *203*, 115866. [CrossRef]
26. Radulescu, C.; Olteanu, R.L.; Buruleanu, C.L.; Tudorache, M.N.; Dulama, I.D.; Stirbescu, R.M.; Bucurica, I.A.; Stanescu, S.G.; Banica, A.L. Polyphenolic screening and the antioxidant activity of grape pomace extracts of romanian white and red grape varieties. *Antioxidants* **2024**, *13*, 1133. [CrossRef]
27. Wei, X.; Ju, Y.; Ma, T.; Zhang, J.; Fang, Y.; Sun, X. New perspectives on the biosynthesis, transportation, astringency perception and detection methods of grape proanthocyanidins. *Crit. Rev. Food. Sci. Nutr.* **2021**, *61*, 2372–2398. [CrossRef]
28. Su, C.; Kang, J.; Liu, S.; Li, C. Exploring the influence of fruit ripeness on the microbiome, bioactive components, and flavor profiles of naturally fermented noni (*Morinda citrifolia* L.) juice. *Food Chem.* **2025**, *482*, 144192. [CrossRef]
29. Niu, X.; Tao, Y.; Wang, Q.; Xu, M.; Zhang, F.; Xie, Y.; Xiao, H. Postharvest ripening-induced modification of cell wall polysaccharide affects plum phenolic bioavailability. *Food Chem.* **2025**, *479*, 143780. [CrossRef]
30. Caffrey, A.J.; Lerno, L.A.; Zweigenbaum, J.; Ebeler, S.E. Direct Analysis of glycosidic aroma precursors containing multiple aglycone classes in vitis vinifera berries. *J. Agric. Food. Chem.* **2020**, *68*, 3817–3833. [CrossRef]
31. Duan, Y.; Liu, Z.; Zhang, Q.; Hu, J.; Zheng, S.; Mao, X.; Wang, Y. Dynamic changes in volatile and non-volatile components of Jinggang honey pomelo (*Citrus maxima* (L.) Osbeck) during growth revealed through an untargeted metabolomics approach. *Food Chem.* **2025**, *478*, 143654. [CrossRef] [PubMed]
32. Lozano, M.; Vidal-Aragón, M.C.; Hernández, M.T.; Ayuso, M.C.; Bernalte, M.J.; Velardo, J.G. Physicochemical and nutritional properties and volatile constituents of six Japanese plum (*Prunus salicina* Lindl.) cultivars. *Eur. Food Res. Technol.* **2009**, *228*, 403–410. [CrossRef]
33. Zhang, Q.; Zhu, S.; Lin, X.; Peng, J.; Luo, D.; Wan, X.; Zhang, Y.; Dong, X.; Ma, Y. Analysis of volatile compounds in different varieties of plum fruits based on headspace solid-phase microextraction-gas chromatography-mass spectrometry technique. *Horticulturae* **2023**, *9*, 1069. [CrossRef]
34. Baz, N.M.; Wang, J.; Zhao, X.; Maqbool, A.; Gao, C.; Wang, P.; Chen, H.; Cao, H. Carotenoid biosynthesis in *Prunus* species: From pathway and accumulation structure to diverse pigmentation. *Mol. Hortic.* **2026**, *6*, 3. [CrossRef]
35. Rizzi, G.P. Formation of strecker aldehydes from polyphenol-derived quinones and α-amino acids in a nonenzymic model system. *J. Agric. Food. Chem.* **2006**, *54*, 1893–1897. [CrossRef] [PubMed]

Disclaimer/Publisher's Note: The statements, opinions and data contained in all publications are solely those of the individual author(s) and contributor(s) and not of MDPI and/or the editor(s). MDPI and/or the editor(s) disclaim responsibility for any injury to people or property resulting from any ideas, methods, instructions or products referred to in the content.

foods

MDPI

Article

Multi-Omics Integration to Investigate the Effects of Variety and Origin on Volatile and Non-Volatile Metabolites in Melons

Junzhe Hua [1], Kemin Mao [1,2], Wenlong Yu [1,2], Zongyang Li [1], Runhan Wen [1], Lingyu Li [1], Liyan Song [3], Yaxin Sang [1,2] and Xianghong Wang [1,2,*]

[1] College of Food Science and Technology, Hebei Agricultural University, No. 2596 Lekai South Street, Baoding 071000, China; 15719016123@163.com (J.H.); keminmao@outlook.com (K.M.); yuwenlong0810@163.com (W.Y.); 13931226615@163.com (Z.L.); 13184750826@163.com (R.W.); lly11022024@163.com (L.L.); sangyx1418@163.com (Y.S.)
[2] Laboratory of Dietary Component Interactions and Precision Nutrition, Baoding 071000, China
[3] Agriculture and Rural Affairs Bureau of Qing County, Cangzhou 062650, China; 15735861061@163.com
* Correspondence: wangshipin2017@163.com; Tel.: +86-(0312)-7528195

Abstract

This study investigated the effects of different cultivation environments on melon quality development and the underlying metabolic regulatory mechanisms. Using 'Yangjiaocui' and 'Boyang 9' melons, we systematically compared their physicochemical properties, nutritional components, volatile compounds, and metabolites under saline–alkali versus normal conditions, employing an integrated multi-omics analytical model. The results showed that saline–alkali cultivation significantly increased several nutritional components (e.g., soluble solids, vitamin C, flavonoids, and polyphenols) compared to normal conditions. Gas chromatography–ion mobility spectrometry (GC-IMS) detected 36 volatiles, predominantly esters and ketones, with 13 key markers such as isovaleric acid isovaleryl ester and ethyl butyrate, effectively discriminating cultivars and growth origins. Liquid chromatography–mass spectrometry (LC-MS) detected 702 metabolites, chiefly organic acids and lipids. KEGG pathway enrichment analysis revealed that flavonoid biosynthesis was the most significantly enriched pathway (enrichment factor ~1, extreme significance), with coordinated regulation of tyrosine and phenylalanine metabolism redirecting metabolic flux toward defensive secondary metabolites. In conclusion, our results suggest that saline–alkali cultivation may contribute to improved nutritional profiles, and multi-omics analysis effectively differentiates melon varieties and origins. This study provides a theoretical basis for understanding the quality, flavor, and metabolite profiles of melon under saline–alkali stress, employing a multi-omics approach.

Keywords: saline–alkali soil; *Cucumis melo* L.; flavor differences; metabolomics; integrative multi-omic

1. Introduction

Melon (*Cucumis melo* L.), an annual herbaceous species within the Cucurbitaceae family, is indigenous to Africa and extensively cultivated throughout Asia. As a globally significant cash crop, it is characterized by a short growth cycle, high benefit-to-cost ratio, and substantial nutritional value, contributing to its considerable consumer popularity [1]. The fruit is distinguished by its crisp texture and pronounced aroma, qualities that endow it with notable economic value and market potential. In Hebei Province, melon cultivation covers an area of 1.546 million mu (approximately 103,000 hectares), yielding an output

value of 14.25 billion CNY. Both the cultivation area and total production rank among the highest in the nation, making melon production a crucial income source for local farmers. However, the extensive diversity among melon varieties leads to considerable variation in quality, flavor, and environmental adaptability. This heterogeneity underscores the necessity for scientific evaluation and selection of high-quality cultivars suited to specific agro-ecological conditions, which has emerged as a key research focus. Among the widely cultivated varieties, 'Yangjiaocui' and 'Boyang 9' represent two mainstream types. 'Yangjiaocui' is characterized by an oblong fruit shape, relatively thick rind, traditional flavor, and distinctive appearance [2]. In contrast, 'Boyang 9' exhibits smooth peel, thick flesh, high sugar content, and a crisp, sweet taste.

Although previous studies have confirmed significant differences in nutritional components (such as minerals and vitamin C) among different melon varieties [3], the current evidence is primarily derived from conventional cultivation. As a typical abiotic stress environment, saline–alkali soil induces specific salt stress and ion toxicity that directly interfere with physiological processes and the biosynthesis of secondary metabolites. These effects are likely to alter the nutritional quality and bioactive composition of melon fruits. Nevertheless, systematic comparisons of varietal adaptation mechanisms and their associated effects on fruit nutritional quality under saline–alkali conditions remain limited. This gap constrains the targeted and effective use of saline–alkali land for quality melon production. Thus, future studies should prioritize evaluating varietal adaptability under saline–alkali stress, clarifying the response of nutritional traits and developing strategies for efficient resource use. Such work will provide theoretical insights into melon salt tolerance physiology and support the sustainable development of specialized melon production in saline–alkali regions.

In recent years, volatile compounds in fruits have been extensively investigated using various analytical techniques, particularly headspace solid-phase microextraction coupled with gas chromatography-mass spectrometry (HS-SPME-GC-MS). Previous studies have characterized volatile profiles in fruits such as peaches [4] and mangoes [5], establishing relationships between specific aroma compounds and flavor quality. For example, Valverde et al. [6] investigated the relationship between aroma components and sensory attributes in melons cultivated in La Mancha, Spain, over three consecutive growing seasons; significant correlations were identified between volatile compounds and specific sensory descriptors such as fruity and floral notes. While existing research has advanced the understanding of melon volatile composition and characteristics, most studies continue to rely exclusively on GC-MS methodologies. Although GC-MS is sensitive, it often requires extensive sample preparation and may fail to detect certain classes of volatiles owing to extraction or ionization biases, potentially leading to an incomplete representation of the volatile profile. Moreover, the flavor profiles of fruits cultivated under saline–alkaline conditions remain largely unexplored. In contrast to GC-MS, GC-IMS requires minimal sample preparation, enables rapid analysis, and is particularly suitable for detecting volatile organic compounds. Thus, applying GC-IMS to characterize the composition and distinctive features of volatile compounds in melons grown under saline–alkaline conditions can yield complementary insights that are not accessible by conventional GC-MS alone.

Non-targeted metabolomics has gained extensive application in fruit research in recent years. It has demonstrated particular significance in quality evaluation, flavor profiling, and metabolite analysis [7]. By enabling comprehensive detection and systematic analysis of metabolites, this approach not only reveals the composition, variation, and dynamic patterns of metabolic profiles but also provides crucial theoretical and technical support for quality assessment, flavor characterization, and breeding of superior fruit varieties. However, the application of non-targeted metabolomics in melon research remains relatively

https://doi.org/10.3390/foods15101746

limited [8]. Existing studies have yet to establish a systematic framework, warranting further development in areas such as metabolite database construction, key metabolic pathway elucidation, and understanding the regulatory mechanisms through which environmental and genetic factors shape the melon metabolome.

This study systematically investigated the physicochemical properties (color, texture, basic nutrients, and mineral elements) of two melon cultivars ('Yangjiaocui' and 'Boyang 9') grown in saline–alkali versus non-saline–alkali soils. Volatile flavor profiles of saline–alkali-grown melons were characterized using GC-IMS coupled with VIP analysis. Non-targeted metabolomics using LC-HRMS with alternating ionization modes identified differentially expressed metabolites. Finally, multi-omics correlation analysis integrated nutritional components, volatiles, and characteristic metabolites to establish associative models, revealing intrinsic relationships among quality parameters. This research provides mechanistic insights into varietal differences under contrasting edaphic conditions, offering a scientific basis for optimizing melon cultivation in saline–alkali soils and supporting the sustainable utilization of marginal land resources in China.

2. Materials and Methods

2.1. Materials and Instruments

As shown in Table 1, Two factors were considered: melon cultivar ('Yangjiaocui' and 'Boyang 9') and soil type (saline–alkali and non-saline–alkali). Saline–alkali soil 'Yangjiaocui' and 'Boyang 9' samples were collected in Qing County, Cangzhou City, Hebei Province in April 2025, with the sampled soil exhibiting a water-soluble salt content of 4.8 g/kg and an alkalinity level of 8%. For non-saline–alkali soil samples, the same procedures were followed using samples collected from Weifang City, Shandong Province (soil: 0.7 g/kg salt, 2% alkalinity). For each soil type and each melon variety, 10 uniformly sized, uniformly mature, and mechanically undamaged melon samples were selected as biological replicates. These samples were stored at –1 ± 0.5 °C for subsequent parameter measurements. A portion of the fresh samples was used to determine indicators such as color, texture, moisture content, and soluble solids. The remaining samples were sliced, freeze-dried, ground into powder, sieved through an 80-mesh screen, and stored at –20 °C for future use. Each biological replicate was measured in triplicate (technical replicates).

Table 1. Melon variety information.

No.	Name	Variety	Origin
1	saline alkali soil "Yangjiaocui" Melon (SASYM)	"Yangjiaocui"	Saline alkali soil in Qing County, Cangzhou City, Hebei Province.
2	non-saline soil "Yangjiaocui" Melon (NSSYM)	"Yangjiaocui"	Non-saline soil in Weifang City, Shandong Province.
3	saline alkali soil "Boyang 9" Melon (SASBM)	"Boyang 9"	Saline alkali soil in Qing County, Cangzhou City, Hebei Province.
4	non-saline soil "Boyang 9" Melon (NSSBM)	"Boyang 9"	Non-saline soil in Weifang City, Shandong Province.

It should be noted that the saline–alkali soil samples (Hebei Province) and non-saline–alkali soil samples (Shandong Province) were collected from two different geographical locations, which may introduce confounding factors such as climate, baseline soil prop-

https://doi.org/10.3390/foods15101746

erties, and local agronomic practices. Therefore, the observed differences between the two cultivation conditions should be interpreted as associative rather than purely causal. Furthermore, detailed records of agronomic practices—including fertilization, irrigation, and pest management—were not available because the samples were collected from local production fields. Consequently, the potential influence of these practices on metabolite profiles cannot be ruled out.

2.2. Experimental Methods

2.2.1. Determination of Physical and Chemical Indicators

The weight of each melon variety was measured using an electronic balance (CP114, OHAUS Corporation, Parsippany, NJ, USA). Transverse and longitudinal diameters were determined with a vernier caliper, and the fruit shape index was calculated according to Formula (1). Color parameters (L^*, a^*, and b^*) were measured using a colorimeter (CR-400 Konica Minnolta, Tokyo, Japan). For texture analysis, a standardized sample ($1 \times 1 \times 0.5$ cm) was excised from the equatorial region of the fruit. A Texture Profile Analysis (TPA) was then performed using a food physical analyzerr (TMS-PRO FoodTechnology Corporation, Sterling, VA, USA). Key texture parameters, including hardness, cohesiveness, springiness, chewiness, gumminess, and resilience, were derived from the resulting force–time curves using the instrument's dedicated software.

$$\text{Fruit shape index} = \frac{\text{Fruit length}}{\text{Fruit width}} \quad (1)$$

2.2.2. Determination of Nutrients

Fruits were longitudinally sectioned, and a pulp sample was excised from the equatorial region near the umbilical end (approximately one-third of the fruit length from the stem end) for the determination of moisture content, total soluble solids (TSS), titratable acidity (TA), soluble sugars (SS), and other related indices. Moisture content was analyzed following the national standard method GB/T 5009.3-2003 "Determination of Moisture Content in Food" [9]. TSS was measured with a handheld refractometer (RSD200), TA was determined by sodium hydroxide titration, and SS content was quantified using the anthrone–sulfuric acid method. The sugar–acid ratio and solid–acid ratio, which are commonly adopted for assessing taste balance in fruits, were subsequently calculated according to Equations (2) and (3), respectively [10].

$$\text{Sugar–acid ratio} = \frac{\text{Soluble sugars}}{\text{Titratable acids}} \quad (2)$$

$$\text{Solid–acid ratio} = \frac{\text{Soluble solids}}{\text{Titratable acids}} \quad (3)$$

2.2.3. Determination of Antioxidant Components

Ascorbic acid content was determined according to the Chinese national standard GB 5009.86-2016 "Determination of Vitamin C in Foods" [11]. Total polyphenol and total flavonoid contents were analyzed following the method described by Ali Guler et al. [12]. Briefly, a gallic acid standard (5 mg) was weighed and used to prepare calibration solutions at concentrations of 0, 8, 12, 16, and 40 mg/mL. For each melon sample, 0.2 g of homogenized tissue was weighed into a 10 mL centrifuge tube, mixed with 3.2 mL of 60% ethanol, and subjected to ultrasonic extraction (60 W, 60 min) with thorough shaking. The mixture was centrifuged at 9000$\times$ g for 5 min, and the supernatant was collected. Subsequently, 10 μL of the extract was combined with 50 μL of Folin–Ciocalteu reagent and allowed to react for 5 min at room temperature in the dark. Then, 750 μL of 7% sodium carbonate solu-

https://doi.org/10.3390/foods15101746

tion was added, and the volume was adjusted to 5 mL with distilled water. After incubation in the dark for 120 min, the absorbance of both samples and standards was measured at 760 nm using a microplate reader (Thermo Fisher Scientific, Waltham, MA, USA). Total flavonoid content was determined using rutin as the standard with absorbance measured at 510 nm.

2.2.4. Determination of Mineral Elements

Microwave-assisted digestion was performed by weighing 0.25 g of melon sample into a digestion vessel, adding 6 mL of nitric acid for pre-digestion over 1 h, followed by the addition of 2 mL of hydrogen peroxide. After the digestion process, the resulting solution was diluted to 50 mL with ultrapure water prior to instrumental analysis.

Auto-sampler parameters: sample lift rate: 2 mL/min (0.5 rps) for 40 s; pre-analysis stabilization: 0.4 rps for 30 s; multi-element simultaneous analysis at 0.1 rps.

Quantitative analysis mode: He gas mode, 3 mass units per acquisition point, 3 data acquisition repetitions; integration time: As = 1 s, Se and Cd = 2 s, Pb = 3 s, other elements = 0.3 s.

Specific mass spectrometer operating parameters: RF power: 1600 W, carrier gas flow rate: 1.0 L/min, peristaltic pump speed: 0.1 rps, nebulizer chamber temperature: 2 °C, oxide index: 0.45%, double charge index: 1.01%.

2.2.5. Determination of Volatile Aroma Compounds

Melon aroma components were determined using a Flavor Spec® gas phase ion mobility spectrometer (G.A.S., Dortmund, North Rhine-Westphalia, Germany). For autosampling, 2.0 g of melon sample was placed in a 20 mL headspace vial. The headspace injection conditions were as follows: incubation at 40 °C for 10 min with a shaking speed of 500 r/min, an injection needle temperature of 85 °C, and an injection volume of 1.0 mL [13].

For GC-IMS conditions, the headspace fraction was extracted using a heated injection needle (Agilent Technologies, Santa Clara, CA, USA) and analyzed for volatile organic compounds (VOCs) using 2-methyl-3-heptanone (chromatographically pure) as the internal standard. GC conditions: column temperature 60 °C and maintained constant; operation time of 40 min, and nitrogen ($\geq$99.999%) as the carrier gas. The carrier gas flow rates were 0–2 min: 2 mL/min; 2–10 min: 2–15 mL/min; 10–25 min: 15–100 mL/min; 25–30 min: 100 mL/min.

Method repeatability and calibration: To assess method repeatability, each melon sample was analyzed in triplicate (technical replicates). The relative standard deviations (RSDs) of retention times and peak intensities for major volatile compounds were below 5% and 10%, respectively, indicating satisfactory repeatability. Calibration was performed using the internal standard method (2-methyl-3-heptanone). A series of standard solutions at five concentration levels was prepared to establish calibration curves for target volatiles, with correlation coefficients (R^2) > 0.99 for all analytes. The limits of detection (LOD) and quantification (LOQ) were calculated as three and ten times the signal-to-noise ratio, respectively.

2.2.6. Qualitative and Quantitative Analysis of Volatile Aroma Compounds

Volatile organic compounds in the samples were collected and analyzed using the VOCal analysis software (Version 4.0.3, G.A.S., Dortmund, North Rhine-Westphalia, Germany) bundled with the instrument. Qualitative analysis of the volatile organic compounds was performed using the NIST and IMS databases integrated within the Library Search software (GCxIMS Library Search V2.2.1). As an internal standard, 2-Methyl-3-heptanone was

https://doi.org/10.3390/foods15101746

employed. The content of each volatile aromatic compound was calculated by comparing its peak area with that of the standard compound, as shown in Equation (4):

$$C = \frac{S_x \times C_0 \times V \times 1000}{S_0 \times m} \quad (4)$$

In the equation: C represented the concentration of the analyte, μg/g; C_0 denoted the mass concentration of the internal standard, mg/mL; S_x and S_0 denoted the chromatographic peak areas of the analyte and internal standard, respectively; m was the sample mass, g; V was the volume of the internal standard, mL; 1000 was the conversion factor.

As this calculation assumes a consistent response factor across all analytes relative to the single internal standard without constructing individual calibration curves, the obtained values are considered semi-quantitative.

2.2.7. Non-Targeted Metabolomics Analysis

Place 100 mg of melon sample into a 2 mL centrifuge tube and add one 6 mm diameter grinding bead. Extract metabolites using 800 μL extraction solution (methanol:water = 4:1 (*v*:*v*)) containing four internal standards (L-2-chlorophenylalanine (0.02 mg/mL), etc.). The mixture was vortexed for 30 s and subjected to ultrasonic extraction at 5 °C and 40 kHz for 30 min. Afterward, the samples were incubated at −20 °C for 30 min and centrifuged at 13,000× *g* for 15 min at 4 °C. The resulting supernatant was carefully transferred and evaporated to dryness under a gentle stream of nitrogen. Transfer the supernatant to an injection vial with an insert tube for instrument analysis. In addition, 20 μL of supernatant was pipetted individually from each sample and then mixed together to serve as a quality control (QC) sample. Each QC sample, matching test samples in volume and processed identically, was inserted every eight test samples during analysis to assess process stability.

Instrument parameters are as follows:

Chromatographic conditions: Sample separation and mass spectrometry detection were performed using two columns (BEHC18 column and BEH Amide column). For the BEHC18 column (100 mm × 2.1 mm i.d., 1.7 μm), mobile phase A was 2% acetonitrile/water (containing 0.1% formic acid), and mobile phase B was acetonitrile (containing 0.1% formic acid). The gradient conditions were: 0–0.5 min held at 2% B, 0.5–7.5 min: linear increase to 35% B, 7.5–13 min: increase to 95% B, 13–14.4 min: hold at 95% B, 14.4–14.5 min: decrease to 2% B, 14.5–16 min: hold at 2% B. Flow rate: 0.40 mL/min. Column temperature: 40 °C.

Mass spectrometry conditions: Sample mass spectrometry signals were acquired using positive and negative ion scanning modes, with a mass range of m/z 70–1050. Ionization voltage: positive ions 3500 V, negative ions −3000 V. Sheath gas 50 psi, auxiliary heating gas 13 psi. Ion source heating temperature 450 °C. Collision energy cycling: 20–40–60 eV. MS1 resolution 70,000, MS2 resolution 17,500.

The LC/MS/MS raw data were preprocessed with Progenesis QI software (Version 3.0, Waters Corporation, Milford, CT, USA). Identification of metabolites was performed by matching MS and MS/MS data against mainstream public databases (such as http://www.hmdb.ca/ (accessed on 11 June 2025); https://metlin.scripps.edu/ (accessed on 12 June 2025), and others) and a self-constructed database supported by Majorbio Biotechnology Co., Ltd. (Shanghai, China) [14,15]. The search parameter was set to signal-to-noise ratio (S/N) ≥ 3, and a result was considered reliable when its S/N exceeded this threshold. Molecular formula prediction was based on the parent ion m/z, possible adduct ions, and isotope peaks from primary mass spectrometry. Metabolites were matched with database entries using a mass deviation threshold of 10 ppm. Daughter ions were matched against the secondary mass spectra of candidate substances, and the weighted mass cosine similarity method was used to select candidate matches. Peak areas served as relative quantitative

values for each metabolite. Subsequently, a three-dimensional CSV data matrix (sample information, metabolite name, and MS response intensity) was exported. Metabolic features detected in at least 80% of any sample set were retained [16]. Missing values were imputed with the minimum value in the matrix, and each metabolic signature was normalized to the sum (sum normalization) to minimize errors from sample preparation and instrument instability, yielding a normalized data matrix. Variables from QC samples with a relative standard deviation (RSD) > 30% were excluded, and the remaining data were log10-transformed to generate the final data matrix for subsequent analysis [17].

For metabolite identification within Progenesis QI (Version 3.0, Waters Corporation, Milford, CT, USA), the primary evaluation criteria are mass deviation, isotopic similarity, and secondary fragment similarity. To ensure accuracy, a threshold of 10 ppm for primary mass deviation is set in the scoring criteria for each rating category; matches with a fragment similarity score greater than 30 are considered valid. Based on the scores of these valid matches, the best match is selected as the qualitative result. According to the metabolomics standards initiative (MSI) [18], the identifications reported in this study correspond to Level 2 (putatively annotated compounds), i.e., based on spectral matching against public and in-house databases without confirmation by authentic standards. To provide further granularity, we divided Level 2 into two subcategories: Bi—identification by experimental spectral matching using MS/MS spectra acquired under identical analytical conditions, and Bii—identification by theoretical spectral matching using in silico predicted fragments or literature spectra. The metabolite numbers presented in this work include both Bi and Bii identifications. The retention criteria on the platform were a Fragmentation Score greater than 35 or a Theoretical Fragmentation Score greater than 40.

2.2.8. Integrated Multi-Omics Analysis

Using the DIABLO framework from the "MixOmics" R package, we applied supervised multi-block partial least squares discriminant analysis (sPLS-DA) [19] to identify discriminative features across multiple datasets that account for inter-group variations. To minimize background interference, the variable importance in projection (VIP) method was employed to select features with VIP scores exceeding 1.0 [20], thereby focusing on the most discriminative high-abundance compounds in melon samples. Feature correlations were visualized using the "plotVar" function, while the "cim" function was applied to examine associations between metabolic components and other variables. Correlation heatmaps were generated using the ComplexHeatmap package for intuitive data representation [21]. Additionally, the "cimDiablo" function effectively highlighted multi-omics molecular expression patterns specific to each melon variety.

2.2.9. Statistical Data

Data processing was performed using Microsoft Excel. One-way analysis of variance (ANOVA) followed by Duncan's multiple range test was conducted with SPSS 23.0, with statistical significance defined at $p < 0.05$. All measurements were carried out in triplicate, and data are presented as mean ± standard deviation. Hierarchical cluster analysis, principal component analysis (PCA), and histogram generation were performed using Origin 2024 and GraphPad Prism 9.5. Further multivariate analysis, including PCA and orthogonal partial least squares-discriminant analysis (OPLS-DA) of volatile compounds, was implemented in SIMCA 14.1. The volatile aroma profiles were visualized using the Reporter plug-in within the Laboratory Analytical Viewer (LAV) software (version 2.2.1, G.A.S., Dortmund, North Rhine-Westphalia, Germany).

https://doi.org/10.3390/foods15101746

3. Results

3.1. Phenotype, Color, Texture of Melon

The appearance and morphology of melons represent fundamental attributes influencing consumer purchase decisions and overall market acceptability (Figure 1a–d). As illustrated in Figure 1e, the transverse diameter of the melons ranged from 28 ± 1.2 mm to 33 ± 1.8 mm, while the longitudinal diameter varied between 23 ± 1.3 mm and 28 ± 2.6 mm, consistent with an elliptical morphology that is commercially preferred for its handling and visual appeal. Color represents another essential criterion for evaluating fruit quality, significantly affecting consumer perception and market value [22]. The *L** value (lightness) ranged from 28.86 to 41.45 (highest in SASYM, lowest in SASBM); *a** values ranged from –7.26 to –1.67, indicating a persistent greenish hue typical of unripe or green-fleshed melons; *b** values ranged from 1.91 to 17.18 (highest in SASYM, lowest in SASBM), suggesting differential carotenoid accumulation that may reflect variations in ripeness and nutritional quality [23] (Figure 1f).

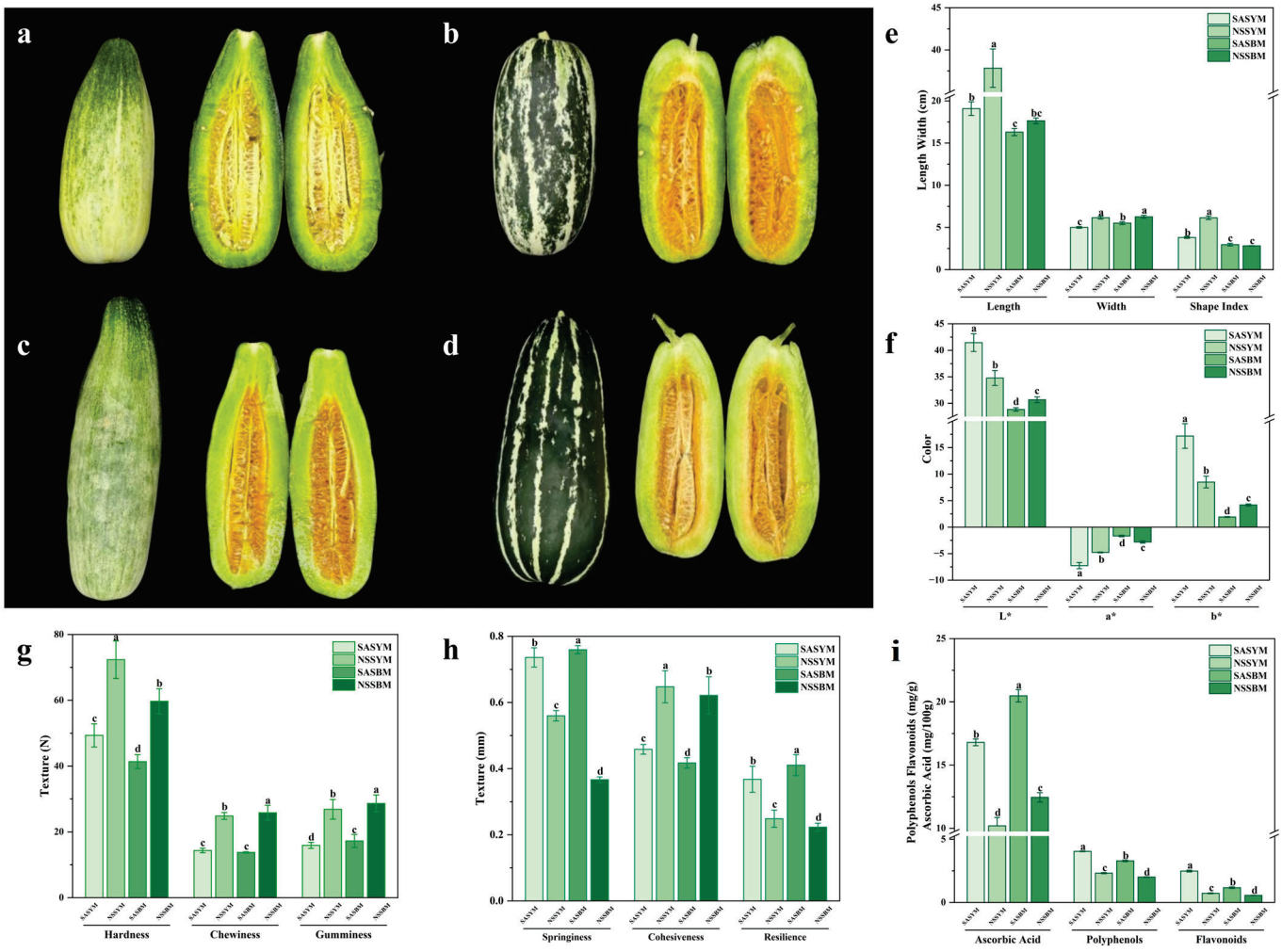


Figure 1. Appearance texture data of four melon varieties. (**a**) SASYM; (**b**) SASBM; (**c**) NSSYM; (**d**) NSSBM; (**e**) Transverse diameter, longitudinal diameter, and shape index of melon; (**f**) Melon color; (**g**) Texture (N); (**h**) Texture (mm). (**i**) Antioxidant composition of four varieties of melon. (Note: Different lowercase letters (a, b, c, d) indicate statistically significant differences between groups ($p < 0.05$); asterisks (*) represent Lab color space indices, including *L** (lightness), *a** (red-green), and *b** (yellow-blue).

https://doi.org/10.3390/foods15101746

The textural properties of the melon samples are summarized in Figure 1g,h. Hardness, defined as the force required to achieve a specified deformation and indicative of tissue density and structural integrity [24], ranged from 41.37 ± 2.09 N to 72.34 ± 5.71 N. Resilience, which reflects the degree of shape recovery after force removal and is associated with freshness and ripeness [25], varied between 0.37 ± 0.01 mm and 0.76 ± 0.01 mm. Chewiness, representing the energy needed to masticate a solid sample to a swallowable consistency and reflecting resistance to sustained deformation [26], was recorded in the range of 13.75 ± 0.2 N to 14.35 ± 0.67 N. Adhesiveness, describing the tendency of food to adhere to oral surfaces and influencing texture perception and flavor release, spanned from 15.9 ± 0.92 N to 26.84 ± 2.58 N. Cohesiveness, indicating the strength of internal bonds and the ability of the material to withstand disintegration, ranged from 0.42 ± 0.02 to 0.65 ± 0.05. Overall, melons grown in saline–alkali soils exhibited lower hardness, chewiness, and adhesiveness, but higher resilience, indicating a crisp, elastic texture with reduced resistance to mastication and minimal surface adhesion. In contrast, non-saline–alkali cultivars generally demonstrated higher hardness, chewiness, and adhesiveness, coupled with relatively lower resilience, suggesting a denser, firmer texture with greater oral resistance and slight stickiness.

3.2. Analysis of Basic Nutritional Components of Melon

Measured parameters for melons cultivated in saline–alkali and non-saline–alkali soils are summarized in Table 2. Water content, a key factor affecting fruit quality, storability, and transportability [27], ranged from 69.39 ± 1.71% to 89.70 ± 0.09%, with higher values observed in non-saline–alkali samples, indicating a notable environmental influence on moisture retention. Soluble solids content, an important indicator of maturity and flavor closely associated with sugars, acids, and minerals, was higher in saline–alkali cultivated melons, likely reflecting stress-induced osmotic adjustment through sugar accumulation [28], as exemplified by 'Yangjiaocui' (11.62 ± 0.08%) and 'Boyang 9' (10.63 ± 0.15%). Soluble sugars, which function as energy sources, osmotic regulators, and participants in antioxidant and ripening-related metabolic pathways [29], were also elevated under saline–alkali conditions, with 'Yangjiaocui' and 'Boyang 9' containing 47.17 ± 0.156% and 44.12 ± 0.418%, respectively, suggesting that such environments may enhance sugar accumulation. Titratable acidity, a critical metric for evaluating sourness and maturation stage, varied between 0.22 ± 0.02% and 0.24 ± 0.01%. The sugar–acid ratio, which significantly influences flavor balance and nutritional synthesis, ranged from 102.76 ± 7.68 to 199.43 ± 6.29. Similarly, the solid–acid ratio, an integrated indicator of sweetness intensity and overall quality, varied from 34.82 ± 1.09 to 49.13 ± 1.38. These findings indicate that saline–alkali cultivation may trigger adaptive stress responses and may enhance certain nutritional parameters. The results suggest that such growing conditions could be associated with increased sweetness and higher nutritional density, but further investigation is needed to establish direct effects on overall fruit quality.

Similar cultivar-dependent variations in antioxidants and fruit quality parameters have been reported in sweet cherry under different ripening phases [30], which is consistent with the possibility that genotype × environment interactions may play a role across different fruit species.

https://doi.org/10.3390/foods15101746

Table 2. Fruit quality indicators in melon.

Varieties	Moisture (%)	Soluble Solids (%)	Soluble Sugars (mg/g)	Titratable Acidity (%)	Sugar–Acid Ratio	Solid–Acid Ratio
SASYM	69.39 ± 1.71 [d]	11.62 ± 0.08 [a]	47.17 ± 0.16 [a]	0.24 ± 0.01 [a]	199.43 ± 6.29 [a]	49.13 ± 1.38 [a]
NSSYM	89.70 ± 0.09 [a]	6.67 ± 0.18 [d]	31.03 ± 0.65 [c]	0.19 ± 0.01 [b]	161.97 ± 4.81 [b]	34.82 ± 1.09 [c]
SASBM	76.42 ± 0.48 [c]	10.63 ± 0.15 [b]	44.12 ± 0.42 [b]	0.23 ± 0.01 [a]	194.47 ± 6.66 [a]	46.85 ± 1.67 [a]
NSSBM	82.05 ± 1.49 [b]	8.74 ± 0.22 [c]	22.14 ± 0.61 [d]	0.22 ± 0.02 [a]	102.76 ± 7.68 [c]	40.54 ± 2.72 [b]

Note: Variety names corresponding to codes are listed in Table 1; different letters within the same column indicate significant differences according to Duncan's multiple range test ($p < 0.05$).

3.3. Content of Total Phenolic, Total Flavonoid, and Vitamin C

Vitamin C, an essential nutrient with demonstrated antioxidant properties, contributes to free radical scavenging, oxidative stress mitigation, iron absorption, and immune function enhancement [31]. The Vitamin C content in saline–alkali soil was 1.5 times higher than that in non-saline–alkali soil ($p < 0.001$), with the highest concentration found in SASBM (20.48 mg/100 g).

Polyphenols and flavonoids in melons exhibit diverse biological activities, including antioxidant effects, prevention of chronic diseases such as cardiovascular conditions and cancer, and regulation of metabolic function [32]. As shown in Figure 1i, The SASYM displayed markedly higher contents of these bioactive compounds, with polyphenol and flavonoid levels reaching 4.04 ± 0.03 mg/g and 2.48 ± 0.07 mg/g, respectively, surpassing those of other tested varieties.

3.4. Melon Mineral Element Analysis

Melons contain abundant mineral elements; we analyzed 18 elements including K, Na, Ca, Mg, P, B, and Fe. As summarized in Table 3, significant differences in mineral content were observed between the 'Yangjiaocui' and 'Boyang 9' varieties. K, Ca, Mg, and P were the predominant minerals (concentrations > 100 mg/kg).

Potassium (K) is essential for cellular function and contributes to taste perception by regulating taste cell membrane potential, thereby enhancing sweetness perception [33]. Consistent with this mechanism, salt–alkali-tolerant varieties exhibited higher K content ('Yangjiaocui': 25,286.23 mg/kg; 'Boyang 9': 27,894.44 mg/kg) and correspondingly higher sweetness. Phosphorus (P) plays a key role in fruit sugar metabolism: it facilitates sugar accumulation, positively correlates with soluble sugar content, and influences fruit firmness and ripening via phosphorus distribution and transport [34]. 'Boyang 9' demonstrated significantly higher P content (2043.39 mg/kg in saline–alkali soil; 2224.21 mg/kg in non-saline–alkali soil) compared to 'Yangjiaocui'. Mg enhances sugar content and fruit quality through its involvement in photosynthesis, carbon–nitrogen metabolism, and sugar accumulation [35], while Mg deficiency adversely affects acidity, firmness, and storage life. Ca contributes to increased fruit firmness, sugar content, and weight, delays softening and senescence, extends shelf life, and improves disease resistance [36]. 'Yangjiaocui' exhibited significantly higher Mg (2086.83 mg/kg in saline–alkali soil; 1935.04 mg/kg in non-saline–alkali soil) and Ca (4611.02 mg/kg in saline–alkali soil; 2884.03 mg/kg in non-saline–alkali soil) content than 'Boyang 9', which may contribute to its superior sweetness and palatability.

https://doi.org/10.3390/foods15101746

Table 3. Comparative analysis of mineral element content in melons.

Mineral Elements	Concentration (mg/kg)			
	SASYM	NSSYM	SASBM	NSSBM
K	25,286.23 ± 190.43 ^{b}	18,187.14 ± 87.15 ^{d}	27,894.44 ± 200.63 ^{a}	22,191.00 ± 210.39 ^{c}
Na	124.45 ± 0.67 ^{a}	58.96 ± 2.51 ^{d}	102.66 ± 2.30 ^{b}	81.26 ± 2.59 ^{c}
Ca	4611.02 ± 24.20 ^{a}	2884.03 ± 51.41 ^{b}	1565.36 ± 10.54 ^{c}	1427.97 ± 9.30 ^{d}
Mg	2086.83 ± 9.50 ^{a}	1935.04 ± 5.76 ^{b}	1495.18 ± 12.48 ^{c}	1333.72 ± 12.79 ^{d}
P	1810.51 ± 29.31 ^{c}	1812.18 ± 10.09 ^{c}	2043.39 ± 13.44 ^{b}	2224.21 ± 18.67 ^{a}
B	10.97 ± 0.39 ^{b}	15.41 ± 1.21 ^{a}	11.36 ± 0.46 ^{b}	12.40 ± 0.81 ^{b}
Fe	19.71 ± 0.60 ^{a}	16.09 ± 0.19 ^{c}	19.60 ± 0.99 ^{a}	17.95 ± 0.33 ^{b}
Sr	26,610.63 ± 345.50 ^{a}	13,951.26 ± 41.18 ^{b}	6680.56 ± 33.87 ^{c}	5991.96 ± 20.19 ^{d}
Mn	4078.69 ± 138.11 ^{b}	7345.58 ± 82.77 ^{a}	3078.03 ± 12.67 ^{c}	3084.84 ± 31.35 ^{c}
Zn	12,291.31 ± 55.94 ^{a}	5620.68 ± 49.75 ^{d}	10,030.32 ± 186.59 ^{b}	7129.09 ± 70.74 ^{c}
Cu	2874.63 ± 26.07 ^{b}	2148.82 ± 1.05 ^{c}	2965.50 ± 31.06 ^{b}	3431.37 ± 133.27 ^{a}
Rb	1374.47 ± 9.88 ^{b}	1007.74 ± 4.80 ^{c}	987.89 ± 7.85 ^{d}	1448.58 ± 13.75 ^{a}
Sn	754.26 ± 18.58 ^{b}	495.19 ± 32.26 ^{d}	872.64 ± 17.51 ^{a}	664.70 ± 16.16 ^{c}
Mo	257.10 ± 8.72 ^{c}	177.89 ± 3.50 ^{d}	480.04 ± 3.85 ^{a}	461.08 ± 6.45 ^{b}
Ni	158.21 ± 1.82 ^{a}	138.39 ± 8.67 ^{b}	113.70 ± 3.65 ^{c}	87.66 ± 1.79 ^{d}
Se	38.05 ± 0.95 ^{a}	30.07 ± 2.67 ^{b}	40.13 ± 1.36 ^{a}	31.44 ± 1.67 ^{b}
Co	30.60 ± 0.74 ^{a}	13.42 ± 0.20 ^{c}	22.77 ± 0.43 ^{b}	13.50 ± 0.54 ^{c}
V	15.29 ± 1.23 ^{b}	15.15 ± 0.20 ^{b}	20.43 ± 1.11 ^{a}	13.43 ± 0.43 ^{c}

Note: Variety names corresponding to codes are listed in Table 1; different letters within the same column indicate significant differences according to Duncan's multiple range test ($p < 0.05$).

3.5. Comprehensive Quality Analysis

3.5.1. Principal Component Analysis

Figure 2a presents a biplot of the principal component analysis, which simultaneously displays the distribution of samples and nutritional components in a reduced two-dimensional space. The first two principal components (PC1 and PC2) collectively explained over half of the total variance, with contribution rates of 55.8% and 28.4%, respectively. Based on the vector lengths and directions in the biplot, PC1 was primarily associated with textural and structural variables (transverse diameter, hardness, and cohesiveness)—the strongest contributors to this component—and clearly separated the saline–alkali soil and non-saline–alkali soil groups along its axis, indicating significant flavor differences among melon varieties under different cultivation conditions. PC2 was mainly characterized by color and morphological parameters (shape index, L^*, and b^*), which qualitatively exhibited the highest loadings on PC2, further distinguishing 'Yangjiaocui' (with higher brightness and yellowness) from 'Boyang 9' (displaying darker appearance and lower lightness) along its direction.

3.5.2. Hierarchical Cluster Analysis

Melon quality indicators exhibit significant diversity and complex interrelationships, making direct comprehensive evaluation prone to information redundancy from overlapping metrics. To establish a streamlined assessment framework, hierarchical clustering was applied to generate a dendrogram based on Euclidean distances between indicators, where smaller distances reflect higher similarity. Using a bottom-up agglomerative approach, the algorithm progressively merged the most similar indicators, yielding distinct clusters that provide an intuitive classification of quality parameters.

https://doi.org/10.3390/foods15101746

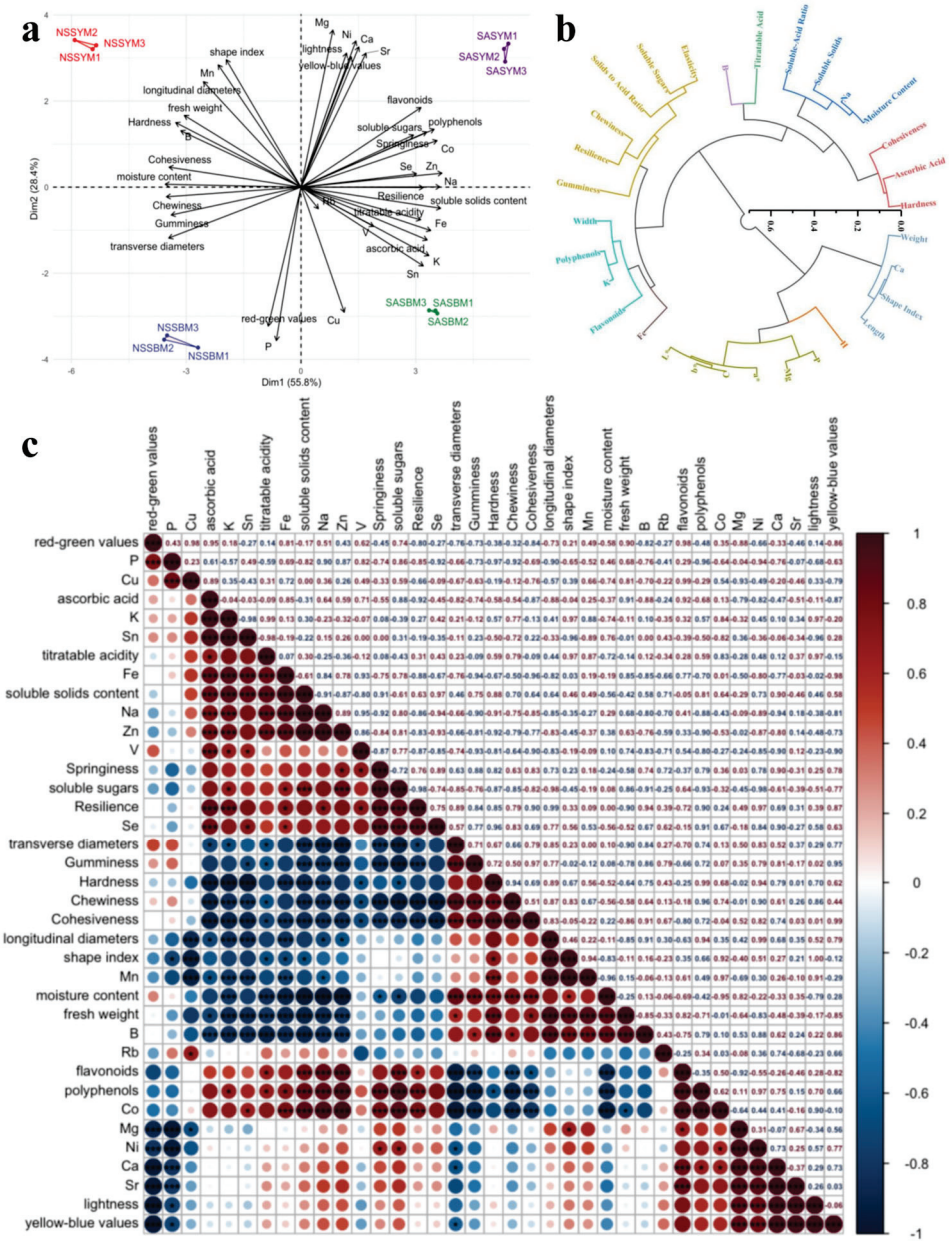


Figure 2. Comprehensive analysis of melon quality. (**a**) Principal Component Analysis Biplot of Fundamental Nutritional Components in Melon. (**b**) Hierarchical cluster analysis of melon indicators. (**c**) Correlation analysis of melon quality indicators. (Circle size indicates correlation magnitude (larger = stronger, smaller = weaker; asterisks indicate significance: * $p < 0.05$, *** $p < 0.001$).

As illustrated in Figure 2b, the clustering outcome, visualized with distinct colors representing separate categories, classified the 31 indicators into 10 independent clusters. From each cluster, the indicator with the smallest Euclidean distance to the cluster centroid (i.e., the most representative variable) was selected as the core parameter. Using this criterion, hardness, chewiness, fruit weight, hue angle, flavonoids, ascorbic acid, firmness-to-acid ratio, iron, magnesium, and boron were identified as the representative core indicators for their respective clusters. These 10 parameters have been established as the fundamental indicators for evaluating the quality of melons.

3.5.3. Correlation Analysis

Pearson correlation analysis of 37 melon quality indicators (Figure 2c) revealed that hardness exhibited significant positive correlations with chewiness, gumminess, and re-

silience, suggesting a positive association between firmer tissue structure and mechanical resistance, deformability recovery, and internal cohesion. Conversely, hardness showed significant negative correlations with moisture content, soluble sugars, titratable acidity, and soluble solids content, which is consistent with the characteristic tissue softening and water loss during fruit maturation. Soluble solids content demonstrated a negative correlation with hardness, chewiness, and gumminess, indicating that higher soluble solids were associated with reduced tissue firmness and elasticity. Its positive correlations with soluble sugars, flavonoids, and polyphenols may be related to sugar accumulation and cell wall modification during ripening. Ascorbic acid was positively correlated with both polyphenols and flavonoids; this correlation may reflect their synergistic interaction in antioxidant metabolism, where Vitamin C directly neutralizes free radicals while concurrently promoting phenolic compound biosynthesis, establishing a complementary redox defense system. Significant positive correlations were observed among mineral elements (K, Na, Ca, Mg, P, B, Fe), suggesting coordinated uptake, translocation, and accumulation of these micronutrients. Collectively, mineral elements showed a negative relationship with water content but positive associations with ascorbic acid, polyphenols, and flavonoids, indicating a correlation between mineral enrichment and cellular dehydration as well as enhanced antioxidant metabolism [37]. These interrelationships form an integrated network connecting textural properties, hydration status, carbohydrate metabolism, antioxidant activity, and mineral nutrition.

3.6. Analysis of Volatile Compounds

3.6.1. Composition and Content of Volatile Compounds

The sensory quality of melon fruits as perceived by consumers is primarily governed by texture, flavor, and visual appearance, with aroma characteristics being largely determined by volatile compounds [38]. Characteristic food aromas are strongly influenced by volatile flavor compounds and their compositional variations, which play a decisive role in consumer preference [39]. GC-IMS analysis of different melon varieties identified 36 volatile components, comprising 20 esters, five ketones, five alcohols, four acids, and two aldehydes (Table 4), indicating the dominance of esters and ketones in the volatile profile. Significant differences in volatile compound content were observed between 'Yangjiaocui' and 'Boyang 9', accounting for their distinct aromatic characteristics. M. Wang et al. [40] utilized GC-MS to investigate melon flavor compounds, revealing that during full ripening, ester levels increase substantially under ethylene-mediated gene regulation. Specifically, ethyl acetate, 2-methylpropyl acetate, and 2-methylbutyl acetate were identified as the principal flavor compounds constituting the core aromatic profile, while variations in ethyl acetate, valeraldehyde, and propionaldehyde serve as specific markers for distinguishing flavor differences among melon varieties [41]. Additionally, a recent GC-IMS analysis of 74 melon varieties identified 56 volatile compounds, with esters being the most abundant class, followed by ketones, aldehydes, and alcohols [42]. However, the volatile profiles of the specific cultivars 'Yangjiaocui' and 'Boyang 9'—particularly their comparative characteristics as revealed by GC-IMS—have not been previously detailed. The present study therefore employs GC-IMS to provide a comprehensive characterization of the volatile components of these two cultivars, thereby filling this gap and offering a more nuanced understanding of their distinct aroma traits.

https://doi.org/10.3390/foods15101746

Table 4. Volatile flavor compounds in muskmelon and their contents.

Variety	Name of Aroma Compound	CAS	Molecular Weight	Retention Index	Drift Time	VIP Value	Concentration (μg/g)			
							SASYM	NSSYM	SASBM	NSSBM
Esters	Acetic acid butyl ester	C107879	116.2	814.9	1.61713	1.14766	110.99 ± 0.29 ^{b}	107.53 ± 0.57 ^{c}	114.42 ± 0.38 ^{a}	113.61 ± 1.80 ^{a}
	Isoamyl isovalerate	C78933	172.3	1079.9	2.02888	1.17549	47.84 ± 1.37 ^{b}	87.68 ± 0.10 ^{a}	47.77 ± 0.68 ^{b}	47.98 ± 0.31 ^{b}
	hexyl isobutyrate	C1629589	172.3	1126	1.46295	1.10407	25.87 ± 0.34 ^{a}	13.41 ± 0.67 ^{c}	21.12 ± 0.73 ^{b}	25.80 ± 0.31 ^{a}
	Isoamyl acetate	C96480	130.2	881.4	1.75135	1.11915	127.42 ± 1.26 ^{c}	126.03 ± 1.77 ^{c}	134.33 ± 0.81 ^{a}	130.60 ± 1.21 ^{b}
	ethyl 2-methylbutanoate	C1003049	130.2	852.2	1.65358	1.06168	131.88 ± 2.90 ^{a}	119.42 ± 0.01 ^{b}	127.60 ± 1.39 ^{a}	131.87 ± 1.04 ^{a}
	heptyl acetate	C40789988	158.2	1110.9	2.03122	1.037	75.99 ± 0.60 ^{a}	78.38 ± 0.02 ^{a}	64.59 ± 1.26 ^{b}	60.92 ± 0.33 ^{c}
	ethyl propanoate	C106354	102.1	708.6	1.45922	1.09909	120.08 ± 0.16 ^{b}	126.34 ± 0.05 ^{a}	114.29 ± 0.15 ^{c}	120.12 ± 1.90 ^{b}
	Octanoic acid, ethyl ester	C106683	172.3	1196.2	1.4753	0.977417	9.40 ± 0.01 ^{a}	5.37 ± 0.09 ^{d}	5.95 ± 0.02 ^{c}	8.77 ± 0.35 ^{b}
	Butyl isopentanoate	C600146	158.2	1045.1	1.38709	0.94597	46.72 ± 3.05 ^{b}	49.30 ± 1.00 ^{b}	59.04 ± 2.79 ^{a}	52.86 ± 4.91 ^{b}
	ethyl hexanoate	C110430	144.2	1003.9	1.79043	0.927371	156.48 ± 4.22 ^{a}	134.94 ± 2.83 ^{c}	114.89 ± 3.83 ^{d}	144.49 ± 3.27 ^{b}
	Butanoic acid, butyl ester	C120923	144.2	999.1	1.33678	0.917529	1.50 ± 0.05 ^{c}	2.50 ± 0.04 ^{a}	2.03 ± 0.12 ^{b}	2.28 ± 0.01 ^{ab}
	amyl acetate	C513860	130.2	916.8	1.76338	0.934788	100.08 ± 1.14 ^{a}	75.51 ± 0.41 ^{bc}	76.33 ± 0.43 ^{b}	74.00 ± 0.14 ^{c}
	ethyl pentanoate	C66251	130.2	902.2	1.68366	0.96603	81.54 ± 1.92 ^{a}	73.74 ± 0.96 ^{b}	37.65 ± 0.98 ^{c}	73.20 ± 1.32 ^{b}
	ethyl butanoate	C110623	116.2	785.1	1.56108	0.847563	90.24 ± 0.92 ^{a}	88.15 ± 0.17 ^{b}	80.17 ± 0.26 ^{c}	89.55 ± 0.06 ^{a}
	isobutyl acetate	C78842	116.2	771.1	1.61651	0.944037	68.46 ± 0.72 ^{d}	73.74 ± 0.42 ^{b}	77.97 ± 0.38 ^{a}	70.82 ± 0.56 ^{c}
	ethyl 2-methylpropanoate	C105577	116.2	750.4	1.56287	0.984759	65.66 ± 0.89 ^{a}	56.77 ± 1.34 ^{b}	53.56 ± 0.74 ^{c}	54.60 ± 0.49 ^{bc}
	Ethyl Acetate	C123386	88.1	632.7	1.3324	0.902905	303.76 ± 1.03 ^{a}	274.72 ± 1.55 ^{d}	284.29 ± 0.15 ^{b}	277.97 ± 0.75 ^{c}
	methyl acetate	C96173	74.1	557.5	1.19916	0.998377	8.81 ± 0.33 ^{a}	4.13 ± 0.08 ^{d}	6.32 ± 0.35 ^{b}	5.83 ± 0.28 ^{c}
	Isobutyl isobutyrate	C78853	144.2	922.2	1.31566	0.9725	3.07 ± 0.24 ^{d}	5.85 ± 0.28 ^{b}	6.38 ± 0.01 ^{a}	4.41 ± 0.11 ^{c}
	(E)-2-Hexenyl acetate	C590863	142.2	1018.7	1.86149	0.976804	153.41 ± 2.31 ^{a}	127.61 ± 1.78 ^{b}	133.60 ± 0.31 ^{b}	144.37 ± 0.24 ^{a}
Ketones	3-hydroxy-2-butanone	C98011	88.1	731.8	1.33931	1.15943	8.53 ± 0.17 ^{b}	7.10 ± 0.19 ^{c}	9.98 ± 0.06 ^{a}	9.69 ± 0.14 ^{a}
	1-octen-3-one	C3268493	126.2	954.8	1.26549	1.10752	12.60 ± 1.55 ^{c}	13.64 ± 1.70 ^{c}	23.07 ± 0.96 ^{a}	19.22 ± 1.66 ^{b}
	Butanone	C620020	72.1	542.9	1.06563	1.01499	8.53 ± 0.17 ^{b}	7.10 ± 0.19 ^{c}	9.98 ± 0.06 ^{a}	9.69 ± 0.14 ^{a}
	2-Nonanone	C107868	142.2	1093.8	1.40458	0.99657	15.52 ± 0.62 ^{a}	9.24 ± 0.38 ^{c}	9.25 ± 0.38 ^{c}	10.14 ± 0.29 ^{b}
	3-Hexanone	C928950	100.2	780.4	1.47442	0.915557	2.30 ± 0.13 ^{a}	1.51 ± 0.11 ^{b}	1.38 ± 0.07 ^{bc}	1.28 ± 0.02^{c}
Alcohols	(Z)-2-Penten1ol	C763326	86.1	740.4	1.45225	0.992235	6.22 ± 0.15 ^{c}	7.59 ± 0.06 ^{b}	9.42 ± 0.25 ^{a}	9.07 ± 0.33 ^{a}
	2-Methyl-2-propanol	C98000	74.1	524.5	1.14467	0.986904	73.77 ± 1.81 ^{a}	68.09 ± 1.26 ^{b}	61.07 ± 0.46 ^{c}	68.99 ± 0.01 ^{b}
	2-methyl-1-propanol	C505102	74.1	1128.3	1.16059	0.895976	30.34 ± 0.86 ^{c}	63.44 ± 0.52 ^{a}	57.57 ± 0.54 ^{b}	24.98 ± 0.81 ^{d}
	(E)-3-hexen-1-ol	C123513	100.2	858.6	1.24261	0.842387	2.00 ± 0.02 ^{d}	3.28 ± 0.10 ^{b}	3.52 ± 0.02 ^{a}	3.08 ± 0.02 ^{c}
	1-pentanol	C107880	88.1	743.7	1.51497	0.757465	2.47 ± 0.14 ^{c}	2.91 ± 0.02 ^{a}	2.75 ± 0.06 ^{b}	2.95 ± 0.05 ^{a}
Acids	Propanoic acid	C57556	74.1	732.7	1.09903	1.07201	1.23 ± 0.01 ^{d}	1.7 ± 0.04 ^{c}	2.55 ± 0.03 ^{a}	2.27 ± 0.02 ^{b}
	(E)-3-hexenoic acid	C116096	114.1	992.1	1.5898	1.02103	5.87 ± 0.26 ^{b}	1.45 ± 0.04 ^{d}	2.54 ± 0.09 ^{c}	7.66 ± 0.09 ^{a}
	Hexanoic acid	C589822	116.2	991.1	1.65646	0.999163	4.44 ± 0.12 ^{a}	1.75 ± 0.11 ^{d}	2.20 ± 0.01 ^{c}	3.91 ± 0.05 ^{b}
	3-Methylbutanoic acid	C111273	102.1	860.1	1.49374	0.937729	3.28 ± 0.01 ^{a}	1.39 ± 0.01 ^{d}	2.12 ± 0.07 ^{b}	1.79 ± 0.07 ^{c}
Aldehydes	Heptanal	C106707	114.2	939.4	1.69925	1.13491	153.28 ± 0.66 ^{b}	127.99 ± 11.33 ^{c}	185.19 ± 10.41 ^{a}	163.71 ± 2.59 ^{b}
	pentanal	C539822	86.1	720.2	1.41772	0.966564	22.38 ± 0.31 ^{a}	16.19 ± 0.24 ^{d}	18.00 ± 0.05 ^{b}	17.30 ± 0.14 ^{c}

Note: Variety names corresponding to codes are listed in Table 1; different letters within the same column indicate significant differences according to Duncan's multiple range test ($p < 0.05$).

As illustrated in Figure 3a, distinct variations in volatile compound composition were observed among the melon varieties. The saline–alkali cultivated 'Yangjiaocui' variety displayed the highest ester content (83.1%), whereas its non-saline–alkali counterpart showed the highest alcohol content (7.3%). The highest proportions of ketones (2.7%) and aldehydes (1.1%) were detected in the saline–alkali grown 'Boyang 9', while the non-saline–alkali 'Boyang 9' exhibited the greatest abundance of acids (1.1%).

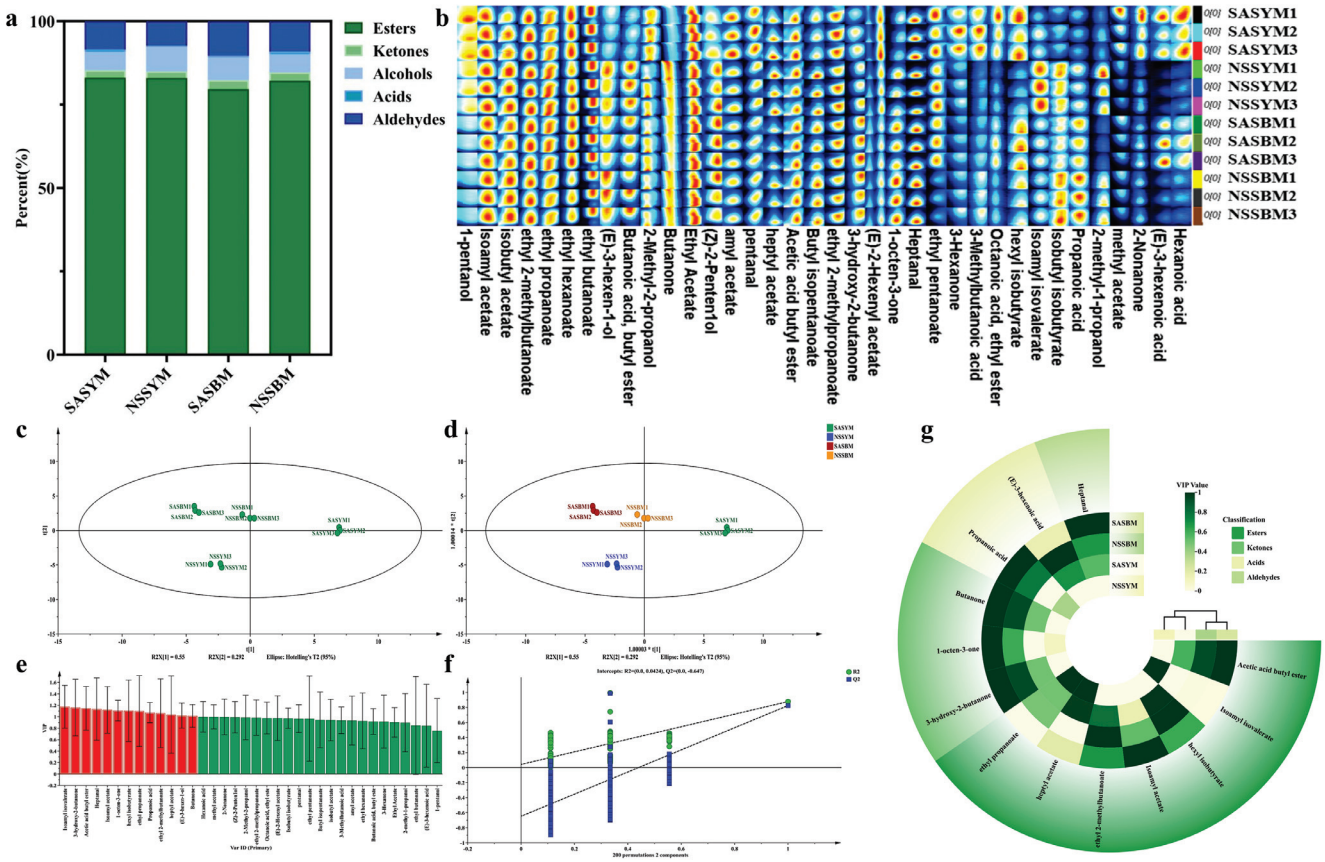


Figure 3. Flavor PCA analysis and cluster heat map. (**a**) Stacked histogram of volatile aroma components composition percentages. (**b**) Flavor fingerprint of melon. (**c**) PCA analysis of volatile aroma components. (**d**) Volatile aroma component OPLS-DA analysis. (**e**) VIP value. (Red represents VIP > 1, green represents VIP < 1). (**f**) Model fit validation. (**g**) Comparative heat map of the content of key volatile aroma components. (Asterisks indicate significance: * $p < 0.05$).

These compositional differences account for the characteristic aroma profiles of each variety. For instance, ethyl valerate contributes sweet, buttery notes reminiscent of apricot and peach with subtle fermented undertones; valeraldehyde provides grassy and apple-like accents; and ethyl acetate delivers aromatic, fruity, and ethereal odors [43]. From a biochemical perspective, these esters are primarily synthesized via alcohol acyltransferase (AAT)-mediated esterification of alcohols and acyl-CoAs, using fatty acids and amino acids as precursors. Further analysis revealed that the characteristic melon-like aroma is primarily attributed to compounds including butyl acetate, 3-hydroxy-2-butanone, and heptanal, which collectively impart sweet, fruity, and fresh herbaceous notes.

3.6.2. Melon Flavor Fingerprinting

The Gallery Plot plugin was utilized to generate and compare fingerprint spectra, effectively highlighting differences in volatile compound composition among the melon samples. Distinctive characteristic fingerprints were established through analysis of specimens representing different varieties and geographical origins. As illustrated in Figure 3b,

https://doi.org/10.3390/foods15101746

each horizontal row corresponds to the complete signal profile of an individual sample, while each vertical column represents the signal distribution of a specific volatile aroma component across all analyzed samples.

Volatile compounds including isovalerate esters, ethyl 2-methylbutanoate, and isobutyrate esters were detected at elevated concentrations in both 'Yangjiaocui' and 'Boyang 9' varieties. These compounds collectively establish an aromatic profile characterized by a sweet fruity foundation, which integrates distinct fruity nuances, such as pineapple, banana, and strawberry, with a mellow sweetness described as both rich and refreshing [44], ultimately defining the characteristic flavor identity of these melon varieties.

Significant differences in volatile organic compound content were observed between saline–alkali and non-saline–alkali soils. Methyl acetate (fruity and floral notes) showed markedly higher concentrations under saline–alkali conditions, as did (E)-3-hexenoic acid (grassy aroma) and 2-nonanone (rose and tea-like notes). These volatiles may function as environmental signaling molecules, and their distribution patterns could potentially influence the sensory properties of the fruits. The results suggest that saline–alkali stress may selectively regulate plant metabolic pathways (e.g., stress-induced shifts in volatile biosynthesis), leading to the specific enrichment of these characteristic aroma compounds. However, further investigation is needed to clarify the exact biological mechanisms underlying these changes.

A principal component analysis model for melon volatiles was established using SIMCA 14.1 software, with 36 aroma components as dependent variables and varieties as independent variables. The first two principal components (PC1 and PC2) collectively explained over half of the variance, with contributions of 55% and 29.2% respectively. 'Yangjiaocui' samples clustered primarily in the first and third quadrants, while 'Boyang 9' samples were mainly distributed in the second quadrant, demonstrating significant flavor differences between varieties.

OPLS-DA exhibited enhanced discriminatory power, effectively separating melon samples by variety. The model yielded an independent variable fit (R^2X) of 0.841, dependent variable fit (R^2Y) of 0.662, and predictive ability (Q^2) of 0.501. While the Q^2 value exceeds the commonly accepted threshold of 0.5, it is only marginally above this limit, suggesting that the model's predictive performance is acceptable but not strong. Furthermore, the moderate discrepancy between R^2Y (0.662) and Q^2 (0.501) indicates a potential risk of slight overfitting, although the difference remains within reasonable bounds for metabolomic datasets with limited sample size [45]. Following 200 permutation tests, the regression line's intersection with the vertical axis below zero (Figure 3f) confirmed the absence of overfitting, validating the model's reliability for melon variety identification based on aroma profiles.

3.6.3. Screening of Key Aroma Compounds

The contribution of volatile flavor compounds to sample classification was evaluated using variable importance in projection (VIP) analysis derived from partial least squares discriminant modeling. Variables with VIP scores exceeding 1.0 are conventionally considered highly influential in the discrimination model [46], a threshold widely adopted in metabolomics studies for identifying discriminatory markers. As illustrated in Figure 3e, screening of volatile compounds from melon samples grown in saline–alkali soil identified 13 compounds with VIP values above 1.0, common to both 'Yangjiaocui' and 'Boyang 9' varieties. These included seven esters, three ketones, two acids, and one aldehyde. These significantly influential compounds were: butyl acetate (VIP = 1.14), isopentyl isovalerate (VIP = 1.17), hexyl isobutyrate (VIP = 1.10), isovalerate (VIP = 1.12), ethyl 2-methylbutyrate (VIP = 1.06), ethyl heptanoate (VIP = 1.04), ethyl propionate (VIP = 1.10), 3-hydroxy-2-

https://doi.org/10.3390/foods15101746

butanone (VIP = 1.16), 1-nonen-3-one (VIP = 1.11), acetone (VIP = 1.01), propionic acid (VIP = 1.07), (E)-hexenoic acid (VIP = 1.02), and heptanal (VIP = 1.13). From a biological perspective, esters are the predominant contributors to melon aroma, imparting sweet and fruity notes; ketones contribute creamy and fruity nuances; and the selected aldehyde (heptanal) is associated with fresh, green herbaceous characteristics [47]. The predominance of esters among the 13 VIP-selected compounds aligns with the well-established role of ester biosynthesis in determining varietal aroma differences. Thus, the selection of these 13 volatiles not only satisfies the statistical criterion (VIP > 1.0) but also reflects their functional relevance to flavor quality, supporting their use as key markers for variety discrimination under saline–alkali cultivation [48].

Further cluster analysis of the 13 key volatile components revealed that these characteristic compounds effectively differentiated the melon samples, as visualized in the cluster heatmap (Figure 3g). Compounds including heptanal, isoamyl acetate, ethyl 2-methylbutanoate, butyl acetate, and ethyl propanoate were consistently present at relatively high concentrations across all varieties. In contrast, marked varietal differences were observed in the abundance of (E)-3-hexenoic acid, propionic acid, 1-octen-3-one, and hexyl isobutyrate. These findings demonstrate that the integration of flavor fingerprinting with multivariate analysis provides an effective methodological framework for discriminating melon varieties and geographical origins.

3.7. Non-Targeted Metabolomics

3.7.1. Overall Metabolome Characteristics

A non-targeted metabolomics approach employing liquid chromatography–high-resolution mass spectrometry in alternating positive and negative ionization modes was utilized to analyze compositional differences in metabolites between saline–alkali and non-saline–alkali soil conditions for both ‘Yangjiaocui’ and ‘Boyang 9’ melon varieties.

As summarized in Figure 4a, a total of 702 distinct compounds were identified across the four sample groups. Under contrasting cultivation conditions, ‘Yangjiaocui’ produced 706 and 740 compounds in saline–alkali and non-saline–alkali soils respectively, while ‘Boyang 9’ yielded 720 and 734 under the same conditions.

Several compounds were consistently detected at elevated levels among all varieties, including 6″-O-malonylhesperidin, scutellarin, and sisudioside. 6″-O-Malonylhesperidin has been reported to possess antioxidant and anti-inflammatory activities, and its malonyl moiety may enhance water solubility and potentially contribute to lipid metabolism regulation [49]. Scutellarin is known to exhibit antioxidant and anti-inflammatory functions; it may also enhance sweet taste perception and could support metabolic health through modulation of gut microbiota and improvement of glucose and lipid profiles [50]. While these bioactivities suggest possible links to the observed quality differences among varieties, direct causal relationships remain to be established. Therefore, the functional implications of the differential accumulation of these flavonoids should be interpreted as hypotheses warranting further investigation.

Classification based on structural characteristics was shown in Figure 4b. The primary metabolites in melons mainly include: 107 organic acids and derivatives (20.9%), 92 lipids and lipid-related molecules (17.97%), 84 phenylpropanoid and polyketide compounds (16.41%), aromatic compounds (70 types, 13.65%), organic oxygen compounds (70 types, 13.43%), organic heterocyclic compounds (46 types, 9.59%), organic nitrogen compounds (18 types, 3.84%), nucleotides and derivatives (11 types, 2.15%), and other compounds across 14 categories.

https://doi.org/10.3390/foods15101746

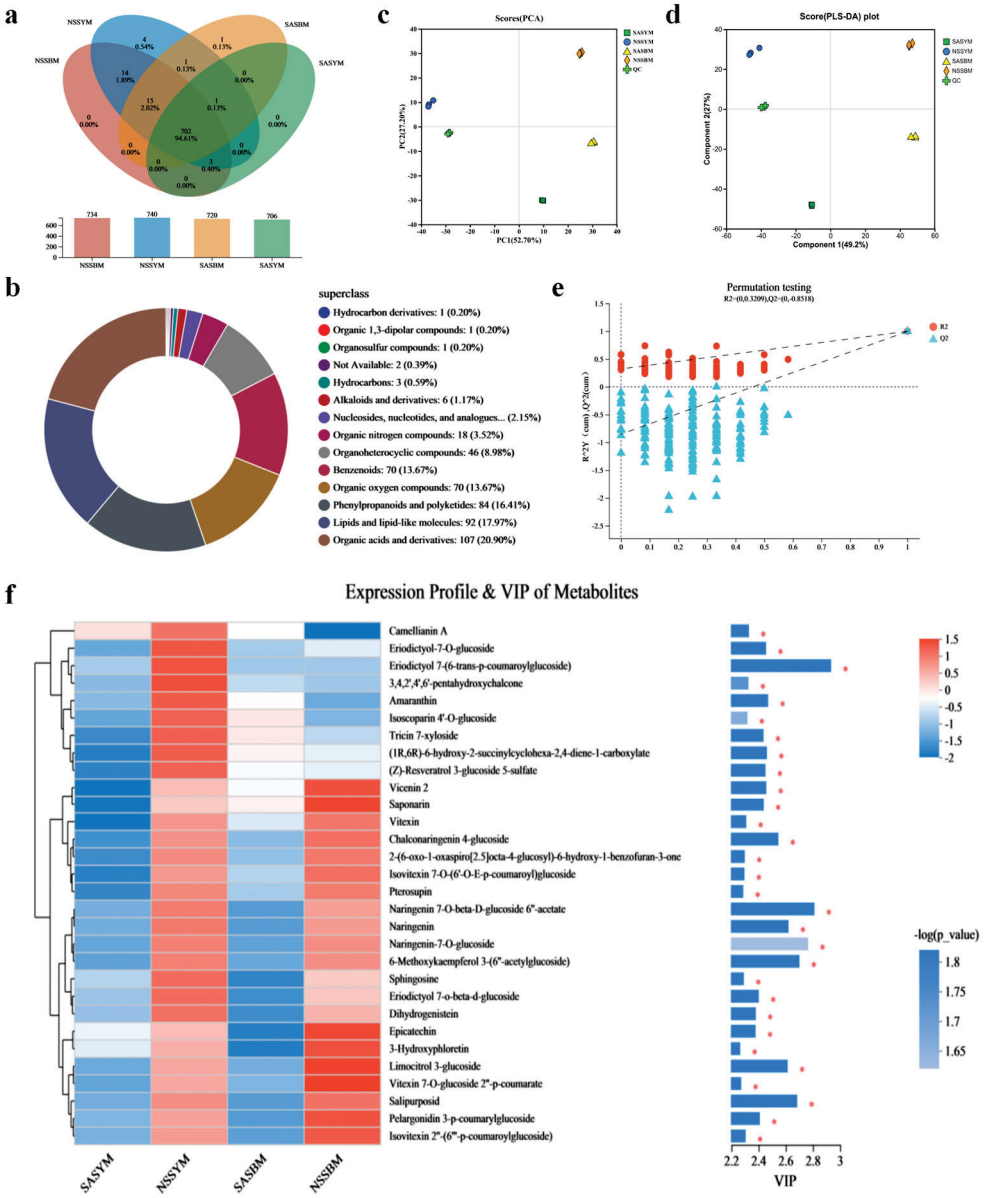


Figure 4. (**a**) Results of Venn analysis. (**b**) Statistical Chart of Compound Classification. (**c**) PCA analysis of metabolic substances in melon. (**d**) PLS-DA analysis. (**e**) Cross-validation diagram of PLS-DA model. (**f**) Analysis of VIP Values. (Asterisks indicate significance: * $p < 0.05$).

3.7.2. Multivariate Statistical Analysis

Metabolomic profiling revealed distinct differentiation in metabolite distribution patterns between saline–alkali and conventional soil conditions, as well as between the 'Yangjiaocui' and 'Boyang 9' varieties.

PCA showed a total explained variance of 80.3% (PC1 = 47.70%, PC2 = 32.60%). Model robustness was assessed by cross-validation ($Q^2 = 0.79$, based on seven-fold cross-validation). Although the goodness-of-fit R^2 reached 1.0 ($p = 0.001$), this near-perfect fit should be interpreted with caution, as it may indicate a risk of overfitting given the high dimensionality of the metabolomics data.

PLS-DA further enhanced the separation. The model parameters were as follows: $R^2X = 0.83$, $R^2Y = 0.99$, $Q^2 = 0.86$. A permutation test ($n = 200$) yielded R^2 intercept = 0.21 and Q^2 intercept = –0.17, indicating that the original model was not overfitted and had good predictive ability. PC1 primarily distinguished samples by soil type (saline–alkali vs.

non-saline–alkali), while PC2 effectively differentiated between the two melon varieties, providing comprehensive insights into the principal factors governing metabolic variation.

Further analysis of intergroup variations in compound content utilizing variable importance in projection (VIP) values is presented in Figure 4f. Under saline–alkali stress conditions, the majority of flavonoid metabolites in melon demonstrated low abundance, whereas these compounds showed elevated expression in non-saline–alkali soil. Key metabolites with VIP values ranging from 2.8 to 2.9 and corresponding −log(p) values approximately between 1.7 and 1.8 included eriodictyol-7-O-glucoside, naringenin-7-O-β-D-glucoside 6″-acetate, naringenin-7-O-glucoside, 6-methoxykaempferol 3-(6″-acetylglucoside), and salipurposide. Their marked intergroup differentiation identifies them as potential biomarkers for distinguishing between saline–alkali and non-saline–alkali cultivation environments.

Under both saline–alkali and non-saline–alkali soil conditions, (Z)-resveratrol 3-glucoside 5-sulfate and vicenin-2—both classified as polyphenolic compounds—were consistently detected at elevated expression levels. Glycosylation enhances their water solubility and bioavailability, and subsequent in vivo enzymatic conversion allows transformation into active molecular forms, thereby supporting sustained and regulated biological activity [51]. The stable accumulation of these polyphenols across different cultivation environments suggests that they represent a constitutive metabolic feature of the two melon varieties, rather than a stress-specific response. Given the established roles of polyphenols in antioxidant defense and their potential contribution to flavor perception, their consistent high expression may underpin baseline fruit quality attributes—such as antioxidant capacity and sensory stability—that persist regardless of soil conditions. This finding underscores the importance of variety-specific metabolic traits in determining fruit quality, independent of environmental salinity.

3.7.3. Metabolite Cluster Analysis

Non-targeted metabolomics coupled with hierarchical cluster analysis was employed to systematically characterize metabolic variations between saline–alkali and non-saline–alkali soil conditions, as well as between the 'Yangjiaocui' and 'Boyang 9' varieties. As demonstrated in Figure 5a, the two varieties exhibit distinctly segregated metabolic profiling patterns.

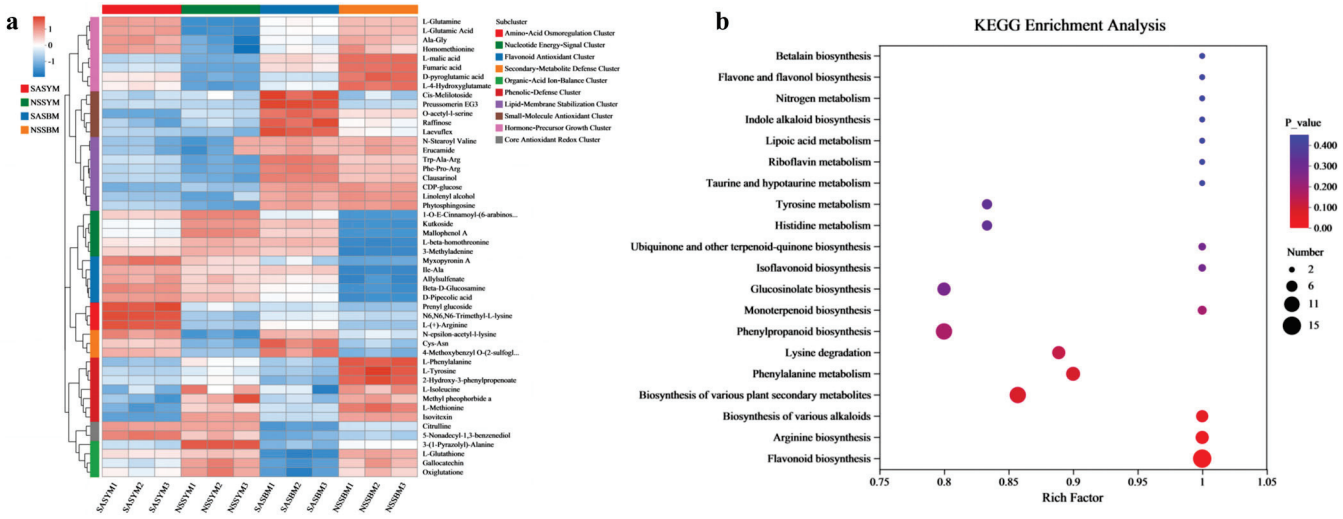


Figure 5. (**a**) Metabolite clustering analysis. (**b**) KEGG pathway enrichment diagram.

Significant increases in the levels of multiple amino acids, including L-glutamine, L-glutamic acid, and Ala-Gly, were detected in SASYM. In contrast, NSSYM exhibited marked reductions in organic acids and specific nucleotide metabolites. Concurrently,

significant accumulations of isoleucine, α-ketoglutarate, and glutathione were observed in NSSYM [52]. Under saline–alkali soil conditions, 'Boyang 9' exhibited significant accumulation of flavonoids and other antioxidant secondary metabolites, including specific flavonoid compounds and quercetin. Furthermore, plants showed concurrent accumulation of organic acids (e.g., azelaic acid and glutaric acid) and additional secondary metabolites. In contrast, 'Boyang 9' cultivated in non-saline–alkali soil showed reduced levels of lipid metabolites, including lipid A and phosphatidylcholine, and significant increases in organic acids such as L-malic acid, fumaric acid, and phenylalanine [53].

3.7.4. Pathway Enrichment Analysis

KEGG pathway enrichment analysis (Figure 5b) indicates that flavonoids, as essential plant secondary metabolites, play pivotal roles in antioxidant defense, disease resistance, and signal transduction. This pathway demonstrated an enrichment factor approaching 1, extreme statistical significance, and the highest number of differentially expressed genes, identifying it as the core mechanism underlying the observed metabolic changes. Concurrently, enrichment results encompassed diverse secondary metabolite pathways including alkaloids, terpenoids, and phenolics, suggesting a comprehensive activation of the plant's defense or adaptive metabolic systems in response to experimental conditions, potentially associated with environmental stress or stage-specific regulation. Tyrosine, as an aromatic amino acid, participates in multiple critical metabolic pathways such as dopamine and phenolic compound biosynthesis, while phenylalanine metabolism serves as the upstream pathway for secondary metabolites including lignin, flavonoids, and phenolic acids. The significant enrichment of both pathways indicates coordinated regulation of upstream metabolism, further explaining the pronounced alterations in downstream products such as flavonoids. The synthesis of various plant secondary metabolites redirects metabolic flux toward flavonoids and other defensive compounds through regulation of aromatic amino acid metabolism, a process that may subsequently influence growth regulation and stress resistance. Although plant hormone signaling pathways showed relatively modest enrichment, differentially expressed hormone-related genes may function as critical regulatory bridges by activating transcription factors that modulate flavonoid biosynthetic genes, thereby orchestrating the integrated response of the aforementioned metabolic network.

3.8. Multi-Omics Integration Analysis

3.8.1. Integrative Cross-Communication of Multiple Omics

Having identified different omics signatures between different samples, our next goal was to explore the interactions of basic nutrients, volatile compounds, and characteristic metabolites, for which we employed DIABLO analysis [54]. This integrated analytical approach effectively captures multi-omics signatures, not only enabling clear discrimination between melon varieties but also elucidating their underlying functional networks (Figure 6a,b).

The arrow plot (Figure 6c) demonstrates that, under different land conditions, 'Boyang 9' showed consistent response patterns in both basic nutrients and volatile metabolites, as indicated by analogous distributions of triangular and circular arrows, suggesting that these two substance categories remain stable across varying habitats. In contrast, the cross-arrow distribution representing metabolic pathways exhibited clear separation, reflecting significant remodeling of core metabolic pathways that distinctly differentiate this cultivar under disparate land conditions. Meanwhile, "Yangjiaocui" displayed distinct typological characteristics across multiple omics levels, including basal nutrients, volatile compounds, and signature metabolites.

https://doi.org/10.3390/foods15101746

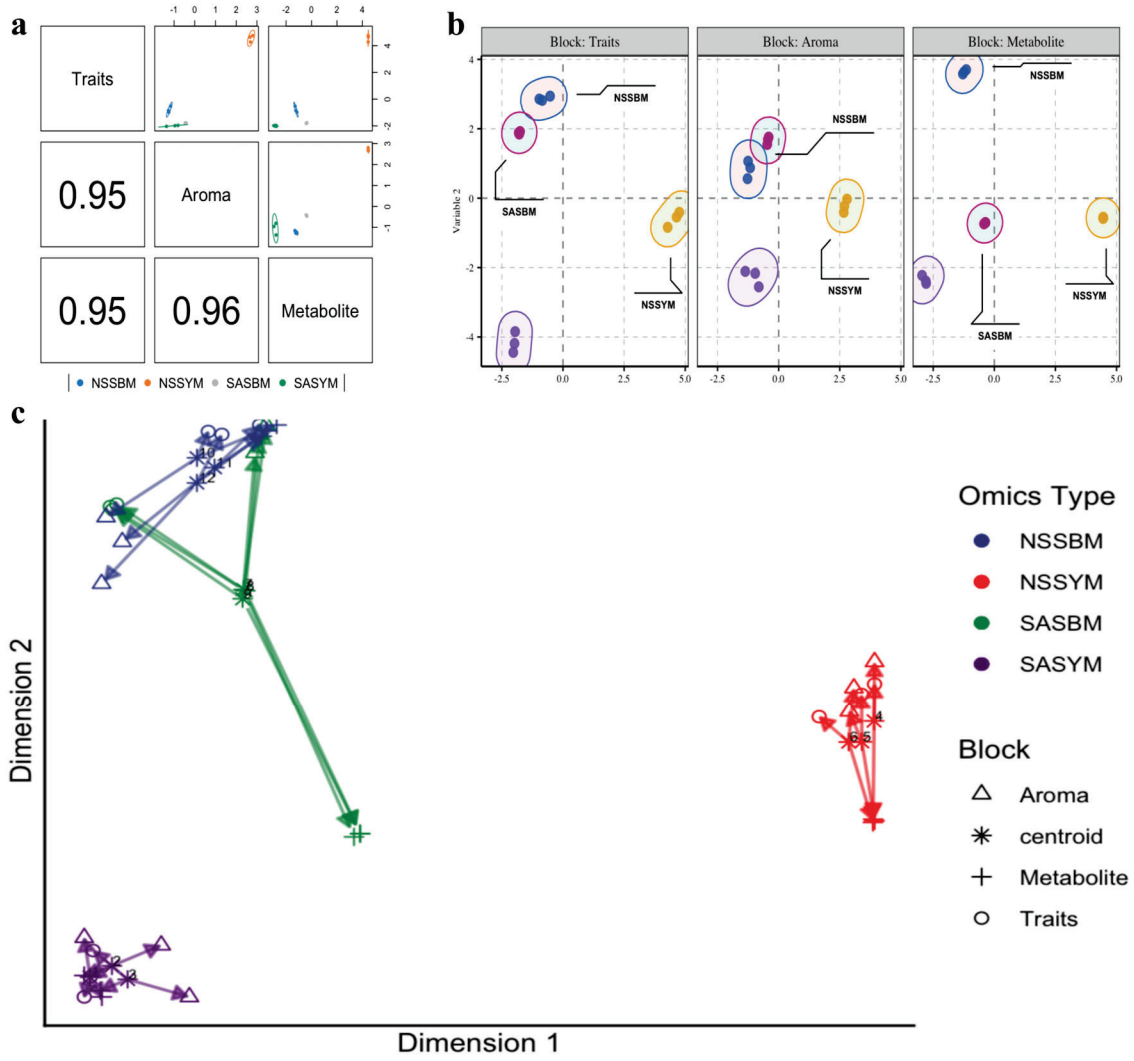


Figure 6. Multi-omics joint analysis. (**a**) Multi-omics DIABLO correlation plot showing Pearson correlations between the first principal component of tri-omics. The correlation among the three datasets supported their integration and the presentation a joint signature; (**b**) Multi-omics joint analysis. Clear discrimination of samples was observed using the signature of basic nutrients, volatile compounds, and characteristics selected by multi-omics DIABLO; (**c**) In the arrow plot, the arrow origin indicates the centroid among all data sets for a given sample, and the tips of the arrows indicate the location of that sample in each block.

3.8.2. Multi-Omics Correlation Analysis of Basic Nutrients, Volatile Compounds, and Characteristic Metabolites in Melon

Fruit morphological characteristics influence flavor metabolism (Figure 7a), where a shape index correlates with enhanced ester production, likely attributable to increased cell volume upregulating the expression or activity of ester synthases. Color parameters (L*, a*, b*) are linked to specific esters like isoamyl isovalerate, isobutyric acid isobutyl ester, and heptanoic acid heptyl ester, suggesting shared regulatory nodes between pigment metabolism (e.g., carotenoids and chlorophyll) and ester biosynthesis. Soluble sugars and solids positively correlated with multiple esters, providing essential carbon precursors. Titratable acidity correlated with esters such as isovaleric acid isovaleryl ester and hexyl isobutyrate, possibly because an acidic microenvironment favors esterification between organic acids and alcohols. Mineral elements function as critical catalytic cofactors in plant metabolism, directly or indirectly regulating the synthesis of flavor compounds. Specifically, trace elements (e.g., Ni, Mn, Cu) showed strong correlations with short-chain

esters, including isobutyric acid isobutyl ester and heptanoic acid ethyl ester, key aroma contributors, potentially by activating acyltransferase-like enzymes. In contrast, alkaline earth metals such as Ca and Sr were associated with propanoic acid, possibly influencing its synthesis and accumulation through calcium-mediated signaling or by maintaining membrane integrity.

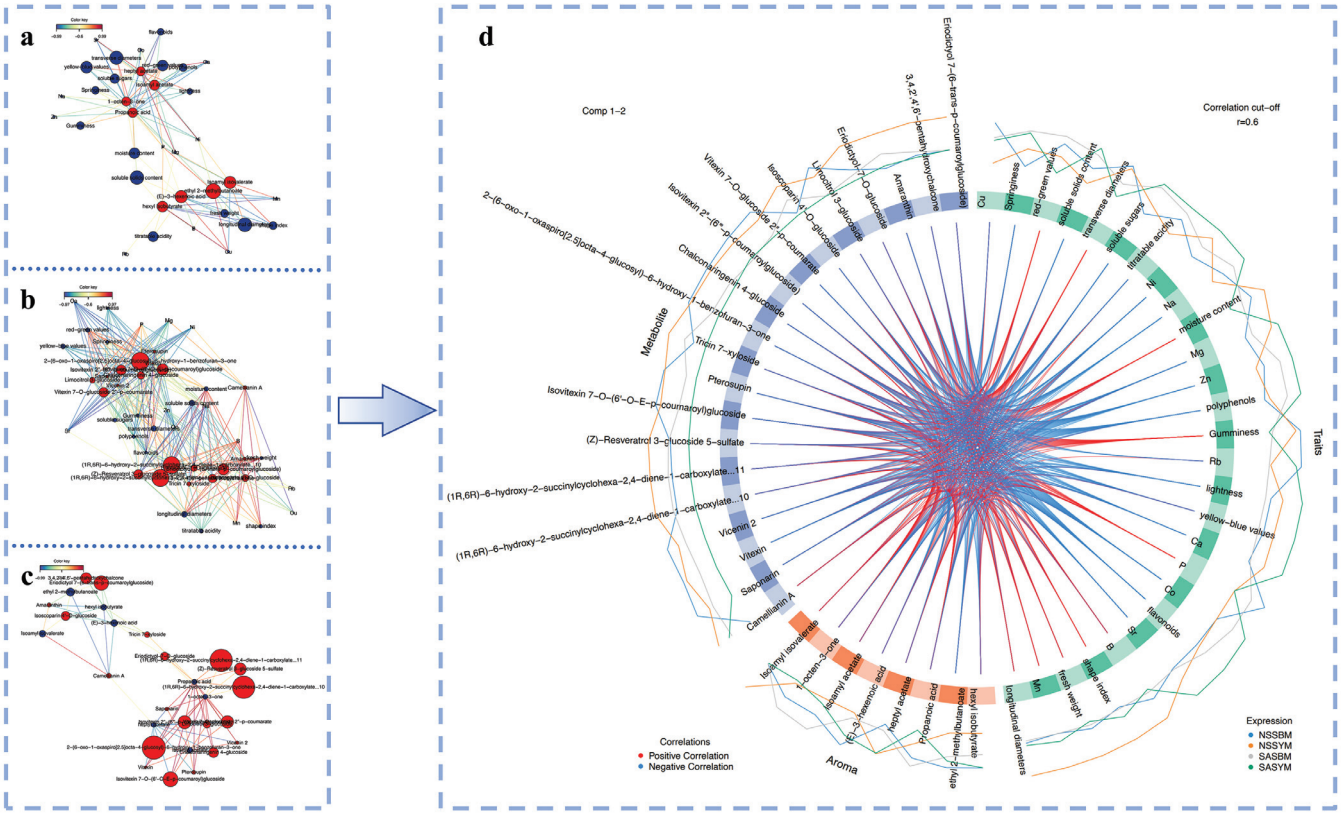


Figure 7. Network analysis of associations among basic nutrients, volatile compounds, and metabolites. (**a**) Association network diagram of basic nutrients and volatile compounds, positive and negative correlations are shown in red and blue; (**b**) Association network diagram of basic nutrients and metabolites, positive and negative correlations are shown in red and blue; (**c**) Association network diagram of volatile compounds and metabolites, positive and negative correlations are shown in red and blue; (**d**) The Circos-plot demonstrated the positive (negative) correlation, denoted as red (blue) lines, between selected multi-omics features. The additional line plots on the outer ring visualize the relative abundance of each feature per experimental group.

Morphological indicators formed a significant positive correlation cluster with flavonoid compounds such as pterostilbene and eriodictyol 7-O-glucoside, suggesting synergistic biosynthesis of multiple flavonoids during fruit development and revealing a close association between fruit morphogenesis and specific flavonoid accumulation. (Figure 7b) In contrast, mineral elements, fresh weight, and color parameters constituted a distinct negative correlation cluster with most flavonoids, reflecting pronounced regulatory relationships among mineral nutrition, biomass accumulation, visual pigmentation, and secondary metabolite biosynthesis. Notably, eriodictyol 7-O-glucoside and soluble solids functioned as central hubs for positive and negative correlations, respectively, implying that their content variations may broadly influence the accumulation patterns of multiple interconnected metabolites.

The metabolic network illustrates co-regulatory relationships between resveratrol glycosides (flavonoid metabolites) and aroma compounds (Figure 7c). Positive correlations (red lines) with volatiles like propionic acid imply co-accumulation, potentially due

to shared pathways or flavonoid degradation. Negative correlations (blue lines) among esters, such as ethyl 2-methylbutyrate, indicate competition for biosynthetic precursors. Compounds such as 2-(6-oxo-1-oxaspiro [2.5]oct-4-yl)-6-hydroxy-1-benzofuran-3-one and Eriodictyol 7-(6-trans-p-coumaroylglucoside) are identified as pivotal hub metabolites. These non-volatile compounds structurally integrate the metabolic network by bridging various aromatic compounds and frequently exist in a glycosidic form, serving as stable precursors that liberate volatile aromas upon hydrolysis. Fundamentally, these relationships arise from interconnected metabolism: the phenylpropanoid pathway yields both flavonoids and benzenoid aromatics, while fatty acid metabolism supports ester synthesis and provides flavonoid precursors.

The Circos diagram of multicomponent VIP values (Figure 7d) reveals distinct disparities in nutritional composition and metabolic profiles among samples. SASYM excels in fundamental nutrients, exhibiting the highest concentrations of polyphenols, flavonoids, and ascorbic acid, alongside the most potent antioxidant activity, while its mineral content, particularly macrominerals such as calcium, magnesium, and potassium, also markedly surpasses other groups, further underscoring its superior nutritional value. In terms of aroma, elevated esters like hexyl isobutyrate impart distinct fruity and floral notes; however, this group shows overall reduced metabolite accumulation, likely due to saline–alkaline stress disrupting regular metabolic pathways and limiting end-product synthesis. NSSYM fruits are characterized by prominent shape and vivid color, growing in neutral or mildly alkaline soils. Although their aromatic intensity is relatively modest, metabolic activity remains unimpeded, leading to generally higher levels of diverse metabolites and reflecting robust metabolic vitality. SASYM also demonstrates excellence in basic nutritional metrics (e.g., polyphenols, flavonoids, ascorbic acid), while its volatile profile, featuring compounds such as 1-octen-3-ol, isoamyl acetate, and propanoic acid, imparts a unique blend of mushroom and fruity aromas. However, similar to SASYM, its overall metabolite levels remain comparatively low. In contrast, NSSBM exhibits high accumulation of multiple metabolites (e.g., vitearin, saponarin, vicenin-2) and active metabolic pathway expression.

4. Discussion

In this study, we explored how saline–alkali versus non-saline–alkali conditions affect melon quality by integrating physicochemical, volatile, and metabolomic data from two cultivars. Cluster analysis condensed 31 quality indicators into ten representative parameters, among which Vitamin C, flavonoids, solid-to-acid ratio, magnesium, and iron were identified as the most informative for quality assessment.

The volatile profiles were dominated by esters and ketones, a pattern broadly consistent with previous melon studies. However, the relatively high proportion of ketones under saline–alkali conditions suggests that environmental stress may shift the volatile bouquet. Multivariate screening (VIP > 1.0) further defined 13 key aroma compounds that effectively discriminate the two cultivars, supporting the utility of GC-IMS for varietal differentiation. Non-targeted metabolomics revealed 702 metabolites, with marked enrichment of polyphenolic compounds such as (Z)-resveratrol-3-glucoside-5-sulfate and vicenin 2. KEGG pathway analysis identified flavonoid biosynthesis as the most significantly enriched pathway, corroborating observations in other salt-stressed crops and pointing to its central role in antioxidant and defense responses. The concurrent activation of alkaloid and terpenoid pathways indicates a systemic reprogramming of plant secondary metabolism. Finally, DIABLO multi-omics integration uncovered an interactive network linking nutritional components, aroma compounds, and metabolites, providing a systems-level perspective on melon quality regulation.

https://doi.org/10.3390/foods15101746

Several limitations must be acknowledged. First, the saline–alkali and non-saline–alkali soils originated from two different provinces, introducing geographic confounding (climate, baseline soil, agronomic practices); therefore, observed differences are associative rather than causal. Second, only two cultivars and one growing season were studied, limiting generalizability. Third, metabolite identification remained at MSI Level 2. Fourth, sensory evaluation was not performed. Fifth, GC-IMS quantification was semi-quantitative. Sixth, because environmental conditions were not fully crossed with location, a two-way ANOVA was not appropriate; we instead used separate one-way ANOVAs. Future factorial experiments at a single location, with more varieties, multiple seasons, and sensory panels, are needed to validate our conclusions.

5. Conclusions

This study systematically compared the physicochemical properties, nutritional components, and volatile aroma compounds (sensory attributes were not formally evaluated) of 'Yangjiaocui' and 'Boyang No. 9' melons grown under different soil conditions. Cluster analysis identified Vitamin C, flavonoids, solid-to-acid ratio, magnesium, and iron as core indicators for evaluating melon quality. Using GC-IMS technology, 36 volatile compounds were characterized, including 20 esters, five ketones, five alcohols, four acids, and two aldehydes. Among these, butyl acetate, 3-hydroxy-2-butanone, and heptanal contributed to fruity and fresh herbal notes. Multivariate statistical analysis (VIP > 1.0) further screened 13 key aroma compounds, such as isoamyl isovalerate (VIP = 1.17) and butyl acetate (VIP = 1.14). Integration of flavor fingerprint profiles, aroma heatmaps, and OPLS-DA models effectively enabled variety discrimination.

Non-targeted metabolomics identified 702 metabolites, including highly expressed polyphenolic compounds such as (Z)-resveratrol-3-glucoside-5-sulfate and vicenin 2. Glycosylation modifications may enhance their water solubility and bioavailability, potentially facilitating sustained enzymatic conversion and release. These compounds have been reported to possess antioxidant, anti-inflammatory, and other bioactivities, although their specific contributions in this study require further validation.

KEGG pathway enrichment analysis indicated that the flavonoid biosynthesis pathway was significantly enriched, with the highest number of differentially expressed genes, suggesting it as a core responsive pathway that may be linked to antioxidant and defense mechanisms. Concurrent activation of alkaloid and terpenoid pathways pointed to a systemic regulation of plant secondary metabolism.

Building on these findings, DIABLO multi-omics integration revealed an interactive network among nutritional components, aroma constituents, and metabolites. It should be noted that the observed differences between saline–alkali and non-saline–alkali conditions may be influenced by geographic and agronomic confounding factors (e.g., sample origin, farming practices); therefore, the associations described here should be interpreted as correlative rather than directly causal. Nonetheless, this comprehensive analytical approach enhances varietal differentiation and provides a system-level perspective on the factors that may govern melon quality formation.

Author Contributions: J.H.: Data curation, Investigation, Methodology, Writing—original draft. K.M.: Software, Data curation, Conceptualization. W.Y.: Methodology, Investigation, Resources. Z.L.: Software, Methodology, Conceptualization. R.W.: Methodology, Data curation. L.L.: Methodology, Data curation. L.S.: Conceptualization, Resources. Y.S.: Resources, Investigation. X.W.: Writing—review & editing, Software, Supervision, Project administration. All authors have read and agreed to the published version of the manuscript.

Funding: This study was financially supported by Hebei Agriculture Research System [Grant number HBCT2023100206], Science Research Project of Hebei Education Department [Grant number YJZ2024001] and the Collaborative Innovation Team for Green and Efficient Vegetable Industry Technology of Hebei Agricultural University [Grant Number 202501TDK04].

Institutional Review Board Statement: Not applicable.

Informed Consent Statement: Not applicable.

Data Availability Statement: The original contributions presented in the study are included in the article, further inquiries can be directed to the corresponding author.

Conflicts of Interest: All authors claim no conflicts of interest.

References

1. Cao, Y.; Yao, D.; Diao, Q.; Tian, S.; Lv, D.; Zhang, W.; Zhang, Y. Integrated physiological, transcriptome and metabolome analysis revealed the response mechanisms of melon to *Podosphaera xanthii*. *Plant Stress* **2025**, *18*, 101070. [CrossRef]
2. Ma, J.; Yuan, G.; Xu, X.; Zhang, H.; Qiu, Y.; Li, C.; Zhang, H. Identification and molecular marker development for peel color gene in melon (*Cucumis melo* L.). *J. Integr. Agric.* **2025**, *24*, 2589–2600. [CrossRef]
3. Mallek-Ayadi, S.; Bahloul, N.; Baklouti, S.; Kechaou, N. Bioactive compounds from *Cucumis melo* L. fruits as potential nutraceutical food ingredients and juice processing using membrane technology. *Food Sci. Nutr.* **2022**, *10*, 2922–2934. [CrossRef]
4. Feng, C.; Ni, Y.; Zhang, Y.; Yang, J.; Xiong, R. Characteristic aroma identification of differentially colored peach fruits based on HS-SPME-GC–MS. *Food Chem.* **2025**, *467*, 142280. [CrossRef] [PubMed]
5. San, A.T.; Joyce, D.C.; Hofman, P.J.; Macnish, A.J.; Webb, R.I.; Matovic, N.J.; Williams, C.M.; De Voss, J.J.; Wong, S.H.; Smyth, H.E. Stable isotope dilution assay (SIDA) and HS-SPME-GCMS quantification of key aroma volatiles for fruit and sap of Australian mango cultivars. *Food Chem.* **2017**, *221*, 613–619. [CrossRef]
6. Valverde, M.A.F.; Sánchez-Palomo, E.; Alises, M.O.; Romero, C.C.; González-Viñas, M.A. Volatile and Sensory Characterization of La Mancha Trujillo Melons over Three Consecutive Harvests. *Foods* **2021**, *10*, 1683. [CrossRef]
7. Chen, J.; Wu, F.; Wang, H.; Guo, C.; Zhang, W.; Luo, P.; Zhou, J.; Hao, W.; Yang, G.; Huang, J. Identification of key taste components in *Baccaurea ramiflora* Lour. fruit using non-targeted metabolomics. *Food Sci. Hum. Wellness* **2023**, *12*, 94–101. [CrossRef]
8. Kaleem, M.M.; Nawaz, M.A.; Ding, X.; Wen, S.; Shireen, F.; Cheng, J.; Bie, Z. Comparative analysis of pumpkin rootstocks mediated impact on melon sensory fruit quality through integration of non-targeted metabolomics and sensory evaluation. *Plant Physiol. Biochem.* **2022**, *192*, 320–330. [CrossRef]
9. *GB/T 5009.3-2003*; Determination of Moisture Content in Food. Standards Press of China: Beijing, China, 2003.
10. He, Y.; Qin, H.; Wen, J.; Cao, W.; Yan, Y.; Sun, Y.; Yuan, P.; Sun, B.; Fan, S.; Lu, W.; et al. Characterization of Key Compounds of Organic Acids and Aroma Volatiles in Fruits of Different *Actinidia argute* Resources Based on High-Performance Liquid Chromatography (HPLC) and Headspace Gas Chromatography–Ion Mobility Spectrometry (HS-GC-IMS). *Foods* **2023**, *12*, 3615. [CrossRef] [PubMed]
11. *GB 5009.86-2016*; Determination of Vitamin C in Foods. Standards Press of China: Beijing, China, 2016.
12. Guler, A. Effects of different maceration techniques on the colour, polyphenols and antioxidant capacity of grape juice. *Food Chem.* **2023**, *404*, 134603. [CrossRef]
13. Wang, Z.; Chen, Y.; Fang, H.; Jia, Y.; Yun, Z.; Wang, L.; Wang, X. Comparative evaluation of physical and chemical properties, nutritional components and volatile substances of 24 chestnut varieties in Yanshan area. *Food Chem.* **2025**, *477*, 143624. [CrossRef]
14. Han, C.; Shi, C.; Liu, L.; Han, J.; Yang, Q.; Wang, Y.; Li, X.; Fu, W.; Gao, H.; Huang, H.; et al. Majorbio Cloud 2024: Update Single-cell and Multiomics Workflows. *iMeta* **2024**, *3*, e217. [CrossRef]
15. Wishart, D.S.; Guo, A.; Oler, E.; Wang, F.; Anjum, A.; Peters, H.; Dizon, R.; Sayeeda, Z.; Tian, S.; Lee, B.L.; et al. HMDB 5.0: The Human Metabolome Database for 2022. *Nucleic Acids Res.* **2022**, *50*, D622–D631. [CrossRef]
16. Yang, J.; Zhao, X.; Lu, X.; Lin, X.; Xu, G. A Data Preprocessing Strategy for Metabolomics to Reduce the Mask Effect in Data Analysis. *Front. Mol. Biosci.* **2015**, *2*, 4. [CrossRef] [PubMed]
17. Dunn, W.B.; Broadhurst, D.; Begley, P.; Zelena, E.; Francis-McIntyre, S.; Anderson, N.; Brown, M.; Knowles, J.D.; Halsall, A.; Haselden, J.N.; et al. Procedures for Large-Scale Metabolic Profiling of Serum and Plasma Using Gas Chromatography and Liquid Chromatography Coupled to Mass Spectrometry. *Nat. Protoc.* **2011**, *6*, 1060–1083. [CrossRef]
18. Fiehn, O.; Robertson, D.; Griffin, J.; Werf, M.; Nikolau, B.; Morrison, N.; Sumner, L.; Goodacre, R.; Hardy, N.; Taylor, C.; et al. The Metabolomics Standards Initiative (MSI). *Metabolomics* **2007**, *3*, 175–178. [CrossRef]
19. Rohart, F.; Gautier, B.; Singh, A.; Cao, K. mixOmics: An R package for 'omics feature selection and multiple data integration. *PLoS Comput. Biol.* **2017**, *13*, e1005752. [CrossRef] [PubMed]

20. Nordlund, Å.; Johansson, I.; Källestål, C.; Ericson, T.; Sjöström, M.; Strömberg, N. Improved ability of biological and previous caries multimarkers to predict caries disease as revealed by multivariate PLS modelling. *BMC Oral Health* **2009**, *9*, 28. [CrossRef]
21. Gu, Z.; Eils, R.; Schlesner, M. Complex heatmaps reveal patterns and correlations in multidimensional genomic data. *Bioinformatics* **2016**, *32*, 2847–2849. [CrossRef]
22. König, L.M.; Koller, J.E.; Villinger, K.; Wahl, D.R.; Ziesemer, K.; Schupp, H.T.; Renner, B. Investigating the Relationship between Perceived Meal Colour Variety and Food Intake across Meal Types in a Smartphone-Based Ecological Momentary Assessment. *Nutrients* **2021**, *13*, 755. [CrossRef]
23. Diao, Q.; Tian, S.; Cao, Y.; Yao, D.; Fan, H.; Zhang, Y. Transcriptome Analysis Reveals Association of Carotenoid Metabolism Pathway with Fruit Color in Melon. *Sci. Rep.* **2023**, *13*, 5004. [CrossRef]
24. Costa, F.; Peace, C.P.; Stella, S.; Serra, S.; Musacchi, S.; Bazzani, M.; Sansavini, S.; Van de Weg, W.E. QTL dynamics for fruit firmness and softening around an ethylene-dependent polygalacturonase gene in apple (*Malusxdomestica* Borkh.). *J. Exp. Bot.* **2010**, *61*, 3029–3039. [CrossRef] [PubMed]
25. Hetzroni, A.; Vana, A.; Mizrach, A. Biomechanical characteristics of tomato fruit peels. *Postharvest Biol. Technol.* **2011**, *59*, 80–84. [CrossRef]
26. Huang, G.; Mcclements, D.; He, K.; Zhang, Z.; Lin, Z.; Xu, Z.; Zou, Y.; Jin, Z.; Chen, L. Review of formation mechanisms and quality regulation of chewiness in staple foods: Rice, noodles, potatoes and bread. *Food Res. Int.* **2024**, *187*, 114459. [CrossRef]
27. Xie, D.; Liu, D.; Guo, W. Relationship of the optical properties with soluble solids content and moisture content of strawberry during ripening. *Postharvest Biol. Technol.* **2021**, *179*, 111569. [CrossRef]
28. Wang, J.; Jin, L.; Zhu, W.; Jin, N.; Sun, Q.; Zhang, Q.; Zhang, W.; Wang, S.; Xie, Y.; Lyu, J.; et al. Effects of exogenous strigolactones on tomato-fruit quality. *Postharvest Biol. Technol.* **2025**, *224*, 113461. [CrossRef]
29. Liu, W.; Yang, J.; Yang, F.; Li, Z.; Ma, Z.; Shao, Y.; Yin, X.; Dong, S.; Sun, Y. High Voltage Electrostatic Field Alters Soluble Sugar Accumulation and Promotes Melon Fruit Growth. *Plant Physiol. Biochem.* **2025**, *229*, 110448. [CrossRef]
30. Mineață, I.; Murariu, O.C.; Sîrbu, S.; Tallarita, A.; Caruso, G.; Jităreanu, C. Effects of Ripening Phase and Cultivar under Sustainable Management on Fruit Quality and Antioxidants of Sweet Cherry. *Horticulturae* **2024**, *10*, 720. [CrossRef]
31. Abeysuriya, H.I.; Bulugahapitiya, V.P.; Jayatissa, L.P. Variation of vitamin C content and antioxidant capacities during the post-harvest storage of fresh fruits under different temperatures. *J. Stored Prod. Res.* **2024**, *109*, 102426. [CrossRef]
32. Gu, C.; Howell, K.; Dunshea, F.; Suleria, H. LC-ESI-QTOF/MS Characterisation of Phenolic Acids and Flavonoids in Polyphenol-Rich Fruits and Vegetables and Their Potential Antioxidant Activities. *Antioxidants* **2019**, *8*, 405. [CrossRef] [PubMed]
33. Huang, X.; Wang, H.; Luo, W.; Xue, S.; Hayat, F.; Gao, Z. Prediction of loquat soluble solids and titratable acid content using fruit mineral elements by artificial neural network and multiple linear regression. *Sci. Hortic.* **2021**, *278*, 109873. [CrossRef]
34. Huang, Y.; Xu, P.; Hou, B.; Shen, Y. Strawberry tonoplast transporter, FaVPT1, controls phosphate accumulation and fruit quality. *Plant Cell Environ.* **2019**, *42*, 2715–2729. [CrossRef]
35. Tian, G.; Qin, H.; Liu, C.; Xing, Y.; Feng, Z.; Xu, X.; Liu, J.; Lyu, M.; Jiang, H.; Zhu, Z.; et al. Magnesium improved fruit quality by regulating photosynthetic nitrogen use efficiency, carbon–nitrogen metabolism, and anthocyanin biosynthesis in 'Red Fuji' apple. *Front. Plant Sci.* **2023**, *14*, 1136179. [CrossRef] [PubMed]
36. Yu, H.; Shi, H.; Ye, A.; Liu, J.; Han, J.; Liu, W. Calcium supplementation strategies for older people: Calcium fortification in whole grain beverages. *Trends Food Sci. Technol.* **2025**, *164*, 105235. [CrossRef]
37. Cao, F.; Guan, C.; Dai, H.; Li, X.; Zhang, Z. Soluble solids content is positively correlated with phosphorus content in ripening strawberry fruits. *Sci. Hortic.* **2015**, *195*, 183–187. [CrossRef]
38. Pang, X.; Zhang, Y.; Qiu, J.; Cao, J.; Sun, Y.; Li, H.; Kong, F. Coupled Multidimensional GC and Odor Activity Value Calculation to Identify Off-Odors in Thermally Processed Muskmelon Juice. *Food Chem.* **2019**, *301*, 125307. [CrossRef]
39. Xu, K.; Jiang, K.; Yang, A.; Zhang, Z.; Lin, Z.; Wang, T.; Xu, L.; Meng, F.; Wang, B. Sensory and chemical characterization of chestnuts processed in different methods using instrumental analyses and the Check-all-that-apply method. *Arab. J. Chem.* **2024**, *17*, 105876. [CrossRef]
40. Wang, M.; Zhang, L.; Boo, K.; Park, E.; Drakakaki, G.; Zakharov, F. PDC 1, a pyruvate/α-ketoacid decarboxylase, is involved in acetaldehyde, propanal and pentanal biosynthesis in melon (*Cucumis melo* L.) fruit. *Plant J.* **2019**, *98*, 112–125. [CrossRef]
41. Li, X.; Zhang, C.; Li, S.; Wang, H.; Yu, P.; Shao, H.; Wang, S.; Wang, H.; Jin, F. Unveiling key aroma-active compounds of two distinct aroma-types oriental melon: An integrated sensomics approach utilizing GC × GC-O-TOF-MS, GC–MS, aroma recombination and omission experiments. *Food Chem. X* **2025**, *28*, 102517. [CrossRef]
42. Jia, Q.; Zhang, L.; Sha, H.; Tian, Y.; Bi, W.; Feng, C.; Yang, T.; Zhang, R.; Yang, N.; Zhu, F.; et al. A Machine Learning Model for Predicting Consumer Preferences of Melon Flavor and Sensory Attributes. *Appl. Food Res.* **2026**, *6*, 102000. [CrossRef]
43. Mayobre, C.; Pereira, L.; Eltahiri, A.; Einat, B.; Lewinsohn, E.; Garcia-Mas, J.; Pujol, M. Genetic dissection of aroma biosynthesis in melon and its relationship with climacteric ripening. *Food Chem.* **2021**, *353*, 129484. [CrossRef] [PubMed]
44. Yu, A.; Yang, Y.; Yang, Y.; Liang, M.; Zheng, F.; Sun, B. Free and Bound Aroma Compounds of Turnjujube (*Hovenia acerba* Lindl.) during Low Temperature Storage. *Foods* **2020**, *9*, 488. [CrossRef]

45. Rivera-Pérez, A.; Romero-González, R.; Garrido Frenich, A. A metabolomics approach based on 1H NMR fingerprinting and chemometrics for quality control and geographical discrimination of black pepper. *J. Food Compos. Anal.* **2022**, *105*, 104235. [CrossRef]
46. Song, X.; Canellas, E.; Nerin, C. Screening of volatile decay markers of minced pork by headspace-solid phase microextraction–gas chromatography–mass spectrometry and chemometrics. *Food Chem.* **2021**, *342*, 128341. [CrossRef]
47. El Hadi, M.; Zhang, F.; Wu, F.; Zhou, C.; Tao, J. Advances in Fruit Aroma Volatile Research. *Molecules* **2013**, *18*, 8200–8229. [CrossRef]
48. Wang, Y.; Jiao, L.; Gui, Y.; Zhao, W.; Chen, L.; Chen, X.; Chen, J.; Li, Y.; Song, L.; Yu, X. Comprehensive Analysis of Volatile Flavor Components in 'Hujing Milu' Peach from Different Regions Using HS-SPME-GC-MS and HS-GC-IMS. *Foods* **2026**, *15*, 1051. [CrossRef]
49. Parhiz, H.; Roohbakhsh, A.; Soltani, F.; Rezaee, R.; Iranshahi, M. Antioxidant and Anti-Inflammatory Properties of the Citrus Flavonoids Hesperidin and Hesperetin: An Updated Review of their Molecular Mechanisms and Experimental Models. *Phytother. Res.* **2015**, *29*, 323–331. [CrossRef]
50. Li, W.; Du, Q.; Li, X.; Zheng, X.; Lv, F.; Xi, X.; Huang, G.; Yang, J.; Liu, S. Eriodictyol Inhibits Proliferation, Metastasis and Induces Apoptosis of Glioma Cells via PI3K/Akt/NF-κB Signaling Pathway. *Front. Pharmacol.* **2020**, *11*, 114. [CrossRef]
51. Han, X.; Sun, X.; Shi, Z.; Fan, X.; Hu, Y.; Chen, C.; Xia, Q.; Sun, Y.; Pan, D. Study on the inhibitory effects and mechanisms of four polyphenolic compounds from perilla extract on advanced glycation end products (AGEs). *Food Chem. X* **2025**, *29*, 102857. [CrossRef]
52. Singh, K.; Jobbágy, K.; Kulman, K.; Pál, M.; Benczur, K.; Mednyánszky, Z.; Simon-Sarkadi, L.; Gulyás, Z.; Polgári, D.; Riyazuddin, R.; et al. Specific redox regulation of carbohydrate, organic acid, amino acid and polyamine levels in maize seedlings. *Plant Stress* **2025**, *18*, 101100. [CrossRef]
53. Lin, Z.; Lei, Y.; Wang, X.; Li, E.; Qin, C.; Qin, J.; Chen, L. Beneficial effects of dietary organic acids on growth and health of juvenile Chinese mitten crab (*Eriocheir sinensis*). *Aquac. Rep.* **2025**, *43*, 102918. [CrossRef]
54. Singh, A.; Shannon, C.P.; Gautier, B.; Rohart, F.; Vacher, M.; Tebbutt, S.J.; Cao, K. DIABLO: An integrative approach for identifying key molecular drivers from multi-omics assays. *Bioinformatics* **2019**, *35*, 3055–3062. [CrossRef] [PubMed]

Disclaimer/Publisher's Note: The statements, opinions and data contained in all publications are solely those of the individual author(s) and contributor(s) and not of MDPI and/or the editor(s). MDPI and/or the editor(s) disclaim responsibility for any injury to people or property resulting from any ideas, methods, instructions or products referred to in the content.

foods

MDPI

Article

Identification of Potential Bioactive Compounds in Strong-Flavor-Type Baijiu via Integration of Widely Targeted Metabolomics and Network Pharmacology

Jinxiao Liu [1], Jia Zheng [2,3,4], Jihong Wu [1,*], Ying Sun [1], Mingquan Huang [1], Jian Su [2,3,4], Fuping Zheng [1] and Dongrui Zhao [1]

[1] Key Laboratory of Brewing Molecular Engineering of China Light Industry, Beijing Technology and Business University, Beijing 100048, China; liujx1218986@163.com (J.L.); btbusunying@163.com (Y.S.); huangmq@th.btbu.edu.cn (M.H.); zhengfp@btbu.edu.cn (F.Z.); zdr@btbu.edu.cn (D.Z.)
[2] Solid-State Fermentation Resource Utilization Key Laboratory of Sichuan Province, Wuliangye Yibin Co., Ltd., Yibin 644000, China; zhengjia@wuliangye.com.cn (J.Z.); sujian@wuliangye.com.cn (J.S.)
[3] Key Laboratory of Wuliangye-Flavor Liquor Solid-State Fermentation, China National Light Industry, Wuliangye Yibin Co., Ltd., Yibin 644000, China
[4] China Engineering Technology Research Center for Baijiu-Making Grains, Wuliangye Yibin Co., Ltd., Yibin 644000, China
* Correspondence: wujihong12@126.com

Abstract

Strong-flavor-type Baijiu, represented by *Wuliangye*—a renowned traditional Chinese alcoholic beverage brewed from five grains (sorghum, rice, glutinous rice, wheat, and corn)—is widely consumed and appreciated for its balanced taste and potential health benefits. While the volatile flavor compounds of Baijiu have been well studied, its bioactive components and their underlying mechanisms remain insufficiently explored. In this study, widely targeted metabolomics techniques were innovatively employed, and 2128 compounds were identified from 10 *Wuliangye* samples, of which 445 were predicted to constitute potential bioactive substances. Network pharmacology analysis further identified four key compounds, namely the four potential bioactive small molecules (fisetin, luteolin, norartocarpetin, and scutellarein), along with ten core targets that were key protein targets interacting with these compounds (SRC, PIK3R1, PTGS1, AKR1B1, STAT3, CYP3A4, ESR1, PIK3CA, PIK3CB, and ALOX15). GO and KEGG enrichment analyses indicated that these targets participated in diverse biological processes, while DO analysis revealed potential associations between these targets and specific diseases. Additionally, molecular docking confirmed the binding patterns between the identified compounds and their targets. Collectively, this study provides systematic chemical information and theoretical screening results for identifying potential bioactive components in strong-flavor-type Baijiu, which may facilitate further studies of their biological functions.

Keywords: bioactive components; network pharmacology; strong-flavor-type Baijiu; widely targeted metabolomics

1. Introduction

Baijiu, a national alcoholic beverage of China with a history spanning over 2000 years, is a typical grain-based distilled spirit. It is produced through a unique solid-state brewing process, including raw material crushing, microbial saccharification by qu, long-term solid-state fermentation in cellars, distillation, aging storage, and scientific blending [1,2]. This

traditional and elaborate brewing procedure promotes the formation of abundant flavor substances and diverse bioactive components, thereby providing a material foundation for its quality and potential health benefits [3]. Advanced and widely used analytical methods have been widely applied to characterize the aroma components of Baijiu [4,5], with over 2700 compounds identified, including volatile phenols, esters, and aldehydes, as well as non-volatile amino acids, polyols, and bioactive peptides [6]. Among the various types of Baijiu, the strong-flavor-type Baijiu is globally renowned for its distinctive brewing process and superior quality, and a total of 861 trace components (e.g., 248 esters, 122 alcohols, and 24 phenols) have been reported in this type [7].

Notably, the quality of Baijiu is determined not only by its volatile flavor substances but also by non-volatile trace components with potential health benefits. With increasing health awareness, research on healthy Baijiu has become a focus. Moderate consumption of Baijiu has been reported to benefit health, which is likely attributed to its bioactive components [7,8]. For example, *Wuliangye* Baijiu, as a representative of strong-flavor-type Baijiu, was shown to promote intestinal homeostasis in mice by regulating intestinal stem cell proliferation, differentiation and gut microbiota composition [9], while pyrazines in sauce-flavor-type Baijiu exhibited anti-inflammatory effects via modulation of the NF-κB/MAPK pathway [10]. However, the molecular mechanisms underlying the bioactivity of these compounds remain insufficiently analyzed. Thus, identifying the functional components in Baijiu and their health benefits is critical for advancing the industry's high-quality development.

In recent years, metabolomics has emerged as a powerful analytical tool for conducting qualitative and quantitative analyses of numerous metabolites in biological samples, thereby offering novel approaches to investigating the functional components within complex systems [11]. Meanwhile, network pharmacology integrates research methods from multiple disciplines, including systems biology, medicinal chemistry, molecular biology, bioinformatics, and computational chemistry. By constructing networks between drugs and biological targets, this approach facilitates a deeper understanding of the mechanisms of action and the multi-target effects of drugs, thereby providing strong support for elucidating the mechanisms of action of functional components [12,13]. Despite their potential, these methods have rarely been applied in Baijiu research.

Prior studies had confirmed that Baijiu and its by-products were rich in bioactive substances, including polyphenols, terpenoids, bioactive peptides, and polysaccharides, which exhibited antioxidant, anti-inflammatory, blood pressure-lowering, and intestinal microbiota-regulating activities [14]. However, obvious limitations remain in the research. Specifically, most studies focus primarily on a single type of bioactive component (e.g., peptides, polysaccharides, or phenolics) and lack systematic profiling of the overall metabolome in Baijiu. Furthermore, the research approaches are predominantly centered on compound identification and in vitro activity validation, with rare involvement of target prediction, signaling pathways, and underlying molecular mechanisms. In particular, comprehensive analysis and mechanistic research of non-volatile bioactive components in strong-flavor Baijiu are still insufficient. For instance, Zeng et al. focused on the preparation, purification, identification, and functional validation of bioactive peptides from Baijiu and its fermentation byproducts, yet comprehensive profiling of the global metabolome was not performed [15]. Hu et al. merely conducted widely targeted metabolomics profiling and in vitro evaluations of the antioxidant and antiglycation activities of Baijiu distillers' grains without exploring potential targets or regulatory pathways [16]. Similarly, Guan et al. only reviewed the extraction and bioactivities of functional components from Baijiu distillers' grains without in-depth mechanistic investigation [17]. In particular, comprehensive profiling and mechanistic studies of non-volatile bioactive components in Baijiu are still

https://doi.org/10.3390/foods15091509

inadequate. Therefore, it is urgent to establish a systematic strategy to globally reveal the bioactive components and their potential health regulatory mechanisms in Baijiu.

Therefore, to address the aforementioned critical limitations, this study integrated widely targeted metabolomics and network pharmacology to identify and analyze bioactive components in *Wuliangye* Baijiu samples. Initially, ultra-high-performance liquid chromatography–electrospray–triple-quadrupole linear ion trap tandem mass spectrometry (UPLC-ESI-Q TRAP-MS/MS) was used for comprehensive metabolite profiling of the *Wuliangye* samples. Subsequently, potential functional components, their targets, and bioactivities were predicted through network pharmacology, followed by compound–target–disease network construction to explore mechanisms. This study overcame the limitations of previous research that only focused on the activity analysis of single components. Furthermore, it addressed the research gap regarding the insufficient mechanistic exploration of non-volatile bioactive components in strong-flavor Baijiu. Consequently, the systematic identification and analysis of functional components in strong-flavor Baijiu and their potential health benefits are of significant importance. These findings will help to scientifically reveal the health attributes of Baijiu, standardize the healthy development of the industry, and meet consumers' growing demand for healthy alcoholic beverages. Thus, exploring the functional components in Baijiu and their associated health benefits is crucial for advancing the industry's high-quality development. Notably, ethanol is the main component of Baijiu. Excessive or long-term consumption of Baijiu may be associated with potential adverse health effects. This study focuses solely on the identification and screening of trace components and their potential physiological activities in Baijiu, which does not reflect the overall effects of Baijiu itself.

2. Materials and Methods

2.1. Wuliangye Baijiu Sample Treatment

The primary objective of this study was to characterize the global profile of bioactive components in *Wuliangye* Baijiu collectively rather than to compare differences among individual products. Thus, a total of 10 distinct *Wuliangye* Baijiu products were procured for this study from Yonghui Supermarket (Beijing, China) and the official *Wuliangye* flagship store on JD.com (Table 1). These samples were then divided into two groups based on product characteristics and research focus. One group consisted of a single sample, WU LIANG YE (Eighth Generation, Yibin, China), which was selected separately due to its distinctive flavor, high market popularity, broad consumer recognition, and superior quality compared to other variants. For this group, 50 mL of Baijiu was subjected to atmospheric distillation at a heating temperature of 90 °C, and the final volume of the sample was reduced to 20 mL. The other group included the remaining nine *Wuliangye* Baijiu products. An amount of 35 mL of each of these 9 products was measured out and then mixed in equal proportions to form a composite sample. This composite sample was then subjected to atmospheric distillation under the same conditions (heating temperature of 90 °C). The final combined volume of the composite sample was 140 mL, corresponding to a concentration factor of 2.25, the same as for the first group. To ensure the repeatability and reliability of the results, three technical replicates were analyzed for each sample during instrumental analysis.

https://doi.org/10.3390/foods15091509

Table 1. Different types of *Wuliangye* Baijiu.

Group	Name	Alcohol Content (*v*/*v* %)	Production Date
1	WU LIANG YE (Eighth Generation)	52	2024/02/05
2	WU LIANG CHUN	52	2024/03/11
	WU LIANG CHEN	52	2021/07/13
	WU LIANG TOU QU	52	2023/09/27
	WU LIANG CHUN (premium)	52	2024/01/08
	WU LIANG TE QU	52	2022/08/30
	FU GUI TIAN XIA JIU	52	2023/12/28
	ZUNJIU	52	2022/03/23
	WU LIANG CHEN (Heritage Series)	52	2021/04/26
	JIAN ZHUANG	52	2024/01/23

2.2. Widely Targeted Metabolomics Analysis and Compounds Database Building

The workflow of this study is presented in Figure 1. The sample preparation and extraction were conducted as previously described, with minor modifications [18]. Briefly, the treated Baijiu samples were freeze-dried and then added to a 70% methanol internal standard extract. The internal standard used was L-2-chlorophenylalanine at a concentration of 1 μg/mL. After lyophilization, the samples were redissolved in the same extractant and concentrated 30-fold for signal correction and quantitative analysis. Notably, this internal standard was not employed for absolute quantitation of metabolites but rather to monitor the stability of the instrumental system throughout the widely targeted metabolomics analysis. The mixture was stirred for 15 min and centrifuged at 12,000 r/min at 4 °C for 3 min. The supernatant was filtered through a microporous membrane (0.22 μm) and then analyzed using a UPLC-ESI-Q TRAP-MS/MS system (UPLC: Nexera X2, Shimadzu, Kyoto, Japan; MS: 6500 Q TRAP, SCIEX, Framingham, MA, USA). Quality control (QC) samples were prepared by mixing equal aliquots of all sample extracts. During instrumental analysis, one QC sample was inserted every 10 injections to monitor system stability and analytical repeatability. For UPLC analysis, an Agilent SB-C18 column (1.8 μm, 2.1 mm × 100 mm) was used. The mobile phase consisted of solvent A (water with 0.1% formic acid) and solvent B (acetonitrile with 0.1% formic acid). The gradient elution program started at 95% A and 5% B, changed to 5% A and 95% B within 9 min, held for 1 min, and then returned to 95% A and 5% B within 1.1 min and held for 2.9 min. The flow rate was maintained at 0.35 mL/min, the column temperature was set to 40 °C, and the injection volume was 2.0 μL. For ESI, the source temperature was 500 °C, the ion spray voltage was 5500 V (positive mode) or −4500 V (negative mode), and gases were set at GSI: 344.74 kPa, GSII: 413.69 kPa, and CUR: 172.37 kPa. The instrument was tuned and calibrated with polypropylene glycol solutions (10.0 and 100 μmol/L) in QQQ and LIT modes. QQQ scans were performed in MRM mode with optimized DP and CE for each transition. The Metware database was used to match parameters, including retention time (RT), secondary mass spectrometry fragment ions, parent ion molecular weight, characteristic fragment ion, DP, and CE of the substances. Metabolites were quantified in multiple reaction monitoring (MRM) mode using triple-quadrupole mass spectrometry.

https://doi.org/10.3390/foods15091509

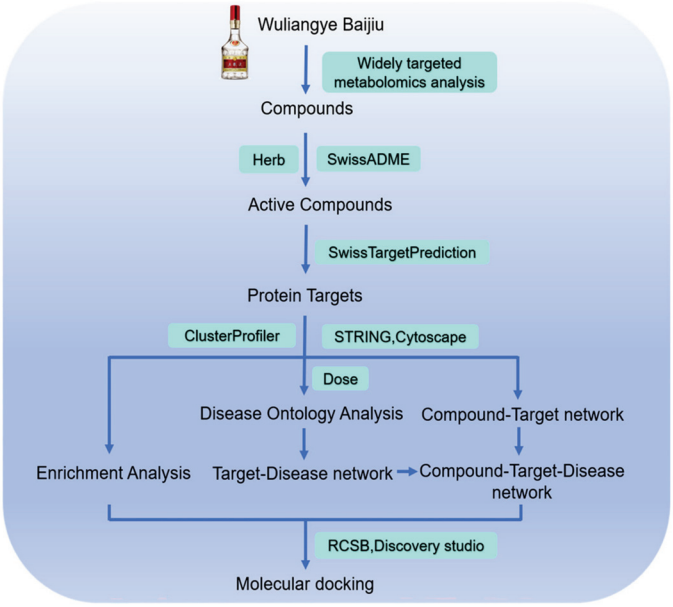


Figure 1. Diagram of the methodology applied in this study.

Metabolite annotation was performed via a widely targeted metabolomics approach based on UPLC-ESI-Q TRAP-MS/MS and multiple reaction monitoring (MRM) scanning, referencing to the Metware database. A strict three-level qualitative identification system was applied: Level 1 (full matching of MS/MS fragment ions and RT, score $\geq$ 0.7), Level 2 (full matching of MS/MS fragment ions and RT, score 0.5–0.7), and Level 3 (consistent matching of Q1, Q3, RT, DP, and CE parameters). The identification level for each metabolite is listed in Table S1.

2.3. Screening Potential Active Compounds and ADMET Evaluation

Traditional Chinese medicine provides a rich foundation for modern drug discovery and development. The Herb database (http://herb.ac.cn) is a specialized high-throughput experimental and reference database for traditional Chinese medicine [19]. ADMET (absorption, distribution, metabolism, excretion, and toxicity) is a key evaluation parameter in druglikeness studies. In this study, the web tool SwissADME (http://www.swissadme.ch/ (accessed on 26 April 2025)) was used to evaluate the ADMET parameters. SwissADME provided information regarding various chemical properties of small molecules, including ADME parameters, physicochemistry, druglikeness, pharmacokinetics, and medicinal chemistry friendliness properties [20]. The potential active compounds were screened based on the following criteria [21]: (1) the compound components must be retrievable from the Herb database, (2) a minimum of two "YES" results for druglikeness properties (Lipinski, Ghose, Veber, Egan, Muegge), (3) the gastrointestinal absorption (GI) level must be "high".

2.4. Target Prediction and Interaction Network Construction

The SwissTargetPrediction (http://www.swisstargetprediction.ch/) is a powerful online tool which predicts potential protein targets by comparing the two-dimensional (2D) and three-dimensional (3D) structural similarities between the query molecule and known ligands [22]. Here, SwissTargetPrediction was used to predict the targets of each potential active compound. The SMILES identifiers of the filtered compounds were imported into SwissTargetPrediction with the "Homo sapiens" setting. A higher probability of a protein target generally correlates with greater accuracy of the prediction. Therefore, a probability threshold of 0.4 was set to filter out more credible protein targets and enable a reliable

compound–target (C-T) network. Given that protein–protein interaction (PPI) networks can complement and improve a C-T network, a PPI network was constructed using STRING (https://string-db.org/). The filtered protein targets were imported into STRING with "Homo sapiens" as the "organism" and the "minimum required interaction score" set to "highest confidence (0.900)" [23].

2.5. Topological Analysis of Compound–Target Network

The network was visualized using Cytoscape v.3.10.3 [24]. To identify the key active compounds and core targets, CytoHubba was employed. CytoHubba can comprehensively evaluate the key nodes in the network through various topological analysis methods [23,25]. The top 10 core nodes of the C-T network were analyzed using 10 different methods, including edge percolated component, maximum neighborhood component, density of maximum neighborhood component, maximal clique centrality, and six centralities (degree, closeness, betweenness, bottleneck, eccentricity, and stress). Subsequently, the final core components were determined by selecting nodes that were consistently identified as significant by at least three of the topological analysis methods [26].

2.6. GO and KEGG Enrichment Analyses

To explore the biological effects of the filtered protein targets, the R package clusterProfiler was used to conduct GO enrichment analysis and KEGG pathway analysis [27]. The *p*-value was adjusted using the Benjamini–Hochberg method, and results with a *p*-value < 0.05 were considered significant. Then, ClueGO and CluePedia, two Cytoscape plugins, were employed to further visualize and interpret the enrichment results. The relationships between pathways and the enrichment of genes within those pathways were more intuitively displayed by integrating ClueGO and CluePedia [28]. For this analysis, the filtered target gene symbols were input into the "Functional analysis" mode, and the "Homo sapiens (9606)" option was selected. The p-value was corrected using a two-sided hypergeometric test and the Bonferroni step down method.

2.7. Disease Ontology Analysis

The Human Disease Ontology (DO; https://www.disease-ontology.org) database is a comprehensive knowledge base that contains a variety of human diseases, thereby providing standardized disease classification and descriptions [29]. DO enrichment analysis is a method employed to identify the gene sets related to specific diseases. Potential biological significance and disease associations can be revealed through DO analysis. Here, the DO analysis was performed using the R package DOSE [30]. For the analysis, the Benjamini–Hochberg method was used to adjust the p-value, with significance set at a *p*-value of less than 0.05.

2.8. Compound–Target–Disease Network Construction

Based on the establishment of the C-T network and DO analysis, the complex relationships between active compounds, protein targets, and diseases were visualized using Cytoscape. In the compound–target–disease (C-T-D) network, nodes represent active compounds, protein targets, or diseases, while edges represent the interactions among them. The importance of compounds and targets was assessed; the higher the degree, the greater its importance.

2.9. Molecular Docking Analysis

To validate the reliability of the C-T association, molecular docking analysis was performed using the filtered active compounds and targets. Briefly, the docking process was carried out as follows: (1) the 3D structure of the compound (ligand) in SDF format

was downloaded from the PubChem database, (2) the crystal structure of the protein target (receptor) in PDB format was downloaded from the RCSB website, (3) the original co-crystallized ligand and water molecules from the receptor were removed using discovery Studio 2019 (DS) software; then, molecular docking was performed with the ligand. For each ligand, ten binding poses were generated. The CDOCKER energy (based on the CHARMm force field) was used as the scoring function to evaluate the relative binding affinity between ligands and the target.

2.10. Data Processing

Pie charts were constructed using GraphPad, and network diagrams were generated using Cytoscape. The GO and KEGG databases were utilized for the annotation of metabolic pathways.

3. Results and Discussion

3.1. Identification of the Metabolites of Wuliangye Baijiu

Based on the mass-to-charge ratio in the Metware database, a total of 2128 metabolites were identified in *Wuliangye* Baijiu (as detailed in Table S1) for the first time, including 281 terpenoids, 276 alkaloids, 234 lipids, 212 amino acids and derivatives, 210 flavonoids, 196 phenolic acids, 112 organic acids, 69 lignans and coumarins, 50 nucleotides and derivatives, 30 quinones, six tannins, five steroids, and 447 unclassified compounds. The comprehensive effect of these compounds might contribute to both the flavor and health effects of Baijiu, as further analyzed below.

Terpenoids constituted the largest proportion among the ten kinds of *Wuliangye* Baijiu samples, which was likely due to the unique brewing process and raw material selection, as reported by Feng et al., that systematically tracked and analyzed terpenoid compounds throughout the brewing process of strong-aroma Baijiu. That process involved raw materials, daqu (a type of fermentation starter), cellar mud, wine dregs, and base Baijiu [31]. Meanwhile, a total of 55 terpenoids were identified in Moutai Baijiu—a typical representative of soy-sauce-flavor-type Baijiu, which were regarded to provide more elegant and delicate aroma to Moutai Baijiu [32]. Therefore, these terpenoids might not only endow *Wuliangye* Baijiu with a unique fragrance but may also offer health benefits such as antibacterial [33], antioxidant [34], anticancer [35], and stomach protection [36]. Alkaloids—a class of basic nitrogen—constituted the second-most abundant group after terpenoids in *Wuliangye* Baijiu. Most alkaloids exhibited significant physiological activity, making them effective components in many medicinal plants. For example, narciclasine had shown significant mitosis-blocking activity in various cancer cell lines [37]. Betaine exerts anti-inflammatory effects in numerous diseases by improving sulfur amino acid metabolism to combat oxidative stress, inhibiting NF-κB signaling and NLRP3 inflammasome activation, regulating energy metabolism, and alleviating endoplasmic reticulum stress and apoptosis [38]. Dopamine can modulate immune cells in the brain and periphery, while immune cells can also indirectly affect distant tissues through dopaminergic regulation [39]. Free fatty acids are the main lipids in *Wuliangye* Baijiu. These compounds are not only precursors for the formation of the main aromatic fatty acids esters in the liquor but also play an important role in the formation of the aroma and aftertaste of the Baijiu [40]. Myristoleic acid can inhibit the activation of Src and Pyk2 and block the rearrangement of the cytoskeleton and the formation of actin rings. As a result, it can suppress the maturation of osteoclasts and bone resorption, exhibiting potential therapeutic value in the prevention of osteoporosis and other bone metabolic diseases [41]. Punicic acid exerts positive effects against neurodegenerative diseases by reducing oxidative damage and inflammation through the upregulation of peroxisome proliferator-activated receptors. Additionally,

https://doi.org/10.3390/foods15091509

it decreases the formation of beta-amyloid deposits and tau hyperphosphorylation by increasing the expression of GLUT4 protein and inhibiting calpain hyperactivation [42]. Similarly, other polyunsaturated fatty acids have been shown to exert positive effects on cardiovascular diseases [43], the nervous system [44], and overall immunity [45].

In addition, amino acids and derivatives, flavonoids, and phenolic acids collectively accounted for a significant proportion (29.1%) of the substances detected in *Wuliangye* Baijiu. Proteins in the raw materials were broken down by microorganisms into amino acids during the brewing process of Baijiu, which were subsequently converted into flavor-specific esters and other compounds during fermentation, thereby enhancing the aromatic complexity of the Baijiu [46]. Amino acids themselves possessed umami, sweet, bitter, astringent, and sour taste properties, thereby directly influencing the mouthfeel and flavor profile [47]. Flavonoids, representing 10% of the compounds in *Wuliangye* Baijiu, are bioactive substances with notable antioxidant [48], antibacterial [49], and antiviral properties [50]; they can react with other compounds in the Baijiu to form new flavor substances [51]. Phenolic compounds contributed aromas, such as smoky, muddy and fruity, to Baijiu [52,53], playing critical roles in its aroma, taste, and stability. Phenolic acids like guaiacol derivatives acted as natural free radical scavengers with potent reactive oxygen species (ROS) elimination capabilities, offering antioxidant effects and potential cardiovascular disease prevention [54].

In contrast, organic acids, lignans and coumarins, nucleotides and derivatives, quinones, tannins, and steroids were present in relatively low concentrations in *Wuliangye* Baijiu. Despite their relatively low content, these compounds might still play significant roles in the overall flavor, taste, and potential health benefits of Baijiu. Organic acids provide a refreshing sour taste and interact with alcohols and esters in the Baijiu to enhance the complexity and layering of the taste [55]. Quinones exhibit redox properties and participate in the oxidation reactions of the Baijiu, influencing its color and stability [56]. Lignans and coumarins, nucleotides and derivatives, tannins, and steroids were all reported to possess antioxidant and antibacterial bioactivities, but further research is required to explore their specific roles and underlying mechanism in Baijiu.

Collectively, these results indicated that the active compounds in *Wuliangye* Baijiu possessed a range of potential biological activities. It should be noted that these conclusions were based on prior studies and in silico analysis, with no experimental validation conducted in the present study. The potential effects of these compounds after ingestion, digestion, and absorption in vivo warrant further investigation.

3.2. Prediction of Potential Active Compounds and Their Pharmacological Properties

After screening the Herb database and analyzing the data with SwissADME, a total of 445 potential active compounds were identified based on the screening criteria outlined in Section 2.3 (listed in Table S2). Alkaloids, phenolic acids, terpenoids, and flavonoids accounted for 52.2% of the total active components and were the main active compounds in *Wuliangye* Baijiu. The relative proportions of these potential active compounds within *Wuliangye* Baijiu were visually represented in Figure 2. The analysis revealed that the average molecular weight of these potential active compounds was approximately 218.13, with a range from 88.15 to 678.81. According to the predicted pharmacological properties, 65.62% (292/445) of the active compounds exhibited high water solubility, 67.87% (302/445) could penetrate the blood–brain barrier, 88.31% (393/445) were not substrates of P-glycoprotein, and 35.06% (156/445) of the active compounds fully complied with Lipinski's rule of five, indicating their high druglikeness.

https://doi.org/10.3390/foods15091509

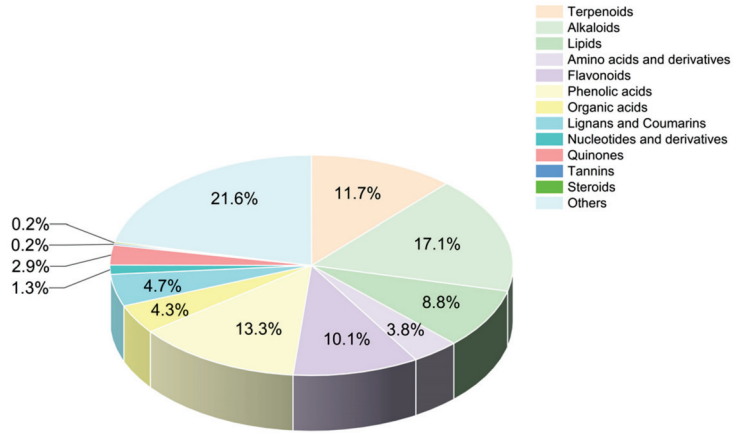


Figure 2. Pie chart of the number of different types of potential active compounds in *Wuliangye* Baijiu.

3.3. Compound–Target Interaction Network

To gain further insight into the mechanisms of these potential active compounds in the human body, the possible protein targets were predicted. Targets with a probability of ≥0.4 were selected to construct a C-T network (Table S3). The results revealed that 207 targets were associated with 127 active compounds. To further explore the key components in *Wuliangye* Baijiu, topological analysis was performed using multiple methods, with the results presented in Table 2. Furthermore, the common components identified by at least three topological methods are listed in Table S4. In total, four key active compounds, including fisetin, luteolin, norartocarpetin, and scutellarein, together with ten core targets (SRC, PIK3R1, PTGS1, AKR1B1, STAT3, CYP3A4, ESR1, PIK3CA, PIK3CB, and ALOX15), were obtained, which was an important new discovery in this study. In the C-T network, fisetin, luteolin, norartocarpetin, and scutellarein were connected to multiple target proteins. Similarly, the ten core target proteins were linked to various active compounds. Therefore, these compounds and targets were recognized as key contributors to the active effects of *Wuliangye* Baijiu.

Table 2. Top 10 core compositions of the compound–target (C-T) network.

Betweenness	Bottleneck	Closeness	Degree	DMNC	Eccentricity	EPC	MCC	MNC	Stress	Rank
Fisetin	Fisetin	Fisetin	Fisetin	EGFR	CA13	Fisetin	SRC	SRC	PTGS1	1
PTGS1	Scutellarein	Norartocarpetin	Norartocarpetin	HSD17B3	CA5A	Luteolin	PIK3R1	Fisetin	Fisetin	2
Nuciferine	ALOX5	Luteolin	Luteolin	IGF1R	AKT1	SRC	EGFR	ESR1	ALOX15	3
DRD4	DRD4	Scutellarein	SRC	PTK2	CA9	PIK3R1	PTK2	AKR1C3	Luteolin	4
Luteolin	PTGS1	CA2	STAT3	CYP2C9	CA14	Norartocarpetin	IGF1R	PIK3R1	CYP3A4	5
MAOA	AKR1B1	AKR1B1	CYP3A4	PIK3R1	CA6	STAT3	PIK3CA	PIK3CA	(9Z,12Z,15Z)—octadecatrienoic acid	6
Norartocarpetin	(9Z,12Z,15Z)—octadecatrienoic acid	SRC	Scutellarein	Nicotine	CA3	PIK3CA	PIK3CB	CYP3A4	FABP4	7
Resveratrol	Nuciferine	CA12	ESR1	CHRNA7	SRC	ESR1	CYP2C19	STAT3	FABP3	8
AKR1B1	CA2	MAOA	AKR1C3	CHRNA3	CA1	Scutellarein	CYP2C9	ALOX15	ALOX5	9
SLC6A4	ACHE	CA7	PIK3R1	CHRNB4	ADORA2A	PIK3CB	ALOX15	PIK3CB	Linoleate	10

In addition, it was noteworthy that luteolin, norartocarpetin, and scutellarein belong to the flavonoid class of compounds. Fisetin, a natural flavonoid polyphenolic compound widely distributed in fruits, vegetables, and natural plants, had been shown to promote the activation of Caspase-3 to induce apoptosis by regulating the PI3K/ AKT/NF-κB axis [57]. It can mediate the TLR4/Src pathway to inhibit the expression of the NF-κB p65 and MAPK signaling pathways, thus alleviating lipopolysaccharide-induced renal inflammation in mice and reducing the expression of inflammatory factors [58]. Moreover, fisetin treatment had also been reported to alleviate cognitive deficits in aged SAMP8 mice, while restoring their impaired synaptic function and stress response, indicating that it had certain antiaging effects [59]. Luteolin, another natural flavonoid compound, also exhibited a wide range of health benefits. Specifically, it alleviated CCl4-induced liver inflammation and fibrosis in mice by inhibiting macrophage infiltration and modulating

M1 macrophage polarization via the Notch1 signaling pathway [60]. Additionally, luteolin inhibited the production of proinflammatory mediators (IL-1β, IL-6, IL-8, IL-17, IL-22, TNF-α, and COX-2) and regulated various signaling pathways (NF-κB, JAK-STAT, and TLR signaling pathways) to modulate numerous inflammatory processes in the skin [61]. Norartocarpetin, a compound in Artocarpus communis that demonstrates antioxidant and antityrosinase activity, downregulated the expression of phospho-cAMP response element-binding (phospho-CREB) and microphthalmia-associated transcription factor (MITF), which reduced the synthesis of tyrosinase and intracellular melanin content, thereby inhibiting melanogenesis [62]. Scutellarin exerted antitumor effects by inducing autophagy and apoptosis in tumor cells, as well as inhibiting proliferation, migration, and invasion of tumor cells [63]. Additionally, scutellarin was an effective GABA-T (Gamma-Aminobutyric Acid Transaminase) inhibitor, with an IC50 value of (12.8 ± 1.0) mmol/L, and its inhibitory effect on SSADH (succinic semialdehyde dehydrogenase) was more obvious, with an IC50 value of only (7.20 ± 0.9) mmol/L, which revealed its neuroprotective potential in ischemic brain injury, epilepsy, and other diseases [64]. Collectively, these findings suggest that the four flavonoid compounds might exhibit a range of physiological activities as functional components in *Wuliangye* Baijiu. However, their actual activities in Baijiu and the related mechanisms were not experimentally verified in this study. It should also be noted that flavonoid concentrations in distilled spirits are generally low. Therefore, their actual concentrations, physiological relevance, and biological activities after oral administration and alcohol metabolism will require further verification in subsequent studies.

3.4. Enrichment Analysis of the Core Protein Targets

To explore the biological functions of the protein targets, 207 protein targets were imported into clusterProfiler for GO and KEGG enrichment analysis. The detailed results are respectively listed in Tables S5 and S6. A total of 1376 biological processes, 57 molecular functions, 190 cellular components, and 255 signaling pathways were obtained. The top ten significantly enriched GO terms and the top twenty significantly enriched KEGG pathways were visualized in Figure 3A,B, respectively. To further analyze the interactions between these protein targets and their functions in different pathways, ClueGO and CluePedia were used to cluster GO and KEGG terms with similar functions together. The terms were then merged and filtered to select the more representative ones. The relationships between gene functions were more intuitively displayed using network visualization, and the results are shown in Figure 4A–D. From this analysis, the conclusion could be easily obtained that for BP, the potential biological effects of the impact were related to regulation of miRNA transcription, nuclear receptor activity, voltage-gated cation channel activity, regulation of long-term synaptic potentiation, regulation of MAP kinase activity, ligand-gated cation channel activity, regulation of axon regeneration, G protein-coupled serotonin receptor activity, regulation of phosphatidylinositol 3-kinase activity, Gq/11-coupled serotonin receptor activity, sodium: chloride symporter activity, the prostaglandin biosynthetic process, the release of sequestered calcium ion into cytosol, activation of cysteine-type endopeptidase activity involved in the apoptotic process, and regulation of telomerase activity (Figure 4A). For CC, the potential biological effects of the impact were related to the synaptic membrane, cytoplasmic side of the membrane, protein kinase complex, dendrite, and membrane raft (Figure 4B). For MF, the potential biological effects of the impact were related to voltage-gated cation channel activity, negative regulation of protein kinase activity, regulation of cysteine-type endopeptidase activity involved in the apoptotic process, positive regulation of phospholipase activity, ligand-gated cation channel activity, positive regulation of lipid kinase activity, positive regulation of cyclin-dependent protein serine/threonine kinase activity, positive regulation of protein kinase

activity, and regulation of protein tyrosine kinase activity (Figure 4C). In addition, the highly enriched signal pathways were mainly involved in the PPAR signaling pathway, gap junction, adherens junction, serotonergic synapse, calcium signaling pathway, cAMP signaling pathway, neuroactive ligand–receptor interaction, dopaminergic synapse, steroid hormone biosynthesis, nitrogen metabolism, and chemical carcinogenesis (Figure 4D). These results may be related to the potential biological functions of *Wuliangye* Baijiu.

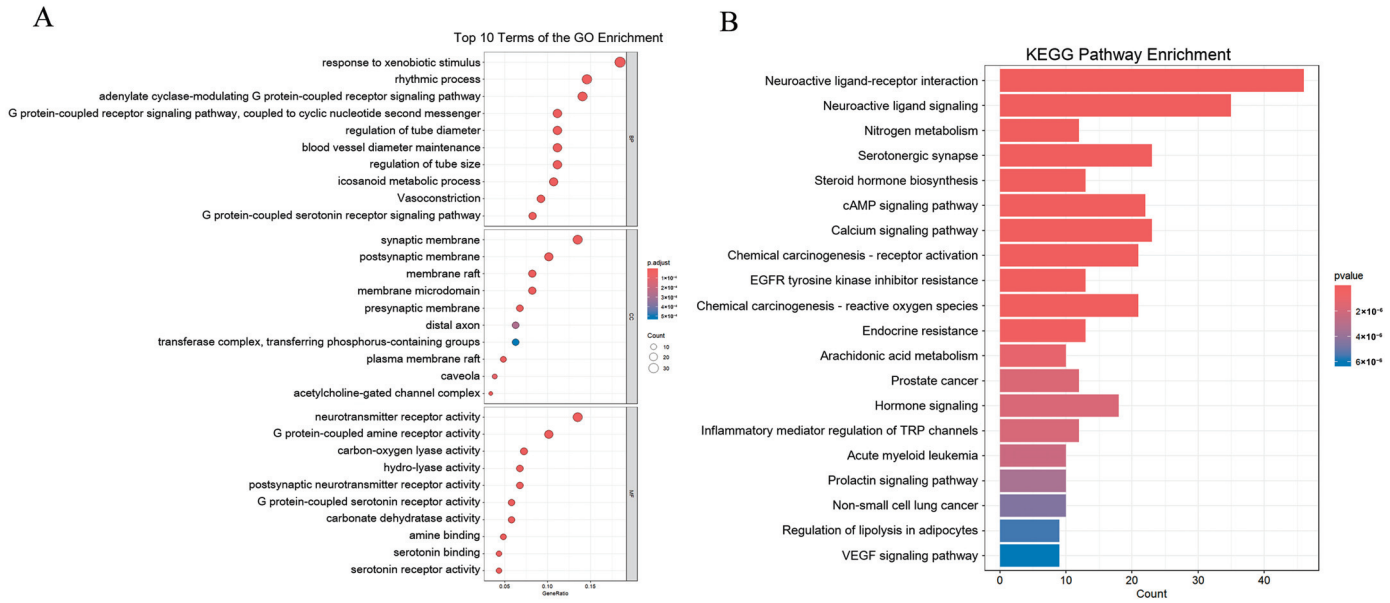


Figure 3. (**A**) Bar chart of GO enrichment analysis (top 10 in every category) of the targets (p.adjust < 0.05); (**B**) dotplot of top 20 signal pathways based on KEGG enrichment analysis (p.adjust < 0.05).

Moreover, the enrichment analysis also indicated that the functional components in *Wuliangye* Baijiu might broadly affect cellular physiological functions through various mechanisms involving cell signal transduction and regulation, gene expression and transcriptional control, neurophysiological functions, and cellular metabolism and apoptosis, as well as inflammation and immune responses. These functional components significantly influenced cellular response to external stimuli through the modulation of key signaling pathways, including the PPAR signaling pathway, calcium signaling pathway, and cAMP signaling pathway. These signaling pathways played crucial roles in fundamental processes, including cell proliferation, differentiation, metabolism, and apoptosis. For instance, PPARγ promoted lipid synthesis and fat storage by inducing the expression of adipocyte-specific genes such as FAS in adipose tissue, which helped regulate fatty acid metabolism and energy storage to maintain the homeostasis of adipose tissue [65]. Regulation of the calcium signaling pathway activates the influx of calcium ions into cells. Inhibition of calcium ion channels in satellite cells has been shown to significantly impact cellular activation and proliferation [66]. Additionally, functional components also regulated the activity of voltage-gated and ligand-gated ion channels, affecting the ion balance inside and outside of the cell. This regulation subsequently influenced neural signal conduction [67] and muscle contraction [68], both of which are vital for maintaining normal cellular physiological functions. With respect to neurophysiological function, these functional components significantly influenced neural signal transduction by modulating neuroactive ligand–receptor interactions, serotonin receptor activity, and dopaminergic synaptic function. These modulatory effects are of great importance for maintaining the normal function of the nervous system [69]. In cellular metabolism and apoptosis, functional components regulate the activity of PI3K, phospholipase, and lipase, which influences metabolic processes within

the cell. These modulatory effects impact not only cellular energy metabolism [70] but also cell survival and apoptosis [71].

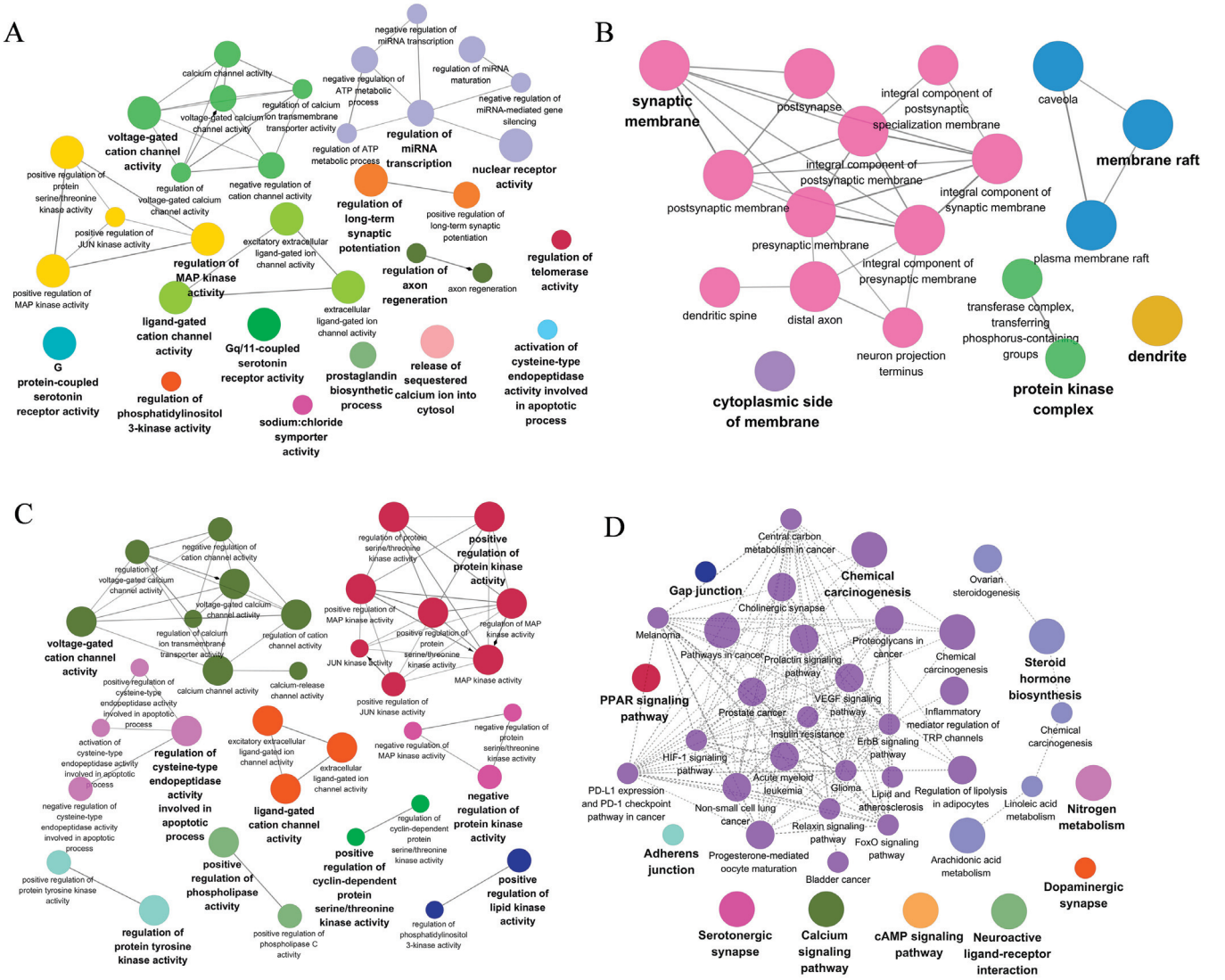


Figure 4. (**A**) Enrichment analysis of protein targets in biological process; (**B**) enrichment analysis of protein targets in cellular component; (**C**) enrichment analysis of protein targets in molecular function; (**D**) enrichment analysis of protein targets in metabolic pathways. Nodes represent significantly enriched GO terms, with size proportional to the number of enriched target genes (larger nodes = more genes). Node colors distinguish distinct functional clusters of related GO terms. Edges indicate shared target genes. All GO terms shown in the network were screened with an adjusted p-value < 0.05 to ensure statistical significance.

3.5. Disease Ontology Analysis

DO analysis enabled the identification of genes associated with specific diseases and facilitated the construction of disease-related gene or protein networks. In this study, the set of 207 protein targets was imported into DOSE for DO enrichment analysis to explore the diseases they may affect. The results showed that the 207 protein targets were associated with 311 diseases (Table S7). To more systematically understand the relationships between these diseases and their hierarchical positions within disease classification, the diseases were further categorized into primary and secondary entries, as detailed in Table S7. The 311 diseases were classified into 29 secondary entries and seven primary entries (Figure 5). Of the 207 protein targets, 57.8% targets were related to anatomical entity disease, 22.5% to

cellular proliferation disease, 14.4% to mental health disease, 2.8% to metabolism disease, 1.6% to infectious agent disease, 0.3% to genetic disease, and 0.3% to syndromes. In the secondary disease categories, the top four diseases were cancer, cardiovascular system disease, nervous system disease, and gastrointestinal system disease, which collectively accounted for 50.48% of the target-associated diseases. Taken all together, these computational predictions suggest that the active compounds in *Wuliangye* Baijiu may be potentially associated with regulating the development of cancer, cardiovascular system disease, nervous system disease, and gastrointestinal system disease by modulating protein targets. It should be emphasized that these were theoretical inferences from network pharmacology and thus require future experimental validation.

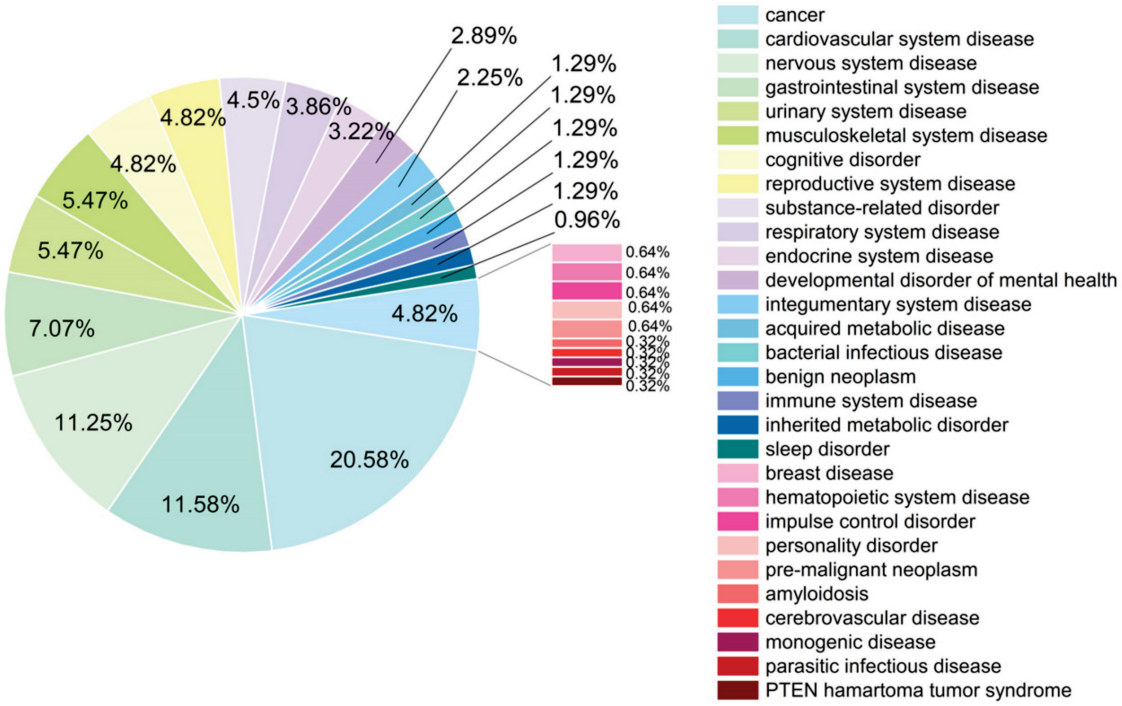


Figure 5. Pie plot of disease ontology terms of 207 targets. Percentages were calculated based on 311 disease entries and rounded for clarity. The total sum may not equal 100% due to rounding.

3.6. Compound–Target–Disease Network Analysis

Based on the C-T network obtained in Section 3.3 and the gene–disease relationships obtained in Section 3.5, a C-T-D network (Figure 6) was successfully constructed using the ten core targets (SRC, PIK3R1, PTGS1, AKR1B1, STAT3, CYP3A4, ESR1, PIK3CA, PIK3CB, and ALOX15) as connecting nodes. The resulting network comprised 62 nodes and 117 edges. In addition to the four key compounds, the ten core targets were also potential targets for multiple compounds. In primary disease classification, the diseases associated with the targets were anatomical entity disease, metabolism disease, cellular proliferation disease, mental health disease, and syndromes. In secondary disease classification, SRC was associated with the regulation of seven diseases, PIK3R1 with six diseases, PTGS1 with seven diseases, AKR1B1 with five diseases, STAT3 with 16 diseases, CYP3A4 with two diseases, ESR1 with 12 diseases, PIK3CA with seven diseases, PIK3CB with six diseases, and ALOX15 with four diseases. Notably, STAT3 and ESR1 were associated with the greatest number of disease types. STAT3 was a transcriptional regulatory factor with DNA-binding activity which regulated various biological processes, including cell proliferation, differentiation, autophagy, apoptosis, and inflammation. It regulated the growth hormone of lysine via the JAK2-STAT pathway, thereby promoting the transcription and expression of

genes involved in cell growth and metabolism in adipose tissue, liver, muscle, and bone [72]. Additionally, STAT3 has been shown to regulate Ca^{2+} flux by downregulating endoplasmic reticulum IP3R3, preventing the excessive release of proapoptotic factors, and modulating the activity of Bcl-2 family proteins to exert antiapoptotic functions [73]. Furthermore, STAT3 also regulated T cell responses to external stimuli, including proinflammatory cytokines and chemokines [74]. ESR1 is a member of the steroid hormone nuclear receptor family of transcription factors and exhibits broad functions. Specifically, it can inhibit lipid formation and white fat deposition by binding to target genes or regulating the transcription factors of key genes in adipocyte differentiation to reduce their phosphorylation [75]. ESR1 also regulates the expression of related genes, including Col1a1, Col1a2, and Col3a1, to protect the liver from fibrosis [76]. Collectively, the interactions of these protein targets and their compounds may contribute to the potential regulatory effects of *Wuliangye* Baijiu.

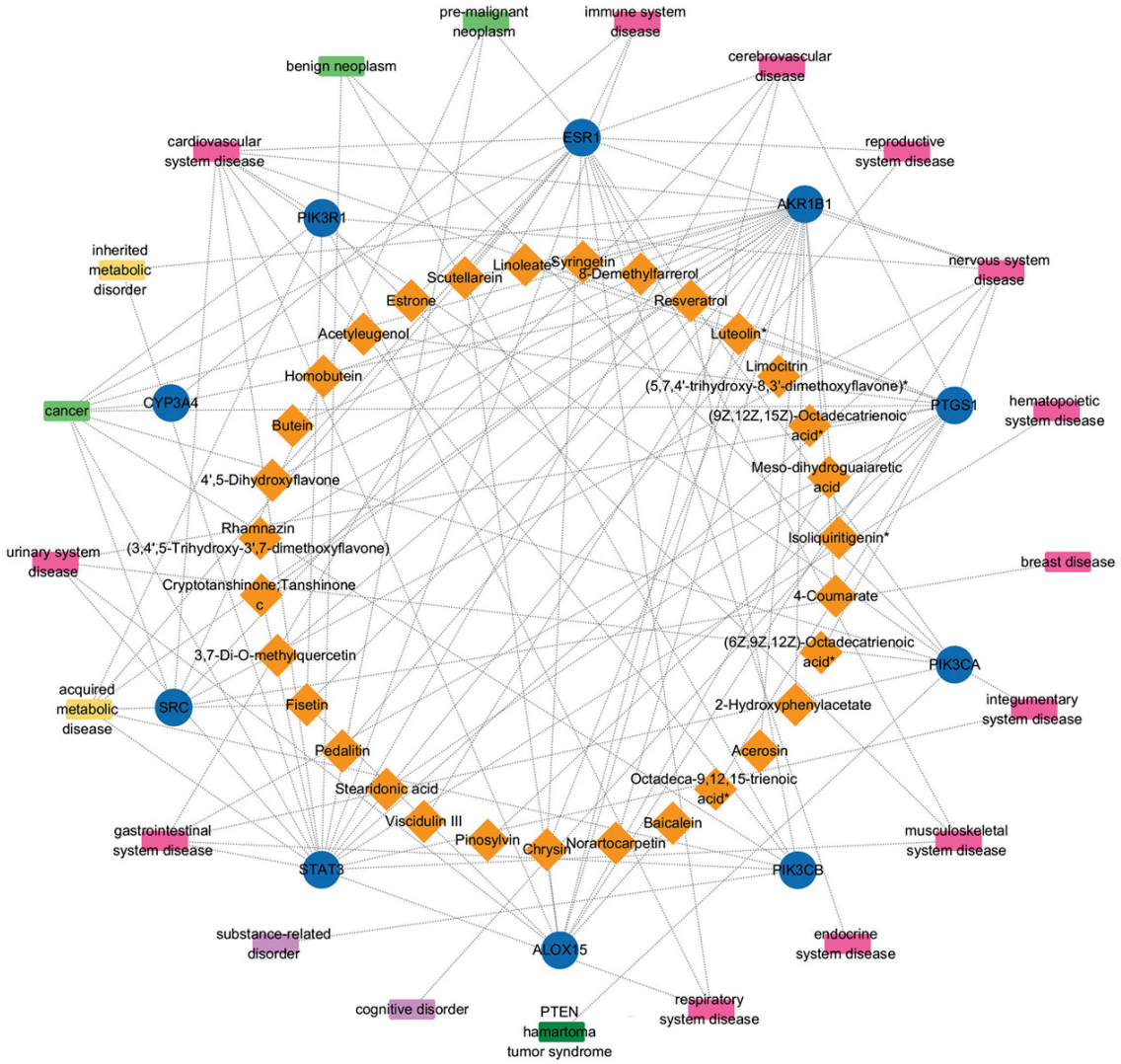


Figure 6. Compound–target–disease (C-T-D) networks of 10 core targets of *Wuliangye* Baijiu. Orange diamond nodes represent key active compounds, blue circular nodes represent core target proteins, and colored rectangular nodes represent related disease categories. Edges denote interactions or associations between nodes: compound–target edges indicate predicted binding, and target–disease edges indicate biological associations. * indicates that the corresponding compound has indistinguishable stereoisomers.

3.7. Molecular Docking Verification

Elucidating the molecular recognition mechanisms and associated intermolecular interactions through simulation of the spontaneous binding process of biomolecules was crucial for understanding compound–target interaction [77]. The interactions between the receptor and ligand typically included hydrogen bonds, electrostatic interactions, van der Waals forces, and hydrophobic interactions. The CDOCKER energy score was employed as a relative scoring metric to assess the potential binding affinity between small-molecule ligands and the target protein. It should be clearly stated that the CDOCKER energy score represents a relative empirical metric for ranking the binding affinity of ligands to the target protein. This score does not represent the true thermodynamic ΔG (Gibbs free energy) value. A more negative CDOCKER energy value generally indicates a stronger predicted binding capacity of the ligand to the target [78]. Based on the four key active compounds and the ten core targets, a total of 45 compound–target docking pairs were identified. The docking results of the computational docking simulation study are shown in Table S9. To assess the reliability of the docking protocol, redocking validation of the co-crystallized ligands was performed for six of the ten core targets (excluding PIK3R1, STAT3, CYP3A4, and PIK3CB). The root mean square deviation (RMSD) values of these six validated targets were all below 2.0 Å, confirming the reliability of the docking results for these targets. For the remaining four targets (PIK3CB, PIK3R1, STAT3, and CYP3A4), high-quality, drug-like co-crystallized ligands suitable for redocking validation could not be identified in the PDB database (available structures only contained cofactors, small-molecule additives, or modified residues), so redocking validation could not be performed. Therefore, the docking results of these four targets should be considered as predictive and require further experimental verification in the future.

The docking results showed that all the CDOCKER energy values were less than 0 kcal/mol^{-1}, except for the docking of stearidonic acid with PTGS1, indicating that the ten core targets exhibited good docking characteristics and binding affinity with their active compounds. Notably, the CDOCKER energy values of the complexes formed between the key compounds and their respective core targets were all lower than -30 kcal/mol^{-1}, indicating high binding affinities and stability between them. The binding affinities of the ten compounds–targets were attributed to hydrogen bonds, hydrophobic interactions, and van der Waals forces from multiple amino acid residues (Figure 7). Taking Fisetin-ALOX25 as an example, fisetin interacted with Lys141, Asp161, Ala25, and Val27 through hydrogen bonds and contacts with amino acid residues Ile160, Lys52, Lys141 through hydrophobic interactions. These interactions collectively promoted the tight binding between the compounds and their targets.

Overall, the molecular docking results indicated that the majority of target–compound pairs exhibited favorable binding characteristics, with the exception of the interaction between stearidonic acid and PTGS1. In particular, the complexes formed between the key compounds and their core targets exhibited tight association through various types of interactions. Notably, the docking results of the six validated targets (with RMSD < 2.0 Å) were reliable, while the results of the four targets without redocking validation were predictive and needed further experimental confirmation. These findings were consistent with the results of the preceding network pharmacology analyses, further supporting the potential of these compounds as functional components in *Wuliangye* Baijiu.

https://doi.org/10.3390/foods15091509

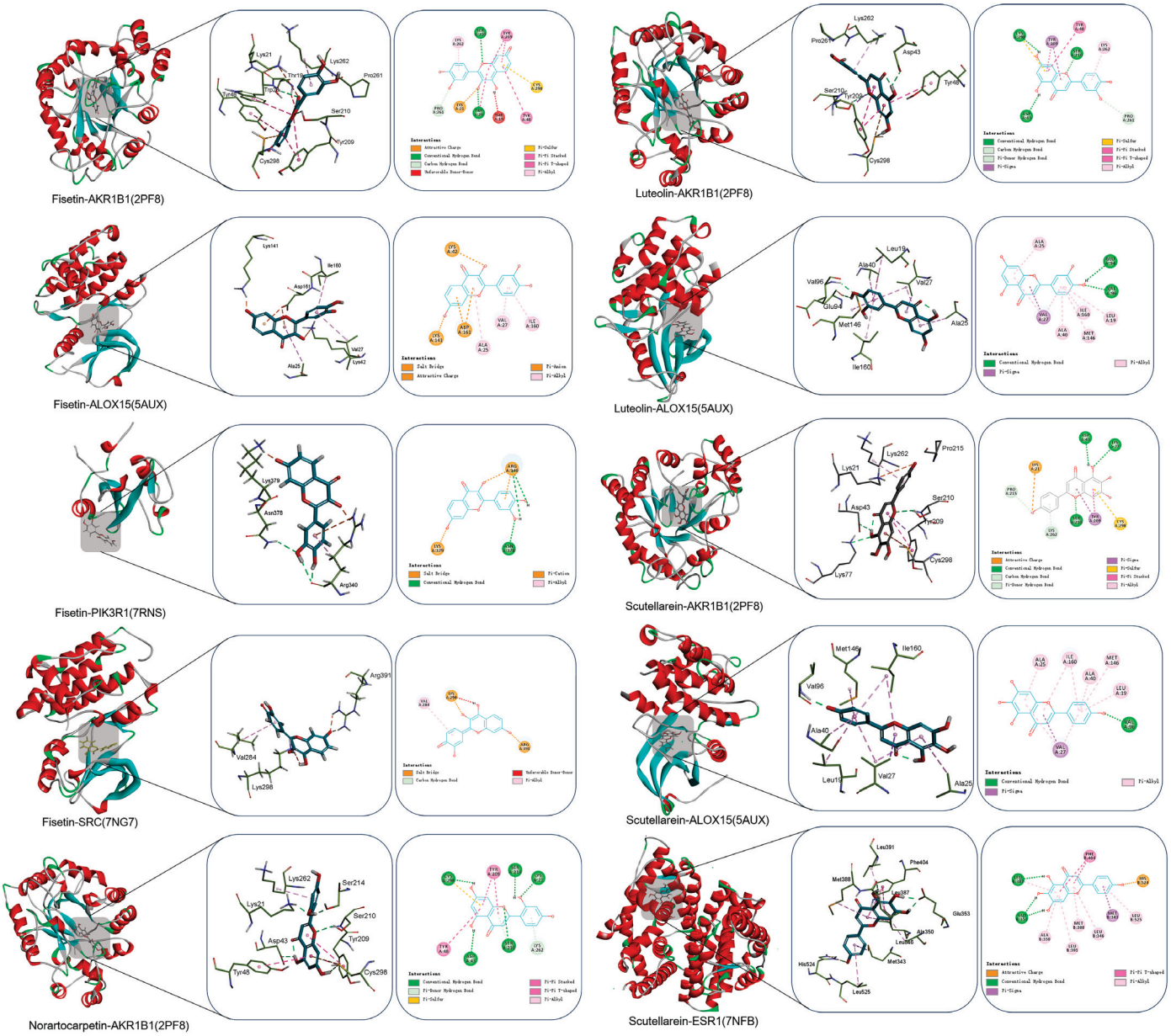


Figure 7. Molecular binding pattern of the ten complexes.

4. Conclusions

This study innovatively integrated widely targeted metabolomics and network pharmacology approaches, establishing a novel systematic analytical method for identifying functional components in Baijiu. Through this approach, four key active compounds, including fisetin, luteolin, norartocarpetin, and scutellarein, were identified for the first time. Then, network pharmacology revealed their potential interactions with multiple biological targets. Moreover, ten core targets, including SRC, PIK3R1, PTGS1, AKR1B1, STAT3, CYP3A4, ESR1, PIK3CA, PIK3CB, and ALOX15, were ultimately identified. These targets played critical roles in diverse physiological and pathological processes involving inflammation, oxidative stress, cell signaling, immune response, and other aspects. Both network analysis and subsequent molecular docking validation revealed complex interactions between the key active compounds and their targets, which may theoretically contribute to the potential health-related properties of *Wuliangye* Baijiu.

However, it should be acknowledged that the present research is mainly based on in vitro analysis and computational simulation, lacking the separation and extraction of

these bioactive compounds, as well as more comprehensive in vivo studies. Therefore, further research is warranted to elucidate the specific efficacy and potential mechanisms of these compounds.

Supplementary Materials: The following supporting information can be downloaded at: https://www.mdpi.com/article/10.3390/foods15091509/s1, Table S1: a list of 2128 compounds from *Wuliangye* Baijiu; Table S2: the physicochemical properties, pharmacokinetics parameters, and druglikeness of 445 potential active compounds; Table S3: a list of the interactions between 127 active compounds and 207 targets; Table S4: the shared compositions of the targets and the active compounds in *Wuliangye* Baijiu; Table S5: the list of biological processes (BPs), molecular function (MF), and cellular components (CCs) category terms from GO enrichment analysis; Table S6: the list of key pathway terms from KEGG enrichment analysis; Table S7: the list of significant DO terms and their parent terms; Table S8: The list of the compound–target–disease network based on 10 key targets; Table S9: The parameter and result of molecular docking.

Author Contributions: Conceptualization, J.L. and J.W.; methodology, J.L.; software, J.Z.; validation, J.L., J.Z. and M.H.; formal analysis, Y.S.; investigation, F.Z.; resources, J.S.; data curation, J.L.; writing—original draft preparation, J.L.; writing—review and editing, J.W.; visualization, M.H.; supervision, D.Z.; project administration, J.S.; funding acquisition, J.W. All authors have read and agreed to the published version of the manuscript.

Funding: This research was funded by the National Key Research and Development Program of China (2022YFD2101205) and the Open Foundation of Key Laboratory of Wuliangye-flavor Liquor Solid-state Fermentation, China National Light Industry (2023JJ005).

Institutional Review Board Statement: Not applicable.

Informed Consent Statement: Not applicable.

Data Availability Statement: The original contributions presented in this study are included in the article and Supplementary Materials. Further inquiries can be directed to the corresponding author.

Conflicts of Interest: The authors declare that this study received funding from the Open Foundation of Key Laboratory of Wuliangye-flavor Liquor Solid-state Fermentation, China National Ligh Industry (2023JJ005). The funder was not involved in the study design, collection, analysis, interpretation of data, the writing of this article, or the decision to submit it for publication. Authors Jia Zheng and Jian Su were employed by the Wuliangye Yibin Co., Ltd. Their contributions to the manuscript were: software, validation, resources, and project administration. The remaining authors declare that the research was conducted in the absence of any commercial or financial relationships that could be construed as potential conflicts of interest.

Abbreviations

The following abbreviations are used in this manuscript:

NF-κB	nuclear factor-κB
PI3K	phosphatidylinositol-3 kinase
AKT	protein kinase B
GO	Gene ontology
KEGG	Kyoto Encyclopedia of Genes and Genomes
DO	Disease ontology
MAPK	mitogen-activated protein kinase
SRC	Tyrosine-protein kinase SRC
PIK3R1	PI3-kinase p85-alpha subunit
PTGS1	Cyclooxygenase-1
AKR1B1	Aldose reductase
STAT3	Signal transducer and activator of transcription 3
CYP3A4	Cytochrome P450 3A4

ESR1	Estrogen receptor alpha
PIK3CA	PI3-kinase p110-alpha subunit
PIK3CB	PI3-kinase p110-beta subunit
ALOX15	Arachidonate 15-lipoxygenase

References

1. Liu, H.; Sun, B. Effect of Fermentation Processing on the Flavor of Baijiu. *J. Agric. Food Chem.* **2018**, *66*, 5425–5432. [CrossRef]
2. Pan, F.; Qiu, S.; Lv, Y.; Li, D. Exploring the controllability of the Baijiu fermentation process with microbiota orientation. *Food Res. Int.* **2023**, *173*, 113249. [CrossRef]
3. Ding, H.; Ao, L.; Deng, B.; Ao, Z.; Song, C.; Liu, M.; Lin, F. Analysis of Trace Healthy Components in Chinese Baijiu. *China Brew.* **2018**, *37*, 11–14. [CrossRef]
4. Qin, D.; Duan, J.; Li, H.; Zheng, F.; Cheng, H.; Ye, X.; Sun, B. Characterization and comparison of the aroma-active compounds on different grades of sesame-flavor Baijiu by headspace solid-phase microextraction and gas chromatography-olfactometry-mass spectrometry. *Food Sci. Hum. Wellness* **2023**, *12*, 79–88. [CrossRef]
5. Duan, J.; Cheng, W.; Lv, S.; Deng, W.; Hu, X.; Li, H.; Sun, J.; Zheng, F.; Sun, B. Characterization of key aroma compounds in soy sauce flavor Baijiu by molecular sensory science combined with aroma active compounds reverse verification method. *Food Chem.* **2024**, *443*, 138487. [CrossRef] [PubMed]
6. Wang, L.; Tang, P.; Zhang, P.; Lu, J.; Chen, Y.; Xiao, D.; Guo, X. Unraveling the aroma profiling of Baijiu: Sensory characteristics of aroma compounds, analytical approaches, key odor-active compounds in different Baijiu, and their synthesis mechanisms. *Trends Food Sci. Technol.* **2024**, *146*, 104376. [CrossRef]
7. Wang, J.; Chen, H.; Wu, Y.; Zhao, D. Uncover the flavor code of strong-aroma Baijiu: Research progress on the revelation of aroma compounds in strong-aroma Baijiu by means of modern separation technology and molecular sensory evaluation. *J. Food Compos. Anal.* **2022**, *109*, 104499. [CrossRef]
8. Wu, J.; Huang, M.; Zheng, F.; Sun, J.; Sun, X.; Li, H.; Sun, B. Research Progress of Healthy Baijiu. *J. Food Sci. Technol. China* **2019**, *37*, 17–23. [CrossRef]
9. Zhu, H.; Gu, B.; Zhao, D.; Ma, Y.; Mehmood, M.A.; Li, Y.; Yang, K.; Wang, Y.; He, M.; Zheng, J.; et al. Wuliangye strong aroma Baijiu promotes intestinal homeostasis by improving gut microbiota and regulating intestinal stem cell proliferation and differentiation. *J. Sci. Food Agric.* **2024**, *104*, 7417–7428. [CrossRef]
10. Luo, Q.; Liu, J.; Liu, Z.G. Study on the Anti-Inflammatory Effect of Bioactive Substances in sauce-flavored Liquor on Human Gastric Epithelial Cells Induced by Helicobacter Pylori Metabolites. *Food Ferment. Technol.* **2020**, *56*, 11–17.
11. Zhao, X.; Wang, Z.; Tang, F.; Cai, W.; Peng, B.; Shan, C. Exploring jujube wine flavor and fermentation mechanisms by HS-SPME-GC-MS and UHPLC-MS metabolomics. *Food Chem. X* **2024**, *21*, 101115. [CrossRef]
12. Hopkins, A.L. Network pharmacology: The next paradigm in drug discovery. *Nat. Chem. Biol.* **2008**, *4*, 682–690. [CrossRef] [PubMed]
13. Reddy, A.S.; Zhang, S. Polypharmacology: Drug discovery for the future. *Expert. Rev. Clin. Pharmacol.* **2013**, *6*, 41–47. [CrossRef] [PubMed]
14. Li, A.; Li, H.; Wang, C.; Qin, J.; Han, X.; Wang, D.; Hao, F. Research Progress of Bioactive Components in Baijiu: A Minireview. *Nutr. Food Sci. Int. J.* **2020**, *10*, 555790.
15. Zeng, Y.; Hu, S.; Liu, H.; Huang, M. Progress in bioactive peptides in Baijiu, fermented grains, and distiller's grains. *China Brew.* **2025**, *44*, 1–7. [CrossRef]
16. Hu, S.; Zeng, Y.; Liu, H.; Huang, M.; Li, H.; Deng, W.W.; Wu, J.; Li, H.; Sun, X. Systematic profiling and bioactivity evaluation of Jiuzao from light flavor Baijiu: A by-product rich in bioactive compounds. *Food Chem.* **2025**, *494*, 13. [CrossRef]
17. Guan, C.; Zhou, F.; Ma, P.; Sun, J.; Chen, T.; Liu, D.; Qiu, S. High-Value Applications of Bioactive Polysaccharides and Functional Components from Baijiu Distillers' Grains: A Review. *Agriculture* **2026**, *16*, 527. [CrossRef]
18. Xi, Q.; Tian, X.; Zhou, T.; Liu, S.; Li, Q.; Wang, Z. Widely targeted metabolomics analysis of metabolite changes during wolfberry wine brewing. *Food Sci. China* **2024**, *45*, 141–149. [CrossRef]
19. Fang, S.; Dong, L.; Liu, L.; Guo, J.; Zhao, L.; Zhang, J.; Bu, D.; Liu, X.; Huo, P.; Cao, W.; et al. HERB: A high-throughput experiment- and reference-guided database of traditional Chinese medicine. *Nucleic Acids Res.* **2021**, *49*, D1197–D1206. [CrossRef]
20. Daina, A.; Michielin, O.; Zoete, V. SwissADME: A free web tool to evaluate pharmacokinetics, drug-likeness and medicinal chemistry friendliness of small molecules. *Sci. Rep.* **2017**, *7*, 42717. [CrossRef]
21. Li, D.; Chen, R.; Xu, X.; Hou, Y.; Li, Z.; Huang, C.; Zhang, G.; Wang, B.; Li, B.; Chu, X. Integrated metabolomics and network pharmacology to reveal the mechanisms of Shexiang Baoxin pill against atherosclerosis. *Phytomedicine* **2024**, *135*, 156138. [CrossRef] [PubMed]
22. Daina, A.; Michielin, O.; Zoete, V. SwissTargetPrediction: Updated data and new features for efficient prediction of protein targets of small molecules. *Nucleic Acids Res.* **2019**, *47*, W357–W364. [CrossRef] [PubMed]

23. Zhou, Y.; Lin, S.; Zhong, X.; Huang, F.; Huang, J.; Xu, L. Oleanolic acid combined with aspirin plays antitumor roles in colorectal cancer via the Akt/NFκB/IκBα/COX2 pathway. *Cell Death Discov.* **2024**, *10*, 504. [CrossRef] [PubMed]
24. Shannon, P.; Markiel, A.; Ozier, O.; Baliga, N.S.; Wang, J.T.; Ramage, D.; Amin, N.; Schwikowski, B.; Ideker, T. Cytoscape: A software environment for integrated models of biomolecular interaction networks. *Genome Res.* **2003**, *13*, 2498–2504. [CrossRef]
25. Chin, C.H.; Chen, S.H.; Wu, H.H.; Ho, C.W.; Ko, M.T.; Lin, C.Y. CytoHubba: Identifying hub objects and sub-networks from complex interactome. *BMC Syst. Biol.* **2014**, *8*, S11. [CrossRef]
26. Wang, X.; Zhao, W.; Zhang, X.; Wang, Z.; Han, C.; Xu, J.; Yang, G.; Peng, J.; Li, Z. An integrative analysis to predict the active compounds and explore polypharmacological mechanisms of Orthosiphon stamineus Benth. *Comput. Biol. Med.* **2023**, *163*, 107160. [CrossRef]
27. Wu, T.; Hu, E.; Xu, S.; Chen, M.; Guo, P.; Dai, Z.; Feng, T.; Zhou, L.; Tang, W.; Zhan, L.; et al. ClusterProfiler 4.0: A universal enrichment tool for interpreting omics data. *Innovation* **2021**, *2*, 100141. [CrossRef]
28. Mlecnik, B.; Galon, J.; Bindea, G. Comprehensive functional analysis of large lists of genes and proteins. *J. Proteom.* **2018**, *171*, 2–10. [CrossRef]
29. Schriml, L.M.; Munro, J.B.; Schor, M.; Olley, D.; McCracken, C.; Felix, V.; Baron, J.A.; Jackson, R.; Bello, S.M.; Bearer, C.; et al. The Human Disease Ontology 2022 update. *Nucleic Acids Res.* **2022**, *50*, D1255–D1261. [CrossRef]
30. Yu, G.; Wang, L.G.; Yan, G.R.; He, Q.Y. DOSE: An R/Bioconductor package for disease ontology semantic and enrichment analysis. *Bioinformatics* **2015**, *31*, 608–609. [CrossRef]
31. Feng, M.X.; Gan, L.Y.; Zhao, Q.; Chen, Y.; Xiao, D.; Guo, X. Terpenoid Compounds and Traceability Analysis During the Brewing Process of Luzhou-Flavored Baijiu. *Food Sci. China* **2023**, *44*, 254–261. [CrossRef]
32. Wang, L.; Hu, G.; Lei, L.; Lin, L.; Wang, D.; Wu, J. Identification and Aroma Impact of Volatile Terpenes in Moutai Liquor. *Int. J. Food Prop.* **2015**, *19*, 1335–1352. [CrossRef]
33. Antoniuk, O.; Maranha, A.; Salvador, J.A.R.; Empadinhas, N.; Moreira, V.M. Bi- and tricyclic diterpenoids: Landmarks from a decade (2013—2023) in search of leads against infectious diseases. *Nat. Prod. Rep.* **2024**, *41*, 1858–1894. [CrossRef] [PubMed]
34. Yang, K.; Han, Q.T.; Xing, R.X.; Li, Z.Y.; Xu, L.T.; Chen, L.Z.; Xiang, L.; Ren, D.M.; Hu, Q.W.; Wang, X.N.; et al. Sphaeropsidin A covalently binds to Cys 151 of Keap1 to attenuate LPS-induced acute pneumonia in mice. *Redox Biol.* **2025**, *82*, 103621. [CrossRef]
35. Wang, D.D.; Zhang, R.; Tang, L.Y.; Wang, L.N.; Ao, M.R.; Jia, J.M.; Wang, A.H. Identification of diterpenoids from Salvia castanea Diels f. tomentosa Stib and their antitumor activities. *Bioorg Chem.* **2024**, *151*, 107701. [CrossRef]
36. Deng, R.; Chen, X.; Zhao, S.; Zhang, Q.; Shi, Y. The effects and mechanisms of natural products on Helicobacter pylori eradication. *Front. Cell. Infect. Microbiol.* **2024**, *14*, 1360852. [CrossRef]
37. Plazas, E.; Avila, M.M.; Munoz, D.R.; Cuca, S.L. Natural isoquinoline alkaloids: Pharmacological features and multi-target potential for complex diseases. *Pharmacol. Res.* **2022**, *177*, 106126. [CrossRef]
38. Zhao, G.; He, F.; Wu, C.; Li, P.; Li, N.; Deng, J.; Zhu, G.; Ren, W.; Peng, Y. Betaine in Inflammation: Mechanistic Aspects and Applications. *Front. Immunol.* **2018**, *9*, 1070. [CrossRef]
39. Matt, S.M.; Gaskill, P.J. Where Is Dopamine and how do Immune Cells See it?: Dopamine-Mediated Immune Cell Function in Health and Disease. *J. Neuroimmune Pharmacol.* **2020**, *15*, 114–164. [CrossRef]
40. Xiao, D.G. Discussion on the formation mechanism of esters during Baijiu Brewing. *Liquor. Mak. Sci. Technol.* **2022**, 17–24. [CrossRef]
41. Kwon, J.O.; Jin, W.J.; Kim, B.; Kim, H.H.; Lee, Z.H. Myristoleic acid inhibits osteoclast formation and bone resorption by suppressing the RANKL activation of Src and Pyk2. *Eur. J. Pharmacol.* **2015**, *768*, 189–198. [CrossRef]
42. Guerra-Vazquez, C.M.; Martinez-Avila, M.; Guajardo-Flores, D.; Antunes-Ricardo, M. Punicic acid and its role in the prevention of neurological disorders: A review. *Foods* **2022**, *11*, 252. [CrossRef] [PubMed]
43. Golanski, J.; Szymanska, P.; Rozalski, M. Effects of omega-3 polyunsaturated fatty acids and their metabolites on haemostasis-current perspectives in cardiovascular disease. *Int. J. Mol. Sci.* **2021**, *22*, 2394. [CrossRef] [PubMed]
44. Giblin, A.; Cammack, A.J.; Blomberg, N.; Anoar, S.; Mikheenko, A.; Carcole, M.; Atilano, M.L.; Hull, A.; Shen, D.; Wei, X.; et al. Neuronal polyunsaturated fatty acids are protective in ALS/FTD. *Nat. Neurosci.* **2025**, *28*, 737–747. [CrossRef] [PubMed]
45. Munteanu, C.; Schwartz, B. The relationship between nutrition and the immune system. *Front. Nutr.* **2022**, *9*, 1082500. [CrossRef]
46. Niu, Y.; Qiao, M.; Ye, Y.; Li, T.; Xu, L.; Xu, L.; Xiao, Z. Effects of amino acids on the release of acidic odor compounds in Langjiu and its potential mechanisms. *J. Food Compos. Anal.* **2025**, *137*, 106987. [CrossRef]
47. Bachmanov, A.A.; Bosak, N.P.; Glendinning, J.I.; Inoue, M.; Li, X.; Manita, S.; McCaughey, S.A.; Murata, Y.; Reed, D.R.; Tordoff, M.G.; et al. Genetics of amino acid taste and appetite. *Adv. Nutr.* **2016**, *7*, 806S–822S. [CrossRef]
48. Zhang, L.; Xu, L.Y.; Tang, F.; Liu, D.; Zhao, X.L.; Zhang, J.N.; Xia, J.; Wu, J.J.; Yang, Y.; Peng, C.; et al. New perspectives on the therapeutic potential of quercetin in non-communicable diseases: Targeting Nrf2 to counteract oxidative stress and inflammation. *J. Pharm. Anal.* **2024**, *14*, 100930. [CrossRef]
49. Peng, Y.; Qu, R.; Xu, S.; Bi, H.; Guo, D. Regulatory mechanism and therapeutic potentials of naringin against inflammatory disorders. *Heliyon* **2024**, *10*, e24619. [CrossRef]

50. Di Petrillo, A.; Orru, G.; Fais, A.; Fantini, M.C. Quercetin and its derivates as antiviral potentials: A comprehensive review. *Phytother. Res.* **2022**, *36*, 266–278. [CrossRef]
51. Shi, N.; Pei, X.X.; Li, M.Y.; Chen, W.T.; Li, H.Q.; Yang, G.S.; Duan, C.Q.; Wang, J. Metabolomics of *Vitis davidii* Foex. grapes from southern China: Flavonoids and volatiles reveal the flavor profiles of five spine grape varieties. *Food Chem.* **2024**, *454*, 139732. [CrossRef]
52. Li, Q.Z.; Wang, J.R.; Zhang, X.L.; Fu, C.; Wang, C.; Xu, N.; Lv, W. Research progress on the flavor substance 4-Vinylguaiacol. *China Brew.* **2021**, *40*, 15–19. [CrossRef]
53. Sun, X.T.; Wang, Z.Y.; Liu, M.; Ao, L.; Sun, B.; Sun, J.; Zheng, F.; Huang, M.; Li, H. Determination of tetramethylpyrazine, 4-Methylguaiacol and 4-ethylguaiacol in 67 Baijiu samples by vortex-assisted liquid-liquid microextraction combined with GC-MS. *Food Sci.* **2017**, *38*, 73–79. [CrossRef]
54. Zhou, J.; Guan, J.; Wei, H.; Cao, J.; Chen, M.; Zhang, M.; Fang, S. Research progress on health factors in Baijiu. *Brew. Sci. Technol.* **2017**, 90–94. [CrossRef]
55. Yan, Y.; Zou, M.; Tang, C.; Ao, H.; He, L.; Qiu, S.; Li, C. The insights into sour flavor and organic acids in alcoholic beverages. *Food Chem.* **2024**, *460*, 140676. [CrossRef]
56. Waterhouse, A.L.; Miao, Y. Can chemical analysis predict wine aging capacity? *Foods* **2021**, *10*, 654. [CrossRef]
57. Zhang, X.J.; Jia, S.S. Fisetin inhibits laryngeal carcinoma through regulation of AKT/NF-κB/mTOR and ERK1/2 signaling pathways. *Biomed. Pharmacother.* **2016**, *83*, 1164–1174. [CrossRef]
58. Ren, Q.; Guo, F.; Tao, S.; Huang, R.; Ma, L.; Fu, P. Flavonoid fisetin alleviates kidney inflammation and apoptosis via inhibiting Src-mediated NF-κB p65 and MAPK signaling pathways in septic AKI mice. *Biomed. Pharmacother.* **2020**, *122*, 109772. [CrossRef]
59. Currais, A.; Farrokhi, C.; Dargusch, R.; Armando, A.; Quehenberger, O.; Schubert, D.; Maher, P. Fisetin reduces the impact of aging on behavior and physiology in the rapidly aging SAMP8 mouse. *J. Gerontol. A Biol. Sci. Med. Sci.* **2018**, *73*, 299–307. [CrossRef]
60. Li, X.; Jin, Q.; Yao, Q.; Xu, B.; Li, L.; Zhang, S.; Tu, C. The flavonoid quercetin ameliorates liver inflammation and fibrosis by regulating hepatic macrophages activation and polarization in mice. *Front. Pharmacol.* **2018**, *9*, 72. [CrossRef]
61. Gendrisch, F.; Esser, P.R.; Schempp, C.M.; Wolfle, U. Luteolin as a modulator of skin aging and inflammation. *Biofactors* **2021**, *47*, 170–180. [CrossRef] [PubMed]
62. Ko, H.H.; Tsai, Y.T.; Yen, M.H.; Lin, C.C.; Liang, C.J.; Yang, T.H.; Lee, C.W.; Yen, F.L. Norartocarpetin from a folk medicine Artocarpus communis plays a melanogenesis inhibitor without cytotoxicity in B16F10 cell and skin irritation in mice. *BMC Complement. Altern. Med.* **2013**, *13*, 348. [CrossRef] [PubMed]
63. Tuli, H.S.; Bhushan, S.; Kumar, A.; Aggarwal, P.; Sak, K.; Ramniwas, S.; Vashishth, K.; Behl, T.; Rana, R.; Haque, S.; et al. Autophagy induction by scutellaria flavones in cancer: Recent advances. *Pharmaceuticals* **2023**, *16*, 302. [CrossRef] [PubMed]
64. Tao, Y.H.; Jiang, D.Y.; Xu, H.B.; Yang, X.L. Inhibitory effect of Erigeron breviscapus extract and its flavonoid components on GABA shunt enzymes. *Phytomedicine* **2008**, *15*, 92–97. [CrossRef]
65. Gilardi, F.; Winkler, C.; Quignodon, L.; Diserens, J.G.; Toffoli, B.; Schiffrin, M.; Sardella, C.; Preitner, F.; Desvergne, B. Systemic PPARγ deletion in mice provokes lipoatrophy, organomegaly, severe type 2 diabetes and metabolic inflexibility. *Metabolism* **2019**, *95*, 8–20. [CrossRef]
66. Hara, M.; Tabata, K.; Suzuki, T.; Do, M.K.; Mizunoya, W.; Nakamura, M.; Nishimura, S.; Tabata, S.; Ikeuchi, Y.; Sunagawa, K.; et al. Calcium influx through a possible coupling of cation channels impacts skeletal muscle satellite cell activation in response to mechanical stretch. *Am. J. Physiol. Cell Physiol.* **2012**, *302*, C1741–C1750. [CrossRef]
67. Beg, A.A.; Jorgensen, E.M. EXP-1 is an excitatory GABA-gated cation channel. *Nat. Neurosci.* **2003**, *6*, 1145–1152. [CrossRef]
68. Roberts, J.A.; Evans, R.J. Cysteine substitution mutants give structural insight and identify ATP binding and activation sites at P2X receptors. *J. Neurosci.* **2007**, *27*, 4072–4082. [CrossRef]
69. Masato, A.; Plotegher, N.; Boassa, D.; Bubacco, L. Impaired dopamine metabolism in Parkinson's disease pathogenesis. *Mol. Neurodegener.* **2019**, *14*, 35. [CrossRef]
70. Caron, A.; Richard, D.; Laplante, M. The roles of mTOR complexes in lipid metabolism. *Annu. Rev. Nutr.* **2015**, *35*, 321–348. [CrossRef]
71. Goncalves, M.D.; Hopkins, B.D.; Cantley, L.C. Phosphatidylinositol 3-Kinase, Growth Disorders, and Cancer. *N. Engl. J. Med.* **2018**, *379*, 2052–2062. [CrossRef]
72. Wojcik, M.; Krawczynska, A.; Antushevich, H.; Herman, A.P. Post-receptor inhibitors of the GHR-JAK2-STAT pathway in the growth hormone signal transduction. *Int. J. Mol. Sci.* **2018**, *19*, 1843. [CrossRef]
73. Avalle, L.; Camporeale, A.; Morciano, G.; Caroccia, N.; Ghetti, E.; Orecchia, V.; Viavattene, D.; Giorgi, C.; Pinton, P.; Poli, V. STAT3 localizes to the ER, acting as a gatekeeper for ER-mitochondrion Ca^{2+} fluxes and apoptotic responses. *Cell Death Differ.* **2019**, *26*, 932–942. [CrossRef]
74. Yoshida, N.; He, F.; Kyttaris, V.C. T cell-specific STAT3 deficiency abrogates lupus nephritis. *Lupus* **2019**, *28*, 1468–1472. [CrossRef]

75. Palmisano, B.T.; Zhu, L.; Stafford, J.M. Role of estrogens in the regulation of liver lipid metabolism. *Adv. Exp. Med. Biol.* **2017**, *1043*, 227–256. [CrossRef]
76. Li, T.; Wang, G.; Zhao, H.; Liu, F.; Deng, Z.; Chen, D.; Zhou, X.; Cao, Y.; Fu, W.; Zhang, H.; et al. Estrogen receptor 1 signaling in hepatic stellate cells designates resistance to liver fibrosis. *Cell Discov.* **2025**, *11*, 37. [CrossRef]
77. Dror, R.O.; Green, H.F.; Valant, C.; Borhani, D.W.; Valcourt, J.R.; Pan, A.C.; Arlow, D.H.; Canals, M.; Lane, J.R.; Rahmani, R.; et al. Structural basis for modulation of a G-protein-coupled receptor by allosteric drugs. *Nature* **2013**, *503*, 295–299. [CrossRef]
78. Hsin, K.Y.; Matsuoka, Y.; Asai, Y.; Kamiyoshi, K.; Watanabe, T.; Kawaoka, Y.; Kitano, H. SystemsDock: A web server for network pharmacology-based prediction and analysis. *Nucleic Acids Res.* **2016**, *44*, W507–W513. [CrossRef] [PubMed]

Disclaimer/Publisher's Note: The statements, opinions and data contained in all publications are solely those of the individual author(s) and contributor(s) and not of MDPI and/or the editor(s). MDPI and/or the editor(s) disclaim responsibility for any injury to people or property resulting from any ideas, methods, instructions or products referred to in the content.

foods

MDPI

Article

Decoding the Flavor Code of Fresh and Dried *Tengjiao* (*Zanthoxylum armatum* DC.) for Preparing Fried *Tengjiao* Oil Through Molecular Sensory Science

Tianyu Dong, Panpan Wu, Jie Sun *, Haitao Chen * and Shuqi Wang

Beijing Key Laboratory of Flavor Chemistry, Beijing Technology and Business University, Beijing 100048, China; dty19991030@163.com (T.D.); 18617240636@163.com (P.W.); wangshuqi@btbu.edu.cn (S.W.)
* Correspondence: sunjie@btbu.edu.cn (J.S.); chenht@th.btbu.edu.cn (H.C.)

Abstract

Fried *Tengjiao* oil is commonly used for seasoning spicy dishes, and both fresh and dried *Tengjiao* are used in its preparation. However, the flavor differences between fried *Tengjiao* oils prepared from these two types of raw materials have not yet been studied. The aim of this study was to compare and analyze the flavor differences between fresh fried *Tengjiao* oil (FFTO) and dried fried *Tengjiao* oil (DFTO). In this study, molecular sensory science was employed to reveal the flavor differences between the two at the molecular level. FFTO had a stronger pepper and spice aroma, while DFTO exhibited a more marked oily aroma. A total of 82 volatile compounds were identified via SAFE-GC-MS (solvent-assisted flavor evaporation–gas chromatography–mass spectrometry). Based on AEDA (aroma extract concentration analysis), 36 aroma-active compounds with FD $\geq$ 27 were accurately quantified. Following the AEDA, OAV analysis, and recombination experiments and omission tests, linalool and β-caryophyllene were identified as key flavor compounds in FTOs. α-thujone, 3-buten-1-yl isothiocyanate, citronellal, linalyl acetate, and 3-phenylpropionitrile were key flavor compounds in FFTO, and *β*-pinene, *α*-terpinene, *β*-phellandrene, and 3-ethyl-2,5-dimethylpyrazine were key flavor compounds in DFTO. Finally, chiral analysis suggests that the ratio of linalool enantiomers may be the potential cause of the flavor differences between FFTO and DFTO. This study provides theoretical guidance for the industrial production of FTO.

Keywords: fried *Tengjiao* (*Zanthoxylum armatum* DC.) oil; molecular sensory science; key flavor compounds; partial least squares regression (PLSR); enantiomer

1. Introduction

Zanthoxylum armatum DC. (ZA), also known as *Tengjiao*, is a small tree or shrub belonging to the genus Zanthoxylum in the Rutaceae family [1]. ZA is originally from China, primarily distributed in southwestern regions such as Sichuan, Chongqing, and Guizhou [2]. In addition, it also has a certain range of distribution in Japan, Republic of Korea, Nepal, India, and Pakistan [3]. It is one of the most widely used seasonings and also possesses certain medicinal value, being used to treat conditions such as colds, toothaches, fevers, indigestion, and cholera [4]. When it comes to Chinese ZA, Sichuan ZA is particularly famous for its special flavor and quality. Specifically, Meishan City in Sichuan Province is situated at the junction of the Sichuan Basin and the Western Sichuan Plateau. Its climate is mild, with pleasant weather year-round, abundant rainfall, and

ample sunshine, making it particularly suitable for the growth of Sichuan peppers. Hongya County, under the jurisdiction of Meishan City, has a high forest coverage rate and is well known as a "natural oxygen bar" and the "hometown of *Tengjiao*". As a result, Hongya *Tengjiao* is widely used in Sichuan cuisine and processed to make products such as *Tengjiao* oil and *Tengjiao* sauce.

In Chinese cuisine, both fresh and dried ZA are commonly used as ingredients in cooking, endowing dishes with a fresh, green aroma and a numbing, spicy taste. With the innovative development of the restaurant industry, *Tengjiao* has found increasingly diverse applications in culinary products. For instance, fried *Tengjiao* oil (FTO) can be used to season rice noodles, hot pot, and other dishes. Additionally, the special green pepper roasted fish is particularly popular among young consumers. It is noteworthy that both dried and fresh *Tengjiao* are utilized in these cooking processes. Therefore, the scientific basis for using both of them simultaneously in the cooking process is an area worth exploring.

Currently, research on ZA has primarily centered on its biological activity, volatile flavor compounds, fagaramide (the numbing component), and extraction processes. Previous studies have demonstrated that ZA exhibits anti-inflammatory, antioxidant, antispasmodic, antibacterial, antiprotozoal, antiviral, anthelmintic, antinociceptive, antiproliferative, antidiabetic, antidepressant, antipyretic, cytotoxicity, hepatoprotective, insecticidal, larvicidal, phytotoxicity, piscicidal, and repellent activities [2,4]. As for flavor, research has focused on processing methods for extracting ZA oil, identifying its key flavor compounds, and comparing flavor differences between ZA and *Zanthoxylum bungeanum* Maxim (ZB). Hu et al. found that ZA oil extract via ultrasound-assisted extraction exhibits the highest levels of aromatic and numbing components, as well as superior stability [5]. Meanwhile, the high-temperature frying method is easy to use and relatively low-cost. It uses high temperature to rupture the cell walls of ZA, releasing aromas that dissolve into the vegetable oil [6]. Linalool, D-limonene, sabinene, myrcene, β-phellandrene, and geraniol and linalyl acetate were identified as the main odorants in ZA oil [5,7,8]. Specifically, linalool, sabinene, linalyl acetate, and piperitone were markers for distinguishing between ZA oil samples and ZB samples [8,9]. Among α-, β-, γ-, and δ-sanshool and their derivatives, it was found that hydroxyl-α-sanshool significantly enhances the phenomenon of a numbing sensation in ZA [10–12]. There is no doubt that the difference between fresh (FFTO) and dried (DFTO) fried *Tengjiao* oil might be related to the *Tengjiao* drying process. During the drying process of Sichuan pepper, alcohols may be converted into terpenes, resulting in a decrease in alcohol content and an increase in terpene content [13]. The drying method is a key factor affecting the volatile compounds in ZA and ZB. In particular, hot-air drying at lower temperatures helps preserve its key flavor compounds [14]. In fried *Tengjiao* oil (FTO), the frying process significantly transforms the composition and proportions of flavor compounds through thermal degradation, oxidative reactions, and interactions with the oil medium. It is found that frying time and temperature have a significant impact on flavor quality [15,16]. For example, high temperatures might accelerate the thermal degradation, thermal oxidation, and isomerization of linalool and other compounds [17]. However, the flavor differences between FFTO and DFTO, as well as the reasons for these flavor differences, have not yet been systematically studied by scholars.

Molecular sensory science is currently the dominant and systematic approach for analyzing the flavor of food. It has been developed by Peter Schieberle's research team and has a history of approximately 18 years [18]. It is a multidisciplinary technology for researching food flavor quality at the molecular level. It employs chromatography, mass spectrometry, and sensory evaluation techniques, combined with olfactory assessment and odor activity value (OAV) to screen aroma compounds, and validates key flavor compounds

https://doi.org/10.3390/foods15081326

through recombination and omission experiments [19]. Molecular sensory science has been applied in the flavor analysis of ZA and ZB. For example, Sun et al. identified β-phellandrene, *p*-cymene, acetic acid octyl ester, octanal, citronellol, and sabinene as the major factors responsible for the flavor differences between Hancheng and Hanyuan fried ZB oils through molecular sensory science technology [20]. Additionally, linalool, linalyl acetate, and 1,8-cineole have been identified as flavor difference markers for ZB oils and *Zanthoxylum schinifolium* sieb. et Zucc. (ZS) oils using molecular sensory science technology [21]. It is noteworthy that in nature, the chiral structure of flavor components influences the overall flavor profile of food. For example, the odor profiles of different menthol isomers exhibit significant differences [22]. Previous studies have examined the enantiomeric ratio of limonene and linalool in fried ZB oil, revealing that S-(−)-limonene and S-(+)-linalool align more closely with the aromatic attributes of these compounds in fried ZB oil [20]. However, the effect of enantiomeric ratios of terpenoids in FTO and the differences between FFTO and DFTO enantiomers on flavor has not yet been studied.

In this study, volatile organic compounds (VOCs) in FFTO and DFTO were extracted via solvent-assisted flavor evaporation (SAFE). Then, gas chromatograph–mass spectrometry (GC-MS) and gas chromatography–olfactometry–mass spectrometry (GC-O-MS) combined with aroma extract concentration analysis (AEDA) were employed for the qualitative and quantitative analysis of volatile flavor compounds in FTO. Subsequently, odor activity values (OAVs) were calculated to determine the contribution of each VOC to the overall aroma of the FTO samples. After that, recombination and omission experiments were performed to identify and validate key flavor compounds. In particular, the enantiomers of limonene and linalool in FTOs were detected to determine their respective contributions to the flavor profile of FTOs.

2. Materials and Methods

2.1. Materials

Hongya Tengjiao samples (from Hongya County, Meishan, China) were obtained from Chengdu Zhuojia Trading Co., Ltd. (Chengdu, China). Rapeseed oil was obtained from Yihai Kerry Grain and Oil Co., Ltd. (Chongqing, China).

2.2. Chemical Standards

Linalyl acetate (95%) was purchased from Acros Organics (Shanghai, China). Germacrene D (>90%), γ-terpinene (>95%), 5-hexenenitrile (>95%), 3-buten-1-yl isothiocyanate (>96%), *cis*-linalool oxide (>97%), 4-octanol (>97%), 2-methylpyrazine (>98%), ethylbenzene (>99.7%), thujone (≥70%), (*E*,*E*)-2,4-decadienal (≥97%), 4-pentenoic acid (≥98%), *o*-xylene (≥99%), *p*-xylene (≥99.8%), β-myrcene (90%), terpinen-4-ol (95%), camphene (95%), 3-phenylpropionitrile (97%), 3-butenenitrile (97%), styrene (99%), 2-acetylfuran (99%), and methyl phenylacetate (99%) were purchased from Aladdin (Shanghai, China). (*E*)-2-Octenal was purchased from Alfa Aesar (Shanghai, China). 4-Octanone (98%), amylene hydrate (99%), furfuryl alcohol (99%) and phenylethyl alcohol (99%) were purchased from Adamas-beta (Shanghai, China). β-Pinene (>95%), 2(5H)-furanone (95%), linalool (98%), and 1-butanol (99.5%) were purchased from Innochem (Beijing, China). (*E*,*E*)-2,4-Heptadienal (90%), (*E*)-2-heptenal (95%), 2-acetyl pyrrole (98%), 1-penten-3-ol (98%), 2-pentyl-furan (98%), phenethyl acetate (98%), 2,5-dimethyl pyrazine (99%), methyl cyclopentenolone (99%), butyric acid (99%), and acetic acid (99.8%) were purchased from J&K Scientific (Beijing, China). α-Phellandrene (≥85%), 1-propanol (≥99.8%), α-caryophyllene (93%), myrtenol (95%), *trans*-β-ocimene (95%), β-Phellandrene (98%), 3-ethyl-2,5-dimethylpyrazine (98%), and pentanal (98%) were purchased from Macklin (Beijing, China). Dichloromethane (99.5%), 5-methyl

furfural (>98%), α-pinene (98%), β-caryophyllene (98%), and eucalyptol (99%) were purchased from Mreda (Beijing, China). n-Alkanes (C_6–C_{30}) and *p*-cymene (99%) were purchased from Sigma-Aldrich (Shanghai, China). Indole (>90%), α-terpinene (>90%), terpinolene (>90%), *trans*,*trans*-2,4-decadienal (>90%), piperitone (>94%), *trans*-2-pentenal (>95%), limonene (>95%), heptanal (>95%), nonanal (>95%), (*E*)-2-hexenal (>95%), hexanal (>98%), octanal (>98%), furfural (>98%), citronellal (>98%), N-methyl-2-pyrrolidone (>99%), γ-butyrolactone (>99%), and benzaldehyde (98%) were purchased from TCI (Shanghai, China). 2-Hydroxy-3-Methyl-2-cyclopentenone (98%) was purchased from Energy Chemical (Shanghai, China). α-Terpineol (≥96%), α-thujone (≥98%), and sabinene (≥98%) were purchased from Yuanye (Shanghai, China).

2.3. FTO Sample Preparation

Preparation of dried *Tengjiao*: Fresh *Tengjiao* (80 g) fruits were weighed and placed in an odorless, uncovered glass Petri dish. Subsequently, they were dried in a Non-Standard Type 10 Electric Heating Dryer Control System (Changzhou Erle Drying Equipment Co., Ltd., Changzhou, China) for 10 h (55–65 °C, 1 m/s).

Preparation of FTO Samples: Our group has conducted in-depth research into the optimal processing conditions for frying pepper oil. We referred to the method that our group previously used to prepare fried pepper oil, with slight modifications [15,23]: 150 g of rapeseed oil was poured into a 500 mL glass flask, which was then placed in an oil bath for heating while the temperature of the rapeseed oil was monitored. At the same time, magnetic stirring was carried out to ensure even heating. When the oil temperature stabilized at 130 °C, the *Tengjiao* fruit (80 g, in fresh *Tengjiao* quality) was added to the oil, and frying began. When the frying time reached 20 min, the flask was quickly removed and the heating process was stopped. The *Tengjiao* fruits were then filtered out, and the FTO was cooled in an ice-water bath. The prepared FTO samples were set aside in a −40 °C refrigerator. All samples were prepared in triplicate for subsequent determination experiments.

2.4. Quantitative Descriptive Analysis (QDA)

The sensory evaluation panel was assembled from members of the Beijing Key Laboratory of Flavor Chemistry at Beijing Technology and Business University. The panel comprised 12 panelists, including 5 males and 7 females, all between the ages of 20 and 30. The odor of the experimental samples posed no danger or discomfort to the participants. Furthermore, the participants signed written consent forms after being fully informed of the details, and they had the right to withdraw from the experiment at any time. The sensory evaluations were conducted in a specialized sensory evaluation room maintained at 25 °C and free of odors. Before the formal experiment began, the sensory panel underwent professional training. This sensory evaluation experiment was approved under Certificate No. 139 of 2025 issued by the Scientific Research Ethics Committee of Beijing Technology and Business University.

Firstly, 2 g of FTO was added to a 10 mL, odorless, transparent glass vial with a cap. Based on the participants' discussions regarding the flavor characteristics of FFTO and DFTO, the aroma descriptors for FTO were determined based on the frequency of occurrence of the descriptors. Ultimately, a total of eight descriptors—oil, pepper, spice, roasted, herbal, wood, citrus-like, and green notes—were identified. The panelists were required to rate the intensity of each descriptor on a 10-point linear scale ranging from 0 to 9 (from completely imperceptible to strongly perceptible).

2.5. Isolation of Volatiles by SAFE

FTO (50 g) was placed in a separating funnel (500 mL), followed by CH_2Cl_2 solvent (200 mL) and internal standard (4-octanol, 82.2 mg/mL, 20 μL) for extraction. Liquid–liquid extraction was carried out using a GGC-C separating funnel vertical shaker (Beijing Guohuan High-tech Automation Technology Research Institute, Beijing, China) at 300 r/min for 20 min. Then, the sample was transferred to a SAFE dropping funnel for high-vacuum distillation. When the pressure of the whole device dropped to 1×10^{-5} mbar, we slowly rotated the piston of the dropping funnel to start distillation. After the distillation was essentially complete, an empty distillation was performed for 40 min to fully extract the volatile compounds from FTO. After that, FTO volatile component extracts were obtained. After the temperature of the extract was stabilized to room temperature, the appropriate amount of anhydrous Na_2SO_4 was added to remove the water. The final distillate was concentrated to 1 mL using a Vigreux column (50 cm × 1 cm) (Beijing Jingxing Glassware Co., Ltd., Beijing, China) and BF-2000 nitrogen drying instrument (Beijing Bafang Century Technology Co., Ltd., Beijing, China). The concentrate was stored in a −40 °C freezer for later detection.

2.6. GC-MS Analysis

GC-MS analysis was performed using a Thermo Fisher Trace 1300 gas chromatograph (Thermo Fisher Scientific, Waltham, MA, USA) combined with a Thermo Fisher mass spectrometer (Thermo Fisher Scientific, Waltham, MA, USA). Separation was performed using a TG-Wax column (30 m × 0.25 mm i.d., 0.25 μm, Thermo Fisher Scientific, Waltham, MA, USA).

The program referred to the method of Sun et al., with slight modifications [20]. Helium was used as the carrier gas and delivered at a fixed flow rate of 1.2 mL/min to the column. For the TG-Wax column, the oven temperature was initially 40 °C, followed by a 1 min hold; increased to 140 °C at a rate of 2 °C/min, followed by a 1 min hold; and finally increased to 220 °C at a rate of 6 °C/min, followed by a 1 min hold. The mass detector conditions were as follows: ionization energy, 70 eV; MS transfer line temperature, 230 °C; ion source temperature, 250 °C; mass range, m/z 40–350; and solvent delay, 4 min.

2.7. GC-O-MS

GC-O-MS analysis was achieved using a GC-MS (7890B Gas Chromatography System equipped with 5977B GC/MSD (Agilent Technologies Inc., Santa Clara, CA, USA)) with an olfactometer detector (ODP 3; Gerstel, Mulheim an der Ruhr, Germany). The GC-MS analysis conditions were consistent with those described in Section 2.6. For olfactometer detector, the transmission line temperature was 250 °C and the exit temperature was 120 °C. During the analysis, these flavor compounds were split at a 1:1 ratio via a three-way valve and directed into the mass spectrometry detector and the olfactory interface. In particular, during the olfactory experiments, a continuous supply of moist air was used to prevent the participants' nasal passages from drying out. In addition, a GC-O-MS evaluation panel consisting of three experts selected from the panel in Section 2.4 recorded the time, intensity, and characteristics of each odor. The three experts showed qualities such as strong concentration, a keen sense of smell, and familiarity with and sensitivity to the odor characteristics of FTO. During the data verification phase, each compound had to be identified by at least two experts before it could be deemed to be an aroma-active compound.

We combined aroma extract concentration analysis (AEDA) with GC-O-MS to investigate the sensory characteristics and intensity of various volatile compounds in FTO. The flavor dilution (FD) factor for the highest concentration sample (undiluted FTO concen-

https://doi.org/10.3390/foods15081326

trate) was designated as 1. Serial dilutions were performed at a ratio of V (undiluted FTO concentrate):V (dichloromethane) = 1:3. Each dilution was subjected to an olfactory assessment, with the detected odors and corresponding retention times recorded. When the dilution ratio reached a level where the odor could no longer be detected by smell, the process could be stopped. The above analysis results were expressed as FD factors.

2.8. Qualitative and Quantitative Analysis

The volatile compounds in FTOs were identified using the NIST 17 library (MS) retention index (RI) combined with standards (Std). First, semi-quantitative analysis was applied to compounds identified by GC-MS. For compounds with FD $\geq$ 27 in the AEDA process, precise quantification was performed by an internal standard curve method based on semi-quantitative results.

2.9. OAV Analysis

In molecular sensory science and technology, OAV is one of the key indexes for evaluating the contribution of various volatile compounds to the overall aroma of a sample. OAV is defined as the ratio of the concentration of a substance to its odor threshold in water or oil [24]. It is calculated by the formula $OAV_i = c_i/OT_i$; among them, OAV_i is the aroma activity value of each ingredient, Ci is the content of each aroma component in the sample (mg/kg), and OT_i is the aroma threshold value of each ingredient (mg/kg). The thresholds in this study were obtained from *Odor thresholds* [25].

2.10. Recombination and Omission Experiments

Before the recombination experiment, we first prepared an odorless matrix as the solvent. For the preparation method for the odorless matrix, we referred to the previous program used by our group, with minor modifications [23]. The rapeseed oil was heated in an oil bath at 130 °C for 20 min. After the rapeseed oil had cooled to room temperature, it was first mixed with 100 mL of dichloromethane for liquid–liquid extraction (30 min) to remove the flavor compounds from the rapeseed oil. Dichloromethane was then removed by rotary evaporation, and extraction was continued with 100 mL of n-pentane. The above process was repeated three times. Finally, the extracted rapeseed oil was transferred into an open beaker, and the residual solvent was removed using a magnetic stirrer (IKA RH D S025) at 60 °C, 300 r.

Based on the quantitative results, aroma recombination for FFTO and DFTO was performed. Aroma compounds with an OAV > 1 were used and added to the odorless FPO matrix. The recombinant samples were evaluated using the attributes employed in sensory evaluation. After this, a triangle test was implemented to verify the significant differences between the omitted and recombinant samples.

2.11. Detection of Enantiomers

Analysis of the enantiomers was performed using a GC-MS (Thermo Fisher Trace 1310 gas chromatograph (Thermo Fisher Scientific, Waltham, MA, USA) combined with a Thermo Fisher mass spectrometer (Thermo Fisher Scientific, Waltham, MA, USA). Separation was performed using a BGB-176SE column (30 m $\times$ 0.25 mm i.d., 0.25 μm, BGB-Analytik AG, Switzerland). Helium was used as the carrier gas and delivered at a fixed flow rate of 2 mL/min to the column. Other chromatographic and mass spectrometry conditions were the same as for 2.4 GC-MS. Qualitative analysis was performed using mass spectrometry (MS) and standards (S), while quantitative analysis was conducted using semi-quantitative methods.

https://doi.org/10.3390/foods15081326

2.12. Statistical Analysis

Experimental data were collected and organized using Excel (Microsoft Office 2016, Redmond, WA, USA). The results of the experiments were expressed as the mean of three experiments ± standard deviation. The *t*-test function was used to analyze significant differences using Excel (Microsoft Office 2016, Redmond, WA, USA). Aroma profile, bar chart and Venn diagram were plotted using Origin version 2025b (OriginLab Corporation, Northampton, MA, USA). PLSR analysis was conducted using XLSTAT version 2019 (Addinsoft, New York, NY, USA). Heat map was created by TBtools-II 2.081software (https://github.com/CJ-Chen/TBtools, accessed on 28 November 2025).

3. Results and Discussion

3.1. Sensory Profiles of DFTO and FFTO

In order to illustrate the flavor differences between FFTO and DFTO more clearly, the aroma profiles are presented using a radar chart (Figure 1). Based on evaluation and screening by sensory panels, eight aroma attributes were used to describe the flavor characteristics of FTOs. They were oil, pepper, spice, roasted, herbal, wood, citrus-like, and green. FFTO and DFTO had similar sensory attributes, but the intensity of each attribute was different, resulting in distinct flavors. The intensity of pepper aroma and spice aroma in FFTO (pepper, 7.58; spice, 6.96) was significantly higher than that in DFTO (pepper, 5.17; spice, 4.58). Meanwhile, the intensity of the oil aroma in DFTO (7.46) was obviously higher than that in FFTO (5.96). The intensity of other aroma attributes (roasted, herbal, wood, citrus-like, and green) showed minimal variation between FFTO and DFTO. It is worth noting that the intensity of these aroma attributes was slightly higher in FFTO than in DFTO. Overall, FFTO exhibited a higher overall aroma intensity than DFTO, particularly in terms of the pepper and spice aroma. The cause of this result might be the loss or transformation of some volatile compounds during the drying process or the frying process of *Tengjiao*.

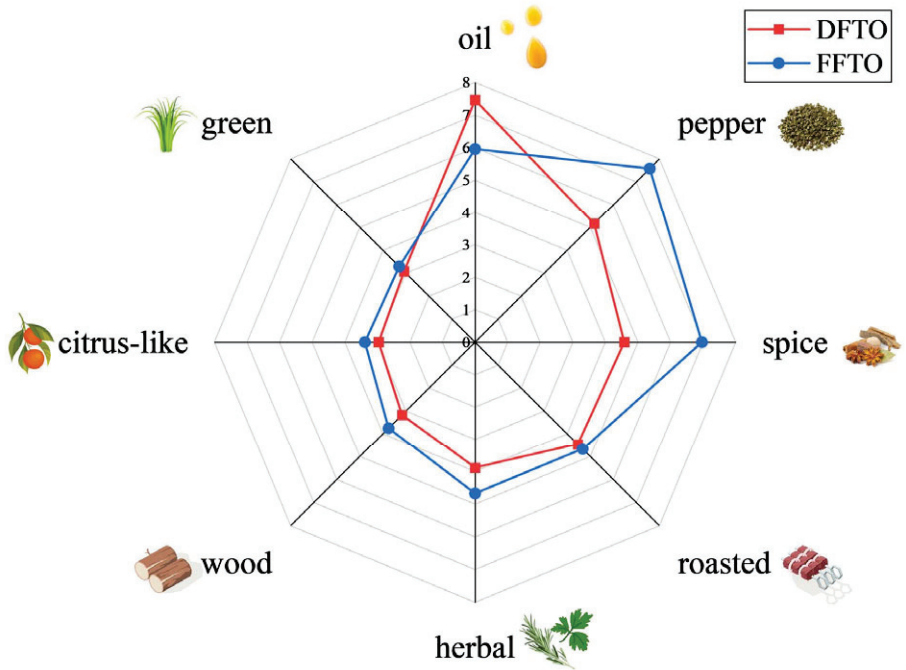


Figure 1. Aroma profiles of DFTO and FFTO by sensory evaluation. (Each of the 12 participants completed one evaluation. A *t*-test was performed. Oil, pepper, and spice: $p < 0.05$. FFTO, fresh fried *Tengjiao* oil; DFTO, dried fried *Tengjiao* oil.)

3.2. Identification of Volatile Compounds in FTOs by GC-MS

A total of 82 volatile compounds (22 alkenes, 13 alcohols, 18 aldehydes, 7 ketones, 3 acids, 5 esters, 1 ether, 9 heterocycles, and 4 nitriles) were identified in FTOs (Table A1). The number of volatile compounds in FFTO and DFTO was not significantly different, with 61 and 64 compounds, respectively. Among them, they shared as high as 43 volatile compounds (Figure 2a). These compounds might contribute to the characteristic flavor profile of FTO, such as its pepper and spice aroma. However, 18 volatile compounds were unique to FFTO, while 21 volatile compounds were unique to DFTO. These compounds might be the main reason for the flavor distinctions between FFTO and DFTO. In terms of compound types, most types of compounds did not differ significantly (alkenes, ketones, acids, esters, ether, and nitriles). Notably, FFTO contained a greater variety of alcohols, while DFTO contained a greater variety of aldehydes and heterocyclic compounds (Figure 2b). This might be due to the relatively high content of terpenols in fresh *Tengjiao* berries, which undergo transformation and degradation during the drying process [13]. Moreover, the drying process also resulted in the formation of more aldehydes and heterocyclic compounds in *Tengjiao* [26]. It is noteworthy that only two heterocyclic compounds were present in FFTO, whereas eight were found in DFTO, with seven of them newly generated. They were 2-pentyl-furan, 2-methylpyrazine, 2,5-dimethyl pyrazine, 3-ethyl-2,5-dimethylpyrazine, 2-acetylfuran, N-methyl-2-pyrrolidone, 2(5H)-furanone, and 2-acetyl pyrrole. In this case, pyrazine and pyrrole might originate from the Maillard reaction [27,28], while furan could come from lipid oxidation [29].

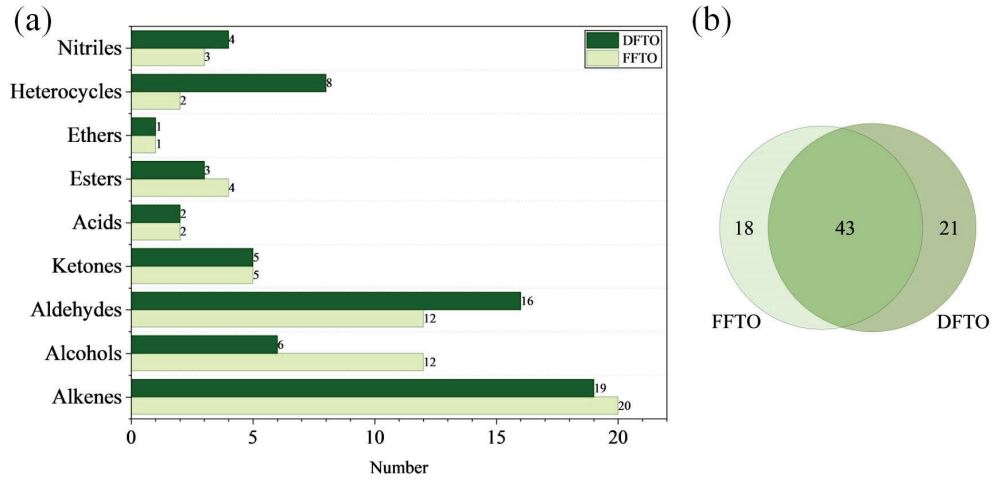


Figure 2. Comparison of volatile compounds in FFTO and DFTO. (**a**) Classification and number of volatile compounds in FTOs. (**b**) Venn diagram of FFTO and DFTO volatile compounds. (FFTO, fresh fried *Tengjiao* oil; DFTO, dried fried *Tengjiao* oil).

In terms of the number of various compounds, alkenes, aldehydes, and alcohols were more abundant in FTOs. The abundance of alkenes, alcohols, and aldehydes was consistent with previous studies [1]. The alkenes and alcohols may mainly originate from *Tengjiao*, while the aldehydes may primarily come from rapeseed oil [30]. Among these, terpenes might give FTO its characteristic floral (linalool, etc.), woody (caryophyllene, etc.), citrus (limonene, etc.) and other flavors. Meanwhile, aldehydes might impart FTO with rich green (hexanal, etc.) and oily (2,4-decadienal, etc.) aromas. In summary, based on the number of compounds, alkenes, aldehydes, and alcohols played a key role in the formation of FTO flavor. Heterocyclic compounds, alcohols, and aldehydes may be the primary factors causing the flavor differences between FFTO and DFTO. This conclusion still required validation through further quantitative experiments.

https://doi.org/10.3390/foods15081326

3.3. Aroma Intensity of Each Compound Determined by AEDA

In order to determine whether volatile compounds in FTOs have aroma activity and consequently influence the flavor of FTOs, we performed an analysis by GC-O-MS combined with AEDA. In FFTO and DFTO, there were 44 and 49 aroma-active compounds, respectively (Table 1). A total of 37 and 36 aroma-active compounds were successfully identified through MS, RI or S qualification, respectively (Figure 3a).

Table 1. The results of AEDA for FFTO and DFTO.

RT	Compound	CAS	Log_3FD		Odor Description
			FFTO	DFTO	
6	Hexanal	66-25-1	1	2	green, sweet
6.5	β-Pinene	127-91-3	6	-	lemon, pine, sweet, bitter
7.07	Sabinene	3387-41-5	7	6	sweet, bitter, wood
8.95	β-Myrcene	123-35-3	7	6	herb, pepper, green
9.31	α-Terpinene	99-86-5	4	-	sweet, lemon
10.18	Limonene	5989-27-5	9	7	citrus, herb
10.36	Eucalyptol	470-82-6	6	3	green, mint, pepper
10.49	β-Phellandrene	555-10-2	0	3	mint, sweet
11.62	4-Octanone	589-63-9	-	2	sweet, fruit
12.41	γ-Terpinene	99-85-4	4	3	pepper, citrus, spice
13.13	Styrene	100-42-5	-	3	sweet
14.26	Terpinolene	586-62-9	-	3	sweet, pine
14.6	Unknown		-	3	roast
14.89	Octanal	124-13-0	7	4	green, sweet
15.5	Unknown		-	5	mold, mushroom
16.61	(*E*)-2-Heptenal	18829-55-5	7	5	fruit, sour, chocolate
19.464	Allo-ocimene	673-84-7	-	4	pepper, stinky
19.5	Neo-alloocimene	7216-56-0	3	-	bitter, pepper, stinky, lemon
20.25	Unknown		-	3	floral, green, wine
20.77	Nonanal	124-19-6	2	3	fat, floral, pepper, nut
21.6	α-Thujone	546-80-5	8	-	green, lemon
22.51	(E)-2-Octenal	2548-87-0	4	3	spice, herb, nut
22.75	Thujone	1125-12-8	8	8	cucumber, green
23.22	3-Ethyl-2,5-diMethylpyrazine	13360-65-1	-	6	sesame, sweet, oil, roast
23.33	cis-Linalool Oxide	5989-33-3	3	-	pepper, sweet
24.4	3-Buten-1-yl Isothiocyanate	3386-97-8	-	3	floral, alcohol
24.3	Acetic acid	64-19-7	6	3	vinegar, sour
24.86	trans-Sabinene hydrate	17699-16-0	4	-	milk, sweet
25.72	Citronellal	106-23-0	4	-	leaf, pepper
26.217	Unknown		-	4	moldy
26.31	(*E*,*E*)-2,4-Heptadienal	4313-03-5	-	0	green, almond, nut, oil
27.11	2-Acetylfuran	1192-62-7	5	3	balsamic, pepper
27.72	Benzaldehyde	100-52-7	7	7	bitter, sauce
28.528	Unknown		-	2	sesame, almonds, oil
30.3	Linalool	78-70-6	10	8	floral, lavender, lemon, sweet
30.43	Linalyl acetate	115-95-7	3	-	sweet, floral
31.03	5-Methyl furfural	620-02-0	-	0	almond milk, sweet, spicy
31.41	β-Caryophyllene	87-44-5	3	2	spice, bitter, floral
32.5	Terpinen-4-ol	562-74-3	1	4	must, smoke
33.23	Myrtenal	564-94-3	3	-	burnt
33.48	γ-Butyrolactone	96-48-0	-	2	peanuts, rice
34.269	Butyric Acid	107-92-6	3	-	cheese, sour, sweet
34.69	trans-2-Decenal	3913-81-3	-	1	sour, pepper, green, cilantro
35.38	α-Caryophyllene	6753-98-6	2	-	pepper, wood
36.5	Furfuryl alcohol	98-00-0	3	3	burnt, rice, bean, yeast powder
37.1	Unknown		3	3	fermented black beans, soy sauce, sour
37.94	α-Terpineol	98-55-5	1	0	anise, oil, almonds
38.192	Unknown		3	-	fermentation

https://doi.org/10.3390/foods15081326

Table 1. *Cont.*

RT	Compound	CAS	Log_3FD		Odor Description
			FFTO	DFTO	
38.55	Piperitone	89-81-6	3	-	lemon, pepper, green, paste
40.267	(*E*)-4-Undecenal	68820-35-9	-	1	stinky, salted fish, sour
40.512	Unknown		2	4	rice, bean, stinky
43.19	Unknown		3	4	green, sour
43.61	trans,trans-2,4-Decadienal	25152-84-5	3	9	fat, oil, pepper
43.943	Allylacetic acid	591-80-0	-	8	fruit, sweet
44.81	2-Hydroxy-3-Methyl-2-cyclopentenone	765-70-8	-	3	wood, bitter, floral
44.84	Methyl cyclopentenolone	80-71-7	3	-	pepper, green lemon
45.383	Unknown		3	8	dust, wheat
46.022	Unknown		3	0	sweet
46.47	Unknown		-	5	bitter, burnt
51.96	2-Acetyl pyrrole	1072-83-9	-	8	roast
54.53	3-Phenylpropionitrile	645-59-0	3	3	spice
54.64	Unknown		-	6	sweet, wheat
55.31	cis-Nerolidol	142-50-7	1	-	spice, floral
58.38	Unknown		3	8	Perilla, plastic
63.68	Indole	120-72-9	1	-	mothball

"-" indicates that the compound was not detected. The experiment was conducted once by each of the three participants. (FFTO, fresh fried *Tengjiao* oil; DFTO, dried fried *Tengjiao* oil; AEDA, aroma extract concentration analysis; RT, retention time; FD, flavor dilution).

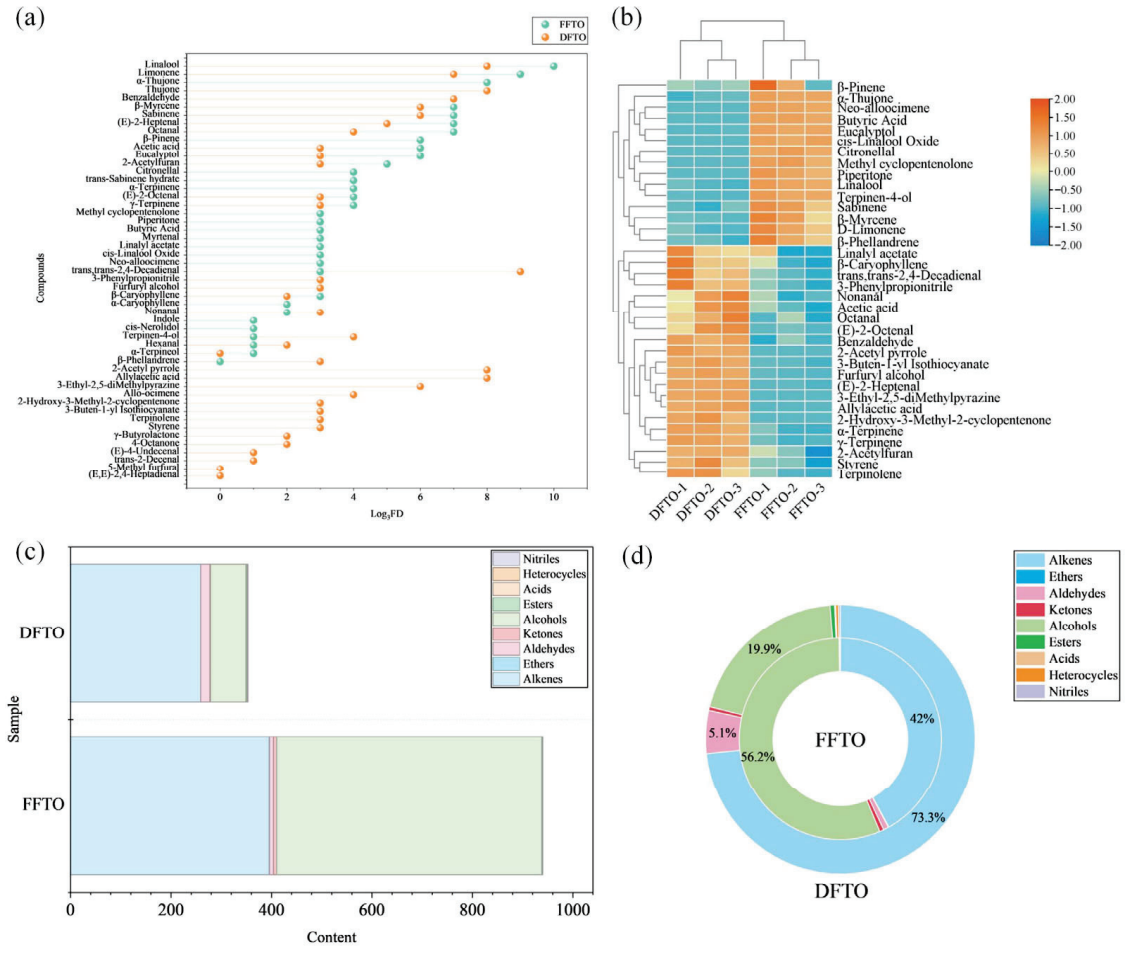


Figure 3. Comparison of aroma-active compounds in FFTO and DFTO. (**a**) FD factors of aroma-active compounds in FTOs. (**b**) Content of aroma-active compounds in FTOs (FD $\geq 3^3$). (**c**) Comparison of aroma-active compound content in FTOs (FD $\geq 3^3$). (**d**) Percentage distribution of various aroma-active compounds. (FFTO, fresh fried *Tengjiao* oil; DFTO, dried fried *Tengjiao* oil).

https://doi.org/10.3390/foods15081326

In FFTO, there was 1 compound with FD = 3^{10} (linalool), 1 compound with FD = 3^9 (limonene), 2 compounds with FD = 3^8 (thujone and α-thujone), 5 compounds with FD = 3^7 (sabinene, β-myrcene, octanal, (*E*)-2-heptenal, and benzaldehyde), 3 compounds with FD = 3^6 (β-pinene, eucalyptol, and acetic acid), 1 compound with FD = 3^5 (2-acetylfuran), 5 compounds with FD = 3^4 (α-terpinene, γ-terpinene, (*E*)-2-octenal, *trans*-sabinene hydrate, and citronellal), and 11 compounds with FD = 3^3 (neo-alloocimene, *cis*-linalool oxide, linalyl acetate, β-caryophyllene, myrtenal, butyric acid, furfuryl alcohol, piperitone, *trans*,*trans*-2,4-decadienal, methyl cyclopentenolone, and 3-phenylpropionitrile). Additionally, six unknown compounds had FD = 3^3. These aroma-active compounds might contribute to flavor formation in FFTO. Linalool had the highest FD factor and exhibited floral, lavender, lemon, and sweet aromas. It has been demonstrated to be a key flavor compound in Sichuan pepper and related products across a multitude of studies [20,31,32]. Limonene has the second-highest FD factor, exhibiting citrus and herb flavor characteristics. It has also been demonstrated to be one of the key flavor compounds in Sichuan peppers and related products [20,33]. It exhibits extremely high aroma intensity in FFTO, but its contribution to the overall flavor profile requires further verification.

In DFTO, there was 1 compound with FD = 3^9 (*trans*,*trans*-2,4-decadienal), 4 compounds with FD = 3^8 (thujone, linalool, allylacetic acid and 2-acetyl pyrrole), 2 compounds with FD = 3^7 (limonene and benzaldehyde), 2 compounds with FD = 3^6 (sabinene, β-myrcene and 3-ethyl-2,5-dimethylpyrazine), 1 compound with FD = 3^5 ((*E*)-2-heptenal), 3 compounds with FD = 3^4 (octanal, allo-ocimene and terpinen-4-ol), and 13 compounds with FD = 3^3 (eucalyptol, β-phellandrene, γ-terpinene, styrene, terpinolene, nonanal, (*E*)-2-octenal, 3-buten-1-yl isothiocyanate, acetic acid, 2-acetylfuran, furfuryl alcohol, 2-hydroxy-3-methyl-2-cyclopentenone, and 3-phenylpropionitrile). In addition, two unknown compounds had FD = 3^8, one unknown compound had FD = 3^6, two unknown compounds had FD = 3^5, three unknown compounds had FD = 3^4, and three unknown compounds had FD = 3^3. These aroma-active compounds might contribute to flavor formation in DFTO. *trans*,*trans*-2,4-Decadienal was the volatile compound with the highest FD factor in DFTO, exhibiting characteristic fat, oil, and pepper odors. It most likely originated from rapeseed oil. It has been shown in previous research to be an important product of the thermal oxidation of linoleic acid [29]. Thujone exhibited a green, cucumber-like odor, allylacetic acid exhibited a fruity sweet aroma, and 2-acetyl pyrrole exhibited a roasted aroma. From the perspective of aroma intensity, they might contribute to flavor formation in DFTO.

In particular, aroma-active compounds such as linalool, limonene, and thujone showed higher FD factors in both FTO samples, potentially making significant contributions to the flavor of FTOs. In summary, 29 and 27 aroma-active compounds with FD > 3^3 were successfully identified in FFTO and DFTO, respectively, and they may be closely related to the flavor of FTOs. Of course, this still requires verification through further analysis and experimentation.

3.4. Content of Aroma-Active Compounds

To precisely determine the content of each aroma-active compound, we employed the standard curve method to quantify 36 aroma-active compounds (FD $\geq 3^3$) that had already been qualitatively identified using standards (Table 2). Based on the *t*-test results for each aroma-active compound, 20 compounds showed significant differences between FFTO and DFTO ($p < 0.05$). These compounds may contribute to the flavor profile differences between FFTO and DFTO. To show the differences in the content of FFTO and DFTO aroma-active compounds more intuitively, we created a heat map (Figure 3b). The heat map clearly demonstrates that there are significant differences between FFTO and DFTO.

https://doi.org/10.3390/foods15081326

We can obviously divide the heat map into two parts. In the upper half, 15 compounds (*β*-pinene to *β*-phellandrene) have higher concentrations in FFTO, while in the lower half, 21 compounds (linalyl acetate to terpinolene) have higher concentrations in DFTO. This result might be due to the degradation and transformation of volatile compounds during the drying process of the *Tengjiao* fruit. In terms of the total amount of aroma-active compounds, the content in FFTO was significantly higher than that in DFTO, with FFTO content even exceeding that of DFTO by more than two times (Figure 3c). Both FTO samples contained abundant alkenes and alcohols. Notably, the alcohol and alkene contents were significantly reduced in the DFTO. In FFTO, the most abundant aroma-active compounds were alcohols (56.2%) and alkenes (42%), whereas in DFTO, the most abundant aroma-active compounds were alkenes (73.3%), alcohols (19.9%), and aldehydes (5.1%) (Figure 3d). In summary, FFTO and DFTO shared similar types of aroma-active compounds, but exhibited significant differences in the content of each component. This difference in content might be the underlying reason for the difference in flavor between the two.

Table 2. The results of OAV for FFTO and DFTO.

No.	Compound	Standard Curve	R^2	Content/(μg/g)		Odor Thresholds/ (μg/g)	OAV	
				FFTO	DFTO		FFTO	DFTO
1	*β*-Pinene	$y = 0.9756x - 0.0067$	0.9965	3.307 ± 0.464	2.926 ± 0.031	1.5	2.20	1.95
2	Sabinene	$y = 0.6253x + 0.1179$	0.9945	140.049 ± 17.954	75.993 ± 4.924	0.98	142.91	77.54
3	*β*-Myrcene	$y = 1.0413x - 0.0245$	0.9967	19.607 ± 1.573	15.209 ± 0.146	0.915	21.43	16.62
4	*α*-Terpinene *	$y = 0.907x - 0.0014$	0.995	1.095 ± 0.201	3.553 ± 0.236	0.085	12.88	41.80
5	Limonene	$y = 0.5897x + 0.0358$	0.9981	209.395 ± 18.876	139.328 ± 5.053	1.2	174.50	116.11
6	Eucalyptol *	$y = 0.4856x + 0.0006$	0.9954	0.834 ± 0.035	0.065 ± 0.009	0.015	55.60	4.33
7	*β*-Phellandrene	$y = 0.7298x - 0.0088$	0.9948	18.256 ± 1.53	13.289 ± 0.384	0.036	507.11	369.14
8	*γ*-Terpinene *	$y = 0.8966x - 0.0007$	0.992	1.87 ± 0.18	5.754 ± 0.447	2.89	0.65	1.99
9	Styrene *	$y = 0.8342x + 0.0003$	0.9961	0.341 ± 0.1	0.841 ± 0.124	3.1	0.11	0.27
10	Terpinolene	$y = 0.9671x - 0.0047$	0.9941	0.947 ± 0.066	1.436 ± 0.153	0.2	4.74	7.18
11	Octanal	$y = 0.2807x - 0.0001$	0.9924	0.358 ± 0.088	0.762 ± 0.145	0.32	1.12	2.38
12	(*E*)-2-Heptenal *	$y = 0.2824x - 0.0008$	0.9987	1.005 ± 0.076	5.564 ± 0.144	14	0.07	0.40
13	Neo-alloocimene *	$y = 2.6262x - 0.0019$	0.9924	0.027 ± 0.001	-	-	-	-
14	Nonanal	$y = 0.0934x - 0.003$	0.9912	5.491 ± 0.867	10.052 ± 2.408	13.5	0.41	0.74
15	*α*-Thujone *	$y = 0.4749x - 0.0004$	0.9997	5.69 ± 0.309	0.606 ± 0.138	0.36	15.81	1.68
16	(*E*)-2-Octenal	$y = 0.3507x - 0.0002$	0.9919	0.148 ± 0.015	0.418 ± 0.094	7	0.02	0.06
17	3-Ethyl-2,5-diMethylpyrazine *	$y = 0.7952x - 0.0004$	0.9991	-	0.228 ± 0.004	0.024	-	9.50
18	*cis*-Linalool oxide *	$y = 0.2468x + 0.0001$	0.9971	0.792 ± 0.044	-	6	0.13	-
19	3-Buten-1-yl Isothiocyanate *	$y = 0.6187x - 0.0002$	0.9953	0.134 ± 0.011	0.38 ± 0.017	0.017	7.88	22.35
20	Acetic acid	$y = 0.6379x - 0.0021$	0.9933	0.18 ± 0.046	0.379 ± 0.078	0.5	0.36	0.76
21	Citronellal *	$y = 0.3727x - 0.0003$	0.9995	0.295 ± 0.019	-	0.046	6.41	-
22	2-Acetylfuran	$y = 0.6467x + 0.0004$	0.9961	0.163 ± 0.117	0.465 ± 0.01	10	0.02	0.05
23	Benzaldehyde *	$y = 0.7671x - 0.0005$	0.9994	0.091 ± 0.016	0.183 ± 0.008	0.06	1.52	3.05
24	Linalool *	$y = 0.4882x + 0.3236$	0.9944	520.354 ± 68.832	68.403 ± 8.984	0.037	14,063.62	1848.73
25	Linalyl acetate	$y = 0.2163x - 0.0002$	0.991	1.099 ± 0.315	1.513 ± 0.218	1	1.10	1.51
26	*β*-Caryophyllene	$y = 0.3392x - 0.0005$	0.9943	0.496 ± 0.109	0.815 ± 0.128	0.064	7.75	12.73
27	Terpinen-4-ol *	$y = 0.4935x - 0.0005$	0.9993	6.576 ± 0.746	0.487 ± 0.051	0.59	11.15	0.83
28	Butyric acid *	$y = 0.9269x - 0.0006$	0.9961	0.025 ± 0.001	-	0.109	0.23	-
29	Furfuryl alcohol *	$y = 0.2295x + 0.0001$	0.9975	0.546 ± 0.019	1.466 ± 0.048	1.9	0.29	0.77
30	Piperitone *	$y = 0.5743x - 0.0007$	0.9962	0.268 ± 0.031	-	0.68	0.39	-
31	*trans*,*trans*-2,4-Decadienal	$y = 0.3071x - 0.001$	0.9912	0.587 ± 0.079	1.139 ± 0.213	2.5	0.23	0.46
32	Allylacetic acid *	$y = 0.5277x - 0.0014$	0.9937	-	0.11 ± 0.006	-	-	-
33	2-Hydroxy-3-Methyl-2-cyclopentenone	$y = 0.2072x - 0.0003$	0.9959	-	0.957 ± 0.177	2	-	0.48
34	Methyl cyclopentenolone *	$y = 0.1751x - 0.0002$	0.9982	0.345 ± 0.036	-	2	0.17	-
35	2-Acetyl pyrrole *	$y = 0.4903x + 1 \times 10^{-5}$	0.999	-	0.425 ± 0.039	58.58525	-	0.01
36	3-Phenylpropionitrile	$y = 0.748x - 0.0001$	0.9996	0.398 ± 0.068	0.852 ± 0.132	0.015	26.53	56.80

"-" indicates that the compound was not detected or the odor threshold was not found. "*" indicates that $p < 0.05$ in the *t*-test, indicating a statistically significant difference. The contents are expressed as the average of three experiments, presented as the mean ± standard deviation. (FFTO, fresh fried *Tengjiao* oil; DFTO, dried fried *Tengjiao* oil; OAV, odor activity value).

3.5. Correlation Between Major Aroma-Active Compounds and Aroma Attributes

To further investigate the relationship between aroma-active compounds and aroma attributes in FFTO and DFTO, we performed partial least squares regression (PLSR) analysis. The X-matrix was designed to represent the aroma-active compounds in FTOs, while the Y-matrix was designed for sensory attributes. As shown in Figure 4a, most of the X-matrix and Y-matrix are located around the circle $r^2 = 1$, which indicates that the PLSR model can adequately explain the above variables [34]. FFTO and DFTO exhibit distinct

differences, distributed in the second and third quadrants and the first and fourth quadrants, respectively. Additionally, this figure also provides clearer sensory evaluation results: FFTO exhibits more pronounced notes of green, pepper, spice, roasted, herbal, wood, and citrus-like aromas, while DFTO displays a more pronounced oil aroma. Specifically, compounds 1 (*β*-pinene), 3 (*β*-myrcene), 7 (*β*-phellandrene), 2 (sabinene), 5 (limonene), 24 (linalool), 30 (piperitone), 27 (terpinen-4-ol), 15 (*α*-thujone), 34 (methyl cyclopentenolone), 13 (neo-alloocimene), 6 (eucalyptol), 28 (butyric acid), 21 (citronellal), and 18 (*cis*-linalool oxide) show a significant positive correlation with FFTO, while compounds 25 (linalyl acetate), 26 (*β*-caryophyllene), 22 (2-acetylfuran), 31 (*trans*,*trans*-2,4-decadienal), 36 (3-phenylpropionitrile), 20 (acetic acid), 9 (styrene), 11 (octanal), 4 (*α*-terpinene), 14 (nonanal), 23 (benzaldehyde), 10 (terpinolene), 8 (*γ*-terpinene), 35 (2-acetyl pyrrole), 19 (3-buten-1-yl isothiocyanate), 12 ((*E*)-2-heptenal), 16 ((*E*)-2-octenal), 29 (furfuryl alcohol), 32 (allylacetic acid), 33 (2-hydroxy-3-methyl-2-cyclopentenone), and 17 (3-ethyl-2,5-dimethylpyrazine) show significant positive correlations with DFTO. Visually, the active compounds in quadrants 1 and 4 may be related to oil aroma. However, the remaining aroma attributes are clustered in the central region of the third and fourth quadrants. These flavor attributes may be associated with the aroma-active compounds in the third and fourth quadrants. However, the complex relationships among them cannot be further confirmed. This also suggested that relying only on the content of aroma-active compounds and the intensity of aroma attributes, combined with statistical methods, can only tentatively establish the association between aroma-active compounds and aroma attributes and cannot not fully describe the relationship between them. Moreover, aroma-active compounds 17 (3-ethyl-2,5-dimethylpyrazine), 28 (butyric acid), 13 (neo-alloocimene), 12 ((*E*)-2-heptenal), 6 (eucalyptol), 32 (allylacetic acid), 18 (*cis*-linalool oxide), 29 (furfuryl alcohol), 21 (citronellal), 15 (*α*-thujone), 19 (3-buten-1-yl isothiocyanate), 35 (2-acetyl pyrrole), 34 (methyl cyclopentenolone), 30 (piperitone), 27 (terpinen-4-ol), 8 (*γ*-terpinene), 4 (*α*-terpinene), 24 (linalool), 33 (2-hydroxy-3-methyl-2-cyclopentenone), 23 (benzaldehyde), 5 (limonene), and 2 (sabinene) exhibited variable importance for projection (VIP) values greater than 1 (Figure 4b), suggesting a strong association with the flavor of FTOs [23,35]. Of course, the above inference still requires further sensory verification to support it.

3.6. Aroma Contribution of Each Compound Determined by OAV

In FFTO and DFTO, there were 18 and 17 compounds with OAV > 1, respectively (Table 2). These aroma-active compounds may significantly contribute to the flavor of FTOs [36]. Among these, the OAVs for *β*-pinene, sabinene, *β*-myrcene, *α*-terpinene, limonene, eucalyptol, *β*-phellandrene, terpinolene, octanal, *α*-thujone, 3-buten-1-yl isothiocyanate, benzaldehyde, linalool, linalyl acetate, and *β*-caryophyllene in both FFTO and DFTO were all greater than 1. This indicates that these compounds likely make significant contributions to the flavor characteristics of FTO and are important constituents of the *Tengjiao* flavor profile. Specifically, citronellal and terpinen-4-ol exhibited OAVs greater than 1 only in FFTO, while *γ*-terpinene showed OAVs greater than 1 only in DFTO. Therefore, these three aroma compounds may be the factors responsible for the difference in FFTO and DFTO flavors. Higher OAV indicates a greater contribution to the overall flavor profile of the sample. In FFTO, linalool (OAV = 14,063.62), *β*-phellandrene (OAV = 507.11), limonene (OAV = 174.50), sabinene (OAV = 142.91), eucalyptol (OAV = 55.60), 3-phenylpropionitrile (OAV = 26.53), *β*-myrcene (OAV = 21.43), *α*-thujone (OAV = 15.81), *α*-terpinene (OAV = 12.88), and terpinen-4-ol (OAV = 11.15) may play a key role in the overall flavor profile of FFTO. In DFTO, linalool (OAV = 1848.73), *β*-phellandrene (OAV = 369.14), limonene (OAV = 116.11), sabinene (OAV = 77.54), 3-phenylpropionitrile (OAV = 56.80), *α*-terpinene (OAV = 41.80), 3-buten-1-yl isothiocyanate (OAV = 22.35),

https://doi.org/10.3390/foods15081326

β-myrcene (OAV = 16.62), and β-caryophyllene (OAV = 12.73) may play a key role in the overall flavor profile of DFTO. In short, the above aroma-active compounds might theoretically make significant contributions to the flavor of FTOs. However, further sensory experiments are required for support and validation.

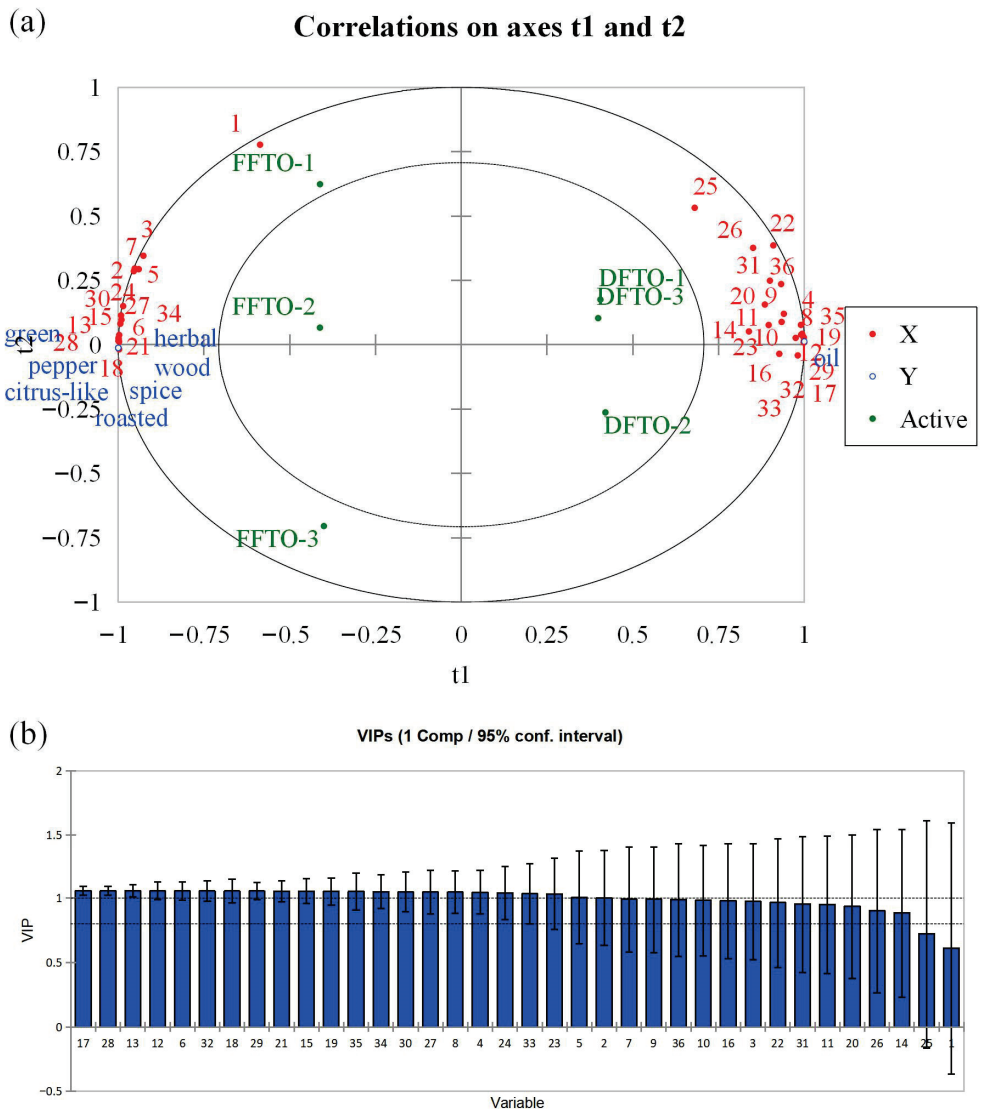


Figure 4. Correlation analysis of FTOs by partial least squares regression (PLSR). (**a**) Correlation loadings of the PLSR model between sensory attributes and aroma-active compounds in fried *Tengjiao* oils (FTOs). (**b**) Variable importance for the projection (VIP) scores and 95% confidence intervals (bootstrap method) of aroma-active compounds for the first component in the PLSR model.

3.7. Determination and Verification of Key Flavor Compounds by Recombination Experiments and Omission Tests

Currently, recombination experiments and omission tests are widely applied in food flavor research and serve as one of the primary methods for identifying key flavor compounds [37]. Based on the OAV analysis results, we conducted reconstruction experiments using aroma-active compounds with OAV > 1 from both FFTO and DFTO, as well as those for which OAV calculation was not performed due to missing threshold values. The amounts of each aroma-active compound added in the experiment were based on the quantitative results provided in Table 2 via standard curve analysis. The results of the recombinant experiment are shown in Figure 5. In Figure 5a, the recombinant model (R-FFTO) exhibits slightly stronger green, citrus-like, herbal, and pepper notes than FFTO,

while its oil, spice, roasted, and wood notes are slightly weaker than FFTO. In Figure 5b, the recombinant model (R-DFTO) exhibits slightly stronger green, citrus-like, wood, herbal, spice, and pepper notes than DFTO, while its oil and roasted notes are slightly weaker than DFTO. The recombinant models are in general agreement with the aroma profile of FTOs, indicating that the recombinations were successful.

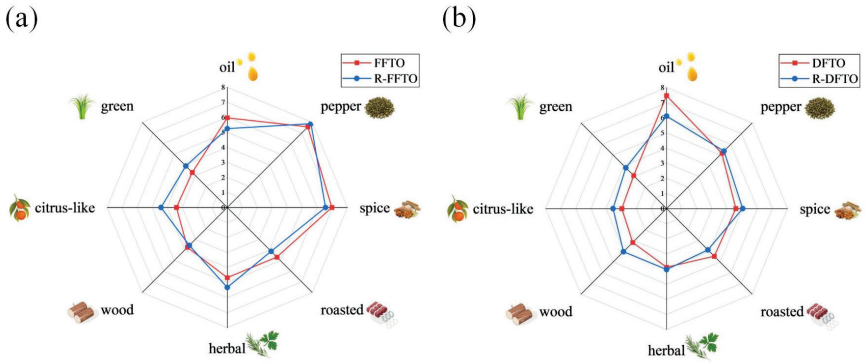


Figure 5. Aroma profiles of FTOs compared to recombinant models. (**a**) FFTO and recombinant model–FFTO (R-FFTO). (A *t*-test was performed: No attributes with $p < 0.05$). (**b**) DFTO and recombinant model–DFTO (R-DFTO). (A *t*-test was performed. oil: $p < 0.05$. FFTO, fresh fried *Tengjiao* oil; DFTO, dried fried *Tengjiao* oil; R-FFTO, recombinant fresh fried *Tengjiao* oil; R-DFTO, recombinant dried fried *Tengjiao* oil).

Subsequently, we conducted omission tests on R-FFTO and R-DFTO, respectively. Specifically, to further validate the key flavor compounds of FTOs, 22 compounds in recombination experiments were filtered for omission testing, and one of the odorants was omitted from each set of models (M1–M22) (Table 3). A sensory panel of 20 professionally trained panelists was organized to evaluate the difference in aroma between the recombinant model and M1–M22 through a triangle test. This sensory evaluation experiment has also been approved and licensed by the Scientific Research Ethics Committee (Reference number: No. 139 in 2025) mentioned in Section 2.4. As shown in Table 3, in FFTO and DFTO, seven and six compounds showed significance in the triangle test results, respectively. In FFTO, linalool*** (floral, lavender, lemon, sweet), *α*-thujone*** (green, lemon), linalyl acetate*** (sweet, floral), 3-buten-1-yl isothiocyanate* (floral, alcohol), citronellal* (leaf, pepper), *β*-caryophyllene* (spice, bitter, floral), and 3-phenylpropionitrile* (spice) were key flavor compounds that played important roles in flavor formation. In DFTO, *β*-caryophyllene*** (spice, bitter, floral), linalool** (floral, lavender, lemon, sweet), *β*-pinene* (lemon, pine, sweet, bitter), *α*-terpinene* (sweet, lemon), *β*-phellandrene* (mint, sweet) and 3-ethyl-2,5-dimethylpyrazine* (sesame, sweet, oil, roast) were key flavor compounds that played important roles in flavor formation. In particular, linalool and *β*-caryophyllene were significant in both FFTO and DFTO, indicating that they are important flavor compounds within the characteristic flavor profile of *Tengjiao*. The linalool content in DFTO was significantly lower than that in FFTO, indicating that most of the linalool degraded and transformed during the drying process. This further results in a reduction in the characteristic Sichuan pepper flavor in DFTO. Under the influence of thermal oxidation, the C^+ of linalool could undergo cyclization to form monoterpenes, such as *α*-terpineol, limonene, and terpinolene, and the C^+ group could further rearrange to form myrcene and *β*-ocimene [17]. *β*-pinene, *α*-terpinene, *β*-phellandrene, *α*-thujone, 3-buten-1-yl isothiocyanate, citronellal, linalyl acetate, 3-phenylpropionitrile, and 3-ethyl-2,5-dimethylpyrazine were the differential key flavor compounds between FFTO and DFTO. *α*-Thujone exhibited extremely high significance only in FFTO, and its concentration was also significantly higher in FFTO than in DFTO; this might be the reason for the slightly stronger green aroma

in FFTO. The difference between the OAV analysis results and those from the omission experiment might be attributable to the complex interactions within the food system [38]. In particular, limonene—which has a high OAV among FTOs—was not identified by most participants in the three-point test. It is possible that the combined effects of other compounds have replaced its own effects.

Table 3. The significance of each compound in the omission tests.

No.	Compound	Number of Correct Answers		Significance	
		FFTO	DFTO	FFTO	DFTO
M1	β-Pinene	8/20	11/20	NS	*
M2	Sabinene	6/20	8/20	NS	NS
M3	β-Myrcene	8/20	6/20	NS	NS
M4	α-Terpinene	4/20	11/20	NS	*
M5	Limonene	4/20	9/20	NS	NS
M6	Eucalyptol	3/20	6/20	NS	NS
M7	β-Phellandrene	9/20	11/20	NS	*
M8	Terpinolene	4/20	6/20	NS	NS
M9	Octanal	5/20	6/20	NS	NS
M10	Neo-alloocimene	7/20	-	NS	-
M11	α-Thujone	15/20	8/20	***	NS
M12	3-Buten-1-yl Isothiocyanate	12/20	6/20	*	NS
M13	Citronellal	11/20	-	*	-
M14	Benzaldehyde	8/20	2/20	NS	NS
M15	Linalool	16/20	13/20	***	**
M16	Linalyl acetate	14/20	5/20	***	NS
M17	β-Caryophyllene	11/20	14/20	*	***
M18	Terpinen-4-ol	6/20	-	NS	-
M19	3-Phenylpropionitrile	11/20	4/20	*	NS
M20	γ-Terpinene	-	5/20	-	NS
M21	3-Ethyl-2,5-diMethylpyrazine	-	11/20	-	*
M22	Allylacetic acid	-	4/20	-	NS

"-" indicates that the compound was not detected or the odor threshold was not found. The experiment is based on the sensory analysis method—the triangle test (GB/T 12311-2012 [39]). The experiment was conducted once by each of the 20 participants. *** 0.1% significance level. ** 1% significance level. * 5% significance level. NS, no significant difference. (FFTO, fresh fried *Tengjiao* oil; DFTO, dried fried *Tengjiao* oil).

3.8. The Enantiomeric Ratio and Its Effect on FTOs' Flavor

To explore the effect of the enantiomeric ratio in FPO on its flavor profile, we determined the enantiomeric ratios of limonene and linalool, which are abundant in FPO (Table 4). The *t*-test results indicate that there is a significant difference in the enantiomers of linalool between FFTO and DFTO. It has been demonstrated that the processing of tea leaves affects the enantiomeric ratio of chiral compounds within them, which in turn influences the flavor profile [40]. In FTOs, the ratio of (S)-(−)-limonene to (R)-(+)-limonene in FFTO and DFTO was similar, with both being close to 7:3. Due to the high proportion of (S)-(−)-limonene, FFTO and DFTO exhibited a herbal and citrus-like aroma, consistent with our AEDA results. Meanwhile, linalool showed a significant difference in enantiomeric ratio. In both FFTO and DFTO, (R)-(−)-linalool was dominant, accounting for 81.68% in FFTO and 90.83% in DFTO. Due to its high proportion of (R)-(−)-linalool, FFTO and DFTO exhibited distinct sweet and floral notes [20] from linalool, consistent with our AEDA results. In sensory evaluation, the citrus-like attributes of FFTO and DFTO were not significantly different, with FFTO exhibiting a slightly higher level than DFTO. This difference may be attributable to other aroma-active compounds present in FTO, such as γ-terpinene. In addition, FFTO had a slightly stronger wood aroma than DFTO, which may be related to the higher proportion of (S)-(+)-linalool in FFTO compared to DFTO. In addition, FFTO had a slightly stronger wood aroma than DFTO, which may be related to the higher proportion

of (S)-(+)-linalool in FFTO compared to DFTO. The main difference between the FFTO and DFTO preparation processes lay in the hot-air drying of the *Tengjiao* fruits. During hot-air drying, linalool may undergo a transformation [17], from which we can infer that hot-air drying may promote the conversion of (S)-(+)-linalool to (R)-(−)-linalool, resulting in the difference in enantiomeric ratio.

Table 4. The enantiomeric ratio of limonene and linalool in FFTO and DFTO.

Compound	CAS	Odor Description [15]	Enantiomeric Ratio (%)	
			FFTO (%)	DFTO (%)
(S)-(−)-Limonene	5989-54-8	lemon-like, piney	70.11 ± 2.61	70.96 ± 0.82
(R)-(+)-Limonene	5989-27-5	citrus-like	29.89 ± 2.61	29.98 ± 0.82
(S)-(+)-linalool *	126-90-9	woody, lavender-like	18.32 ± 2.34	9.17 ± 1.2
(R)-(−)-linalool *	126-91-0	sweet, floral, petitgrain-like	81.68 ± 2.34	90.83 ± 1.2

"*" indicates that $p < 0.05$ in the *t*-test, indicating a statistically significant difference. The contents are expressed as the average of three experiments, presented as the mean ± standard deviation. (FFTO, fresh fried *Tengjiao* oil; DFTO, dried fried *Tengjiao* oil).

4. Conclusions

In this study, we compared the flavor differences between FFTO and DFTO by molecular sensory science. First, sensory evaluation was used to compare the flavor profiles of the two samples. In terms of overall flavor profile, FFTO had stronger pepper and spice notes, while DFTO exhibited a more marked oily aroma. Recombination experiments and omission tests were conducted based on the AEDA and OAV results. Linalool and β-caryophyllene were both key flavor compounds within the characteristic flavor profile of 2 FTOs. α-Thujone, 3-buten-1-yl isothiocyanate, citronellal, linalyl acetate, and 3-henylpropionitrile were key flavor compounds in FFTO, and β-pinene, α-terpinene, β-phellandrene, and 3-ethyl-2,5-dimethylpyrazine were key flavor compounds in DFTO. Furthermore, chiral analysis revealed that the predominant enantiomers in FTO were primarily (R)-(−)-linalool and (S)-(−)-limonene. In conclusion, in this experiment, we determined and compared the differences in key flavor compounds between FFTO and DFTO and analyzed the enantiomeric ratios of limonene and linalool. Based on the results, we explained the reasons for using both fresh and dried *Tengjiao* in spicy dishes from a flavor perspective. This study provides theoretical guidance for the production of spicy dishes. In the future, we can perform more in-depth research, such as exploring how the ratio of fresh *Tengjiao* to dried *Tengjiao* affects the flavor of dishes. This study provides preliminary insights into the flavor differences between FFTO and DFTO at the molecular level. However, the exact mechanism has not yet been elucidated. A clear mechanism will provide valuable guidance for quality control in FTO.

Author Contributions: Conceptualization, J.S. and H.C.; methodology, T.D.; software, P.W.; validation, S.W., J.S. and H.C.; formal analysis, P.W.; investigation, P.W.; resources, J.S.; data curation, P.W.; writing—original draft preparation, T.D.; writing—review and editing, J.S.; visualization, H.C.; supervision, S.W.; project administration, H.C.; funding acquisition, J.S. All authors have read and agreed to the published version of the manuscript.

Funding: This research was funded by Yunnan Province Major Science and Technology Special Project on Biological Breeding and Deep Processing of Agricultural Products, grant number 202502AE090034.

Institutional Review Board Statement: The study was conducted in accordance with the Declaration of Helsinki and approved by the Ethics Committee of Beijing Technology and Business University (protocol code No. 139 of 2025, approved on 4 June 2025).

Informed Consent Statement: Informed consent was obtained from all subjects involved in the study.

Data Availability Statement: The original contributions presented in this study are included in the article. Further inquiries can be directed to the corresponding authors.

Conflicts of Interest: The authors declare no conflicts of interest.

Abbreviations

The following abbreviations are used in this manuscript:

ZA	*Zanthoxylum armatum* DC.
FTO	Fried *Tengjiao* oil
FFTO	Fresh fried *Tengjiao* oil
DFTO	Dried fried *Tengjiao* oil
ZB	*Zanthoxylum bungeanum* Maxim.
OAV	Odor activity value
ZS	*Zanthoxylum schinifolium* sieb. et Zucc.
VOCs	Volatile organic compounds
SAFE	Solvent-assisted flavor evaporation
GC-MS	Gas chromatography–mass spectrometry
QDA	Quantitative descriptive analysis
AEDA	Aroma extract concentration analysis
FD	Flavor dilution
PLSR	Partial least squares regression
VIP	Variable importance for the projection

Appendix A

Table A1. The results of GC-MS for FFTO and DFTO.

RT	Compound	CAS	FFTO	DFTO	Identification
3.66	Pentanal	110-62-3		√	MS, RI, S
4.23	tert-Amyl alcohol	75-85-4	√	√	MS, RI, S
4.32	α-Pinene	80-56-8	√	√	MS, RI, S
4.46	α-Phellandrene	99-83-2	√	√	MS, S
4.83	1-Propanol	71-23-8	√		MS, RI, S
5.31	Camphene	79-92-5	√		MS, RI, S
6	Hexanal	66-25-1	√	√	MS, RI, S, O
6.5	β-Pinene	127-91-3	√	√	MS, RI, S, O
7.07	Sabinene	3387-41-5	√	√	MS, RI, S, O
7.4	Ethylbenzene	100-41-4		√	MS, RI, S
7.55	trans-2-Pentenal	1576-87-0		√	MS, RI, S
7.62	*p*-Xylene	106-42-3	√	√	MS, RI, S
8.29	1-Butanol	71-36-3	√		MS, RI, S
8.88	1-Penten-3-ol	616-25-1		√	MS, RI, S
8.95	β-Myrcene	123-35-3	√	√	MS, RI, S, O
9.31	α-Terpinene	99-86-5	√	√	MS, RI, S, O
9.58	*o*-Xylene	95-47-6	√	√	MS, RI, S
9.74	3-Butenenitrile	109-75-1		√	MS, RI, S
9.83	Heptanal	111-71-7		√	MS, RI, S
10.18	Limonene	5989-27-5	√	√	MS, RI, S, O
10.36	Eucalyptol	470-82-6	√	√	MS, RI, S, O
10.49	β-Phellandrene	555-10-2	√	√	MS, RI, S, O
11.21	(*E*)-2-Hexenal	6728-26-3		√	MS, RI, S
11.62	4-Octanone	589-63-9	√	√	MS, RI, S, O
12.02	2-pentyl-Furan	3777-69-3		√	MS, RI, S
12.23	*trans*-β-Ocimene	3779-61-1	√		MS, RI, S
12.41	γ-Terpinene	99-85-4	√	√	MS, RI, S, O
13.13	Styrene	100-42-5	√	√	MS, RI, S, O
13.4	2-Methylpyrazine	109-08-0		√	MS, RI, S
13.67	*p*-Cymene	99-87-6	√	√	MS, RI, S
14.12	3-Methylcrotononitrile	4786-24-7	√	√	MS
14.26	Terpinolene	586-62-9	√	√	MS, RI, S, O
14.89	Octanal	124-13-0	√	√	MS, RI, S, O
16.25	2,5-Dimethyl pyrazine	123-32-0		√	MS, RI, S

Table A1. *Cont.*

RT	Compound	CAS	FFTO	DFTO	Identification
16.61	(*E*)-2-Heptenal	18829-55-5	√	√	MS, RI, S, O
17.54	6-Methyl-5-hepten-2-one	110-93-0		√	MS, RI, S
18	5-Hexenenitrile	5048-19-1	√	√	MS, RI, S
19.464	2,6-DiMethyl-2,4,6-octatriene	673-84-7		√	MS, O
19.5	Neo-alloocimene	7216-56-0	√		MS, S, O
20.77	Nonanal	124-19-6	√	√	MS, RI, S, O
21.6	*α*-Thujone	546-80-5	√	√	MS, RI, S, O
22.51	(*E*)-2-Octenal	2548-87-0	√	√	MS, RI, S, O
22.75	Thujone	1125-12-8	√	√	MS, RI, S, O
23.22	3-Ethyl-2,5-diMethylpyrazine	13360-65-1		√	MS, RI, S, O
23.33	*cis*-Linalool Oxide	5989-33-3	√		MS, RI, S, O
24.3	Acetic acid	64-19-7	√	√	MS, S, O
24.4	3-Buten-1-yl Isothiocyanate	3386-97-8	√	√	MS, RI, S, O
24.86	*trans*-Sabinene hydrate	17699-16-0	√		MS, O
25	Furfural	98-01-1	√	√	MS, RI, S
25.72	Citronellal	106-23-0	√		MS, RI, S, O
26.31	(*E*,*E*)-2,4-Heptadienal	4313-03-5	√	√	MS, RI, S, O
27.11	2-Acetylfuran	1192-62-7	√	√	MS, RI, S, O
27.72	Benzaldehyde	100-52-7	√	√	MS, RI, S, O
30.3	Linalool	78-70-6	√	√	MS, RI, S, O
30.43	Linalyl acetate	115-95-7	√	√	MS, RI, S, O
31.03	5-Methyl furfural	620-02-0	√	√	MS, RI, S, O
31.41	*β*-Caryophyllene	87-44-5	√	√	MS, RI, S, O
32.5	Terpinen-4-ol	562-74-3	√	√	MS, RI, S, O
33.23	Myrtenal	564-94-3	√		MS, RI, O
33.48	Gamma Butyrolactone	96-48-0		√	MS, S, O
34.269	Butyric Acid	107-92-6	√		MS, S, O
34.69	*trans*-2-Decenal	3913-81-3		√	MS, RI, S, O
35.38	*α*-Caryophyllene	6753-98-6	√	√	MS, RI, S, O
35.41	N-Methyl-2-pyrrolidone	872-50-4		√	MS, RI, S
36.5	Furfuryl alcohol	98-00-0	√	√	MS, RI, S, O
37.62	Germacrene D	23986-74-5	√	√	MS, RI, S
37.94	*α*-Terpineol	98-55-5	√	√	MS, RI, S, O
38.55	Piperitone	89-81-6	√		MS, RI, S, O
40.267	(*E*)-4-Undecenal	68820-35-9		√	MS, O
40.38	2(5H)-Furanone	497-23-4		√	MS, RI, S
41.24	Methyl phenylacetate	101-41-7	√		MS, RI, S
42.9	Myrtenol	515-00-4	√		MS, RI, S
43.61	*trans*,*trans*-2,4-Decadienal	25152-84-5	√	√	MS, RI, S, O
43.943	Allylacetic acid	591-80-0		√	MS, S, O
44.1	Phenethyl acetate	103-45-7	√		MS, RI, S
44.81	2-Hydroxy-3-Methyl-2-cyclopentenone	765-70-8		√	MS, RI, S, O
44.84	Methyl cyclopentenolone	80-71-7	√		MS, RI, S, O
49.04	Phenylethyl Alcohol	60-12-8	√		MS, RI, S
51.96	2-Acetyl pyrrole	1072-83-9		√	MS, RI, S, O
54.53	3-Phenylpropionitrile	645-59-0	√	√	MS, RI, S, O
55.31	cis-Nerolidol	142-50-7	√		MS, O
63.68	Indole	120-72-9	√		MS, RI, S, O

"√" indicates that the compound was detected.

References

1. Wang, Y.; Wu, Q.; Jiang, L.; Ma, D.; Yu, J.; Cui, Q.; Huo, X.; Shen, G.; Zhou, M.; Liu, H.; et al. Characteristic of essential oil in *Zanthoxylum armatum* DC. leaves and application in flavor oil. *Food Chem. X* **2025**, *28*, 102519. [CrossRef]
2. Yang, H.; Zhuo, Z.; Qian, Q.; Yang, Y.; Xu, D. Multi-omics strategy to reveal the numbing taste of *Zanthoxylum armatum* DC. at different developmental stages. *Ind. Crop. Prod.* **2024**, *221*, 119405. [CrossRef]
3. Xu, D.; Wang, C.; Zhuo, Z.; Ye, M.; Pu, B. Extraction, purification and antioxidant activity of polysaccharide from cold pressed oil cake of 'Tengjiao' seed. *Int. J. Biol. Macromol.* **2020**, *163*, 508–518. [CrossRef]
4. Devi, M.L.; Das, S. Traditional uses, phytochemistry, biological activities, and molecular studies of *Zanthoxylum armatum* DC.: A review. *Next Res.* **2025**, *2*, 100445. [CrossRef]
5. Hu, F.; Zhang, A.; Ji, Z.-L.; Thakur, K.; Zhang, J.-G.; Wei, Z.-J. Effects of different extraction methods on the volatile components and numbing substances in red *Huajiao* (*Zanthoxylum bungeanum* Maxim.) and green Huajiao (*Zanthoxylum armatum* DC.). *Food Chem. X* **2025**, *29*, 102820. [CrossRef]

6. Liu, H.; Zhan, P.; Wang, P.; Geng, J.; He, W.; Tian, H. Huajiao Extract Oil: A Comprehensive Review of Its Biological Activities, Extraction Techniques, and Utilization in Food Industry. *Food Rev. Int.* **2025**, *41*, 3569–3588. [CrossRef]
7. Liu, Y.; Li, Q.; Yang, W.; Sun, B.; Zhou, Y.; Zheng, Y.; Huang, M.; Yang, W. Characterization of the potent odorants in *Zanthoxylum armatum* DC Prodr. pericarp oil by application of gas chromatography–mass spectrometry–olfactometry and odor activity value. *Food Chem.* **2020**, *319*, 126564. [CrossRef]
8. Li, J.; Zhang, Y.; Cui, Q.; Zhang, Z.; Hou, X. Quality Control of Fried Pepper Oils Based on GC-MS Fingerprints and Chemometrics. *Foods* **2025**, *14*, 1624. [CrossRef]
9. Fei, X.; Qi, Y.; Lei, Y.; Wang, S.; Hu, H.; Wei, A. Transcriptome and Metabolome Dynamics Explain Aroma Differences between Green and Red Prickly Ash Fruit. *Foods* **2021**, *10*, 391. [CrossRef]
10. Liu, J.; Wan, J.; Zhang, Y.; Hou, X.; Shen, G.; Li, S.; Luo, Q.; Li, Q.; Zhou, M.; Liu, X.; et al. The establishment of comprehensive quality evaluation model for flavor characteristics of green Sichuan pepper (*Zanthoxylum armatum* DC.) in Southwest China. *Food Chem. X* **2023**, *18*, 100721. [CrossRef]
11. Cheng, J.; Hou, X.; Cui, Q.; Shen, G.; Li, S.; Luo, Q.; Zhou, M.; Chen, H.; Zhang, Z. Separation and Purification of Hydroxyl-α-Sanshool from *Zanthoxylum armatum* DC. by Silica Gel Column Chromatography. *Int. J. Mol. Sci.* **2023**, *24*, 3156. [CrossRef]
12. Ji, Y.; Li, S.; Ho, C.-T. Chemical composition, sensory properties and application of Sichuan pepper (*Zanthoxylum* genus). *Food Sci. Hum. Well.* **2019**, *8*, 115–125. [CrossRef]
13. Wang, J.; Zhu, X.; Ye, J.; Zhu, X.; Hou, X.; Shen, G.; Cui, Q.; Yu, J.; Liu, H.; Wen, C.; et al. Moisture dynamics and flavor evolution in green Sichuan pepper during processing: An LF-NMR/MRI approach. *Food Chem.* **2026**, *498*, 147151. [CrossRef]
14. Zhao, C.; Zhang, F.; Chen, S.; Hu, W.; Dong, L.; Zhao, Y.; Han, M.; Li, Z. Effects of drying methods on the quality of Hanyuan *Zanthoxylum bungeanum* based on physicochemical and functional metabolite analysis. *LWT* **2023**, *180*, 114674. [CrossRef]
15. Liu, R.J.; Qi, N.; Sun, J.; Chen, H.T.; Zhang, N.; Sun, B.G. Effects of Frying Conditions on Volatile Composition and Odor Characteristics of Fried Pepper (*Zanthoxylum bungeanum* Maxim.) Oil. *Foods* **2022**, *11*, 1661. [CrossRef]
16. Zhang, W.; Bi, T.; Liu, E.; Xiong, Y.; Yang, Y.; Liu, Q.; Xie, Y.; Li, T.; Yuan, Y. The role of frying time in shaping the flavor characteristics of chili rapeseed oil. *Int. J. Gastron. Food Sci.* **2025**, *41*, 101220. [CrossRef]
17. Zhang, J.; Zhang, M.; Chen, K.; Bhandari, B.; Deng, D. Impact of cooking methods on the quality, sensory and flavor compounds of Sichuan pepper oleoresin. *Food Chem.* **2023**, *427*, 136639. [CrossRef]
18. Steinhaus, P.; Schieberle, P. Characterization of the Key Aroma Compounds in Soy Sauce Using Approaches of Molecular Sensory Science. *J. Agric. Food Chem.* **2007**, *55*, 6262–6269. [CrossRef]
19. He, W.; Chen, X.; Sun, J.; Chen, H.; Sun, B. Unveiling key aroma compounds formation during the roasting process of Yunnan Arabica coffee using molecular sensory science approaches. *Food Chem.* **2025**, *494*, 145853. [CrossRef]
20. Sun, J.; Sun, B.G.; Ren, F.Z.; Chen, H.T.; Zhang, N.; Zhang, Y.Y. Characterization of Key Odorants in Hanyuan and Hancheng Fried Pepper (*Zanthoxylum bungeanum*) Oil. *J. Agric. Food Chem.* **2020**, *68*, 6403–6411. [CrossRef]
21. Ni, R.; Yan, H.; Tian, H.; Zhan, P.; Zhang, Y. Characterization of key odorants in fried red and green huajiao (*Zanthoxylum bungeanum* maxim. and *Zanthoxylum schinifolium* sieb. et Zucc.) oils. *Food Chem.* **2022**, *377*, 131984. [CrossRef]
22. Wang, M.; Wen, F.; Zhang, L.; Sun, B.; Xie, J.; Sun, S.; Zhang, Y. Decoding the Molecular Mechanisms of Menthol Isomer Perception Based on Computational Simulations. *Foods* **2025**, *14*, 2494. [CrossRef]
23. Dong, T.; Tian, Z.; Wang, S.; Sun, J.; Chen, H.; Wang, S.; Sun, B. Identification of key off-flavor compounds during storage of fried pepper (*Zanthoxylum bungeanum* Maxim.) oils by sensory-directed flavor analysis and partial least squares regression (PLSR). *J. Food Compos. Anal.* **2024**, *131*, 106268. [CrossRef]
24. Tian, P.; Zhan, P.; Tian, H.; Wang, P.; Lu, C.; Zhao, Y.; Ni, R.; Zhang, Y. Analysis of volatile compound changes in fried shallot (*Allium cepa* L. var. aggregatum) oil at different frying temperatures by GC–MS, OAV, and multivariate analysis. *Food Chem.* **2021**, *345*, 128748. [CrossRef] [PubMed]
25. Gemert, L.J.V. *Odour Thresholds*; Oliemans Punter & Partners BV: Utrecht, The Netherlands, 2011.
26. Chen, P.; Zhao, S.; Li, C.; Zhang, T.; Xing, Y.; Zhang, K.; Lv, J.; Zhu, W. Changes and Analytical Techniques in Volatile Flavor Compounds in Dried Agricultural Products: A Review. *Foods* **2025**, *14*, 3531. [CrossRef]
27. Adams, A.; Polizzi, V.; van Boekel, M.; De Kimpe, N. Formation of Pyrazines and a Novel Pyrrole in Maillard Model Systems of 1,3-Dihydroxyacetone and 2-Oxopropanal. *J. Agric. Food Chem.* **2008**, *56*, 2147–2153. [CrossRef] [PubMed]
28. Yaylayan, V.A.; Keyhani, A. Elucidation of the mechanism of pyrrole formation during thermal degradation of 13C-labeled l-serines. *Food Chem.* **2001**, *74*, 1–9. [CrossRef]
29. Zhang, Q.; Ke, J.; Long, P.; Wen, M.; Han, Z.; Zhang, L.; Zhu, M. Formation of Furan from Linoleic Acid Thermal Oxidation: (E,E)-2,4-Decadienal as a Critical Intermediate Product. *J. Agric. Food Chem.* **2024**, *72*, 4384–4392. [CrossRef]
30. Dong, T.; Wang, S.; Wu, P.; Sun, J.; Chen, H.; Wang, S. Unraveling the influence of storage condition on off-flavor generation in fried pepper (*Zanthoxylum bungeanum* Maxim.) oil during storage through molecular sensory science and simulation experiment. *Food Chem.* **2026**, *508*, 148415. [CrossRef]

31. Su, K.; Sun, S.; Chen, R.; Ren, M.; Wang, Y.; Bi, S.; Liu, Y. Identification of key aroma-active compounds in five types of Zanthoxylum bungeanum Maxim. essential oils using a molecular sensory approach. *J. Food Compos. Anal.* **2025**, *145*, 107816. [CrossRef]
32. Zhu, X.; Wu, D.; Zhao, L.; Wen, C.; Yong, C.; Kan, Q. Unveiling the flavor and quality variations in dried *Zanthoxylum bungeanum* maxim from China's diverse regions. *Food Chem. X* **2025**, *25*, 102017. [CrossRef]
33. Lu, L.; Wang, M.; Cui, R.; Zhu, Y.; Liu, S.; Yin, Z.; Gao, D. Discrimination and characterization analysis of key flavor compounds from Tianshui *Zanthoxylum bungeanum* shells and seeds by GC×GC-TOFMS and chemometrics. *Food Chem. X* **2025**, *29*, 102765. [CrossRef]
34. Pu, D.; Zhang, H.; Zhang, Y.; Sun, B.; Ren, F.; Chen, H.; Xie, J. Characterization of the oral breakdown, sensory properties, and volatile release during mastication of white bread. *Food Chem.* **2019**, *298*, 125003. [CrossRef] [PubMed]
35. Xiang, Q.; Xia, Y.; Song, J.; Nazmus Saqib, M.; Zhong, F. Characterization of the key nonvolatile metabolites in Cheddar cheese by partial least squares regression (PLSR), reconstitution, and omission. *Food Chem.* **2023**, *403*, 134034. [CrossRef] [PubMed]
36. Wang, M.-Q.; Ma, W.-J.; Shi, J.; Zhu, Y.; Lin, Z.; Lv, H.-P. Characterization of the key aroma compounds in Longjing tea using stir bar sorptive extraction (SBSE) combined with gas chromatography-mass spectrometry (GC–MS), gas chromatography-olfactometry (GC-O), odor activity value (OAV), and aroma recombination. *Food Res. Int.* **2020**, *130*, 108908. [CrossRef] [PubMed]
37. He, Y.; Liu, Y.; Sun, J.; Qiao, M.; Wang, L.; Zhao, Q.; Xiao, D.; Guo, X. Characterization of the key aroma-active compounds causing the Douchi aroma in high-temperature Daqu via integrated molecular sensory science, metabolomics, and molecular docking. *Food Chem.* **2025**, *493*, 146125. [CrossRef]
38. Chen, C.; Sheng, M.; Yuan, H.; Pan, X.; Tian, H.; Lou, X. Perceptual interaction of aroma compounds and their effects on the enhancement of flavor quality in foods: A review. *Trends Food Sci. Tech.* **2025**, *165*, 105315. [CrossRef]
39. *GB/T 12311-2012*; Sensory Analysis Method—Triangle Test. China Standard Press: Beijing, China, 2012.
40. Shao, C.-Y.; Zhang, Y.; Lv, H.-P.; Zhang, Z.-F.; Zeng, J.-M.; Peng, Q.-H.; Zhu, Y.; Lin, Z. Aromatic profiles and enantiomeric distributions of chiral odorants in baked green teas with different picking tenderness. *Food Chem.* **2022**, *388*, 132969. [CrossRef]

Disclaimer/Publisher's Note: The statements, opinions and data contained in all publications are solely those of the individual author(s) and contributor(s) and not of MDPI and/or the editor(s). MDPI and/or the editor(s) disclaim responsibility for any injury to people or property resulting from any ideas, methods, instructions or products referred to in the content.

foods

MDPI

Article

Characterization of Retronasal Aroma Differences in High- and Low-Alcohol Jiangxiangxing Baijiu Using Temporal Sensory Evaluation, Retronasal Olfactory Thresholds, and Dose-over-Threshold Analysis

Jun Zhang [1], Yehui Han [1], Xiaolong You [2,3], Xiaochun Zhu [2,3], Youlan Sun [2,3], Feng Hu [2,3], Xiaowei Yu [1,*], Shuang Chen [1,*] and Yan Xu [1]

[1] Laboratory of Brewing Microbiology and Applied Enzymology, State Key Laboratory of Food Science & Resources, Key Laboratory of Industrial Biotechnology of Ministry of Education, School of Biotechnology, Jiangnan University, 1800 Lihu Ave, Wuxi 214122, China; zjchem163@163.com (J.Z.); dblhui2@163.com (Y.H.); yxu@jiangnan.edu.cn (Y.X.)

[2] Guizhou Xijiu Co., Ltd., Xishui 564622, China; youxiaolong1122@163.com (X.Y.); luqintian2022@163.com (X.Z.); 15761699434@163.com (Y.S.); hufeng2025xj@163.com (F.H.)

[3] Key Laboratory of Quality and Safety of Jiangxiangxing Baijiu, State Administration for Market Regulation, Guiyang 550025, China

* Correspondence: yuxw@jiangnan.edu.cn (X.Y.); shuangchen@jiangnan.edu.cn (S.C.); Tel.: +86-0510-85918201 (X.Y.)

Abstract

Retronasal aroma strongly influences the flavor quality of low-alcohol Jiangxiangxing Baijiu. This study investigated the retronasal aroma differences between high- and low-alcohol samples (Sample-High and Sample-Low). Dynamic sensory evaluation revealed roasted, grain, floral and fruity, hay, and caramel notes were more pronounced in Sample-High, whereas Sample-Low exhibited stronger fatty and smoky notes, indicating insufficient retronasal aroma richness in Sample-Low. Analysis of 67 compounds showed no significant concentration differences, yet their retronasal olfactory thresholds varied markedly between alcoholic systems (ratio 1.04–4.75), leading to higher dose-over-threshold (DoT) values for several compounds in Sample-Low. Further analysis of the DoT distribution intervals showed Sample-High presented a more balanced distribution, whereas Sample-Low was strongly driven by several high-contribution compounds, which reduced the relative contributions of others. This unbalanced distribution may underlie the lower retronasal aroma richness observed in Sample-Low. These findings provide a new perspective for understanding retronasal aroma in low-alcohol Jiangxiangxing Baijiu.

Keywords: low-alcohol; retronasal aroma; temporal sensory evaluation; retronasal olfactory thresholds; dose-over-threshold

1. Introduction

Jiangxiangxing Baijiu, as one of the important categories within the Chinese distilled liquor system, has received widespread attention owing to its distinctive and rich flavor characteristics. The formation of its characteristic style is closely associated with the numerous flavor compounds generated during its unique brewing process, which collectively shape its sensory profile and further influence consumer perception of overall quality and typicity [1–3]. Aroma, as one of the important components of the overall flavor of *Jiangxiangxing* Baijiu, shapes the initial olfactory impression of consumers and plays a

critical role in their perception of product quality and preference. As consumer preferences diversify, the market for lower-alcohol Baijiu has shown steady growth, accompanied by heightened expectations for aroma quality. Against this background, clarifying how alcohol concentration influences the olfactory characteristics of Baijiu has become a central scientific topic of shared concern for both academia and industry.

Current studies in Baijiu flavor chemistry have mainly concentrated on identifying aroma compounds and assessing their contributions to overall sensory perception. These studies have predominantly focused on high-alcohol Baijiu (typically $\geq$50% vol) and have been limited to the orthonasal olfactory pathway. However, human olfaction involves both orthonasal and retronasal pathways [4,5]. Compared with orthonasal perception, retronasal olfaction provides a more accurate representation of the dynamic evolution of aroma during the consumption of Baijiu, thereby playing a pivotal role in defining the overall sensory experience. Nevertheless, systematic studies on the retronasal olfactory characteristics of Baijiu remain scarce. Among the few available studies, some have concentrated exclusively on single-alcohol systems [6], whereas others have lacked an integrated framework linking alcohol content variation with the functional roles of aroma perception [7,8]. To date, the influence of alcohol concentration on the dynamic evolution of retronasal aroma in Baijiu remains poorly elucidated, revealing a distinct knowledge gap in Baijiu flavor research. Notably, the perceptual differences between high- and low-alcohol *Jiangxiangxing* Baijiu are closely associated with variations in the differential contributions of key aroma compounds. From the perspective of flavor chemistry, the potential retronasal impact of individual compounds can be quantitatively assessed using the dose-over-threshold (DoT). Among relevant parameters, the retronasal olfactory threshold (ROT) serves as a key indicator for quantitative evaluation, indirectly reflecting the intrinsic capacity of individual compounds to contribute to retronasal aroma. However, research on the ROT of key aroma compounds in Baijiu remains considerably limited. First, existing data are primarily based on single-alcohol systems [6,9]. Second, the number of compounds with established ROT values is insufficient for comprehensive comparison. Critically, no systematic studies have yet explored how ethanol concentration influences the ROT of key aroma compounds. These limitations obscure the chemical basis of post-ingestive retronasal differences between high- and low-alcohol *Jiangxiangxing* Baijiu and hamper flavor optimization of low-alcohol products. Therefore, clarifying the ROT and DoT of key aroma compounds across different alcohol levels can bridge the existing research gap and provide essential theoretical and practical insights into the chemical basis of retronasal sensory differences among Baijiu with different alcohol levels.

Therefore, to clarify the retronasal aroma differences between high- and low-alcohol *Jiangxiangxing* Baijiu, this study aimed to: (1) characterize these differences across different stages using temporal sensory evaluation methods; (2) determine the ROT of selected aroma compounds in 40% vol and 50% vol ethanol aqueous solution systems; and (3) elucidate the chemical basis of these retronasal aroma differences by integrating compound DoT values across high- and low-alcohol systems with the differential patterns of potential aroma contribution distributions within each system. This study establishes a theoretical foundation for quality improvement and precise flavor modulation in low-alcohol *Jiangxiangxing* Baijiu, highlighting both its academic significance and practical relevance.

2. Materials and Methods

2.1. Baijiu Samples

Given the limited availability of commercially available low-alcohol *Jiangxiangxing* Baijiu products, 39% vol and 53% vol were selected as practical comparison points to provide a clearer contrast between typical low- and high-alcohol products on the market.

https://doi.org/10.3390/foods15071156

Two *Jiangxiangxing* Baijiu samples from a distillery in Southwest China were therefore used in this study: a low-alcohol sample (39% vol, labeled Sample-Low) and a high-alcohol sample (53% vol, labeled Sample-High). Although some co-authors are affiliated with the company, it provided only access to analytical instruments and technical personnel, and had no involvement in the selection of the samples or alcohol levels. Both products have been marketed for years and thus show a certain degree of market representativeness in flavor profile. Samples were stored at 20 °C in a temperature-controlled room throughout the experiment.

2.2. Reagents and Chemicals

All compounds used in the sensory experiments were food-grade, with detailed provided in Table S1. Food-grade ethanol (95% vol) was supplied by Shanghai Titan Co., Ltd. (Shanghai, China), and purified water was obtained from Hangzhou Wahaha Group Co., Ltd. (Hangzhou, China).

2.3. Sensory Analysis

2.3.1. Sensory Panel

Referring to a previous study [10], a sensory panel consisting of 36 assessors had already been established. Based on this panel, 23 assessors (13 males and 10 females, aged 25–30 years) were pre-selected as the core candidate semi-trained panel for the present study.

All were current graduate students from Jiangnan University (Wuxi, China) with over two years of experience in Baijiu sensory evaluation. In addition, six senior certified Baijiu tasters from renowned domestic distilleries, each possessing over ten years of sensory experience, were invited to provide expert guidance, participate in descriptor discussion, and assist in the performance evaluation of the semi-trained panelists. These tasters were not included in the formal sensory dataset used for statistical analysis. All candidate semi-trained panelists and senior tasters were in good health, had normal olfactory function, and no history of alcohol allergy.

Before the formal experiment, the training program was refined based on prior curricula, and a short-term professional course consisting of three two-hour sessions was conducted, focusing on the identification of sensory attributes and the establishment of reference standards (Table S2). To avoid potential bias from prior knowledge, semi-trained members were not informed of the chemical composition of each reference during training. Moreover, some high- and low-alcohol Jiangxiangxing Baijiu samples with typical aroma characteristics were used to strengthen their ability to identify these sensory features under varying ethanol concentrations. Following the training, the 23 semi-trained panelists underwent a comprehensive performance evaluation and were confirmed as qualified for the formal sensory experiments. Written informed consent was obtained from all participants prior to the study, and appropriate remuneration was provided upon completion. The study was reviewed and approved by the Human Research Ethics Committee of Jiangnan University.

The formal sensory evaluation was conducted in the professional sensory laboratory of the Synergistic Innovation Centre at Jiangnan University. The testing environment was maintained at 25 ± 1 °C, with clean and odor-free air. The panelists performed evaluations in individual sensory booths while wearing nose clips before sample intake. Each sample (2 mL) was accurately measured and served in standardized tasting glasses labeled with random three-digit codes, which were presented in a randomized order. To verify within-panelist consistency and sample repeatability, the same Baijiu sample (identified by different random codes) was presented three times during the evaluation

https://doi.org/10.3390/foods15071156

sequence. After completing each set of samples, panelists rinsed their mouths with an aqueous ethanol solution of about 3% vol for approximately 10 s, followed by thorough rinsing with purified water at room temperature. The entire rinsing procedure lasted about 1 min, after which a mandatory rest period of at least 10 min was required before evaluating the next sample.

2.3.2. Retronasal Dual-Mode Temporal Check-All-That-Apply (RDM-TCATA) Analysis

The development of dynamic sensory analysis techniques has greatly advanced the characterization of the temporal evolution of sensory attributes during consumption. While the check-all-that-apply method allows for comprehensive collection of retronasal aroma descriptors, it fails to capture their temporal evolution. In contrast, temporal check-all-that-apply integrates the time dimension, enabling dynamic tracking of aroma evolution [11]. Given the inherent complexity and temporal variability of retronasal aroma perception during Baijiu consumption, this study developed an innovative dual-mode system, RDM-TCATA, to capture retronasal aroma attributes and their temporal citation dynamics under different evaluation modes.

To establish descriptors scientifically aligned with the retronasal aroma characteristics of Sample-High and Sample-Low, six senior certified Baijiu tasters participated in on-site evaluations and discussions based on actual samples. Through consensus among all panelists, a final predefined list of retronasal aroma descriptors was developed and later applied in the RDM-TCATA experiments. Following previous studies [12,13], this study also considered three evaluation intervals, attack (A, 0–15 s), evolution (E, 16–60 s), and finish (F, 61–150 s), to investigate the dynamic changes in retronasal aroma perception across different post-ingestion stages in samples. Prior to the experiment, panelists received supplementary training to standardize descriptor definitions and software operation procedures, thereby ensuring consistency in evaluation criteria. The experiment was conducted in two consecutive stages. In the first stage (Mode 1), panelists used specialized software to record retronasal aroma descriptors. Within 150 s after swallowing each sample, they selected and logged perceived retronasal aroma descriptors in real time from a predefined descriptor list. After completing all evaluations, the citation proportion for each attribute was calculated as the percentage of its selections relative to the total number of records within a specific time segment. This metric was used to characterize the perceived frequency of each attribute across different stages and to identify representative retronasal descriptors for further analysis. In the second stage, the descriptors selected during the first stage were used as evaluation indicators for the Mode 2 experiment. During this process, panelists continuously recorded their perceived retronasal aroma attributes in real time through specialized software, enabling the generation of time–citation proportion curves for each sensory attribute. Each sample was evaluated in triplicate by every panelist to ensure data reliability.

2.3.3. Retronasal Dual-Attribute Time–Intensity (RDA-TI) Analysis

From the perspective of temporal changes in sensory intensity, traditional time–intensity methods effectively capture the evolution of a single attribute over time but are limited by their time-consuming procedures [14]. As an advanced extension, dual-attribute time–intensity improves the efficiency of temporal sensory data collection [15]. The RDA–TI method developed in this study enabled real-time monitoring of dynamic changes in retronasal aroma intensity, providing a quantitative approach to compare the temporal evolution of sensory intensity between high- and low-alcohol samples. Before the experiment, six experienced tasters conducted multiple rounds of on-site discussions and sensory validations using experimental samples. Based on these sessions and the initial

perceptual data distributions obtained from the pre-experiment sensory panel, intensity grading standards and corresponding value ranges for each key retronasal aroma descriptor were systematically established. To account for differences in perceived intensity levels among various aroma attributes, attribute-specific maximum intensity thresholds were defined, and values exceeding these limits were fixed in the software. Panelists were instructed to rate intensities strictly within the range of 0 to the respective threshold, thereby standardizing the evaluation scale and minimizing scoring variability caused by individual differences in maximum intensity perception. During data acquisition, the system operated with a 2 s refresh cycle. After swallowing each sample, panelists continuously rated the aroma intensities of two randomly paired attributes in real time on the evaluation scale. After data acquisition, key parameters were extracted from the TI curves, including the time to reach maximum intensity (T_{max}), maximum intensity (I_{max}), total duration (T_{tot}), area under the curve (AUC), duration of the 90% maximum intensity plateau ($Plateau_{90\%}$), and the decay time constant after reaching peak intensity (τ). These parameters were used mainly to characterize and compare the dynamic retronasal aroma patterns of high- and low-alcohol samples under different temporal dimensions. Previous studies have shown that the temporal decay of retronasal aroma attributes after reaching maximum intensity can be approximated by an exponential function [16–18]. Accordingly, based on this pattern, the post-peak intensity decay of each retronasal aroma attribute was fitted using an exponential model (Equation (1)). The τ was subsequently derived from the fitted model (Equation (2)), where a larger value indicates stronger temporal persistence of the corresponding aroma attribute. In Equation (1), y denotes the perceived aroma intensity, x represents the time variable, a corresponds to the coefficient related to the initial intensity, b indicates the decay rate constant, and c defines the time offset.

$$y = a \cdot e^{b \cdot (x-c)} \tag{1}$$

$$\tau = \frac{1}{|b|} \tag{2}$$

2.4. Determination of Concentrations of Representative Compounds in Samples

Given the large number of aroma compounds previously identified in high- and low-alcohol *Jiangxiangxing* Baijiu, a total of 67 representative compounds from 11 chemical categories were selected for detailed analysis. The selection was based on a combination of considerations, including relatively high concentrations, significant odor activity values, distinctive physicochemical properties, and the ability of the compounds to represent the major aroma categories. It should be noted that conventional odor activity values are derived from orthonasal olfactory thresholds and were therefore used in this study only as a preliminary screening criterion, rather than as a decisive indicator of retronasal relevance. Accordingly, although some compounds with limited orthonasal prominence but potentially greater retronasal importance may not have been fully captured, this strategy still allowed broad coverage of the major aroma categories while maintaining experimental feasibility. This selection strategy was similar to approaches reported in the literature [19], with only minor differences. The quantification of aroma compounds in this study was based on a multi-technique analytical framework established in our previous studies [10,20]. Specifically, direct injection coupled with gas chromatography–flame ionization detection was used for volatile abundant components; dispersive liquid–liquid microextraction coupled with gas chromatography–mass spectrometry was used for volatile phenols and acidics; headspace solid-phase microextraction coupled with comprehensive two-dimensional gas chromatography–time-of-flight mass spectrometry was used for volatile trace components; headspace solid-phase microextraction coupled

https://doi.org/10.3390/foods15071156

with gas chromatography–pulsed flame photometric detection and solid-phase extraction coupled with ultra-performance liquid chromatography–tandem mass spectrometry were used for major volatile sulfur compounds; and 2,4-dinitrophenylhydrazine derivatization coupled with ultra-performance liquid chromatography–tandem mass spectrometry was used for volatile aldehydes and ketones. In this work, only the specific operations for the analysis of furans and lactones were supplemented, employing dispersive liquid–liquid microextraction coupled with gas chromatography–tandem mass spectrometry to further enhance the overall quantitative analytical framework.

A total of 4 mL of Baijiu sample was mixed with 16 mL of saturated sodium chloride solution and 4 mL of an ethyl acetate–acetone mixture (1:1, *v*/*v*) in a 50 mL glass vial. Subsequently, 20 μL of the internal standard solution (guaiacol-d3, 100 mg/L) was added. The mixture was vortexed at 500 rpm for 10 min to ensure efficient extraction, and then allowed to stand for 10 min. The upper organic phase was collected, dehydrated with anhydrous sodium sulfate, and concentrated under a gentle stream of nitrogen to approximately 250 μL for instrumental analysis. The concentrated extract was analyzed using a gas chromatograph coupled with a triple quadrupole mass spectrometer (8890 GC–7000E MS/MS, Agilent Technologies, Santa Clara, CA, USA) equipped with a DB-FFAP capillary column (60 m × 0.32 mm × 0.25 μm; Agilent Technologies, USA). High-purity helium (≥99.999%) was used as both the carrier gas (1.4 mL/min) and quenching gas (2.25 mL/min), while nitrogen served as the collision gas (1.5 mL/min). The injector temperature was maintained at 250 °C, and 1 μL of the concentrated extract was injected in splitless mode with a solvent delay of 8 min. The oven temperature program was as follows: initial temperature of 40 °C held for 2 min, ramped at 4 °C/min to 150 °C and held for 2 min, then increased at 6 °C/min to 230 °C and held for 15 min. The ion source, transfer line, and quadrupoles 1 and 2 were maintained at 230 °C, 250 °C, 150 °C, and 150 °C, respectively. Mass spectrometric detection was performed in electron ionization (EI, 70 eV) mode using dynamic multiple reaction monitoring (dMRM) for data acquisition. For method development, target compounds were initially analyzed in full-scan mode to determine their retention times and precursor ions, with the most intense precursor–product ion pairs selected based on signal abundance. Product ion scans were subsequently performed at a collision energy of 10 eV to identify the most responsive fragment ions. Subsequently, the MRM parameters were automatically optimized over a collision energy range of 0–25 eV using MassHunter Workstation software (v12.1, Agilent, Palo Alto, CA, USA). The two transitions exhibiting the highest signal intensities and their corresponding optimal collision energies were selected for quantification. The MS/MS parameters and quantitative calibration curves for all compounds were summarized in Table S3.

2.5. Determination of ROT of Representative Compounds in High- and Low-Alcohol Systems

As emphasized in the Introduction, the determination of ROT is critically important. Accordingly, the ROTs of 67 aroma compounds were systematically measured using the three-alternative forced-choice method according to ISO 13301:2018 [21]. Food-grade compounds were dissolved in anhydrous ethanol to prepare initial stock solutions, ensuring complete solubility. Preliminary experiments were conducted to determine the detectable concentration range of each compound in the target ethanol aqueous solution systems (40% or 50% vol). Based on these results, an intermediate concentration was selected as the reference point, and six concentration levels were prepared using a three-fold serial dilution. The 40% vol and 50% vol ethanol aqueous solution systems were used here as standardized reference conditions for controlled threshold determination and comparative screening of compounds with potential retronasal relevance at two representative alcohol levels, rather than to fully reproduce the real Baijiu matrix. The use of whole-number

https://doi.org/10.3390/foods15071156

alcohol levels also facilitates comparison with future threshold studies and improves cross-study comparability. Each gradient sample was paired with a blank solution of 40% vol or 50% vol to form a test set, with 2 mL of each sample dispensed into coded cups labeled with random three-digit numbers. During the formal experiment, panelists wore nose clips before taking each sample and removed them only after the sample was placed in the mouth. Throughout the test, samples were evaluated in ascending order of concentration to prevent interference from residual high-intensity stimuli. Specifically, panelists were instructed to take the sample into their mouths within 0–2 s and distribute it evenly. They then kept their mouths closed and breathed naturally, spitting out the sample at the 5 s. Between 5 and 10 s, panelists focused on perceiving aromas through the retronasal pathway and identified the sample containing the target compound. To minimize sensory fatigue and adaptation, panelists rested for 10 min after rinsing their mouths, as previously described, before evaluating the next set of samples. Finally, the geometric mean of the individual best-estimate thresholds obtained from the 23 qualified semi-trained panelists was calculated and used as the final ROT for each compound under the specified alcohol concentration.

2.6. Statistical Analysis

The relative standard deviations of compound concentrations in different samples were evaluated. Cluster analysis and heatmap visualization of different aroma descriptors were performed using Tbtools (v2.450) [22]. Differences in elicitation proportions between the two samples were assessed in XLSTAT (version 2019.2.2, Addinsoft, Paris, France) using Fisher's test at a significance level of 5%. The key parameters extracted from the TI curves were analyzed using DPS software (Version 9.01, Hangzhou, China) by one-way analysis of variance followed by Duncan's multiple range test. Horizontal bar charts were generated on the NGplot platform [23]. Subsequently, a two-tailed Welch's *t*-test was conducted to assess the significance of DoT differences for individual compounds between the two alcohol-level systems.

3. Results and Discussion

3.1. Analysis of Time–Citation Proportion Differences in High- and Low-Alcohol Systems

Based on the analysis of Model 1, the distribution of retronasal aroma descriptors for Sample-Low and Sample-High across stages A, E, and F was clearly defined (Figure 1a). From the citation frequencies of aroma attributes, ten main retronasal aroma descriptors with relatively high citation rates were identified, including grain, floral and fruity, acidic, alcoholic, roasted, hay, caramel, smoky, fatty, and grassy notes. The total number of selected attributes was consistent with recommended guidelines [24]. Overall, these descriptors broadly correspond to the major aroma dimensions reported in previous studies on the characteristic sensory profile of Jiangxiangxing Baijiu [25]. According to the data distribution, a 6% citation threshold was applied to determine the dominant retronasal aroma attributes most frequently reported by panelists over time (Figure 1b). This threshold was based on the overall distribution of citation frequencies and those observed in the F phase. While effective, it was an empirical decision. Results indicated that during the A phase, eight notes in Sample-High exceeded the threshold, whereas only six were observed in Sample-Low, suggesting a greater diversity of retronasal aroma perception in the initial stage of Sample-High. In the E phase, the number of frequently cited notes was similar between the two samples, with eight notes identified in Sample-High and seven in Sample-Low. In the F phase, the overall citation frequency of notes decreased, yet Sample-High still maintained five notes above the threshold (floral and fruity, roasted, caramel, hay, and grain), while Sample-Low retained four (roasted, caramel, hay, and grain). This finding suggested that Sample-High maintained a higher level

https://doi.org/10.3390/foods15071156

of aromatic diversity in the lingering stage of retronasal perception. However, the current results only reflect the frequency of attribute citations, without considering their time–citation proportions within the perceptual process.

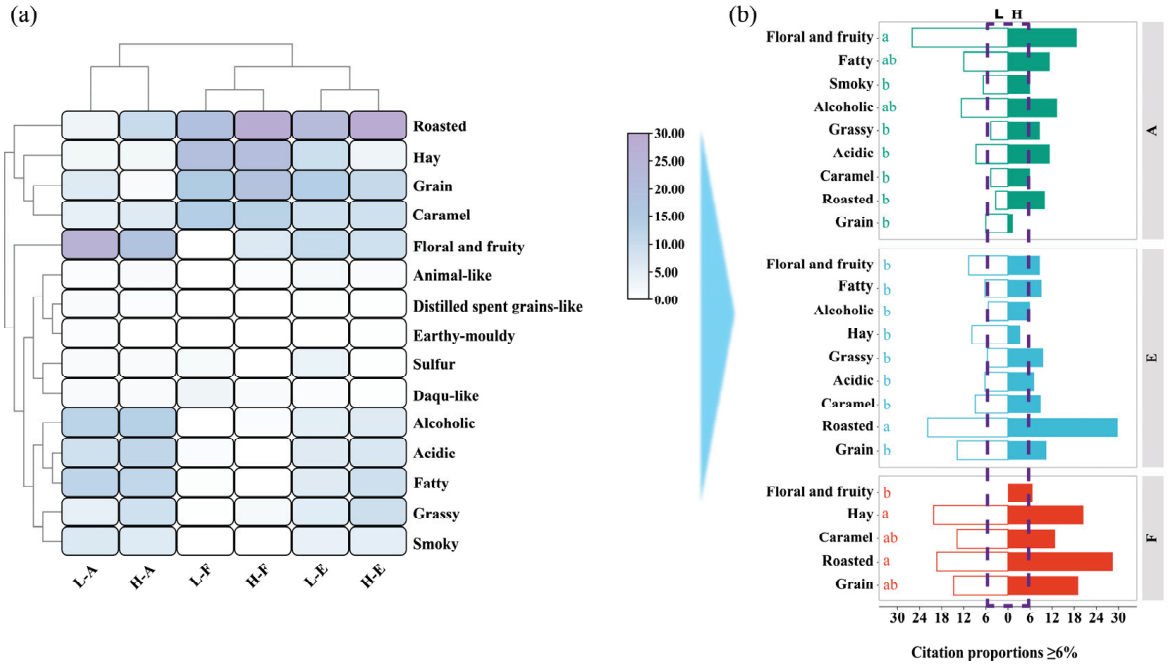


Figure 1. Differences in retronasal aroma descriptors between Sample-Low and Sample-High across stages A, E, and F. In both (**a**,**b**), L represents Sample-Low, H represents Sample-High, while A, E, and F correspond to the attack phase (0–15 s), evolution phase (16–60 s), and finish phase (61–150 s), respectively. Lowercase letters (a, b.) indicated significant differences among groups ($p < 0.05$).

A Model 2 experiment was further conducted to analyze the temporal dynamics of the time–citation proportions for each note (Figure 2). Results showed that during the A phase, the citation proportions of both Sample L and Sample H gradually increased, indicating that retronasal aroma perception developed rapidly during the initial swallowing phase. In contrast, Sample H showed stronger simultaneous enhancement and interaction among multiple attributes, exhibiting a multidimensional release pattern. Sample L was dominated by the smoky note, with weaker contributions from other aromas, reflecting limited overall aroma synergy. This stage underscored the distinct differences between the two samples in their aroma release rhythm and coordination patterns, although no clear difference was detected in their overall citation proportions. Stage E represented the critical phase of aroma evolution, during which the differences between the two samples became more pronounced. The dominant sensory profile of Sample-High featured smoky, floral and fruity, roasted, caramel, grain, and hay notes, creating a complex and well-layered aromatic structure. In contrast, Sample L was initially dominated by the smoky note, which was rapidly replaced by roasted and caramel notes, followed by a gradual increase in the citation proportions of hay and grain notes in the later stages. Significance analysis ($p < 0.05$, Figure 2c) showed that during the early phase (20–30 s), smoky and floral and fruity notes were more pronounced in Sample-High, while the roasted note prevailed in Sample-Low. In the middle phase (30–40 s), the hay note became more pronounced in Sample-Low. In the later phase (50–60 s), fatty and floral and fruity notes became more perceptible in Sample-Low, whereas caramel notes in Sample-High continued to increase steadily. During the F phase, corresponding to the decline of retronasal aroma perception, time–citation proportions exhibit an overall downward trend. In Sample-High, hay, caramel, grain, and roasted notes remained consistently dominant during the later stage. In contrast, Sample-Low showed greater fluctuations in aroma dominance. Although

hay and grain notes were briefly dominant, they faded quickly, leaving a simpler and less persistent afterodor. The significance difference curves (Figure 2c) revealed notable differences between the two samples in caramel, hay, and grain notes ($p < 0.05$), with Sample-High exhibiting a richer and more persistent perceptual profile.

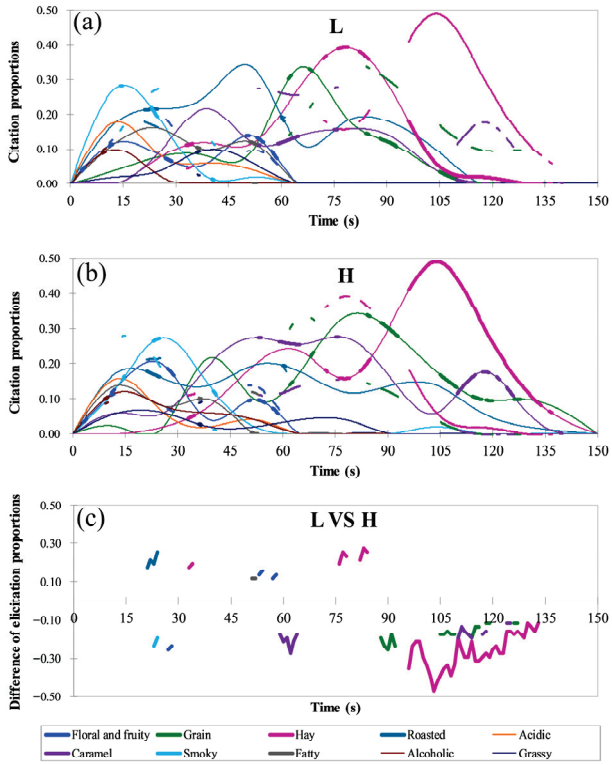


Figure 2. Differences in the time–citation proportions of important retronasal attributes between Sample-Low and Sample-High. Here, L represents Sample-Low and H represents Sample-High. When key reference curves are displayed, the corresponding attribute curves are shown in bold. Panels (**a**–**c**) represent the time–citation proportion curves of different retronasal attributes for Sample-Low, Sample-High, and the differences in elicitation proportions between the two samples, respectively. Differences in elicitation proportions were assessed using Fisher's test ($p < 0.05$) and interpreted mainly in the context of the overall temporal evolution pattern of each attribute.

In summary, the RDM-TCATA analysis indicated that Sample-High exhibited a more pronounced advantage in retronasal aroma performance, aligning with previous reports of enhanced aroma quality in high-alcohol wines [26]. Furthermore, these results indicate that ethanol content plays a key role in determining the richness and temporal persistence of retronasal aromas. Similarly, studies on rum have shown that ethanol concentration strongly affects its temporal sensory dynamics, underscoring the central role of ethanol in shaping the time-dependent perception of distilled spirits [27]. In this study, the RDM-TCATA results were used primarily to identify retronasal attributes showing differentiated temporal patterns between the two samples. Accordingly, the differences are better understood at the level of overall temporal evolution rather than isolated time points, and individual significant findings should therefore be interpreted with caution. In addition, it should be acknowledged that the RDM–TCATA approach has limited capacity to capture changes in perceived aroma intensity. Accordingly, a time–intensity experiment was subsequently conducted to further quantify the dynamic changes in retronasal notes.

3.2. Analysis of Time–Intensity Differences in High- and Low-Alcohol Systems

Based on the time–intensity sensory evaluation, the quantitative results offered a clearer representation of the differences between Sample-High and Sample-Low in aroma

intensity, duration, and decay behavior (Figure 3). The T_{tot} data (Figure 3a) revealed that the total durations of hay, grain, roasted, and caramel notes in Sample-High each exceeded 50 cycles, whereas only three notes in Sample-Low reached this level, and six had values below 30 cycles. Notably, the fruit and floral note exhibited the shortest duration, suggesting that higher ethanol concentrations markedly suppressed its perception, a trend consistent with previous research findings [28]. Moreover, reducing alcohol content has been reported to diminish the perceived persistence of wine in the mouth [29], whereas a higher ethanol content prolongs the finish duration [30]. Consequently, the greater proportion of short-lived aromas in Sample-Low likely accelerated flavor decay, explaining its weaker and shorter retronasal impression.

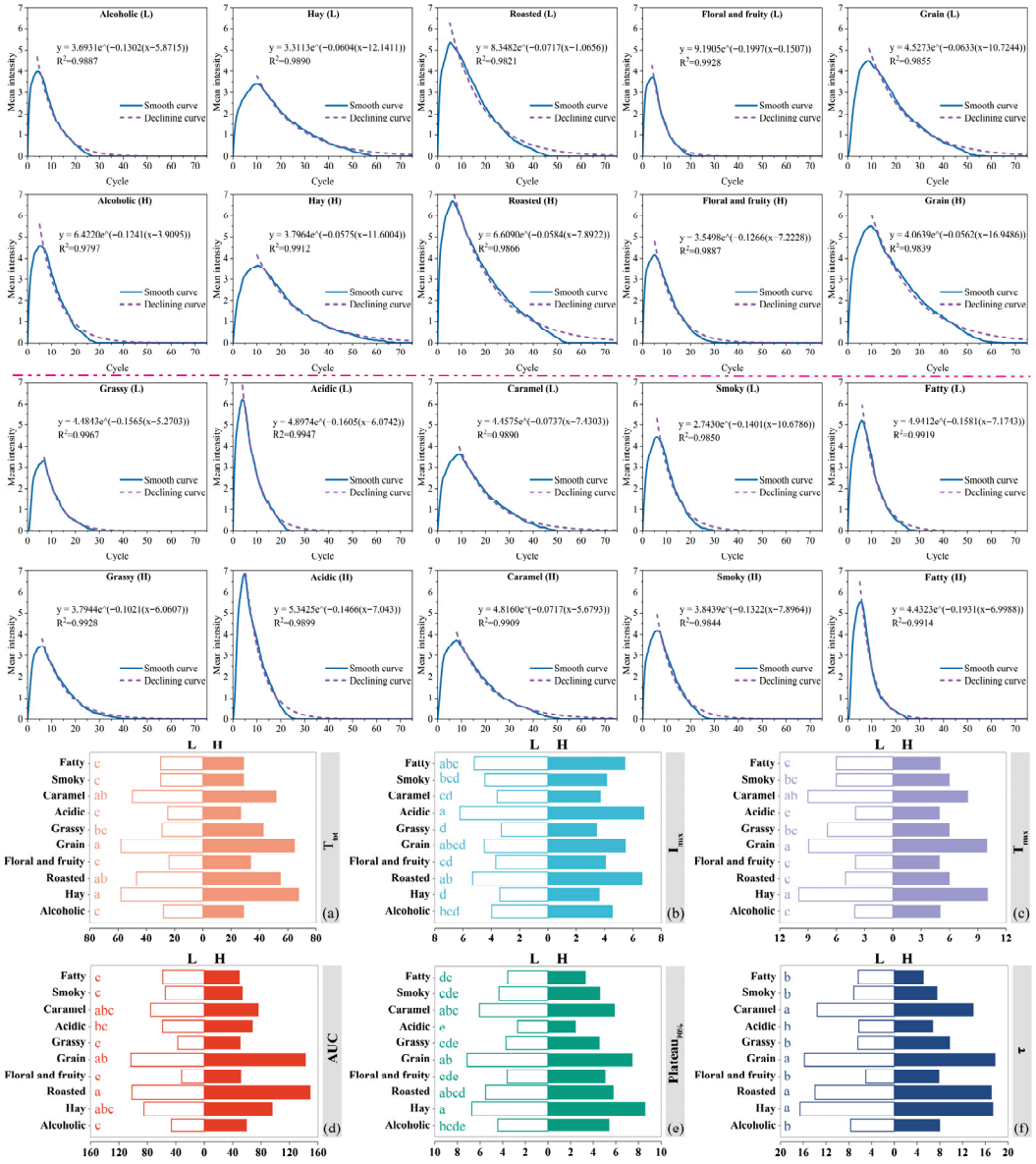


Figure 3. Time–intensity fitting curves and differences in key parameters of important retronasal notes between Sample-Low and Sample-High. Here, L represents Sample-Low and H represents Sample-High. Subfigures (**a**), (**b**), (**c**), (**d**), (**e**), and (**f**) represent the intensity parameters T_{tot}, I_{max}, T_{max}, AUC, $Plateau_{90\%}$, and τ, respectively. Lowercase letters (a, b, c, etc.) next to aroma attributes indicate the grouping of between-sample differences under the corresponding TI parameter. Earlier letters (a > b > c > d > e) indicate relatively larger between-sample differences.

https://doi.org/10.3390/foods15071156

The I_{max} and T_{max} data demonstrated that Sample-High exhibited a distinct advantage in some notes (Figure 3b,c). Notably, the roasted, grain, alcoholic, floral and fruity, acidic, and hay notes exhibited both higher I_{max} values and longer T_{max} durations in Sample-High. For instance, the roasted and grain notes showed over a 20% increase in I_{max}, with their T_{max} extended by nearly one cycle. This indicated that these notes in Sample-High not only reached higher perceived intensity but also sustained their peak perception longer, thereby enhancing the persistence and complexity of retronasal aroma perception. In contrast, Sample-Low exhibited lower I_{max} values, with only the smoky note showing a slight increase. Except for grassy, fatty, and caramel notes, the T_{max} values of all others occurred earlier than those in Sample-High. Thus, compared with the low-alcohol sample, the high-alcohol sample showed greater aroma intensity and a later peak perception, suggesting a richer and longer-lasting retronasal experience under the present sample conditions.

AUC, an integrated index of intensity and duration, further confirmed these differences. Previous studies reported that high-alcohol samples could extend the T_{tot} of certain aroma features, leading to larger AUC values [31]. Accordingly, Figure 3d consistently showed that, except for fatty and smoky notes, all others in Sample-High displayed higher AUC than those in Sample-Low, with increases exceeding 37% for floral and fruity, roasted, grain, and grassy notes. Notably, the notes of roasted and grain not only remained longer but also accumulated to higher perceived intensities, further highlighting the superiority of Sample-High in retronasal aroma longevity and complexity.

The $Plateau_{90\%}$ data indicated that Sample-High maintained higher intensities for most key aroma attributes over a longer duration (Figure 3e). The intensities of floral and fruity, hay, grassy, and alcoholic notes increased by more than 20%, while the persistence of negative attributes, such as fatty, was reduced. In contrast, Sample-Low exhibited only slight advantages in fatty, acidic, and caramel notes. These findings further confirmed the overall superiority of Sample-High in aroma stability and sensory quality.

The τ data further revealed that the decay of some notes in Sample-High occurred more gradually than in Sample-Low (Figure 3f). Specifically, the τ values of grain, hay, and roasted exceeded 17, while floral and fruity as well as grassy notes increased by more than 50% compared to Sample-Low. These results suggested that higher ethanol content slowed the decline of aroma intensity after its peak and enhanced the persistence and complexity of retronasal aroma. In contrast, Sample-Low exhibited a faster decline in several notes, with only the fatty note presenting a higher τ value, which may negatively affect the perception of retronasal aroma. The distinct trends observed across different aroma characteristics suggested that aroma persistence may be associated with the structural properties of the corresponding compounds [32]. Furthermore, these findings reinforce the important role of ethanol in modulating the persistence of retronasal aroma [33].

Analysis of the differences in intensity parameters (I_{max}, T_{max}, $Plateau_{90\%}$, T_{tot}, AUC, and τ) revealed that roasted, grain, floral and fruity, hay, and caramel notes were more prominent in Sample-High, whereas fatty and smoky notes dominated in Sample-Low. These differences indicate that most notes in Sample-High exhibited greater intensity, longer persistence, and richer cumulative perception, reflecting its overall advantage in retronasal aroma performance. This TI-based interpretation is better understood in terms of the integrated pattern across multiple temporal dimensions rather than any single parameter alone. Comparisons within each parameter primarily reflected the relative magnitude of between-sample differences among aroma attributes, and should be interpreted with caution because no additional global multiple-comparison correction was applied.

https://doi.org/10.3390/foods15071156

3.3. Analysis of Retronasal Aroma Differences Based on Compound DoT in High- and Low-Alcohol Systems

To investigate how ethanol concentration influences retronasal aroma perception in Baijiu, this study systematically evaluated the ROT and DoT of 67 compounds in high- and low-alcohol systems, as summarized in Table 1. From the perspective of compound concentration, the overall difference between the two samples was consistently minimal. The concentrations of 52 compounds varied by only 1- to 2-fold, which suggested that these changes were unlikely to be the main factor underlying the marked difference in retronasal aroma detected between the samples. In contrast, the ROT results revealed pronounced differences among compounds from different categories in response to ethanol concentration. For most compounds, ROT values in the low-alcohol system were substantially lower than those in the high-alcohol system, with ROT ratios ranging from 1.04 to 4.75, as illustrated in Figure 4a. These findings indicated that the effect of ethanol on the release of compounds with different structures was not uniform, and that more compounds in the low-alcohol system were likely to be detected at lower concentrations. However, whether this trend resulted in a richer retronasal aroma experience was further examined. The DoT of each compound was calculated from its concentration and corresponding ROT value, as summarized in Table 1. It should be noted that DoT is better regarded as a potential indicator whose primary value lies in identifying compounds with relatively high potential retronasal aroma contribution, rather than in precisely quantifying sensory contribution in the real sample matrix. Because the ROTs were obtained in simplified ethanol aqueous solution systems at 40% vol and 50% vol, rather than in systems exactly matching the two actual Baijiu samples, the resulting DoTs are more appropriately interpreted as approximate comparative measures. Although their absolute values may involve some deviation, they remain informative for compound screening, relative comparison, and trend assessment.

To reduce the impact of extreme DoT values on the interpretation of overall trends, the original DoT data were log-transformed (DoT_{log}) to decrease high-value variability and enhance the visibility of mid- to low-value ranges, thereby improving the comparability of potential aroma contributions between the two systems. Based on these calculations, the logarithmic differences between the two systems were expressed as ΔDoT_{log}. As shown in Figure 4b, most compounds had ΔDoT_{log} below 0, which suggested that Sample-Low likely possessed a higher potential retronasal aroma contribution. However, sensory evaluation revealed that Sample-High exhibited a richer and more balanced retronasal aroma, whereas Sample-Low showed brief intensity in certain notes but lacked overall fullness. This discrepancy between prediction and observation suggested that the retronasal aroma difference could not be fully explained by a simple linear summation of individual compound DoT values. Previous studies have shown that aroma perception in alcoholic beverages arises from complex mixtures of odorants, and perceptual interactions such as masking, addition, or other non-linear effects may influence the final sensory expression [34–36].

https://doi.org/10.3390/foods15071156

Table 1. ROT and DoT for aroma compounds of different classes under high- and low-alcohol systems.

Compounds [a]	Class	C (L) [b]	C (H) [c]	ROT (H) μg/L [d]	ROT (L) μg/L [e]	Retronasal Aroma Descriptor	DoT (L) [f]	DoT (H) [g]	*p* [h]	DoT_n (L) [i]	DoT_n (H) [j]
1,1-Diethoxyethane	Acetals	149,452.39 ± 11,411.11	435,348.42 ± 34,132.36	883.09	223.67	fruit, cream	668.19	492.98	**	0.60	0.60
Decanoic acid [a]	Acids	1425.82 ± 184.14	1074.84 ± 60.99	31,327.90	6594.08	rancid, fat	0.22	0.03	**	0.01	0.00
Butanoic acid [a]	Acids	46,685.81 ± 101.04	38,312.72 ± 1529.98	9875.25	4256.91	rancid, cheese, sweat	10.97	3.88	***	0.22	0.15
Acetic acid	Acids	2,409,795.19 ± 153,437.86	2,063,417.79 ± 13,878.84	253,501.50	157,897.33	sour, pungent	15.26	8.14	**	0.25	0.21
4-Methylpentanoic acid	Acids	600.66 ± 38.69	441.44 ± 7.97	1438.68	1116.50	pungent, cheese	0.54	0.31	**	0.03	0.02
Propanoic acid	Acids	50,268.83 ± 1066.78	74,224.91 ± 142.52	9722.62	5397.24	cheesy, vinegar	9.31	7.63	**	0.21	0.20
3-Methylbutanoic acid	Acids	118,549.15 ± 6248.04	127,666.2 ± 2249.81	2626.34	2217.93	sweat, rancid	53.45	48.61	*	0.36	0.37
2-Heptanol	Alcohols	2326.4 ± 179.37	2923.97 ± 118.95	104.87	42.01	fresh lemon, green	55.38	27.88	**	0.37	0.32
1-Octen-3-ol	Alcohols	171.74 ± 13.45	107.89 ± 6.57	59.49	47.91	mushroom, earthy, green	3.58	1.81	**	0.13	0.10
2-Nonanol [a]	Alcohols	131.47 ± 5.24	165.51 ± 12.85	440.99	191.29	cucumber, waxy	0.69	0.38	***	0.04	0.03
2-Methyl-1-butanol	Alcohols	92,689.18 ± 212.39	105,362.93 ± 3273.49	22,386.71	21,246.19	alcoholic, greasy, whiskey	4.36	4.71	*	0.15	0.16
2-Phenylethanol	Alcohols	6377.23 ± 119.55	10,561.51 ± 611.56	646.40	543.83	floral, rose	11.73	16.34	**	0.23	0.27
1-Propanol	Alcohols	931,570.55 ± 59,199.51	2,397,456.14 ± 76,087.82	401,520.03	387,082.17	alcoholic, fusel	2.41	5.97	***	0.10	0.18
Nonanal [a]	Aldehydes	74.04 ± 3.15	84.62 ± 13.48	52.53	31.10	citrus, green, fatty	2.38	1.61	*	0.10	0.09
(2E,4E)-2,4-Decadienal [a]	Aldehydes	22.50 ± 0.20	22.86 ± 0.11	0.89	0.61	fried, wax, fat	36.74	25.77	***	0.33	0.31
3-Methylbutanal	Aldehydes	19,398.22 ± 244.48	27,313.17 ± 649.54	4.28	2.15	ethereal, aldehydic	9028.69	6378.09	***	0.84	0.84
Benzeneacetaldehyde	Aldehydes	2550.34 ± 153.62	3045.70 ± 182.35	243.63	144.97	honey, sweet	17.59	12.50	**	0.26	0.25
(2E)-2-Dodecenal [a]	Aldehydes	17.52 ± 1.52	27.04 ± 3.44	44.20	24.57	green, fat, sweet	0.71	0.61	-	0.04	0.04
Hexanal [a]	Aldehydes	2038.49 ± 16.79	2320.17 ± 1.05	19.82	16.29	grass, green	125.12	117.05	**	0.44	0.46
Vanillin	Aldehydes	35.48 ± 0.37	44.95 ± 0.30	134.09	104.06	vanilla, sweet, creamy	0.34	0.34	-	0.02	0.02
(2E,6Z)-nona-2,6-dienal [a]	Aldehydes	127.46 ± 11.37	142.19 ± 5.90	0.08	0.07	cucumber, wax, green	1857.81	1856.79	-	0.69	0.72

https://doi.org/10.3390/foods1

Table 1. *Cont.*

Compounds [a]	Class	C (L) [b]	C (H) [c]	ROT (H) μg/L [d]	ROT (L) μg/L [e]	Retronasal Aroma Descriptor	DoT (L) [f]	DoT (H) [g]	p [h]	DoT_n (L) [i]	DoT_n (H) [j]
Acetaldehyde	Aldehydes	458,591.06 ± 34,549.68	950,408.08 ± 21,672.7	43,756.79	25,262.99	pungent, ether, aldehydic	18.15	21.72	*	0.27	0.30
Octanal [a]	Aldehydes	37.33 ± 6.49	64.81 ± 9.07	5.48	4.74	fatty, soapy, green	7.19	10.99	**	0.19	0.24
(2E)-2-Nonenal [a]	Aldehydes	37.55 ± 1.19	191.16 ± 40.71	0.29	0.12	tallowy, fatty, oily	308.28	662.69	*	0.52	0.62
Propanal [a]	Aldehydes	2264.21 ± 191.67	5257.72 ± 52.92	3149.05	2982.54	solvent, pungent	0.76	1.67	***	0.04	0.09
Decanal [a]	Aldehydes	129.96 ± 16.12	935.1 ± 46.88	32.35	29.52	soap, orange peel, tallow	4.40	28.90	**	0.15	0.32
Ethyl octanoate	Esters	12,210.55 ± 699.37	6138.81 ± 340.49	265.85	77.75	fruity, wine, waxy	157.05	23.09	***	0.46	0.30
Ethyl 4-methylpentanoate	Esters	1344.25 ± 67.00	857.04 ± 54.06	5.14	1.72	fruit	759.39	166.64	***	0.61	0.49
Ethyl hexanoate	Esters	294,241.98 ± 9033.42	134,574.16 ± 8287.64	568.21	303.92	apple peel, sweet, pineapple	968.15	236.84	***	0.63	0.53
Isoamyl acetate	Esters	2060.18 ± 90.02	2638.53 ± 154.39	81.51	22.38	sweet, fruity, banana	92.04	32.37	***	0.41	0.34
Ethyl 2-methylpentanoate [a]	Esters	119.31 ± 1.30	56.92 ± 3.05	3.85	2.85	fruity, apple, pineapple	41.81	14.78	***	0.34	0.26
Ethyl 3-methylpentanoate [a]	Esters	23.22 ± 1.56	36.15 ± 2.14	0.31	0.08	pineapple, fruity	301.05	116.48	***	0.52	0.46
Ethyl valerate	Esters	11,057.26 ± 359.02	7149.27 ± 463.12	73.28	60.86	yeast, fruit	181.70	97.57	***	0.47	0.44
Ethyl benzoate	Esters	743.03 ± 42.15	1350.99 ± 91.42	105.37	31.39	fruity, wintergreen, green	23.67	12.82	***	0.29	0.25
Ethyl hexahydrobenzoate [a]	Esters	10.14 ± 0.67	11.93 ± 0.06	0.10	0.05	fruity, cheese, winey	208.69	113.67	**	0.49	0.45
Ethyl butanoate	Esters	20,515.93 ± 44.94	27,966.09 ± 717.59	160.58	77.61	fruity, sweet, ethereal	264.35	174.15	***	0.51	0.50
Ethyl propionate [a]	Esters	42,989.38 ± 2008.04	65,936.26 ± 1695.25	2262.08	1040.67	sweet, fruity, rum	41.31	29.15	**	0.34	0.33
Ethyl isobutyrate	Esters	20,028.77 ± 422.82	22,663.58 ± 1108.25	7.37	4.91	sweet, ethereal, fruity	4080.62	3075.88	**	0.76	0.77
Ethyl heptanoate	Esters	11,844.43 ± 893.35	10,927.09 ± 125.92	56.92	47.40	fruity, pineapple, cognac	249.89	191.96	*	0.50	0.50
Ethyl cinnamate	Esters	1193.60 ± 2.42	1621.04 ± 2.00	182.50	108.05	honey, cinnamon	11.05	8.88	***	0.22	0.22
Ethyl 3-phenylpropanoate	Esters	1917.16 ± 120.82	1886.19 ± 114.35	24.49	20.93	hyacinth, rose, honey	88.29	77.01	-	0.41	0.42

https://doi.org/10.3390/foods1

Table 1. *Cont.*

Compounds [a]	Class	C (L) [b]	C (H) [c]	ROT (H) μg/L [d]	ROT (L) μg/L [e]	Retronasal Aroma Descriptor	DoT (L) [f]	DoT (H) [g]	*p* [h]	DoT_n (L) [i]	DoT_n (H) [j]
Ethyl phenylacetate	Esters	451.70 ± 28.5	837.00 ± 1.92	527.59	345.77	fruit, sweet	1.31	1.59	*	0.07	0.09
Ethyl 2-methylbutanoate	Esters	9614.45 ± 330.95	16,099.75 ± 1101.4	0.81	0.75	apple, green	12,829.86	19,045.46	***	0.87	0.95
Ethyl lactate	Esters	765,379.29 ± 45,931.29	1,888,738.75 ± 118,713.16	337,505.73	203,269.09	sharp, fruity, buttery	3.77	5.60	***	0.14	0.18
Ethyl 3-methylbutanoate	Esters	3681.74 ± 46.98	9298.84 ± 543.61	3.75	3.12	sweet, apple, pineapple	1178.83	2479.18	**	0.65	0.75
Ethyl acetate	Esters	1,039,920.63 ± 24,334.54	2,312,802.78 ± 48,024.14	40,873.88	39,300.22	pineapple, fruity, sweet	26.46	56.58	***	0.30	0.39
Furfural	Furans and Lactones	141,564.18 ± 12,358.4	195,686.68 ± 11,173.81	1079.97	310.94	sweet, woody, baked bread	455.28	181.20	**	0.56	0.50
γ-Nonanolactone [a]	Furans and Lactones	18.33 ± 3.31	53.85 ± 10.05	43.10	11.97	coconut, peach	1.53	1.36	-	0.08	0.08
4-Hydroxy-2,5-dimethylfuran-3-one [a]	Furans and Lactones	7.94 ± 0.62	11.38 ± 0.62	6.34	5.02	sweet, candy, caramel	1.58	1.74	-	0.08	0.09
4-Hydroxy-2,3-dimethyl-2H-furan-5-one [a]	Furans and Lactones	795.24 ± 123.49	1609.56 ± 189.61	13.74	11.26	caramel, sugar, herb	64.52	110.56	**	0.38	0.45
4-Undecanolide [a]	Furans and Lactones	294.89 ± 8.52	791.34 ± 23.49	24.26	21.95	peach, creamy, fatty	13.43	32.62	***	0.24	0.34
5-Ethyl-3-hydroxy-4-methyl-2(5H)-furanone [a]	Furans and Lactones	0.12 ± 0.06	23.65 ± 2.91	2.03	1.14	caramel, sugar, herb	0.11	11.68	**	0.00	0.24
Acetophenone	Ketones	523.44 ± 25.55	364.66 ± 27.63	346.17	92.63	flower, almond, sweet	5.65	1.05	***	0.17	0.07
Acetoin	Ketones	7511.67 ± 7.59	15,714 ± 829.2	2514.87	810.28	sweet, buttery, creamy	9.27	6.25	**	0.21	0.19
3-Methylnonane-2,4-dione [a]	Ketones	0.57 ± 0.15	0.61 ± 0.10	2.44	1.91	hay, caramel, burnt	0.30	0.25	-	0.01	0.02
4-Methylphenol	Phenols	309.49 ± 10.21	75.66 ± 3.42	80.94	28.86	medicine, phenol, smoke	10.72	0.93	***	0.22	0.06
3-Methylphenol [a]	Phenols	3364.86 ± 253.56	1048.36 ± 21.06	466.79	185.69	fecal, plastic	17.39	2.25	***	0.26	0.11
4-Ethylphenol	Phenols	9.22 ± 0.19	9.59 ± 0.38	34.75	31.71	phenol, spice, musk	0.29	0.28	-	0.01	0.02

https://doi.org/10.3390/foods1

Table 1. *Cont.*

Compounds [a]	Class	C (L) [b]	C (H) [c]	ROT (H) μg/L [d]	ROT (L) μg/L [e]	Retronasal Aroma Descriptor	DoT (L) [f]	DoT (H) [g]	p [h]	DoT_n (L) [i]	DoT_n (H) [j]
2-Methoxyphenol	Phenols	28.01 ± 1.64	54.74 ± 0.86	86.56	74.77	smoke, sweet, medicine	0.37	0.63	***	0.02	0.04
2,6-Dimethylpyrazine	Pyrazines	618 ± 52.27	649.75 ± 39.72	1934.71	954.76	nut, cocoa, roast beef	0.65	0.34	**	0.04	0.02
2,3,5-Trimethylpyrazine	Pyrazines	694.95 ± 9.93	1390.96 ± 88.58	5339.62	1920.19	nutty, roasted, musty	0.36	0.26	**	0.02	0.02
2-Methyl-3-furanthiol	Sulfides	4.74 ± 0.01	2.41 ± 0.11	0.02	0.02	sulfury, meaty, fish	263.95	125.40	***	0.51	0.46
Furfuryl mercaptan	Sulfides	36.79 ± 1.69	36.49 ± 1.25	0.0011	0.0007	sulfury, roasted, burnt	52,096.09	32,573.59	***	1.00	1.00
Dimethyl trisulfide	Sulfides	3.20 ± 0.26	4.09 ± 0.14	0.05	0.04	sulfur, fish, cabbage	79.11	76.80	-	0.40	0.42
β-Damascenone [a]	Terpenes	1.24 ± 0.03	1.66 ± 0.04	2.10	0.62	apple, rose, honey	1.99	0.79	***	0.09	0.05
Linalool	Terpenes	104.03 ± 18.64	89.59 ± 0.69	9.49	8.22	flower, wood	12.66	9.44	-	0.23	0.22
Geosmin	Terpenes	102.34 ± 7.35	376.28 ± 22.72	26.69	10.72	musty, earthy, soil	9.55	14.10	**	0.21	0.26

Annotation: [a] Compounds, compounds marked with "a" were supplementally quantified, while those unmarked were referenced from previous studies [10,20]. [b] C (L), average concentration of triplicates of Sample-Low. [c] C (H), average concentration of triplicates of Sample-High. The letters [d] and [g] represent the retronasal olfactory threshold and dose-over-threshold in 50% vol ethanol aqueous solution, respectively. The letters [e] and [f] represent the retronasal olfactory threshold and dose-over-threshold in 40% vol ethanol aqueous solution, respectively. [h] p, *, **, and *** indicate DoT significance at $p < 0.05$, $p < 0.01$, and $p < 0.001$, respectively. The letters [i] and [j] represent the normalized distribution of the logarithmic DoT values of the compounds in low-alcohol and high-alcohol systems, respectively.

https://doi.org/10.3390/foods1

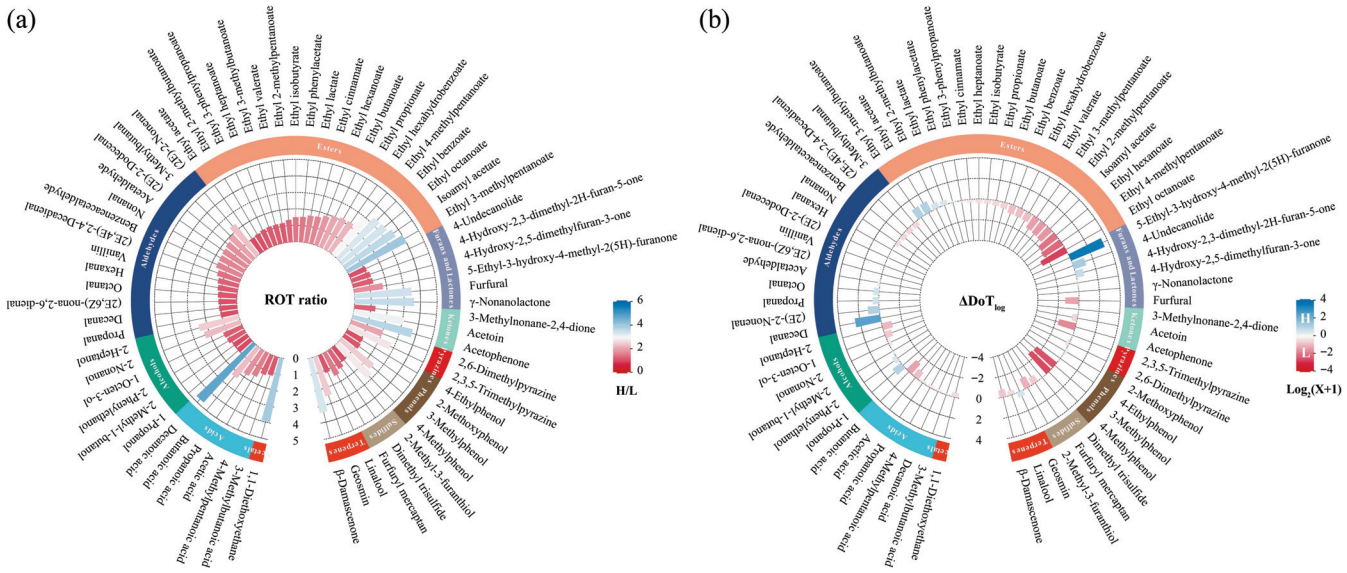


Figure 4. Differences in ROT and DoTlog values among various classes of aroma compounds between the high- and low-alcohol systems. (**a**) ROT ratios of different classes of compounds in 40% vol and 50% vol ethanol aqueous solutions; (**b**) logarithmic differences in DoT values of individual compounds between high- and low-alcohol systems.

By applying min–max normalization to the DoT_{log} values in each system, we obtained DoT_n, which reflected the relative contribution pattern of each compound within each system. This metric was used to first examine the within-system distribution pattern of contribution levels and then compare the distributional features between Sample-Low and Sample-High, with the final interpretation made in combination with the overall trend of ΔDoT_{log}. Thus, DoT_n was used mainly to characterize distributional features rather than to directly represent absolute DoT-related magnitudes between the two systems. As shown in Figure 5a,b, the DoT_n density distribution of these compounds differed between the two systems. To compare their potential aroma contribution distributions more clearly, we conducted a segmented DoT_n analysis based on compound abundance and contribution proportion (Figure 5c,d). The results showed that within the 0.50–1.00 interval, Sample-Low contained 15 compounds, which was higher than the 10 compounds in Sample-High. In addition, the DoT_n weight proportion of Sample-Low in this interval reached 48.11%, exceeding the 36.04% in Sample-High. This may provide a plausible perceptual explanation for the lower retronasal aroma richness of Sample-Low. Previous work on odor-mixture processing indicates that when one component is much stronger than the others, it may cover the odor quality of the remaining components, a phenomenon described as complete overshadowing or masking [37–39]. Accordingly, the more concentrated contribution of a limited number of high-DoTn compounds in Sample-Low may have influenced the overall retronasal percept and reduced the perceptual expression of other aroma-active compounds, thereby weakening the overall aroma balance. In contrast, within the medium contribution interval (0.25–0.50), Sample-High contained 25 compounds and showed a DoT_n weight proportion of 46.54%, both of which were higher than the 18 compounds and 32.37% in Sample-Low. This distributional difference suggested that the retronasal aroma of Sample-High was supported by a broader group of medium contribution components, which could have reduced the chance of a small group of compounds becoming overly dominant and helped maintain a more balanced aroma profile. Within the low contribution interval (0.00–0.25), the two samples showed similar numbers of compounds with 34 in Sample-Low and 32 in Sample-High, and comparable weight proportions of 19.52% and 17.42%, respectively. These minor differences were likely to have exerted only a limited influence

on the retronasal aroma distinctions between the two systems. Overall, the relatively high proportion of strongly contributing compounds and the limited presence of medium-contribution components in Sample-Low made its aroma system more prone to being strongly driven by a small number of compounds. In contrast, Sample-High displayed a more balanced contribution profile, which may help support greater retronasal aroma richness and harmony. Building on the understanding of the overall aroma contribution, the next step focused on the pronounced notes to analyze potential aroma compounds driving these sensory differences.

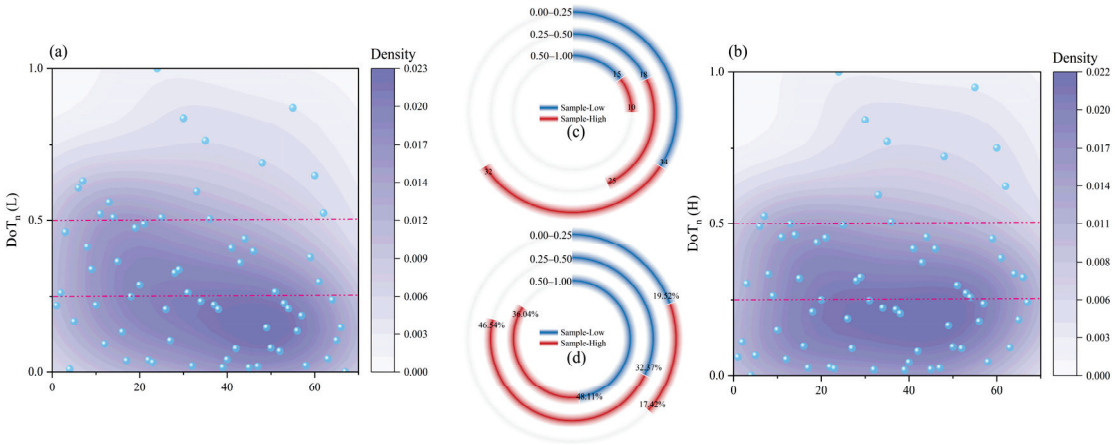


Figure 5. Differences in DoTn distribution characteristics of aroma compounds between the high- and low-alcohol systems. (**a**,**b**) show the DoTn distribution densities of compounds in the low- and high-alcohol systems, respectively. (**c**,**d**) show the differences in the number of compounds and their relative contribution proportions across different DoTn intervals in the two systems, respectively.

The floral and fruity note mainly originated from esters [40]. As shown in Figure 4a, the ROT values of esters varied significantly between the two ethanol systems, with the ratio of the high- and low-alcohol systems ranging from 1.04 to 4.02. In contrast with ethyl propionate, ethyl acetate, and ethyl lactate, which had ROT values above 10 μg/L, the ROT values of ethyl hexahydrobenzoate, ethyl 3-methylpentanoate, and ethyl 2-methylbutanoate were below 10 μg/L, which suggested that these esters were more easily perceived retronasally. Further analysis demonstrated that compounds with ROT ratios greater than 2 were predominantly distributed among those with lower ROT values. The ΔDoT_{log} results indicated that most compounds exhibited values below 0, theoretically suggesting that the floral and fruity notes were more pronounced in Sample-Low. Despite the differences in time–citation proportion during the E stage, the sensory evaluation demonstrated that Sample-High performed better overall across the intensity parameters. An examination of the DOT_n distribution further showed that Sample-Low contained more compounds within the high-contribution interval (0.50–1.00) and had a higher cumulative potential contribution of 53.19%. This pattern indicated that the floral and fruity note of Sample-Low was more likely to be dominated by a limited group of strongly contributing compounds, reflecting a tendency toward extreme-value driving. In contrast, Sample-High contained more compounds within the medium-contribution interval (0.25–0.50) and presented a larger potential contribution proportion of 51.10%. This distribution pattern suggested that the floral and fruity note of Sample-High was primarily shaped by the collective contributions of multiple medium-strength components. Within the low-contribution interval (0–0.25), the differences between the two samples were relatively small and likely exerted only a limited influence. Taken together, the results suggested that the aroma richness of the floral and fruity notes did not result from the dominance of a few strong contributors. Instead, it was driven by the balanced contributions of multiple

https://doi.org/10.3390/foods15071156

components. It should be noted that the floral and fruity note in both ethanol system was short-lived, which was likely due to the rapid release of these compounds in the oral cavity and their low binding affinity to the mucosal surface [41]. In addition, its sensory expression may also be modulated, to some extent, by perceptual interactions among coexisting compounds. Previous research has shown that 1-propanol can weaken floral and fruity perception and suppress the volatilization of some ester compounds [42]. Other studies have further shown that long-chain fatty acids and their ethyl esters could modulate the retronasal persistence of fruity esters [43].

Pyrazines are typically associated with roasted notes. In this study, 2,6-dimethylpyrazine and 2,3,5-trimethylpyrazine were selected as representative compounds. Meanwhile, because furfuryl mercaptan exhibits sulfury, roasted, and burnt characteristics [44], it might have acted synergistically with pyrazines to enhance the roasted impression within the complex aroma matrix. According to the ROT analysis, both 2,6-dimethylpyrazine and 2,3,5-trimethylpyrazine exhibited ROT ratios above 2, suggesting that increasing ethanol concentration suppressed their release in the high-alcohol system, thereby reducing their accessibility to the olfactory system. In contrast, the ROT of furfuryl mercaptan was extremely low in both systems, with values of 0.0011 μg/L and 0.0007 μg/L, respectively, indicating that it could be perceived readily even at trace levels. All three compounds showed negative ΔDoT_{log} values, theoretically indicating a stronger roasted note in Sample-Low. However, the sensory results did not fully align with this prediction. Sample-Low only exhibited a rapid rise in the citation proportion of the roasted note during the E stage, which differed significantly from Sample-High. In contrast, Sample-High maintained a longer persistence of roasted characteristics during the F stage, and multiple intensity parameters confirmed that it demonstrated a more pronounced retronasal roasted characteristic across several sensory dimensions. To further clarify this difference, the DOT_n distribution showed that furfuryl mercaptan occupied an overwhelmingly dominant position within the 0.50–1.00 interval, with its potential contribution accounting for 95.80% in Sample-High and 94.66% in Sample-Low. The two pyrazine compounds were mainly distributed in the 0.00–0.25 interval, contributing only 4.20% and 5.34%, respectively. This distribution pattern indicated that the potential roasted contribution was driven primarily by compounds with high contribution levels within the current analytical framework. The overall trend supported the conclusion that Sample-High exhibited a more pronounced retronasal roasted characteristic. Notably, most pyrazines in Baijiu occurred at subthreshold levels, implying that their direct aroma contributions were limited, yet they might have participated in roasted note formation through synergistic enhancement [45]. Studies have also shown that the roasted note is not determined solely by the concentration of pyrazines, but rather arises from the complex interactions among key volatile compounds [46]. Therefore, the potential synergistic effects of multiple subthreshold pyrazines in Baijiu deserve further investigation in future studies.

Furans and lactones are characterized by distinctive caramel-like and fruity notes [47,48]. This study examined the caramel note by comparing the potent aroma contributions of furfural, 4-hydroxy-2,5-dimethylfuran-3-one, 4-hydroxy-2,3-dimethyl-2H-furan-5-one, and 5-ethyl-3-hydroxy-4-methyl-2(5H)-furanone between high- and low-alcohol systems. The ROT analysis showed that furfural had a markedly higher ROT value in the high-alcohol system, which suggested that increasing ethanol concentration exerted a certain suppressive effect on its olfactory perception. In contrast, the other three compounds exhibited consistently low and stable ROT values across both systems, indicating that they could be perceived at relatively low concentrations and were not substantially affected by ethanol level. According to the ΔDoT_{log} results, the theoretical aroma contribution trends of these compounds showed clear differentiation. Except for furfural, all compounds exhibited

positive values, suggesting that Sample-High may have a theoretical advantage in aroma contribution. In agreement with the sensory observations, Sample-High showed a significantly higher time–citation proportion during the F stage than Sample-Low, displaying overall stronger perceptual intensity, slower attenuation, and greater aroma accumulation. Sample-Low showed only slight advantages in $Plateau_{90\%}$ and T_{max}, indicating that Sample-High demonstrated a more persistent and stable olfactory performance for the caramel note. The distribution of compound DoT_n values further revealed differences in the contribution interval patterns between the two samples. Within the high-contribution interval (0.50–1.00), only Sample-Low contained a single compound, which accounted for 54.99%, suggesting that the caramel note was more susceptible to being strongly driven by high-contribution components. In contrast, Sample-High contained no compounds in this interval but included more components in the medium-contribution range (0.25–0.50) than Sample-Low, with a markedly higher cumulative potential contribution of 73.89%, compared with 37.27% in Sample-Low. This pattern indicated that the caramel note of Sample-High was primarily shaped by compounds with medium contribution levels. In the low-contribution interval (0–0.25), both samples contained the same number of compounds, although Sample-High exhibited a larger contribution proportion. Integrating the sensory observations with the potential contribution distribution indicated that caramel note perception of Sample-Low was likely dominated by a few high-contribution compounds, producing a rapid but relatively transient caramel impression. In Sample-High, the broader distribution of several medium-contribution components formed a more dispersed contribution pattern, which helped sustain a stronger and longer-lasting caramel perception.

Previous studies have reported that 3-methylnonane-2,4-dione possesses a strawlike aroma characteristic [49] and originates from furanoid fatty acids [50]. Based on its aroma characteristics, the hay note detected in the samples was likely attributed to this compound. ROT analysis showed that 3-methyl-2,4-nonanedione had low ROTs in both the high- and low-alcohol systems (2.44 and 1.91 μg/L, respectively), suggesting that it can be readily perceived. The negative ΔDoT_{log} value suggested that, theoretically, the aroma contribution of this compound was slightly greater in the low-alcohol system. From the sensory perspective, the citation proportion of the hay note in Sample-Low was temporarily and significantly higher than that in Sample-High during the middle of the E stage and the early phase of the F stage. This trend was consistent with the theoretical prediction. However, in the later phase of the E stage, the citation proportion of the hay note in Sample-High gradually increased, becaming significantly higher than that in Sample-Low during the middle and late phases of the F stage. All intensity parameters also supported the superior performance of Sample-High. The DoT_n value of this compound in Sample-High was slightly higher than that in Sample-Low, which suggested a certain advantage in its relative aroma contribution within the high-alcohol system. This observation aligned with the stronger hay note perception of Sample-High during the later phase of the E stage. On the whole, although increasing ethanol concentration might slightly suppress the monomeric activity of this compound, it would not necessarily diminish its relative contribution weight in the high-alcohol system. The low-alcohol system may promote a more intense and immediate aroma generated by 3-methylnonane-2,4-dione, whereas the high-alcohol system could enhance its persistence, resulting in a more stable and longer lasting retronasal perception.

Aldehydes are key contributors to the aroma profile of Baijiu. Short-chain saturated aldehydes (e.g., acetaldehyde) produce pungent and aldehydic notes, medium- to long-chain aldehydes (e.g., hexanal) impart grassy nuances, aromatic aldehydes (e.g., benzeneacetaldehyde) deliver honey- and sweet-like notes, and unsaturated aldehydes (e.g., (2E,6Z)-nona-2,6-dienal) contribute cucumber- and green-like aromas. Moreover,

many long-chain saturated and unsaturated aldehydes exhibit fatty characteristics [20]. These observations indicated that chain length and saturation were critical structural factors influencing the aroma expression of aldehydes. From the sensory perspective, the time–citation proportion of the fatty note in Sample-Low was significantly higher than that in Sample-High during the later phase of the E stage, indicating a broader perception plateau and greater persistence. Sample-High showed an advantage only in I_{max}, whereas its overall duration was comparatively weaker. To investigate the underlying chemical basis, several compounds associated with the fatty note were selected in this study, including octanal, nonanal, decanal, (2E)-2-nonenal, (2E)-2-dodecenal, and (2E,4E)-2,4-decadienal [20]. ROT analysis demonstrated that these aldehydes generally had low ROT values, which further declined in the low-alcohol system, yielding ratios between the two systems ranging from 1.10 to 2.37. Among them, (2E)-2-nonenal and (2E)-2-dodecenal showed the most pronounced reductions, which suggested that the volatility of medium- to long-chain unsaturated aldehydes might be strongly suppressed in the high-alcohol system. In contrast, long-chain saturated and polyunsaturated aldehydes showed only minor variations, which indicated lower sensitivity to alcohol concentration. In terms of total DoT, the combined proportion of these compounds in Sample-High reached 1.18%, which was notably higher than that in Sample-Low (0.47%). This theoretically suggested that Sample-High possessed a more pronounced fatty characteristic. However, this trend did not fully align with the actual sensory results. Analysis of the DoT_n distribution showed that both samples contained one compound in the high-contribution interval (0.50–1.00), with comparable contribution proportions, although Sample-Low showed a slightly higher value than Sample-High (39.37% vs. 38.24%). In the medium-contribution interval (0.25–0.50), Sample-High contained more compounds and exhibited a substantially higher cumulative contribution (39.15% vs. 24.67%), which might have contributed to its greater peak intensity. Conversely, Sample-Low showed a higher contribution proportion in the low-contribution interval (0.00–0.25), accounting for 35.95%, compared with 22.60% in Sample-High. Overall, the potential contribution pattern in Sample-Low was more broadly distributed, with aroma contributions spread more evenly across intervals. This distribution trend corresponded well with its broader and more persistent perceptual plateau observed in the sensory evaluation.

Phenols are typically associated with smoky characteristics, and previous studies have identified 2-methoxyphenol as a key compound responsible for the grain-like note [51]. In this study, 3-methylphenol, 4-methylphenol, 2-methoxyphenol, and 4-ethylphenol were selected as representative compounds to investigate their potential contributions to smoky or grain notes under different alcohol systems. ROT analysis showed that, except for 3-methylphenol, the remaining compounds generally had low ROT values. Among those, 2-methoxyphenol was scarcely affected by alcohol concentration, suggesting strong stability within the system, whereas 4-methylphenol and 3-methylphenol exhibited relatively high ROT ratios, implying that their release and perception were more susceptible to modulation by alcohol concentration. Based on the ΔDoT_{log} results, all compounds except 2-methoxyphenol showed negative values, which suggested that 3-methylphenol, 4-methylphenol, and 4-ethylphenol might enhance the smoky note of Sample-Low. In contrast, 2-methoxyphenol might contribute to a stronger grain note in Sample-High. Previous studies have reported that 2-methoxyphenol could be readily adsorbed onto the oral mucosa and remain there for an extended period, thereby contributing significantly to aroma persistence [41]. This unique retention property provides a chemical basis for its ability to sustain aroma longevity within the system. Based on the DoT_n distribution characteristics, the compounds associated with the smoky note in Sample-Low were mainly distributed within the 0.00–0.50 range, with the 0.25–0.50 interval contributing 52.77%. This

https://doi.org/10.3390/foods15071156

indicated a more dispersed contribution pattern, which corresponded well with its stronger persistence and greater aroma accumulation observed in the sensory evaluation. In contrast, all contributions in Sample-High were confined to the 0.00–0.25 interval (100%), forming a highly concentrated low-contribution profile. Although this pattern supported a higher citation proportion during the early E stage, Sample-High exhibited markedly weaker persistence and lower aroma accumulation compared with Sample-Low. For the grain note, 2-methoxyphenol remained within the low-contribution interval in both systems. Analysis of the DoT_n differences further revealed a positive value, indicating a greater relative contribution weight in the high-alcohol system. This suggested that 2-methoxyphenol might play a more prominent role in Sample-High, consistent with its superior performance in the corresponding intensity parameters.

This study was intended to characterize retronasal aroma differences between representative high- and low-alcohol Jiangxiangxing Baijiu samples. However, because the present design did not include multiple independent samples within each alcohol level, the observed differences should be interpreted as differences between representative products associated with alcohol-level variation under the tested conditions, rather than as strictly controlled single-factor effects. Future studies using a broader set of independent samples or controlled dilution-based designs are needed to further validate these findings.

4. Conclusions

This study comprehensively investigated the dynamic retronasal aroma differences between high- and low-alcohol *Jiangxiangxing* Baijiu from two dimensions: time–citation proportion and time–intensity. The results showed that Sample-High exhibited greater retronasal aroma richness than Sample-Low. Significant differences in citation proportions were mainly observed for roasted, floral and fruity, smoky, hay, fatty, caramel, and grain notes, and the intensity-related results further indicated that roasted, grain, floral and fruity, hay, and caramel notes were more prominent in Sample-High, whereas fatty and smoky notes were more pronounced in Sample-Low. Overall, these sensory results reflected the relatively weaker retronasal aroma richness of Sample-Low. At the chemical level, this study found that the concentrations of 67 compounds did not differ significantly between the samples, which suggested that differences in compound concentration alone were unlikely to fully account for the retronasal aroma differences observed between the two samples. In contrast, most compounds showed lower ROTs in the low-alcohol system, and several compounds therefore exhibited larger DoTs under this condition. Further analysis of the DoTn distribution showed that, for most differential notes, Sample-Low contained a higher proportion of high-contribution compounds, making its aroma profile more susceptible to being driven by a small number of dominant components. In contrast, Sample-High presented a more balanced contribution structure, which was associated with superior retronasal aroma performance. Collectively, this study suggests that alcohol-level differences were closely associated with retronasal aroma perception in representative Jiangxiangxing Baijiu samples, and provides new insight into the sensory and perceptual differences between high- and low-alcohol products. At the same time, as the present comparison was based on representative samples from two common alcohol-level categories in the Baijiu market, the findings should be interpreted with appropriate caution. However, the overall trends were broadly consistent with previous reports concerning alcohol-level effects on aroma perception. Future studies using a wider range of alcohol-level gradients may provide further insight into how alcohol level shapes retronasal aroma perception.

Supplementary Materials: The following supporting information can be downloaded at https://www.mdpi.com/article/10.3390/foods15071156/s1, Table S1: List of food-grade standard

compounds; Table S2: Different aroma descriptors and references; Table S3: Compounds and analytical parameters of GC-MS/MS.

Author Contributions: Conceptualization, J.Z. and S.C.; Data curation, J.Z. and S.C.; Methodology, J.Z. and S.C.; Resources, S.C., X.Y. (Xiaowei Yu) and Y.X.; Supervision, X.Y. (Xiaowei Yu), Y.X. and X.Z.; Writing—original draft, J.Z., S.C., X.Y. (Xiaolong You), X.Z., Y.S., F.H. and Y.H.; Writing—review and editing, J.Z., S.C., X.Z., Y.H., Y.X. and X.Y. (Xiaowei Yu). All authors have read and agreed to the published version of the manuscript.

Funding: This research was funded by the Postgraduate Research & Practice Innovation Program of Jiangsu Province (KYCX23_2497).

Institutional Review Board Statement: This study does not involve clinical research or the collection of sensitive personal information, and it is not associated with any commercial interests. All participants involved in the sensory evaluation were adults. Their data were anonymized prior to analysis, and participants were informed of their right to withdraw from the study at any time. The study was conducted in accordance with the Declaration of Helsinki, and ethical approval for this research was obtained from the Human Research Ethics Committee of Jiangnan University (approval no. JNU202409RB0032, approval date 27 September 2024).

Informed Consent Statement: Informed consent was obtained from all subjects involved in the study.

Data Availability Statement: The original contributions presented in this study are included in the article/Supplementary Materials. Further inquiries can be directed to the corresponding authors.

Conflicts of Interest: Xiaolong You, Xiaochun Zhu, Youlan Sun and Feng Hu were employed by Guizhou Xijiu Co., Ltd., Xishui, Guizhou, China, and are also affiliated with the Key Laboratory of Quality and Safety of Jiangxiangxing Baijiu, State Administration for Market Regulation, Guiyang, China. These authors contributed to manuscript preparation and/or supervision as described in the Author Contributions Section. The authors declare that the research was conducted in the absence of any commercial or financial relationships that could be construed as a potential conflict of interest.

Abbreviations

The following abbreviations are used in this manuscript:

ROT	Retronasal olfactory threshold
DoT	Dose-over-threshold
RDM-TCATA	Retronasal dual-mode temporal check-all-that-apply
RDA-TI	Retronasal dual-attribute time–intensity

References

1. Zheng, X.-W.; Han, B.-Z. Baijiu, Chinese liquor: History, classification and manufacture. *J. Ethn. Foods* **2016**, *3*, 19–25. [CrossRef]
2. Jin, G.; Zhu, Y.; Xu, Y. Mystery behind Chinese liquor fermentation. *Trends Food Sci. Technol.* **2017**, *63*, 18–28. [CrossRef]
3. Liu, Q.; He, D.; Ma, Y.; Wang, H.; Li, Y.; Cheng, Y.; Huang, Y. Sensory profile and the contribution of key aroma compounds in Jiang-flavor rounded-base Baijiu produced in the Chishui river basin. *LWT* **2023**, *189*, 115474. [CrossRef]
4. Rozin, P. "Taste-smell confusions" and the duality of the olfactory sense. *Percept. Psychophys.* **1982**, *31*, 397–401. [CrossRef]
5. Shepherd, G.M. Smell images and the flavour system in the human brain. *Nature* **2006**, *444*, 316–321. [CrossRef]
6. Wang, L.; Zhu, L.; Zheng, F.; Zhang, F.; Shen, C.; Gao, X.; Sun, B.; Huang, M.; Li, H.; Chen, F. Determination and comparison of flavor (retronasal) threshold values of 19 flavor compounds in Baijiu. *J. Food Sci.* **2021**, *86*, 2061–2074. [CrossRef]
7. Chen, L.; Yan, R.; Zhao, Y.; Sun, J.; Zhang, Y.; Li, H.; Zhao, D.; Wang, B.; Ye, X.; Sun, B. Characterization of the aroma release from retronasal cavity and flavor perception during baijiu consumption by Vocus-PTR-MS, GC×GC-MS, and TCATA analysis. *LWT Food Sci. Technol.* **2023**, *174*, 114430. [CrossRef]
8. Chen, L.; Zhao, Y.; Chen, X.; Zhang, Y.; Li, H.; Zhao, D.; Wang, B.; Ye, X.; Sun, B.; Sun, J. Peanut pairing Baijiu: To enhance retronasal aroma intensity while reducing Baijiu aftertaste. *J. Agric. Food Chem.* **2024**, *72*, 14851–14864. [CrossRef]
9. Yu, Y.; Yan, Y.; Wu, L.; Nie, Y.; Chen, S.; Xu, Y. Retronasal sensory characterization of aroma compounds in Baijiu by detection threshold measurement, retronasal OAVs, and time-intensity evaluation. *J. Food Sci.* **2024**, *89*, 1684–1700. [CrossRef] [PubMed]

10. Zhang, J.; Lu, J.; Yu, X.; Chen, S.; Xu, Y. Characterization of aroma differences in Jiangxiangxing Baijiu with varying ethanol concentrations: Emphasis on olfactory threshold changes of aroma compounds. *Food Chem.* **2025**, *469*, 142506. [CrossRef] [PubMed]
11. Castura, J.C.; Antúnez, L.; Giménez, A.; Ares, G. Temporal check-all-that-apply (TCATA): A novel dynamic method for characterizing products. *Food Qual. Prefer.* **2016**, *47*, 79–90. [CrossRef]
12. Visalli, M.; Mahieu, B.; Thomas, A.; Schlich, P. Concurrent vs. retrospective temporal data collection: Attack-evolution-finish as a simplification of Temporal Dominance of Sensations? *Food Qual. Prefer.* **2020**, *85*, 103956. [CrossRef]
13. Pierguidi, L.; Spinelli, S.; Monteleone, E.; Dinnella, C. The combined use of temporal dominance of sensations (TDS) and discrete time-intensity (DTI) to describe the dynamic sensory profile of alcoholic cocktails. *Food Qual. Prefer.* **2021**, *93*, 104281. [CrossRef]
14. Keefer, H.R.M.; Rovai, D.; Drake, M. A timely application—Temporal methods, past, present, and future. *J. Food Sci.* **2023**, *88*, A21–A52. [CrossRef] [PubMed]
15. Duizer, L.M.; Bloom, K.; Findlay, C.J. Dual-attribute time-intensity sensory evaluation: A new method for temporal measurement of sensory perceptions. *Food Qual. Prefer.* **1997**, *8*, 261–269. [CrossRef]
16. Gotow, N.; Moritani, A.; Hayakawa, Y.; Akutagawa, A.; Hashimoto, H.; Kobayakawa, T. Development of a time–intensity evaluation system for consumers: Measuring bitterness and retronasal aroma of coffee beverages in 106 untrained panelists. *J. Food Sci.* **2015**, *80*, S1343–S1351. [CrossRef] [PubMed]
17. Gotow, N.; Omata, T.; Uchida, M.; Matsuzaki, N.; Takata, S.; Hagiwara, I.; Kobayakawa, T. Multi-sip time–intensity evaluation of retronasal aroma after swallowing Oolong tea beverage. *Foods* **2018**, *7*, 177. [CrossRef]
18. Valentová, H.; Skrovánková, S.; Panovská, Z.; Pokorný, J. Time–intensity studies of astringent taste. *Food Chem.* **2002**, *78*, 29–37. [CrossRef]
19. Goodstein, E.S.; Bohlscheid, J.C.; Evans, M.; Ross, C.F. Perception of flavor finish in model white wine: A time-intensity study. *Food Qual. Prefer.* **2014**, *36*, 50–60. [CrossRef]
20. Zhang, J.; Yu, X.; Chen, S.; Xu, Y. Characterization of key aroma compounds contributing to oxidized oil-like off-odor in Jiangxiangxing Baijiu. *Food Chem.* **2025**, *483*, 144250. [CrossRef]
21. *ISO 13301:2018*; Sensory Analysis—Methodology—General Guidance for Measuring Odour, Flavour and Taste Detection Thresholds by a Three-Alternative Forced-Choice (3-AFC) Procedure. ISO: Geneva, Switzerland, 2018.
22. Chen, C.; Chen, H.; Zhang, Y.; Thomas, H.R.; Frank, M.H.; He, Y.; Xia, R. TBtools: An Integrative Toolkit Developed for Interactive Analyses of Big Biological Data. *Mol. Plant* **2020**, *13*, 1194–1202. [CrossRef]
23. NewMer Bioinformation Technology Co., Ltd. NGplot. Available online: https://www.bioinforw.com/ldm/webdraw (accessed on 21 August 2025).
24. Pineau, N.; de Bouillé, A.G.; Lepage, M.; Lenfant, F.; Schlich, P.; Martin, N.; Rytz, A. Temporal dominance of sensations: What is a good attribute list? *Food Qual. Prefer.* **2012**, *26*, 159–165. [CrossRef]
25. Wang, L.; Gao, Y.; Wu, L.; Chen, S.; Xu, Y. Characterization of Key Aging Aroma Compounds in Aged Jiangxiangxing Baijiu and Their Formation Influencing Factors during the Storge Process. *J. Agric. Food Chem.* **2024**, *72*, 1695–1707. [CrossRef]
26. Meillon, S.; Viala, D.; Medel, M.; Urbano, C.; Guillot, G.; Schlich, P. Impact of partial alcohol reduction in Syrah wine on perceived complexity and temporality of sensations and link with preference. *Food Qual. Prefer.* **2010**, *21*, 732–740. [CrossRef]
27. Harwood, W.S.; Parker, M.N.; Drake, M. Influence of ethanol concentration on sensory perception of rums using temporal check-all-that-apply. *J. Sens. Stud.* **2020**, *35*, e12546. [CrossRef]
28. King, E.S.; Dunn, R.L.; Heymann, H. The influence of alcohol on the sensory perception of red wines. *Food Qual. Prefer.* **2013**, *28*, 235–243. [CrossRef]
29. Meillon, S.; Urbano, C.; Schlich, P. Contribution of the Temporal Dominance of Sensations (TDS) method to the sensory description of subtle differences in partially dealcoholized red wines. *Food Qual. Prefer.* **2009**, *20*, 490–499. [CrossRef]
30. Baker, A.K.; Ross, C.F. Sensory Evaluation of Impact of Wine Matrix on Red Wine Finish: A Preliminary Study. *J. Sens. Stud.* **2014**, *29*, 139–148. [CrossRef]
31. Baker, A.K.; Ross, C.F. Wine finish in red wine: The effect of ethanol and tannin concentration. *Food Qual. Prefer.* **2014**, *38*, 65–74. [CrossRef]
32. Muñoz-González, C.; Brule, M.; Martin, C.; Feron, G.; Canon, F. Molecular mechanisms of aroma persistence: From noncovalent interactions between aroma compounds and the oral mucosa to metabolization of aroma compounds by saliva and oral cells. *Food Chem.* **2022**, *373*, 131467. [CrossRef]
33. Muñoz-González, C.; Pérez-Jiménez, M.; Criado, C.; Pozo-Bayón, M.Á. Effects of ethanol concentration on oral aroma release after wine consumption. *Molecules* **2019**, *24*, 3253. [CrossRef]
34. Ma, Y.; Xu, Y.; Tang, K. Olfactory perception complexity induced by key odorants perceptual interactions of alcoholic beverages: Wine as a focus case example. *Food Chem.* **2025**, *463*, 141433. [CrossRef] [PubMed]
35. Ferreira, V.; de-la-Fuente-Blanco, A.; Sáenz-Navajas, M.-P. A New Classification of Perceptual Interactions between Odorants to Interpret Complex Aroma Systems. Application to Model Wine Aroma. *Foods* **2021**, *10*, 1627. [CrossRef]

36. Niu, Y.; Yao, Z.; Xiao, Z.; Zhu, G.; Zhu, J.; Chen, J. Sensory evaluation of the synergism among ester odorants in light aroma-type liquor by odor threshold, aroma intensity and flash GC electronic nose. *Food Res. Int.* **2018**, *113*, 102–114. [CrossRef]
37. Thomas-Danguin, T.; Sinding, C.; Romagny, S.; El Mountassir, F.; Atanasova, B.; Le Berre, E.; Le Bon, A.-M.; Coureaud, G. The perception of odor objects in everyday life: A review on the processing of odor mixtures. *Front. Psychol.* **2014**, *5*, 1–18. [CrossRef]
38. Kay, L.M.; Crk, T.; Thorngate, J. A Redefinition of Odor Mixture Quality. *Behav. Neurosci.* **2005**, *119*, 726–733. [CrossRef]
39. Cain, W.S.; Drexler, M. Scope and evaluation of odor counteraction and masking. *Ann. N. Y. Acad. Sci.* **1974**, *237*, 427–439. [CrossRef]
40. Niu, Y.; Zhu, Q.; Xiao, Z. Characterization of perceptual interactions among ester aroma compounds found in Chinese Moutai Baijiu by gas chromatography-olfactometry, odor Intensity, olfactory threshold and odor activity value. *Food Res. Int.* **2020**, *131*, 108986. [CrossRef] [PubMed]
41. Esteban-Fernández, A.; Rocha-Alcubilla, N.; Muñoz-González, C.; Moreno-Arribas, M.V.; Pozo-Bayón, M.Á. Intra-oral adsorption and release of aroma compounds following in-mouth wine exposure. *Food Chem.* **2016**, *205*, 280–288. [CrossRef]
42. Zhao, H.; Chai, L.-J.; Zhang, W.; Zhang, X.-J.; Lu, Z.-M.; Wang, S.-T.; Shen, C.-H.; Shi, J.-S.; Xu, Z.-H. Changes in flavor profile of sauce-flavor baijiu: Perceptual interactions between 1-propanol and aroma compounds. *Food Chem. X* **2025**, *25*, 102153. [CrossRef] [PubMed]
43. Zhou, X.; Lyu, J.; Zhang, D.; Xu, Y.; Tang, K. Retronasal persistence of fruity esters modulated by palmitic acid and ethyl palmitate: A dynamic dual-monitoring approach. *Food Biosci.* **2026**, *77*, 108349. [CrossRef]
44. Hofmann, T.; Schieberle, P. Chemical interactions between odor-active thiols and melanoidins involved in the aroma staling of coffee beverages. *J. Agric. Food Chem.* **2002**, *50*, 319–326. [CrossRef]
45. Yan, Y.; Chen, S.; Nie, Y.; Xu, Y. Quantitative analysis of pyrazines and their perceptual interactions in soy sauce aroma type Baijiu. *Foods* **2021**, *10*, 441. [CrossRef]
46. Niu, M.; Ma, L.; Yang, Y.; Jia, J.; Xiang, L.; Tu, T.; Zhao, X.; Shen, C.; Wang, S. Uncovering the key volatile compounds affecting the roasted aroma in sauce-flavor baijiu and their perceptual interactions. *LWT* **2025**, *237*, 118705. [CrossRef]
47. Nogueira, J.P.; Souza, I.H.d.S.; Andrade, J.K.S.; Narain, N. Status of research on lactones used as aroma: A bibliometric review. *Food Biosci.* **2022**, *50*, 102004. [CrossRef]
48. Qian, X.; Lan, Y.; Han, S.; Liang, N.; Zhu, B.; Shi, Y.; Duan, C. Comprehensive investigation of lactones and furanones in icewines and dry wines using gas chromatography-triple quadrupole mass spectrometry. *Food Res. Int.* **2020**, *137*, 109650. [CrossRef]
49. Kato, Y.; Yuasa, Y. Practical synthesis of 3-methylnonane-2,4-dione, an intense strawlike and fruity flavored compound. *J. Agric. Food Chem.* **2001**, *49*, 3864–3866. [CrossRef] [PubMed]
50. Kao, J.-W.; Wu, X.; Hammond, E.G.; White, P.J. The impact of furanoid fatty acids and 3-methylnonane-2,4-dione on the flavor of oxidized soybean oil. *J. Am. Oil Chem. Soc.* **1998**, *75*, 831–835. [CrossRef]
51. Yang, Y.; Ni, D.; Lin, L.; Wang, D.; Wang, L. Odor activity study on the aroma compounds of steamed sorghum. *Food Ferment. Ind.* **2018**, *44*, 222–226.

Disclaimer/Publisher's Note: The statements, opinions and data contained in all publications are solely those of the individual author(s) and contributor(s) and not of MDPI and/or the editor(s). MDPI and/or the editor(s) disclaim responsibility for any injury to people or property resulting from any ideas, methods, instructions or products referred to in the content.

foods

MDPI

Article

Investigating the Impact of Different Drying Methods on the Aroma of Citri Reticulatae Pericarpium Using GC–MS/GC–IMS and E-Nose Technology

Aygul Alim, Chengfei Huang, Xin Zhao, Saren Gaowa, Runrong Zhang, Junrong Zhang, Xueqing Zhang, Yuanbao Jin and Wenzhong Hu *

School of Life Science, Zhuhai College of Science and Technology, No. 8 Anji East St., Jinwan Dist, Zhuhai 519041, China; aygulalim@sina.com (A.A.); ysxy@zcst.edu.cn (C.H.); 23383@zcst.edu.cn (X.Z.); kuailexiaosa@sina.com (S.G.); zrr163@126.com (R.Z.); zhangjunrong@zcst.edu.cn (J.Z.); 17666276137@163.com (X.Z.); jinyuanbao@zcst.edu.cn (Y.J.)

* Correspondence: hwz@dlnu.edu.cn

Abstract

Drying and storage conditions play a critical role in shaping the quality of aged citrus peel. This study investigated the effects of different processing strategies on the volatile composition, microstructure, and sensory characteristics of five-year-aged Citrus Reticulata 'Chachi' Peel (CRP). Four treatments were evaluated using SPME/GC–MS, GC–IMS, electronic nose analysis, sensory assessment, scanning electron microscopy (SEM), and multivariate statistical tools. GC–IMS identified 96 volatile compounds, demonstrating that aging combined with varied drying–storage conditions promoted the formation of diverse aroma-active substances. Terpenes and related compounds predominated, with the indoor-dried and warehouse-stored XH sample showing significantly higher concentrations of key terpenoids and sesquiterpenes, including α-terpineol, γ-muurolene, germacrene, β-selinenol, α-farnesene, and nerolidol. These compounds contributed to enhanced citrus, floral, fruity, and woody notes. Principal component analysis of electronic nose data (93.46% cumulative variance) clearly distinguished XH from other samples. Sensory results supported instrumental findings, indicating stronger fruity and sweet attributes in XH and C, while sun-dried samples exhibited more hay-like characteristics. SEM revealed better structural integrity in indoor-dried samples, potentially facilitating volatile retention. Overall, indoor drying and controlled storage improved aroma complexity and sensory quality, providing a scientific basis for optimized CRP processing.

Keywords: volatile compounds; sensory evaluation; multivariate analysis; aroma profile; drying

1. Introduction

Citrus Reticulata Peel (CRP) is extensively produced in Guangdong, Fujian, Sichuan, Chongqing, and Zhejiang provinces in southern China [1]. As a well-recognized traditional Chinese medicinal herb, the quality of CRP is enhanced with prolonged aging, which is attributed to the temporal variations in its volatile oil components [2]. CRP contains over 300 volatiles (terpenes, alcohols, etc.). Researchers used electronic nose/tongue with chemometrics for rapid identification of its cultivars and aging years; GC–MS and UHPLC-Q-TOF-MS identified key volatiles including β-myrcene and limonene [3]. Citri Reticulatae Pericarpium (CRP), a widely recognized medicinal and edible homologous herb, has

garnered considerable research interest due to its diverse biological properties, including hypolipidemic, anti-inflammatory, antidepressant, and antihypertensive effects [4–6], with high value in functional foods and daily chemical industries. Its quality and market value largely depend on characteristic aroma, closely related to processing techniques, making aroma retention crucial for industrial production and societal demand. Current CRP research mainly focuses on active components and pharmacology, while the impact of drying on aroma remains underexplored. As a critical processing step, inappropriate drying causes volatile oil loss and structural damage [7,8]. Conventional thermal and sun drying destroys cell structures, leading to shrinkage and accelerated aroma degradation, impairing CRP's quality and commercial value. Flavonoids and volatile oils are key CRP quality markers [9], and hot-air drying is superior to sun drying in retaining them [10]. However, existing studies lack systematic characterization combining aroma, sensory properties, and microstructure, leaving a research gap.

Nevertheless, the impact of different drying methods on CRP aroma profiles and related sensory evaluations has been rarely reported. This study selected five-year-stored CRP with different drying methods, integrating GC–IMS, GC–MS, sensory evaluation, electronic nose, and SEM for analysis; PLSR explored aroma–sensory correlations. It supplements theoretical understanding and provides a scientific basis for optimizing drying technologies and selecting high-quality CRP raw materials, supporting the efficient development of the CRP industry. This study provides a scientific basis for sample selection in CRP drying processes and CRP essential oil extraction.

2. Materials and Methods

2.1. Samples and Chemicals

Citrus Reticulata Peel (CRP) samples subjected to different drying and storage conditions—designated as XH, A, B, and C—were all aged for five years. The control sample (XHCRP) was dried under controlled temperature and humidity conditions and stored in a standard warehouse. Sample A was naturally sun-dried and subsequently stored in stacked piles, while sample B was naturally sun-dried and then stored in a standard warehouse. Sample C was dried using hot-air treatment and stored indoors. This study conducted a comparative analysis of commercially processed products rather than a controlled experiment, acknowledging that their proprietary processing parameters constitute a methodological limitation. All samples were purchased from Xinhui Village, Jiangmen City, Guangdong Province, China. Reference standards, including 2-methyl-3-heptanone (GR), n-alkanes (C7–C30) (GR), and n-hexane (GR), were obtained from Sigma-Aldrich (St. Louis, MO, USA).

2.2. Solid-Phase Microextraction (SPME)

A 3 g portion of each sample, along with 1 μL of the internal standard 2-methyl-3-heptanone (analytical standard, ≥99.5%; Sigma-Aldrich, St. Louis, MO, USA) was diluted with dichloromethane (HPLC-grade, ≥99.9%; Sigma-Aldrich, USA) to a final concentration of 0.816 μg/μL and was placed into a 20 mL sealed vial. The vial was equilibrated in a water bath at 55 °C for 20 min. a CAR/DVB/PDMS-coated SPME fiber (65 μm; Supelco Inc., Bellefonte, PA, USA, a subsidiary of Merck KGaA, Darmstadt, Germany)was used and exposed to the headspace for 40 min to adsorb volatile compounds. The fiber was subsequently placed into the gas chromatograph (GC) injection port, where thermal desorption was carried out at 250 °C for 5 min with a split ratio of 5:1 [11].

https://doi.org/10.3390/foods15071117

2.3. Analysis of Aroma Compounds in the Samples by GC–IMS and GC–MS

GC–IMS analysis was carried out with a FlavourSpec® instrument (G.A.S, Dortmund, Germany). GC–IMS operating conditions: An MXT-5 capillary column (15 m × 0.53 mm ID) was employed, and the column temperature was maintained at 40 °C. The total analysis time was 32 min. High-purity nitrogen (N_2, ≥99.999%) was used as the carrier gas, and the IMS drift tube temperature was set to 45 °C. The carrier gas flow rate was initially set at 2.00 mL/min and held for 2 min, then increased linearly to 100.00 mL/min over 0–30 min, after which this flow rate was maintained for an additional 10 min [11].

A GC–MS system (Shimadzu, QP2010 Ultra, Kyoto, Japan) was applied for qualitative and quantitative analysis. Gas chromatography–olfactometry–mass spectrometry (GC–MS) conditions: For GC analysis, a DB-5 capillary column was used with helium (purity > 99.99%) as the carrier gas at a constant flow rate of 1.2 mL/min and a split ratio of 5:1. The oven temperature program started at 40 °C and was held for 3 min, followed by an increase to 200 °C at a rate of 5 °C/min (without holding), and then ramped to 230 °C at 10 °C/min with a final hold of 3 min. MS analysis was performed using electron impact (EI) ionization at 70 eV. The ion source temperature was set to 230 °C, the mass scan range was 40–300 m/z, and the solvent delay time was 4 min [12].

Qualitative and quantitative analysis of aroma compounds: For qualitative identification, the mass spectra of volatile aroma compounds were initially matched against the NIST 2.0 mass spectral library. Retention index (RI) values were then verified using standard odor descriptions, and key aroma compounds were further confirmed based on the odor characteristics of corresponding reference standards. RI values were calculated using a homologous series of n-alkanes according to the following equation:

$$RI = 100N + 100n\,(t_{Ra} - t_{RN})/(t_{R(N+n)} - t_{RN}) \quad (1)$$

where N represents the carbon number of the lower n-alkane; n is the carbon number difference between the two bracketing n-alkanes; and t_{Ra}, t_{RN}, and $t_{R(N+n)}$ correspond to the retention times of the target aroma compound, the lower n-alkane, and the higher n-alkane, respectively.

Relative quantification was carried out using an internal standard method by comparing the chromatographic peak area of each volatile compound with that of the internal standard. The relative concentration was calculated using the following equation:

$$C_i = C_{IS} \times A_i/A_{IS}\ (\mu g/g) \quad (2)$$

where C_i is the relative concentration of the aroma compound, C_{IS} is the relative concentration of the internal standard, A_i is the peak area of the aroma compound, and A_{IS} is the peak area of the internal standard. Using an internal standard, semi-quantitative analysis was conducted to initially screen key aroma compounds [13].

2.4. Sensory Evaluation

Descriptive sensory analysis: Approximately 15 g of each sample was weighed and transferred into a clean, odor-free 40 mL headspace vial. Sensory evaluation was carried out by a trained panel consisting of 12 assessors (7 females and 5 males, mean age 30 years) in a quiet, odor-controlled sensory laboratory. Panelists were instructed to abstain from eating for at least one hour before the session. To ensure independent assessments, communication among panelists was not permitted during evaluation. Reference samples included five types of authentic CRP and pure chemical standards representing key aroma attributes. Specifically, D-limonene (citrus, 0.1% *v*/*v*), ethyl butanoate (fruity, 0.05% *v*/*v*), linalool (floral, 0.1% *v*/*v*), ethyl butanoate (sweet, 0.05% *v*/*v*), octanal (hay-like, 0.05% *v*/*v*), and

https://doi.org/10.3390/foods15071117

citric acid (sour, 0.5% *w*/*v*) were employed as reference standards, following established citrus aroma sensory protocols [14]. Each sample was evaluated in triplicate, with results reported as mean values. The primary aroma descriptors for the citrus peel included fruity, sweet, sour, floral, hay-like, and citrus notes, while refreshing and pleasant characteristics were also assessed using the same 10-point scale [12].

2.5. Discrimination of CRP Based on E-Nose Analysis

An E-nose with a gas sensor array (Sensigent, Cyranose 320, Baldwin Park, CA, USA) was used for odor detection. A 3.5 g portion of the CRP sample was transferred into a 50 mL headspace vial, which was subsequently capped, sealed, and equilibrated at 26 °C for 30 min prior to analysis. The electronic nose operating conditions were as follows: cleaning time of 120 s, zeroing time of 5 s, pre-injection time of 8 s, measurement time of 60 s, and a carrier gas flow rate of 400 mL/min. Under these conditions, variations in the conductivity ratio (G/G_0) were recorded, where G and G_0 denote the responses of the metal oxide sensor to the sample gas and the clean gas, respectively. All measurements were performed in triplicate, and the mean values were calculated for subsequent plotting and analysis using Origin software. Unlike principal component analysis (PCA), which is primarily used for data reduction, this method focuses on classification by maximizing inter-group separation while minimizing variability within groups.

2.6. Scanning Electron Microscope

The CRP microstructures of the four samples were examined using a JSM-6510LV (JEOL, Tokyo, Japan) scanning electron microscope (SEM). For surface analysis, a small section of each CRP was excised from the central region for imaging at magnifications of 200× and 500×. Each specimen was mounted onto the sample stage with conductive adhesive, ensuring a flat orientation to achieve optimal electrical conductivity. Prior to imaging, the samples were coated with a thin layer of gold using an ion sputter coater. Morphological observations were conducted at an accelerating voltage of 20 kV [15].

2.7. Statistical Analysis

For GC–MS-derived data, statistical differences among samples were evaluated using analysis of variance (ANOVA) followed by Duncan's multiple range test. Principal component analysis (PCA) was applied to illustrate sample clustering and to elucidate the contributions of odor-active compounds to overall flavor profiles. GC–IMS data were processed using Laboratory Analytical Viewer (LAV) software (Version 2.7) equipped with three plug-ins, including the GC × IMS Library Search, allowing for multidimensional analysis of samples. Statistical analyses were conducted using IBM SPSS Statistics 22.0 (Chicago, IL, USA). Quantitative results are presented as mean ± standard error of the mean (SEM), with significance set at $p < 0.05$. Heatmaps were constructed using Origin 2019 software. Partial least-squares regression (PLSR) was conducted to correlate volatile compound profiles (X-matrix) with sensory attributes (Y-matrix) of XHCRP. The optimal number of latent variables was determined using leave-one-out cross-validation (LOOCV) to assess the model's predictive performance and prevent overfitting [16].

3. Results and Discussion

3.1. Analysis of Volatile Components in CRP Based on GC–IMS

Significant differences were observed in both the composition and relative abundance of volatile compounds among the four CRP samples. Compounds showing pronounced variation were categorized into seven regions (a, b, c, d, e, f, and h) for detailed discussion (Figure 1). Substances identified in region a were detected across all four dried

https://doi.org/10.3390/foods15071117

citrus peel samples and primarily consisted of aldehydes, alcohols, and ketones. Specifically, 2,4-heptadienal (Z,Z), hexanal, and (Z)-3-hexenol contributed strong grassy notes. Limonene and Z-4-decenal imparted characteristic lemon-citrus aromas. β-Pinene exhibited a resinous scent, whereas α-pinene presented a typical pinene odor, and camphene produced a faint camphor-like aroma. δ-Heptanolide was associated with a coconut oil-like note, while 1-phenylethyl acetate contributed a fresh floral aroma. 2-Formyl-5-methylthiophene was characterized by a woody fragrance, and (R)-α-pinene imparted an aromatic, mint-like note. Octanal displayed a pungent, sharp, and waxy aroma. Fruity notes were attributed to 2-heptanone, (E)-2-hexen-1-ol, ethyl 2-methylbutyrate, and isobutyl propanoate. In addition, triethylamine exhibited an ammonia-like odor; 2-methylpentanal imparted a roasted peanut-like aroma; acetic acid was characterized by an irritating odor; 3-methylbutanoic acid exhibited an unpleasant rancid smell; and 2-butoxyethanol contributed a mild aroma.

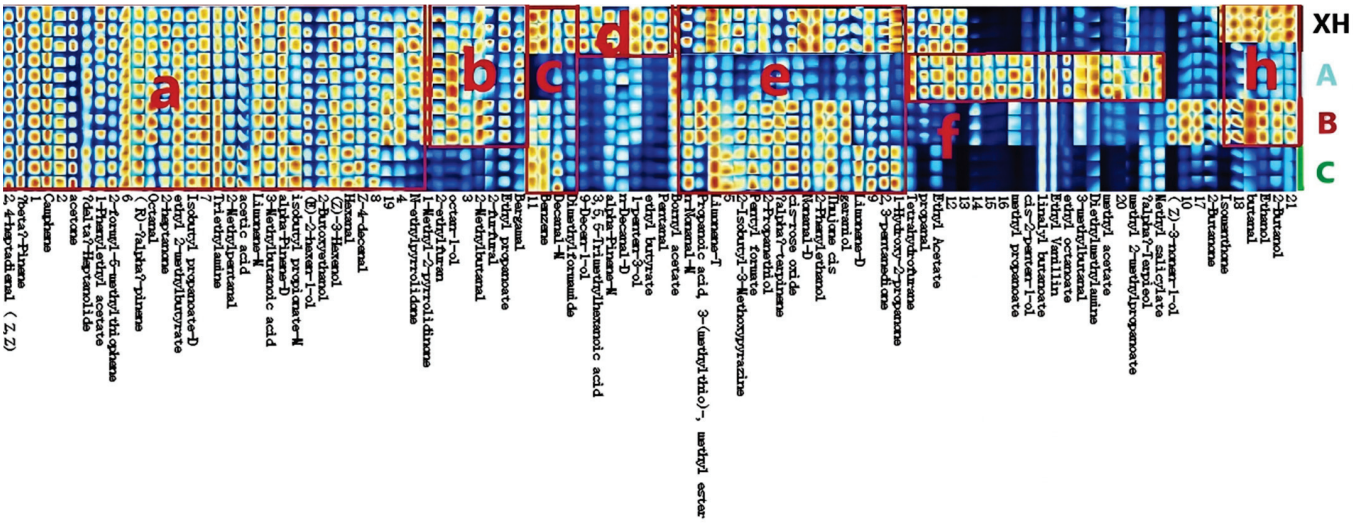


Figure 1. Gallery plot (fingerprint) of CRP samples. (The regions a, b, c, d, e, f, and h in the figure were used to analyze the differences in aroma compounds.)

The compounds identified in region b were commonly found in the XH, A, and B dried citrus peel samples at relatively high concentrations. Among them, 1-ethyl-2-pyrrolidinone had a slight ammonia-like odor; 2-ethylfuran exhibited a roasted aroma; octan-1-ol carried a citrus note; 2-ethylbutanal produced an irritating smell; 2-furfural had a distinctive benzaldehyde-like scent; and ethyl propanoate and Bergamal contributed fruity flavors.

The compounds detected in region c were prevalent in the XH, B, and C dried citrus peel samples with relatively high levels. Benzene exhibited an aromatic odor, while decanal emitted a sweet fragrance reminiscent of orange and lemon.

The compounds in region d were unique to the XH samples and present at relatively high concentrations. Dimethylformamide had an ammonia-like odor; 9-decen-1-ol gave a floral aroma; α-pinene exhibited its characteristic pine scent; Decanal was characterized by a sweet fragrance reminiscent of orange and lemon; 1-penten-3-ol and ethyl butyrate offered fruity notes; and pentanal possessed a distinctive aroma. Unlike other drying methods that easily cause the loss of unique volatile compounds [16], the specific drying and aging processes adopted for the XH samples effectively retained these characteristic aroma substances, resulting in their uniqueness in region d.

The compounds identified in region e were detected in the XH, B, and C samples at relatively high levels, predominantly consisting of esters, aldehydes, and ketones. Specifically, bornyl acetate imparted a cool pinewood aroma; propanoic acid, 3-(methylthio)-, methyl ester and pentyl formate contributed fruity notes; limonene, α-terpinene, and nonanal

https://doi.org/10.3390/foods15071117

provided citrusy, lemon-like scents; 2-isobutyl-3-ethoxypyrazine had a green pepper aroma; 2-propanethiol produced an unpleasant odor; cis-rose oxide offered a green floral fragrance reminiscent of rose cortex; 2-phenylethanol and geraniol conveyed floral aromas; and cis-thujone presented a cedar and arborvitae scent [12]. In contrast to tray drying (TD), which was found to cause severe loss of esters and aldehydes in citrus peels [17], the XH, B, and C samples retained significantly higher levels of these aroma-active compounds, suggesting that their drying methods are more superior in preserving the aromatic quality of CRP.

The compounds in region f were detected at relatively high concentrations in both the XH and A samples.Limonene displayed a fresh lemon fragrance, 2,3-pentanedione gave a creamy aroma, and 1-hydroxy-2-propanone emitted a caramel-like scent. Wang et al. [16] demonstrated that drying temperature is a critical factor affecting the content of volatile compounds in citrus peels, and the high abundance of characteristic compounds in the XH and A samples might be associated with their moderate drying temperature.

The compounds in region h were found in the XH and B dried citrus peel samples at relatively high levels. Tetrahydrofuran exhibited an ether-like odor, while propanal had a pungent smell. Ethyl acetate, methyl propanoate, cis-2-penten-1-ol, and methyl 2-ethylpropanoate contributed fruity aromas; linalyl butanoate and 3-ethylbutanal provided a bergamot-like scent; ethyl vanillin offered a vanilla bean fragrance; ethyl octanoate produced a sweet, brandy-like aroma; methyl acetate had a fragrant odor; and α-terpineol emitted a floral scent. Additionally, methyl salicylate conveyed a wintergreen leaf flavor, (Z)-3-nonen-1-ol presented a mushroom-like taste, isomenthone and 2-butanol had minty aromas, and butanal and ethanol emitted sharp, irritating odors.

A total of 96 characteristic target volatile compounds were successfully identified from the topographic plots using the GC × IMS Library Figure 2 (Table 1). Compared with the volatile profile of fresh CRP, the drying and aging processes led to the formation of a substantial number of new volatile compounds. Overall, the results shown in Figure 2 indicate that the aroma profile of CRP—primarily composed of terpenes, alcohols, aldehydes, and a minor proportion of furans—undergoes significant alterations depending on the drying method. Its aroma profiles were distinctly different from those of citrus peels dried by vacuum infrared drying (VID) and vacuum microwave drying (VMD). Bozkir et al. [18] reported that VID and VMD can better retain volatile compounds than TD, but the XH and B samples in this study showed a more abundant aroma profile, especially in fruity and floral compounds.

Table 1. Aroma compounds of CRP identified by HS-GC-IMS.

No	Compounds	CAS	Formula	MW	RI	Rt [Sec]	Dt [a.u.]
1	2,4-Heptadienal (Z,Z)	5910-85-0	$C_7H_{10}O$	110.2	992.3	594.363	1.19059
2	β-Pinene	127-91-3	$C_{10}H_{16}$	136.2	977.9	566.167	1.21609
3	**1**	unidentified	*	0	951.8	518.266	1.70461
4	Camphene	79-92-5	$C_{10}H_{16}$	136.2	962	536.412	1.21286
5	**2**	unidentified	*	0	723.4	252.033	1.67446
6	Acetone	67-64-1	C_3H_6O	58.1	495.2	146.309	1.11905
7	Bornyl acetate	76-49-3	$C_{12}H_{20}O_2$	196.3	1278.1	1177.504	1.2262
8	δ-Heptanolide	3301-90-4	$C_7H_{12}O_2$	128.2	1159.2	887.495	1.22255
9	1-Phenylethyl acetate	93-92-5	$C_{10}H_{12}O_2$	164.2	1164.5	898.869	1.05253
10	2-Formyl-5-methylthiophene	13679-70-4	C_6H_6OS	126.2	1128.1	824.217	1.17103
11	9-Decen-1-ol	13019-22-2	$C_{10}H_{20}O$	156.3	1241.8	1079.988	1.43873
12	Decanal-M	112-31-2	$C_{10}H_{20}O$	156.3	1190.7	956.519	1.53577
13	**3**	unidentified	*	0	1189	952.599	1.63795
14	n-Decanal-D	112-31-2	$C_{10}H_{20}O$	156.3	1187.9	950.307	2.05673
15	Isomenthone	491-07-6	$C_{10}H_{18}O$	154.3	1160.2	889.571	1.33675

Table 1. *Cont.*

No	Compounds	CAS	Formula	MW	RI	Rt [Sec]	Dt [a.u.]
16	**4**	unidentified	*	0	1171.7	914.221	1.49666
17	3,5,5-Trimethylhexanoic acid	3302-10-1	$C_9H_{18}O_2$	158.2	1155.6	880	1.45377
18	n-Nonanal-M	124-19-6	$C_9H_{18}O$	142.2	1098.3	767.915	1.47012
19	Bergamal	106-72-9	$C_9H_{16}O$	140.2	1054.8	692.577	1.17614
20	Limonene-D	138-86-3	$C_{10}H_{16}$	136.2	1028.6	650.698	1.28874
21	1-Methyl-2-pyrrolidinone	872-50-4	C_5H_9NO	99.1	1043.4	674.026	1.4377
22	Propanoic acid, 3-(methylthio)-, methyl ester	13532-18-8	$C_5H_{10}O_2S$	134.2	1042	671.786	1.60356
23	Limonene-T	138-86-3	$C_{10}H_{16}$	136.2	1022.6	641.537	1.65772
24	Octanal	124-13-0	$C_8H_{16}O$	128.2	1007.7	619.164	1.8037
25	α-Pinene	7785-70-8	$C_{10}H_{16}$	136.2	932.4	485.322	1.73124
26	2-Heptanone	110-43-0	$C_7H_{14}O$	114.2	891	422.145	1.72079
27	α-Pinene-M	80-56-8	$C_{10}H_{16}$	136.2	941.5	500.568	1.28888
28	**5**	unidentified	*	0	1054.8	692.542	1.72524
29	**6**	unidentified	*	0	917	460.665	2.17224
30	Ethyl 2-methylbutyrate	7452-79-1	$C_7H_{14}O_2$	130.2	843.6	366.191	1.6433
31	Isobutyl propanoate-D	540-42-1	$C_7H_{14}O_2$	130.2	858.4	382.786	1.71212
32	**7**	unidentified	*	0	869.3	395.468	1.94579
33	**8**	unidentified	*	0	824.3	345.527	2.18164
34	Pentyl formate	638-49-3	$C_6H_{12}O_2$	116.2	767.5	290.448	1.66879
35	Ethyl propanoate	105-37-3	$C_5H_{10}O_2$	102.1	739.2	265.196	1.4493
36	Triethylamine	121-44-8	$C_6H_{15}N$	101.2	780.2	302.466	1.21725
37	2-Methylpentanal	123-15-9	$C_6H_{12}O$	100.2	755.4	279.37	1.21857
38	**9**	unidentified	*	0	707.3	239.372	1.21721
39	Pentanal	110-62-3	$C_5H_{10}O$	86.1	688.2	225.179	1.42501
40	2,3-Pentanedione	600-14-6	$C_5H_8O_2$	100.1	675.4	218.86	1.21358
41	Benzene	71-43-2	C_6H_6	78.1	648.7	206.176	1.08117
42	Acetic acid	64-19-7	$C_2H_4O_2$	60.1	627.3	196.55	1.14892
43	2-Butanone	78-93-3	C_4H_8O	72.1	591.6	181.459	1.24433
44	**10**	unidentified	*	0	600.5	185.105	1.41118
45	Tetrahydrofurane	109-99-9	C_4H_8O	72.1	623.4	194.865	1.23708
46	Propanal	123-38-6	C_3H_6O	58.1	509.8	151.175	1.15704
47	**11**	unidentified	*	0	459.7	135.148	1.14505
48	Ethyl acetate	141-78-6	$C_4H_8O_2$	88.1	564.2	170.712	1.33808
49	1-Penten-3-ol	616-25-1	$C_5H_{10}O$	86.1	685.5	223.861	1.35015
50	2-Methylbutanal	96-17-3	$C_5H_{10}O$	86.1	674.2	218.256	1.16324
51	Ethanol	64-17-5	C_2H_6O	46.1	435.2	127.946	1.04191
52	1-Hydroxy-2-propanone	116-09-6	$C_3H_6O_2$	74.1	650.9	207.195	1.04046
53	Ethyl butyrate	105-54-4	$C_6H_{12}O_2$	116.2	783.4	305.614	1.56114
54	**12**	unidentified	*	0	740.5	266.306	1.58684
55	Dimethylformamide	68-12-2	C_3H_7NO	73.1	783.4	305.64	1.26047
56	Hexanal	66-25-1	$C_6H_{12}O$	100.2	792	313.653	1.29176
57	**13**	unidentified	*	0	480.3	141.51	1.28705
58	Cis-2-penten-1-ol	1576-95-0	$C_5H_{10}O$	86.1	771.3	293.941	1.44934
59	Linalyl butanoate	78-36-4	$C_{14}H_{24}O_2$	224.3	1411	1614.95	1.22539
60	Ethyl vanillin	121-32-4	$C_9H_{10}O_3$	166.2	1410.9	1614.415	1.29612
61	Cis-rose oxide	3033-23-6	$C_{10}H_{18}O$	154.3	1098.4	768.11	1.80756
62	Nonanal-D	124-19-6	$C_9H_{18}O$	142.2	1098	767.429	1.93877
63	Limonene-M	138-86-3	$C_{10}H_{16}$	136.2	1025.7	646.169	1.219
64	(Z)-3-nonen-1-ol	10340-23-5	$C_9H_{18}O$	142.2	1126.1	820.319	1.38669
65	**14**	unidentified	*	0	1155.3	879.303	1.08637

Table 1. *Cont.*

No	Compounds	CAS	Formula	MW	RI	Rt [Sec]	Dt [a.u.]
66	**15**	unidentified	*	0	473	139.235	1.20457
67	2-Ethylfuran	3208-16-0	C_6H_8O	96.1	707.2	239.293	1.30514
68	2-Furfural	98-01-1	$C_5H_4O_2$	96.1	843.9	366.528	1.32698
69	**16**	unidentified	*	0	418.7	123.311	1.09023
70	3-Methylbutanal	590-86-3	$C_5H_{10}O$	86.1	649.4	206.481	1.40303
71	4-Ketoisophorone	1125-21-9	$C_9H_{12}O_2$	152.2	1132.4	832.856	1.33188
72	**17**	unidentified	*	0	1140.2	848.361	1.78974
73	**18**	unidentified	*	0	1160	889.197	1.59659
74	2-Isobutyl-3-methoxypyrazine	24683-00-9	$C_9H_{14}N_2O$	166.2	1170.7	912.184	1.84124
75	(E)-2-hexen-1-ol	928-95-0	$C_6H_{12}O$	100.2	859.5	384.065	1.55833
76	2-Propanethiol	75-33-2	C_3H_8S	76.2	569.2	172.629	1.14739
77	3-Methylbutanoic acid	503-74-2	$C_5H_{10}O_2$	102.1	886.5	416.454	1.21233
78	Octan-1-ol	111-87-5	$C_8H_{18}O$	130.2	1042.9	673.228	1.46523
79	Methyl acetate	79-20-9	$C_3H_6O_2$	74.1	518.3	154.058	1.19534
80	**19**	unidentified	*	0	700.9	234.457	1.61102
81	Methyl 2-methylpropanoate	547-63-7	$C_5H_{10}O_2$	102.1	683.3	222.734	1.45116
82	Geraniol	106-24-1	$C_{10}H_{18}O$	154.3	1253.4	1110.237	1.22551
83	Alpha-pinene-D	80-56-8	$C_{10}H_{16}$	136.2	939.9	497.835	1.65887
84	α-Terpinene	99-86-5	$C_{10}H_{16}$	136.2	1017.8	634.162	1.72181
85	Isobutyl propionate-M	540-42-1	$C_7H_{14}O_2$	130.2	858.4	382.774	1.28135
86	Butanal	123-72-8	C_4H_8O	72.1	612.1	189.978	1.29234
87	2-Phenylethanol	60-12-8	$C_8H_{10}O$	122.2	1127.6	823.422	1.67124
88	Z-4-decenal	21662-09-9	$C_{10}H_{18}O$	154.3	1184.9	943.394	1.94593
89	Methyl salicylate	119-36-8	$C_8H_8O_3$	152.1	1196.8	970.594	1.15109
90	**20**	unidentified	*	0	1146.2	860.634	1.24883
91	Thujone cis	546-80-5	$C_{10}H_{16}O$	152.2	1099.7	770.466	1.87156
92	2-Butoxyethanol	111-76-2	$C_6H_{14}O_2$	118.2	900.2	435.207	1.21228
93	N-ethylpyrrolidone	2687-91-4	$C_6H_{11}NO$	113.2	1165.9	901.886	1.15055
94	(Z)-3-hexenol	928-96-1	$C_6H_{12}O$	100.2	853.9	377.686	1.21998
95	2-Butanol	78-92-2	$C_4H_{10}O$	74.1	597.5	183.888	1.3279
96	**21**	unidentified	*	0	582	177.606	1.11674

"*" Not identified in the standard library; chemical formula unknown.

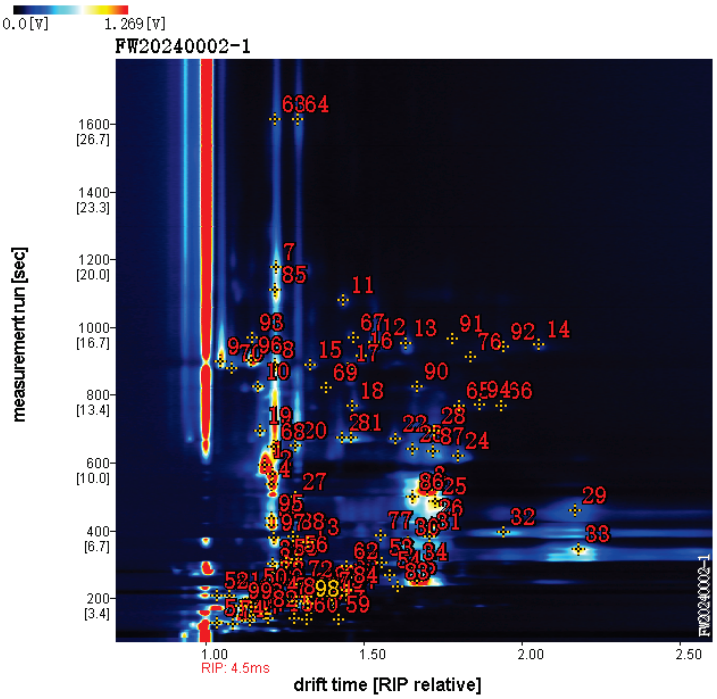


Figure 2. Qualitative analysis of CRP by GC–IMS.

3.2. Identification and Quantification of Volatile Components by GC–MS

The primary compounds were identified using the SPME/GC–MS internal standard method, and their corresponding aroma profiles were obtained from the Flavornet database. Differences among the various samples were then analyzed (Figure 3). The results revealed significant variations in the aroma components of CRP subjected to different drying methods, with both the types and concentrations of compounds changing noticeably. As illustrated in the figure, the XH samples generally exhibited higher concentrations of several key compounds, including α-terpineol (floral and woody), γ-muurolene (woody and spicy), 2-dodecenal (sweet), germacrene (woody and spicy), β-selinenol (woody and green), α-farnesene (woody), nerolidol, and m-camphorene. Compared with samples A, B, and C, Xinhui tangerine peel contained a greater diversity of volatile compounds, predominantly esters, alcohols, ketones, aldehydes, and terpenoids, with smaller amounts of acids and heterocyclic compounds. XHCRP was characterized by prominent citrus, sweet fruity, and floral aromas, along with cool notes reminiscent of mint and pine. The broader range of volatile compounds (esters, alcohols, ketones, aldehydes, terpenoids, acids, and heterocyclics) in XHCRP contributes to these complex aroma profiles, enhancing its market quality. Consequently, XHCRP surpasses the other samples in both flavor and overall quality, exhibiting unique aroma characteristics with strong commercial potential [19]. Consistent with this finding, Zheng et al. also verified that the drying regime is a critical factor regulating the bioactive and volatile components in Citri Reticulatae Pericarpium, which directly determines its sensory quality and market value [20].

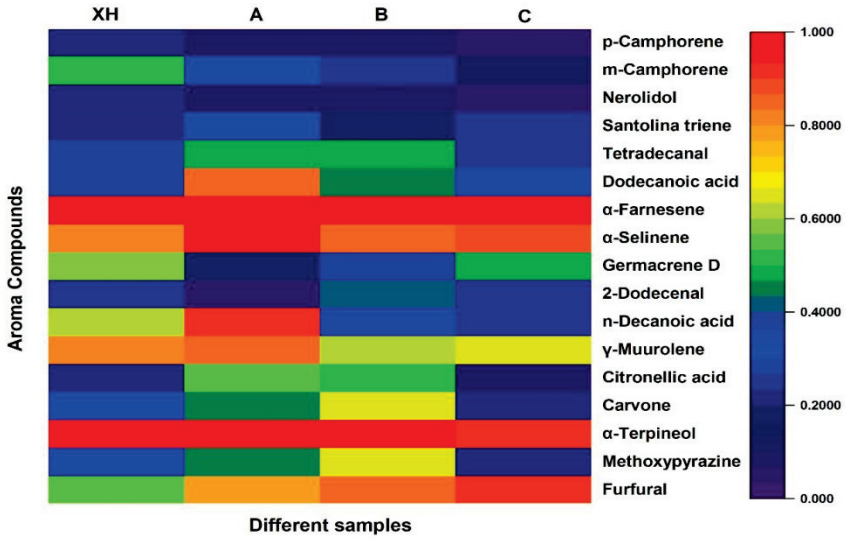


Figure 3. Determination of volatile components by GC–MS.

Specifically, during the drying phase, the dynamic evolution of flavor metabolites, including the synthesis of new aroma compounds and the conversion of their precursor substances, is closely associated with the changes in microbial diversity induced by different drying conditions, which further regulates the formation of CRP aroma profiles [8]. Different drying techniques affect the formation of aroma compounds by altering the drying rate and physical structure of CRP, and they can significantly influence the content of total volatile oil and the composition of volatile organic compounds (VOCs), with thermal drying and non-thermal drying methods leading to distinct differences in aroma-related components [21]. Additionally, the oil cell number, which is affected by drying techniques, can indirectly regulate the accumulation and release of key aroma substances, further participating in the formation of the unique aroma of XHCRP [21].

https://doi.org/10.3390/foods15071117

3.3. Sensory Evaluation and Emotion Evaluation

The radar chart illustrating the aroma quality of CRP from different samples (Figure 4) shows that the overall characteristic aroma sub-attributes included fruity, sweet, sour, floral, hay-like, and citrus notes. A 10-point scale was used to evaluate the refreshing and pleasant sensations associated with the aromas. Sensory evaluation results indicated that the XH sample and sample C were primarily characterized by fruity, citrus, and sweet aromas. This is likely because both samples underwent indoor drying followed by indoor storage, which helped preserve a higher concentration of volatile compounds compared to the other samples. Samples A and B displayed more pronounced hay-like and citrus aromas. Regarding aroma pleasantness and refreshing quality, the XH, C, and A samples received higher sensory scores. Overall, the XH sample showed a distinct advantage in aroma-related sensory evaluation [22].

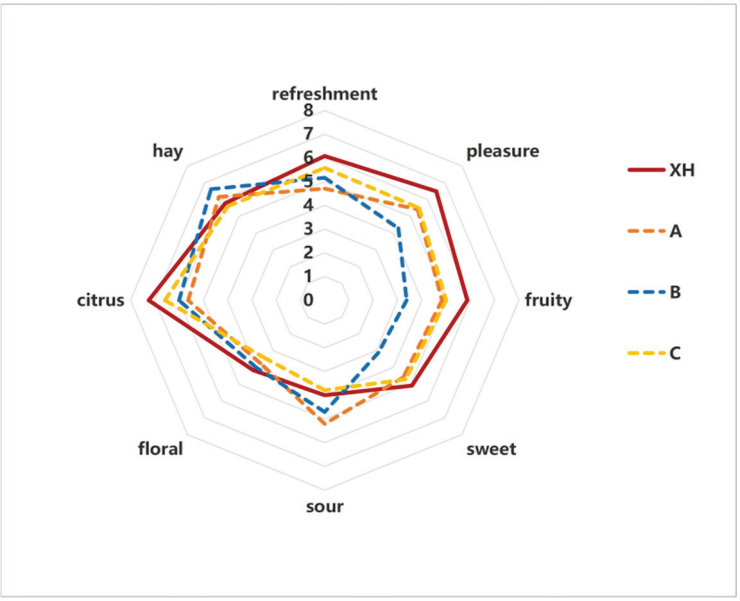


Figure 4. Radar chart of sensory evaluation of different CRP samples.

3.4. Electronic Nose Analysis

To investigate the response patterns of the 10 sensors in the electronic nose toward CRP samples under different storage conditions, the sensor signals were analyzed to determine each sensor's response value. The sensor response values were evenly arranged along the circumference of the plot, and the maximum response of each sensor was extracted to generate the radar chart shown in Figure 5. This analysis revealed that the CRP samples contained a diverse array of odor-active compounds. Among the five CRP samples with different storage conditions, sensors W5S (sensitive to nitrogen oxides), W1S (methyl groups), and W1W (sulfides) exhibited the highest response intensities. Sensors W2W (aromatic compounds and organic sulfides) and W2S (alcohols, aldehydes, and ketones) showed moderate responsiveness, while W6S (hydrides), W1C (benzene), W5C (short-chain alkanes), and W3C (aromatic ammonia) displayed the lowest sensitivity. Regarding the samples, XH demonstrated the strongest overall aroma intensity, followed by C and B, with A showing the weakest aromatic profile.

https://doi.org/10.3390/foods15071117

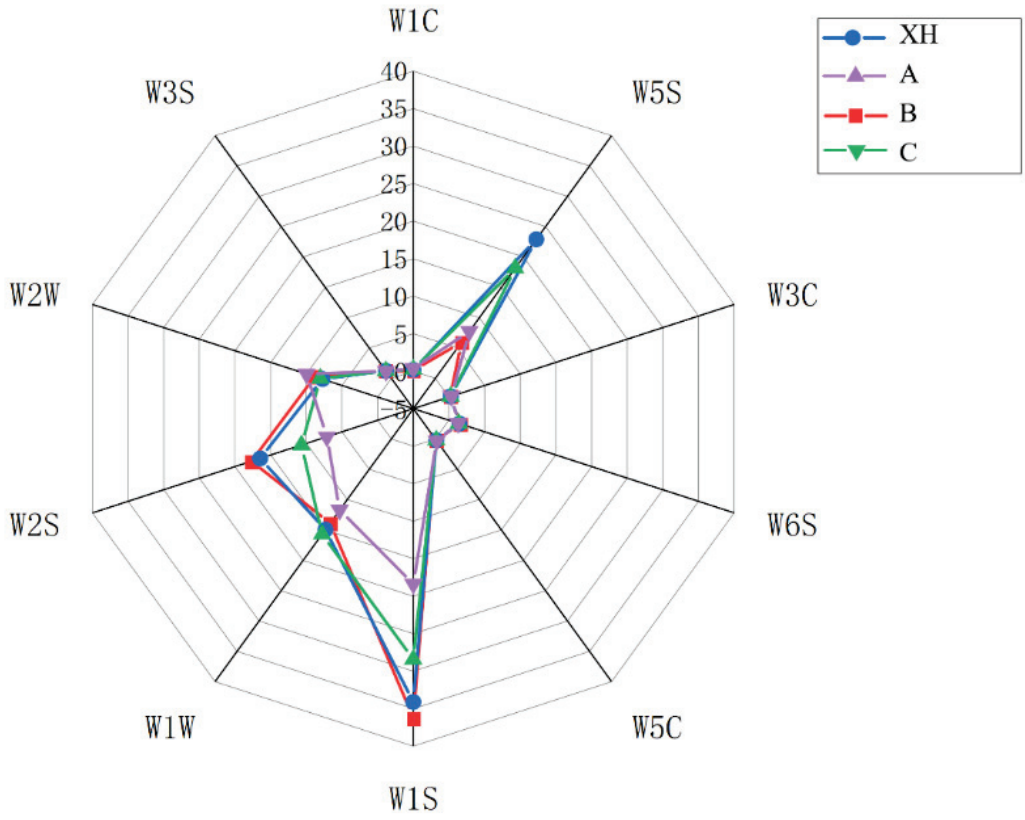


Figure 5. Electronic nose radar map of CRP.

As shown in the PCA plot (Figure 6), XHCRP is positioned in the lower region, distinctly separated from the other samples, indicating its unique flavor profile and low similarity to the others. In contrast, samples A, B, and C cluster closely together, reflecting their high flavor similarity.

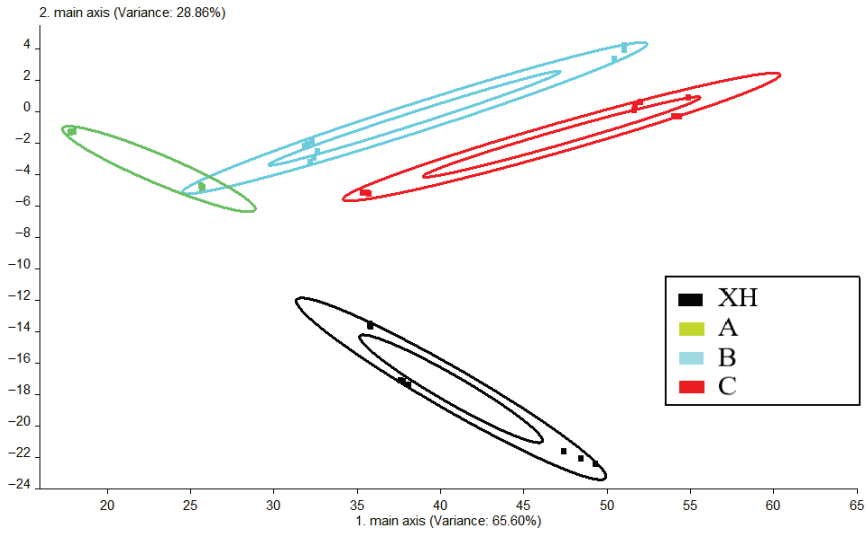


Figure 6. PCA of CRP samples.

3.5. Scanning Electron Microscopy and Microstructure Analysis of CRP

Figure 7 presents the surface morphology of CRP samples from different vintages at magnifications of 200 μm (XH-1, A-1, B-1, C-1) and 500 μm (XH-2, A-1, B-2, C-2). As the peel ages, pericarp cells deteriorate rapidly, and plastids and vacuoles gradually disintegrate, accompanied by respiration and other physiological processes [23]. The pericarp tissue

shrinks, its initially loose structure collapses and becomes scattered, and small, sporadically distributed pores appear on the surface. Regarding stomata, the surfaces of samples XH and C, despite exhibiting numerous wrinkles, retain some fullness and three-dimensionality; their stomata collapse into concave shapes with pore sizes larger than those of samples A and B. In sample B (naturally sun-dried), surface wrinkles are more pronounced, shrinkage is greater, and stomatal pores decrease in size. The stomata of the stored XH sample are concave with raised areas surrounding them, whereas those of sample C enlarge significantly, showing a concave center with raised surrounding areas.

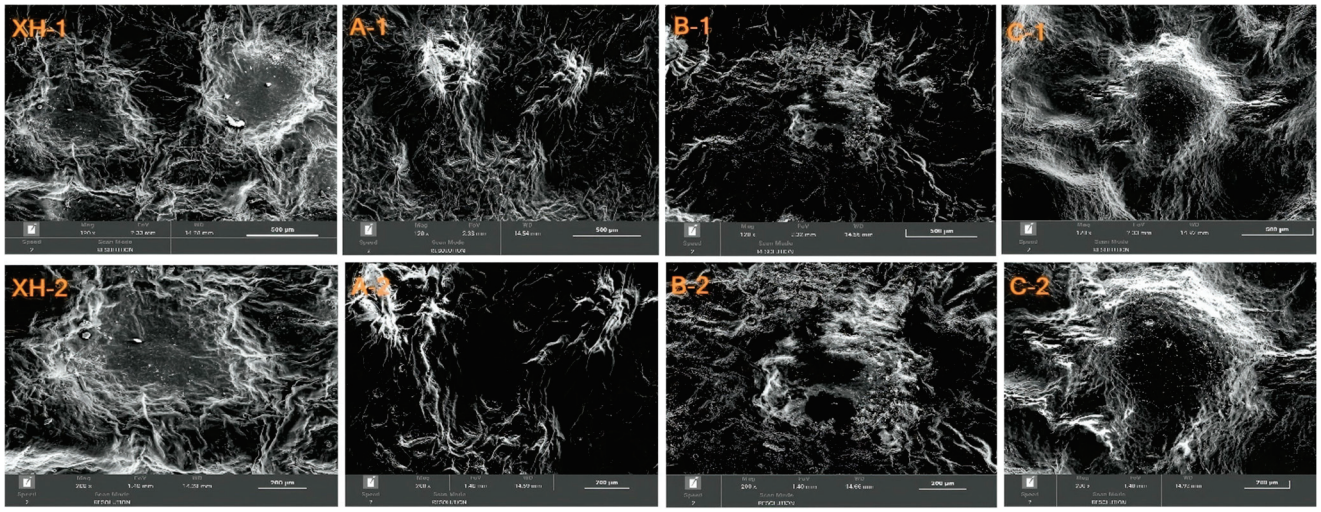


Figure 7. Scanning electron microscope (SEM) microstructure of CRP.

These structural variations could be partially explained by the decomposition of non-volatile components in the pericarp during long-term aging, which can be transformed into aroma-contributing small molecules and thus lead to modifications in tissue structure and stomatal morphology [20]. Meanwhile, enzymatic browning also plays an important role: under aerobic conditions, enzymes react with corresponding substrates and catalyze the formation of quinones, which further polymerize or combine with amino compounds to generate brown pigments, resulting in pericarp browning [14,24]. During such processes, the pericarp tissue gradually softens, stomatal structures become indistinct, and the overall tissue becomes looser, which is consistent with previous observations in stored CRP [20].

3.6. Correlation Between the Content of Aroma Compounds and Odor During the Storage Period Analyzed by PLSR

Figure 8 depicts the relationship between various aroma compounds and the odor attributes of the XH CRP sample, as determined by a PLSR model. The upper-left quadrant of Figure 8 highlights significant correlations ($p < 0.05$) between the aroma compounds and specific odor characteristics. Sour and hay-like odors were positively associated with compounds such as methoxypyrazine, D-(+)-carvone, decanoic acid, and santolina triene. Conversely, compounds in the upper-right quadrant, including α-terpineol, tetradecanal, and 2-dodecenal, exhibited negative correlations with these two odor attributes. In the lower-right quadrant, aroma compounds like germacrene, β-selinenol, α-farnesene, santolina triene, nerolidol, and furfural showed positive correlations with fresh, citrus, pleasant, fruity, and sweet odors. Meanwhile, compounds in the lower-left quadrant displayed negative correlations with these odor attributes.

https://doi.org/10.3390/foods15071117

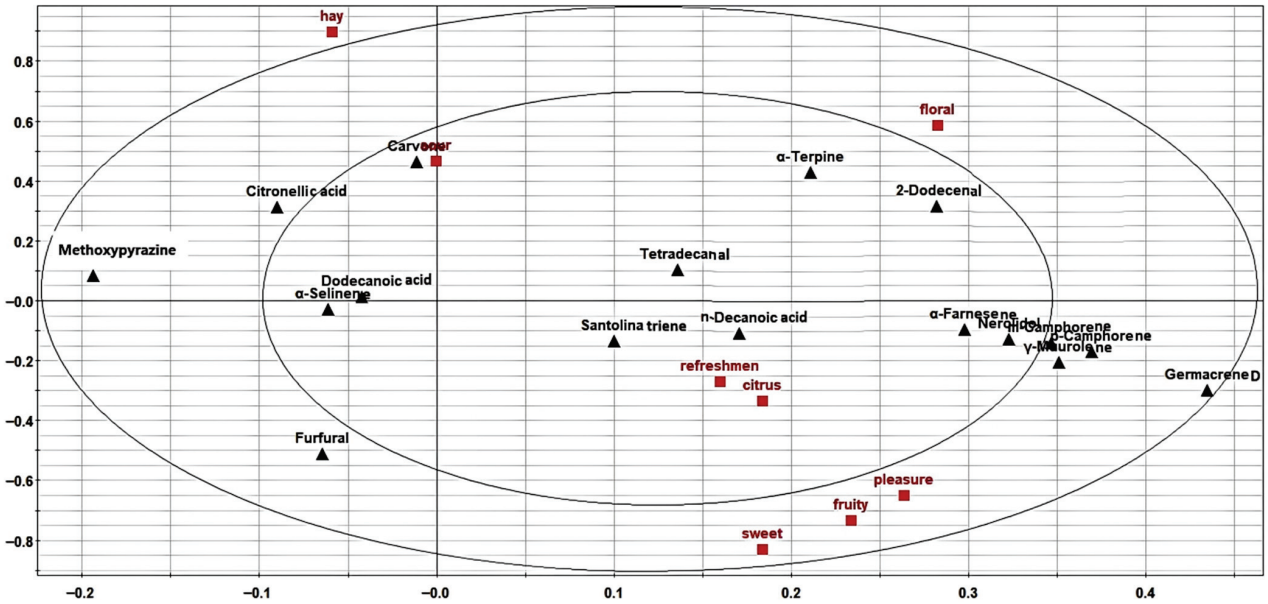


Figure 8. Correlation of aroma compounds and odor by PLSR.

4. Conclusions

This study comprehensively analyzed the aroma profiles, flavor variations, surface microstructure, and aroma–sensory relationships of CRP from different sources, processing methods, and vintages, using integrated techniques including SPME/GC–MS, sensory evaluation, electronic nose detection, and multivariate models (PCA and PLSR). Drying methods affected CRP volatile components: indoor-dried and stored XHCRP had a broader volatile spectrum and higher concentrations of key aroma compounds (e.g., α-terpineol and γ-muurolene), with distinctive aromas. Sensory evaluation and electronic nose confirmed XH's superior aroma quality; PCA distinguished XH from other samples, which clustered closely due to similar flavors. Additionally, CRP microstructure changed notably with aging, showing pericarp cell deterioration, structural collapse, and varied stomatal morphology, mainly driven by non-volatile decomposition and enzymatic browning. It should be noted that the observed differences in the samples were influenced by the combined effects of different drying methods and five-year natural aging. Therefore, the variations in flavor components and sensory characteristics cannot be attributed solely to drying processes but rather to the integrated effects of drying treatment and long-term storage.

This study innovatively integrates multiple analytical techniques to clarify the synergistic effects of sources, processing methods, and vintages on CRP quality, while establishing the relationship between aroma compounds and sensory attributes—filling the research gap of insufficient systematic characterization of CRP from multi-dimensional perspectives. Practically, it provides a solid scientific basis for the selection of raw materials in relevant application fields: guiding the development of safe, clean, and hygienic drying methods for CRP production, and offering theoretical support for the targeted production of CRP-derived products with characteristic aromas, including essential oils, incense, and functional perfumes. This research further promotes the standardized and high-quality production of CRP and expands its application value in related industries, bringing practical benefits to production practices and industrial upgrading.

Author Contributions: A.A.: Funding acquisition, writing—review and editing, writing—original draft, methodology, and data curation. C.H.: Writing—investigation, and data curation. X.Z. (Xin Zhao): Writing—original draft, and conceptualization. S.G.: Conceptualization and data curation. R.Z.: Writing—original draft, and data curation. J.Z.: Writing—review and editing, and data curation.

X.Z. (Xueqing Zhang): Writing—original draft. Y.J.: Data curation. W.H.: Writing—review and editing, writing—original draft, and data curation. All authors have read and agreed to the published version of the manuscript.

Funding: This work was supported by the "Mechanism research on potential antidepressant effects of aroma compounds from Guangdong tangerine peel" characteristic innovation project of ordinary universities in Guangdong province (2024KTSCX018) and "Tri-level Talents Development Project" of Zhuhai College of Science and Technology.

Institutional Review Board Statement: Ethical review and approval were waived for this study due to the following reasons: This study focuses on analyzing aroma components of 5-year aged dried Citri Reticulatae Pericarpium samples via GC–MS/GC–IMS, E-nose and sensory evaluation (panelists received pre-experiment training). It involves no human or animal subjects, nor any behaviors that may endanger the rights and interests of individuals, groups or society. In line with Ethics Committee of Zhuhai College of Science and Technology, general academic norms and relevant national laws, studies of this type (without involving human/animal subjects) are exempt from ethical review.

Informed Consent Statement: Informed consent was obtained from all subjects involved in the study.

Data Availability Statement: The original contributions of this study are presented in this article. Further inquiries can be directed to the corresponding author.

Conflicts of Interest: The authors declare no conflicts of interest.

References

1. Zhang, H.; Cui, J.; Tian, G.; DiMarco-Crook, C.; Gao, W.; Zhao, C.; Li, G.; Lian, Y.; Xiao, H.; Zheng, J. Efficiency of four different dietary preparation methods in extracting functional compounds from dried tangerine peel. *Food Chem.* **2019**, *289*, 340–350. [CrossRef]
2. Fu, M.; Wang, Y.; Yu, Y.; Wen, J.; Cheong, M.S.; Cheang, W.S.; Wu, J. Changes of volatile substance composition during processing of nine-processed tangerine peel (Jiuzhi Chenpi) determined by gas chromatography-ion mobility spectrometry. *Front. Nutr.* **2022**, *9*, 963655. [CrossRef]
3. Li, X.; Yang, Y.; Zhu, Y.; Ben, A.; Qi, J. A novel strategy for discriminating different cultivation and screening odor and taste flavor compounds in Xinhui tangerine peel using E-nose, E-tongue, and chemometrics. *Food Chem.* **2022**, *384*, 132519. [CrossRef]
4. Yu, Z.; Wu, Y.; Ma, Y.; Cheng, Y.; Song, G.; Zhang, F. Systematic analysis of the mechanism of aged citrus peel (Chenpi) in oral squamous cell carcinoma treatment via network pharmacology, molecular docking and experimental validation. *J. Funct. Foods* **2022**, *91*, 105012. [CrossRef]
5. Zou, J.; Wang, J.; Ye, W.; Lu, J.; Li, C.; Zhang, D.; Liu, Z. Citri Reticulatae Pericarpium (Chenpi): A multi-efficacy pericarp in treating cardiovascular diseases. *Biomed. Pharmacother.* **2022**, *154*, 113626. [CrossRef]
6. Wang, J.; Hao, J.; Miao, D.; Xiao, P.; Jiang, X.; Hu, L. Compound chenpi tea consumption reduces obesity-related metabolic disorders by modulating gut microbiota and serum metabolites in mice. *J. Sci. Food Agric.* **2024**, *104*, 431–442. [CrossRef]
7. Talens, C.; Arboleya, J.; Castro-Giraldez, M.; Fito, P. Effect of microwave power coupled with hot air drying on process efficiency and physico-chemical properties of a new dietary fibre ingredient obtained from orange peel. *LWT* **2017**, *77*, 110–118. [CrossRef]
8. Sun, W.; Li, M.J.; Zhang, Y.; Ai, Z.P.; Lei, D.W.; Pei, Y.P.; Liu, Y.H. Effect of different drying techniques on drying characteristics, physical quality, and active components of *Citri reticulatae pericarpium*, and the correlation between physiochemical quality. *Ind. Crops Prod.* **2023**, *204*, 117350. [CrossRef]
9. Li, D.; Mujumdar, A.S.; Wen, Y. Hot air impingement drying kinetics and quality attributes of orange peel. *J. Food Process. Preserv.* **2020**, *44*, e14294. [CrossRef]
10. Zheng, H.; Su, Z.C.; Huang, S.T.; Li, D.L.; Yuan, Z.D.; Xu, J.C. 4-vinylguaiacol in citri reticulatae 'chachiensis' pericarpium volatile oil: A microbial-mediated aging marker enhances glucose metabolism. *Foods* **2025**, *14*, 3489. [CrossRef]
11. Sireyil, G.; Alim, A. Effects of onion paste on flavor of a different kind of bread (naan) analyzed with E-Nose and GC–IMS. *J. Food Process. Preserv.* **2022**, *46*, e16457. [CrossRef]
12. Alim, A.; Huang, C.F.; Zhao, X.; Sarengaowa; Zhang, R.R.; Zhang, J.R.; Zhang, X.Q.; Jin, Y.B.; Wu, G.R.; Hu, W.Z. GC–IMS/GC–MS/E-nose and molecular simulation analysis of the effects of aging duration on the aroma of Citri Reticulatae Pericarpium and its associated antidepressant effect. *J. Agric. Food Res.* **2025**, *2*, 102359. [CrossRef]
13. Alim, A.; Song, H.; Liu, Y.; Zou, T.; Zhang, Y.; Zhang, S.; Raza, A. Research of beef-meaty aroma compounds from yeast extract using carbon module labeling (CAMOLA) technique. *LWT* **2019**, *112*, 108239. [CrossRef]

14. González-Mas, M.C.; Rambla, J.L.; López-Gresa, M.P.; Blázquez, M.A.; Granell, A. Volatile Compounds in Citrus Essential Oils: A Comprehensive Review. *Front. Plant Sci.* **2019**, *10*, 12. [CrossRef] [PubMed]
15. Ullah, F.; Papini, A.; Shah, S.N.; Zaman, W.; Sohail, A.; Iqbal, M. Seed micromorphology and its taxonomic evidence in subfamily Alsinoideae (Caryophyllaceae). *Microsc. Res. Tech.* **2019**, *82*, 250–259. [CrossRef]
16. Dong, T.; Tian, Z.; Wang, S.; Jie, S.; Hai, C.; Shu, W.; Bao, S. Identification of key off-flavor compounds during storage of fried pepper (*Zanthoxylum bungeanum* Maxim.) oils by sensory-directed flavor analysis and partial least squares regression (PLSR). *J. Food Compos. Anal.* **2024**, *131*, 14. [CrossRef]
17. Wang, J.; Wang, H.; Xiao, W. Effects of drying temperature on the drying characteristics and volatile profiles of Citrus reticulata Blanco peels under two stages of maturity. *Dry. Technol.* **2022**, *40*, 15. [CrossRef]
18. Bozkir, H.; Yeliz, T.; Erten, S. Effects of tray drying, vacuum infrared drying, and vacuum microwave drying techniques on quality characteristics and aroma profile of orange peels. *J. Food Process Eng.* **2021**, *44*, e13611. [CrossRef]
19. Qin, K.; Zheng, L.; Cai, H.; Cao, G.; Lou, Y.; Lu, T.; Cai, B. Characterization of chemical composition of Pericarpium Citri reticulatae volatile oil by comprehensive two-dimensional gas chromatography with high-resolution time-of-flight mass spectrometry. *Evid.-Based Complement. Altern. Med.* **2013**, *237541*, 11. [CrossRef]
20. Zheng, G.; Chao, Y.; Liu, M.; Yang, Y.; Zhang, D.; Wang, K.; Tao, Y.; Zhang, J.; Li, Y.; Wei, M. Evaluation of dynamic changes in the bioactive components in Citri Reticulatae Pericarpium (*Citrus reticulata* 'Chachi') under different harvesting and drying conditions. *J. Sci. Food Agric.* **2021**, *101*, 3280–3289. [CrossRef] [PubMed]
21. Hu, Y.; Hu, D.L.; Yin, L.; Deng, Z.; Cheng, Y.Y.; Li, H.X.; Wang, F.; Liu, Y.P. Dynamic profiling of bioactive compounds, flavor metabolites, and quality-related microorganisms during the freshening-drying-aging process of Citri reticulatae pericarpium: Implications for quality formation mechanisms. *Food Chem. X* **2025**, *30*, 102906. [CrossRef] [PubMed]
22. Yang, D.; Wu, X.; Shi, H.; Zhang, J.; Wang, C. Essential aroma substances and release pattern of Xin hui Chenpi. *Beverage Plant Res.* **2022**, *2*, 177–184. [CrossRef]
23. Xu, G.; Zhao, J.Y.; Yao, J.Q.; Xu, Y.; Yuan, X.H.; Pan, S.Y. Effects of aging on the fine structure, chain conformation, and morphology of Chenpi polysaccharides. *Carbohydr. Polym.* **2025**, *349*, 122970. [CrossRef]
24. Yi, Z.B.; Yu, Y.; Liang, Y.Z.; Zeng, B. In vitro antioxidant and antimicrobial activities of the extract of Pericarpium Citri Reticulatae and its main flavonoids. *LWT* **2008**, *41*, 597–603. [CrossRef]

Disclaimer/Publisher's Note: The statements, opinions and data contained in all publications are solely those of the individual author(s) and contributor(s) and not of MDPI and/or the editor(s). MDPI and/or the editor(s) disclaim responsibility for any injury to people or property resulting from any ideas, methods, instructions or products referred to in the content.

foods

MDPI

Article

Integrated Molecular Informatics and Sensory-Omics Study of Core Trace Components and Microbial Communities in Sauce-Aroma High-Temperature Daqu from Chishui River Basin

Dandan Song [1], Lulu Song [1], Xian Zhong [1], Yashuai Wu [2], Yuchao Zhang [1] and Liang Yang [1,*]

[1] School of Brewing Engineering, Moutai Institute, Renhuai 564501, China; songdd0330@163.com (D.S.); songlulu@mtxy.edu.cn (L.S.); zhongxian2025@163.com (X.Z.); zyc10271027@163.com (Y.Z.)
[2] School of Food Science and Engineering, South China University of Technology, Guangzhou 510640, China; wyss995418706@163.com
* Correspondence: moutaiyl0725@163.com; Tel.: +86-18786819825

Abstract

Flavor-relevant trace volatiles and microbial communities were examined in six sauce-aroma high-temperature Daqu samples. Headspace solid-phase microextraction coupled with gas chromatography–mass spectrometry (HS-SPME-GC-MS) quantified 210 trace volatile compounds across 14 chemical classes. Orthogonal partial least squares discriminant analysis (OPLS-DA) with variable importance in projection (VIP) screening was integrated with sensory scoring, correlation analysis, and molecular docking to an olfactory receptor model. Volatile profiles showed clear stratification in total abundance. Pyrazines dominated the high-total group. Tetramethylpyrazine served as a major driver. Sensory evaluation indicated that aroma explained overall quality best. (E)-2-pentenal and dimethyl trisulfide showed significant positive associations with aroma and overall scores. In the olfactory receptor, the polar residue module that provides directional constraints for Daqu odor activation was formed by Ser75, Ser92, Ser152, Ser258, Thr74, Thr76, Thr98, Thr200, Gln99, and Glu94. The hydrogen-bond or charge network was further reinforced by Arg150, Arg262, Asn194, His180, His261, Asp182, and Gln181. The core discriminant set comprised acetic acid, hexanoic acid, (E)-2-pentenal, nonanal, decanal, dimethyl trisulfide, trans-3-methyl-2-n-propylthiophane, 2-hexanone oxime, ethyl linoleate, propylene glycol, 2-ethenyl-6-methylpyrazine, 4-methylquinazoline, 5-methyl-2-phenyl-2-hexenal, and 1,2,3,4-tetramethoxybenzene. Sequencing revealed higher bacterial diversity than fungal. *Bacillus* and *Kroppenstedtia* were dominant bacterial genera. *Aspergillus*, *Paecilomyces*, *Monascus*, and *Penicillium* were major fungal genera. Correlation patterns suggested that *Bacillus* and *Monascus* were positively linked to acetic acid and 1,2,3,4-tetramethoxybenzene. Together, these results connected chemical fingerprints, sensory performance, receptor-level plausibility, and microbial ecology. Concrete targets are provided for quality control of high-temperature Daqu.

Keywords: sauce-aroma high-temperature Daqu; core trace components; core microorganisms; Baijiu; molecular informatics and sensory omics

1. Introduction

Baijiu is a traditional distilled spirit that is produced from cereal grains through solid-state fermentation and distillation. It is widely regarded as the national liquor of China. It is also described as one of the six major distilled spirits worldwide. Among the aroma

types of Baijiu, sauce-aroma Baijiu is considered a highly representative type [1–4]. Its style is characterized by a prominent sauce-like aroma, elegant finesse, a full-bodied mouthfeel, a long finish, and a persistent aroma in the empty glass. Consumer demand remains strong. In recent years, the sauce-aroma sector has expanded rapidly and become one of the most prominent sectors in the industry. In 2024, national sauce-aroma Baijiu production capacity was approximately 650,000 kL. Sales revenue was approximately 240 billion CNY, and profit was approximately 97 billion CNY. In 2024, the total output of the Baijiu industry above designated size was 4,145,000 kL, with sales revenue of 796.38 billion CNY and total profit of 250.87 billion CNY. Based on these figures, sauce-aroma Baijiu contributed about 15.7% of capacity, about 30.1% of industry revenue, and about 38.7% of industry profit (https://assets.kpmg.com/content/dam/kpmg/cn/pdf/zh/2025/06/mid-term-research-report-on-the-chinese-baijiu-market-2025.pdf, accessed on 27 January 2026). The Chishui River Basin has attracted multiple leading sauce-aroma Baijiu producers [5–7]. Four sauce-aroma enterprises have annual revenues above 10 billion CNY. The distinctive quality of sauce-aroma Baijiu and rising market demand keep the sector at the center of attention in the Baijiu industry.

Sauce-aroma Baijiu brewing is exemplified by the production area in the Chishui River Basin of Guizhou Province, with Moutai Town as the core [8,9]. This region is often described as a prime zone for sauce-aroma Baijiu production [5]. The traditional process is distinctive and highly complex [10]. It requires a 1-year cycle with two feedings, nine steamings, eight fermentation rounds, and seven liquor collections. The process is known in the industry as "12987" [11–13]. Within this long process, sauce-aroma high-temperature Daqu is regarded as the core of the brewing [14]. Sauce-aroma high-temperature Daqu is produced from grains such as wheat [5]. It relies on natural inoculation under open conditions and is formed under a high-temperature environment [13]. The maximum temperature during Daqu production can exceed 60 °C. Sauce-aroma high-temperature Daqu serves as the main carrier of microorganisms required for fermentation. It also serves as a saccharifying and fermenting agent [14,15]. It is an important source of flavor precursors. Many studies have indicated that sauce-aroma high-temperature Daqu plays a key role in the formation of the characteristic flavor of sauce-aroma Baijiu [8]. Microbial consortia enriched in Daqu provide functional strains and enzyme systems for sauce-aroma fermentation. Daqu quality is directly linked to the yield and quality of the final Baijiu. Dominant microorganisms in Daqu are often the core functional microorganisms for aroma formation and enzyme production [16–22]. They directly influence the formation of the final flavor profile.

The Chishui River Basin, with Moutai Town as the core, is distinguished by a river-valley basin setting and a long-established brewing landscape that together create a relatively closed and stable local microclimate, typically characterized by warm and humid conditions with comparatively low wind speed, which favors the persistence, dispersal, and long-term domestication of fermentation-related microorganisms in and around production spaces [23,24]. In addition to climatic stability, regional hydrogeochemical features further strengthen this uniqueness, as the basin has been reported as the core area for sauce-aroma Baijiu, and its water chemistry (for example, near-neutral pH and abundant trace elements) is considered supportive of microbial growth and metabolic activity, thereby providing a consistent ecological backdrop for open fermentation [23,25]. Under such conditions, the open and highly interactive production ecology of sauce-aroma Baijiu becomes especially consequential: high-temperature Daqu making and subsequent solid-state fermentation are extensively exposed to ambient air and surrounding environments, allowing environmental microorganisms to repeatedly enter and be selected across cycles, and accumulating a place-linked microbial reservoir that is difficult to reproduce in non-local settings [26]. Re-

https://doi.org/10.3390/foods15030599

cent evidence from source-tracking and environmental microbiome investigations supports that microbes from surrounding matrices can contribute to Daqu community assembly and that airborne microbiomes in the Chishui River Basin core production areas show structured [27–32] community patterns shaped by environmental factors, reinforcing the concept that regional environmental ecology is a key driver of microbial community stability and, ultimately, characteristic flavor expression [8]. Collectively, the coupling of the basin-specific geography and microclimate, water- and soil-related geochemical context [6], and centuries of open, multi-round brewing practices forms a distinctive microbial "terroir" in Moutai Town, which is widely regarded as a fundamental basis for sauce-aroma Baijiu flavor formation and a major reason why authentic sensory typicity is challenging to replicate outside the core Chishui River Basin region [33–40].

Under the coordinated action of diverse microorganisms in solid-state fermentation, Chinese Baijiu develops a highly complex chemical matrix, yet only a subset of compounds ultimately drives sensory identity. In Baijiu manufacture, Daqu is not a passive additive but a core starter that supplies functional microbiota, enzyme systems, and flavor precursors, enabling the characteristic "simultaneous saccharification and fermentation" strategy and supporting the initiation and stability of fermented-grain (Jiupei) fermentation [13]. For sauce-aroma Baijiu in particular, the workflow includes mixing fermented grains with Daqu and water, performing high-temperature stacking on the workshop floor for several days, and then transferring the stacked grains to a mud-sealed cellar for extended anaerobic fermentation before distillation, followed by grading and storage [25]. Because Daqu governs the early establishment of microbial consortia and enzyme activities that drive starch degradation [41], amino acid release, and precursor formation, variations in Daqu quality can propagate through fermentation and translate into differences in product quality and manufacturing robustness, which is why the use of high-quality Daqu is essential for producing commercially acceptable Baijiu [16–18,20,21,33,42].

High-temperature Daqu should also be distinguished clearly from other starter types. Daqu is commonly categorized by its maximum fermentation temperature into high-temperature Daqu (typically associated with sauce-aroma or Maotai-flavor Baijiu), medium-temperature Daqu (commonly used for strong-aroma Baijiu), and low-temperature Daqu (commonly used for light-aroma Baijiu), reflecting different incubation regimes that select different microbial communities and functional profiles [13,27]. Sauce-aroma high-temperature Daqu is characteristically produced from wheat and incubated at higher temperatures, often reaching 60–65 °C under open conditions, which enriches thermotolerant microorganisms and promotes the formation of enzymes and metabolites that support the subsequent high-temperature stacking and cellar fermentation stages typical of sauce-aroma Baijiu production [25]. Given the long production cycle and the strong dependence of sauce-aroma-style expression on microbial metabolism, a systematic framework that links Daqu microbiota with characteristic trace aroma compounds is needed. Therefore, this study focuses on identifying key functional microorganisms and core flavor-related trace components in sauce-aroma high-temperature Daqu and integrating chemical, microbiological, and sensory evidence to improve interpretability and practical relevance [13,27].

Based on this context, an integrated molecular informatics and sensory-omics strategy was applied to sauce-aroma high-temperature Daqu from the Chishui River Basin. The objective was to systematically identify key odor-active substances and core functional microorganisms. The material basis and microbial mechanisms underlying the characteristic aroma were also examined. Molecular-level flavor analysis was coupled with human sensory evaluation. The internal links among the regional environment, process parameters, and flavor characteristics were thereby clarified more comprehensively. Molecular informatics enabled the acquisition of large-scale volatile data. Sensory-omics evaluation supported

https://doi.org/10.3390/foods15030599

assessment of contributions to overall aroma. This strategy was expected to pinpoint the most representative odorants in Daqu and to locate the core functional microorganisms that drove their formation. The outcomes were expected to support the optimization and standardization of traditional sauce-aroma processes. Brewing practice was expected to shift from experience-based operation toward more precise and rational guidance.

2. Materials and Methods

2.1. Samples and Reagents

Samples were collected in Moutai Town, Renhuai, Zunyi, Guizhou Province, located in the core production area of sauce-aroma Baijiu in the Chishui River Basin. Six distilleries were randomly selected along the river continuum (from upstream to downstream) and were coded as Daqu_A, Daqu_B, Daqu_C, Daqu_D, Daqu_E, and Daqu_F. Within each distillery, 3 Daqu rooms were randomly selected, and within each Daqu room, 3 Daqu bricks were randomly selected (6 distilleries × 3 rooms × 3 bricks, n = 54 bricks in total). Bricks from the same distillery were crushed and homogenized, and 3 representative composite samples were obtained per distillery, resulting in 18 representative samples overall (n = 18). To facilitate parallel multi-omics measurements and clearly distinguish experimental variants and analytical branches, a study flowchart summarizing sampling, pooling, and downstream processing was added (Figure 1).

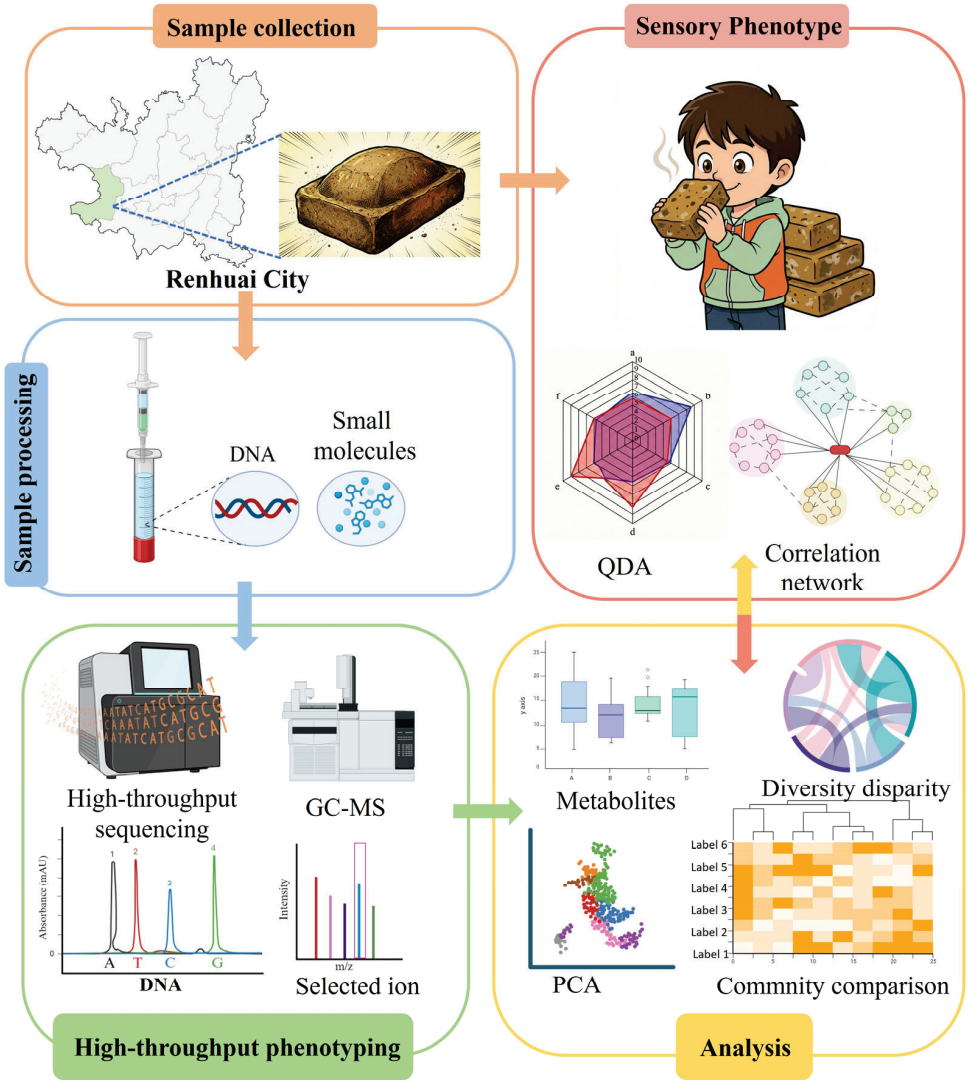


Figure 1. Workflow of this study. QDA: quantitative descriptive analysis.

High-temperature sauce-aroma Daqu was produced under routine commercial solid-state fermentation conditions using 100% wheat as the sole substrate. During the stacking stage, the internal fermentation temperature increased to a peak of 60–65 °C, which was consistent with the typical peak-temperature window reported for high-temperature Daqu manufacture. Throughout stacking, the relative humidity was maintained at 10–40% (i.e., under low-humidity/low-moisture conditions), aligning with the general low-moisture nature of Daqu solid-state fermentation, where moisture content is reported to decline substantially during production. The solid-state fermentation lasted for exactly 40 days, matching the commonly described ~40-day high-temperature fermentation period for Jiang-/sauce-flavor Daqu prior to subsequent storage/maturation. Finally, all samples were collected at the mature harvest stage (post-maturation) to ensure that the profiled microbial communities and volatile signatures represent the final, stabilized starter state actually used for Baijiu brewing after fermentation and storage.

Each representative sample was divided into 2 portions: one portion was stored at 4 °C for metabolome evaluation, and the other portion was stored at −80 °C for microbial community analysis. All authentic standards had a minimum purity of 97% and were purchased from J & K (Beijing, China) and Sigma-Aldrich (Shanghai, China). 4-octanol, 2-ethylbutyric acid, and amyl acetate were used as internal standards, and ultrapure water was obtained from a Milli-Q system.

2.2. Experimental Procedures

2.2.1. Pretreatment of Sauce-Aroma High-Temperature Daqu

Volatile compounds were enriched and extracted by HS-SPME. A 2 g Daqu sample was weighed into a 20 mL headspace vial containing 6 mL saturated NaCl solution. High-temperature Daqu samples were collected as mature (post-maturation) Daqu bricks from routine commercial production, then crushed and homogenized to obtain representative composite materials. The samples were handled "as received" on a wet-weight basis (i.e., no additional oven drying or dehydration treatment was applied after collection), consistent with how mature Daqu is used directly as a starter in Baijiu brewing. A 10 μL mixed standard solution was added. The final concentration was 20 μg/mL. The vial was capped and sealed. Equilibration was performed at 40 °C for 20 min. A 50/30 μm DVB/CAR/PDMS fiber was used. The fiber was exposed to the vial headspace. Extraction was performed with stirring at a temperature below 40 °C for 40 min. Desorption was performed immediately in the GC inlet at 250 °C for 5 min.

2.2.2. HS-SPME and GC-MS Conditions for Sauce-Aroma High-Temperature Daqu

Volatile compounds were analyzed by a GC-MS system (7890B GC System, 5977A MSD). A DB-FFAP capillary column was used (60 m × 250 μm × 0.25 μm, Agilent Technologies, Santa Clara, CA, USA). Helium was used as the carrier gas with a purity of 99.999%. The flow rate was kept constant at 2.0 mL/min. The inlet temperature was set to 250 °C. The oven program was as follows. The initial temperature was held at 40 °C for 3 min. The temperature was increased to 150 °C at 2 °C/min and held for 2 min. The temperature was increased to 230 °C at 7 °C/min and held for 8 min. The transfer line temperature was set to 250 °C. The ion source temperature was set to 230 °C. EI was operated at 70 eV. The scan range was m/z 35–450 amu. Injection was performed in splitless mode. Qualitative identification was performed by matching mass spectra to the NIST (version, 2020) library. Quantification was performed by the internal standard method.

2.2.3. Molecular Docking

Molecular docking was performed in Maestro 14.5. The receptor was the cryo-EM structure of the human olfactory receptor OR51E2 deposited in the RCSB PDB as 8F76.

https://doi.org/10.3390/foods15030599

The structure was an active conformation with a propionate-bound fatty acid odorant. It was also in complex with miniGs. Receptor preparation was performed with the Protein Preparation Wizard workflow. Hydrogen atoms were added. Bond orders and formal charges were assigned. Missing side chains were completed. The hydrogen-bond network was optimized. Restrained minimization was performed under the OPLS4 force field to reduce local strain while maintaining the global conformation of the transmembrane helices. Crystallization additives and free water molecules unrelated to the binding cavity were removed. Structural water molecules that were located deep in the pocket and contributed to bridging polar interactions were retained when cavity geometry was not affected [43–47].

Ligand conformations and protonation states were generated by LigPrep with Epik. Three-dimensional structures were standardized. Major ionization states and tautomers within the specified pH window were enumerated. Relevant stereoisomers were retained to cover possible orientations and conformational heterogeneity. The receptor grid was defined by using the co-crystallized ligand position in 8F76 as a geometric reference. The center and boundary of the orthosteric pocket were defined within the transmembrane bundle. The grid box covered the main cavity and the adjacent narrow channel. Hydrophobic coordination and polar anchoring were both sampled. Docking was performed with the standard Glide small-molecule protocol [46,48]. The ligand vdW scaling factor was set to 0.80. A partial charge cutoff of 0.15 was applied to improve tolerance for flexible ligands and to increase pose diversity. Sampling was performed in SP mode with post-docking minimization and pose rescoring. Top-ranked poses were rechecked in XP mode when needed. Docking score and Emodel were considered during evaluation. GlideScore approximated binding free-energy trends. Emodel supported the selection of reasonable poses among multiple poses of the same ligand. The reported ecoul and evdw terms were used to separate electrostatic and van der Waals contributions. The final poses were analyzed in Maestro. Hydrogen bonds, salt bridges, π-related interactions, and hydrophobic contacts were recorded. These results supported residue-level mechanistic interpretation in subsequent analyses [47,49].

2.2.4. Sensory Evaluation of Sauce-Aroma High-Temperature Daqu

The sensory attributes of mature sauce-aroma high-temperature Daqu were considered an intuitive signal of whether Daqu making met the process requirements. They were also regarded as an early indicator of subsequent style stability in sauce-aroma Baijiu. Because aroma and appearance were easily affected by ambient odors, noise, and lighting, sensory evaluation was conducted under controlled conditions. The facility followed general principles for a sensory analysis laboratory. It included separate functional areas, such as a testing area and a sample preparation area. This layout reduced the impact of sample preparation on air quality and background odors in the testing area. Environmental controllability and consistency were emphasized during evaluation. Temperature and humidity in the testing area were set to ensure assessor comfort and to meet sample handling needs. Noise was controlled at 40 dB or lower. Lighting was adjustable and was typically set at 6500 K. Illuminance was maintained within 200 lx to 400 lx. External odors were controlled by ventilation and filtration. Residual odors were minimized to reduce carryover between samples.

A trained sensory panel was formed. The panel consisted of 10 assessors, including 5 males and 5 females, aged 20–29 years. Routine training focused on descriptor recognition, scale use, and sensory memory retention. These measures ensured comparability in discrimination for samples evaluated within the same batch. Samples were presented with random codes and a balanced serving order. Within the same session, assessors completed visual inspection, aroma evaluation, and cross-section observation. During evaluation,

surface color and mold growth distribution were examined first. Representative bricks were then fractured to assess cross-section color uniformity, pore structure, and mycelial appearance. Aroma was assessed with brief and repeated sniffs to capture dominant notes and potential off-odors. A weighted scoring method was applied. Surface color, aroma, and cross-section were used as core dimensions. A higher weight was assigned to aroma to align with practical needs in quality assessment of sauce-aroma high-temperature Daqu (Table 1).

Table 1. Sensory dimension scoring criteria for sauce-aroma high-temperature Daqu.

Sensory Dimension	Score	Evaluation Focus	Scoring Criteria
Surface color	20 points	Overall surface color and uniformity, degree of yellow-brown or dark-brown, proportion of gray-white, abnormal mold bloom and cracks	Premium grade: Surface was mainly yellow-brown or dark-brown, 17–20 points. Good grade: Surface was largely yellow-brown or dark-brown with only a small amount of gray-white, 14–16 points. Standard grade: Surface appeared gray-white or showed a high proportion of gray-white, 12–13 points. Further deductions were applied when obvious abnormal mold spots or abnormal dampness were present.
Aroma	60 points	Clarity and harmony of sauce aroma, Daqu aroma, douchi aroma, or toasted aroma; intensity of composite aroma; off-odor and moldy spoilage cues	Premium grade: Sauce aroma, Daqu aroma, and douchi aroma were prominent, and composite aroma was evident, 54–60 points. Good grade: Sauce aroma, Daqu aroma, and toasted aroma were relatively clear, and composite aroma was distinct, 42–53 points. Standard grade: Daqu aroma and sauce aroma were present, But composite aroma was weak, and minor off-odors could occur, 36–41 points. Samples with obvious off-odors were downgraded further.
Cross-section	20 points	Consistency of cross-section color, gray-white or gray-yellow appearance, uniformity of pores and structure, extent of mycelial appearance, dryness of the core	Premium grade: Cross-section color was consistent, mycelia were obvious, and the core was relatively dry, 17–20 points. Good grade: Cross-section was relatively consistent, mycelia were fairly obvious, and the core contained a small amount of moisture, 14–16 points. Standard grade: Cross-section consistency was moderate, and contaminating microbes could be observed or the core moisture was high, 12–13 points. Further deductions were applied when contamination and a wet core were evident.
Overall grade	100	Overall sensory quality score	Premium grade: Total score was greater than 90 points. Good grade: Total score was 70–90 points. Standard grade: Total score was 60–70 points. Samples below 60 points were considered unqualified.

2.3. Metagenomic Sequencing

Total DNA in Daqu was extracted using the QIAGEN DNeasy mericon Food Kit (QIAGEN, Hilden, Germany) according to the manufacturer's instructions. DNA quality was evaluated by 1% agarose gel electrophoresis. DNA concentration was measured with a NanoDrop™ One spectrophotometer (Thermo Fisher Scientific, Waltham, MA, USA). This ensured suitability for subsequent sequencing. The extracted DNA was used to construct metagenomic sequencing libraries. All libraries were sequenced on an Illumina NovaSeq X Plus platform (Illumina Inc., San Diego, CA, USA). Sequencing was completed by Shanghai Majorbio Bio-pharm Technology Co., Ltd. (Shanghai, China). A 150 bp paired-

end mode was applied to provide sufficient coverage for downstream microbial community structure analysis.

Quality-filtered reads were assembled using MEGAHIT (v1.1.2). Short reads were merged into longer contigs by a fast assembly algorithm. Contigs were filtered by length. Contigs with a length of at least 300 bp were retained as the final assembly. Open reading frames (ORFs) were predicted on the assembled contigs using Prodigal (v2.6.3). Prodigal identified gene regions across different taxa. Putative protein-coding sequences were extracted. Only ORFs with a length of at least 100 bp were retained to improve prediction reliability.

A non-redundant gene catalog was constructed using CD-HIT (v4.7) to reduce sequence redundancy and improve analytical efficiency. Gene sequences were clustered at 90% sequence identity and 90% coverage. Each cluster contained a representative sequence. This provided a streamlined and reliable gene catalog for subsequent analyses.

2.4. Statistical Analysis

Statistical computing was performed mainly in R (v4.5.x, R Foundation). Mixed-effects models were fitted using lme4. Estimated marginal means and post hoc contrasts were obtained using emmeans. Reproducible hypothesis testing and regression analyses were cross-checked in Python (v3.15.0). One-way ANOVA and correlation analyses were performed using IBM SPSS Statistics 24. Adjusted *p*-values were reported. Data visualization and curve fitting were performed in GraphPad Prism 9 and OriginPro 2021. Heatmaps and clustering plots were generated using TBtools(v2.119).

3. Results and Discussion

3.1. Volatile Components in Daqu Determined by HS-SPME-GC-MS

As shown in Table S1, HS-SPME-GC-MS was used to qualitatively and quantitatively determine 210 volatile trace components in six Daqu groups (A–F; n = 3 per group). Fourteen chemical classes were covered. Aldehydes and ketones, esters, alcohols, aromatic compounds, and pyrazine were among the most abundant classes in high-temperature sauce-aroma Daqu by number of compounds.

At the total level, the summed concentration of volatile components in the six Daqu groups showed clear stratification. All concentrations were reported in μg/g. The mean value of group A was 303.69 ± 12.51. Group B was 199.41 ± 44.73. Group C was 123.76 ± 6.63. Group D was 479.11 ± 37.76. Group E was 498.30 ± 43.97. Group F was 467.03 ± 43.77. One-way ANOVA indicated a significant difference in total volatile concentration among groups ($p < 0.05$). Multiple comparisons showed no significant differences among D–F ($p > 0.05$). These three groups were significantly higher than A, B, and C ($p < 0.05$). Group A was significantly higher than B and C ($p < 0.05$). No significant difference was observed between B and C ($p > 0.05$). This result indicated a high-total group (D, E, and F), an intermediate group (A), and a low-total group (B and C) for the overall accumulation of volatile products in the sauce-aroma high-temperature Daqu.

After total abundance was decomposed by class, differences in dominant classes became more concentrated. Groups D, E, and F were dominated by pyrazines. The proportions of pyrazines in total volatiles reached 65.69%, 57.54%, and 54.03%, respectively. Group A also showed a high proportion of pyrazines at 46.44%, but the overall intensity was lower than that of D, E, and F. In contrast, the main contributions in group C were from other compounds and alcohols. Their proportions were 28.43% and 27.44%, respectively. Pyrazines accounted for only 10.54%. Statistical testing at the class level showed significant differences among samples for pyrazines, alcohols, fatty acids, aldehydes and ketones, and esters ($p < 0.05$). Only the total phenols did not differ significantly ($p = 0.136$).

https://doi.org/10.3390/foods15030599

In the stacked solid-state fermentation system of sauce-aroma high-temperature Daqu, volatile phenols often showed a non-significant pattern. This pattern did not imply a weak flavor role. It reflected buffered net accumulation driven by formation and consumption mechanisms. Key precursors of phenols were often cell wall-bound phenolic acids such as ferulic acid. These precursors required release by microbial esterase systems. Volatile phenols such as 2-methoxy-4-vinylphenol could then be formed via phenolic acid decarboxylases. This route had enzymatic support in bacteria and yeasts. Bacillus was also reported to decarboxylate ferulic acid to 4-vinylguaiacol. However, the high-temperature and oxygen-rich solid-state environment of Daqu also enhanced the subsequent conversion and fate of volatile phenols. Oxidative enzymes could catalyze one-electron oxidation and coupling polymerization. This shifted monomeric phenols toward higher polymers. As a result, free phenolic monomers captured by headspace sampling did not accumulate readily. In addition, 4-vinylguaiacol and its precursors could exert inhibitory effects on microorganisms. Prior studies also suggested that conversion yield and final concentration could be constrained by toxicity and metabolic stress. This further reduced the magnitude of between-sample differences. Even when microecology and metabolic intensity differed among Daqu samples, phenol formation was constrained by precursor supply. Phenol depletion was also reinforced by oxidative polymerization and metabolic conversion. Group differences, therefore, remained difficult to distinguish [50–57]. A p-value above 0.05 was consistent with the dynamic behavior of phenols in sauce-aroma high-temperature Daqu.

At the individual-compound level, differences in pyrazines were mainly driven by tetramethylpyrazine. The mean levels of tetramethylpyrazine in A, B, C, D, E, and F were 112.13, 12.48, 4.77, 258.24, 220.80, and 195.80, respectively. This compound accounted for a high proportion in both total volatiles and within pyrazines. Its proportions within pyrazines reached 79.51% in A, 82.05% in D, 77.01% in E, and 77.59% in F. Its proportions in total volatiles were 36.92%, 53.90%, 44.31%, and 41.92%, respectively. The difference among Daqu groups was significant ($p < 0.05$). The trend was consistent with the class-level difference for pyrazines. In addition, 2,3,5-trimethylpyrazine remained at high levels in D, E, and F at 31.98, 36.82, and 36.09. These values were significantly higher than B and C at 5.32 and 4.06. The difference was also significant ($p < 0.05$). These compounds jointly formed a pyrazine framework for the high-total group.

For alcohols, the ranking across the six groups differed from that of pyrazines. The total alcohols were highest in F at 69.09. This level was significantly higher than most comparisons with A, B, C, D, and E ($p < 0.05$). A representative compound was phenethyl alcohol. Its mean value in F reached 51.07. This level was significantly higher than A, B, C, and D ($p < 0.05$). Group D was also significantly lower than E ($p < 0.05$). Phenethyl alcohol was often associated with floral or honey-like notes in prior studies on alcoholic beverages and Daqu making. It therefore provided strong interpretive value for flavor differences among Daqu samples.

Fatty acids highlighted the distinctive feature of group A. The total fatty acids in A were 30.37. This value was significantly higher than B, C, D, and F. It was also significantly higher than E ($p < 0.05$). Hexanoic acid reached 18.43 in A and 13.20 in E. It was not detected in B, C, D, and F. This led to a very significant difference for this compound ($p < 0.01$). The branched-chain acid 3-methylbutanoic acid was detected in all groups. Its level differed significantly among groups ($p < 0.05$). Groups A, D, and E were relatively higher, and F was lower. Because fatty acids and their esterification products often shape body and aftertaste, these acid-end differences provided a quantitative anchor for differences in flavor profiles.

The overall contribution of esters also showed a statistical difference ($p < 0.05$). Total esters were higher in A and F at 14.88 and 14.45. They were lower in C and D at 6.65 and 6.41. Ethyl hexadecanoate was among the major quantified ester peaks. It was close to 6.2

https://doi.org/10.3390/foods15030599

in A and F. It was about 2.07 in C. It was about 4.17 in D. The compound itself did not show a significant difference ($p = 0.225$). This suggested that ester differences were more likely driven by the combined effects of multiple medium- and low-abundance esters rather than by a single ester component.

Phenols were mainly contributed by 2-methoxy-4-vinylphenol. Its mean value was about 33.5 in B and E. It was about 27.75 in D. It was about 7.2 in A and F. It was only 0.18 in C. The difference did not reach significance ($p = 0.133$). This was consistent with the p-value for total phenols. The result was mainly influenced by increased within-group variation in B. Prior work indicated that volatile phenols often had high odor potency. They were also important in Daqu volatile profiles. Compounds such as 2-methoxy-4-vinylphenol were commonly discussed as key phenols. Stronger statistical discrimination for phenols would therefore require reduced within-group variance or increased replicate numbers. This would reduce cases in which a clear trend was observed but significance was not reached.

Sulfides showed a highly concentrated distribution. The mean sulfides in D reached 3.85. Groups A, C, and E were only 0.01 to 0.04. Sulfides were not detected in B and F. The class-level difference was highly significant ($p < 0.05$). This difference was almost entirely contributed by benzyl methyl sulfide. Its value was 3.85 in D. It was not detected in the other samples. Given the threshold sensitivity of sulfur volatiles, the enrichment in D should be regarded as a strong distinguishing signal. In the next step, specific trace components in each group are further analyzed to assess their importance.

3.2. Importance Analysis of Trace Components in Sauce-Aroma High-Temperature Daqu

As shown in File S1a, the model achieved an R2X of 0.934, an R2Y of 0.995, and a Q2 of 0.981. Values of R2 and Q2 above 0.5 indicated acceptable model performance. After 200 permutation tests, File S1 showed that the intercept of the Q2 regression line with the y-axis was below 0. This result indicated the absence of overfitting. Model validation was considered effective. The model was therefore considered suitable for analyzing key odor-active substances in sauce-aroma high-temperature Daqu. Trace components with VIP > 1 in the sauce-aroma high-temperature Daqu are shown in Table 2.

Table 2. VIP values of trace components in different sauce-aroma high-temperature Daqu samples (>1.000).

Number	Compound Name	VIP
1	2-Pentanol	1.263
2	Butyl acrylate	1.260
3	(Z)-Oxacyclopentadec-6-en-2-one	1.241
4	γ-Linolenic acid	1.232
5	5-Butyl-4-methyl-2(3H)-furanone	1.226
6	Hexanoic acid	1.210
7	trans-3-Methyl-2-n-propylthiophane	1.190
8	Ethyl octanoate	1.184
9	Benzoic acid	1.178
10	1-Pentanol	1.176
11	4-Octanone	1.176
12	2-Pentylfuran	1.174
13	Ethyl 2-methylbutanoate	1.174
14	1,2,3,4,5-Pentamethoxybenzene	1.173
15	3-Octanol	1.173
16	1,4-Dimethoxybenzene	1.172
17	Ethyl 4-methylpentanoate	1.171
18	2-Hexanone oxime	1.161
19	(E)-2-Pentenal	1.149

Table 2. *Cont.*

Number	Compound Name	VIP
20	(E)-2-Nonenal	1.143
21	Dimethyl trisulfide	1.142
22	Cyclohept-4-en-1-ol	1.136
23	Methyl 3,4-dimethylbenzoate	1.133
24	2-Methylpropanal	1.109
25	β-Methylcinnamaldehyde	1.109
26	2-Ethenyl-6-methylpyrazine	1.105
27	2-Propanamine	1.105
28	Allyl acetate	1.104
29	Acetic acid	1.098
30	Propylene glycol	1.097
31	Octanal	1.095
32	4,5-Dihydro-5,5,7-trimethyl-6H-[1,2,5] oxadiazolo[3,4-b] [1,4] diazepine	1.092
33	2-Hydroxy-3-pentanone	1.091
34	Benzyl methyl sulfide	1.089
35	1,2,3-Trimethoxybenzene	1.088
36	1,3-Hexadienylbenzene	1.087
37	Octyloxirane	1.085
38	2-Phenyl-1H-imidazole	1.085
39	2-Phenylethyl nicotinate	1.084
40	Ethyl 2-methylpropanoate	1.084
41	2-Dodecanone	1.083
42	2,3,5-Trimethyl-6-propylpyrazine	1.082
43	2-Nonanone	1.082
44	2-Methyl-1-propanol	1.080
45	Methyl linoleate	1.080
46	7-Oxooctanoic acid	1.075
47	Propionic acid	1.075
48	Ethyl 4-hydroxybenzoate	1.072
49	Methyl 6-nonynoate	1.069
50	N, N-Dimethylmethylamine	1.069
51	4-Methylhexanoic acid	1.067
52	Angelic acid	1.064
53	Cyclotridecanone	1.061
54	Methyl anthranilate	1.060
55	Hexanal	1.058
56	Menthol	1.057
57	Decyloctyl ether	1.056
58	Ethyl pentadecanoate	1.055
59	Acetaldehyde	1.051
60	Octanoic acid	1.051
61	2-Methylpropanoic acid	1.046
62	(Z)-Undec-6-en-2-one	1.040
63	Ethyl valerate	1.039
64	Ethyl oleate	1.039
65	Ethyl linoleate	1.038
66	Ethyl butyrate	1.035
67	(E)-2-Methyl-2-pentenoic acid	1.035
68	2-Phenylethyl 2-methylpropanoate	1.031
69	1-Pentadecene	1.030
70	Nonanal	1.028
71	3-Methylbutanoic acid	1.025
72	Nonanoic acid	1.024
73	3-Methyl-1-butanol	1.024
74	3,7-Dimethyl-1,6-octadien-3-yl formate	1.024

Table 2. *Cont.*

Number	Compound Name	VIP
75	2-Octanone	1.024
76	4-Methylquinazoline	1.022
77	3-Methyl-2,5-piperazinedione	1.021
78	(Z)-Benzaldehyde oxime	1.016
79	Decanal	1.015
80	Ethyl acetate	1.014
81	2-Methylhexanoic acid	1.013
82	Acetone	1.012
83	N-(2-Methylpropyl) acetamide	1.012
84	3-Methyltridecane	1.012
85	2-Acetyl-3,4,6-trimethylpyrazine	1.010
86	2-(Phenylpiperidin-1-ylmethyl) cyclohexanol	1.007
87	5-Methyl-2-phenyl-2-hexenal	1.007
88	1,2,3,4-Tetramethoxybenzene	1.003
89	Methylpyrazine	1.003
90	2,3-Butanedione	1.000

The Daqu-making temperature of sauce-aroma high-temperature Daqu could reach 60–65 °C. A multi-stage temperature rise and fall occurred under open stacking conditions. Microbial succession, enzyme release, and thermal reactions occurred in parallel. Systematic differences in volatile profiles among samples were therefore expected. Among trace components with VIP > 1, the highest contributors were not confined to a single class. They were jointly represented by nitrogen-containing heterocycles, fatty acids and related esters, lipid oxidation-related aldehydes and ketones, sulfur-containing compounds, and limited phenols and aromatic ethers. This pattern suggested that group discrimination mainly reflected differences in Maillard reaction intensity and pathways during high-temperature stacking. It also reflected differences in microbial supply of acids and esters. Additional differences were associated with lipid oxidation and amino acid degradation that affected aldehydes, ketones, and sulfur compounds.

In Table 2, the most characteristic markers of sauce-aroma high-temperature Daqu were pyrazines and derivatives. These included methylpyrazine, 2,3-dimethylpyrazine, 2,5-dimethylpyrazine, trimethylpyrazine, and tetramethylpyrazine. They also included highly substituted pyrazines with ethenyl, propyl, or acetyl substituents. Pyrazines typically convey roasted, nutty, cocoa-like, and toasted-cereal notes. This profile matched the stylistic basis of sauce-aroma Daqu, in which Daqu aroma and roasted notes were both emphasized. Tetramethylpyrazine was repeatedly highlighted in recent studies on sauce-aroma high-temperature Daqu and sauce-aroma Baijiu. It was regarded as a representative key flavor substance. Nut-like and baked notes could be imparted. Its formation was supported by both Maillard reactions and microbial synthesis during Daqu making, stacking fermentation, and solid-state fermentation. Table 2 also included 2-ethenyl-6-methylpyrazine, 2,3,5-trimethyl-6-propylpyrazine, and 2-acetyl-3,4,6-trimethylpyrazine. These higher substitution patterns suggested that differences were not limited to total pyrazines. Differences in substituent spectra were also likely. Substituent changes could markedly affect odor threshold, volatility, and aroma texture [14,25,58]. Highly substituted pyrazines often enhanced the depth of toasted and roasted nut-like notes. Certain samples could therefore present a stronger roasted base and a longer-lingering finish. Consistent with this view, studies on sauce-aroma Baijiu also reported that pyrazines were a key flavor framework. The pyrazine spectrum could diverge under different production areas or process conditions.

Typical aldehydes, ketones, and unsaturated aldehydes were also observed. This included acetaldehyde, hexanal, octanal, nonanal, decanal, trans-2-pentenal, trans-2-nonenal, 4-octanone, 2-nonanone, and 2-dodecanone. These compounds often produced a sharper aroma outline. Freshness and brightness could be provided at low levels. Oxidative notes and irritation could emerge at high levels. Trans-2-nonenal was often used as an indicator of lipid oxidation in food and beverage systems. It could present cucumber-like notes and cardboard-like oxidized off-odors. Its appearance as a VIP variable, therefore, suggested meaningful differences in lipid oxidation degree, precursor supply, or clearance rates across samples. Straight-chain aldehydes such as hexanal and octanal were more often associated with grassy and fatty notes. They could arise from autoxidation and enzymatic oxidation of raw material lipids. They could also be linked to the oxidative environment during high-temperature stacking. Strong aeration and heat release occurred during stacking. When oxygen participation increased, lipid oxidation chain reactions were more likely to proceed. Aldehydes could therefore become key variables for sample discrimination. In parallel, carbonyl compounds such as 2,3-butanedione and 2-hydroxy-3-pentanone also showed VIP > 1. They were often associated with buttery, creamy, and sweet notes in fermented foods. Softer roundness could be provided on top of a strong roasted base. Daqu aroma could therefore appear fuller and less harsh [22].

Acids and esters occupy a prominent position in Table 2. Acetic acid, propionic acid, hexanoic acid, octanoic acid, nonanoic acid, and multiple branched-chain acids were included. Paired esters included ethyl acetate, ethyl butyrate, ethyl valerate, ethyl octanoate, ethyl 2-methylbutanoate, ethyl 2-methylpropanoate, and ethyl 4-methylpentanoate. In sauce-aroma high-temperature Daqu, these variables often carried integrated information on microbial metabolism and enzymatic conversion. The acid side was commonly linked to carbon flux partitioning by lactic acid bacteria and other bacteria. It was also linked to amino acid degradation and lipid hydrolysis. Sensory cues could include acidic notes, fermentation impressions, sweaty notes, or cheese-like notes. Esters could partly soften acid sharpness. Fruity and sweet lift could be provided. Medium- and short-chain ethyl esters such as ethyl butyrate, ethyl valerate, and ethyl octanoate often contributed pineapple-like, apple-like, and composite fruity notes to Daqu and Baijiu systems. In sauce-aroma systems, fruity notes did not need to be exaggerated. Moderate fruity notes more often acted as support and elevation. Roasted Daqu aroma and sauce aroma could appear cleaner, with clearer layering. Acid–ester spectra as discriminant variables often implied differences in the balance between acid supply and esterification capacity. These differences could arise from microecological composition [34]. They could also reflect differences in enzyme activity windows shaped by stacking temperature curves.

Table 2 also shows phenols and aromatic ethers with clear smoky and spicy cues. 2-methoxy-4-vinylphenol is of particular interest. In many fermented and baked foods, this compound often presents clove-like and spicy notes with some smokiness. The roasted base can be extended toward a more penetrating spicy direction. In sauce-aroma high-temperature Daqu, such phenolic volatiles were often linked to the release of precursors such as ferulic acid and subsequent decarboxylation. They were also linked to thermal reaction pathways under high-temperature conditions. Co-occurrence with polymethoxy aromatic compounds such as 1,4-dimethoxybenzene, 1,2,3-trimethoxybenzene, and 1,2,3,4,5-pentamethoxybenzene suggested sweet, medicinal, or woody base notes. Thresholds and contribution patterns differed across compounds. Their appearance as VIP variables indicated measurable differences in woody sweetness and spiciness across samples. Sensory evaluation of sauce-aroma high-temperature Daqu often emphasized the purity of Daqu aroma and control of off-notes. Differences in this variable set, therefore, carried practical interpretive value. A cleaner spicy character could be indicated. Excessive

smokiness or medicinal intensity could also occur under imbalance. Further judgment required integration with sensory descriptors and threshold calculations [59].

Sulfur-containing compounds were few but highly distinctive. Dimethyl trisulfide and benzyl methyl sulfide were particularly notable. Dimethyl trisulfide was often regarded as a typical high-impact sulfur odorant. Garlic-like, onion-like, and cooked cabbage-like notes could be expressed. Effects on overall aroma were often driven by a low threshold and strong impact. Stacking fermentation of sauce-aroma high-temperature Daqu occurred under high temperatures and complex nitrogen sources. Degradation of sulfur-containing amino acids and derivative reactions were therefore more likely to occur. High temperatures also promoted the formation of sulfur-containing heterocycles related to Maillard reactions. Studies on the identification of sauce-aroma high-temperature Daqu and related Baijiu reported that high-temperature fermentation produced more Maillard-derived products. These included pyrazines, aldehydes, furans, and sulfur-containing heterocycles such as thiophenes. This direction was consistent with the presence of thiophane signals in the VIP list. In sauce-aroma Daqu flavor construction, sulfur compounds often acted as finishing touches. Very low levels could enhance maturity and complexity. Levels above an appropriate range could shift toward irritation and unclean impressions. Sulfur compounds as discriminant variables, therefore, implied stable differences in sulfur precursor release, redox microenvironments, or downstream clearance mechanisms across samples.

Compounds with VIP > 1 also included furan and lactone structures related to lipid oxidation or thermal reactions. 2-pentylfuran and 5-butyl-4-methyl-2(3H)-furanone were representative. 2-pentylfuran was used in many foods as an indicator of lipid oxidation. Aroma could include green bean-like and green notes with nutty nuances. In Daqu aroma, such cues often appeared as a fresh, fatty character or a slight green edge. 5-butyl-4-methyl-2(3H)-furanone tended toward sweet and coconut-like lactone notes. Coconut-like cues were often noted in barrel-aged systems. Its presence as a VIP variable in Daqu could indicate differences in tendencies for lipid cleavage and cyclization toward lactones. A softer or more woody–sweet underpinning could therefore emerge at the base of Daqu aroma. These components were usually not the sole dominant aroma sources in sauce-aroma high-temperature Daqu. When combined with pyrazines, phenols, and acid–ester components, they often shaped whether Daqu aroma leaned toward a clean, roasted, nutty style or a sweeter, mature style. This shift could further affect the construction of the sauce-aroma framework during subsequent stacking fermentation [25,60].

Based on the clear separation in OPLS-DA and the structural composition of VIP compounds, differences among sauce-aroma high-temperature Daqu samples could be interpreted as coordinated shifts across multiple pathways. Differences in pyrazines and highly substituted derivatives indicated differences in Maillard reactions and nitrogen-related metabolism during high-temperature stacking. This direction aligned closely with the typical roasted Daqu aroma. Differences in aldehydes, ketones, and furans more strongly reflected differences in lipid oxidation and thermal cracking. Unsaturated aldehydes as oxidation markers suggested that some samples were more prone to oxidative edge notes. Sensory evaluation was still needed to judge whether this reflected freshness or oxidized off-odors. Differences in acids and esters reflected differences in the balance between acid formation and esterification capacity. These differences often determined fermentation thickness and the degree of fruity lift. Phenolic spiciness and smoky cues represented by 2-methoxy-4-vinylphenol, together with sulfur impact represented by dimethyl trisulfide, acted as variables that shaped flavor individuality. A stronger aroma texture could be created on top of a similar roasted framework.

It should be noted that VIP > 1 reflected contribution to supervised classification. It did not mean that each variable had significant differences in univariate tests. These VIP trace

components will be correlated with sensory evaluation in subsequent analyses. A closed loop from mechanism to sensory performance and quality control will be constructed. Key odor-active substances in sauce-aroma high-temperature Daqu will be further screened.

3.3. Sensory Evaluation Analysis of Sauce-Aroma High-Temperature Daqu

Quantitative sensory evaluation was conducted for six groups of sauce-aroma high-temperature Daqu, covering surface color, aroma, cross-section, and overall score. As shown in Figure 2 and Table S2, the overall score ranged from 80.6 to 93.5 (A: 93.5; B: 80.6), with a between-group span of 12.9, indicating recognizable grade differences in overall sensory quality among Daqu from different sources or process conditions. The combinations across the four dimensions were not randomly distributed, and a relatively stable grouping pattern was observed, suggesting systematic sensory differences rather than incidental fluctuation. Surface color, aroma, and cross-section have also been widely used as core sensory indices in Daqu quality identification, and sensory evaluation is commonly regarded as a dominant basis for Daqu quality determination.

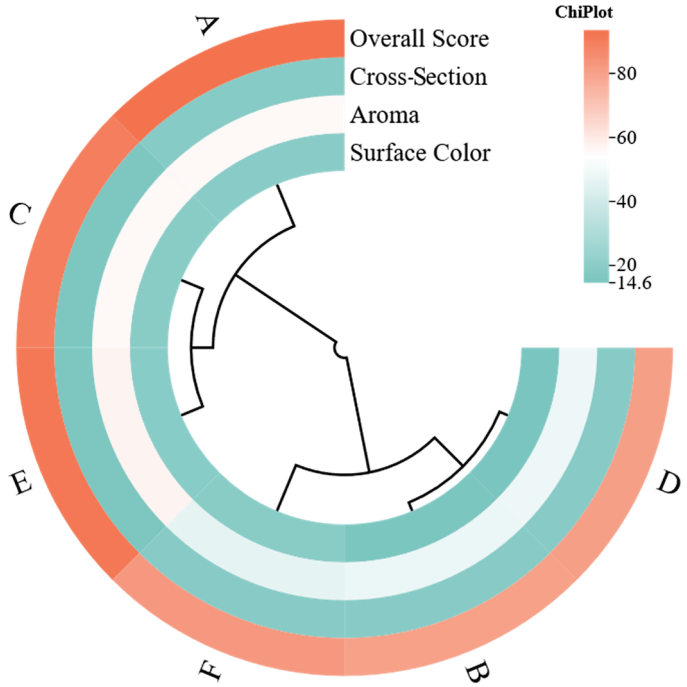


Figure 2. Overall sensory evaluation scores of sauce-aroma high-temperature Daqu.

At the individual-dimension level, aroma showed the strongest discriminability, with scores ranging from 45.9 to 57.9 (range: 12.0), and its ranking closely matched the overall score. Groups A, C, and E showed high aroma scores (56.5, 56.3, and 57.9), with corresponding overall scores of 93.5, 90.2, and 91.8, whereas groups B, D, and F showed lower aroma scores (47.5, 48.2, and 45.9), with overall scores between 80.6 and 82.8. In Figure 2, the aroma band shows clear stratification in both the color scale and the dendrogram, consistent with the notion that aroma is the most critical quality cue in Daqu sensory systems and is often assigned a higher weight, thereby driving the overall score more strongly.

Surface color also differed across samples, ranging from 14.6 to 18.9 (span: 4.3). Groups A, C, E, and F clustered between 18.5 and 18.9, indicating closer alignment with typical high-quality Daqu in apparent maturity and integrated surface coloration, while groups B and D scored 14.8 and 14.6, suggesting relatively insufficient maturity and surface coloration. The surface color band in Figure 2 similarly positions B and D at the low end, supporting their lower overall scores. Notably, group F showed a relatively strong surface color score

https://doi.org/10.3390/foods15030599

(18.5) but a modest overall score (82.8), implying that the limiting factor was more likely aroma rather than appearance.

The cross-section dimension was not fully aligned with the overall score. Groups A, B, D, and F scored similarly (18.1–18.4), while groups C and E were lower (15.2 and 15.1), yet their overall scores remained high (90.2 and 91.8). In Figure 2, C and E exhibit a lighter cross-section band but a high overall-score band, suggesting that cross-section was not the dominant driver of overall evaluation in this sample set, and its impact was likely outweighed by advantages in aroma and surface color under the current weighting framework. The previous literature indicates that cross-section mainly reflects internal structure and mycelial status, whereas aroma is more directly linked to flavor potential and practical value, so these indices often serve different roles in comprehensive judgment.

Based on the clustering structure in Figure 2, the six groups were classified into two major clusters. Groups A, C, and E formed one branch, sharing high surface color and aroma with overall performance above 90; although cross-section decreased in C and E, overall quality remained in a higher tier. Groups B and D formed another branch, showing low surface color and aroma, and although cross-section scores were higher, overall scores remained slightly above 80. Group F clustered closer to B and D, consistent with its low aroma score: despite relatively high surface color and cross-section, insufficient aroma limited the overall score and prevented entry into the high-score group. Overall, the clustering pattern highlighted that the upper bound of sensory quality for sauce-aroma high-temperature Daqu was primarily driven by aroma intensity and aroma cleanness, while appearance and cross-section more often determined basic qualification and structural stability, showing diminishing marginal effects on improving overall score. This also provides a clear direction for subsequent association analysis between sensory outcomes and differences in volatile components.

3.4. Correlation Analysis Between Sensory Scores and Key Trace Components in Sauce-Aroma High-Temperature Daqu

As shown in Table 3, trace components with VIP > 1 were not uniformly coupled with sensory dimensions. Clear directional preferences were observed. For correlation coefficients, the number of variables with an absolute value greater than 0.5 reached 31, 29, 31, and 28 in surface color, aroma, cross-section, and overall score, respectively. This pattern suggested that sensory differences in sauce-aroma high-temperature Daqu were not driven by a few single compounds. They were more likely shaped by coordinated shifts across several chemical modules. It should be noted that the sample size comprised six Daqu groups. The significance threshold for correlation tests was therefore more difficult to reach. A limited number of variables with $p < 0.05$ was consistent with statistical expectations. Under this constraint, five variables still reached significance for the overall score. Four variables were significant for aroma. Three variables were significant for surface color. Three variables were significant for cross-section. This distribution suggested that the overall score and aroma were more readily captured by volatile profiles. Cross-section and surface color were more likely external manifestations of process state and structural maturity [40,60–62]. Significant coupling emerged only when specific compounds stably indicated these states.

https://doi.org/10.3390/foods15030599

Table 3. Correlation analysis between sensory scores and key trace components in sauce-aroma high-temperature Daqu.

Compound Name	r: Surface Color	r: Aroma	r: Cross-Section	r: Overall Score	*p*: Surface Color	*p*: Aroma	*p*: Cross-Section	*p*: Overall Score
2-Pentanol	0.357	0.404	0.263	0.577	0.488	0.427	0.615	0.230
Butyl acrylate	0.357	0.404	0.263	0.577	0.488	0.427	0.615	0.230
(Z)-Oxacyclopentadec-6-en-2-one	0.357	0.404	0.263	0.577	0.488	0.427	0.615	0.230
γ-Linolenic acid	0.357	0.404	0.263	0.577	0.488	0.427	0.615	0.230
5-Butyl-4-methyl-2(3H)-furanone	0.238	0.538	−0.118	0.553	0.650	0.271	0.824	0.255
Hexanoic acid	**0.537**	**0.709**	**−0.181**	**0.801**	**0.272**	**0.115**	**0.732**	**0.055**
trans-3-Methyl-2-n-propylthiophane	**0.528**	**0.689**	**−0.131**	**0.794**	**0.281**	**0.130**	**0.805**	**0.059**
Ethyl octanoate	0.134	0.314	0.230	0.404	0.801	0.544	0.662	0.427
Benzoic acid	0.310	0.386	−0.616	0.298	0.550	0.450	0.193	0.566
1-Pentanol	0.310	0.386	−0.616	0.298	0.550	0.450	0.193	0.566
4-Octanone	0.642	0.346	0.167	0.599	0.169	0.502	0.752	0.209
2-Pentylfuran	0.416	0.158	−0.471	0.165	0.412	0.765	0.345	0.755
Ethyl 2-methylbutanoate	0.310	0.386	−0.616	0.298	0.550	0.450	0.193	0.566
1,2,3,4,5-Pentamethoxybenzene	0.310	0.386	−0.616	0.298	0.550	0.450	0.193	0.566
3-Octanol	−0.032	−0.183	0.742	0.025	0.952	0.728	0.091	0.963
1,4-Dimethoxybenzene	0.310	0.386	−0.616	0.298	0.550	0.450	0.193	0.566
Ethyl 4-methylpentanoate	0.310	0.386	−0.616	0.298	0.550	0.450	0.193	0.566
2-Hexanone oxime	**0.542**	**0.744**	**−0.348**	**0.789**	**0.266**	**0.090**	**0.500**	**0.062**
(E)-2-Pentenal	**0.717**	**0.926**	**−0.504**	**0.978**	**0.109**	**0.008**	**0.308**	**0.001**
(E)-2-Nonenal	0.399	0.429	0.195	0.597	0.433	0.396	0.712	0.211
Dimethyl trisulfide	**0.685**	**0.866**	**−0.409**	**0.937**	**0.133**	**0.026**	**0.421**	**0.006**
Cyclohept-4-en-1-ol	−0.497	−0.162	0.028	−0.321	0.316	0.759	0.958	0.534
Methyl 3,4-dimethylbenzoate	0.310	0.386	−0.616	0.298	0.550	0.450	0.193	0.566
2-Methylpropanal	0.453	−0.105	−0.239	−0.002	0.367	0.843	0.648	0.997
β-Methylcinnamaldehyde	0.427	0.519	−0.541	0.485	0.399	0.291	0.267	0.329
2-Ethenyl-6-methylpyrazine	**0.373**	**0.706**	**−0.866**	**0.548**	**0.467**	**0.117**	**0.026**	**0.260**
2-Propanamine	−0.302	−0.129	0.483	−0.093	0.561	0.808	0.332	0.860
Allyl acetate	−0.227	0.049	0.463	0.093	0.665	0.926	0.356	0.860
Acetic acid	**0.433**	**0.914**	**−0.483**	**0.871**	**0.391**	**0.011**	**0.332**	**0.024**
Propylene glycol	**0.194**	**0.515**	**−0.849**	**0.312**	**0.713**	**0.296**	**0.032**	**0.548**
Octanal	0.528	0.624	−0.242	0.702	0.282	0.185	0.644	0.120
4,5-Dihydro-5,5,7-trimethyl-6H-[1,2,5] oxadiazolo[3,4-b] [1,4] diazepine	−0.654	−0.350	0.323	−0.470	0.159	0.497	0.532	0.347
2-Hydroxy-3-pentanone	0.710	0.278	−0.012	0.510	0.114	0.593	0.983	0.301
Benzyl methyl sulfide	−0.654	−0.350	0.323	−0.470	0.159	0.497	0.532	0.347
1,2,3-Trimethoxybenzene	0.413	0.317	−0.541	0.292	0.416	0.540	0.268	0.574

https://doi.org/10.3390/foods1

Table 3. *Cont.*

Compound Name	r: Surface Color	r: Aroma	r: Cross-Section	r: Overall Score	*p*: Surface Color	*p*: Aroma	*p*: Cross-Section	*p*: Overall Score
1,3-Hexadienylbenzene	−0.654	−0.350	0.323	−0.470	0.159	0.497	0.532	0.347
Octyloxirane	−0.654	−0.350	0.323	−0.470	0.159	0.497	0.532	0.347
2-Phenyl-1H-imidazole	−0.033	0.312	−0.180	0.228	0.950	0.547	0.732	0.664
2-Phenylethyl nicotinate	−0.654	−0.350	0.323	−0.470	0.159	0.497	0.532	0.347
Ethyl 2-methylpropanoate	−0.654	−0.350	0.323	−0.470	0.159	0.497	0.532	0.347
2-Dodecanone	−0.654	−0.350	0.323	−0.470	0.159	0.497	0.532	0.347
2,3,5-Trimethyl-6-propylpyrazine	−0.165	0.094	0.456	0.155	0.754	0.859	0.363	0.769
2-Nonanone	−0.699	−0.301	0.559	−0.375	0.122	0.562	0.249	0.463
2-Methyl-1-propanol	−0.248	−0.677	0.316	−0.631	0.635	0.140	0.542	0.180
Methyl linoleate	0.222	−0.361	0.662	−0.071	0.672	0.482	0.152	0.893
7-Oxooctanoic acid	−0.418	−0.102	0.454	−0.119	0.410	0.847	0.366	0.823
Propionic acid	0.101	0.142	0.346	0.264	0.849	0.789	0.502	0.613
Ethyl 4-hydroxybenzoate	−0.654	−0.350	0.323	−0.470	0.159	0.497	0.532	0.347
Methyl 6-nonynoate	−0.654	−0.350	0.323	−0.470	0.159	0.497	0.532	0.347
N, N-Dimethylmethylamine	0.149	−0.054	−0.352	−0.095	0.778	0.919	0.494	0.858
4-Methylhexanoic acid	−0.634	−0.276	0.594	−0.319	0.176	0.597	0.214	0.538
Angelic acid	0.491	−0.109	0.486	0.210	0.323	0.837	0.329	0.690
Cyclotridecanone	−0.536	−0.212	0.418	−0.273	0.273	0.687	0.409	0.601
Methyl anthranilate	−0.020	0.155	−0.424	0.019	0.970	0.769	0.402	0.971
Hexanal	−0.239	0.300	0.163	0.238	0.648	0.564	0.757	0.649
Menthol	0.493	−0.074	0.481	0.242	0.321	0.889	0.334	0.644
Decyloctyl ether	0.592	0.514	−0.431	0.571	0.216	0.296	0.394	0.237
Ethyl pentadecanoate	0.472	0.690	−0.546	0.659	0.344	0.129	0.263	0.155
Acetaldehyde	0.556	−0.116	−0.229	0.028	0.251	0.827	0.663	0.957
Octanoic acid	0.412	0.179	0.213	0.374	0.417	0.734	0.685	0.465
2-Methylpropanoic acid	0.097	0.798	−0.434	0.655	0.856	0.057	0.390	0.158
(Z)-Undec-6-en-2-one	−0.595	−0.272	0.387	−0.358	0.213	0.603	0.448	0.486
Ethyl valerate	0.446	0.308	0.106	0.476	0.376	0.552	0.841	0.340
Ethyl oleate	0.202	−0.291	0.575	−0.037	0.701	0.576	0.232	0.944
Ethyl linoleate	**0.975**	**0.511**	**−0.325**	**0.735**	**0.001**	**0.300**	**0.530**	**0.096**
Ethyl butyrate	0.462	0.690	−0.724	0.606	0.356	0.129	0.104	0.202
(E)-2-Methyl-2-pentenoic acid	0.465	−0.085	−0.172	0.040	0.353	0.873	0.744	0.940
2-Phenylethyl 2-methylpropanoate	0.451	0.674	−0.677	0.600	0.370	0.142	0.140	0.208
1-Pentadecene	−0.418	−0.206	0.444	−0.218	0.409	0.696	0.378	0.679
Nonanal	**0.807**	**0.766**	**−0.608**	**0.832**	**0.052**	**0.076**	**0.201**	**0.040**
3-Methylbutanoic acid	−0.179	0.381	0.049	0.304	0.735	0.456	0.926	0.558

https://doi.org/10.3390/foods1

Table 3. *Cont.*

Compound Name	r: Surface Color	r: Aroma	r: Cross-Section	r: Overall Score	*p*: Surface Color	*p*: Aroma	*p*: Cross-Section	*p*: Overall Score
Nonanoic acid	−0.334	0.011	0.197	−0.054	0.518	0.983	0.708	0.918
3-Methyl-1-butanol	0.060	−0.445	0.101	−0.364	0.910	0.376	0.850	0.478
3,7-Dimethyl-1,6-octadien-3-yl formate	−0.251	−0.052	0.465	−0.009	0.632	0.922	0.353	0.986
2-Octanone	0.072	0.411	−0.659	0.225	0.892	0.418	0.154	0.669
4-Methylquinazoline	**−0.921**	**−0.532**	**0.465**	**−0.696**	**0.009**	**0.277**	**0.353**	**0.125**
3-Methyl-2,5-piperazinedione	0.333	0.531	−0.646	0.433	0.519	0.278	0.166	0.390
(Z)-Benzaldehyde oxime	0.333	0.531	−0.646	0.433	0.519	0.278	0.166	0.390
Decanal	**0.501**	**0.740**	**−0.830**	**0.637**	**0.311**	**0.092**	**0.041**	**0.174**
Ethyl acetate	0.555	0.397	−0.587	0.405	0.253	0.436	0.221	0.426
2-Methylhexanoic acid	0.367	−0.396	0.021	−0.230	0.474	0.437	0.969	0.661
Acetone	0.333	0.531	−0.646	0.433	0.519	0.278	0.166	0.390
N-(2-Methylpropyl) acetamide	0.333	0.531	−0.646	0.433	0.519	0.278	0.166	0.390
3-Methyltridecane	−0.062	0.239	−0.400	0.088	0.906	0.648	0.432	0.868
2-Acetyl-3,4,6-trimethylpyrazine	0.333	0.531	−0.646	0.433	0.519	0.278	0.166	0.390
2-(Phenylpiperidin-1-ylmethyl) cyclohexanol	0.333	0.531	−0.646	0.433	0.519	0.278	0.166	0.390
5-Methyl-2-phenyl-2-hexenal	**−0.511**	**−0.887**	**0.423**	**−0.890**	**0.301**	**0.018**	**0.403**	**0.017**
1,2,3,4-Tetramethoxybenzene	**−0.998**	**−0.602**	**0.511**	**−0.776**	**0.000**	**0.206**	**0.300**	**0.070**
Methylpyrazine	0.191	−0.173	−0.035	−0.102	0.717	0.743	0.948	0.848
2,3-Butanedione	0.695	0.241	−0.007	0.472	0.126	0.646	0.990	0.345

Note: r: Surface Color, r: Aroma, r: Cross-section, and r: Overall Score represented the correlations between each trace component and the corresponding sensory dimension score. p: Surface Color, p: Aroma, p: Cross-section, and p: Overall Score represented the significance of the correlations between each trace component and the corresponding sensory dimension score. The compounds shown in bold and with blue shading in the table are the core compounds identified after screening of Daqu and are highlighted accordingly.

https://doi.org/10.3390/foods1

A, C, and E showed higher aroma and overall scores. B, D, and F showed lower values. This pattern was broadly consistent with the direction of significant variables. Molecules that were significantly positively associated with aroma and overall score mainly clustered in lipid oxidation-related aldehydes, high-impact sulfur compounds, and fermentative organic acids. These modules often increased brightness and diffusivity. They also enhanced the maturity notes and fermentation character. They were therefore reflected as positive contributors in the comprehensive evaluation. In contrast, molecules that were significantly negatively associated with aroma or overall score showed a stronger idiosyncratic odor background. Aromatic compounds and nitrogen-containing heterocycles with cocoa-like or medicinal tendencies could act as off-direction signals within the Daqu aroma framework of sauce-aroma high-temperature Daqu. Sensory scores were therefore reduced. Meanwhile, significant negative associations in the cross-section dimension were presented by propylene glycol, decanal, and specific pyrazines. This pattern more likely reflected tension between internal structural maturity and volatile accumulation. When certain metabolic and thermal reactions were stronger, the idealized internal-tissue state did not necessarily improve in parallel.

On this basis, 14 key trace components served as a core bridge linking chemical fingerprints to sensory differences in sauce-aroma high-temperature Daqu. They covered the most information-dense part of the correlation and significance results. They also aligned with the mechanistic narrative in which microbial metabolism and thermal reactions occurred concurrently during high-temperature stacking fermentation.

Hexanoic acid (r aroma 0.709, p 0.115; r overall score 0.801, p 0.055) showed a consistent positive trend for aroma and overall score. Statistical significance at 0.05 was not reached. Correlation strength remained high. Hexanoic acid carried a typical fatty and cheese-like background. Fermentation thickness could be directly enhanced. It could also act as an esterification precursor in subsequent brewing systems. The high correlation with overall score, therefore, suggested that high-scoring Daqu had a stronger acid supply and a more robust flavor foundation [63–65].

trans-3-Methyl-2-n-propylthiophane (r aroma 0.689, p 0.130; r overall score 0.794, p 0.059) also showed a positive but non-significant association. Sulfur-containing heterocycles often had very low olfactory thresholds and strong diffusion. Trace-level changes could alter mature aroma depth and complexity. In sauce-aroma systems, sulfur compounds were not required to be abundant. An appropriate window was more critical. Subtle mature, meaty, or onion-garlic accents could be provided. The Daqu aroma could be shifted from simple roasting toward a more three-dimensional sauce-aroma precursor profile. The formation mechanisms and low-threshold contributions of sulfur volatiles in Baijiu were also emphasized in existing reviews [66–68].

2-Hexanone oxime (r aroma 0.744, p 0.090; r overall score 0.789, p 0.062) showed a strong positive trend for aroma and overall score. Oximes were often viewed as derivative forms of carbonyls or as reaction companions. Under complex solid-state fermentation and high-temperature conditions, this compound more likely served as an indirect indicator of active carbonyl metabolism and nitrogen-related reactions. Some oximes were described as green-leafy, fresh, or slightly earthy. This orientation complemented the fresh edge required in sauce-aroma high-temperature Daqu. The positive trend, therefore, remained mechanistically plausible [69–71].

(E)-2-Pentenal (r aroma 0.926, p 0.008; r overall score 0.978, p 0.000744) was among the clearest positive signals for aroma and overall score. Correlation strength and significance were both high. This aldehyde was often described as green, pungent, and partly fruity. It was commonly linked to lipid oxidation or thermal reactions in food systems. Combined with the aroma advantage of high-scoring groups in the sensory heatmap, an interpretation

was supported. At an appropriate level, it likely provided lifted brightness and diffusive freshness. The roasted base was therefore less dull. The overall score was consequently increased [72].

Dimethyl trisulfide (r aroma 0.866, p 0.026; r overall score 0.937, p 0.006) also showed significant positive associations. It represented a typical high-impact variable. Dimethyl trisulfide often carried cooked onion–garlic- and cabbage-like sulfur notes. The threshold was extremely low. Minor changes could reshape the aroma profile. In sauce-aroma high-temperature Daqu, this sulfur note was not necessarily expressed as a foul odor. It was more often reflected as reinforcement of mature aroma and a sauce-like background. When coexisting with pyrazines and carbonyls, roasted notes could be pushed from planar to layered. The strong positive association with the overall score, therefore, showed high mechanistic consistency [66–68].

Ethyl linoleate (r surface color 0.975, p 0.000925; r overall score 0.735, p 0.096) showed an extremely strong and significant positive association with surface color. It served as one of the clearest indicators of coloration in this dataset. Fatty acid ethyl esters often reflected integrated outcomes of lipid release, ethanol supply, and the esterification environment. Higher surface color scores often indicated more coordinated temperature rise and subsequent drying. Lipid-related precursor formation and esterification stability were also favored. This result suggested that surface color was not only an appearance index. It could also covary with lipid-related flavor potential [63,64].

Nonanal (r aroma 0.766, p 0.076; r overall score 0.832, p 0.040) reached a significant positive association with overall score. Nonanal often conveyed waxy and fatty notes with citrus-like and green nuances. At very low levels, it could enhance aromatic bloom. The significant positive association, therefore, suggested that high-scoring Daqu had better aroma diffusion and a cleaner fresh edge. Daqu aroma appeared brighter and cleaner. The overall evaluation was consequently improved [73,74].

Decanal (r cross-section −0.830, p 0.041; r aroma 0.740, p 0.092) showed a significant negative association with cross-section. This finding required attention. Decanal was also linked to lipid oxidation. In this dataset, a clear inverse coupling with the cross-section score was observed. When decanal increased, cross-section performance tended to decline. A more reasonable explanation was supported. Cross-section scoring emphasized compactness and uniformity. These traits could correspond to a more stable internal microenvironment and more controlled oxidation. Decanal elevation reflected more active oxidation chain reactions. Mechanistic tension, therefore, existed. This finding indicated that cross-section was not an independent index in which higher values always implied improvement. Trade-offs with parts of the volatile profile were possible [73–75].

4-Methylquinazoline (r surface color −0.921, p 0.009; r overall score −0.696, p 0.125) showed a significant negative association with surface color. 4-Methylquinazoline was reported to have medicinal tendencies. Its presence was often linked to nitrogen-containing heterocycle formation. A stronger heterocycle background could be formed under high-temperature reactions and nitrogen participation. In the evaluation framework of sauce-aroma high-temperature Daqu, ideal color implied maturity without overprocessing. When such heterocycles increased with stronger high-temperature reactions, reduced color scores and style deviation could occur. The significant negative association was therefore consistent [64,76].

5-Methyl-2-phenyl-2-hexenal (r aroma −0.887, p 0.018; r overall score −0.890, p 0.017) was among the most explicit negative flavor signals in this dataset. This compound was often described as cocoa-like with an aldehydic background. Within the Daqu aroma framework of sauce-aroma high-temperature Daqu, excessive cocoa-like or sweet aldehydic notes could indicate style deviation. When combined with sulfur notes and acidic notes,

a less clean composite tone could form. Significant negative associations with aroma and overall score, therefore, suggested that this variable required constraint [64,77,78].

1,2,3,4-Tetramethoxybenzene (r surface color −0.998, p 0.000006; r aroma −0.602, p 0.206) showed an extremely strong and significant negative association with surface color. It was almost a reverse marker for color evaluation. Polymethoxy aromatics often conveyed sweet, woody, or medicinal tendencies. They were more likely signals derived from plant phenolic structures. This result suggested that accumulation of such aromatic ethers was linked to surface coloration deviating from the ideal state of high-scoring samples. Differences in phenolic release, thermal reaction routes, or microbial degradation could underlie this association. These differences were captured by surface color evaluation [79].

2-Ethenyl-6-methylpyrazine (r cross-section −0.866, p 0.026; r aroma 0.706, p 0.117) showed a significant negative association with cross-section. A strong positive trend was observed for aroma. Pyrazines represented a key roasted and nutty flavor framework in sauce-aroma high-temperature Daqu. They were also widely regarded as key nitrogenous odorants in Baijiu flavor research. This result suggested that enhanced pyrazine spectra improved aroma. Alignment with the ideal cross-section structure was not guaranteed. This tension matched the realistic state of high-temperature stacking fermentation. When thermal reactions and nitrogen metabolism intensified, internal structure did not necessarily shift toward a more regular aesthetic standard [69,79,80].

Acetic acid (r aroma 0.914, p 0.011; r overall score 0.871, p 0.024) was another significant positive core variable. Acetic acid directly contributed to fermentative acidity and freshness. It also acted as an esterification substrate that influenced ester formation. Significant positive associations with aroma and overall score, therefore, indicated a more active and balanced basal metabolic network in high-scoring Daqu. This signal was consistent with the general understanding that microbial metabolism dominated flavor formation in Baijiu brewing systems [63,64].

Propylene glycol (r cross-section −0.849, p 0.032; r aroma 0.515, p 0.296) showed a significant negative association with cross-section. Propylene glycol was a polyol. It was often linked to carbon flux allocation and protective metabolism under osmotic and moisture stress in microorganisms. In solid-state fermentation, it was often associated with local moisture retention and polyol accumulation. Cross-section scoring emphasized dryness, uniformity, and maturity of internal tissues. Elevated polyols could reflect stronger water retention or a shift toward polyol metabolism. An inverse relationship with cross-section evaluation was therefore plausible [64,81].

These 14 trace components covered core nodes of significant associations. They also included both positive flavor frameworks and potential negative deviation signals. For sauce-aroma high-temperature Daqu from the Chishui River Basin, this combination corresponded to a key stylistic tension. Advantages in roasted and mature notes, driven by high-temperature reactions needed to be balanced. Appropriate brightness from lipid oxidation-related aldehydes was required. Three-dimensional maturity could be enhanced by sulfur volatiles. Fermentative character and freshness were maintained by organic acids. Excessive accumulation of aromatic aldehydes and certain nitrogen heterocycles could induce style deviation. These components could therefore be defined as a core flavor set for sauce-aroma high-temperature Daqu from the Chishui River Basin. Molecular docking and molecular dynamics will be introduced in subsequent work. The binding and activation of olfactory receptor proteins by these key odorants will be explored. This approach will advance sensory differences from statistical association to mechanistic evidence at the receptor level.

https://doi.org/10.3390/foods15030599

3.5. Mechanisms by Which 14 Core Trace Components Activated the Olfactory Receptor

As shown in Table 4, the 14 core trace components exhibited a clear gradient of docking affinity and interaction modes. Acetic acid showed the strongest binding tendency (docking score = −6.655) with a highly negative electrostatic term (glide ecoul = −14.562), suggesting stabilization dominated by hydrogen bonding/polar interactions and plausibly supporting the baseline perception of fermentative acidity and freshness in Daqu aroma. In contrast, 4-methylquinazoline (−4.714) and 1,2,3,4-tetramethoxybenzene (−3.845) belonged to the high-affinity group with strongly negative van der Waals terms (glide evdw = −15.929 and −18.566), indicating hydrophobic matching and shape complementarity that could contribute medicinal/woody–warm nuances and enhance aroma texture/aftertaste. A second high-impact route involved sulfur compounds, where dimethyl trisulfide (−3.950; glide evdw = −13.611) and trans-3-methyl-2-n-propylthiophane (−3.774; glide evdw = −13.695) showed stable hydrophobically driven binding consistent with their low-threshold potential to intensify mature, onion–garlic/meaty accents and increase aroma depth; similarly, 2-ethenyl-6-methylpyrazine (−3.414; glide evdw = −13.849) supported a hydrophobic binding mode consistent with reinforcement of roasted/nutty recognition. Compounds in the moderate range were more likely to modulate aroma contour: hexanoic acid (−2.121; glide ecoul = −5.397; glide evdw = −13.009) combined polar anchoring with hydrophobic fitting, consistent with fatty/cheese-like fullness, while (E)-2-pentenal (−1.027; glide evdw = −10.705) and nonanal (−0.508; glide evdw = −14.471) plausibly contributed brightness and diffusion (green/fresh and waxy nuances). 2-hexanone oxime showed notable hydrophobic embedding (markedly negative glide evdw) and was interpreted mainly as a subtle modifier (fresh/herbal smoothing) rather than a dominant identity cue. Decanal displayed unfavorable binding (docking score = 1.952), which does not exclude sensory contribution but suggests the selected receptor model may not preferentially recognize decanal and that perception may rely on other receptor subtypes, reinforcing that sauce-aroma high-temperature Daqu aroma is encoded by multi-receptor, multi-molecule integration rather than a single-ligand pathway. A detailed interpretation is provided in File S2.

Table 4. Docking scores of 14 core trace components for activation of the olfactory receptor.

Compound Name	Docking Score	Glide Ecoul	Glide Emodel	Glide Evdw
Acetic acid	−6.655	−14.562	−41.101	−4.830
4-Methylquinazoline	−4.714	−0.531	−21.129	−15.929
5-Methyl-2-phenyl-2-hexenal	−4.578	−0.318	−20.426	−17.022
Propylene glycol	−4.022	−10.972	−21.636	−8.251
Dimethyl trisulfide	−3.950	−0.414	−16.924	−13.611
1,2,3,4-Tetramethoxybenzene	−3.845	−0.720	−21.225	−18.566
trans-3-Methyl-2-n-propylthiophane	−3.774	−0.534	−15.895	−13.695
2-Ethenyl-6-methylpyrazine	−3.414	−1.282	−17.958	−13.849
Hexanoic acid	−2.121	−5.397	−18.345	−13.009
2-Hexanone oxime	−1.666	−0.736	−16.098	−14.212
(E)-2-Pentenal	−1.027	−0.136	−9.989	−10.705
2-Hexanone oxime	−0.871	−0.726	−13.351	−12.092
Nonanal	−0.508	−0.645	−13.211	−14.471
Decanal	1.952	−0.735	−14.879	−17.428

Note: Docking Score was the primary metric for ligand ranking and selection. Lower values indicated better evaluation. Units were kcal/mol (same below). Glide Ecoul was the Coulombic (electrostatic) interaction energy between the receptor and ligand. Glide Emodel was used for pose selection and stability comparison within the same ligand. It was mainly applied to rank and select among different poses of the same ligand. Glide Evdw was the van der Waals interaction energy between the receptor and ligand derived from the force field vdW term.

The docking results suggest that key Daqu volatiles follow a recognition logic that combines polar anchoring with hydrophobic compaction after entering the olfactory-

receptor binding cavity. Polar functional groups (carboxyl, hydroxyl, oxime, and carbonyl) tend to be directionally constrained at the pocket's polar boundary, where hydrogen-bonding and dipole stabilization are provided by polar residues (e.g., Ser75/Ser92/Ser152, Thr74/Thr76/Thr98/Thr200, Gln99, and Glu94). When needed, electrostatic or hydrogen-bond networks are reinforced by charged/polar residues (e.g., Arg150/Arg262, Asn194, His180/His261, Asp182, Gln181, and Ser258), thereby reducing ligand conformational freedom. The pocket core remains predominantly hydrophobic and is formed mainly by aliphatic residues (Leu/Ile/Val/Ala/Pro/Met), enabling continuous van der Waals contacts that govern compaction, residence time, and chain-length matching. Aromatic/heterocyclic ligands can further gain specificity through π-related contacts with aromatic residues (e.g., Phe93/Phe101/Phe102 and Tyr197), consistent with shape complementarity. Sulfur-containing ligands may exploit sulfur polarizability to form S/π interactions near aromatic residues (e.g., Phe93/Phe101/Phe102) and Met100, and may also form directional sulfur-related contacts with oxygen-containing groups of Glu94, supporting stable binding even for weakly polar ligands.

More negative docking scores generally indicate more favorable binding trends, but they are best interpreted as relative rankings within the same receptor/modeling system, rather than absolute binding affinities, due to known limitations and biases of scoring functions. Importantly, this docking analysis is computational and unvalidated experimentally in the present study, and it reflects a single-receptor, single-ligand scenario; it does not capture mixture effects (competition/antagonism) that are common in odor coding, nor does it model matrix-dependent transformations that occur during brewing. Under the canonical pathway, once polar anchoring and hydrophobic compaction support productive binding, the transmembrane bundle may undergo conformational rearrangement toward an active state, couple to Gαolf, activate adenylyl cyclase III, increase cAMP, and amplify olfactory signaling; however, receptor subtype diversity and alternative signaling routes are not addressed here. Detailed interaction maps and full residue lists are provided in File S2.

3.6. Microbial Community Composition Analysis of Sauce-Aroma High-Temperature Daqu

Microorganisms were major constituents of Daqu. They served as producers of hydrolytic enzymes and key contributors to characteristic flavor compounds. Therefore, microbial diversity and composition in sauce-aroma high-temperature Daqu were investigated. High-throughput sequencing was applied for profiling and subsequent analysis.

In general, α-diversity was evaluated using the Chao, Shannon, and Simpson indices to assess community richness and evenness (Figure 3a,b). The results indicated that bacterial richness and diversity were higher than those of fungi. This observation was consistent with the common description of sauce-aroma high-temperature Daqu as bacterial-dominated Daqu. A plausible explanation was that the fermentation temperature exceeded 60 °C. During the high-temperature stage, most fungi were inactivated, whereas thermotolerant bacteria were retained. To determine whether microbial composition differed among samples, PCoA was used to compare community structures (Figure 3c). Significant differences were observed for both bacteria and fungi based on ANOSIM. For bacteria, r = 0.865 and $p = 0.001$. For fungi, r = 0.967 and $p = 0.001$. These compositional differences were expected to drive divergence in metabolic phenotypes across Daqu.

At the phylum level, the dominant bacterial phyla mainly comprised *Bacillota* and *Actinomycetota* (Figure 3d). The relative abundance of *Bacillota* ranged from 65.64% to 98.83%. *Actinomycetota* followed with 0.85% to 33.84%.

At the genus level, the dominant bacteria included *Kroppenstedtia*, *Bacillus*, *Lentibacillus*, *Oceanobacillus*, *Desmospora*, *Pallidibacillus*, *Saccharopolyspora*, *Scopulibacillus*, and *Virgibacillus*.

This pattern was broadly consistent with earlier metagenomic surveys of sauce-aroma high-temperature Daqu.

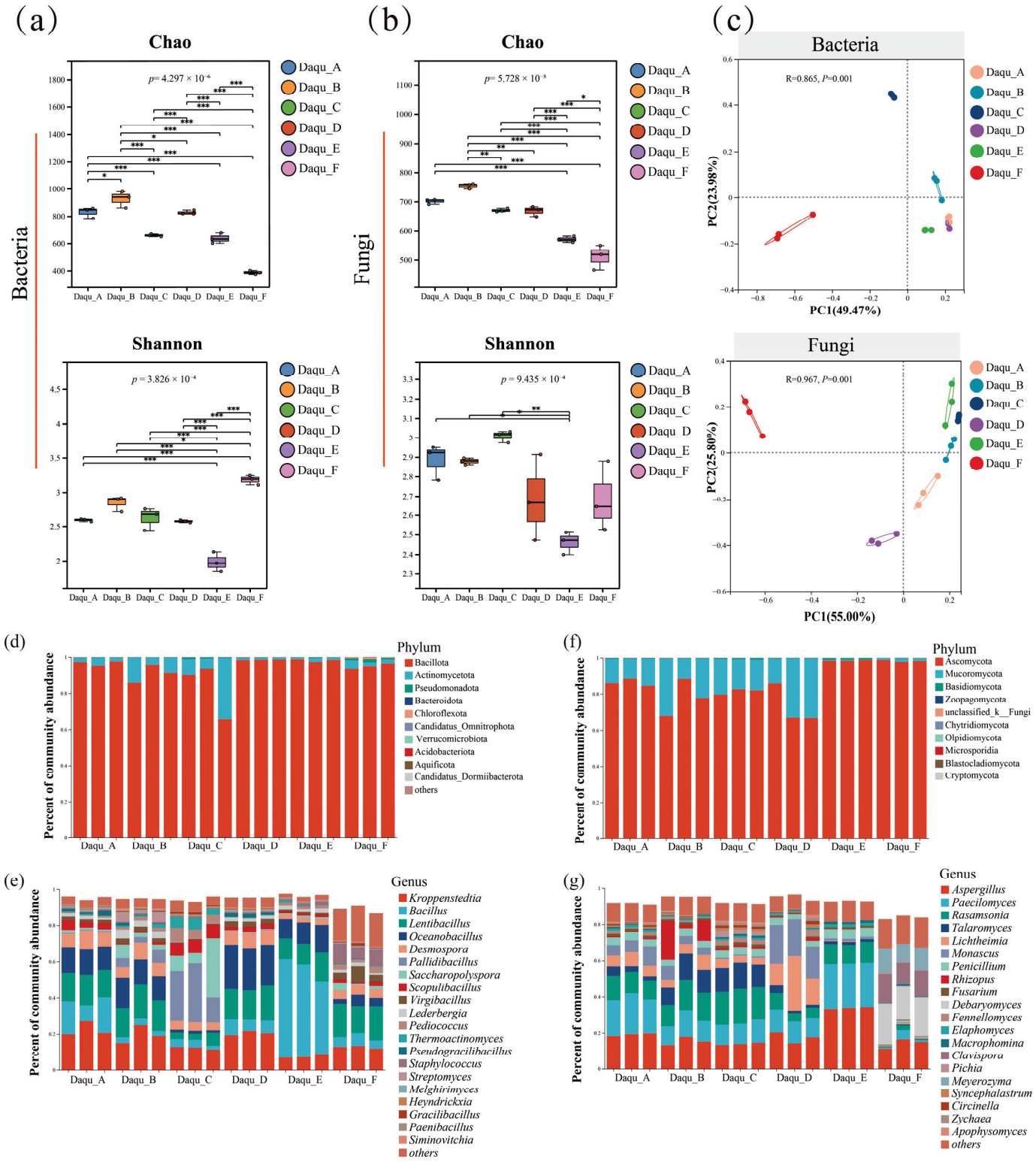


Figure 3. The differences in microbial diversity and structural composition within high-temperature Daqu. (**a**) Microbial diversity of bacteria; (**b**) microbial diversity of fungi; (**c**) PCoA analysis; (**d**) microbial structure composition of bacteria at the phylum level; (**e**) microbial structure composition of bacteria at the genus level; (**f**) microbial structural composition of fungi at phylum level; (**g**) microbial structural composition of fungi at genus level. Note: $p < 0.05$ (*), $p < 0.01$ (**), $p < 0.001$ (***).

https://doi.org/10.3390/foods15030599

Across all samples, *Bacillus* and *Kroppenstedtia* were the major dominant genera. *Bacillus* accounted for a substantial proportion, with a relative abundance of 2.16% to 54.56%. It was regarded as a functional cornerstone due to roles in secreting proteases and amylases, and in generating flavor precursors. *Kroppenstedtia* showed stable abundance at 6.82% to 27.15%. This genus was considered an indicator microorganism for sauce-aroma high-temperature Daqu. High prevalence was typically associated with the high-temperature fermentation environment and with the formation of pyrazine flavor compounds. Beyond these core genera, multiple thermotolerant or halotolerant genera were detected. This pattern supported the presence of a complex cooperative microbial network. *Lentibacillus*, *Oceanobacillus*, *Virgibacillus*, *Scopulibacillus*, and *Pallidibacillus* suggested natural selection under high temperature and high osmotic pressure during fermentation. The detection of *Saccharopolyspora* and *Desmospora* suggested active biosynthesis of secondary metabolites. These metabolites may have contributed to aging-related properties and characteristic aroma formation. Although genus-level relative abundances fluctuated among samples, core taxa such as *Bacillus* and *Kroppenstedtia* remained dominant. This result indicated strong directional selection imposed by the fermentation process, which supported stability and adaptability of key functional taxa. Such stability was closely linked to processing conditions, fermentation environment, and regional features.

For fungi, the dominant phyla mainly comprised *Ascomycota* and *Mucoromycota* (Figure 3f). *Ascomycota* was overwhelmingly dominant, with a relative abundance of 66.7% to 98.8%. *Mucoromycota* and *Basidiomycota* showed lower abundance and larger variation across samples. In particular, *Ascomycota* remained the leading phylum in all samples. In Daqu_A and Daqu_F, the relative abundance was 84.57% to 88.45% and 97.89% to 98.84%, respectively. As major fungal groups during Daqu fermentation, members of *Ascomycota* played important roles in organic matter degradation, fermentation participation, and synthesis of flavor components.

At the genus level, the major fungal genera included *Aspergillus*, *Paecilomyces*, *Rasamsonia*, *Talaromyces*, *Lichtheimia*, *Monascus*, and *Penicillium* (Figure 3g). Clear differences in relative abundance were observed among samples, reflecting diversity in fungal community structures. *Aspergillus* showed notable abundance, particularly in Daqu_A at 18.39% to 19.78%. *Aspergillus* was known to secrete abundant hydrolases such as amylases and proteases. These enzymes efficiently degraded starch and proteins into reducing sugars and amino acids. Such metabolites provided essential carbon and nitrogen sources for yeasts and other functional microbes. In addition, its metabolism could generate various volatiles and directly enrich the flavor profile.

Paecilomyces showed stable abundance in most samples. In Daqu_A and Daqu_E, it reached 18.76% to 22.49% and 24.36% to 24.69%, respectively. This genus contributed to organic-matter degradation and played important roles in producing 2-phenylethanol, benzaldehyde, and benzeneacetic acid ester-related compounds, and in maintaining fermentation stability. *Monascus* showed distinctive roles in Daqu. Its pigment-producing capacity and involvement in amino acid metabolism may influence flavor and color. Its metabolites also suggested potential health-related effects such as antioxidant and antimicrobial activities. *Rasamsonia* showed relatively high abundance, particularly in Daqu_B and Daqu_C at 11.79% to 16.56% and 17.99% to 19.30%. These taxa may have participated in biosynthesis of secondary metabolites during fermentation. *Talaromyces* and *Lichtheimia* were lower in abundance, indicating more limited roles in certain samples. In Daqu_F, *Lichtheimia* was 0.27% to 0.77%, indicating low activity.

Overall, strong differences were observed at the fungal genus level. Although *Aspergillus* and *Paecilomyces* were core dominant genera, their abundances varied among samples. Other genera such as *Rasamsonia* and *Talaromyces* dominated in specific

https://doi.org/10.3390/foods15030599

samples. This pattern indicated that microbial communities during Daqu fermentation were shaped by multiple environmental factors and showed strong regional and process-dependent features.

3.7. Correlations Between Dominant Bacterial and Fungal Genera and 14 Key Compounds in Sauce-Aroma High-Temperature Daqu Samples

Correlations between dominant bacterial and fungal genera and the 14 key compounds were analyzed to clarify the complex links between microbial communities and flavor and aroma compounds in Daqu fermentation. The results indicated that bacteria and fungi not only produced specific compounds through metabolism, but also shaped flavor formation through interspecies interactions during fermentation.

As shown in Figure 4, the correlation analysis suggested that *Aspergillus*, *Paecilomyces*, *Monascus*, *Bacillus*, *Kroppenstedtia*, and *Lentibacillus* exerted marked influences on flavor generation during Daqu fermentation. In the bacterial analysis, *Bacillus* exhibited significant positive correlations with several key compounds, particularly with acetic acid. This pattern indicated that metabolically active *Bacillus* might have promoted acetic acid formation. As an important organic acid in Daqu fermentation, acetic acid directly affected sourness and flavor complexity. In addition, a positive association between *Bacillus* and 1,2,3,4-tetramethoxybenzene suggested that this genus might have facilitated the formation of aromatic compounds, thereby enhancing the layering of Daqu aroma. In contrast, *Lentibacillus* showed negative correlations with multiple flavor compounds such as (E)-2-pentenal and dimethyl trisulfide. This negative relationship implied that *Lentibacillus* might have suppressed the formation of these compounds via metabolic regulation, thereby influencing overall flavor.

In the fungal analysis, *Monascus* showed a significant positive correlation with acetic acid. This result suggested that *Monascus* might have promoted acetic acid formation through its metabolic activity, which strengthened sourness and increased aroma intensity. A positive association between *Monascus* and 1,2,3,4-tetramethoxybenzene also suggested that this fungus might have enhanced the generation of certain aromatic compounds, adding complex aromatic layers to the flavor profile. By contrast, *Paecilomyces* and *Penicillium* exhibited negative correlations with flavor compounds such as 5-methyl-2-phenyl-2-hexenal and decanal. This pattern indicated that these fungi might have inhibited the formation of these compounds through metabolism, thereby modulating aroma characteristics [82].

Members of the genus *Virgibacillus* are ubiquitous bacteria in Daqu, with previous surveys highlighting them as dominant taxa in high-temperature Daqu (HTD). Specifically, research into the microecological divergence of black, yellow, and white Daqu indicated a markedly higher relative abundance of *Virgibacillus* in yellow Daqu compared to the other two types. While the functional contributions of *Virgibacillus* to fermentation are not yet fully elucidated, initial findings suggest it is among six "chameleon microorganisms" that play a fundamental role in the microecological differentiation of HTD [14,83,84].

The analysis of positively correlated microorganisms indicated that *Bacillus* and *Monascus* played promoting roles in flavor formation. *Bacillus* appeared to enhance sourness and enrich flavor layering by promoting acetic acid formation. *Monascus* appeared to deepen sourness and aroma by promoting the formation of acetic acid and aromatic compounds such as 1,2,3,4-tetramethoxybenzene. These metabolic activities contributed substantially to sourness, aroma, and overall flavor complexity. Although *Paecilomyces* and *Penicillium* showed negative correlations with certain flavor compounds, this pattern did not indicate irrelevance. Instead, negatively correlated genera such as *Paecilomyces* and *Penicillium* might have regulated flavor balance by constraining the synthesis of specific

https://doi.org/10.3390/foods15030599

compounds. Even with inhibitory tendencies, these fungi still contributed to shaping the overall aroma and flavor characteristics [85].

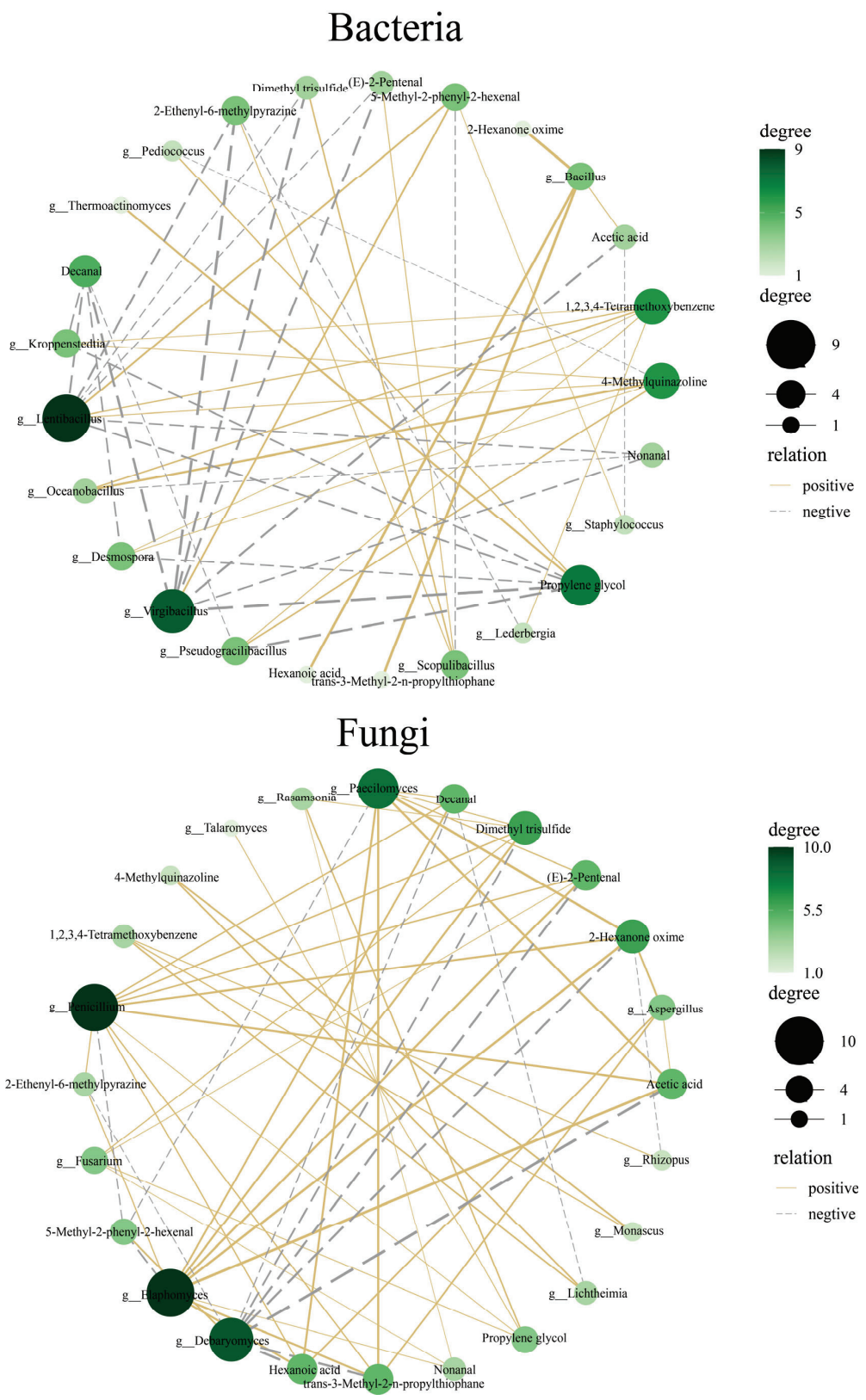


Figure 4. Correlation analysis network diagrams: The correlation network between dominant microbials and compounds of Daqu. The size of the circles is linked to the number of the edge of compounds. The thickness of lines is proportional to the value of spearman's correlation ($|\varrho| > 0.6$, $p < 0.05$).

Significantly, in open, spontaneous Daqu manufacture, environmental microorganisms can be introduced transiently, including taxa that are often treated as spoilage-associated indicators in fermented foods (e.g., members of *Enterobacteriaceae*). However, sauce-aroma high-temperature Daqu undergoes a pronounced high-temperature stage (commonly reaching 60–70 °C) together with progressive dehydration/low moisture, which collectively imposes a strong selective pressure that favors thermotolerant functional groups (e.g., *Bacillus* and other heat-adapted taxa) while suppressing the outgrowth of many mesophilic, spoilage-associated organisms [86–88]. Although heat-resistant *Enterobacteriaceae* variants can still be detected in some Daqu fermentations (indicating that high temperature is not an absolute sterilization step), their persistence is typically constrained by the combined effects of thermal stress, low water activity, and competitive starter ecology [89]. In our metagenomic profiles of mature (post-maturation) Daqu, spoilage-associated bacterial groups (e.g., *Enterobacteriaceae*) were nearly undetectable, which we interpret as a "clean" microbial signature and a practical quality indicator: it suggests that the starter has passed through the intended high-temperature selective barrier and reached a stable ecological state more likely to support consistent enzymatic functionality and reduce the likelihood of atypical fermentation trajectories or off-note risk in subsequent brewing [24,82,90,91].

Overall, correlation analysis between dominant bacterial and fungal genera and 14 key compounds revealed a complex relationship between microbial ecology and flavor and aroma compounds. The results indicated that bacteria and fungi not only produced specific compounds, but also influenced flavor formation through interactions within the community. On this basis, the following key microorganisms showing significant influences during fermentation were identified. (1) *Aspergillus* played an important role in fermentation and significantly affected flavor characteristics by promoting the formation of sourness- and aroma-related compounds. (2) *Paecilomyces* regulated flavor balance through negative correlations with multiple flavor compounds and served an important modulatory role. (3) *Monascus* positively contributed to the formation of acetic acid and aromatic compounds, thereby enhancing sourness and deepening aroma. (4) *Bacillus* contributed substantially to sourness and flavor complexity by promoting acetic acid formation. (5) *Kroppenstedtia* and *Lentibacillus* influenced flavor compound synthesis through metabolic activity and modulated flavor layering.

3.8. Discussion

A growing body of Baijiu and Daqu research has moved from single-layer profiling toward integrated flavoromics, yet many studies still treat volatile fingerprints, sensory outcomes, and process drivers as loosely connected endpoints. Against this backdrop, the present work positions sauce-aroma high-temperature Daqu quality as a stratified chemical phenotype, where a 210-compound headspace volatile matrix separates into abundance tiers and highlights pyrazines as a dominant signature. This aligns with reports that high-temperature Daqu tends to be enriched in Maillard-derived nitrogen heterocycles, with tetramethylpyrazine repeatedly recognized as a hallmark contributor to roasted and nutty impressions in sauce-flavor systems [92,93]. At the same time, the emphasis on aldehydes and sulfur volatiles as quality-associated variables is consistent with broader sauce-flavor Baijiu literature showing that carbonyls and trace sulfur odorants, despite low concentrations, can exert disproportionate sensory leverage because of low thresholds and high diffusivity [3,35].

The microbial results also resonate with well-established ecological principles of Daqu fermentation, where bio-heat and dehydration create strong selection that favors thermotolerant bacterial consortia and reduces fungal breadth, producing community trajectories that are reproducible across regions and process variants [94,95]. Dominance of *Bacillus* in

high-temperature Daqu has been widely reported and is typically interpreted through its enzyme secretion capacity and its role in generating precursor pools that feed downstream aroma formation, while *Kroppenstedtia* and related thermophiles are often discussed as environment-adapted taxa associated with high-temperature niches and characteristic flavor directionality in sauce-flavor production chains [94–96]. What this study adds relative to many sequencing surveys is the explicit linkage between dominant genera and discriminant odorants, which parallels newer work that couples microbiome shifts to volatile outputs during Daqu or heap fermentation but usually stops at correlation and pathway inference [93,97,98]. A critical reading suggests that the reported genus compound associations are best viewed as hypotheses about metabolic routing and community-level division of labor, and future causal confirmation would benefit from time-resolved multi-omics, isolate-based reconstructions, or controlled consortia fermentations that can separate production from consumption and adsorption effects [93,97].

The most distinctive scientific move is the attempt to bridge statistical discrimination and sensory coupling with receptor-level plausibility, shifting the discussion from what correlates with quality to what could be physically recognized by an odor receptor pocket under realistic chemical constraints. Traditional aroma studies in Daqu frequently rely on HS-SPME GC MS combined with GC olfactometry and OAV-based prioritization, which is powerful for identifying odor-active molecules but does not directly test whether a proposed marker set is compatible with receptor-binding logic [69]. In contrast, docking-guided interpretation follows an emerging computational chemical-senses literature where structure-based models, dynamics, and virtual screening are used to rationalize ligand recognition and to propose testable residue-level hypotheses, while also acknowledging that odor coding is multi-receptor and mixture-dependent [99–101]. Taken together, this study is scientifically unique because it connects chemical fingerprints, sensory relevance, microbial ecology, and receptor-scale mechanisms into a single quality control narrative, yielding a compact set of actionable targets that are not only statistically discriminant but also mechanistically interpretable and, therefore, more transferable across batches, sites, and process adjustments [97,99].

4. Limitations and Prospects

This study was designed as a focused, proof-of-concept mapping between trace volatiles, sensory performance, and microbial ecology, yet its statistical inferences should be interpreted as hypothesis-generating, because the dataset contains only six independent Daqu groups and the overall sensory scores are concentrated in a relatively high band from 80.6 to 93.5 on a 100-point scale. Looking ahead, expanding the sampling space across production sites, seasons, batches, and process windows is the most direct way to improve power and transportability, which is consistent with broader evidence that Daqu microbiota and flavor phenotypes are strongly temperature- and process-driven and can vary systematically under different incubation trajectories.

Because the commercial target is marketable Baijiu, an important next step is to connect Daqu markers to the sensory and chemical outcomes of the liquor itself rather than relying on Daqu sensory outcomes alone, especially since many volatiles can be lost during fermentation and distillation while additional compounds can be induced or amplified across the saccharification, fermentation, and post-distillation stages. A staged validation design could track the same batches from Daqu to fermented grains to base Baijiu and, when possible, to aged liquor, testing whether the proposed discriminant set predicts downstream aroma quality and whether any markers function as stable proxies or only as early process indicators. Embedding sensory methods that mirror distillery practice would further strengthen interpretability, since industry scoring systems integrate cues that reflect

production realities, and aligning laboratory panels with those criteria helps ensure that chemical signatures are evaluated against a commercially meaningful definition of quality.

The current scope also emphasizes headspace volatiles and amplicon profiling, so future work can broaden the mechanistic foundation by adding affordable but informative measurements, such as proximate composition, acidity and pH, soluble carbohydrates, residual starch, nonvolatile fermentation products, and especially enzyme activities that are widely recognized as critical functional outputs of Daqu microbiota. In parallel, Daqu is a dynamic culture with succession over time, so time-resolved sampling across incubation and maturation would help separate transient blooms from stable functional states, an issue repeatedly highlighted in high-temperature Daqu succession studies. Finally, the olfactory receptor modeling can be framed as a mechanistic plausibility layer that prioritizes ligands and residues for targeted validation rather than as a standalone proof of odor coding, since docking scores require experimental corroboration and odor perception is shaped by multi-receptor, mixture-dependent interactions. Future directions that fit naturally with the present framework include testing a small receptor panel with heterologous expression, using mutagenesis to probe key polar residues, and applying mixture models or competitive binding concepts to evaluate non-additivity in complex matrices.

5. Conclusions

In this study, volatile profiles and microbial communities were jointly characterized in six groups of sauce-aroma high-temperature Daqu. A total of 210 volatile trace compounds were quantified by HS-SPME-GC-MS. Fourteen chemical classes showed significant stratification across samples. The high-abundance group was dominated by pyrazines, and the separation was largely driven by tetramethylpyrazine and 2,3,5-trimethylpyrazine. OPLS-DA and VIP indicated that discriminatory signals originated from pyrazine derivatives, lipid oxidation-related aldehydes and ketones, acids and their ethyl esters, sulfur-containing compounds, and selected aromatic compounds. In sensory evaluation, aroma best explained the overall score. (E)-2-pentenal and dimethyl trisulfide were significantly and positively correlated with aroma and overall score. Receptor docking suggested that polar small molecules and hydrophobic heterocycles jointly contributed to olfactory recognition. Sequencing results showed higher bacterial diversity than fungal diversity. Dominant bacterial genera were *Bacillus*, *Kroppenstedtia*, and *Lentibacillus*. Dominant fungal genera included *Aspergillus*, *Paecilomyces*, *Monascus*, and *Penicillium*. Correlation patterns suggested that *Bacillus* and *Monascus* were more likely to promote the accumulation of acetic acid and aromatic compounds.

By integrating chemical fingerprints, sensory coupling, and microbial evidence, the core trace compounds were identified as acetic acid, hexanoic acid, (E)-2-pentenal, nonanal, decanal, dimethyl trisulfide, trans-3-methyl-2-n-propylthiophane, 2-hexanone oxime, ethyl linoleate, propylene glycol, 2-ethenyl-6-methylpyrazine, 4-methylquinazoline, 5-methyl-2-phenyl-2-hexenal, and 1,2,3,4-tetramethoxybenzene. The core microorganisms were identified as *Bacillus*, *Kroppenstedtia*, *Lentibacillus*, *Aspergillus*, *Paecilomyces*, *Monascus*, and *Penicillium*.

Supplementary Materials: The following supporting information can be downloaded at: https://www.mdpi.com/article/10.3390/foods15030599/s1. File S1. OPLS-DA of different sauce-aroma high-temperature Daqu samples (a) and model cross-validation results (b). File S2. Mechanisms by which 14 core trace components activated the olfactory receptor. Figure S1. These photos show the olfactory receptor (a) and its microscopic molecular interaction forces (b). The schematic diagrams of interactions between the olfactory receptor and the following compounds are provided in subfigures (c) to (p), respectively: Hexanoic acid, trans-3-Methyl-2-n-propylthiophane, 2-Hexanone oxime, (E)-2-Pentenal, Dimethyl trisulfide, Ethyl linoleate, Nonanal, Decanal, 4-Methylquinazoline,

5-Methyl-2-phenyl-2-hexenal, 1,2,3,4-Tetramethoxybenzene, 2-Ethenyl-6-methylpyrazine, Acetic acid, and Propylene glycol. Table S1. Concentrations of volatile components in high-temperature Daqu. Table S2. Detailed sensory evaluation dataset for sauce-aroma high-temperature Daqu.

Author Contributions: Conceptualization, D.S. and L.Y.; methodology, X.Z., Y.W. and Y.Z.; software, Y.W., Y.Z. and L.S.; validation, Y.W. and X.Z.; formal analysis, Y.W. and L.Y.; investigation, Y.Z. and L.S.; resources, D.S., X.Z., Y.W., Y.Z., L.S. and L.Y.; data cu-ration, D.S., X.Z. and L.S.; writing—original draft preparation, Y.W. and L.Y.; writing—review and editing, Y.W., Y.Z., L.S. and L.Y.; visualization, X.Z. and L.S.; supervision, L.Y. and D.S. All authors have read and agreed to the published version of the manuscript.

Funding: This research was funded by the Science and Technology Innovation Team of Moutai Institute (MTXYTD202501); Guizhou Provincial Basic Research Program (Natural Science) (QianKeHeJiChu-ZD[2025]018); The Fund of Zunyi Technology and Big data Bureau, Moutai Institute Joint Science and Technology Research and Development Project (ZunShiKeHe HZ Zi[2023]112); Research Foundation for Scientific Scholars of Moutai Institute (mygccrc[2022]011, mygccrc[2022]013); Moutai Institute & Guangdong Li'er'an Chemical Industry Group Co., Ltd. (XYNJ20240104). The APC was funded by the same funding sources listed above.

Institutional Review Board Statement: This study involves a sensory evaluation of fermented products. It does not collect sensitive personal information or involve any commercial interests. All participants are adults, and their data are anonymized. Participants were fully informed and provided written informed consent prior to participation, and they may withdraw at any time. The study complies with the Measures for the Ethical Review of Life Sciences and the regulations on Medical Research Involving Human Subjects issued by the National Health Commission (Document No. 4), specifically Article 32. Our study qualifies for an exemption from ethics review because it poses no potential risk to participants.

Informed Consent Statement: Informed consent was obtained from all subjects involved in the study.

Data Availability Statement: The original contributions presented in this study are included in the article/Supplementary Materials. Further inquiries can be directed to the corresponding author.

Conflicts of Interest: The authors declare no conflicts of interest.

Abbreviations

The following abbreviations are used in this manuscript:

AC III	Adenylyl cyclase III
ANOSIM	Analysis of similarities
bp	base pairs
cAMP	cyclic adenosine monophosphate
CD-HIT	Cluster Database at High Identity with Tolerance
Ecoul	Coulomb (electrostatic) interaction energy term
EI	electron ionization
Emodel	Glide Emodel
Evdw	van der Waals interaction energy term
GC-MS	gas chromatography–mass spectrometry
Gαolf	alpha subunit of the olfactory G protein, G(olf)
HS-SPME-GC-MS	headspace solid-phase microextraction–gas chromatography–mass spectrometry
MEGAHIT	MEGAHIT (metagenome assembly program name)
miniGs	engineered mini Gs protein
m/z	mass-to-charge ratio
NIST	National Institute of Standards and Technology
OPLS-DA	orthogonal partial least squares discriminant analysis
OPLS4	Optimized Potentials for Liquid Simulations 4
ORF/ORFs	open reading frame(s)

OR51E2	olfactory receptor family 51 subfamily E member 2
PCoA	principal coordinates analysis
RCSB PDB	Research Collaboratory for Structural Bioinformatics Protein Data Bank
RMSD	root mean square deviation
SP (Glide)	standard precision
SPME	solid-phase microextraction
VIP	variable importance in projection
vdW	van der Waals

References

1. Wang, J.; Li, Q.; Sun, Y.; Liu, J.; Jiang, Z.; Zheng, Z.; Liu, L.; Min, X.; Yu, Y.; Zheng, Q. Why does distilled liquor (Baijiu) have a yellowish color: A comprehensive analysis. *Food Chem.* **2025**, *463*, 141469. [CrossRef] [PubMed]
2. Ali, A.; Wu, Y.; Li, W.; Chen, X.; Patil, P.J.; Han, M.; Shah, H.; Zhao, L.; Li, X. Biotechnological approaches for targeted strain screening and enhancement of Daqu for quality baijiu production. *Food Biosci.* **2024**, *61*, 104885. [CrossRef]
3. Huang, Y.; Wang, L.; Li, Y.; Chen, Y.; Chen, G.; Jia, L.; Ge, Y. Comparative analysis of key flavor compounds in various baijiu types using E- nose, HS-SPME-GC-MS/MS, and HS-GC-IMS technologies. *Food Chem. X* **2025**, *29*, 102689. [CrossRef]
4. Wang, L.; Tang, P.; Zhang, P.; Lu, J.; Chen, Y.; Xiao, D.; Guo, X. Unraveling the aroma profiling of Baijiu: Sensory characteristics of aroma compounds, analytical approaches, key odor-active compounds in different Baijiu, and their synthesis mechanisms. *Trends Food Sci. Technol.* **2024**, *146*, 104376. [CrossRef]
5. Gong, J.; Ma, Y.; Li, L.; Cheng, Y.; Huang, Y. Comparative characterization and contribution of key aroma compounds in the typical base liquor of Jiang-flavor Baijiu from different distributions in the Chinese Chishui River basin. *Food Chem. X* **2023**, *20*, 100932. [CrossRef]
6. Liu, S.; Jiang, Z.; Ma, D.; Liu, X.; Li, Y.; Ren, D.; Zhu, Y.; Zhao, H.; Qin, H.; Huang, M.; et al. Distance decay pattern of fermented-related microorganisms in the sauce-flavor Baijiu producing region. *Food Biosci.* **2023**, *51*, 102305. [CrossRef]
7. Pan, F.; Qiu, S.; Lv, Y.; Li, D. Exploring the controllability of the Baijiu fermentation process with microbiota orientation. *Food Res. Int.* **2023**, *173*, 113249. [CrossRef]
8. Zhou, J.; Li, X.; Li, S.; Ding, H.; Lang, Y.; Xu, P.; Wang, C.; Wu, Y.; Liu, X.; Qiu, S. Airborne microorganisms and key environmental factors shaping their community patterns in the core production area of the Maotai-flavor Baijiu. *Sci. Total Environ.* **2024**, *912*, 169010. [CrossRef]
9. Ren, T.; Su, W.; Mu, Y.; Qi, Q.; Zhang, D. Study on the correlation between microbial communities with physicochemical properties and flavor substances in the Xiasha round of cave-brewed sauce-flavor Baijiu. *Front. Microbiol.* **2023**, *14*, 1124817. [CrossRef] [PubMed]
10. Niu, J.; Yang, Y.; Zhao, L.; Cao, N.; Xiong, X.; Yun, Z.; Yang, F.; Xu, Y.; Tu, H.; Zhong, K.; et al. Sensory Lexicon Construction and Quantitative Descriptive Analysis of Jiang-Flavor Baijiu. *Food Sci. Nutr.* **2025**, *13*, e4652. [CrossRef]
11. Chen, C.; Ni, D.; Yang, Y.; Tian, J.; Yang, F.; Ye, X. Characterizing the microbial community constructure and the metabolites among different colour Moutai Daqu. *Food Chem. X* **2025**, *26*, 102223. [CrossRef]
12. Ding, H.; Yang, J.; Cheng, M.; Li, X.; Zeng, M.; Yang, W.; Wu, Q.; Luo, X.; Zhao, J.; Li, X.; et al. Comparative characterization of key compounds of Sauce-flavored rounded-Baijiu in northern and southern China and the potential possibility of similar quality of their combined products. *Food Chem. X* **2024**, *24*, 101970. [CrossRef]
13. Li, H.; Liu, S.; Liu, Y.; Hui, M.; Pan, C. Functional microorganisms in Baijiu Daqu: Research progress and fortification strategy for application. *Front. Microbiol.* **2023**, *14*, 1119675. [CrossRef]
14. Shi, W.; Chai, L.; Fang, G.; Mei, J.; Lu, Z.; Zhang, X.; Xiao, C.; Wang, S.; Shen, C.; Shi, J.; et al. Spatial heterogeneity of the microbiome and metabolome profiles of high-temperature Daqu in the same workshop. *Food Res. Int.* **2022**, *156*, 111298. [CrossRef]
15. Zhu, Q.; Chen, L.; Peng, Z.; Zhang, Q.; Huang, W.; Yang, F.; Du, G.; Zhang, J.; Wang, L. Analysis of environmental driving factors on Core Functional Community during Daqu fermentation. *Food Res. Int.* **2022**, *157*, 111286. [CrossRef] [PubMed]
16. Du, J.; Zhang, Y.; Ning, Z.; Jiang, S.; Liu, J.; Ni, X.; Li, Q.; Yang, Q. Comparative analysis of pyrazine compounds in soy sauce aroma Baijiu from different regions and their impact on flavor profiles. *J. Food Compos. Anal.* **2025**, *148*, 108447. [CrossRef]
17. Zhao, Y.; Tian, S.; Zhang, S.; Yu, Y.; Wu, Q. Antioxidant peptides from the mixed-distillate of Baijiu fermented grains and soy sauce residue interact with flavor substances in sauce-aroma Baijiu. *LWT-Food Sci. Technol.* **2025**, *228*, 117955. [CrossRef]
18. Zhao, T.; Chen, S.; Li, H.; Xu, Y. Identification of 2-Hydroxymethyl-3,6-diethyl-5-methylpyrazine as a Key Retronasal Burnt Flavor Compound in Soy Sauce Aroma Type Baijiu Using Sensory-Guided Isolation Assisted by Multivariate Data Analysis. *J. Agric. Food. Chem.* **2018**, *66*, 10496–10505. [CrossRef]

19. Huang, Y.; Tian, J.; Hu, X.; Yang, H.; Xie, L.; Zhou, Y.; Xia, Y.; Huang, D.; He, K. Predicting the composition of aroma components in Baijiu using hyperspectral imaging combined with a replication allocation strategy-enhanced stacked ensemble learning model. *Spectrochim. Acta Part A Mol. Biomol. Spectrosc.* **2025**, *341*, 126398. [CrossRef]
20. Li, C.; Zhang, X.; Wang, S.; Lu, Z.; Chai, L.; Xu, H.; Shi, J.; Wang, S.; Yang, B.; Shen, C.; et al. Investigation on quality discrepancies of Soy Sauce Aroma Baijiu: Flavor chemical characteristics in single-source and cross-source samples. *Food Control* **2025**, *175*, 111305. [CrossRef]
21. Zhao, Y.; Huang, X.; Wang, J.; Zhang, X.; Wang, Z.; Tian, S.; Yu, Y.; Wu, Q.; Li, X. Enrichment of oligopeptides in sauce-aroma Baijiu by optimized distillation with soy sauce byproduct and their effect on Baijiu flavor. *LWT* **2024**, *201*, 116208. [CrossRef]
22. Wang, L.; Shen, Y.; Wang, X.; Gan, L.; Zhong, K.; He, Q.; Luo, A.; Gao, H. The spatial differences of the Chinese sauce aroma liquor Daqu and identification by FT-MIR spectroscopy. *Food Control* **2023**, *154*, 109990. [CrossRef]
23. Wu, X.; Zhao, X.; Wang, L.; Chen, B.; Li, F.; Tang, Z.; Wu, F. Unraveling the regional environmental ecology dominated baijiu fermentation microbial community succession and associated unique flavor. *Front. Microbiol.* **2024**, *15*, 1487359. [CrossRef]
24. Wang, L.; Cheng, Y.; Hu, X.; Huang, Y. Analysis of bacterial diversity and functional differences of Jiang-flavored Daqu produced in different seasons. *Front. Nutr.* **2023**, *9*, 1078132. [CrossRef] [PubMed]
25. Niu, J.; Yang, S.; Shen, Y.; Cheng, W.; Li, H.; Sun, J.; Huang, M.; Sun, B. What Are the Main Factors That Affect the Flavor of Sauce-Aroma Baijiu. *Foods* **2022**, *11*, 3534. [CrossRef]
26. Gong, L.; Qin, S.; Zheng, X.; Zhao, J.; Liu, M.; Zhao, M. Traceability between microbial community and environmental microbial Community in Maotai-flavor Daqu. *Food Chem. X* **2025**, *27*, 102321. [CrossRef] [PubMed]
27. Tu, W.; Cao, X.; Cheng, J.; Li, L.; Zhang, T.; Wu, Q.; Xiang, P.; Shen, C.; Li, Q. Chinese Baijiu: The Perfect Works of Microorganisms. *Front. Microbiol.* **2022**, *13*, 91904. [CrossRef]
28. Hu, Y.; Lei, X.; Zhang, X.; Guan, T.; Wang, L.; Zhang, Z.; Yu, X.; Tu, J.; Peng, N.; Liang, Y.; et al. Characteristics of the Microbial Community in the Production of Chinese Rice-Flavor Baijiu and Comparisons with the Microflora of Other Flavors of Baijiu. *Front. Microbiol.* **2021**, *12*, 673670. [CrossRef]
29. Xu, Y.; Zhao, J.; Liu, X.; Zhang, C.; Zhao, Z.; Li, X.; Sun, B. Flavor mystery of Chinese traditional fermented baijiu: The great contribution of ester compounds. *Food Chem.* **2022**, *369*, 130920. [CrossRef]
30. Zhang, P.; Liu, Y.; Li, H.; Hui, M.; Pan, C. Strategies and Challenges of Microbiota Regulation in Baijiu Brewing. *Foods* **2024**, *13*, 1954. [CrossRef] [PubMed]
31. Chen, Y.; Li, K.; Liu, T.; Li, R.; Fu, G.; Wan, Y.; Zheng, F. Analysis of Difference in Microbial Community and Physicochemical Indices Between Surface and Central Parts of Chinese Special-Flavor Baijiu Daqu. *Front. Microbiol.* **2021**, *11*, 592421. [CrossRef]
32. Xu, Y.; Wu, M.; Niu, J.; Lin, M.; Zhu, H.; Wang, K.; Li, X.; Sun, B. Characteristics and Correlation of the Microbial Communities and Flavor Compounds during the First Three Rounds of Fermentation in Chinese Sauce-Flavor Baijiu. *Foods* **2023**, *12*, 207. [CrossRef]
33. Duan, J.; Yang, S.; Li, H.; Qin, D.; Shen, Y.; Li, H.; Sun, J.; Zheng, F.; Sun, B. Why the key aroma compound of soy sauce aroma type baijiu has not been revealed yet? *LWT* **2022**, *154*, 112735. [CrossRef]
34. Wang, L.; Shen, Y.; Chen, B.; Nie, H.; Gan, L.; Luo, A.; He, Q.; Zhong, K.; Gao, H. Spatial environments of stack and layer shape the quality of Chinese sauce aroma Daqu: Characteristics, functions, and relationships. *Int. J. Food Microbiol.* **2025**, *440*, 111287. [CrossRef] [PubMed]
35. Wu, J.; Chen, R.; Li, X.; Fu, Z.; Xian, C.; Zhao, W.; Zhao, C.; Wu, X. Comprehensive identification of key compounds in different quality grades of soy sauce-aroma type baijiu by HS-SPME-GC-MS coupled with electronic nose. *Front. Nutr.* **2023**, *10*, 1132527. [CrossRef]
36. Huang, H.; Wu, Y.; Chen, H.; Hou, Y.; Wang, J.; Hong, J.; Zhao, D.; Sun, J.; Huang, M.; Sun, B. Identification of regionalmarkers based on the flavor molecular matrix analysis of sauce-aroma style baijiu. *J. Sci. Food Agric.* **2023**, *103*, 7434–7444. [CrossRef] [PubMed]
37. Xu, L.; Du, R.; Wu, Q.; Xu, Y. Species-level distribution of microbiota with secondary metabolic potential in Chinese Baijiu fermentation. *Food Biosci.* **2024**, *59*, 104231. [CrossRef]
38. Yan, Y.; Chen, S.; Nie, Y.; Xu, Y. Quantitative Analysis of Pyrazines and Their Perceptual Interactions in Soy Sauce Aroma Type Baijiu. *Foods* **2021**, *10*, 441. [CrossRef]
39. Wang, X.; Liu, G.; Chen, Y.; Dong, W.; Su, Z.; Liu, M.; Xu, N.; Song, X.; Lv, H.; Feng, X.; et al. Construction of synthetic microbial community for pyrazines metabolism in sauce-flavor Baijiu. *Syst. Microbiol. Biomanuf.* **2025**, *5*, 679–691. [CrossRef]
40. Tang, Q.; Zhang, Y.; Huang, J.; Zhou, R. Synthetic and natural microbial communities in high-temperature Daqu production: Insights into metabolic pathways and volatile organic compounds. *Food Res. Int.* **2025**, *219*, 116962. [CrossRef]
41. Shang, C.; Li, Y.; Zhang, J.; Gan, S. Analysis of Bacterial Diversity in Different Types of Daqu and Fermented Grains from Danquan Distillery. *Front. Microbiol.* **2022**, *13*, 883122. [CrossRef]
42. Ren, Q.; Jiang, F.; Zhang, Q.; Wang, L.; Zhou, Z.; Zhao, Z.; Li, L.; Yang, F. Study on the Influence of Sorghum Waxy Characteristics on the Fermentation and Flavor of Sauce-Aroma Baijiu. *J. Am. Soc. Brew. Chem.* **2025**, *83*, 499–510. [CrossRef]

43. Xiao, Z.; Li, Q.; Niu, Y.; She, Y.; Sun, Z.; Zhang, J.; Wang, Z.; Zhou, R.; Zhu, J. Mechanism of the interaction between olfactory receptors and characteristic aroma compounds in sweet orange juice. *LWT* **2024**, *207*, 116660. [CrossRef]
44. Harini, K.; Sowdhamini, R. Computational Approaches for Decoding Select Odorant-Olfactory Receptor Interactions Using Mini-Virtual Screening. *PLoS ONE* **2015**, *10*, e0131077. [CrossRef]
45. Wen, F.; Wang, M.; Zhang, L.; Duan, W.; Sun, B.; Xie, J.; Huang, M.; Sun, S.; Yang, R.; Zhang, Y. Molecular Mechanism Analysis of the Activation of Human Olfactory Receptor OR9Q2 by 4-Methylphenol. *Foods* **2025**, *14*, 3738. [CrossRef]
46. Wu, Y.; Yin, R.; Guo, L.; Song, Y.; He, X.; Huang, M.; Ren, Y.; Zhong, X.; Zhao, D.; Li, J.; et al. The Identification and Analysis of Novel Umami Peptides in Lager Beer and Their Multidimensional Effects on the Sensory Attributes of the Beer Body. *Foods* **2025**, *14*, 2743. [CrossRef] [PubMed]
47. Wu, Y.; Yin, R.; Gao, Z.; Guo, L.; Song, Y.; Zhao, D.; Sun, J.; Huang, M.; Sun, B. Mining umami peptides in lager and multidimensional sensory evaluation of the beer body integrating computational biology with modern sensomics. *Food Chem. X* **2025**, *31*, 103132. [CrossRef]
48. Unver, Y.; Tuluk, M.; Kahriman, N.; Emirik, M.; Bektas, E.; Direkel, S. New Chalcone Derivatives with Schiff Base-Thiophene: Synthesis, Biological Activity, and Molecular Docking Studies. *Russ. J. Gen. Chem.* **2019**, *89*, 794–799. [CrossRef]
49. Khan, H.; Sabbah, D.A.; Zafar, M.; Mubarak, M.S. Molecular modeling studies of coruscanone (A) core nucleus as potential antifungal agents. *Life Sci.* **2018**, *209*, 332–340. [CrossRef]
50. Coghe, S.; Benoot, K.; Delvaux, F.; Vanderhaegen, B.; Delvaux, F.R. Ferulic acid release and 4-vinylguaiacol formation during brewing and fermentation: Indications for feruloyl esterase activity in *Saccharomyces cerevisiae*. *J. Agric. Food Chem.* **2004**, *52*, 602–608. [CrossRef] [PubMed]
51. Chen, Y.; Qin, C.; Li, Q.; Hu, K.; Li, J.; Liu, S. Research Progress in Phenolic Acid Decarboxylase Derived from Microorganisms. *Food Sci.* **2024**, *45*, 323–332.
52. Mukai, N.; Masaki, K.; Fujii, T.; Kawamukai, M.; Iefuji, H. PAD1 and FDC1 are essential for the decarboxylation of phenylacrylic acids in *Saccharomyces cerevisiae*. *J. Biosci. Bioeng.* **2010**, *109*, 564–569. [CrossRef] [PubMed]
53. Mukai, N.; Masaki, K.; Fujii, T.; Iefuji, H. Single nucleotide polymorphisms of PAD1 and FDC1 show a positive relationship with ferulic acid decarboxylation ability among industrial yeasts used in alcoholic beverage production. *J. Biosci. Bioeng.* **2014**, *118*, 50–55. [CrossRef]
54. Liu, S.; Bischoff, K.M.; Anderson, A.M.; Rich, J.O. Novel Feruloyl Esterase from *Lactobacillus fermentum* NRRL B-1932 and Analysis of the Recombinant Enzyme Produced in *Escherichia coli*. *Appl. Environ. Microbiol.* **2016**, *82*, 5068–5076. [CrossRef] [PubMed]
55. Sun, L.; Lv, S.; Yu, F.; Li, S.; He, L. Biosynthesis of 4-vinylguaiacol from crude ferulic acid by *Bacillus licheniformis* DLF-17056. *J. Biotechnol.* **2018**, *281*, 144–149. [CrossRef] [PubMed]
56. Aljawish, A.; Chevalot, I.; Jasniewski, J.; Paris, C.; Scher, J.; Muniglia, L. Laccase-catalysed oxidation of ferulic acid and ethyl ferulate in aqueous medium: A green procedure for the synthesis of new compounds. *Food Chem.* **2014**, *145*, 1046–1054. [CrossRef]
57. Richard, P.; Viljanen, K.; Penttila, M. Overexpression of PAD1 and FDC1 results in significant cinnamic acid decarboxylase activity in Saccharomyces cerevisiae. *AMB Express* **2015**, *5*, 1046–1054. [CrossRef]
58. Tang, J.; Tang, X.; Tang, M.; Zhang, X.; Xu, X.; Yi, Y. Analysis of the Bacterial Communities in Two Liquors of Soy Sauce Aroma as Revealed by High-Throughput Sequencing of the 16S rRNA V4 Hypervariable Region. *BioMed Res. Int.* **2017**, *2017*, 6271358. [CrossRef]
59. Yang, L.; Fan, W.; Xu, Y. GC × GC-TOF/MS and UPLC-Q-TOF/MS based untargeted metabolomics coupled with physicochemical properties to reveal the characteristics of different type daqus for making soy sauce aroma and flavor type baijiu. *LWT* **2021**, *146*, 111416. [CrossRef]
60. Xiao, Z.; Yu, D.; Niu, Y.; Ma, N.; Zhu, J. Characterization of different aroma-types of chinese liquors based on their aroma profile by gas chromatography-mass spectrometry and sensory evaluation. *Flavour Frag. J.* **2016**, *31*, 217–227. [CrossRef]
61. Song, X.; Zhu, L.; Jing, S.; Li, Q.; Ji, J.; Zheng, F.; Zhao, Q.; Sun, J.; Chen, F.; Zhao, M.; et al. Insights into the Role of 2-Methyl-3-furanthiol and 2-Furfurylthiol as Markers for the Differentiation of Chinese Light, Strong, and Soy Sauce Aroma Types of Baijiu. *J. Agric. Food. Chem.* **2020**, *68*, 7946–7954. [CrossRef]
62. Zhu, C.; Wei, J.; Yang, Y.; Ge, X.; Yang, M.; Wu, Q.; Huang, Y. Regional fingerprint, enrichment and flavor contribution of Bacillus community in Daqu for Chinese Baijiu. *Food Res. Int.* **2025**, *211*, 116460. [CrossRef]
63. Xu, J.; Zhang, T.; Chen, H.; Dai, Y.; Li, Z.; He, J.; Ju, R.; Hou, A. Study on the Fermented Grain Characteristics and Volatile Flavor Substances during the Tuqu Fermentation of Hunan Light-Flavor Baijiu. *Foods* **2024**, *13*, 899. [CrossRef] [PubMed]
64. Tang, P.; Wang, L.; Zhao, Q.; Lu, J.; Qiao, M.; Li, C.; Xiao, D.; Guo, X. Characterization of key aroma compounds and relationship between aroma compounds and sensory attributes in different quality of high temperature Daqu. *LWT* **2024**, *194*, 115801. [CrossRef]
65. Shui, M.; Feng, T.; Tong, Y.; Zhuang, H.; Lo, C.; Sun, H.; Chen, L.; Song, S. Characterization of Key Aroma Compounds and Construction of Flavor Base Module of Chinese Sweet Oranges. *Molecules* **2019**, *24*, 2384. [CrossRef] [PubMed]

66. Duan, J.; Cheng, W.; Lv, S.; Deng, W.; Hu, X.; Li, H.; Sun, J.; Zheng, F.; Sun, B. Characterization of key aroma compounds in soy sauce flavor baijiu by molecular sensory science combined with aroma active compounds reverse verification method. *Food Chem.* **2024**, *443*, 138487. [CrossRef]
67. Yang, S.; Zhang, G.; Xu, L.; Duan, J.; Li, H.; Sun, J.; Sun, B. Investigation on the interaction between 1,3-dimethyltrisulfide and aroma-active compounds in sesame-flavor baijiu by Feller Additive Model, Odor Activity Value and Partition Coefficient. *Food Chem.* **2023**, *410*, 135451. [CrossRef]
68. Sun, J.; Wang, Z.; Sun, B. Low Quantity but Critical Contribution to Flavor: Review of The Current Understanding of Volatile Sulfur-containing Compounds in Baijiu. *J. Food Compos. Anal.* **2021**, *103*, 104079. [CrossRef]
69. Wang, Z.; Wang, S.; Liao, P.; Chen, L.; Sun, J.; Sun, B.; Zhao, D.; Wang, B.; Li, H. HS-SPME Combined with GC-MS/O to Analyze the Flavor of Strong Aroma Baijiu Daqu. *Foods* **2022**, *11*, 116. [CrossRef]
70. Niu, M.; Ma, L.; Yang, Y.; Jia, J.; Xiang, L.; Tu, T.; Zhao, X.; Shen, C.; Wang, S. Uncovering the key volatile compounds affecting the roasted aroma in sauce-flavor baijiu and their perceptual interactions. *LWT* **2025**, *237*, 118705. [CrossRef]
71. Yu, G.; Jia, X. Unlocking key odor-active compounds in cold-pressed, roasted, microwaved and steam-exploded flaxseed oils using a sensomics approach. *LWT* **2025**, *231*, 118347. [CrossRef]
72. Abeyrathne, E.D.N.S.; Nam, K.; Ahn, D.U. Analytical Methods for Lipid Oxidation and Antioxidant Capacity in Food Systems. *Antioxidants* **2021**, *10*, 1587. [CrossRef]
73. Buettner, A.; Schieberle, P. Evaluation of key aroma compounds in hand-squeezed grapefruit juice (*Citrus paradisi* Macfayden) by quantitation and flavor reconstitution experiments. *J. Agric. Food Chem.* **2001**, *49*, 1358–1363. [CrossRef]
74. Kim, M.; Sowndhararajan, K.; Choi, H.J.; Park, S.J.; Kim, S. Olfactory Stimulation Effect of Aldehydes, Nonanal, and Decanal on the Human Electroencephalographic Activity, According to Nostril Variation. *Biomedicines* **2019**, *7*, 57. [CrossRef]
75. Pignoli, G.; Bou, R.; Rodriguez-Estrada, M.T.; Decker, E.A. Suitability of saturated aldehydes as lipid oxidation markers in washed turkey meat. *Meat Sci.* **2009**, *83*, 412–416. [CrossRef]
76. Cicha-Wojciechowicz, D.; Frank, S.; Steinhaus, M.; Majcher, M.A. Key Odorants Forming Aroma of Polish Mead: Influence of the Raw Material and Manufacturing Processes. *J. Agric. Food Chem.* **2024**, *72*, 10548–10557. [CrossRef]
77. Chen, G.; Xue, Y.; Zhu, G.; Xie, H.; Zhang, J.; Xiao, W.; He, C.; Huang, J.; Liu, Z.; Wang, C. Characterization of the influence of extraction factors on instant Pu-erh tea: Focusing on changes in sensory quality and aroma profile. *Food Chem. X* **2024**, *24*, 101925. [CrossRef]
78. Han, W.; Zihan, C.; Hui, Q.; Mengyang, H.; Guoli, X.; Xingfei, L.; Yuqing, C.; Yi, D.; Suyi, Z.; Jing, Y.; et al. Seasonal influence on the microbial diversity and flavor substances in the strong flavor Daqu fermentation. *Food Chem. Mol. Sci.* **2025**, *11*, 100332. [CrossRef] [PubMed]
79. Ma, S.; Shang, Z.; Chen, J.; Shen, Y.; Li, Z.; Huang, D.; Luo, H. Differences in structure, volatile metabolites, and functions of microbial communities in Nongxiangxing daqu from different production areas. *LWT* **2022**, *166*, 113784. [CrossRef]
80. Zhu, B.; An, H.; Li, L.; Zhang, H.; Lv, J.; Hu, W.; Xue, F.; Liu, L.; He, S.; Li, D. Characterization of Flavor Profiles of Cigar Tobacco Leaves Grown in China via Headspace-Gas Chromatography-Ion Mobility Spectrometry Coupled with Multivariate Analysis and Sensory Evaluation. *ACS Omega* **2024**, *9*, 15996–16005. [CrossRef] [PubMed]
81. Tao, Y.; Bu, C.; Zou, L.; Hu, Y.; Zheng, Z.; Ouyang, J. A comprehensive review on microbial production of 1,2-propanediol: Micro-organisms, metabolic pathways, and metabolic engineering. *Biotechnol. Biofuels* **2021**, *14*, 216. [CrossRef]
82. Xu, T.; Zhu, A.; Zhong, S.; Wang, Y.; Wang, C.; Zhang, J.; Chen, Y.; Wang, R.; Zhang, C. Physicochemical properties and bioturbation analysis of high-temperature Daqu by functional microflora. *Front. Microbiol.* **2025**, *16*, 1601675. [CrossRef]
83. Yang, L.; Fan, W.; Xu, Y. Chameleon-like microbes promote microecological differentiation of Daqu. *Food Microbiol.* **2023**, *109*, 104144. [CrossRef]
84. Yang, L.; Fan, W.; Xu, Y. Qu-omics elucidates the formation and spatio-temporal differentiation mechanism underlying the microecology of high temperature Daqu. *Food Chem.* **2024**, *438*, 137988. [CrossRef] [PubMed]
85. An, Y.; Qian, Y.; Chen, S.; Qian, M.C. Aroma Comparison of Tibetan "Qjngke" Liquor with Other Chinese Baijiu. In *Sex, Smoke, and Spirits: The Role of Chemistry*; Guthrie, B., Beauchamp, J.D., Buettner, A., Toth, S., Qian, M.C., Eds.; American Chemical Society: Washington, DC, USA, 2019; pp. 225–252.
86. Yi, Z.; Jin, Y.; Xiao, Y.; Chen, L.; Tan, L.; Du, A.; He, K.; Liu, D.; Luo, H.; Fang, Y.; et al. Unraveling the Contribution of High Temperature Stage to Jiang-Flavor Daqu, a Liquor Starter for Production of Chinese Jiang-Flavor Baijiu, with Special Reference to Metatranscriptomics. *Front. Microbiol.* **2019**, *10*, 472. [CrossRef] [PubMed]
87. Wang, L. Research trends in Jiang-flavor baijiu fermentation: From fermentation microecology to environmental ecology. *J. Food Sci.* **2022**, *87*, 1362–1374. [CrossRef] [PubMed]
88. Wen, Z.; Han, P.; Han, D.; Song, L.; Wei, Y.; Zhu, H.; Chen, J.; Guo, Z.; Bai, F. Microbial community assembly patterns at the species level in different parts of the medium temperature Daqu during fermentation. *Curr. Res. Food Sci.* **2024**, *9*, 100883. [CrossRef]
89. Wang, Z.; Li, P.; Luo, L.; Simpson, D.J.; Ganzle, M.G. Daqu Fermentation Selects for Heat-Resistant *Enterobacteriaceae* and *Bacilli*. *Appl. Environ. Microbiol.* **2018**, *84*, e01483-18. [CrossRef]

90. Dong, W.; Yu, X.; Wang, L.; Zou, M.; Ma, J.; Liu, J.; Feng, Y.; Zhao, S.; Yang, Q.; Hu, Y.; et al. Unveiling the microbiota of sauce-flavor Daqu and its relationships with flavors and color during maturation. *Front. Microbiol.* **2024**, *15*, 1345772. [CrossRef]
91. Ali, A.; Wu, Y.; Li, W.; Duan, Z.; Zhang, R.; Liu, J.; Patil, P.J.; Shah, H.; Li, X. Insight into microorganisms and flavor substances in traditional Chinese fermented food starter: Daqu. *Process Biochem.* **2024**, *146*, 433–450. [CrossRef]
92. Luo, Y.; Liao, H.; Luo, Y.; Gao, L.; Xia, X. Temperature-driven microbial assembly and flavor compound dynamics in high-temperature Daqu: Adaptive co-evolution for efficient Tetramethylpyrazine production. *Int. J. Food Microbiol.* **2025**, *441*, 111325. [CrossRef]
93. Tang, P.; Li, Q.; Shan, Q.; Qin, L.; Kang, X.; Li, C.; Xiao, D.; Guo, X. Physicochemical properties, microbial community evolution, and flavor compounds during the mechanized production of Jiangxiangxing high-temperature daqu. *LWT* **2025**, *232*, 118418. [CrossRef]
94. Xiao, C.; Lu, Z.; Zhang, X.; Wang, S.; Ao, L.; Shen, C.; Shi, J.; Xu, Z. Bio-Heat Is a Key Environmental Driver Shaping the Microbial Community of Medium-Temperature Daqu. *Appl. Environ. Microbiol.* **2017**, *83*, e01550–e01617. [CrossRef] [PubMed]
95. Yuan, H.; Zheng, J.; Ding, L.; Wang, H.; Jiang, Q.; Zhang, C.; Xie, T.; Nan, G.; Li, L.; Lou, K. Temperature-Driven Divergence in Microbial Consortia and Physicochemical Functionality: A Comparative Study of High- and Medium-Temperature Daqu. *Microorganisms* **2025**, *13*, 1312. [CrossRef] [PubMed]
96. Zou, T.; Mu, Y.; Qi, Q.; Ren, T.; Su, W. Analysis of microbial community succession and its metabolic characteristics in the first and second rounds of cave-brewed sauce-flavor Baijiu. *Food Biosci.* **2024**, *60*, 104485. [CrossRef]
97. Shi, G.; Fang, C.; Xing, S.; Guo, Y.; Li, X.; Han, X.; Lin, L.; Zhang, C. Heterogenetic mechanism in high-temperature Daqu fermentation by traditional craft and mechanical craft: From microbial assembly patterns to metabolism phenotypes. *Food Res. Int.* **2024**, *187*, 114327. [CrossRef]
98. Cheng, W.; Chen, X.; Lan, W.; Liu, G.; Xue, X.; Li, R.; Pan, T.; Li, N.; Zhou, D.; Chen, X. Insights into the influence of physicochemical parameters on the microbial community and volatile compounds during the ultra-long fermentation of compound-flavor Baijiu. *Front. Microbiol.* **2023**, *14*, 1272559. [CrossRef]
99. Odoemelam, C.S.; Steuber, V.; Schmuker, M. Computational modelling of olfactory receptors. *Biochim. Et Biophys. Acta (BBA)-Gen. Subj.* **2025**, *1869*, 130825. [CrossRef]
100. Yuan, S.; Dahoun, T.; Brugarolas, M.; Pick, H.; Filipek, S.; Vogel, H. Computational modeling of the olfactory receptor Olfr73 suggests a molecular basis for low potency of olfactory receptor-activating compounds. *Commun. Biol.* **2019**, *2*, 141. [CrossRef]
101. Zeng, S.; Zhang, L.; Li, P.; Pu, D.; Fu, Y.; Zheng, R.; Xi, H.; Qiao, K.; Wang, D.; Sun, B.; et al. Molecular mechanisms of caramel-like odorant-olfactory receptor interactions based on a computational chemistry approach. *Food Res. Int.* **2023**, *171*, 113063. [CrossRef]

Disclaimer/Publisher's Note: The statements, opinions and data contained in all publications are solely those of the individual author(s) and contributor(s) and not of MDPI and/or the editor(s). MDPI and/or the editor(s) disclaim responsibility for any injury to people or property resulting from any ideas, methods, instructions or products referred to in the content.

foods

MDPI

Article

Diversity of Volatile Profiles and Nutritional Traits Among 29 Cucumber Cultivars

Panling Lu [1,†], Chunfang Wang [2,†], Yongxue Zhang [1], Haijun Jin [1], Shaofang Wu [1], Xiaotao Ding [1,*] and Hongmei Zhang [1,*]

[1] Shanghai Key Laboratory of Protected Horticultural Technology, Horticulture Research Institute, Shanghai Academy of Agricultural Sciences, 1000 Jinqi Road, Fengxian District, Shanghai 201403, China; lpl2245@163.com (P.L.); zhangyongxue@saas.sh.cn (Y.Z.); jinhaijun@saas.sh.cn (H.J.); sfwu@saas.sh.cn (S.W.)

[2] Crop Breeding & Cultivation Research Institute, Shanghai Academy of Agricultural Sciences, 1000 Jinqi Road, Fengxian District, Shanghai 201403, China; fhwcf@126.com

* Correspondence: dingxiaotao@saas.sh.cn (X.D.); zhanghongmei@saas.sh.cn (H.Z.); Tel.: +86-13564084520 (H.Z.)

† These authors contributed equally to this work.

Abstract

Twenty-nine samples of two cucumber types (*Cucumis sativus* L.) were evaluated to determine the amino acid, tannin, soluble protein, soluble sugar, Vc, nitrate nitrogen contents and volatile organic compounds (VOCs). Cucumber variety differences in amino acid, tannin, soluble proteins, et al., were significant ($p < 0.05$). The VOCs were derived by headspace solid-phase microextraction (HS-SPME) coupled with gas chromatography–mass spectrometry (GC-MS). A total of 67 VOCs were identified, including 24 aldehydes, 13 alcohols, 12 ketones, 12 alkenes and 6 other compounds. (E, Z)-2,6-Nonadienal, (E)-2-Nonenal and (E)-6-Nonenal were the three most abundant volatiles. A total of 21 VOCs were present in all 29 cultivars. An average of 45 kinds of VOCs were identified in each cultivar. Principal component analysis (PCA) clustered the 29 cucumber cultivars into five groups. Partial least-squares-discriminant analysis (PLS-DA) indicated that the European type was separated from the South China type across PLS1. Furthermore, 25 key differential volatiles for distinguishing 29 cultivars and 23 key differential volatiles for differentiating between South China and European types were identified, respectively. These results provide information for the development of new cultivars with high nutritional quality and intense flavor.

Keywords: cucumber; volatile compounds; Fruit quality; cultivars; HS-SPME-GC-MS

1. Introduction

Cucumber (*Cucumis sativus* L.), a member of the Cucurbitaceae family, is a globally cultivated and consumed vegetable [1]. Cucumber is very popular because of its distinctive flavor and nutritional value, which are rich in beneficial nutrients, including vitamin C, sugars, proteins, amino acids, flavonoids, and polyphenolic compounds, which contribute to human health [2]. Aroma, a crucial component of fruit flavor, is closely linked to volatile organic compounds (VOCs), and is vital for fruit quality assessment and breeding [3,4]. In recent years, with increasing consumer demand for better flavor in cucumbers, growing research is being conducted on cucumber volatile compounds [5,6]. A comprehensive analysis of the volatile compounds in cucumbers will not only provide a theoretical foundation for flavor quality improvement but also offer guidance for optimizing postharvest preservation techniques and processing technologies.

Since the 1960s, there has been significant attention on the research and regulation of flavor compounds in cucumbers [7,8]. The aromatic compounds in cucumbers are primarily composed of volatile organic substances such as aldehydes, alcohols, ketones, and esters [9]. Among them, aldehydes are the main flavor compounds in cucumbers, accounting for 56.30–83.92% of the total volatile substances, followed by alcohols [10]. Studies have shown that C6 and C9 volatile compounds are the main components of cucumber aroma [2]. C6 volatile compounds impart the characteristic fresh green and grassy notes, while C9 aldehyde has a floral aroma [11], the ratio of these two groups of components plays a decisive role in the flavor of cucumbers [12]. It has been determined based on flavor threshold and content that (E, Z)-2,6-Nonadienal and (E)-2-Nonenal are the primary aroma-active compound in cucumber fruit, playing a dominant role in its characteristic flavor [13–15]. Plant VOCs can be roughly divided into three main categories based on their synthesis pathways: the terpenoids pathway, amino acid pathway and fatty acids pathway [5,6,12]. The main aromatic compounds in cucumbers are aldehydes and alcohols, primarily produced through the fatty acid metabolic pathway. The unique aroma of cucumber is primarily derived from linoleic acid and linolenic acid, which are oxygenated under the catalysis of LOX (lipoxygenase), introducing molecular oxygen at the C13 or C9 position to form 13-hydroperoxy linolenic acid (13-HPOT) or 9-hydroperoxy linolenic acid (9-HPOT). These compounds are then converted by hydroperoxide lyase (HPL) into short-chain aldehydes and oxoacids, ultimately producing the pleasant, fresh cucumber fragrance [16,17].

Aroma is strongly dependent on genotypes. Long-term selection and breeding practices have led to the development of distinct cucumber ecotypes and market classes, such as Chinese Long (North or South China type, Japanese Long), European Long (English or Dutch cucumber), and North American slicing or pickling cucumbers [18]. In studies on cucumber fruit flavor, significant differences have been observed in flavor intensity among different cucumber genotypes. Zhang et al. analyzed the aroma compounds of three cucumber types (European greenhouse, Northern Chinese-type, and Southern Chinese-type) and found that different varieties of cucumber contain different types and amounts of VOCs [5]. Aroma is also closely related to their varietal characteristics, ripeness, and postharvest handling [17,19,20].

Various methods are available for determining volatile organic compounds (VOCs), such as dynamic headspace extraction [21], stir bar sorptive technique [22,23], and solid-phase microextraction (SPME) [24]. Solid-phase microextraction (SPME), as a simple and solvent-free technique for volatile compound extraction, has been widely used in conjunction with gas chromatography–mass spectrometry (GC-MS) for the qualitative and quantitative analysis of volatile compounds in fruits and vegetables [25,26].

Optimizing flavor is one of the primary objectives in breeding superior cucumber varieties and developing processed products. Therefore, it is essential to investigate volatile flavor compounds across different cucumber genotypes to further understand and exploit genetic resources. Current research on cucumber fruit aroma compounds has primarily focused on the identification of flavor substances within the fruit [27], the dynamic changes in aromatic compounds during different developmental stages [17], and the key factors influencing fruit flavor quality [15]. While existing studies have characterized volatile profiles in various cucumber cultivars, our understanding of the organic volatile composition in diverse breeding materials remains incomplete. Research on cucumber volatiles has largely been limited to a few cultivars, and studies systematically comparing different cucumber types are lacking. In this study, headspace solid-phase microextraction (HS-SPME) coupled with gas chromatography–mass spectrometry (GC-MS) was used to analyze the composition and concentration of volatile compounds in 29 cucumber cultivars (16 European

types and 13 South China types). The objectives were to (1) assess aroma quality at the cultivar level, (2) evaluate inter-varietal differences, thereby providing a scientific basis for future cultivation and breeding strategies, and (3) identify the essential differences in volatile compounds between European and South China cucumber types, providing the chemical rationale for their unique flavor characteristics. These findings offer critical data for mining, utilizing, and enhancing proprietary, high-quality cucumber germplasm.

2. Materials and Methods

2.1. Plant Materials

In this study, 29 Cucumber cultivars (19 inbreds and 10 F1 hybrids) were grown in the plastic greenhouse at Zhuanghang Comprehensive Experimental Station, Shanghai Academy of Agricultural Sciences, China. All cucumber cultivars were grown in a single greenhouse under standardized conditions, with soil, water, and fertilizer management maintained constant. Among them, C-1 to C-4, C-6, C-9, C-11, C-13, C-14, C-17, C-18, C-27 to C 30, C-32, C-45, C-47, and C-48 were inbreds, and CP-2, CP-3, CP-8, CP-9, CP-18, CP-22, CP-23, CP-24, CP-31, and CP-44 were hybrids. More details and pictures of cucumber fruits are listed in Figure 1 and Table S1. The fruits were harvested at 10–12 days after flowering. Nine fruits for each cultivar were harvested, each replicate containing 3 fruits. The cucumber fruit was divided into three segments based on length, and then intermediate segments were chopped into small pieces and immediately frozen in liquid nitrogen, and stored at −80 °C until analysis.

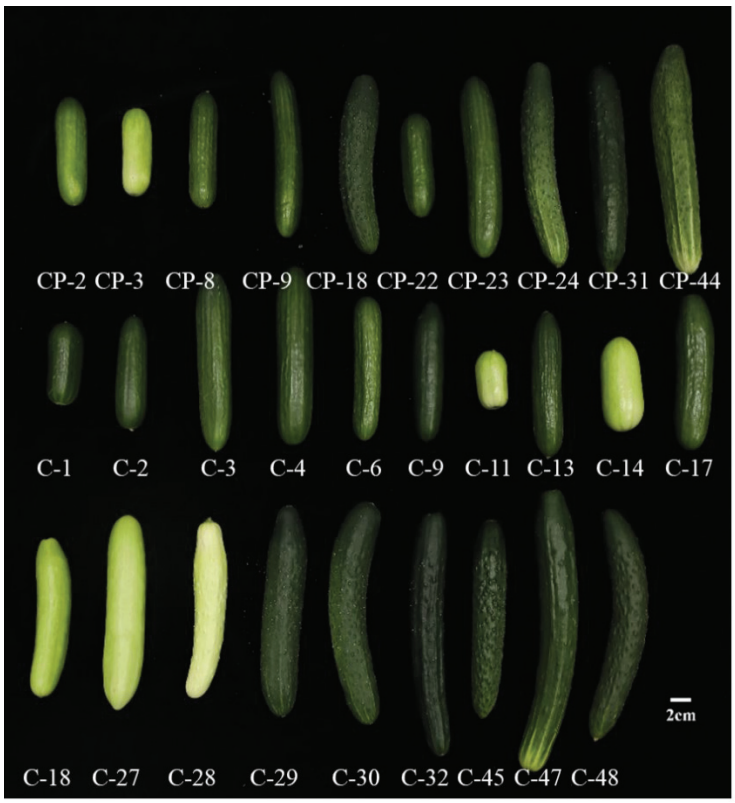


Figure 1. Materials of 29 cucumber cultivars used in this study.

2.2. Physiological Characteristics Measurement

The single fruit weight was measured by an electronic balance, fruit length and flesh thickness were determined with a straight ruler, and fruit diameter was measured by a vernier caliper. Total soluble solids (TSS) content was measured using a digital refractometer. The amino acid (ninhydrin method), tannin (Folin–Ciocalteu method), soluble

protein (Coomassie Brilliant Blue method), soluble sugar (anthrone–sulfuric acid method), Vc (2,6-dichlorophenol-indophenol titration), and nitrate nitrogen contents (salicylic acid colorimetric method) were determined using assay kits (Suzhoukeming, Suzhou, China), following the manufacturer's protocols.

2.3. HS-SPME Analysis

Before analysis, the samples were ground by a cryogenic grinding machine (JX-FSTPRP-I, Shanghai Jingxin Industrial Development Co., Ltd., Shanghai, China). The HS-SPME analysis was performed following the study described by Wei et al. [28], and the appropriate adjustments were made. For the extraction of volatile compounds, 7 g of the ground sample was added into a 20 mL vial and 1 g of NaCl and 8 μL 2-octanol solution (100 μg/L, added as internal standard) were also added. All the extractions were performed using SPME fiber composed of 50/30 μm carboxen divinylbenzene polydimethylsiloxane (CAR/DVB/PDMS) (Supelco Inc., Bellefonte, PA, USA). The extraction fiber was heated and aged for 5 min in the aging device in advance. Samples were equilibrated at 40 °C for 15 min with agitation. The fiber was inserted into the headspace of the capped vial to adsorb volatile substances for 30 min. After extraction, the fiber underwent thermal desorption in the GC inlet at 260 °C for 5.0 min.

2.4. GC–MS Analysis

GC-MS conditions were according to the procedure described by Xu et al. [29]. A GC–MS system (7890B-5977B, Agilent Technologies Inc., Palo Alto, CA, USA) equipped with a DB-WAX capillary column (30 m × 250 μm × 0.25 μm) was used for analysis. The GC temperature was programmed as follows: 40 °C held for 5 min, raised to 220 °C at 5 °C/min, then increased at 20 °C/min to 250 °C and held for 2.5 min. Helium, the carrier gas, was circulated at 1.0 mL/min at a constant flow rate in splitless mode. The temperature of the ion source was 230 °C and transfer line was 260 °C. Blank runs were conducted during sample analyses. MS fragmentation was performed under an electron ionization of 70 eV with the scan range of 29–450 m/z.

2.5. Identification and Quantification of Volatile Compounds

MassHunter software (B.07.05.2479) was used to collect the data from the GC-MS; every composition was analyzed by the computer workstation's automatic deconvolution system (AMDIS) and volatile compounds were identified by the database of NIST/EPA/NIH Mass Spectral Library (NIST 2014) according to its mass fragmentation pattern from the spectra database. Only substances with an MS matching score greater than 70% were retained. The concentration of each compound in cucumber was calculated using the internal standard method with reference to Wei's method. The calculation formula is as follows: C_x (μg/Kg) = $S_x \times C_i/S_i/1000$. C_x represents the concentration of the aroma substance; S_x represents the peak area of the aroma substance; C_i represents the concentration of internal standard 2-octanol; S_i represents the peak area of internal standard 2-octanol.

2.6. Statistical Analysis

All the data were the means of three biological replicates. Excel 2021 software was used for statistical analysis and charting of data. SPSS 22.0 software was employed for analyzing data using Duncan's multiple range tests of variance ($p < 0.05$) and significance test. The heatmap of the major volatiles was produced by TBtools-II, and the PCA and PLS-DA were produced by the online website of MetaboAnalyst 6.0 (https://www.metaboanalyst.ca).

3. Results and Discussion

3.1. Comparison of Nutrient Contents

The levels of Vc, amino acids, soluble solids, soluble sugars, soluble proteins, tannins, and nitrites in cucumbers are important indicators for evaluating their nutritional quality. The soluble solids content directly affects the nutritional quality of cucumber fruits. Meanwhile, the contents of Vc, soluble sugars, and soluble protein indirectly influence the nutritional quality of the fruits [30]. Enhancing the content of beneficial components such as Vc, amino acids, and soluble sugars, while reducing the levels of tannins and nitrites, is a primary focus in cucumber quality breeding and high-quality cultivation practices [31]. There was diversity in these nutrient contents among 29 cucumber cultivars (Table 1). The Vc and amino acids contents varied from 31.14 to 182.57 mg/kg FW and 224.54 to 782.02 mg/kg FW, with a mean of 82.32 mg/kg FW and 422.68 mg/kg FW. The soluble proteins, soluble sugars, and SSC ranged from 0.34 to 2.22 mg/g FW, 11.51 to 29.06 mg/g FW, and 3.6 and 5.37, with a mean of 0.98 mg/g FW, 19.37 mg/g FW and 4.26, respectively. The tannins and nitrate nitrogen ranged from 38.39 to 98.14 mg/kg FW and 41.97 to 237.13 mg/kg FW; the average values were 69.98 mg/kg FW and 112.92 mg/kg FW, respectively. These values are consistent with the results reported in other studies [31–33].

Table 1. Comparison of nutrient contents in 29 cucumber cultivars.

Name	Amino Acid (mg/kg)	Tannin (mg/kg)	Soluble Protein (mg/g)	SSC (° Brix)	Soluble Sugar (mg/g)	Vc (mg/kg)	Nitrate Nitrogen (mg/kg)
C-1	593.26 ± 8.39 ^{bcd}	53.77 ± 4.74 ^{lm}	0.86 ± 0.06 ^{fghi}	4.57 ± 0.15 ^{bcd}	25.21 ± 2.32 ^{bc}	71.48 ± 0.98 ^{ijkl}	95.68 ± 3.29 ^{gh}
C-2	527.80 ± 8.00 ^{bcde}	54.34 ± 1.35 ^{klm}	0.78 ± 0.03 ^{hi}	4.3 ± 0.1 ^{def}	25.89 ± 1.78 ^{ab}	69.36 ± 2.22 ^{jkl}	123.75 ± 3.92 ^{de}
C-3	782.02 ± 30.45 ^{a}	76.82 ± 4.37 ^{defg}	0.84 ± 0.04 ^{ghi}	5.17 ± 0.15 ^{a}	18.34 ± 1.11 ^{hijkl}	76.48 ± 4.66 ^{hijk}	97.19 ± 1.03 ^{gh}
C-4	625.58 ± 33.06 ^{b}	93.82 ± 3.67 ^{ab}	0.84 ± 0.03 ^{ghi}	3.97 ± 0.06 ^{fghijk}	22.63 ± 0.83 ^{bcdef}	85.68 ± 2.84 ^{ghi}	92.10 ± 4.29 ^{ghi}
C-6	609.39 ± 47.84 ^{bc}	62.52 ± 5.13 ^{hijkl}	0.86 ± 0.08 ^{fghi}	4.37 ± 0.06 ^{cde}	23.28 ± 0.49 ^{bcdef}	80.04 ± 2.40 ^{hijk}	93.76 ± 6.92 ^{gh}
C-9	487.10 ± 47.52 ^{ef}	79.84 ± 6.38 ^{cdef}	0.72 ± 0.02 ^{hij}	3.97 ± 0.06 ^{fghijk}	21.77 ± 0.15 ^{cdefg}	95.53 ± 6.20 ^{fg}	41.97 ± 3.92 ^{l}
C-11	609.43 ± 63.54 ^{bc}	98.14 ± 4.02 ^{a}	1.22 ± 0.02 ^{bcd}	4.77 ± 0.06 ^{b}	22.65 ± 0.91 ^{bcdef}	69.43 ± 5.91 ^{jkl}	145.80 ± 2.50 ^{cd}
C-13	518.46 ± 2.02 ^{cde}	57.08 ± 3.73 ^{klm}	0.54 ± 0.09 ^{ijk}	3.93 ± 0.06 ^{fghijk}	19.49 ± 0.97 ^{fghij}	65.61 ± 3.40 ^{klm}	88.42 ± 2.61 ^{ghi}
C-14	256.07 ± 64.92 ^{ij}	78.52 ± 5.39 ^{cdef}	0.43 ± 0.02 ^{jk}	3.90 ± 0.10 ^{ghijk}	17.83 ± 0.50 ^{hijkl}	31.14 ± 1.75 ^{q}	58.84 ± 3.53 ^{jkl}
C-17	408.23 ± 18.32 ^{fgh}	63.17 ± 5.21 ^{ghijkl}	0.37 ± 0.01 ^{k}	3.70 ± 0.10 ^{jk}	20.09 ± 1.61 ^{efghi}	51.67 ± 4.46 ^{mno}	89.98 ± 9.56 ^{ghi}
C-18	424.34 ± 11.85 ^{efg}	71.36 ± 4.47 ^{efghij}	0.56 ± 0.04 ^{ijk}	4.53 ± 0.06 ^{bcd}	24.02 ± 1.46 ^{bcd}	58.98 ± 4.61 ^{lmn}	123.43 ± 1.01 ^{def}
C-27	298.36 ± 13.82 ^{ij}	75.64 ± 5.84 ^{defgh}	0.75 ± 0.11 ^{hij}	5.37 ± 0.15 ^{a}	25.22 ± 0.72 ^{bc}	33.03 ± 3.16 ^{pq}	78.42 ± 2.16 ^{hij}
C-28	265.45 ± 35.51 ^{ij}	72.92 ± 5.64 ^{defghi}	1.05 ± 0.08 ^{efgh}	4.73 ± 0.23 ^{bc}	29.06 ± 2.35 ^{a}	41.02 ± 3.25 ^{opq}	100.85 ± 6.99 ^{fgh}
C-29	282.34 ± 30.04 ^{ij}	79.58 ± 5.50 ^{cdef}	0.71 ± 0.39 ^{ij}	4.03 ± 0.06 ^{efghij}	17.29 ± 1.32 ^{hijkl}	49.95 ± 1.05 ^{no}	92.56 ± 10.67 ^{ghi}
C-30	494.31 ± 33.40 ^{def}	55.05 ± 5.49 ^{klm}	0.59 ± 0.01 ^{ijk}	3.60 ± 0.10 ^{k}	18.79 ± 1.19 ^{ghijk}	50.38 ± 2.45 ^{mno}	56.68 ± 4.57 ^{jkl}
C-32	446.48 ± 34.15 ^{efg}	38.39 ± 1.11 ^{n}	0.55 ± 0.04 ^{ijk}	4.23 ± 0.15 ^{defgh}	20.22 ± 0.64 ^{defgh}	41.70 ± 4.18 ^{opq}	60.96 ± 3.00 ^{jkl}
C-45	468.09 ± 6.18 ^{ef}	61.14 ± 5.85 ^{ijklm}	0.65 ± 0.06 ^{ijk}	4.00 ± 0.10 ^{efghij}	17.19 ± 0.86 ^{hijkl}	49.81 ± 4.96 ^{no}	61.47 ± 1.15 ^{jkl}
C-47	451.30 ± 21.62 ^{efg}	91.57 ± 3.76 ^{abc}	0.34 ± 0.01 ^{k}	3.77 ± 0.06 ^{ijk}	19.68 ± 0.77 ^{fghij}	47.12 ± 3.10 ^{nop}	55.63 ± 5.09 ^{kl}
C-48	626.22 ± 36.11 ^{b}	64.47 ± 2.07 ^{ghijkl}	1.18 ± 0.05 ^{def}	4.53 ± 0.15 ^{bcd}	23.74 ± 1.10 ^{bcde}	150.19 ± 5.94 ^{b}	70.19 ± 6.22 ^{ijk}
CP-2	349.86 ± 27.48 ^{ghi}	67.80 ± 6.81 ^{fghijk}	1.36 ± 0.06 ^{bcd}	4.30 ± 0.20 ^{def}	15.26 ± 0.94 ^{klmn}	81.11 ± 6.42 ^{ghij}	198.67 ± 13.93 ^{b}
CP-3	511.60 ± 49.47 ^{cdef}	76.14 ± 2.35 ^{defgh}	2.20 ± 0.15 ^{a}	4.73 ± 0.12 ^{bc}	16.05 ± 1.34 ^{jklm}	132.55 ± 5.90 ^{c}	237.13 ± 5.14 ^{a}
CP-8	300.42 ± 30.41 ^{ij}	85.48 ± 2.56 ^{abcd}	1.46 ± 0.12 ^{bc}	4.20 ± 0.26 ^{defgh}	11.51 ± 1.46 ^{n}	123.22 ± 2.67 ^{cd}	202.94 ± 4.89 ^{b}
CP-9	276.46 ± 5.35 ^{ij}	71.28 ± 2.22 ^{efghij}	1.53 ± 0.03 ^{b}	4.30 ± 0.10 ^{def}	14.75 ± 1.3 ^{lmn}	182.57 ± 8.01 ^{a}	158.24 ± 7.41 ^{c}
CP-18	284.37 ± 22.95 ^{ij}	58.36 ± 3.18 ^{jklm}	1.20 ± 0.15 ^{bcd}	4.20 ± 0.10 ^{defgh}	17.68 ± 0.89 ^{hijkl}	124.43 ± 4.32 ^{cd}	144.82 ± 10.7 ^{cd}
CP-22	272.12 ± 16.28 ^{ij}	47.95 ± 1.77 ^{mn}	1.50 ± 0.16 ^{bc}	3.97 ± 0.12 ^{fghijk}	12.75 ± 0.38 ^{mn}	113.82 ± 7.22 ^{de}	185.12 ± 5.54 ^{b}
CP-23	318.35 ± 12.67 ^{hij}	53.18 ± 5.42 ^{lm}	1.12 ± 0.09 ^{efg}	4.27 ± 0.06 ^{defg}	15.18 ± 0.93 ^{klmn}	115.87 ± 2.32 ^{de}	204.91 ± 5.82 ^{b}
CP-24	255.73 ± 19.64 ^{ij}	80.05 ± 2.45 ^{cdef}	1.48 ± 0.09 ^{bc}	4.3 ± 0.26 ^{def}	12.55 ± 1.32 ^{mn}	103.29 ± 6.99 ^{ef}	125.64 ± 10.35 ^{d}
CP-31	290.10 ± 55.53 ^{ij}	82.45 ± 2.65 ^{bcde}	1.30 ± 0.04 ^{bcd}	4.10 ± 0.10 ^{efghi}	16.32 ± 1.00 ^{ijklm}	88.37 ± 4.66 ^{fgh}	87.60 ± 8.430 ^{ghi}
CP-44	224.54 ± 10.60 ^{j}	78.70 ± 1.38 ^{cdef}	1.29 ± 0.04 ^{bcd}	3.87 ± 0.06 ^{hijk}	17.32 ± 0.58 ^{hijkl}	103.48 ± 9.75 ^{ef}	101.83 ± 17.84 ^{efg}

Note: Values are expressed as "average concentration ± SD", and each includes three replicates. Different letters (a, b, c, d, e, f, g, h, I, j, k, l, m, n, o, p, q) indicate statistically significant differences ($p < 0.05$) among columns based on Duncan's test following the same format.

3.2. Identification of Volatile Compounds

Cucumber fruits are deeply loved by people for their unique aroma, and flavor compounds are an important indicator for evaluating fruit quality [5]. With the advancement of detection technologies, an increasing number of aromatic substances in cucumbers have been identified. GEORGIOS et al. employed capillary gas chromatography–mass spectrometry (GC/MS) to analyze the volatile components of three Greek cucumber varieties, identifying a total of 21 aroma compounds [34]. Min et al. identified 84 VOCs in 69 cucumber genotypes, including 15 unknown compounds [35]. In this study, 67 volatile

compounds were detected, including 24 aldehydes, 13 alcohols, 12 ketones, 12 alkenes, and 6 other compounds (Table 2). An average of 45 kinds of VOCs were identified in each cultivar. CP-44 had the most VOCs (51), while C-4 and C-14 had the fewest VOCs (38). More than 50 types of VOCs were identified in C-27 (50). Fewer than 45 types of VOCs were identified in C-2 (43), C-4 (38), C-6 (40), C-14 (38), CP-2 (40), CP-8 (44), CP-22 (42), and CP-23 (43) (Table 3); 21 VOCs were present in all cultivars, including Hexanal, (E)-2-Hexenal, 2-Octanone, Nonanal, (E, Z)-2,6-Nonadienal, (E)-2-Nonenal, et al. (Table S2).

Table 2. Average contents of volatile compounds (n = 3, equivalent of 2-octanol) and their distribution ranges (in parenthesis) of 29 cucumber cultivars.

Code [a]	Compounds	CAS [b]	RT (min) [c]	Average Content (μg/kg FW)
Aldehydes				
A1	Butanal, 3-methyl-	000590-86-3	4.568	6.01 (0–15.7)
A2	Pentanal	000110-62-3	4.563	1.1 (0–9.57)
A3	2-Butenal	004170-30-3	6.08	5.1 (0–15.9)
A4	Hexanal	000066-25-1	7.729	55.50 (32.87–85.95)
A5	2-Pentenal, (E)-	001576-87-0	8.885	0.94 (0–8.72)
A6	2-Pentenal, 2-methyl-	000623-36-9	9.852	2.11 (0–9.53)
A7	Heptanal	000111-71-7	11.047	1.38 (0–6.65)
A8	2-Hexenal, (E)-	006728-26-3	11.804	49.68 (34.32–76.08)
A9	Nonanal	000124-19-6	17.283	60.31 (39.09–142.35)
A10	5-Ethylcyclopent-1-enecarboxaldehyde	036431-60-4	17.566	8.02 (4.13–12.53)
A11	4-Nonenal, (E)-	002277-16-9	18.488	0.44 (0–7.08)
A12	6-Nonenal, (E)-	002277-20-5	18.718	82.20 (0–184.01)
A13	2,4-Heptadienal, (E,E)-	004313-03-5	19.63	60.17 (24.96–91.60)
A14	Benzaldehyde	000100-52-7	20.221	15.99 (0–23.01)
A15	2-Nonenal, (E)-	018829-56-6	20.923	200.70 (93.36–380.42)
A16	2,6-Nonadienal, (E,Z)-	000557-48-2	22.192	302.59 (163.06–479.77)
A17	1-Cyclohexene-1-carboxaldehyde, 2,6,6-trimethyl-	000432-25-7	22.831	11.62 (6.04–22.03)
A18	2,4-Nonadienal, (E,E)-	005910-87-2	24.695	13.54 (0–27.94)
A19	Tridecanal	010486-19-8	27.423	3.96 (1.64–7.61)
A20	4-Oxononanal	1000314-10-4	27.564	4.99 (0–17.03)
A21	Tetradecanal	000124-25-4	29.638	9.04 (3.81–18.59)
A22	Pentadecanal	002765-11-9	31.79	51.99 (18.07–108.02)
A23	cis,cis-7,10,-Hexadecadienal	056829-23-3	35.112	1.29 (0–4.08)
A24	cis-9-Hexadecenal	056219-04-6	36.147	2.51 (0.66–7.01)
Alcohols				
L1	Ethanol	000064-17-5	3.733	3.45 (2.49–6.85)
L2	1-Hexanol	000111-27-3	16.078	13.88 (2.83–32.62)
L3	3-Hexen-1-ol, (E)-	000928-97-2	16.859	1.53 (0–3.24)
L4	1-Hexanol, 2-ethyl-	000104-76-7	19.752	0.48 (0–2.04)
L5	Linalool	000078-70-6	21.221	7.64 (0–18.67)
L6	1-Octanol	000111-87-5	21.518	1.22 (0–3.86)
L7	1-Nonanol	000143-08-8	23.905	15.92 (0–44.2)
L8	3-Nonen-1-ol, (Z)-	010340-23-5	24.407	25.84 (17.55–38.05)
L9	(6Z)-Nonen-1-ol	035854-86-5	25.154	26.48 (8.42–55.49)
L10	3,6-Nonadien-1-ol, (E,Z)-	056805-23-3	25.851	18.01 (0–42.49)
L11	2,6-Nonadien-1-ol	028069-72-9	26.222	0.42 (0–7.65)
L12	Benzyl alcohol	000100-51-6	28.359	0.75 (0–5.19)
L13	11,11-Dimethyl-4,8-dimethylenebicyclo[7.2.0]undecan-3-ol	079580-01-1	36.557	1.03 (0–4.2)
Ketones				
K1	2,3-Pentanedione	000600-14-6	6.807	0.13 (0–1.9)
K2	3-Octanone	000106-68-3	13.063	6.97 (0–12.07)
K3	2-Octanone	000111-13-7	13.98	1.38 (0.79–2.18)
K4	5-Hepten-2-one, 6-methyl-	000110-93-0	15.463	0.7 (0–3.76)
K5	3-Octen-2-one	001669-44-9	17.434	8.21 (0–15.91)
K6	3,5-Octadien-2-one	038284-27-4	20.352	52.86 (37.61–72.36)
K7	3,5-Octadien-2-one, (E,E)-	030086-02-3	21.592	18.29 (0–46.01)
K8	.alpha.-Ionone	000127-41-3	28.018	1.1 (0–2.92)
K9	5,9-Undecadien-2-one, 6,10-dimethyl-, (E)-	003796-70-1	28.125	0.07 (0–0.76)
K10	trans-.beta.-Ionone	000079-77-6	29.838	11.25 (5.25–19.65)
K11	3-Buten-2-one, 4-(2,2,6-trimethyl-7-oxabicyclo[4.1.0]hept-1-yl)-	023267-57-4	30.877	1.83 (0–3.83)
K12	2(3H)-Furanone, dihydro-5-pentyl-	000104-61-0	31.492	0.15 (0–1.68)

Table 2. *Cont.*

Code [a]	Compounds	CAS [b]	RT (min) [c]	Average Content (μg/kg FW)
Alkenes				
O1	1-Octene	000111-66-0	2.64	1.61 (0–2.8)
O2	Decane	000124-18-5	5.28	0.13 (0–2.79)
O3	(1R)-2,6,6-Trimethylbicyclo[3.1.1]hept-2-ene	007785-70-8	5.651	0.96 (0–15.84)
O4	Dodecane	000112-40-3	11.633	0.1 (0–1.42)
O5	Tridecane	000629-50-5	14.819	0.41 (0–2.51)
O6	1,6-Dioxaspiro[4.4]nonane, 2-ethyl-	038401-84-2	15.985	0.08 (0–1.03)
O7	Tetradecane	000629-59-4	17.737	0.3 (0–3.54)
O8	Caryophyllene	000087-44-5	22.446	6.03 (0–28.34)
O9	Humulene	006753-98-6	24.051	9.63 (0–26.8)
O10	Nonadecane	000629-92-5	29.35	1.14 (0–2.12)
O11	Caryophyllene oxide	001139-30-6	30.755	5.39 (0–19.7)
O12	(+)-epi-Bicyclosesquiphellandrene	054274-73-6	34.332	0.33 (0–1.59)
Others				
E1	2(4H)-Benzofuranone, 5,6,7,7a-tetrahydro-4,4,7a-trimethyl-	015356-74-8	37.22	1.07 (0–6.22)
E2	Furan, 2-ethyl-	003208-16-0	3.997	7.81 (2.23–16.33)
E3	Furan, 2-pentyl-	003777-69-3	12.306	15.38 (2.06–41.29)
E4	cis-2-(2-Pentenyl)furan	070424-13-4	14.409	10.36 (0–29.52)
E5	Furan, 2-(2-propenyl)-	075135-41-0	22.636	1.3 (0–2.59)
E6	Furan, 2-(1-pentenyl)-, (E)-	036144-40-8	28.769	3.13 (0–5.3)

[a] Compound codes, [b] CAS number, [c] Retention time (min).

Table 3. Number of volatile compounds and total content of volatiles identified in the 29 cucumber cultivars.

NO	Cultivars	Number of Volatile Compounds	Total Content (μg/kg FW)
1	CP-3	45	1187.8 ± 133.89^{efgh}
2	CP-8	44	1047.63 ± 56.3^{hi}
3	CP-9	46	916.15 ± 73.22^{ij}
4	CP-22	42	1146.39 ± 37.35^{fgh}
5	CP-23	43	1116.71 ± 104.9^{gh}
6	C-1	45	1167.1 ± 74.95^{efgh}
7	C-2	43	1236.5 ± 51.64^{defg}
8	C-3	46	1121.65 ± 75.33^{gh}
9	C-4	38	1332.14 ± 28.61^{cde}
10	C-6	40	1142.65 ± 50.04^{fgh}
11	C-9	45	1802.38 ± 53.11^{a}
12	C-11	47	1390.91 ± 42.11^{cd}
13	C-13	44	1172.3 ± 18.71^{efgh}
14	C-14	38	1564.49 ± 112.04^{b}
15	C-17	48	1473.07 ± 155.47^{bc}
16	C-18	47	1571.32 ± 78.57^{b}
17	C-27	50	1296.37 ± 97.21^{def}
18	C-28	45	1630.5 ± 188.25^{b}
19	C-29	45	1086.09 ± 71.26^{gh}
20	C-30	46	1042.61 ± 107.14^{hi}
21	C-32	49	1294.13 ± 98.03^{def}
22	C-45	48	1037.35 ± 105.59^{hi}
23	C-47	45	1562.69 ± 81.07^{b}
24	C-48	49	1099.04 ± 126.96^{gh}
25	CP-2	40	1076.46 ± 111.91^{ghi}
26	CP-18	47	1374.38 ± 61.57^{cd}
27	CP-24	47	1059.67 ± 20.6^{hi}
28	CP-31	45	771.34 ± 66.75^{j}
29	CP-44	51	1125.12 ± 76.06^{fgh}

Note: Values are expressed as "average concentration ± SD", and each includes three replicates. Different letters (a, b, c, d, e, f, g, h, i, j) indicate statistically significant differences ($p < 0.05$) among columns based on Duncan's test.

The formation of cucumber aroma is attributed to a combination of various volatile compounds, with the composition and concentration of these aromatic substances demon-

strating distinct patterns across different varieties [9]. In this study, the VOCs of the 29 varieties showed significant differences, ranging from 771.34 ± 66.75 μg/kg FW to 1802.38 ± 53.11 μg/kg FW (Table 3). C-9 had the highest content of VOCs, followed by C-28 (1630.5 ± 188.25 μg/kg FW) and C-18 (1571.32 ± 78.57 μg/kg FW), while CP-31 (771.34 ± 66.75 μg/kg FW) had the lowest content. C-9 were 2.3-fold greater than those in CP-31. An analysis of total volatile compounds in 15 F1 cucumber hybrids derived from 4 maternal and 10 paternal parents by Min et al. revealed that the total volatile content in the F1 generation was lower than the mid-parent value, particularly in terms of ethanol content [35]. In this study, CP-31 (a hybrid cultivar) exhibited the lowest volatile content, while C-9 (an inbred line) showed the highest volatile content, which is consistent with the aforementioned research findings.

3.3. Composition and Concentration of Volatile Compounds

Aldehydes, alcohols, ketones, alkenes, and other VOCs were identified in 29 cucumber cultivars; the composition and concentration of VOCs are shown in Table S3. For all cultivars, the main types were aldehydes and alcohols (Table 4), which contributed to 80–90% of the total volatile content (Table S4), similar to previous studies [15]. While the consensus is that aldehydes and alcohols are the main substances responsible for the formation of cucumber flavor, this does not mean that other volatile compounds can be overlooked [14]. This is because aroma depends not only on the concentration of volatiles but also on their thresholds [36]. Among these VOCs, major volatiles (16 types, average content > 15 μg/kg FW) are presented in Figure 2. As shown in Table 2, (E, Z)-2,6-Nonadienal (A16), (E)-2-Nonenal (A15), (E)-6-Nonena (A12), Nonanal (A9), (E, E)-2,4-Heptadienal (A13), Hexanal (A4), Pentadecanal (A22), and 3,5-Octadien-2-one (K6) were the most abundant volatiles (average content > 50 μg/kg FW) in 29 cucumber cultivars.

Table 4. Total content (μg/kg FW) of each type of volatiles in 29 cucumber cultivars.

Cultivars	Aldehydes	Alcohols	Ketones	Alkenes	Others
C-1	895.1 ± 54.65 ^{hijkl}	80.14 ± 10.55 ^{kl}	113.30 ± 12.88 ^{defg}	49.41 ± 1.60 ^{b}	29.17 ± 3.45 ^{efgh}
C-2	1002.69 ± 41.44 ^{gfh}	70.35 ± 1.64 ^{l}	118.88 ± 5.63 ^{cde}	3.93 ± 0.57 ^{ij}	40.65 ± 4.35 ^{bcde}
C-3	860.42 ± 57.35 ^{ijklm}	78.76 ± 4.89 ^{kl}	98.15 ± 8.86 ^{gh}	37.00 ± 1.52 ^{cd}	47.33 ± 3.10 ^{bc}
C-4	1097.62 ± 38.57 ^{def}	86.13 ± 2.46 ^{jkl}	99.72 ± 3.38 ^{fgh}	20.53 ± 21.02 ^{ef}	28.16 ± 9.2 ^{efghi}
C-6	980.68 ± 50.43 ^{fghi}	73.18 ± 0.70 ^{kl}	72.89 ± 2.87 ^{jk}	0.83 ± 0.07 ^{j}	15.08 ± 0.99 ^{ghi}
C-9	1531.18 ± 36.56 ^{a}	99.48 ± 7.18 ^{hij}	104.92 ± 6.8 ^{efgh}	32.76 ± 2.29 ^{d}	34.06 ± 1.59 ^{cdef}
C-11	1094.46 ± 39.67 ^{def}	90.62 ± 5.64 ^{ijk}	125.65 ± 3.73 ^{bcd}	46.45 ± 0.49 ^{b}	33.74 ± 0.50 ^{cdef}
C-13	966.76 ± 16.87 ^{ghij}	68.68 ± 3.70 ^{l}	108.40 ± 2.74 ^{efgh}	3.49 ± 0.12 ^{ij}	24.98 ± 1.61 ^{efghi}
C-14	1312.05 ± 95.82 ^{b}	118.93 ± 2.55 ^{fgh}	66.81 ± 1.79 ^{kl}	23.39 ± 0.95 ^{e}	43.32 ± 13.43 ^{bcd}
C-17	1143.73 ± 113.81 ^{cde}	71.69 ± 3.12 ^{l}	139.37 ± 7.73 ^{ab}	43.76 ± 2.56 ^{bc}	74.52 ± 30.13 ^{a}
C-18	1224.38 ± 60.35 ^{bc}	85.43 ± 6.44 ^{jkl}	134.24 ± 6.55 ^{ab}	73.59 ± 4.37 ^{a}	53.68 ± 4.45 ^{b}
CP-3	955.40 ± 108.83 ^{ghijk}	111.63 ± 10.12 ^{fgh}	77.38 ± 10.12 ^{jk}	23.12 ± 2.78 ^{e}	20.25 ± 2.65 ^{fghi}
CP-8	828.83 ± 45.95 ^{klmno}	119.53 ± 9.39 ^{fgh}	81.21 ± 0.85 ^{ijk}	9.95 ± 0.28 ^{ghi}	8.13 ± 0.1 ^{i}
CP-9	701.32 ± 58.68 ^{p}	108.67 ± 5.28 ^{gh}	78.15 ± 9.06 ^{jk}	12.52 ± 0.71 ^{fgh}	15.47 ± 1.08 ^{ghi}
CP-22	886.13 ± 29.44 ^{hijklm}	122.15 ± 4.57 ^{fgh}	114.17 ± 7.22 ^{def}	12.79 ± 0.49 ^{fgh}	11.14 ± 4.18 ^{hi}
CP-23	892.26 ± 88.23 ^{hijkl}	97.87 ± 5.97 ^{hij}	103.91 ± 9.10 ^{efgh}	7.66 ± 0.90 ^{hij}	15.00 ± 1.26 ^{ghi}
C-27	925.38 ± 60.8 ^{ghijk}	104.86 ± 6.29 ^{ghi}	139.89 ± 8.48 ^{ab}	36.29 ± 3.07 ^{cd}	89.95 ± 22.21 ^{a}
C-28	1201.66 ± 136.22 ^{bcd}	179.85 ± 21.47 ^{bc}	131.08 ± 15.93 ^{abc}	36.77 ± 3.74 ^{cd}	81.15 ± 11.37 ^{a}
C-29	782.44 ± 60.44 ^{lmnop}	112.17 ± 3.86 ^{fgh}	104.69 ± 8.91 ^{efgh}	33.51 ± 1.83 ^{d}	53.27 ± 3.81 ^{b}
C-30	711.16 ± 73.91 ^{op}	190.02 ± 14.81 ^{ab}	84.07 ± 9.19 ^{ij}	23.14 ± 2.51 ^{e}	34.22 ± 7.59 ^{cdef}
C-32	850.30 ± 62.87 ^{jklmn}	202.17 ± 16.08 ^{a}	141.72 ± 9.64 ^{a}	16.85 ± 1.51 ^{efg}	83.09 ± 7.96 ^{a}
C-45	745.79 ± 68.30 ^{nop}	144.67 ± 16.58 ^{e}	77.42 ± 7.76 ^{jk}	24.14 ± 4.39 ^{e}	45.32 ± 9.20 ^{bcd}
C-47	1188.44 ± 55.88 ^{cd}	105.51 ± 5.34 ^{ghi}	119.72 ± 6.72 ^{cde}	70.88 ± 5.73 ^{a}	78.15 ± 7.50 ^{a}
C-48	780.50 ± 84.15 ^{lmnop}	131.27 ± 7.32 ^{ef}	95.14 ± 17.85 ^{hi}	43.42 ± 4.72 ^{bc}	48.73 ± 14.68 ^{bc}
CP-2	886.40 ± 76.29 ^{hijklm}	104.18 ± 23.57 ^{ghi}	56.86 ± 5.22 ^{l}	9.10 ± 2.59 ^{ghij}	19.92 ± 6.38 ^{fghi}
T CP-18	1041.32 ± 43.66 ^{efg}	162.39 ± 10.68 ^{d}	104.52 ± 5.24 ^{efgh}	14.30 ± 0.76 ^{fgh}	51.85 ± 2.61 ^{b}
CP-24	759.19 ± 22.22 ^{mnop}	165.94 ± 1.46 ^{cd}	112.88 ± 1.90 ^{defg}	11.83 ± 0.41 ^{ghi}	9.82 ± 1.29 ^{i}
CP-31	548.39 ± 52.23 ^{q}	128.54 ± 4.54 ^{efg}	75.36 ± 6.67 ^{jk}	10.44 ± 0.78 ^{ghi}	8.62 ± 2.86 ^{i}
CP-44	790.52 ± 54.65 ^{lmnop}	170.87 ± 8.07 ^{cd}	105.24 ± 6.26 ^{efgh}	24.87 ± 1.51 ^{e}	33.61 ± 5.69 ^{cdef}

Note: Values are expressed as "average concentration ± SD", and each includes three replicates. Different letters (a, b, c, d, e, f, g, h, I, j, k, l, m, n, o, p, q) indicate statistically significant differences ($p < 0.05$) among columns based on Duncan's test.

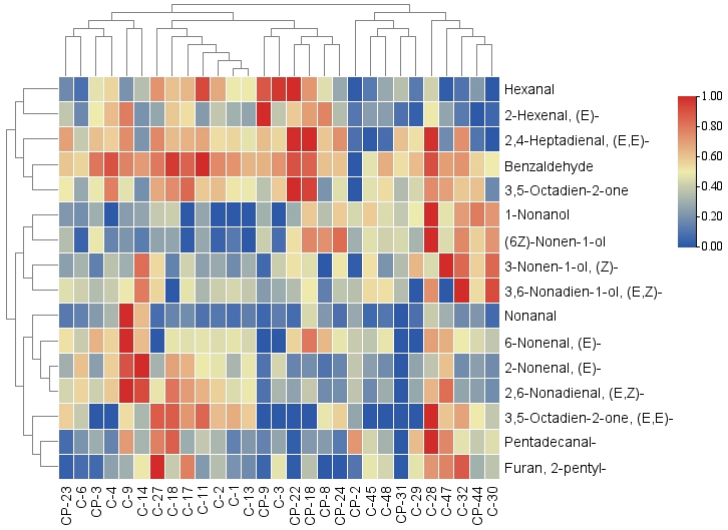


Figure 2. Contents (as shown by heatmap) and hierarchical cluster analysis of the major volatiles (average content > 15 μg/kg FW) in the fruits of 29 cucumber cultivars.

3.3.1. Aldehydes

Aldehydes were the most abundant volatiles in cucumber; among all cultivars, twenty-four aldehydes were identified (Table 2), accounting for between 65.71% (C-32) and 85.83% (C-6) (Table S4); the average value was 76.64%, which is similar to previous studies [10,15]. The content of aldehydes varies significantly among different cucumber cultivars; the highest total aldehyde content was observed in C-9 (1531.18 ± 36.56 μg/kg FW), accounting for 84.95% of the total VOCs, while the lowest was found in CP-31 (548.39 ± 52.23 μg/kg FW), making up 71.10% of the total VOCs (Table S4). Among the aldehydes, (E, Z)-2,6-Nonadienal (A16) was the most abundant (163.06 ± 13.57 to 479.77 ± 5.25 μg/kg FW), followed by (E)-2-Nonenal (A15) (93.36 ± 10.27 to 380.42 ± 36.91 μg/kg FW) and (E)-6-Nonenal (A12) (0 to 184.01 ± 5.67 μg/kg FW) (Table S3). A total of nine aldehydes had average concentrations exceeding 15 μg/kg FW including the three mentioned above, as well as Hexanal (A4), (E)-2-Hexenal (A8), Nonanal (A9), (E, E)-2,4-Heptadienal (A13), Benzaldehyde (A14), and Pentadecanal (A22) (Table 2 and Table S3). Among these aldehydes, eleven compounds were identified in all cultivars (Table S2). (E, Z)-2,6-Nonadienal is primarily responsible for cucumber's flavor, imparting a fresh cucumber scent, and (E)-2-Nonenal is the second most important odor compound in cucumbers [37]. These two compounds have low odor thresholds and significantly influence the flavor of cucumber fruits [38]. In this study, C-9 had a higher content of (E, Z)-2,6-Nonadienal than other cucumber cultivars, up to 479.77 ± 5.24 μg/kg FW. C-14 had a higher content of (E)-2-Nonenal, up to 380.42 ± 36.91 μg/kg FW. Previous studies have indicated that a higher ratio of (E, Z)-2,6-Nonadienal to (E)-2-Nonenal correlates with a more intense fresh cucumber-like flavor [17]. The highest and lowest ratios were found in CP-24 and C-17, respectively. The average ratio is slightly smaller in European-type cucumbers compared to the South China type, but the difference is not significant. Hao et al.'s study demonstrated that (E)-6-Nonenal, Hexanal, (E)-2-Hexenal, Nonanal, and (E,E)-2,4-Heptadienal are also characteristic aroma compounds in cucumber, based on odor activity value (OAV) calculations [10,17]. The flavor of cucumbers is closely related to their genotypes. JO et al. found that the contents of most aldehydes, including 2,6-Nonadienal, Propanal, Pentanal, 2,4-Nonadienal, 2-Octenal, Tetradecanal, Hexadecanal, Hexanal, and 2-Hexenal, were relatively lower in the Korean group of cucumbers compared to other types such as Japanese, Chinese, and European cucumbers [9]. In our study, we did not find a similar pattern, which is likely attributable to the large sample size of the same cucumber type.

3.3.2. Alcohols

In this study, a total of thirteen alcohols were detected, accounting for 4.87% (C-17) to 18.23% (C-30) of the total VOCs, with an average contribution of 9.84% (Table S4). Alcohol content varied considerably among different cultivars. The highest total alcohol content was observed in C-32 (202.17 ± 16.08 μg/kg FW, 15.62% of total VOCs), while the lowest was in C-13 (68.68 ± 3.7 μg/kg FW, 5.86% of total VOCs). 1-Nonanol (L7), (Z)-3-Nonen-1-ol (L8), (6Z)-Nonen-1-ol (L9), and (E, Z)-3,6-Nonadien-1-ol (L10) were the main alcohol compounds (Table 2, >15 μg/kg). Among these, (6Z)-Nonen-1-ol and (Z)-3-Nonen-1-ol exhibited the highest concentrations, at 26.48 μg/kg FW (ranging from 8.42 ± 1.3 to 55.49 ± 7.37) and 25.84 μg/kg FW (ranging from 17.55 ± 5.89 to 38.05 ± 2.21), respectively. Four alcohols were detected in all cultivars, including Ethanol (L1), 1-Hexanol (L2), (Z)-3-Nonen-1-ol (L8), and (6Z)-Nonen-1-ol (L9) (Table 2 and Table S3). Previous studies indicate that (6Z)-Nonen-1-ol and (E, Z)-3,6-Nonadien-1-ol contribute floral notes, and (E)-2-hexene-1-ol and (E)-3-hexene-1-ol possess a distinctive grassy aroma [17]. Therefore, alcohols also have a large influence on cucumber flavor.

3.3.3. Ketones

Ketones have a floral and fruity sweet flavor [39]. Twelve ketones were identified, contributing between 4.27% (C-14) and 10.95% (C-32) of the total VOCs, with an average of 8.42% (Table S4). C-32 had the highest content (141.72 ± 9.64 μg/kg FW, 10.95% of total volatiles) of all ketones, followed by C-27 (139.89 ± 8.48 μg/kg FW, 10.79% of total volatiles) and C-17 (139.37 ± 7.73 μg/kg FW, 9.46% of total volatiles), whereas C-14 had the lowest total ketones (66.81 ± 1.79 μg/kg FW, 4.27% of total volatiles) (Table S4). 3,5-Octadien-2-one and (E, E)-3,5-Octadien-2-one were the main ketones (Table 2, >15 μg/kg), accounting for 69.30% of all ketones. 2-Octanone, 3,5-Octadien-2-one, and trans-beta-Ionone were the three ketones present in all cucumber cultivars.

3.3.4. Alkenes

A total of 12 alkenes compounds were detected in 29 cucumber fruits, accounting for 0.07% (C-6) to 4.68% (C-18) of the total VOCs, with an average of 2.04% (Table S4). C-18 had the highest total olefins (73.59 ± 4.37 μg/kg FW, 4.68% of total volatiles), while C-6 had the lowest total alkenes (0.83 ± 0.07 μg/kg FW, 0.07% of total volatiles). The principal alkenes were Caryophyllene and Humulene; however, they were not identified in all cucumber cultivars, and no alkenes present in all cucumber cultivars.

3.3.5. Others

One ester and five furans were found, constituting 0.78% to 6.94% of the total volatile substances (Table S4). Esters constitute the main body of aromatic compounds and impart the characteristic aroma to various fruits and vegetables such as apples and melons [40,41]. Furan is an oxygen-containing heterocyclic compound that imparts fruity and fresh aromas [42]. 2-pentyl-Furan (F2) had the highest content, ranging from 2.06 ± 0.23 μg/kg in cultivar CP-8 to 41.29 ± 11.43 μg/kg in cultivar C-27 (Tables 2 and S3). 2-ethyl-Furan(F1) and 2-pentyl-Furan (F2) were detected in all cultivars. It has been reported that the furan compound contents in cucumbers of the North China type and South China type are higher than in the European type [43], but no similar pattern was observed in this study.

3.4. Analysis of Volatile Compounds

Principal component analysis (PCA) is an unsupervised clustering method, often used to provide a partial visualization of data in dimensionality reduction plots, and it has been widely applied in the study of volatile components [44,45]. Principal component

analysis (PCA) was performed to confirm the differences in 67 VOCs among 29 breeding lines cultivar. Overall, 67 VOCs could be simplified into four principal components (PCs), with a cumulative variance contribution rate of 53.7%. The first two principal components (PCs) accounted for 33.9%, PC1 and PC2 represented 20.5% and13.4% of the total variance, respectively (Figure 3A). The 29 cultivars were divided into five groups based on the relationship between scores and loadings (Figure 3B). The first group included three cultivars (C-27, C-28, C-47), which contained high relative contents of Pentadecanal (A22), Tridecanal (A19), cis-9-Hexadecenal (A24), and cis-2-(2-Pentenyl) furan (E4). The second group contained one cultivar (C-18) characterized by high relative contents of (E, Z)-2,6-Nonadienal (A16) and (E)-2-Nonenal (A15). The third group contained twelve cultivars (C-1, C-2, C-3, C-4, C-9, C-11, C-13, C-14, C-17, CP-2, CP-3, CP-23) characterized by high relative contents of (+)-epi-Bicyclosesquiphellandrene (O12). The fourth group contained four cultivars (CP-8, CP-9, CP-22, CP-31) characterized by high relative contents of 2-Pentenal, 2-methyl- (A6), and 2-Butenal (A3). The fifth group contained eight cultivars (C-29, C-30, C-32, C-48, C-45, CP-18, CP-24, CP-44) characterized by high relative contents of 1-Octanol (L6), 1-Nonanol (L7), 1-Hexanol (L2), and 3-Hexen-1-ol, (E)- (L3). It is worth noting that the cultivars of the European type and South China type exhibit distinct separation, although a small number of varieties still show overlap (Figure 3C). The cultivars of the South China type were characterized by high relative contents of Pentadecanal (A22), Tridecanal (A19), cis-9-Hexadecenal (A24) and cis-2-(2-Pentenyl) furan (E4), 1-Octanol (L6), 1-Nonanol (L7), 1-Hexanol (L2) and 3-Hexen-1-ol, and (E)- (L3) (Figure 3D). Varieties within the same group do not necessarily belong to the same ecotype; the third and fourth groups contain both European-type and South China-type. A similar result was also observed by Shi et al. [26] and Min et al. [35].

Partial least-squares-discriminant analysis (PLS-DA), a supervised classification technique, is widely applied to create multivariate models that predict features, differentiate samples, and screen for key biomarker variables [46]. Therefore, PLS-DA was performed to elucidate the differences among 29 cultivars in more detail. The results of the permutation test (R2 = 0.717, Q2 = 0.681) and (R2 = 0.833, Q2 = 0.783) demonstrated that both models exhibited favorable fitting without the risk of overfitting. $Q2 > 0.5$ is generally considered to indicate that the model has good predictive ability [47]. Previous studies show that PLS-DA model analysis could cluster cucumbers together depending on the geographical group to which they belong [9]. In this study, PLS-DA models from VOC analysis revealed that the cucumber fruit clustered together depending on the types. The European type was separated from the South China type across PLS1 (18.2%) (Figure 4A). The result of the loading plot was consistent with the PCA loading plot. The cultivars of South China-types have high relative contents of Pentadecanal (A22), Tridecanal (A19), et al., while European types have high relative contents of 2,4-Nonadienal, (E,E)- (A18) and (+)-epi-Bicyclosesquiphellandrene (O12) (Figure 4B). In the PLS-DA model, the VIP (Variable Importance in Projection) score estimates the importance of each x-variable in the predictive model for each x-variable and summarizes the contribution of variables to the model [48]. Typically, a VIP value greater than 1 is considered the criterion for variable selection [49]. The VIP plot of 29 cultivars indicates that 25 compounds with a VIP value larger than 1.0 were selected as the most discriminant VOCs, including 6 aldehydes, 7 alcohols, 3 ketones, 3 alkenes, and 6 others (Table S5). The VIP identified 23 compounds as key differential VOCs in different types of cucumbers (Table S6; Figure 4C), including 1-Nonanol, cis-9-Hexadecenal, Pentadecanal, et al. The content of 1-Nonanol, (E,E)-2,4-Nonadienal, Linalool, Hexanal, Tridecane, and 1-Octenewere higher in European type, while the content of 1-Nonanol, cis-9-Hexadecenal, cis,cis-7,10,-Hexadecadienal, Tetradecanal, et al. were higher in the South China type. Jo et al. [9]. conducted a

comparative analysis of cucumber varieties from Korea, Europe, and Thailand, 22 and 17 significantly discriminant metabolites in the peel and pulp were identified by PLS-DA analysis, respectively. Some of these differential metabolites are consistent with the findings of this study, such as (E,E)-2,4-Nonadienal, Hexanal, and others.

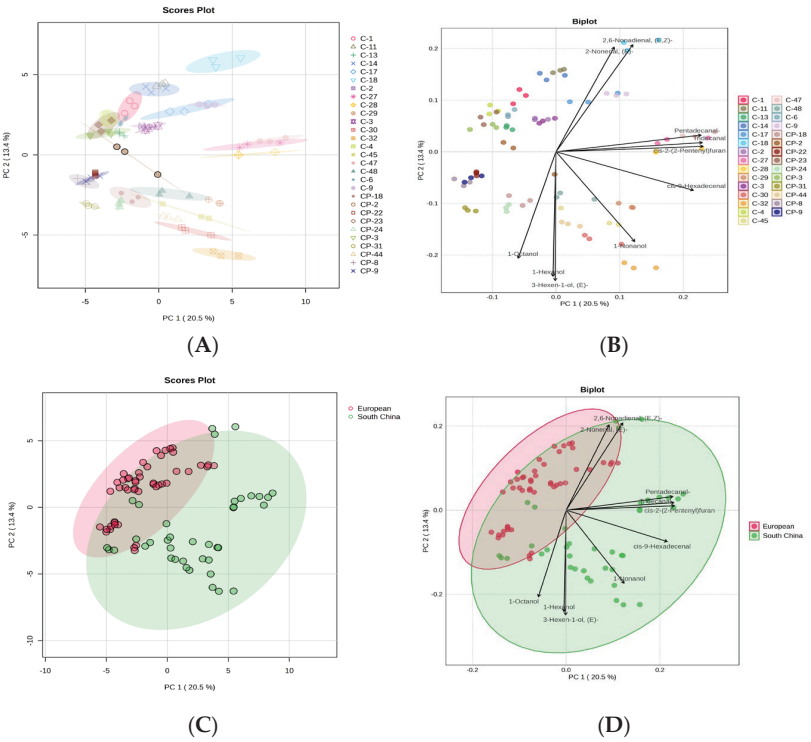


Figure 3. PCA score plots of 29 cucumber cultivars based on all VOC data. (**A**,**C**) shows the PCA scores scatter plot. (**B**,**D**) shows the PCA loading plots.

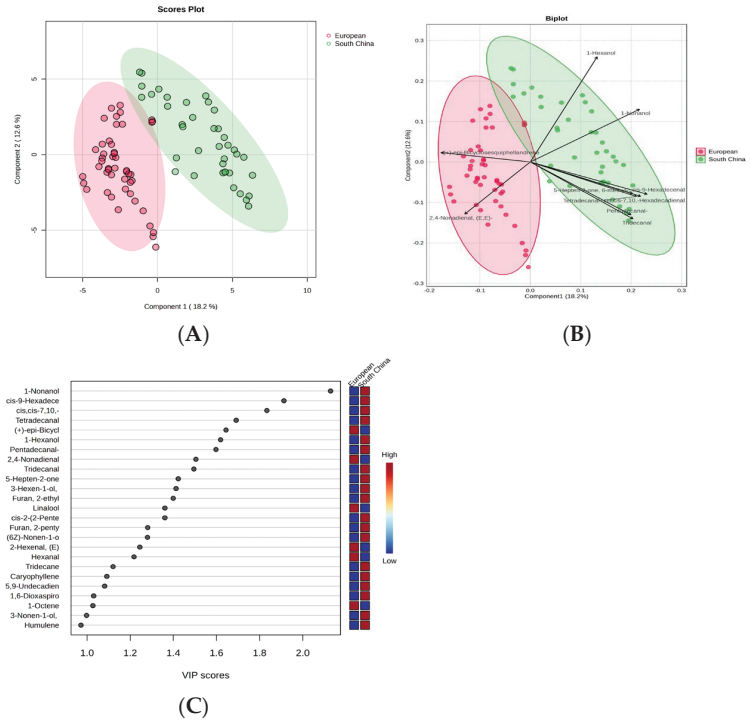


Figure 4. PLS-DA score plots of 29 cucumber cultivars of two types based on all VOC data. (**A**) shows the PLS-DA scores scatter plot. (**B**) shows the PLS-DA loading plots. (**C**) VOCs with VIP values larger than 1.0.

Through PCA and PLS-DA analysis, potential volatile substances in different varieties can be purposefully identified, thereby uncovering differential information among different varieties. This will contribute to a comprehensive evaluation of cucumber volatile substances.

4. Conclusions

In this study, the amino acids, tannins, soluble proteins, soluble sugars, Vc, nitrate nitrogen contents, and compositions and content of VOCs in 29 cucumber cultivars were identified. As a result, cucumber variety differences in amino acids, tannins, soluble proteins, et al. were found to be significant ($p < 0.05$). A total of 67 VOCs were identified, including 24 aldehydes, 13 alcohols, 12 ketones, 12 alkenes, and 6 other compounds; 21 VOCs were common in all 29 cultivars, including Hexanal, (E)-2-Hexenal, 2-Octanone, Nonanal, (E, Z)-2,6-Nonadienal, (E)-2-Nonenal, et al. The content and variety of aroma substances differ significantly among different cultivars. An average of 45 kinds of VOCs were identified in each cultivar. CP-44 had the most kinds of VOCs, while C-4 and C-14 had the fewest kinds of VOCs. C-9 had the highest content of VOCs, while CP-31 had the lowest content. PCA clustered the 29 cucumber cultivars into five groups based on the relationship between scores and loadings. At the same time, the cultivars of the European and South China types exhibited distinct separation by PCA and PLS-DA analysis. The cultivars of the South China types showed high relative contents of Pentadecanal (A22), Tridecanal (A19) et al., while European-types had high relative contents of (E,E)-2,4-Nonadienal (A18) and (+)-epi-Bicyclosesquiphellandrene (O12). PLS-DA analysis also identified 25 key differential volatiles for distinguishing 29 cultivars and 23 key differential volatiles for differentiating between South China and European types. These results provide effective information for breeding distinct cucumber varieties, such as intensely aromatic types with high soluble sugar content suitable for fresh consumption, and types with stable flavor profiles and high solid content ideal for processing, thereby catering to diverse consumer preferences.

Supplementary Materials: The following supporting information can be downloaded at: https://www.mdpi.com/article/10.3390/foods14223878/s1, Table S1. Cucumber cultivars used in this study and some basic fruit quality parameters. Table S2. The content (μg/kg FW) of 21 common volatile compounds in 29 cucumber cultivars. Table S3. Relative contents (μg/kg FW) of identified volatiles in the fruits of 29 cucumber cultivars. Table S4. Percentage (%) of each type of volatiles in 29 cucumber cultivars. Table S5. VIP value for sample line. Table S6. VIP value for sample groups of types.

Author Contributions: Conceptualization, P.L. and C.W.; methodology, P.L.; software, C.W.; validation, Y.Z., H.J. and S.W.; formal analysis, P.L. and C.W.; investigation, C.W.; resources, H.Z. and X.D.; data curation, C.W.; writing—original draft preparation, P.L.; writing—review and editing, H.Z. and X.D.; funding acquisition, H.Z. All authors have read and agreed to the published version of the manuscript.

Funding: This research was funded by the Shanghai Agricultural Science and Technology Innovation Project (2023-02-08-00-12-F04581) and Shanghai Academy of Agricultural Sciences, Smart Agriculture Research Center (HUNONGKE CENTER [2025] 002).

Institutional Review Board Statement: Not applicable.

Informed Consent Statement: Not applicable.

Data Availability Statement: The datasets generated for this study are available on request to the corresponding author.

Conflicts of Interest: The authors declare no conflicts of interest.

References

1. Williams, C.; Weng, Y.; Du, X. Sensory profiles of 10 cucumber varieties using a panel trained with chemical references. *ACS Food Sci. Technol.* **2022**, *2*, 815–824. [CrossRef]
2. Li, X.; Sun, Y.; Wang, X.; Dong, X.; Zhang, T.; Yang, Y.; Chen, S. Relationship between key environmental factors and profiling of volatile compounds during cucumber fruit development under protected cultivation. *Food Chem.* **2019**, *290*, 308–315. [CrossRef] [PubMed]
3. Yang, S.; Hao, N.; Meng, Z.; Li, Y.; Zhao, Z. Identification, comparison and classification of volatile compounds in peels of 40 apple cultivars by HS–SPME with GC–MS. *Foods* **2021**, *10*, 1051. [CrossRef] [PubMed]
4. Ye, Z.; Shang, Z.; Zhang, S.; Li, M.; Zhang, X.; Ren, H.; Hu, X.; Yi, J. Dynamic analysis of flavor properties and microbial communities in Chinese pickled chili pepper (*Capsicum frutescens* L.): A typical industrial-scale natural fermentation process. *Food Res. Int.* **2022**, *153*, 110952. [CrossRef] [PubMed]
5. Zhang, J.; Gu, X.; Yan, W.; Lou, L.; Xu, X.; Chen, X. Characterization of differences in the composition and content of volatile compounds in cucumber fruit. *Foods* **2022**, *11*, 1101. [CrossRef]
6. Wei, G.; Tian, P.; Zhang, F.; Qin, H.; Miao, H.; Chen, Q.; Hu, Z.; Cao, L.; Wang, M.; Gu, X.; et al. Integrative analyses of nontargeted volatile profiling and transcriptome data provide molecular insight into voc diversity in cucumber plants (*Cucumis sativus*). *Plant Physiol.* **2016**, *172*, 603–618. [CrossRef]
7. Forss, D.; Dunstone, E.; Ramshaw, E.; Stark, W. The flavor of cucumbers. *J. Food Sci.* **1961**, *27*, 90–93. [CrossRef]
8. Galliard, D.; Reynolds, J. The formation of cis-3-nonenal, trans-2-nonenal and hexanal from linoleic acid hydroperoxide isomers by a hydroperoxide cleavage enzyme system in cucumber (*Cucumis sativus*) fruits. *Biochim. Biophys. Acta.* **1976**, *441*, 181–192. [CrossRef]
9. Jo, H.; Song, K.; Kim, J.; Lee, C. Non-targeted metabolomic analysis for the comparative evaluation of volatile organic compounds in 20 globally representative cucumber lines. *Front. Plant Sci.* **2022**, *13*, 1028735. [CrossRef]
10. Hao, L.; Chen, S.; Wang, C.; Chen, Q.; Wan, X.; Shen, X.; Chen, Z.; Meng, H. Aroma components and their contents in cucumbers from different genotypes. *J. Northwest A&F Univ. (Nat. Sci. Ed.)* **2013**, *41*, 139–146.
11. Amaro, A.; Beaulieu, J.; Grimm, C.; Stein, R.; Almeida, D. Effect of oxygen on aroma volatiles and quality of fresh-cut cantaloupe and honeydew melons. *Food Chem.* **2012**, *130*, 49–57. [CrossRef]
12. Hadi, M.; Ahmed, M.; Zhang, F.; Wu, F.; Zhou, C.; Tao, J. Advances in fruit aroma volatile research. *Molecules* **2013**, *18*, 8200–8299. [CrossRef]
13. Palma-Harris, C.; Mcfeeters, R.; Fleming, H. Solid-phase microextraction (SPME) technique for measurement of generation of fresh cucumber flavor compounds. *J. Food Sci.* **2001**, *49*, 4203. [CrossRef]
14. Ligor, T.; Buszewski, B. Single-drop microextraction and gas chromatography–mass spectrometry for the determination of volatile aldehydes in fresh cucumbers. *Anal. Bioanal. Chem.* **2008**, *391*, 2283–2289. [CrossRef] [PubMed]
15. Shan, N.; Gan, Z.; Nie, J.; Liu, H.; Wang, Z.; Sui, X. Comprehensive characterization of fruit volatiles and nutritional quality of three cucumber (*Cucumis sativus* L.) genotypes from different geographic groups after bagging treatment. *Foods* **2020**, *9*, 294. [CrossRef] [PubMed]
16. Matsui, K.; Ujita, C.; Fujimoto, S.H.; Wilkinson, J.; Hiatt, B.; Knauf, V.; Kajiwara, T.; Feussner, I. Fatty acid 9- and 13-hydroperoxide lyases from cucumber. *FEBS Lett.* **2000**, *481*, 183–188. [CrossRef] [PubMed]
17. Chen, S.; Zhang, R.; Hao, L.; Chen, W.; Cheng, S. Profiling of volatile compounds and associated gene expression and enzyme activity during fruit development in two cucumber cultivars. *PLoS ONE* **2015**, *10*, e0119444. [CrossRef]
18. Weng, Y. Cucumis sativus chromosome evolution, domestication, and genetic diversity. *Plant Breed. Rev.* **2021**, *44*, 79–111.
19. Gilbert, J.; Guthart, M.; Gezan, S.; Melissa, P.; Schwieterman, M.; Colquhoun, T.; Bartoshuk, L.; Sims, C.; Clark, D.; Olmstead, J. Identifying breeding priorities for blueberry flavor using biochemical, sensory, and genotype by environment analyses. *PLoS ONE* **2015**, *10*, e0138494. [CrossRef]
20. Spadafora, N.; Cocetta, G.; Cavaiuolo, M.; Bulgari, R.; Dhorajiwala, R.; Ferrante, A.; Spinardi, A.; Rogers, H.; Müller, C. A complex interaction between pre-harvest and post-harvest factors determines fresh-cut melon quality and aroma. *Sci. Rep.* **2019**, *9*, 2745. [CrossRef]
21. Lignou, S.; Parker, J.K.; Baxter, C.; Mottram, D.S. Sensory and instrumental analysis of medium and long shelf-life charentais cantaloupe melons (*Cucumis melo* L.) harvested at different maturities. *Food Chem.* **2014**, *148*, 218–229. [CrossRef]
22. de Siqueira, A.C.P.; Dutra Sandes, R.D.; Nogueira, J.P.; Araujo, H.C.S.; de Jesus, M.S.; Rajkumar, G.; Leite Neta, M.T.S.; Narain, N. Volatile profiles of murcott and ponkan mandarins obtained by stir bar sorptive extraction technique and their contributions to the fruit aroma. *J. Food Sci.* **2024**, *89*, 4823–4838. [CrossRef]
23. Lee, J.H.; Lee, Y.Y.; Choi, Y.S.; Jang, H.W. Headspace stir-bar sorptive extraction combined with gas chromatography–mass spectrometry for trace analysis of volatile organic compounds in *Schisandra chinensis* Baillon (omija). *Food Sci. Nutr.* **2023**, *11*, 7396–7406. [CrossRef]

24. El-Akad, R.; El-Din, M.; Farag, M. How does *Lagenaria siceraria* (Bottle Gourd) metabolome compare to *Cucumis sativus* (Cucumber) f. Cucurbitaceae? A multiplex approach of HR-UPLC/MS/MS and GC/MS using molecular networking and chemometrics. *Foods* **2023**, *12*, 771. [CrossRef] [PubMed]
25. Zhong, Y.; Jia, Z.; Zhou, H.; Zhang, D.; Li, G.; Yu, J. Comparative analysis of volatile compounds from four radish microgreen cultivars based on ultrasonic cell disruption and HS-SPME/GC–MS. *Int. J. Mol. Sci.* **2023**, *24*, 14988. [CrossRef] [PubMed]
26. Shi, J.; Wu, H.; Xiong, M.; Chen, Y.; Chen, J.; Zhou, B.; Wang, H.; Li, L.; Fu, X.; Bie, Z.; et al. Comparative analysis of volatile compounds in thirty nine melon cultivars by headspace solid-phase microextraction and gas chromatography-mass spectrometry. *Food Chem.* **2020**, *316*, 126342. [CrossRef] [PubMed]
27. Shang, M.; Wu, Y.; Chen, J.; Lou, Q. Identification and comparison of aroma componentsin peel and flesh of cucumber. *Acta Agric. Boreali-Occident. Sin.* **2021**, *30*, 1365–1373.
28. Wei, S.; Xiao, X.; Wei, L.; Li, L.; Li, G.; Liu, F.; Xie, J.; Yu, J.; Zhong, Y. Development and comprehensive HS-SPME/GC–MC analysis optimization, comparison, and evaluation of different cabbage cultivars (*Brassica oleracea* L. Var. *Capitata* L.) volatile components. *Food Chem.* **2021**, *340*, 128166.
29. Xu, L.; Liu, W.; Pan, Z.; Pang, F.; Zhang, Y.; Liang, J.; Wang, Q.; Wang, J.; Zhao, M.; Qiao, Y.; et al. Characterization and comparative analysis of volatile organic compounds in four aromatic wild strawberry species using HS-SPME-GC-MS. *Food Chem. X* **2025**, *25*, 102092. [CrossRef]
30. Zhang, J.; Feng, S.; Yuan, J.; Wang, C.; Lu, T.; Wang, H.; Yu, C. The formation of fruit quality in *Cucumis sativus* L. *Front. Plant Sci.* **2021**, *12*, 729448.
31. Zhao, C.; Song, S.; Chen, S.; Wang, C.; Zhang, Y.; Tao, W. Evaluation of cucumber nutritional quality based on grey system theory. *J. Northwest A&F Univ. (Nat. Sci. Ed.)* **2015**, *43*, 181–186.
32. Du, X.; Routray, J.; Williams, C.; Weng, Y. Association of refreshing perception with volatile aroma compounds, organic acids, and soluble solids in freshly consumed cucumber fruit. *ACS Food Sci. Technol.* **2022**, *2*, 1495–1506. [CrossRef]
33. Ali, A.; Ghani, M.I.; Ding, H.; Fan, Y.; Cheng, Z.; Iqbal, M. Co-amended synergistic interactions between arbuscular mycorrhizal fungi and the organic substrate-induced cucumber yield and fruit quality associated with the regulation of the am-fungal community structure under anthropogenic cultivated soil. *Int. J. Mol. Sci.* **2019**, *20*, 1539. [CrossRef] [PubMed]
34. Sotiroudis, G.; Melliou, E.; Sotiroudis, T.G.; Chinou, I. Chemical analysis, antioxidant and antimicrobial activity of three greek cucumber (*Cucumis sativus*) cultivars. *J. Food Biochem.* **2010**, *34*, 61–78. [CrossRef]
35. Min, K.; Song, K.; Lim, S.; Yi, G.; Jin Lee, E. Cucurbitacin and volatile compound profiling reveals independent domestication of cucumber (*Cucumis sativus* L.) fruit. *Food Chem.* **2023**, *405*, 135006. [CrossRef]
36. Zhu, Y.; Lv, H.; Shao, C.; Kang, S.; Zhang, Y.; Guo, L.; Dai, W.; Tan, J.; Peng, Q.; Lin, Z. Identification of key odorants responsible for chestnut-like aroma quality of green teas. *Food Res. Int.* **2018**, *108*, 74–82. [CrossRef]
37. Schieberle, P.; Ofner, S.; Grosch, W. Evaluation of potent odorants in cucumbers (*Cucumis sativus*) and muskmelons (*Cucumis melo*) by aroma extract dilution analysis. *J. Food Sci.* **1990**, *55*, 195. [CrossRef]
38. Aboshi, T.; Musya, S.; Sato, H.; Ohta, T.; Murayama, T. Changes of volatile flavor compounds of watermelon juice by heat treatment. *Biosci. Biotechnol. Biochem.* **2020**, *84*, 2157–2159. [CrossRef]
39. Odeyemi, O.; Burke, C.; Bolch, C.; Stanley, R. Evaluation of spoilage potential and volatile metabolites production by shewanella baltica isolated from modified atmosphere packaged live mussels. *Food Res. Int.* **2018**, *103*, 415–425. [CrossRef]
40. Majithia, D.; Metrani, R.; Dhowlaghar, N.; Crosby, K.; Patil, B. Assessment and classification of volatile profiles in melon breeding lines using headspace solid-phase microextraction coupled with gas chromatography-mass spectrometry. *Plants* **2021**, *10*, 2166. [CrossRef]
41. Aprea, E.; Corollaro, M.L.; Betta, E.; Endrizzi, I.; Demattè, M.L.; Biasioli, F.; Gasperi, F. Sensory and instrumental profiling of 18 apple cultivars to investigate the relation between perceived quality and odour and flavour. *Food Res. Int.* **2012**, *49*, 677–686. [CrossRef]
42. Nakamura, A.; Ono, T.; Yagi, N.; Miyazawa, M. Volatile compounds with characteristic aroma of boiled sweet potato (*Ipomoea batatas* L. cv Ayamurasaki, *I. batatas* L. cv Beniazuma and *I. batatas* L. cv Simon 1). *J. Essent. Oil Res.* **2013**, *25*, 497–505. [CrossRef]
43. Liu, C.; He, W.; Liu, Y. Head-space solid phase microextraction and GC-MS analysis of fragrance of cucumber. *Acta Hortic. Sin.* **2002**, *6*, 581–583.
44. Valverde, M.A.F.; Sánchez-Palomo, E.; Alises, M.O.; Romero, C.C.; González-Viñas, M.A. Volatile and sensory characterization of la mancha trujillo melons over three consecutive harvests. *Foods* **2021**, *10*, 1683. [CrossRef]
45. Metrani, R.; Jayaprakasha, G.K.; Patil, B.S. Optimization of experimental parameters and chemometrics approach to identify potential volatile markers in seven Cucumis melo varieties using HS–SPME–GC–MS. *Food Anal. Methods* **2021**, *15*, 607–624. [CrossRef]
46. Kalivodová, A.; Hron, K.; Filzmoser, P.; Najdekr, L.; Janecková, H.; Adam, T. PLS-DA for compositional data with application to metabolomics. *J. Chemom.* **2015**, *29*, 21–28. [CrossRef]

47. Yu, S.; Huang, X.; Wang, L.; Wang, Y.; Jiao, X.; Chang, X.; Tian, X.; Ren, Y.; Zhang, X. Characterization of the volatile flavor profiles of black garlic using nanomaterial-based colorimetric sensor array, HS-SPME-GC/MS coupled with chemometrics strategies. *Food Chem.* **2024**, *458*, 140213. [CrossRef]
48. Deng, H.; He, R.; Long, M.; Li, Y.; Zheng, Y.; Lin, L.; Liang, D.; Zhang, X.; Liao, M.; Lv, X.; et al. Comparison of the fruit volatile profiles of five muscadine grape cultivars (*Vitis rotundifolia* Michx.) using HS-SPME-GC/MS combined with multivariate statistical analysis. *Front. Plant Sci.* **2021**, *12*, 728891. [CrossRef]
49. Park, Y.; Lee, J.; Park, S.; Kim, Y.; Mani, V.; Lee, K.; Kwon, S.; Park, S.; Kim, J. Metabolite changes in soybean (*Glycine max*) leaves during the entire growth period. *ACS Omega* **2023**, *8*, 41718–41727. [CrossRef]

Disclaimer/Publisher's Note: The statements, opinions and data contained in all publications are solely those of the individual author(s) and contributor(s) and not of MDPI and/or the editor(s). MDPI and/or the editor(s) disclaim responsibility for any injury to people or property resulting from any ideas, methods, instructions or products referred to in the content.

foods

MDPI

Article

Dynamics of Lactic Acid Bacteria Dominance in Sour Bamboo Shoot Fermentation: Roles of Interspecies Interactions and Organic Acid Stress

Xinxin Zhang [1], Changfeng Zhang [1], Menglian Gong [1], Pao Li [1], Hui Tang [2], Liwen Jiang [1,2,*] and Yang Liu [1,*]

[1] College of Food Science and Technology, Hunan Agricultural University, Changsha 410128, China; zxxhunauyjs@yeah.net (X.Z.); zhcfhnnd@163.com (C.Z.); gongml88@163.com (M.G.); lipao@mail.nankai.edu.cn (P.L.)

[2] Guangdong Provincial Key Laboratory of Utilization and Conservation of Food and Medicinal Resources in Northern Region, Shaoguan University, Shaoguan 512005, China; lokeytang@163.com

* Correspondence: hnndjlwsp@hunau.edu.cn (L.J.); fs.ly@hunau.edu.cn (Y.L.); Tel.: +86-135-0742-4629 (L.J.); +86-153-8801-1234 (Y.L.)

Abstract

To elucidate the mechanisms underlying the formation of the bacterial community predominantly composed of lactic acid bacteria (LAB) in sour bamboo shoots, the dynamics of the bacterial community structure and the influence of organic acids on the growth of dominant species were investigated. The results showed that the dominant bacteria in sour bamboo shoots changed from *Enterobacteriaceae* at first to LAB after fermentation. Correlation analysis revealed that organic acids, especially lactic acid and acetic acid, had great effects on bacteria. Even low concentrations of organic acids had negative effects on the growth of *Enterobacter asburiae*, while LAB exhibited remarkable tolerance to 8 g/L of organic acids. Notably, *Levilactobacillus spicheri* displayed a normal growth rate during incubation in medium containing 4 g/L of malic acid for 48 h. This study clarified the regulation of organic acids on bacterial community formation and provided a new understanding for bacterial control in traditional fermented foods.

Keywords: sour bamboo shoots; bacterial community succession; lactic acid bacteria; organic acids

1. Introduction

Fermentation is one of the time-honored food processing methods. Studying the microbial community structure and metabolism in fermented foods is important for understanding traditional fermentation processes. Previous studies have shown that the succession of microbial communities was affected by biological and abiotic factors, such as raw materials, environmental conditions, and microbial interactions. Raw material characteristics determine the initial colonization of microorganisms. Song et al. [1] reported that only cabbage- and garlic-derived microorganisms can successfully ferment kimchi. Environmental parameters affecting microbial composition include temperature, acidity, and salt concentration. For example, in non-post-fermented Shuidouchi, microbial diversity increases at moderate temperatures, *Bacillus* and *Aneurinibacillus* increase, and fungi decrease at high temperatures [2]. Pretreatment of fresh corn forage with organic acids in a certain proportion could reduce the abundance of undesirable microorganisms such as *Klebsiella* and *Paenibacillus* in whole-plant corn silage [3]. Under a low salinity environment, *Cardiobacteria* and *Ruminococcus* increased in

Spanish-style green table olives, which promoted metamorphism [4]. Further, the interspecific interactions during fermentation also affect both microbial communities and fermented products. Liu et al. reported that amino acids and nucleosides secreted by *Saccharomyces cerevisiae* in Maotai had a positive effect on *Limosilactobacillus panis* (*Lm. panis*), while the produced ethanol had a negative effect on *Lm. panis* [5].

Sour bamboo shoots are a fermented food produced in southern China, which is also a common condiment in southern dishes. Usually, bamboo shoots (mainly *Dendrocalamus latiflorus*) are cut into pieces or chopped, then sealed and soaked in salt-free water for 30 days or more [6]. Although fresh bamboo shoots harbor diverse bacteria such as *Enterobacter*, *Raoultella*, *Oxyphotobacteria*, and *Enterococcus* [6,7], LAB becomes the dominant bacteria in sour bamboo shoots after a period of fermentation [7–9]. These LAB are considered key bacteria related to the flavor of sour bamboo shoots. In addition to the special aroma provided by volatile substances such as p-cresol and octanoic acid [10], the unique sourness related to organic acids is also an important flavor characteristic of sour bamboo shoots [11–13]. Previous studies have indicated that changes in organic acids (such as malic acid and succinic acid) during the fermentation of sour bamboo shoots are closely related to the metabolism of flavor compounds [9]. Guan et al. [7] also found that lactic acid and acetic acid are positively correlated with the microbial community of sour bamboo shoots in the mid and late stages of fermentation. However, the influence of organic acids on bacterial community succession in fermented bamboo shoots remains unclear.

The changes in microbial communities during sour bamboo fermentation revealed by high-throughput sequencing technologies could document the succession from non-LAB to LAB. However, the intrinsic mechanisms driving this succession have not been elucidated, as the DNA obtained by high-throughput sequencing represents the total bacterial genetic material in the sample and cannot distinguish between live and dead cells. It is necessary to reveal the growth dynamics of key bacterial groups (such as *Levilactobacillus spicheri* and *Enterobacter asburiae*). Further, the influence of organic acids on the proliferation of key bacterial groups could help reveal how organic acids shape the community structure through inhibition and selection. This study aims to reveal how organic acids shape the community structure through inhibition and selection and to provide a theoretical basis for a comprehensive understanding of the microbial community succession in sour bamboo shoots and optimize the process of sour bamboo shoots.

2. Materials and Methods

2.1. Sample Preparation and Fermentation Process

Clay jars were purchased from a local market and used as fermentation containers. The jars were sterilized by flaming: a small volume of ethanol was sprayed into the inner surface and then ignited. After the flame was extinguished, the jars were cooled to room temperature for use. Fresh bamboo shoots harvested from Liuzhou, China, were used as the fermentation substrate. The shoots were peeled, sliced, then put into clay jars and immersed in sterile water at a ratio of 1:1.2. The jars were sealed with water at the edge.

Sampling was conducted aseptically on days 0, 1, 4, 7, 10, 15, 20, 25, and 30 of fermentation. For each sampling, the entire jar was transferred into a laminar flow, and then the external surface of the jar was wiped with 75% (v/v) ethanol and exposed to ultraviolet radiation for 15 min before opening. The sample was then thoroughly homogenized by shaking. The unfermented (day 0) control sample was handled immediately after collection in the same manner as the fermented sample, with sterile water added for analysis. Each sample was divided into three parts.

2.2. Analysis of Microbial Community

DNA extraction: Microbial biomass was collected by centrifuging 25 mL of fermentation brine. DNA was extracted using the Magnetic Soil and Stool DNA Kit (TIANGEN, Beijing, China); 16S rDNA sequencing: target region: V3-V4 hypervariable region of bacterial 16S rRNA gene. Primers: 341F (5′-CCTAYGGGRBGCASCAG-3′) and 806R (5′-GGACTACNNGGGTATCTAAT-3′) were purchased from Sangon Biotech (Shanghai, China). Qualified PCR products were evaluated using an Agilent 2100 Bioanalyzer (Agilent, Santa Clara, CA, USA) and Illumina library quantitative kits (Kapa Biosciences, Woburn, MA, USA), which were further pooled together and sequenced on an Illumina NovaSeq 6000 (Illumina, San Diego, CA, USA).

2.3. Analysis of Physicochemical Properties

The second part was used for the analysis of immediate physicochemical properties. pH was measured using a calibrated pH meter (Lei Ci, Shanghai, China) on each sample. Total acidity was determined by titration with NaOH, expressed as lactic acid equivalent (g/kg). The composition of organic acids was analyzed by High-Performance Liquid Chromatography (HPLC), which was performed according to the research of Tang et al. [12]. HPLC conditions: Instrument: Liquid Chromatograph (Shimadzu, Kyoto, Japan); Column: ZORBAX Eclipse XDB-C18 (4.6 × 250 mm, 5-μm, Agilent, Santa Clara, CA, USA); mobile phase: 0.1% phosphoric acid-methanol = 97.5 + 2.5 (volume ratio), isocratic elution at 0.8 mL/min; detection: UV detector at 210 nm; standards including oxalic acid (99.6%), acetic acid (99.8%), succinic acid (99.5%), and propionic acid (99.5%) were purchased from Macklin (Shanghai, China). Malic acid (98%), L-lactic acid (98%), and citric acid (99.5%) were obtained from Aladdin (Shanghai, China). L-lactic acid was detected as studies have shown that the type of lactic acid in many fermented foods is L-lactic acid [14–16].

The third part was stored at −80 °C for future analysis. These samples were freeze-dried, ground into a powder, and subsequently used for the determination of total sugar and reducing sugar content. Reducing sugar and total sugar: the 3,5-Dinitrosalicylic acid (DNS) colorimetric method [17] was used to determine the reducing sugar before hydrolysis and total sugar after acid hydrolysis.

2.4. Isolation and Functional Validation of Key Strains

2.4.1. Strain Isolation

LAB: MRS agar. *Enterobacteriaceae*: Violet Red Bile Glucose agar (VRBGA). Both culture media were purchased from Huankai Bio-Technology Co., Ltd. (Guangzhou, China). Physiological and biochemical experiments were conducted, including the Calcium dissolution test, Gram staining, litmus milk test, catalase test, oxidase test, gelatin liquefaction test, methyl red test, and indole test. The physiological and biochemical identification of LAB referred to Öz et al. [18] and Shao et al. [19], and *Enterobacteriaceae* referred to Padovani et al. [20]

2.4.2. Mono- and Co-Culture Experiments

Simulated fermentation: LAB and *Enterobacteriaceae* strains were inoculated individually (mono-culture) and in combination (co-culture at a ratio of 1:1) into sterile bamboo shoot medium. The sterilized bamboo shoot medium was prepared by homogenizing fresh bamboo shoots with distilled water at a ratio of 1:1.2 (w/v). The mixture was then autoclaved at 105 °C for 30 min in conical flasks before use. The initial inoculum for all cultures was adjusted to approximately 10^8 CFU/mL by the McNeill turbidimetric method, and the inoculation amount was 0.1%. The cultures were incubated at 37 °C under static conditions. The pH and plate count of the culture broth were measured daily over 7 days

by aseptically sampling the medium. All experiments were performed in triplicate using 250 mL sterile conical flasks containing 100 mL of medium.

2.4.3. Organic Acid Regulation Test

Oxalic acid, malic acid, lactic acid, and acetic acid were selected for tolerance assessment. Stock solutions of each organic acid were prepared, filter-sterilized, and aseptically added to sterile MRS (for LAB) or LB (for *Enterobacteriaceae*) medium to achieve final concentrations of 0, 0.5, 2, 4, and 8 g/L. The isolated strain and static culture were inoculated at 37 °C. Bacterial growth was monitored by measuring the OD_{600} every 12 h for 48 h using a microplate reader (ReadMax 1900, Shangpu, Shanghai, China). All absorbance readings were blank-corrected against the sterile medium. All assays were performed in sterile 96-well plates with three biological replicates, each with three technical replicates.

2.5. Statistical Analysis

All measurements were performed with three replicates, and the results were averaged. Principal Coordinates Analysis (PCoA) among communities was analyzed by R software (version 4.0.3); prediction of microbial community function was conducted using PICRUSt2; Pearson correlation calculation was conducted using an online platform (https://www.omicstudio.cn/tool, accessed on 21 January 2025). Canoco5 (ter Braak and Šmilauer, 2012) was used for Redundancy Analysis (RDA).

3. Results

3.1. Microbial Community Diversity of Sour Bamboo Shoots

Alpha diversity analysis and beta diversity analysis were performed based on the ASV feature sequence and ASV abundance table obtained from 2.2. Alpha diversity's core lies in the comprehensive assessment of species richness, distribution uniformity, and completeness of sequencing data [21]. Figure 1A lists the core analysis parameters, including the observed_otus, Shannon, Simpson, and chao1 (logarithmic normalization of raw data was adopted for plotting). As the fermentation process progressed, chao1 increased, indicating a rise in community richness. In contrast, Shannon decreased, reflecting a reduction in community diversity. Beta diversity refers to the variation in species composition among different environmental communities [22]. PCoA was employed to examine the differences and similarities among samples. PCoA1 and PCoA2 contributed 94.16% and 4.25% to the OTU data difference. As illustrated in Figure 1B, the samples from D4 to D30 were closely clustered, particularly D4 and D7, as well as D15 and D30, indicating similarities in their microbial structures. In contrast, the samples from D0 and D1 were distinctly separated from all other sample groups, suggesting that the microbial composition of these two groups significantly differs from the others.

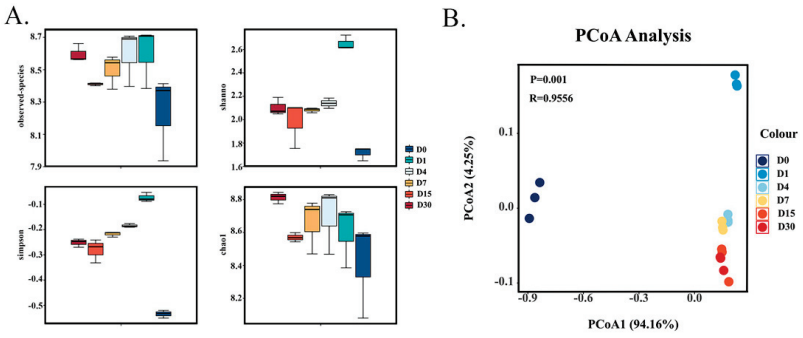


Figure 1. Alpha diversity (**A**) and beta diversity (**B**) of bacterial communities during sour bamboo shoot fermentation at the OTU level: The percentages on the horizontal and vertical axes indicate the degree of explanation of the sample differences by the first and second axes.

3.2. Representative Bacteria of Different Fermentation Stages of Sour Bamboo Shoots

The classification of bacterial biomes across the six sample groups at both the phylum and genus levels is illustrated in Figure 2. At the phylum level (Figure 2A), *Firmicutes* (51.38%), *Proteobacteria* (39.67%), *Bacteroidota* (3.7%), and *Actinobacteriota* (2.68%) together account for approximately 97.4% of the bacterial composition in fresh bamboo shoots (Group D0). As the fermentation time was prolonged, the proportion of Firmicutes gradually increased and came to dominate, rising to over 90%. The proportion of Actinobacteria fell below 1% in the later fermentation stages.

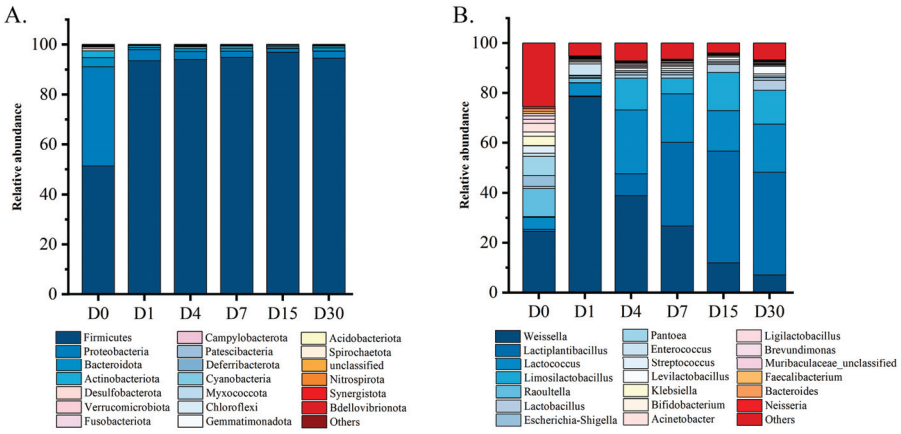


Figure 2. Changes in bacterial community structure at the phylum (**A**) and genus (**B**) levels during sour bamboo shoots fermentation. All measurements were performed with three replicates.

As can be seen from Figure 2B, the microbial composition typically undergoes very active changes during the early stages of fermentation [23]. In the raw materials (D0), *Weissella* was the dominant bacterium (24.55%), which also included many miscellaneous bacteria. With the fermentation process, LAB gradually occupied the absolute advantage. On the 30th day, the relative abundance of LAB was more than 90%. Among LAB, *Weissella* was the dominant bacterium in the early stage of fermentation. The relative abundance of *Weissella* reached 78.49% in D1. This surge was likely attributed to its rapid reproduction and effective utilization of fermentation substrates during the early stages, similar to the transient dominance of *Weissella* observed in the initial phase of kimchi fermentation [24]. After 30 days of fermentation, the abundance of *Weissella* gradually decreased to 7.10%. *Lactococcus* showed a similar trend, with its maximum abundance value appearing at D4, which was 25.58%. At the middle and late stages of fermentation (D15 and D30), *Lactiplantibacillus* became the dominant genus, and its relative abundance remained above 40%. It is worth noting that *Raoultella*, *Escherichia-Shigella*, *Pantoea,* and *Klebsiella*, which are members of the *Enterobacteriaceae* family and classified as facultative anaerobes, exhibited high abundances at D0, with relative percentages of 11.27%, 4.22%, 7.73%, and 3.76%, respectively. This phenomenon may be attributed to either their inherent presence in the raw materials or initial environmental contamination. However, the sum of *Enterobacteriaceae* relative abundances continued to decrease to only 1.34% by D30. It showed that LAB and *Enterobacteriaceae* bacteria grew in opposite directions in sour bamboo shoots; their interaction needed further investigation.

On account of 16S rDNA high-throughput gene recognition of live and dead cells, plate counts of *Enterobacteriaceae* and LAB were performed. In order to understand the growth dynamics of key bacterial groups (LAB and *Enterobacteriaceae*), the live cell counts of them during fermentation were detected (Figure S1). *Enterobacteriaceae* could not be detected after 4 days of fermentation, while LAB rapidly proliferated and stabilized above

3.5×10^6 CFU/mL (the counts were expressed as the log of CFU per milliliter in the figure). It was similar to the diversity changes in *Enterobacteriaceae* and LAB in sour bamboo shoots.

3.3. Functional Potential of Microbial Community

KEGG Ortholog (KO) information corresponding to OTU was obtained by Greengenes ID corresponding to OTU. Abundance of each functional category was calculated according to information from the KEGG database (Kyoto Encyclopedia of Genes and Genomes, http://www.genome.jp/kegg/, accessed on 15 December 2024) and OTU abundance [25]. Figure 3 shows two levels of information of the KEGG metabolic pathway. As can be seen from Figure 3A, the metabolism abundance was the highest at KEGG level 1 compared to environmental information processing and genetic information processing, and there was no significant difference in the relative abundance of metabolism among the sample groups. It indicated that metabolism is an important function during sour bamboo shoots fermentation, which is similar to paocai [26]. As can be seen from Figure 3B, more metabolism functions were identified at KEGG level 2, including amino acid metabolism, carbohydrate metabolism, energy metabolism, cofactors and vitamin metabolism, and nucleotide metabolism, among others. As the fermentation progressed, carbohydrate metabolism became higher and energy metabolism became lower, while the relative abundance of other metabolism pathways did not change significantly. Combined with Figure 2, the increase in carbohydrate metabolism abundance in the community may be related to the proliferation of LAB.

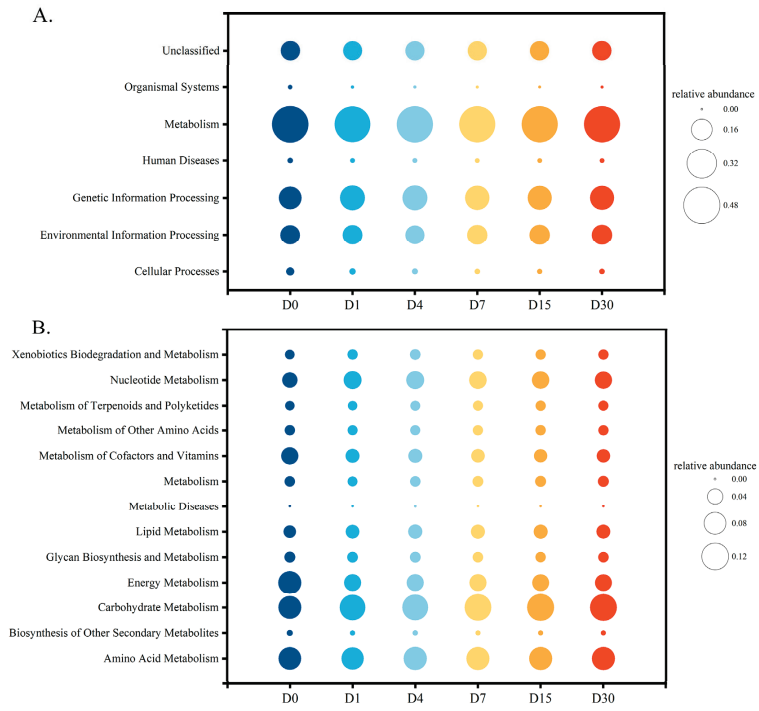


Figure 3. Predicted KEGG functional abundance of the sour bamboo shoot bacterial community based on KEGG level 1 (**A**) and KEGG level 2 (**B**). The size of bubbles corresponds to the relative abundance of functions, and the colors represent different functions.

3.4. Changes in Physicochemical Properties in the Fermentation Process of Sour Bamboo Shoots

As shown in Figure 4A, the final content of reducing and total sugars decreased during fermentation, consistent with Guan et al. [7] and Singhal et al. [27]. This may be due to the increasing abundance of carbohydrate metabolic functions in the community (Figure 3B). However, reducing sugar content increased on day 7, probably because the rate of hydrolysis of total sugar into reducing sugars surpassed the rate of bacterial consumption

of reducing sugars, leading to a transient accumulation of reducing sugars. The pH value of sour bamboo shoots decreased rapidly to 3.84 after the 4th day of fermentation and then tended to be stable. Total acid accumulated continuously and reached 28.35 g/kg but decreased to 26.19 g/kg on day 30.

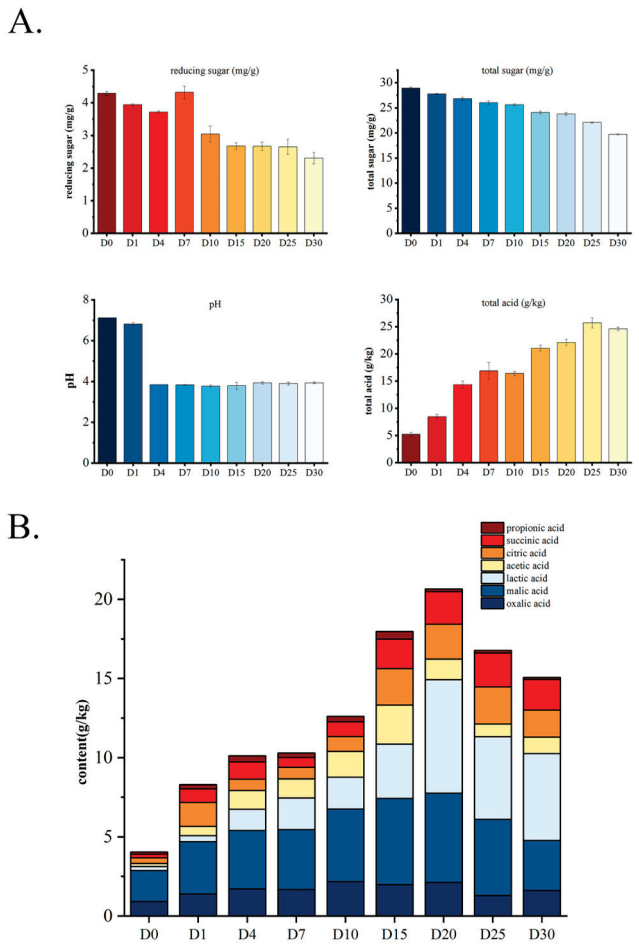


Figure 4. Changes in reducing sugar, total sugar, pH, total acid (**A**), and organic acids (**B**) during sour bamboo shoot fermentation.

According to Figure 4B, the total concentration of these seven organic acids exhibited a nonlinear dynamic characteristic, initially rising and then declining. The continuous accumulation of organic acids in the sour bamboo shoot led to a decrease in pH and an increase in total acids. On day 0, the predominant organic acids in the fermentation brine were oxalic acid, malic acid, and citric acid, indicating their presence in the raw bamboo shoot materials. This finding is consistent with the results reported by other scholars [9,28]. As fermentation progressed, these three organic acids gradually increased, with malic acid peaking on the 20th day at 5.64 g/kg. Subsequently, the decrease in malic acid concentration was potentially due to its involvement in the synthesis of other substances as precursors. Some studies have demonstrated that low-molecular-weight organic acids play a crucial role in various physiological and metabolic processes in plants [29]. However, lactic acid and acetic acid became the primary organic acids in the late stage of fermentation of sour bamboo shoots, and their concentrations reached 1.33 g/kg and 1.18 g/kg, respectively, on day 4. The lactic acid concentration reached a maximum of 7.16 g/kg after 20 days of fermentation and maintained a relatively high level until day 30.

3.5. Association Analysis of Microbial Interaction Networks and Environmental Factors

Pearson and coor.test were used to calculate the correlations among microorganisms and distance matrix correlations between microorganisms and environmental factors, and Figure 5 and a correlation coefficient table (Tables S1 and S2) were obtained. In Figure 5A, the heat map on the right shows the correlation between microorganisms. It reveals that *Weissella* was positively correlated with *Enterococcus* and *Raoultella* and significantly negatively correlated with other LAB ($r < -0.6$) within the sour bamboo shoots system. There was a positive correlation among *Lactiplantibacillus*, *Lactococcus*, *Limosilobacillus*, *Lactobacillus*, and *Levilactobacillus* ($r = 0.36$–0.90). At the same time, these five LAB genera were negatively correlated ($r = -0.70$ to -0.28) with *Enterobacteriaceae*, a negative correlation between LAB and *Enterobacteriaceae* that has also been reported in Mahewu [30], fermented carrot juice [31], and kimchi [32]. From the network diagram on the left in Figure 5A, there are only 11 pairs of statistically significant relationships that exist between the two distance matrices, including 4 correlations with total acid and microbial genera, 2 with pH and microbial genera, 3 with total sugar and microbial genera, and 2 with reducing sugar and microbial genera. This result indicates that pH and total acids are important indicators affecting microorganisms [33,34]; the direct regulation of the acid–base environment on the bacterial structure was significantly stronger than that of the carbon source.

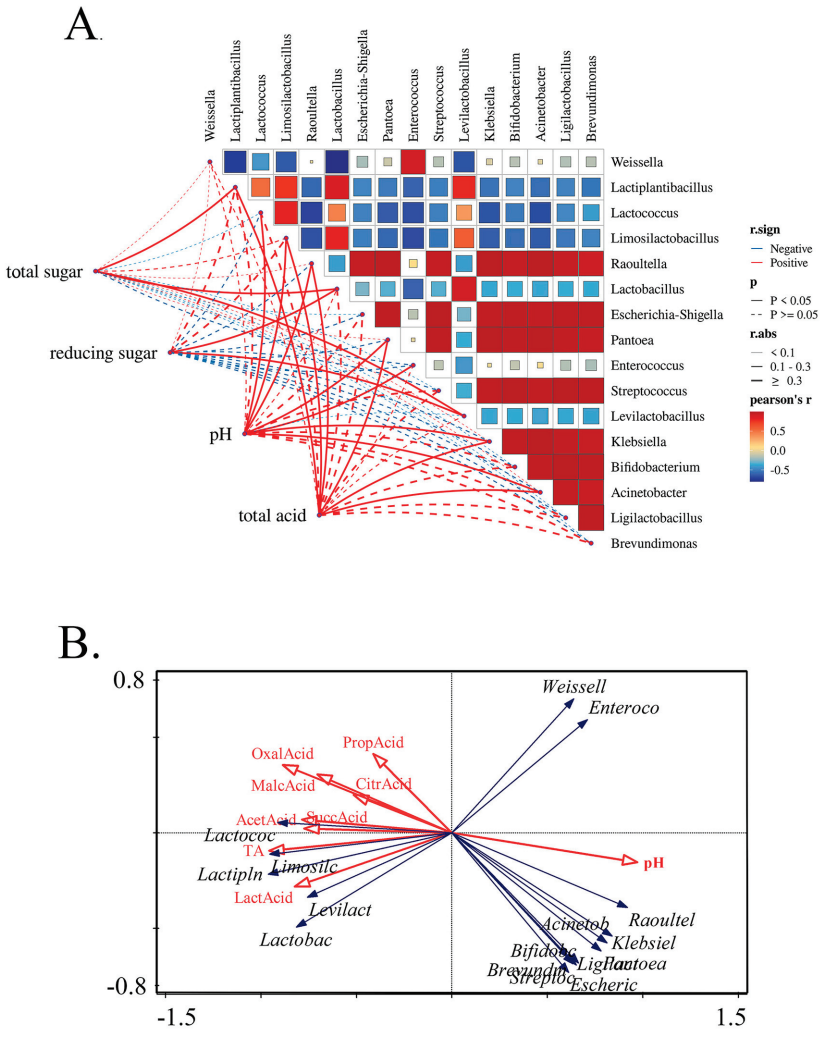


Figure 5. Association analysis of bacterial interaction networks and environmental factors (**A**) and RDA of genus and organic acids (**B**). Blue denotes negative correlation, red represents positive correlation, and $|r| > 0.5$ indicates strong correlation. Lines indicate significance; $p < 0.05$ indicates "r" is statistically significant.

The coor.test revealed overall correlations between environmental factors and bacteria, but it could not resolve interactions or collinearity among environmental factors, which may lead to misjudgments of key drivers. To address this limitation, RDA was further employed to visualize the direction and strength of associations among pH, total acid, and bacteria. In Figure 5B, the obtuse angle between total acid and *Weissella* or *Enterobacteriaceae* indicated negative correlations. The rapid decrease in *Enterobacteriaceae* was also found when the pH of the fermented cereal beverage fell below 4.5 [30]. On the contrary, total acid and organic acids were positively correlated with *Lactiplantibacillus*, *Lactococcus*, *Limosilactobacillus*, *Levilactobacillus,* and *Lactobacillus*. The vectors of lactic acid and acetic acid exhibited the smallest angles with LAB, coupled with significantly longer projection lengths compared to other organic acids, suggesting that they had stronger positive effects on LAB distribution. It is speculated that lactic acid and acetic acid could inhibit miscellaneous bacteria and promote LAB propagation.

3.6. Isolation and Identification of Key Strains and Exploration of Interactions

3.6.1. Isolation and Screening of Strains

To analyze the interactions between key strains, a total of 36 strains were isolated by MRS medium and VRBGA medium and the Gram staining method, among which 28 strains of suspected LAB and 8 strains of suspected *Enterobacteriaceae* were screened (Figure 6A). After physiological and biochemical analysis, ten strains of LAB and four strains of *Enterobacteriaceae* were screened (Figure 6B). They were identified as seven *Lactiplantibacillus plantarum*, one *Lactiplantibacillus pentosus*, two *Levilactobacillus spicheri*, two *Enterobacter ludwigii,* and two *Enterobacter asburiae,* respectively. Further, they were inoculated into sterilized bamboo shoots alone (Figure 6C), and their growth was measured by the plate counting method. Three strains, *Enterobacter asburiae* (*E. asburiae*), *Levilactobacillus spicheri* (*Lv. spicheri*), and *Lactiplantibacillus plantarum* (*Lp. plantarum*), exhibiting the best growth were further investigated (Figure 6D). Several studies have confirmed the safety of *Lv. spicheri* [35] and *Lp. plantarum* [36]. Name abbreviations were based on the proposal of S.D. Todorov et al. [37].

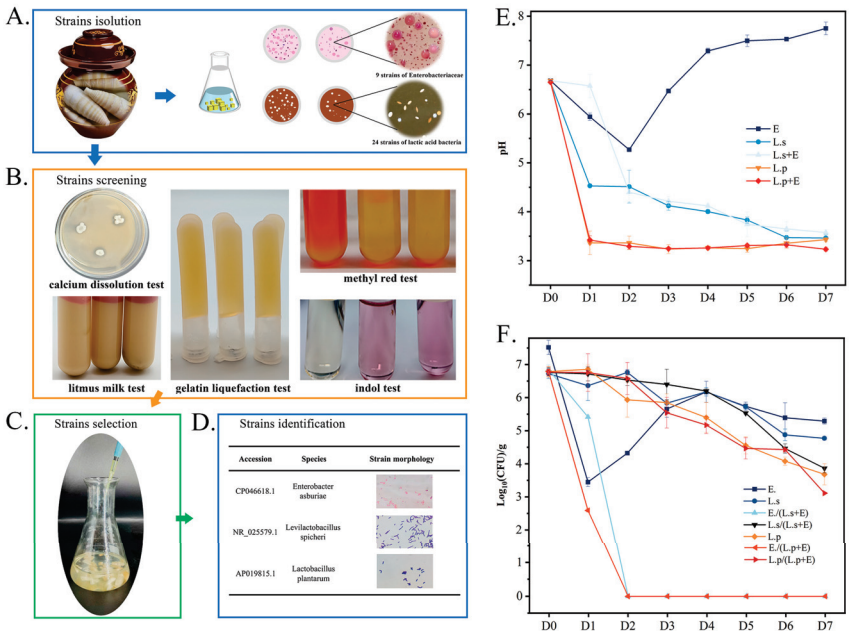


Figure 6. Screening of key strains (**A**–**D**) in sour bamboo shoots and changes in pH (**E**) and population (**F**) of strains in mono-culture and co-culture systems. Considering the size and aesthetic appeal of the figure, *Enterobacter asburiae*, *Levilactobacillus spicheri,* and *Lactiplantibacillus plantarum* are abbreviated as E., L.s, and L.p, respectively.

3.6.2. pH Dynamics and Bacterial Growth in Mono-Culture and Co-Culture Systems

Mono-culture of and co-culture of *Lv. spicheri*, *Lp. plantarum* and *E. asburiae* were carried out in sterilized bamboo shoots for 7 days. As shown in Figure 6E, the pH value decreased at first and then increased in mono-culture of *E. asburiae*, and the system reached a weak alkaline state on the 7th day. The initial pH decrease may be related to the leakage of organic acid from raw materials and the consumption of reducing sugar by *E. asburiae* to produce acid [38–40]. The subsequent pH increase may be caused by *E. asburiae* metabolizing protein. The pH of the system fermented by *Lv. spicheri* and *Lp. plantarum* continuously decreased to 3.46; in particular, the pH of the system fermented by *Lp. plantarum* decreased fast to 3.36 in 1 day, indicating that *Lp. plantarum* had a stronger acid production capacity. The situation was similar to that of naturally fermented products [9,41].

As shown in Figure 6F, the number of colonies increased in the first 2 days and then decreased slowly when *E. asburiae* was cultured alone. However, when co-cultured with *Lv. spicheri* or *Lp. plantarum* for 2 days, the total colonies of *E. asburiae* dropped below the detection limit. This indicates that *E. asburiae* can proliferate independently in mono-culture, while the decrease in pH caused by acid production from LAB in co-culture likely inhibits *E. asburiae* growth [30]. Notably, LAB colony counts initially increased and then decreased in all conditions: *Lv. spicheri* reached its peak on day 2 in mono-culture. Under other conditions, both *Lv. spicheri* and *Lp. plantarum* reached their peak on the first day.. At the late stage of *Lv. spicheri* and *E.asburiae* co-culture, the proliferation of *Lv. spicheri* was lower than that of *Lv. spicheri* mono-culture, probably because *E. asburiae* consumed some nutrients in the bamboo shoot. In addition, the decline rate of *Lv. spicheri* was significantly slower than that of *Lp. plantarum* in both mono-culture and co-culture, suggesting that *Lv. spicheri* may possess stronger acid tolerance.

3.7. Analysis of Concentration-Dependent Effects of Organic Acids on Growth Inhibition and Promotion of Isolated Strains

Since high levels of oxalic acid, malic acid, lactic acid, and acetic acid were observed in sour bamboo shoots, their effect on the growth of strains was further investigated. Figure 7A,D,G show that the inhibition of *E. asburiae* by organic acids differs by type and concentration. Lactic acid and acetic acid exhibited the most potent antimicrobial activity, which led to a decrease of over 75% in biomass compared to the control group. Similarly, oxalic acid also displayed significant dose-responsive inhibition, with 2 g/L and 4 g/L concentrations reducing *E. asburiae* biomass by 64% and 75%, respectively, at 48 h. The 0.5 g/L malic acid treatment led to a marginal *E. asburiae* biomass increase relative to the control in the first 36 h, suggesting potential substrate utilization at lower concentrations. This effect shifted to inhibition with increasing concentrations (above 2 g/L).

As can be seen from Figure 7B,E,H, and J (biomass variation in *Lv. spicheri*) and Figure 7C,F,I,K (biomass variation in *Lp. plantarum*), there were differential regulations of LAB by organic acids. *Lp. plantarum* reached high absorbance faster than *Lv. spicheri*, indicating that *Lp. plantarum* proliferates faster, which may be the reason that *Lp. plantarum* colony count reached the maximum value faster during bamboo shoot fermentation (Figure 6E). Interestingly, low concentrations of organic acids had no inhibitory effect on *Lv. spicheri* and *Lp. plantarum*. After 48 h of fermentation in a 0.5 g/L organic acid fermentation system, the absorbance of *Lv. spicheri* increased by 14% to 21% compared with the organic acid-free control. Notably, the biomass of *Lv. spicheri* showed a certain increase in the presence of 4 g/L of malic acid. Similarly, 2 g/L of organic acid had no effect on *Lp. plantarum* proliferation only in the early stage of fermentation (within 12 h). The inhibitory activity of organic acids on *Lv. spicheri* and *Lp. plantarum* proliferation increased gradually with the increase in organic acid concentration; in particular, oxalic acid and lactic acid showed

the greatest effect on *Lv. spicheri* and *Lp. plantarum*. The growth of *Lv. spicheri* and *Lp. plantarum* was effectively inhibited when the oxalic acid concentration exceeded 2 g/L. *Lv. spicheri* exhibited stronger tolerance to high concentrations (8 g/L) of lactic acid and oxalic acid than *Lp. plantarum*, with the biomass of *Lv. spicheri* decreased by 59% to 76%, while that of *Lp. plantarum* decreased by 84% to 96%. The high tolerance ability of *Lv. spicheri* to lactic acid might be one reason for its slower decrease during sour bamboo fermentation (Figure 6E).

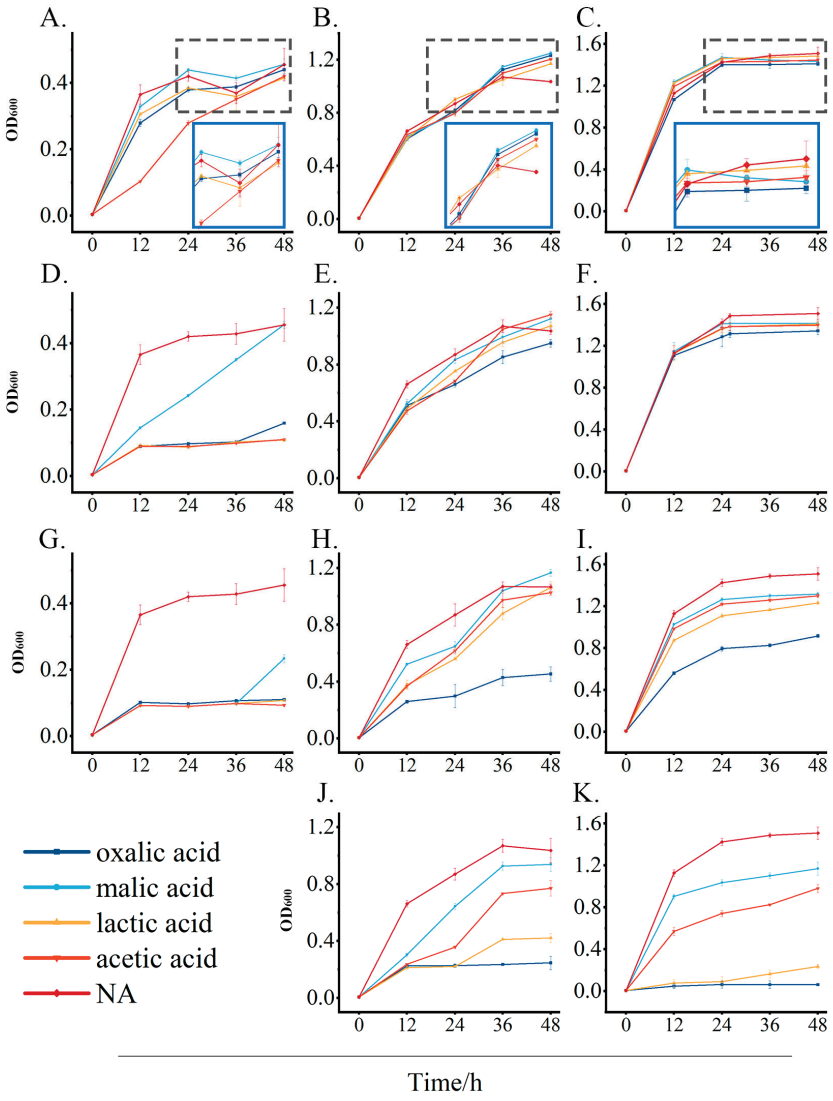


Figure 7. The effects of oxalic acid, malic acid, lactic acid, and acetic acid at concentrations of 0.5‰ (**A**–**C**), 2‰ (**D**–**F**), 4‰ (**G**–**I**), and 8‰ (**J**,**K**) on the growth of *Enterobacter asburiae* (**A**,**D**,**G**), *Levilactobacillus spicheri* (**B**,**E**,**H**,**J**), and *Lactiplantibacillus plantarum* (**C**,**F**,**I**,**K**). Biomass was expressed as OD_{600}, and each measurement was repeated three times. The blue box was an enlarged representation of the black box (**A**–**C**).

4. Discussion

The structure of microbial communities is very important to the quality of fermented products. At the phylum level, Firmicutes were the predominant phylum in sour bamboo shoots, as well as other fermented vegetables [23,42]. At the genus level, it was found that the relative abundance of the *Enterobacteriaceae* family (*Raoultella*, *Escherichia-Shigella*, *Pantoea*, and *Klebsiella*) was the highest in the early stage of fermentation, and the fermentation system dominated by the LAB family (*Lactiplantibacillus*, *Lactococcus*, *Limosilactobacillus*,

and so on) was formed in the late stage of fermentation (Figure 2). These observations were similar to those of a cross-regional study of China's traditional sour bamboo shoot fermentation [8,9,12] and other traditional fermented pickles [43]. However, the 16S rDNA sequencing cannot distinguish between live and dead cells. The detected *Enterobacteriaceae* in the later stage may come from dead cell DNA, which potentially overestimates their viability. This was confirmed by the live cell count data of LAB and *Enterobacteriaceae* (Figure S1).

Obviously, the changes in bacterial community structure, especially the increase in relative abundance of *Lactiplantibacillus*, led to an increase in the abundance of carbohydrate metabolism functions (Figure 3) [44], which further alter the content of lactic acid and acetic acid in sour bamboo shoot (Figure 4). Among them, the production of organic acids is mainly due to the release and permeation of raw materials and the metabolism of microorganisms to carbohydrates [39,45]. The main organic acid changes in the system may be due to LAB metabolizing malic acid, citric acid, and carbohydrates to produce lactic acid and acetic acid [46,47]. In the present study, organic acid profiling focused exclusively on L-lactic acid, and the presence of D-lactic acid was worth further quantifying to evaluate the safety of fermented foods.

Furthermore, the correlation analysis (Figure 5) and in vitro validation experiment collectively suggest that this succession, LAB gradually becoming the dominant bacteria, was likely driven by organic acids (especially lactic acid and acetic acid) produced by the metabolism of LAB. The inhibition of LAB on *E. asburiae* in the co-culture experiment (Figure 6) was likely achieved by creating a low pH and organic acid environment, since organic acids such as lactic acid and acetic acid have been widely proven to be antibacterial substances against *Enterobacteriaceae* [48,49]. Further, the pure culture experiment (Figure 7) confirmed that even low concentrations of organic acids can strongly inhibit the growth of Enterobacteriaceae, which could explain why *Enterobacteriaceae* rapidly die out in natural fermentation as organic acids accumulate.

Differently, organic acids showed dual regulation on LAB (Figure 7). Promotion at low concentrations is more likely due to its ability to reduce environmental pH, creating a competitive advantage for acidophilic LAB. The inhibitory effect of high concentrations of organic acids may be due to the destruction of the integrity of the cell wall structure of LAB. This result was consistent with the similar effect of phenolic acids on LAB reported by Rodríguez et al. [50]. Interestingly, *Lv. spicheri* can still grow normally in 4 g/L of malic acid, which contrasts with most strains that are inhibited under high acidity. This suggests that *Lv. spicheri* may possess unique acid tolerance mechanisms (such as specific stress responses) that allow it to maintain dominance in the harsh environment of the mid-to-late stages of fermentation. *Lv. spicheri* may have potential as a starter culture. However, in vitro culture experiments cannot fully simulate the complex physicochemical microenvironment in natural fermentation. RT-qPCR of key bacterial species combined with macro-transcriptomics could be considered to reveal the functions of active bacterial communities during fermentation.

In summary, the microbial succession during sour bamboo shoot fermentation resulted from interspecies competition and organic acid-mediated stress. It was driven primarily by the dominance of LAB, which outcompeted early-stage *Enterobacteriaceae* through the production of organic acids that both lower pH and generate antimicrobial substances. These findings deepen the understanding of the mechanism of colony formation in traditional food fermentation processes and help to develop functional fermentation agents centered around *Lv. spicheri* to regulate the sour bamboo shoot fermentation process.

5. Conclusions

This study revealed the mechanisms through which LAB achieved dominance during sour bamboo shoot fermentation. The dominant bacteria changed from *Enterobacteriaceae* to LAB (such as *Lactiplantibacillus*, *Lactococcus*, and *Limosilobacillus*) after fermentation. As the fermentation progressed, total sugar and reducing sugar eventually decreased, and total acid increased. Both lactic acid and acetic acid concentrations rapidly exceed 1.00 g/kg, thus inhibiting the proliferation of bacteria, especially *Enterobacteriaceae*. Interestingly, the regulatory effects of organic acids on LAB exhibited significant variations depending on both acid concentration and bacterial strains. The growth of LAB was promoted in a low concentration (0.5 g/L) of organic acids, especially *Lv. spicheri*, which increased by 14–21% in 0.5 g/L of organic acids compared with the organic acid-free control group. In contrast, high concentrations of organic acids (8 g/L) inhibit the growth of LAB, and *Lv. spicheri* showed better tolerance than *L. p* to organic acid. Therefore, this study revealed the nonlinear regulation of organic acid during bacterial community succession in sour bamboo shoots, which provided theoretical support for the regulation of bacterial population in the traditional fermentation system.

Supplementary Materials: The following supporting information can be downloaded at https://www.mdpi.com/article/10.3390/foods14203481/s1. Figure S1: Plate count of *Enterobacteriaceae* and Lactic acid bacteria in sour bamboo shoots with different fermentation days. Table S1: Pearson correlation matrix of inter-genus relationships in sour bamboo shoot fermentation microbiota; Table S2: Correlation analysis between microbial genera and physicochemical parameters via coor.test.

Author Contributions: Conceptualization, L.J. and Y.L.; methodology, X.Z. and Y.L.; validation, X.Z. and C.Z.; formal analysis, X.Z. and P.L.; resources, H.T.; data curation, C.Z. and M.G.; writing—original draft preparation, X.Z.; writing—review and editing, Y.L. and P.L.; visualization, X.Z.; supervision, H.T.; project administration, L.J.; funding acquisition, L.J. and Y.L. All authors have read and agreed to the published version of the manuscript.

Funding: This research was funded by Natural Science Foundation of Hunan Province (2024JJ5186 and 2023JJ30289), Hu-nan Provincial Education Department (22A0156) and Natural Science Foundation of Changsha, China (kq2208074).

Institutional Review Board Statement: Not applicable.

Informed Consent Statement: Not applicable.

Data Availability Statement: The original contributions presented in the study are included in the article/Supplementary Materials. Further inquiries can be directed to the corresponding authors.

Acknowledgments: The authors would like to acknowledge everyone who provided helpful guidance, and we extend our sincere gratitude to Hai Huang and Liuzhou Meishenyuan Food Technology Co., Ltd. for their kind support in supplying the specialized raw materials and would also like to thank the anonymous reviewers for their useful comments.

Conflicts of Interest: The authors declare no conflicts of interest.

References

1. Song, H.S.; Whon, T.W.; Kim, J.; Lee, S.H.; Kim, J.Y.; Kim, Y.B.; Choi, H.; Rhee, J.; Roh, S.W. Microbial niches in raw ingredients determine microbial community assembly during kimchi fermentation. *Food Chem.* **2020**, *318*, 126481. [CrossRef]
2. Chen, Y.; Qin, F.; Dong, M. Dynamic changes in microbial communities and physicochemical characteristics during fermentation of non-post fermented Shuidouchi. *Front. Nutr.* **2022**, *9*, 926637. [CrossRef]
3. Jiang, F.; Cheng, H.; Liu, D.; Wei, C.; An, W.; Wang, Y.; Sun, H.; Song, E. Treatment of whole-plant corn silage with lactic acid bacteria and organic acid enhances quality by elevating acid content, reducing pH, and inhibiting undesirable microorganisms. *Front. Microbiol.* **2020**, *11*, 593088. [CrossRef]

4. De Castro, A.; Sánchez, A.H.; López-López, A.; Cortés-Delgado, A.; Medina, E.; Montaño, A. Microbiota and metabolite profiling of spoiled Spanish-style green table olives. *Metabolites* **2018**, *8*, 73. [CrossRef]
5. Liu, Y.; Wan, B.; Yang, F.; Zhang, X.; Li, J.; Du, G.; Wang, L.; Chen, J. Metabolomics-driven elucidation of interactions between *Saccharomyces cerevisiae* and *Lactobacillus panis* from Chinese Baijiu fermentation microbiome. *Fermentation* **2022**, *8*, 33. [CrossRef]
6. Li, J.; Liu, Y.; Xiao, H.; Huang, H.; Deng, G.; Chen, M.; Jiang, L. Bacterial communities and volatile organic compounds in traditional fermented salt-free bamboo shoots. *Food Biosci.* **2022**, *50*, 102006. [CrossRef]
7. Guan, Q.; Huang, T.; Peng, F.; Huang, J.; Liu, Z.; Peng, Z.; Xie, M.; Xiong, T. The microbial succession and their correlation with the dynamics of flavor compounds involved in the natural fermentation of suansun, a traditional Chinese fermented bamboo shoots. *Food Res. Int.* **2022**, *157*, 111216. [CrossRef] [PubMed]
8. Chen, C.; Cheng, G.; Liu, Y.; Yi, Y.; Chen, D.; Zhang, L.; Wang, X.; Cao, J. Correlation between microorganisms and flavor of Chinese fermented sour bamboo shoot: Roles of *Lactococcus* and *Lactobacillus* in flavor formation. *Food Biosci.* **2022**, *50*, 101994. [CrossRef]
9. Chen, C.; Li, J.; Cheng, G.; Liu, Y.; Yi, Y.; Chen, D.; Wang, X.; Cao, J. Flavor changes and microbial evolution in fermentation liquid of sour bamboo shoots. *J. Food Compos. Anal.* **2023**, *120*, 105273. [CrossRef]
10. Guo, R.; Yu, F.; Wang, C.; Jiang, H.; Yu, L.; Zhao, M.; Liu, X. Determination of the volatiles in fermented bamboo shoots by Head Space–Solid-Phase Micro Extraction (HS-SPME) with Gas Chromatography–Olfactory–Mass Spectrometry (GC-O-MS) and Aroma Extract Dilution Analysis (AEDA). *Anal. Lett.* **2021**, *54*, 1162–1179. [CrossRef]
11. Qian, Q.; Chen, Z.; Li, K.; Xiong, J.; Lu, Y.; Xu, H.; Xu, Z. Guangxi sour bamboo shoots: A study on microbial diversity and flavor characteristics across regions. *J. Food Compos. Anal.* **2024**, *135*, 106641. [CrossRef]
12. Tang, H.; Ma, J.; Chen, L.; Jiang, L.; Kang, L.; Guo, Y.; Men, G.; Nie, D.; Zhong, R. Characterization of key flavor substances and their microbial sources in traditional sour bamboo shoots. *Food Chem.* **2024**, *437*, 137858. [CrossRef] [PubMed]
13. Zhang, X.; Wang, A.; Li, J.; Shan, Y.; Gong, X.; Yao, H.; Zhou, W.; Wang, M.; Liang, B.; Wang, F.; et al. Volatiles and bacterial composition of pickled bamboo shoots within 10 pre-packaged Chinese Luosifen disclosed by GC–MS, GC-IMS, and high-throughput sequencing. *Innov. Food Sci. Emerg. Technol.* **2024**, *96*, 103794. [CrossRef]
14. Danial, A.M.; Medina, A.; Magan, N. *Lactobacillus plantarum* strain HT-W104-B1: Potential bacterium isolated from Malaysian fermented foods for control of the dermatophyte *Trichophyton rubrum*. *World J. Microb. Biot.* **2021**, *37*, 57. [CrossRef]
15. Kim, K.H.; Chun, B.H.; Baek, J.H.; Roh, S.W.; Lee, S.H.; Jeon, C.O. Genomic and metabolic features of *Lactobacillus sakei* as revealed by its pan-genome and the metatranscriptome of kimchi fermentation. *Food Microbiol.* **2020**, *86*, 103341. [CrossRef]
16. Liu, N.; Qin, L.; Miao, S. Regulatory mechanisms of l-lactic acid and taste substances in Chinese acid rice soup (Rice-Acid) fermented with a *Lacticaseibacillus paracasei* and *Kluyveromyces marxianus*. *Front. Microbiol.* **2021**, *12*, 594631. [CrossRef]
17. Chen, G.; Li, W.; Tong, S.; Qiu, Y.; Han, J.; Lv, X.; Ai, L.; Sun, J.; Sun, B.; Ni, L. Effects of the microbial community on the formation of volatile compounds and biogenic amines during the traditional brewing of *Hongqu* rice wine. *Curr. Res. Food Sci.* **2022**, *5*, 1433–1444. [CrossRef]
18. Öz, E.; Kaban, G.; Barış, Ö.; Kaya, M. Isolation and identification of lactic acid bacteria from pastırma. *Food Control* **2017**, *77*, 158–162. [CrossRef]
19. Shao, Y.; Wu, X.; Yu, Z.; Li, M.; Sheng, T.; Wang, Z.; Tu, J.; Song, X.; Qi, K. Gut microbiome analysis and screening of lactic acid bacteria with probiotic potential in Anhui swine. *Animals* **2023**, *13*, 3812. [CrossRef]
20. Padovani, N.F.A.; Santos, T.S.; Almeida, P.; Dias, M.; Mendes, M.A.; Cesar, A.S.M.; Maffei, D.F. *Salmonella* and other Enterobacteriaceae in conventional and organic vegetables grown in Brazilian farms. *Braz. J. Microbiol.* **2023**, *54*, 1055–1064. [CrossRef]
21. Lu, X.; Han, B.; Deng, X.; Deng, S.; Zhang, Y.; Shen, P.; Hui, T.; Chen, R.; Li, X.; Zhang, Y. Pomegranate peel extract ameliorates the severity of experimental autoimmune encephalomyelitis via modulation of gut microbiota. *Gut Microbes* **2020**, *12*, 1857515. [CrossRef]
22. Knuesel, T.; Mohajeri, M.H. The role of the gut microbiota in the development and progression of major depressive and bipolar disorder. *Nutrients* **2022**, *14*, 37. [CrossRef]
23. Cao, X.; Zhao, M.; Zou, S.; Li, Z.; Wu, Y.; Ji, C.; Chen, Y.; Dong, L.; Zhang, S.; Liang, H. Effect of autochthonous lactic acid bacteria-enhanced fermentation on the quality of Suancai. *Foods* **2022**, *11*, 3310. [CrossRef]
24. Jeong, S.H.; Jung, J.Y.; Lee, S.H.; Jin, H.M.; Jeon, C.O. Microbial succession and metabolite changes during fermentation of dongchimi, traditional Korean watery kimchi. *Int. J. Food Microbiol.* **2013**, *164*, 46–53. [CrossRef] [PubMed]
25. Yu, X.; Jiang, W.; Kosik, R.O.; Song, Y.; Luo, Q.; Qiao, T.; Tong, J.; Liu, S.; Deng, C.; Qin, S.; et al. Gut microbiota changes and its potential relations with thyroid carcinoma. *J. Adv. Res.* **2022**, *35*, 61–70. [CrossRef] [PubMed]
26. Liang, H.; Chen, H.; Ji, C.; Lin, X.; Zhang, W.; Li, L. Dynamic and functional characteristics of predominant species in industrial paocai as revealed by combined DGGE and metagenomic sequencing. *Front. Microbiol.* **2018**, *9*, 2416. [CrossRef] [PubMed]
27. Singhal, P.; Satya, S.; Naik, S.N. Fermented bamboo shoots: A complete nutritional, anti-nutritional and antioxidant profile of the sustainable and functional food to food security. *Food Chem. Mol. Sci.* **2021**, *3*, 100041. [CrossRef]

28. Kozukue, E.; Kozukue, N.; Kurosaki, T. Organic acid, sugar and amino acid composition of bamboo shoots. *J. Food Sci.* **1983**, *48*, 935–938. [CrossRef]
29. Sun, J.; Li, Q.; Xu, H.; Zhang, W. Analysis of metabolomic changes in xylem and phloem sap of cucumber under phosphorus stresses. *Metabolites* **2022**, *12*, 361. [CrossRef]
30. Pswarayi, F.; Gänzle, M.G. Composition and origin of the fermentation microbiota of mahewu, a Zimbabwean fermented cereal beverage. *Appl. Environ. Microbiol.* **2019**, *85*, e03130-18. [CrossRef]
31. Wuyts, S.; Van Beeck, W.; Oerlemans, E.F.M.; Wittouck, S.; Claes, I.J.J.; De Boeck, I.; Weckx, S.; Lievens, B.; De Vuyst, L.; Lebeer, S. Carrot juice fermentations as man-made microbial ecosystems dominated by lactic acid bacteria. *Appl. Environ. Microbiol.* **2018**, *84*, e00134-18. [CrossRef]
32. Lee, J.; Heo, G.; Lee, J.W.; Oh, Y.; Park, J.A.; Park, Y.; Pyun, Y.; Ahn, J.S. Analysis of kimchi microflora using denaturing gradient gel electrophoresis. *Int. J. Food Microbiol.* **2005**, *102*, 143–150. [CrossRef] [PubMed]
33. Liu, L.; She, X.; Chen, X.; Qian, Y.; Tao, Y.; Li, Y.; Guo, S.; Xiang, W.; Liu, G.; Rao, Y. Microbiota succession and chemical composition involved in the radish fermentation process in different containers. *Front. Microbiol.* **2020**, *11*, 445. [CrossRef]
34. Wu, R.; Yu, M.; Liu, X.; Meng, L.; Wang, Q.; Xue, Y.; Wu, J.; Yue, X. Changes in flavour and microbial diversity during natural fermentation of suan-cai, a traditional food made in Northeast China. *Int. J. Food Microbiol.* **2015**, *211*, 23–31. [CrossRef]
35. Chiş, M.S.; Păucean, A.; Man, S.M.; Bonta, V.; Pop, A.; Stan, L.; Beldean Tătar, B.V.; Pop, C.R.; Mureşan, V.; Muste, S. Effect of rice flour fermentation with *Lactobacillus spicheri* DSM 15429 on the nutritional features of gluten-free muffins. *Foods* **2020**, *9*, 822. [CrossRef]
36. Aiello, A.; Pizzolongo, F.; De Luca, L.; Blaiotta, G.; Aponte, M.; Addeo, F.; Romano, R. Production of butyric acid by different strains of *Lactobacillus plantarum* (*Lactiplantibacillus plantarum*). *Int. Dairy J.* **2023**, *140*, 105589. [CrossRef]
37. Todorov, S.D.; Baretto Penna, A.L.; Venema, K.; Holzapfel, W.H.; Chikindas, M.L. Recommendations for the use of standardised abbreviations for the former *Lactobacillus* genera, reclassified in the year 2020. *Benef. Microbes* **2023**, *15*, 1–4. [CrossRef] [PubMed]
38. Sun, L.; Bai, C.; Xu, H.; Na, N.; Jiang, Y.; Yin, G.; Liu, S.; Xue, Y. Succession of bacterial community during the initial aerobic, intense fermentation, and stable phases of whole-plant corn silages treated with lactic acid bacteria suspensions prepared from other silages. *Front. Microbiol.* **2021**, *12*, 655095. [CrossRef]
39. Vivijs, B.; Moons, P.; Aertsen, A.; Michiels, C.W. Acetoin synthesis acquisition favors Escherichia coli growth at low pH. *Appl. Environ. Microbiol.* **2014**, *80*, 6054–6061. [CrossRef] [PubMed]
40. Wang, Y.; Wang, C.; Zhou, W.; Yang, F.; Chen, X.; Zhang, Q. Effects of wilting and *Lactobacillus plantarum* addition on the fermentation quality and microbial community of Moringa oleifera leaf silage. *Front. Microbiol.* **2018**, *9*, 1817. [CrossRef]
41. Lu, H.; Huang, C.; Yu, K.; Liu, Z. Effects of mixed inoculation of *Leuconostoc citreum* and *Lactobacillus plantarum* on suansun (Sour bamboo shoot) fermentation. *Food Biosci.* **2022**, *47*, 101688. [CrossRef]
42. Chang, L.; Mu, G.; Wang, M.; Zhao, T.; Tuo, Y.; Zhu, X.; Qian, F. Microbial diversity and quality-related physicochemical properties of spicy cabbage in northeastern China and their correlation analysis. *Foods* **2022**, *11*, 1511. [CrossRef] [PubMed]
43. Xiao, M.; Xiong, T.; Peng, Z.; Liu, C.; Huang, T.; Yu, H.; Xie, M. Correlation between microbiota and flavours in fermentation of Chinese Sichuan Paocai. *Food Res. Int.* **2018**, *114*, 123–132. [CrossRef] [PubMed]
44. Cui, Y.; Wang, M.; Zheng, Y.; Miao, K.; Qu, X. The Carbohydrate metabolism of *Lactiplantibacillus plantarum*. *Int. J. Mol. Sci.* **2021**, *22*, 13452. [CrossRef]
45. Cirlini, M.; Ricci, A.; Galaverna, G.; Lazzi, C. Application of lactic acid fermentation to elderberry juice: Changes in acidic and glucidic fractions. *LWT* **2020**, *118*, 108779. [CrossRef]
46. Briz-Cid, N.; Rial-Otero, R.; Cámara, M.A.; Oliva, J.; Simal-Gandara, J. Dissipation of three fungicides and their effects on anthocyanins and color of Monastrell red wines. *Int. J. Mol. Sci.* **2019**, *20*, 1447. [CrossRef]
47. Gong, L.; Ren, C.; Xu, Y. GlnR negatively regulates glutamate-dependent acid resistance in *Lactobacillus brevis*. *Appl. Environ. Microbiol.* **2020**, *86*, e02615-19. [CrossRef]
48. Kawai, T.; Ohshima, T.; Tanaka, T.; Ikawa, S.; Tani, A.; Inazumi, N.; Shin, R.; Itoh, Y.; Meyer, K.; Maeda, N. *Limosilactobacillus* (*Lactobacillus*) fermentum ALAL020, a probiotic candidate bacterium, produces a cyclic dipeptide that suppresses the periodontal pathogens *Porphyromonas gingivalis* and *Prevotella intermedia*. *Front. Cell. Infect. Microbiol.* **2022**, *12*, 804334. [CrossRef]
49. Liu, G.; Wang, Y.; Li, X.; Hao, X.; Xu, D.; Zhou, Y.; Mehmood, A.; Wang, C. Genetic and biochemical evidence that *Enterococcus faecalis* Gr17 produces a novel and sec-dependent bacteriocin, Enterocin Gr17. *Front. Microbiol.* **2019**, *10*, 1806. [CrossRef]
50. Rodríguez, H.; Curiel, J.A.; Landete, J.M.; de Las Rivas, B.; de Felipe, F.L.; Gómez-Cordovés, C.; Mancheño, J.M.; Muñoz, R. Food phenolics and lactic acid bacteria. *Int. J. Food Microbiol.* **2009**, *132*, 79–90. [CrossRef]

Disclaimer/Publisher's Note: The statements, opinions and data contained in all publications are solely those of the individual author(s) and contributor(s) and not of MDPI and/or the editor(s). MDPI and/or the editor(s) disclaim responsibility for any injury to people or property resulting from any ideas, methods, instructions or products referred to in the content.

foods

MDPI

Article

Multi-Technique Flavoromics for Identifying Key Differential Volatile Compounds Underlying Sensory Profiles in Lager Beers

Yiyuan Chen [1,2,3,†], He Huang [1,2,3,†], Ruiyang Yin [4], Xiuli He [4], Liyun Guo [4], Yumei Song [4], Dongrui Zhao [1,2,3,*], Jinyuan Sun [1,2,3], Jinchen Li [1,2,3], Mingquan Huang [1,2,3] and Baoguo Sun [1,2,3]

[1] China Food Flavor and Nutrition Health Innovation Center, Beijing Technology and Business University, Beijing 100048, China; chenyiyuan_1112@163.com (Y.C.)
[2] Key Laboratory of Brewing Molecular Engineering of China Light Industry, Beijing Technology and Business University, Beijing 100048, China
[3] Beijing Laboratory of Food Quality and Safety, Beijing Technology and Business University, Beijing 100048, China
[4] Technology Center of Beijing Yanjing Beer Co., Ltd., Beijing 101300, China
* Correspondence: zdr@btbu.edu.cn; Tel.: +86-10-68984044; Fax: +86-10-68984890
† These authors contributed equally to this work.

Abstract

In this study, inter-brand variations in volatile flavor compound profiles of four lager beers were systematically investigated by integrating sensory evaluation with GC-MS, GC×GC-TOF-MS, and GC-O-MS. A total of 594 volatile compounds were identified, of which 71 with odor activity values (OAV) ≥ 1 were found to contribute directly to aroma expression. Additionally, 59 compounds with taste activity values (TAV) ≥ 1 were identified and may also contribute to taste perception. Furthermore, 53 aroma-active compounds were confirmed through GC-O-MS, providing additional evidence for their sensory contribution. Partial least squares discriminant analysis (PLS-DA), correlation analysis, and flavor addition experiments revealed brand-specific differential flavor compounds. Ultimately, twenty key differential flavor compounds, encompassing esters, alcohols, aromatic compounds, acids, lactones, and others, were confirmed to contribute to fruity, floral, burnt, and sweet notes. Phenethyl alcohol, with concentrations varying from 1377.1 mg/L in QD to 3297.5 mg/L in HR, showed a more than 2.4-fold difference across brands and was strongly associated with fruity (r = 0.553) and floral (r = 0.564) aroma. These compounds acted in combination to shape distinct aroma profiles. This study provides a molecular-level basis for understanding lager beer flavor and offers practical guidance for targeted flavor modulation in brewing.

Keywords: lager beer; volatile compounds; odor activity value (OAV); taste activity value (TAV); sensory evaluation; multivariate statistical analysis; flavor addition validation

1. Introduction

Lager beer, as one of the most widely consumed beer types globally, owes its market appeal largely to its flavor characteristics, which serve as a decisive factor in consumer preference. It is typically brewed using barley malt as the primary grain source through a multi-stage process involving malting, mashing, wort production, and the addition of hops, along with water and bottom-fermenting yeast [1]. Noticeable differences in flavor are frequently observed among different brands, indicating that the composition and relative concentrations of compounds may play a crucial role in shaping brand-specific profiles.

Volatile compounds, including esters, alcohols, and aromatic compounds, are the primary contributors to beer flavor [2], and variations in their types and concentrations directly influence the complexity and uniqueness of the flavor [3]. These compositional differences are largely influenced by raw materials such as malt and hops, brewing processes, and yeast strains [4–6]. However, the mechanisms through which these factors drive brand-specific differences in the flavor profile have yet to be systematically elucidated. Although prior studies have explored volatile compound compositions, systematic investigations of the chemical basis and sensory implications of brand-specific differences remain limited, hindering precise flavor modulation to meet growing consumer demand for flavor diversification. In recent years, consumer demand for flavor diversification in beer has been increasing, whereas industrial standardization in production may result in flavor homogenization. Therefore, elucidating inter-brand differences in volatile compounds at the molecular level is of great significance for optimizing flavor modulation and enhancing product competitiveness.

Beer represents a complex matrix rich in proteins and other macromolecules. These constituents often interfere with analytical procedures, leading to column blockage and detector contamination, thereby complicating the reliable extraction and characterization of volatile compounds. Thus, several extraction techniques for volatile compounds in beer have been developed, including liquid–liquid extraction (LLE), headspace solid-phase microextraction (HS-SPME) [7], and solvent-assisted flavor evaporation (SAFE) [8]. The combined application of these methods not only enhances the recovery of volatile compounds with different physicochemical properties but also improves analytical accuracy and representativeness, and they have therefore been widely adopted in current flavor research. Richter et al. compared the effects of HS-SPME and SAFE on hop volatiles, finding that SAFE was more suitable for alcohols and acids, while HS-SPME was suitable for highly volatile compounds such as esters; however, the limited surface area in HS-SPME resulted in a 40% reduction in extracted compounds [9]. In recent years, HS-SPME has become the most widely used extraction technique prior to gas chromatography–mass spectrometry (GC-MS) quantification due to its high efficiency and operational simplicity [10]. HS-SPME has been optimized to efficiently extract a broad spectrum of volatile organic compounds from wort, beer fermentation samples, and finished beer [11]. When combined with GC-MS, HS-SPME has been reported to enable the quantification and annotation of numerous volatile compounds, with up to 397 compounds identified across four types of beer [12]. Nevertheless, GC-MS is subject to co-eluting chromatographic peaks, which can interfere with compound identification, and it is unable to detect certain trace-level constituents. Current analytical techniques often focus on single methods, lacking integration of multiple approaches to comprehensively characterize complex volatile compound profiles and their brand-specific differences. Comprehensive two-dimensional gas chromatography–time-of-flight mass spectrometry (GC×GC-TOF MS), which employs two columns with differing polarities for orthogonal separation, can more effectively resolve compounds with similar retention times and mitigate the impact of co-elution on qualitative and quantitative analyses [13]. A total of 215 volatile metabolites were identified in Undaria-based alcoholic beverages using HS-SPME coupled with GC×GC-TOF-MS. Esters were found to be the most abundant chemical class across all samples, followed by alcohols and ketones, suggesting their predominant contribution to the overall aroma profile [14]. Compared with one-dimensional gas chromatography, GC×GC offers higher peak capacity and sensitivity, and has been widely applied to the analysis of volatile compounds in various foods. However, it does not provide information on the odor characteristics of the compounds or their contribution to the sample aroma [15].

Aroma plays a crucial role in maintaining beer quality and appeal. These flavor compounds typically occur at very low concentrations, accounting for less than 3–5% of the total volatiles in beer [16]. Gas chromatography–olfactometry–mass spectrometry (GC-O-MS) is effective in analyzing aroma-active compounds in complex odor mixtures [17] and has been widely applied in the flavor analysis of various foods. Characteristic aroma-active compounds in wheat beer have been identified using GC-O-MS, including 2-methoxyphenol (smoky, phenolic), 2-ethyl-3,6-dimethylpyrazine (earthy), 2,3-diethyl-5-methylpyrazine (earthy), and maltol (caramel-like) [18]. Among the abundant volatile compounds, only a small subset contributes significantly to beer aroma; these are referred to as key flavor compounds or character-impact aroma compounds [15]. Molecular sensory science has been widely employed to systematically analyze beer flavor and describe key aroma-active compounds [19]. In caramel malt beer, compounds such as (E)-β-damascenone, 2-acetyl-1-pyrroline, methional, 2-ethyl-3,5-dimethylpyrazine, and 6-methyl-5-hepten-2-one have been reported to exhibit particularly high odor activity value (OAV), while 2-methoxyphenol showed the highest OAV in roasted malt beer [20]. However, due to interactions among aroma compounds, even after identifying individual aroma-active compounds, it remains necessary to validate flavor similarity with actual samples using standard references. This is essential for understanding the chemical origins of beer flavor [21]. Furthermore, studies on the correlation between sensory attributes and chemical composition often rely on empirical descriptions, lacking systematic integration based on multi-dimensional data encompassing chemical analysis, sensory evaluation, and statistical modeling.

In this context, the present study focuses on four different brands of lager beer with the objective of systematically elucidating the differences in volatile compounds among brands and revealing their intrinsic associations with sensory attributes through multi-technique integration and multi-dimensional data analysis. Specifically, LLE-SAFE and HS-SPME were combined with GC-MS, GC×GC-TOF MS, and GC-O-MS for comprehensive identification of volatile compounds in lager beers. Molecular sensory science was integrated with multivariate statistical analysis to determine potential differentiating compounds, followed by sensory validation to confirm key differential volatiles. This study provides a chemical basis for brand-specific volatile differences, advancing beer flavor chemistry from empirical description toward precise modulation and supporting product differentiation in a competitive market.

2. Materials and Methods

2.1. Sample Collection

Four commercially available lager beers were selected for analysis, each representing a distinct brand and formulation. The samples included U8 from Beijing Yanjing Brewery Co., Ltd., Beijing, China, (coded as YJ), Classic from Tsingtao Brewery Group Co., Ltd., Qingdao, China, (coded as QD), Brave the World from China Resources Beer (Holdings) Co., Ltd., Hong Kong, China, (coded as HR), and Ice Beer from Budweiser Asia Pacific Holdings Ltd., Hong Kong, China, (coded as BW). All beers had an original wort concentration of 8 °P and were brewed using water, malt, and hops as the primary ingredients, with variations in adjuncts such as rice, brewing syrup, hop extract, or yeast depending on the brand-specific recipe. These brands were chosen for their extensive consumer base in China, strong market representation, and regional characteristics, reflecting diverse flavor and brewing processes (e.g., variations in raw materials and yeast strains). This selection effectively captures the diversity of brand-specific volatile compounds and regional flavor profiles.

In addition to these commercial samples, a 10 °P lager beer, produced by Beijing Yanjing Brewery Co., Ltd., Beijing, China, under the product name Qing Shuang Beer, was

acquired for use as the base matrix in subsequent recombination and addition experiments. This beer was chosen because of its relatively simple volatile background, which minimizes sensory interference. The specific brand formulations are provided in Appendix A Table A1. All samples were purchased from local retail outlets within one week of analysis to minimize storage-related changes in volatile composition. The beers were transported under refrigerated conditions to the laboratory and stored at 4 °C until further processing. One bottle was selected from each brand (YJ, QD, HR, and BW) for analysis. Each beer sample was analyzed in technical triplicate to ensure instrumental reproducibility (n = 3).

2.2. Materials

Anhydrous ethanol and dichloromethane (99.9%, chromatographic grade) were purchased from Aladdin Biochemical Technology Co., Ltd. (Shanghai, China). Anhydrous sodium sulfate (99.8%, analytical grade) was obtained from Sinopharm Chemical Reagent Beijing Co., Ltd. Internal standards, including 2-ethylbutyric acid (IS1), 4-octanol (IS2), and ethyl valerate (IS3), all of chromatographic grade with a purity of no less than 97.0%, were supplied by J&K Scientific Ltd. (Beijing, China). A mixture of C3–C30 n-alkanes (chromatographic grade) was purchased from Sigma–Aldrich (St. Louis, MO, USA). Analytical standards for the identification and quantification of trace components were obtained from J&K Scientific Ltd. (Beijing, China), all with a purity of at least 97.0%.

2.3. LLE-SAFE and HS-SPME

Beer samples were first subjected to liquid–liquid extraction (LLE). A volume of 150 mL of beer was placed in a separation vessel, sodium chloride was added, and the sample was extracted three times with dichloromethane, 50 mL each time. The combined extracts were subsequently processed using solvent-assisted flavor evaporation (SAFE). A 500 mL dry round-bottom flask was used as the receiving vessel, the cold trap was filled with liquid nitrogen, and another round-bottom flask was placed in a water bath maintained at 40 °C. The compound turbomolecular pump was activated, and once the absolute pressure of the system reached 1×10^{-4} MPa, the combined LLE extract was slowly introduced into the SAFE apparatus for distillation. The flow rate of the sample was kept constant during operation. The collected distillate was concentrated to 1 mL using a rotary evaporator. All processed samples were stored at −20 °C until subsequent GC-O-MS and GC×GC-TOF MS analyses [22].

To compensate for the loss of low-boiling volatile compounds during LLE, headspace solid-phase microextraction (HS-SPME) was employed for the analysis of volatile components in the beer samples. A 5 mL aliquot of beer was transferred into a 20 mL headspace vial, followed by the addition of 25 μL of internal standard solution (2-ethylbutyric acid, IS1; 4-octanol, IS2; ethyl valerate, IS3) and 1.50 g of sodium chloride to saturation. The vial was immediately sealed with a silicone septum cap. The sample was equilibrated in a water bath at 40 °C for 30 min, after which a 50/30 μm DVB/CAR/PDMS fiber was exposed to the headspace for 40 min at the same temperature. The fiber was then promptly inserted into the gas chromatograph injection port and desorbed at 250 °C for 5 min for analysis [23,24].

2.4. Analytical Instrumentation and Conditions

2.4.1. GC-MS Conditions

Volatile compounds were analyzed using a GC-MS system equipped with a polar DB-FFAP column (60 m × 0.25 mm × 0.25 μm). Each sample (1.0 μL), prepared via HS-SPME, was injected in splitless mode, and each analysis was performed in triplicate. High-purity helium (99.999%) was used as the carrier gas at a constant flow rate of 1.0 mL/min. The injector temperature was set at 250 °C. The column temperature program was as follows:

initial temperature of 40 °C held for 5 min, increased at 5 °C/min to 70 °C and held for 15 min, then increased at 1 °C/min to 100 °C and held for 5 min, followed by an increase at 3 °C/min to 240 °C and held for 10 min. The mass spectrometer was operated in electron impact (EI) mode at 70 eV, with quadrupole and ion source temperatures set at 150 °C and 230 °C, respectively. The scan range was 35–550 amu in full-scan mode, with a solvent delay of 3 min and a transfer line temperature of 245 °C.

2.4.2. GC-O-MS Conditions

GC-O-MS was used to identify potential aroma-active compounds. The DB-FFAP column (60 m × 0.25 mm × 0.25 μm) was used with helium (99.999%) as the carrier gas at a flow rate of 1.0 mL/min. Samples (1.0 μL) were injected in splitless mode, and the effluent was split 1:1 between the mass spectrometer (250 °C) and the olfactometry port (250 °C). Three trained panelists (one male and two females) performed GC-O analysis. During operation, panelists positioned their noses above the olfactometry port to sniff and record the retention time, odor description, and intensity of each eluted compound. Odor intensity was rated on a five-point scale (0 = none, 1 = very weak, 2 = weak, 3 = moderate, 4 = strong, 5 = very strong), and the Osme value for each compound was calculated as the average score from the three panelists. Each sample was analyzed in triplicate. The column oven was initially held at 40 °C, increased at 10 °C/min to 50 °C and held for 20 min, then increased at 1 °C/min to 70 °C and held for 10 min, and finally increased at 3 °C/min to 250 °C and held for 15 min. The mass spectrometer operated in EI mode at 70 eV in full-scan mode over the range m/z 45–550 amu [25].

2.4.3. GC×GC-TOF MS Conditions

A GC×GC-TOF MS system was used for the analysis of trace volatile compounds. The system was equipped with two columns: a DB-Wax column (60 m × 0.25 mm × 0.25 μm) as the first dimension and a DB-17 ms column (1.85 m × 0.18 mm × 0.18 μm) as the second dimension, with a thermal modulator positioned between the columns. Helium (99.999%) was used as the carrier gas at a constant flow rate of 2.1 mL/min. The primary oven temperature program was as follows: initial temperature of 40 °C held for 5 min, increased at 3 °C/min to 230 °C and held for 10 min. The cold zone of the modulator was set to −50 °C. The hot and cold jet temperatures were maintained at 70 °C and 160 °C above the primary oven temperature, with maximum temperatures of 260 °C and 320 °C, respectively. The modulation period was 5 s. For TOF MS detection, the transfer line and ion source temperatures were set to 250 °C and 230 °C, respectively, with electron impact energy at 70 eV. The mass range was m/z 35–350 amu [26].

2.5. Qualitative and Quantitative Analysis

The qualitative identification of volatile compounds in beer was performed using four criteria. For mass spectrometric (MS) identification, background noise was subtracted from chromatograms, and compound spectra were matched against the NIST 2020 library and the LIQUOR (in-house) mass spectral libraries. Only compounds with a match score greater than 80% were retained. For retention index (RI) identification, n-alkanes (C_3–C_{30}) were analyzed before and after sample injection under identical chromatographic conditions, and retention indices were calculated based on retention times. Compounds with RI values within an absolute difference of 30 from literature data were considered identical. For aroma sniffing identification, compounds whose odor characteristics matched those of the reference standards were considered identical. For standard substance identification, standards were analyzed under the same chromatographic conditions as the beer samples. Compounds were confirmed as identical when their characteristic ion peaks and retention times were consistent between the sample and the standard mass spectra.

Quantification of volatile compounds was performed using internal standards in combination with calibration curves. A 3% (v/v) aqueous ethanol solution was used as the matrix, and working standard solutions were prepared at appropriate gradient concentrations based on the levels of each compound in beer. Both the working standards and beer samples were analyzed under the same chromatographic conditions. Calibration curves were constructed by plotting the ratio of the peak area of the compound to that of the internal standard on the x-axis against the compound concentration on the y-axis. Internal standard IS1 was used for acids, IS2 for alcohols, and IS3 for esters and other compounds. Calibration curve information is shown in Appendix A Table A2. All analyses were performed in triplicate [27].

2.6. Odor Activity Value (OAV) and Taste Activity Value (TAV) Calculation

Odor activity values (OAV) and taste activity values (TAV) are defined as the ratios of compound concentrations to their respective odor and taste thresholds [27]. Based on the quantitative results and the published sensory thresholds for each compound in alcoholic beverages, OAV and TAV values were calculated for trace compounds in all representative samples [28,29].

2.7. Flavor Perception Evaluation of Lager Beers

Prior to the experiment, ten trained panelists (five males and five females, aged 21–28 years) with at least one year of experience in sensory evaluation were recruited from the Key Laboratory of Brewing Molecular Engineering of China Light Industry to form a sensory evaluation panel. The sensory quantitative descriptive analysis (SQDA) method was applied to assess the sensory attributes of the beer samples. All panelists completed a two-week structured training program, which included aroma reference compound familiarization, terminology alignment, intensity scaling practice using representative beer samples, and consensus development on aroma descriptors. Frequently occurring descriptive terms were screened and compiled into a standardized list of sensory attributes, based on both training sessions and the aroma descriptions of the beers. The final set of sensory attributes included fruity, floral, woody, husky, grassy, cereal-like, roasted, phenolic, acidic, sulfurous, oily, sweet, and off-flavor notes.

Additionally, three panelists, selected from the SQDA panel based on specialized olfactory training, formed the gas chromatography–olfactometry (GC-O) panel to identify key aroma-active compounds. The smaller GC-O panel size was due to the high level of specialized olfactory expertise required, typically performed by a limited number of highly trained experts to ensure precise olfactory data, whereas SQDA required a larger panel to capture the diversity and statistical significance of sensory attributes [30,31].

Sensory evaluations were conducted in a controlled environment (25 $\pm$ 1 °C and 35–50% relative humidity) within isolated booths to prevent panelist interaction. Each sample (50 mL) was presented in a 100 mL glass bottle coded with a random three-digit number, and each sample was evaluated in triplicate by every panelist (n = 3). The panelists were instructed to rate the intensity of each sensory attribute on a 10-point scale (0 = none, 5 = moderate, 10 = very strong). Sample presentation order was randomized to minimize order effects, and all evaluations were carried out under uniform lighting and ventilation to reduce contextual bias.

To assess whether compounds with an odor activity value (OAV) $\geq$ 1 are sufficient to reproduce the aroma sensory characteristics of different lager beer brands, the set of OAV $\geq$ 1 compounds identified in each of the four beers was selected as the aroma-active component pool for recombination modeling. A 3% (v/v) aqueous ethanol solution was used as the model base, and the selected aroma-active compounds were incorporated

at their experimentally determined concentrations. After equilibration at 25 ± 1 °C for 20 min to ensure homogeneity, four recombined beer aroma models were prepared. Each recombined model and its corresponding original beer sample were evaluated following the same procedure described above, using identical sample presentation, coding, evaluation environment, and scoring method [32].

Although the sensory panel underwent rigorous training to ensure consistency, the small GC-O panel size (3 panelists) may limit the diversity of olfactory data, and the SQDA panel (10 panelists) and its young age range (21–28 years) may not fully reflect the flavor preferences of a broader consumer population.

2.8. Adding Validation Experiment

An addition experiment was conducted to verify the contribution of the screened key differential volatile compounds to the aroma sensory attributes of lager beer [33]. Yanjing Qing Shuang Beer was selected as the base matrix due to its relatively simple volatile background, which minimizes sensory interference and allows clearer identification of the effects of the added compounds. Based on the actual concentrations determined in the tested samples, twenty key differential volatiles were selected and grouped into ten categories according to their chemical classifications: esters, alcohols, aromatics, acids, furans, lactones, sulfur-containing compounds, aldehydes, ketones, and others. This classification strategy, widely applied in sensory science, was adopted to facilitate systematic evaluation and to minimize interpretive bias from cross-category interactions.

All compounds were incorporated into the base matrix at their respective concentrations as measured in the original beer samples. No sensory-based concentration adjustments were made, ensuring that the assessment reflected real-world exposure conditions and enabling objective comparison of class-specific aroma contributions. The spiked samples were evaluated by the same panel of ten trained assessors following the procedure described in Section 2.7.

2.9. Statistical Analysis and Statistical Methods

Statistical analyses were conducted using Excel and IBM SPSS Statistics 26.0 (Chicago, IL, USA). Pearson correlation coefficients were calculated for correlation analysis. A p-value of less than 0.05 was considered statistically significant. Basic data processing was performed in Excel. The results were expressed as mean ± standard deviation (SD), based on three parallel replicates per sample. Data visualization was carried out using Origin 2021 (OriginLab Co., Northampton, MA, USA). Partial least squares discriminant analysis (PLS-DA) was performed using SIMCA 14.1 (Umetrics, Umeå, Sweden) to discriminate among beer samples based on volatile compound profiles and to identify variables contributing most to group separation.

3. Results and Discussion

3.1. Analysis of Distribution Characteristics of Volatile Compounds

Differences in the distribution of compounds among lager beers from different brands were investigated through qualitative analysis, as illustrated in Figure 1a,b. Although the beers originated from different manufacturers, their volatile profile exhibited a similar distribution pattern, dominated by alcohols, esters, and nitrogen-containing compounds. Alcohols were the most diverse group, primarily generated through microbial metabolism and serving as precursors for ester formation. Overall, the numbers of compounds identified in YJ, QD, HR, and BW were 345, 341, 374, and 358, respectively, with HR showing the highest number, followed by BW (Appendix A Table A3).

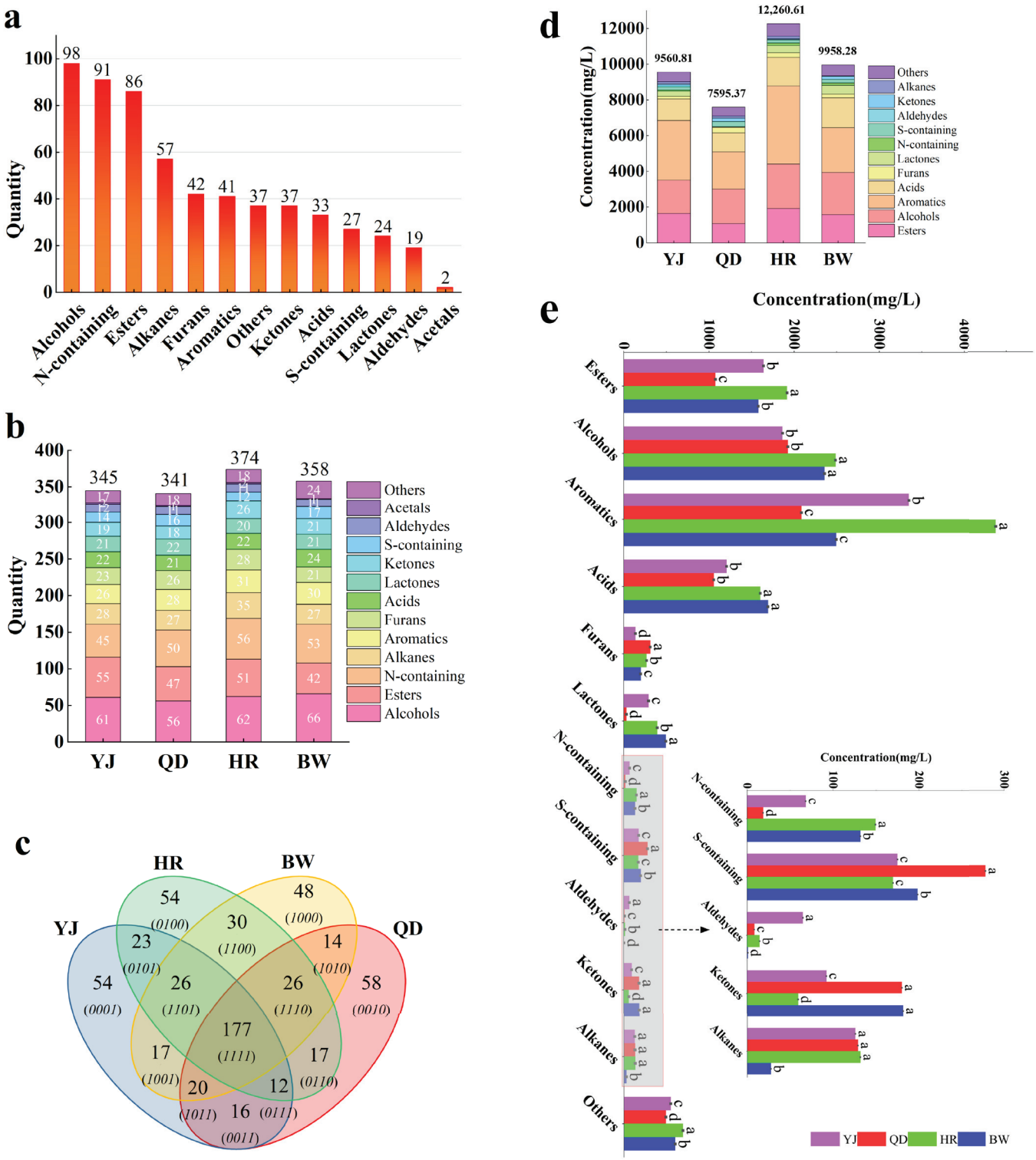


Figure 1. (**a**) Bar chart of identified volatile compounds in different brands of lager beer. (**b**) Stacked bar chart of compound classes in different brands of lager beer. (**c**) Venn diagram of compound classes identified in different brands of lager beer. (**d**) Stacked bar chart of total concentrations of volatile compounds in different brands of lager beer. (**e**) Bar chart of concentrations of volatile compounds in different brands of lager beer. The letters a, b, c, and d represent concentrations with significant differences ($p < 0.05$). The average concentration is highest for letter a and lowest for letter d. Abbreviations YJ, QD, HR, and BW are defined in the manuscript's Abbreviations section: YJ (U8, Beijing Yanjing Brewery Co., Ltd.), QD (Classic, Tsingtao Brewery Group Co., Ltd.), HR (Brave the World, China Resources Beer (Holdings) Co., Ltd.), and BW (Ice Beer, Budweiser Asia Pacific Holdings Ltd.).

Despite the comparable total numbers and categories of compounds, the Venn diagram in Figure 1c revealed significant brand-specific differences. Across the four brands, 177 volatile compounds were shared, while YJ, QD, HR, and BW contained 54, 58, 54, and 48 unique compounds, respectively. Examples of unique compounds include β-butyrolactone, ethyl thioacetate, 3-methylbutanal, ethyl benzoate, nerolidyl formate, and 1-heptanol in YJ; 1,2-butanediol, ethyl 3-methylbutanoate, butyl butanoate, butanoic acid, and 5-methyl-3-heptanone in QD; 2,5-dimethylphenol, 2-n-butylfuran, 5-methyl-2-furfural, and methyl lactate in HR; and resorcinol, ethyl cinnamate, 4-methylpentanoic acid, nonanoic acid, and methyl formate in BW. These compounds exhibit diverse sensory properties and interact with one another, collectively shaping the complexity of lager beer aroma.

Aroma-active compounds were further characterized using LLE-SAFE and gas chromatography–olfactometry (GC-O). In total, 53 aroma compounds were detected across the four beers, comprising 9 aromatics, 9 acids, 7 nitrogen-containing compounds, 7 esters, 5 furans, 4 alkanes, 4 alcohols, 3 lactones, 2 ketones, 2 sulfur-containing compounds, and 1 miscellaneous compound (Appendix A Table A4). Among these, 21 compounds were consistently identified as aroma-active in all beers, including 4-vinylguaiacol, γ-decalactone, phenylacetic acid, 3-methylbutanoic acid, sotolon, 2-phenylethyl acetate, phenylethanol, hexanoic acid, and 1-octen-3-ol, which were deemed as key contributors to the typical sensory profile of lager beers. Acids imparted sour and dark wheat-like notes, such as cis-vaccenic acid and palmitic acid, while some, like acetic acid, produced undesirable sour and muddy odors. Esters generally provided sweet, fruity, and floral notes, with monoethyl succinate contributing malty aromas. Alcohols mainly presented roasted, dark wheat, and husky notes, whereas aromatics, lactones, and ketones often offered sweet and floral attributes, such as γ-decalactone, which imparted gardenia-like sweetness and creamy notes. Most furans gave unpleasant aromas, although sotolon was an exception, imparting a pleasant caramel sweetness.

For quantitative analysis, 150 compounds were selected based on their strong aroma relevance, including 36 esters, 23 alcohols, 19 aromatics, 19 acids, 11 furans, 10 lactones, 9 nitrogen-containing compounds, 9 sulfur-containing compounds, 6 others, 4 aldehydes, 3 ketones, and 1 alkane. Significant differences ($p \leq 0.05$) in the concentrations of individual compounds among the beers were observed, such as ethyl isovalerate, ethyl propanoate, hexyl butanoate, ethyl lactate, γ-decalactone, and furfuryl alcohol. The total concentration of volatile compounds was highest in HR (12260.61 mg/L), followed by BW (9958.28 mg/L), YJ (9560.81 mg/L), and QD (7595.37 mg/L), consistent with their compositional diversity. Esters, alcohols, aromatics, and acids were the dominant quantitative contributors. Ethyl acetate, a major ester, showed the highest concentration among esters in YJ (554.93 ± 7.64a mg/L) and QD (449.33 ± 9.29b mg/L), and was also abundant in HR (515.28 ± 52.73a mg/L) and BW (367.56 ± 6.76c mg/L), second only to ethyl 3-methylbutyrate in the latter two [34]. Ethyl 3-methylbutanoate, known to enhance fruity aromas, was abundant in all beers but declines during storage, potentially impacting flavor stability [35].

Figure 1e illustrated that aromatic compounds contributed most to the between-brand differences, with HR containing the highest total aromatic content (4377.93 mg/L), followed by YJ (3348.73 mg/L), BW (2495.21 mg/L), and QD (2087.12 mg/L). HR also had the highest total concentrations of esters (1917.86 mg/L), alcohols (2485.89 mg/L), and nitrogen-containing compounds (149.26 mg/L), whereas BW contained the highest total acids (1692.25 mg/L) and lactones (493.46 mg/L), and QD exhibited the highest total furans (311.13 mg/L), sulfur-containing compounds (278.57 mg/L), and ketones (180.07 mg/L). Notably, 2-phenylethanol was the most abundant volatile in all beers, with concentrations of 3297.47 ± 217.49a, 2374.06 ± 285.93b, 1760.47 ± 226.12c, and 1377.05 ± 303.76c mg/L

in HR, YJ, BW, and QD, respectively. Other abundant volatiles included 3-methyl-1-butanol, ethyl acetate, glycerol, 2,6-di-tert-butyl-p-cresol, 1-heptene, octanoic acid, ethyl 3-methylbutanoate, and 1-pentanol. However, due to matrix effects, the contribution of each compound to beer flavor cannot be determined solely based on concentration.

3.2. Flavor Expression Evaluation

In order to screen the flavor compounds, odor specific magnitude estimation (Osme), odor activity values (OAV), and taste activity values (TAV) were applied to evaluate flavor expression for volatile compounds.

The Osme method was applied to record the aroma intensity of the aroma-active compounds, and the results were visualized as a heatmap (Figure 2a). Overall, acids, aromatics, and lactones exhibited higher aroma intensities than other classes of aroma-active compounds, followed by furans. Differences in aroma intensity among compounds were observed across the lager beer samples. In YJ, the most intense compounds were γ-decalactone (2.94 ± 0.05 mg/L), 4-vinylguaiacol (23.35 ± 0.29 mg/L), phenylacetic acid (101.22 ± 6.24 mg/L), 3-methylbutanoic acid (18.32 ± 2.46 mg/L), 2-phenylethyl acetate (25.76 ± 3.66 mg/L), acetic acid (17.47 ± 4.32 mg/L), and octanoic acid (413.13 ± 46.23 mg/L). In BW, γ-decalactone (8.77 ± 0.38 mg/L), phenylacetic acid (91.45 ± 3.00 mg/L), and 2-phenylethanol (1760.47 ± 226.12 mg/L) were dominant. In HR, the highest intensities were for γ-decalactone (5.15 ± 0.20 mg/L), acetic acid (12.29 ± 1.60 mg/L), 3-methylbutanoic acid (34.84 ± 1.53 mg/L), 2-phenylethyl acetate (59.37 ± 3.69 mg/L), and 2-phenylethanol (3297.47 ± 217.49 mg/L). In QD, γ-decalactone (3.63 ± 0.43 mg/L), 4-vinylguaiacol (24.23 ± 0.80 mg/L), acetic acid (9.53 ± 2.05 mg/L), and 3-methylbutan-1-ol (421.12 ± 70.96 mg/L) were most pronounced. Compared to YJ, BW showed a 198.30% increase in γ-decalactone concentration, a 9.66% decrease in phenylacetic acid, and a 25.86% decrease in 2-phenylethanol. Relative to YJ, HR exhibited a 75.17% increase in γ-decalactone, a 29.66% decrease in acetic acid, a 90.17% increase in 3-methylbutanoic acid, a 130.51% increase in 2-phenylethyl acetate, and a 38.90% increase in 2-phenylethanol. In comparison to YJ, QD demonstrated a 23.47% increase in γ-decalactone, a 3.77% increase in 4-vinylguaiacol, a 45.45% decrease in acetic acid, and a 25.23% decrease in 3-methylbutan-1-ol. γ-Decalactone consistently showed the highest aroma intensity in all four beers, suggesting its potential importance as a key aroma-active compound in lager beer. Other compounds exhibited sample-specific variations without a consistent trend.

As previously noted, the sensory contribution of volatile compounds in beer depends not only on their concentrations but also on their interactions and the matrix effect. Although GC-O analysis is an effective method for identifying odorants, it does not account for the influence of the beer matrix [25]. To assess the contribution of volatile compounds to lager beer flavor, odor activity values (OAVs) were calculated based on literature-reported aroma thresholds. Compounds with OAV ≥ 1 were considered to contribute directly to beer flavor, and a higher OAV indicated a greater contribution to overall flavor quality. The results (Table A5) showed that a total of 71 flavor compounds with OAV ≥ 1 were identified across the four lager beers, including 21 esters, 11 alcohols, 11 aromatics, 9 acids, 4 furans, 4 lactones, 4 sulfur-containing compounds, 3 aldehydes, 2 ketones, and 2 others. YJ, QD, HR, and BW contained 60, 52, 57, and 55 such compounds, respectively. Among these, 44 compounds were common to all four beers, mainly esters, acids, and aromatics. Acids were primarily associated with cheesy notes, esters were the major flavor contributors in beer with floral and fruity characteristics, and aromatics imparted rose-like notes [3,25]. These findings suggest that esters, acids, and aromatics are the most important flavor groups in lager beer.

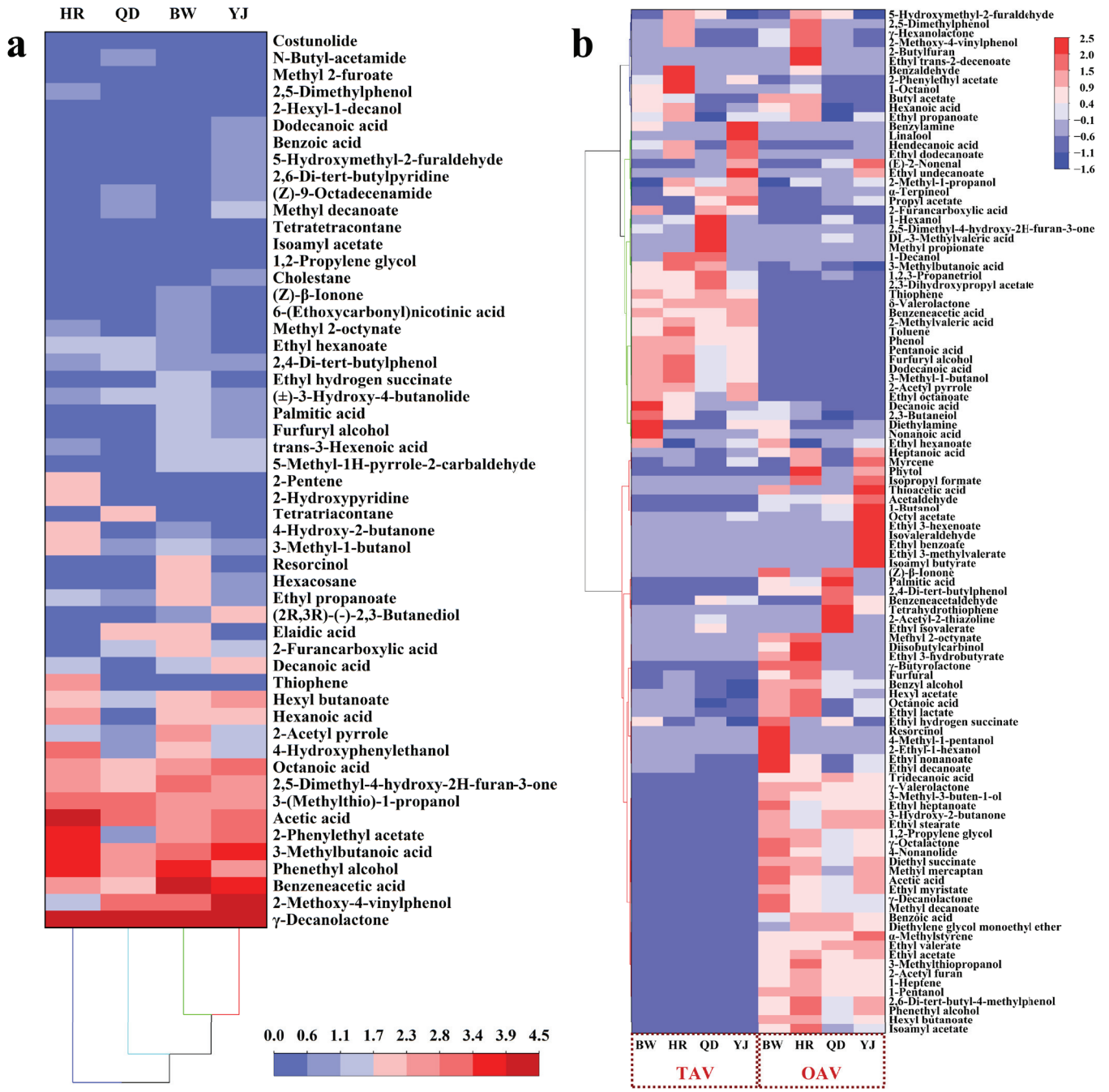


Figure 2. (**a**) Heatmap of Osme results for different brands of lager beer. (**b**) Heatmap of compounds with TAV/OAV ≥ 1. A redder color indicates a higher value. Abbreviations YJ, QD, HR, and BW are defined in the manuscript's Abbreviations section.

The highest OAV differed among samples. In YJ, 3-methylbutyl acetate (2,046,526) ranked first, followed by hexanoic acid (258,687), trans-2-nonenal (149,938), methyl decanoate (19,448), 2-methyl-1-propanol (14,796), and ethyl acetate (11,099). In QD, the top compounds were (Z)-β-ionone (14,243,050), 3-methylbutyl acetate (1,217,009), hexanoic acid (198,095), trans-2-nonenal (41,011), 3-methylbutyl propanoate (31,502), methyl decanoate (16,822), and 2-methyl-1-propanol (12,246). In HR, 3-methylbutyl acetate (4,338,735) was the highest, followed by hexanoic acid (474,974), methyl decanoate (29,701), 2-methyl-1-propanol (15,732), and ethyl acetate (10,306). In BW, (Z)-β-ionone (12,784,795) ranked first, followed by 3-methylbutyl acetate (2,821,490), hexanoic acid (419,423), methyl decanoate (45,970), and ethyl hexanoate (10,366). Some compounds, such as (Z)-β-ionone,

3-methylbutyl propanoate, hexanoic acid, methyl decanoate, and ethyl acetate, consistently exhibited high OAV in all samples, indicating substantial contributions to lager beer aroma. Certain low-abundance compounds, including myrcene, methanethiol, γ-decalactone, 4-vinylguaiacol, phenylacetaldehyde, and 3-methylbutan-1-ol, also had OAV ≥ 1 due to low aroma thresholds, whereas some high-abundance compounds, such as glycerol, 5-hydroxymethyl-2-furfural, monoethyl succinate, and diethyl succinate, showed low OAV due to high thresholds. Overall, these 71 high OAV compounds may constitute the core flavor framework of lager beer.

Odor and taste are two primary drivers of flavor perception that can act independently or interact through cross-modal effects. One such interaction is odor-induced taste perception (OICTP), in which volatile compounds stimulate olfactory receptors in the nasal epithelium retronasally during consumption, altering the taste sensations perceived by the taste buds [36,37]. Taste activity values (TAV) were calculated for volatile compounds, with TAV ≥ 1 indicating a direct contribution to beer taste. The results (Table A5, Figure 2b) showed that 59 compounds had TAV ≥ 1, including 18 esters, 9 alcohols, 9 aromatics, 9 acids, 4 lactones, 4 sulfur-containing compounds, 2 furans, 2 aldehydes, 1 ketone, and 1 other. Among these, 37 were present with TAV ≥ 1 in all four beers. The numbers of compounds with TAV ≥ 1 were 49, 46, 51, and 43 in YJ, QD, HR, and BW, respectively. In YJ, the highest TAV was for hexanoic acid (279,058), followed by trans-2-nonenal (113,953) and 3-methylbutyl acetate (102,326). In QD, hexanoic acid (213,694), 2-acetyl-2-thiazoline (70,957), and 3-methylbutyl acetate (60,850) were highest. In HR, hexanoic acid (512,378), 3-methylbutyl acetate (216,937), and 2-methyl-1-propanol (19,592) ranked highest. In BW, hexanoic acid (452,452), 3-methylbutyl acetate (141,074), and ethyl octanoate (18,693) were most pronounced. Hexanoic acid and 3-methylbutyl acetate thus appear to be the major contributors to taste perception in lager beer. Previous studies have shown that hexanoic acid enhances beer sourness and prolongs its perception, which can affect bitterness perception after swallowing [38]. 3-methylbutyl acetate imparts banana-like and ester aromas, and at higher concentrations it can mask the flavor expression of other compounds, such as 2-methylbutanal, 3-(methylthio)propanal, and phenylacetaldehyde [39]. A total of 33 flavor compounds were identified with both an odor activity value (OAV) ≥ 1 and a taste activity value (TAV) ≥ 1 across the four types of lager beer, including 3-methylbutyl acetate, ethyl hexanoate, 2-methyl-1-propanol, hexanoic acid, γ-decalactone, 2-phenylethanol, 6-methyl-5-hepten-2-one, ethyl pyruvate, among others. These compounds are likely to serve as key contributors to the characteristic flavor profile of lager beers.

3.3. Flavor Perception Evaluation

To investigate the aroma sensory characteristics of different lager beer brands, sequential quantitative descriptive analysis (SQDA) was conducted to assess the aroma profiles and intensity of four beer samples, followed by analysis of variance (Duncan's test) to determine significant differences in aroma attributes. As shown in Figure 3a, the overall aroma profiles of the four beers exhibited notable differences. Significant differences ($p \leq 0.001$) were observed in sweet aroma, burnt aroma, phenolic aroma, and off-flavor attributes, while sulfur aroma and grain aroma differed significantly ($p \leq 0.05$). No significant differences were found for fruity aroma, floral aroma, woody aroma, nut shell, grass aroma, sour aroma, and oil aroma. Specifically, the YJ sample was characterized by pronounced grain aroma and fruity aroma, with noticeable floral aroma, sweet aroma, and burnt aroma; the QD sample showed prominent phenolic aroma, sulfur aroma, and fruity aroma, along with a distinct off-flavor; the HR sample exhibited strong fruity aroma and sweet aroma, with marked floral aroma and burnt aroma; the BW sample displayed intense sweet aroma and burnt aroma, followed by fruity aroma and grain aroma. These differences are closely re-

lated to the composition, concentration, and interactions of volatile compounds, indicating the necessity of molecular-level investigation into their sensory contributions.

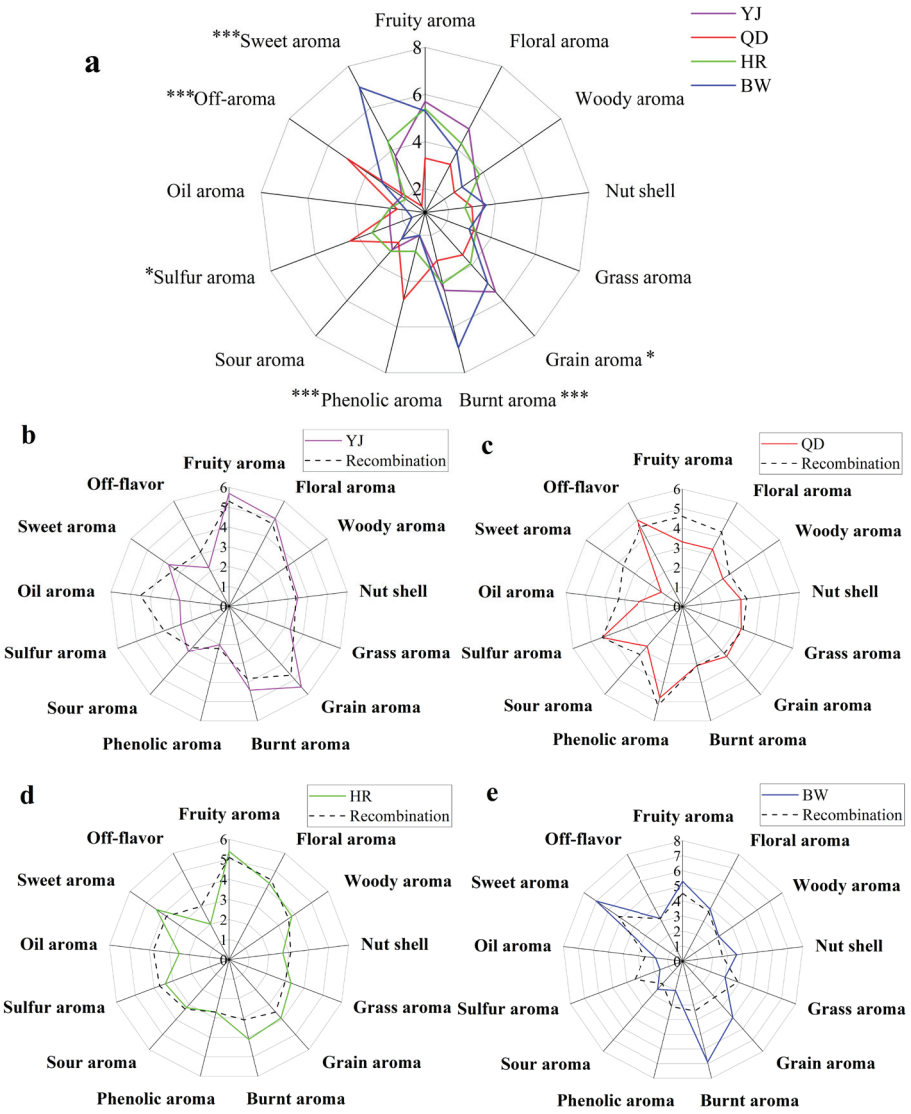


Figure 3. (**a**) Aroma sensory radar chart of different brands of lager beer. Asterisks * and *** indicate significant differences at $p \leq 0.05$ and $p \leq 0.001$, respectively. (**b**–**e**) Comparison of aroma recombination models and original beer samples for lager beer. Radar charts correspond to YJ, QD, HR, and BW, respectively. Abbreviations YJ, QD, HR, and BW are defined in the manuscript's Abbreviations section.

Based on these findings, flavor compounds with OAV ≥ 1 were blended according to their concentrations in the four lager beer samples to prepare simulated recombination models, which were subsequently evaluated by SQDA. The sensory panel assessed the intensity of 13 aroma attributes (fruity aroma, floral aroma, woody aroma, nut shell, grass aroma, grain aroma, burnt aroma, phenolic aroma, sour aroma, sulfur aroma, oil aroma, sweet aroma and off-flavor) for both the original samples and their corresponding recombination models. Results indicated that the aroma profiles of the recombination models were highly similar to those of the original beers, with Pearson correlation coefficients of 0.78, 0.68, 0.74, and 0.64 for YJ, QD, HR, and BW, respectively. As illustrated in Figure 3b, the YJ recombination model successfully reproduced the dominant grain aroma and fruity aroma, as well as distinct floral aroma, sweet aroma, and burnt aroma, showing good similarity in woody aroma, nut shell, grass aroma, phenolic aroma, and sour aroma. Figure 3c shows

that the QD model effectively reproduced the overall aroma profile of the original beer, with a slight enhancement in sweet aroma. Figure 3d indicates that the HR model achieved a high level of similarity to the original. Figure 3e demonstrates that the BW model reproduced most of the original aroma characteristics, although a deviation was noted in burnt aroma intensity.

These results suggest that the primary aroma characteristics of lager beer are shaped by the synergistic effects of the selected flavor compounds. However, despite the overall similarity between the recombination models and the original samples, subtle differences in certain sensory attributes were noted by the panel. These discrepancies may be attributed to the absence of compounds with odor activity values (OAVs) below 1 or non-volatile matrix components that were not included in the models [40]. Notably, in complex multicomponent systems such as beer, aroma perception arises not only from the intensity of individual volatiles but also from their perceptual interactions. Compounds present at sub-threshold levels can influence the perception of other aroma-active compounds through mechanisms such as synergistic enhancement, blending, or masking, thereby contributing to the overall realism and complexity of the aroma profile. Therefore, to improve the fidelity of aroma reproduction, future research should consider incorporating low-OAV compounds into reconstitution models or conducting targeted omission/addition experiments to better understand their functional roles in sensory perception.

3.4. Screening of Potential Differential Compounds by PLS-DA

To identify the key factors contributing to sensory differences among different lager beer brands, supervised partial least squares discriminant analysis (PLS-DA) was employed to extract informative variables from the flavor compound dataset. PLS-DA is a multivariate statistical method that performs dimensionality reduction while establishing a relationship model between variables and sample categories, thereby effectively separating samples in the reduced dimensional space.

To ensure statistical reliability and prevent overfitting, we conducted a 200-iteration permutation test for model validation. As shown in Figure 4a, the four lager beer samples were clearly separated in the two-dimensional score plot. The first and second principal components (R^2X [1] and R^2X [2]) explained 0.483 and 0.243 of the total variance, respectively. The model's explained variance (R^2Y) and predictive ability (Q^2Y) were 0.993 and 0.981, indicating strong explanatory and predictive power. Permutation test results (Figure 4b) showed that all permuted R^2 and Q^2 values were lower than those of the original model, and the intercept of the Q^2 regression line on the vertical axis was below zero ($Q^2Y = -0.55$). These results confirm that the PLS-DA model is statistically robust and free from overfitting.

Variable importance in projection (VIP) scores were calculated to evaluate the contribution of each flavor compound to sample discrimination. Following widely accepted chemometric standards, variables with VIP > 1 were considered significant contributors to inter-brand differentiation [41,42]. As shown in Figure 4c, 25 flavor compounds had VIP > 1, including ethyl hexanoate (VIP = 1.29432), phenylacetic acid (VIP = 1.27321), diacetyl (VIP = 1.26486), 2-methyl-1-propanol (VIP = 1.21913), linalool (VIP = 1.20656), 3-methylbutanoic acid (VIP = 1.18217), ethyl acetate (VIP = 1.13657), 4-vinylguaiacol (VIP = 1.08803), δ-nonalactone (VIP = 1.01653), and γ-decalactone (VIP = 1.01045). Among these, ethyl hexanoate, 4-vinylguaiacol, phenylacetic acid, 3-methylbutanoic acid, γ-decalactone, δ-nonalactone, and diacetyl had previously been identified as aroma-active compounds in the GC-O analysis, suggesting their potential role as key characteristic flavor compounds in lager beer. Nevertheless, these findings derived from mathematical modeling require further validation through sensory evaluation.

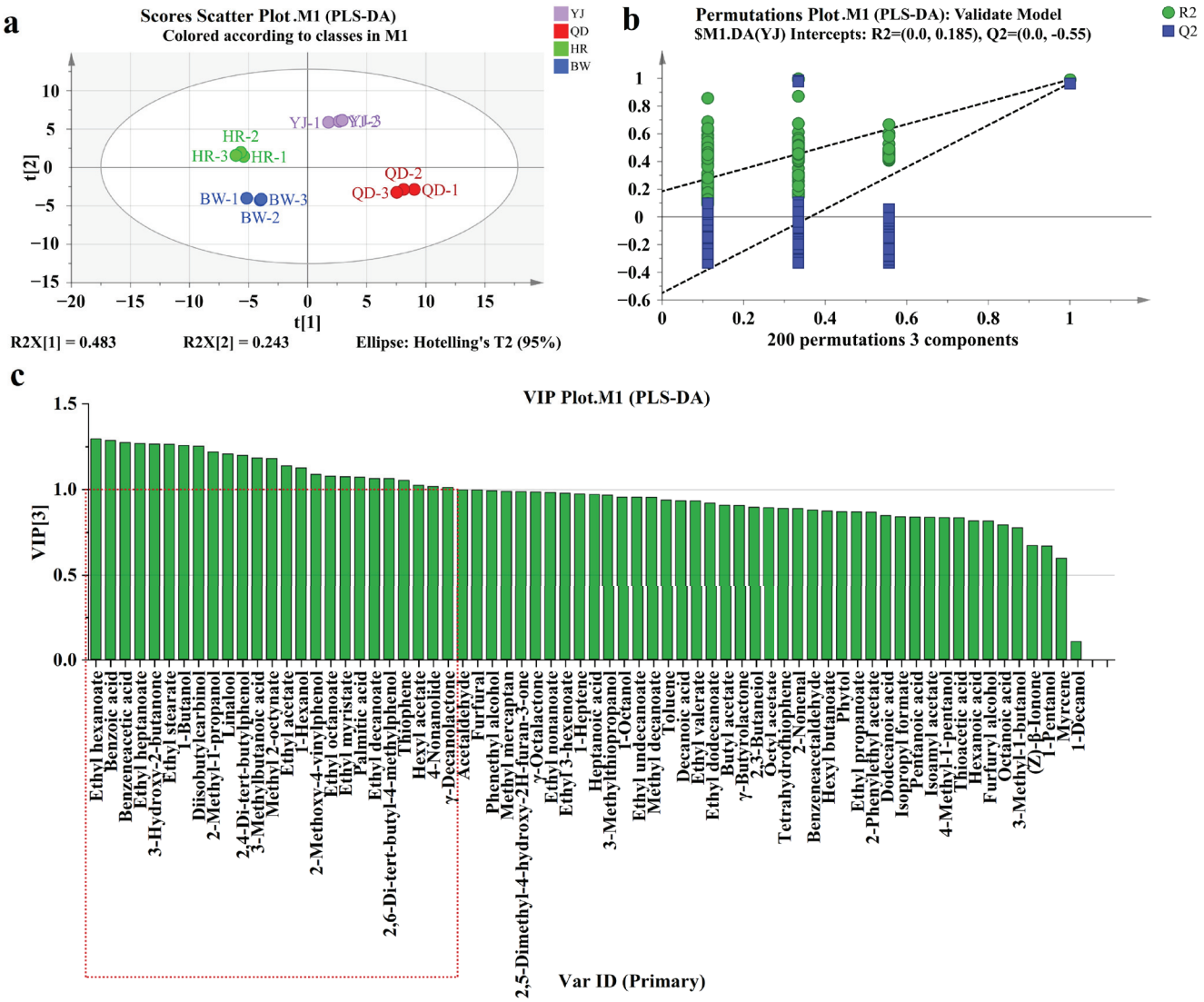


Figure 4. PLS-DA analysis of different brands of lager beer. (**a**) Score scatter plot. (**b**) Permutation test plot. (**c**) VIP score plot. Abbreviations YJ, QD, HR, and BW are defined in the manuscript's Abbreviations section. The red dotted box highlights compounds with a Variable Importance in Projection (VIP) score greater than 1.

3.5. Validation Experiment Analysis

Given the discrepancies among the OAV analysis, Osme results, and PLS-DA outcomes, a comprehensive evaluation was performed to identify the key differential flavor compounds influencing aroma expression in different lager beer brands. A total of 20 compounds were selected, including two esters (ethyl hexanoate, ethyl acetate), two alcohols (2-methyl-1-propanol, linalool), five aromatic compounds (phenethyl alcohol, 2-phenylethyl acetate, benzeneacetaldehyde, 2-methoxy-4-vinylphenol, benzeneacetic acid), four acids (octanoic acid, hexanoic acid, 3-methylbutanoic acid, decanoic acid), one furanone (2,5-dimethyl-4-hydroxy-2h-furan-3-one), two lactones (γ-decanolactone, 4-nonanolide), one sulfur-containing compound (3-methylthiopropanol), one aldehyde (3-methylbutanal), one ketone (3-hydroxy-2-butanone), and one other compound (myrcene).

To verify the specific contributions of these volatile compounds to the sensory quality of lager beer, both Pearson correlation analysis and flavor addition experiments were conducted. Pearson correlation analysis was used to evaluate the relationships between the OAV values of flavor compounds and the sensory scores of beer, thereby providing mathematical evidence of their influence on flavor expression. The flavor addition experi-

ments involved spiking the selected compounds, grouped by chemical category, into the base beer, followed by sensory evaluation using the SQDA method.

The Pearson correlation results between the 20 flavor compounds and 13 aroma attributes of lager beer confirmed their distinct roles in flavor expression (Figure 5a). In the ester group, ethyl hexanoate was positively correlated with burnt aroma (r = 0.623), but moderately negatively correlated with woody aroma and floral aroma, suggesting enhancement of burnt characteristics while diminishing floral and woody impressions. Ethyl acetate showed a significant positive correlation with floral aroma (r = 0.622) and a strong negative correlation with burnt aroma (r = −0.669), indicating a greater contribution to fresh floral characteristics rather than to burnt notes.

For alcohols, linalool exhibited a moderate positive correlation with grain aroma (r = 0.561) and oil aroma (r = 0.467), suggesting that beyond floral enhancement, it may synergize with grain- and lipid-associated volatiles to enhance maltiness and smoothness [43,44].

Among aromatic compounds, phenethyl alcohol was positively correlated with fruity aroma (r = 0.553) and floral aroma (r = 0.564), and strongly negatively correlated with off-flavor (r = −0.642), indicating its role in elevating elegant aromatic notes while suppressing undesirable ones. 2-phenylethyl acetate showed similar correlations (r > 0.51 for fruity aroma and floral aroma; negative with off-flavor), highlighting the stable contribution of aromatic esters to desirable beer aroma profiles.

Within the acid group, octanoic acid was positively correlated with fruity aroma (r = 0.661) and sweet aroma (r = 0.588), and moderately negatively correlated with off-flavor, suggesting a role in imparting mild fruitiness and sweetness.

In the lactone group, γ-decanolactone exhibited extremely strong positive correlations with burnt aroma (r = 0.909) and sweet aroma (r = 0.739), while 4-nonanolide showed high correlations with burnt aroma (r = 0.842) and sweet aroma (r = 0.859), confirming the importance of lactones in sweet and baked-like aroma formation [45,46].

For furanones, 2,5-Dimethyl-4-hydroxy-2H-furan-3-one correlated strongly with phenolic (r = 0.819) and off-flavor (r = 0.864) attributes and negatively with sweet notes, suggesting that while it can add complexity, excessive levels may lead to undesirable flavors [47].

Overall, the Pearson correlation analysis revealed statistically significant relationships between specific volatiles and aroma attributes, indicating that these compounds shape the overall flavor profile of lager beer through both synergistic and antagonistic effects. It is important to clarify that while Pearson correlation analysis provides valuable information about statistical associations between chemical concentrations and sensory attributes, such correlations should not be misinterpreted as direct causal relationships. In this study, compounds showing significant correlations were subjected to additional validation through aroma recombination and flavor addition experiments. These experiments were designed to test the perceptual impact of specific volatiles under controlled conditions, thereby allowing us to move from correlation toward stronger evidence of causality.

The addition experiments (Figure 5b) further demonstrated that different types of volatile compounds contributed distinctly to beer aroma. Esters enhanced fruity, floral, sweet, acidic, and bready notes while reducing woody and phenolic characteristics, with Ethyl acetate and Ethyl hexanoate often exceeding their odor thresholds in beer [3,12]. Alcohols significantly increased floral, fruity, woody, bready, and acidic notes but decreased roasted, sulfur, and grain aromas, with linalool being a hop-derived odorant. Aromatic compounds enhanced floral, sweet, and oily notes, with 2-methoxy-4-vinylphenol identified as a key contributor to clove-like aroma [48]. Acids had limited effects on acidity but markedly increased oily notes and reduced grain aroma. Furanones reduced fruity and

floral impressions. Lactones strongly enhanced sweetness, consistent with γ-decanolactone sensory results; notably, the BW sample showed the highest sweet score and lactone content. Sulfur compounds had minimal effects on sulfur notes but markedly increased off-flavor, possibly due to the sour and earthy odor of 3-methylthiopropanol [49]. Aldehydes enhanced oily and bready notes while suppressing fruitiness. Ketones mainly influenced acidic and sweet notes, whereas other compounds affected fruity and grassy characteristics.

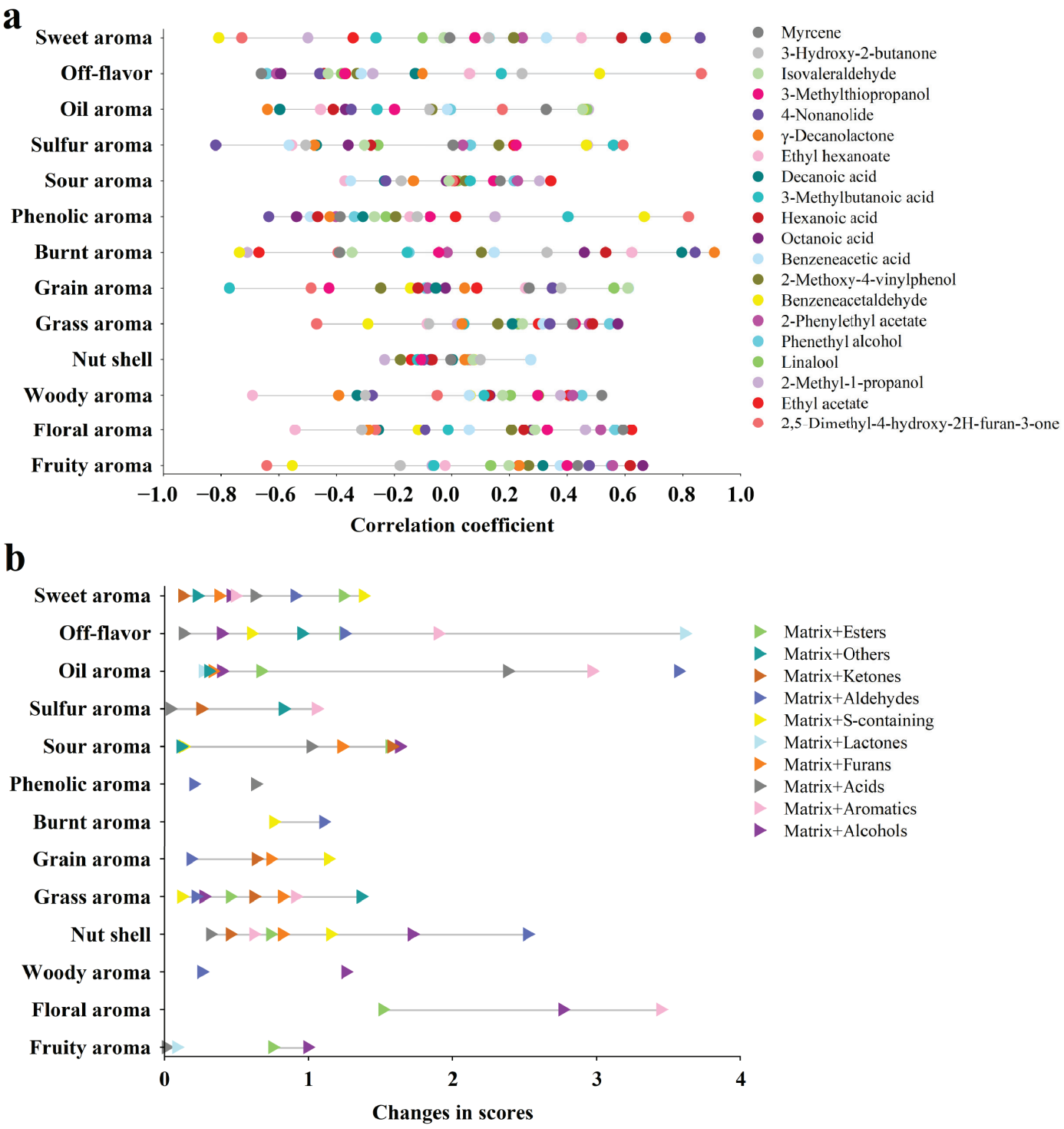


Figure 5. (**a**) Pearson correlation analysis between flavor compounds and sensory attributes. (**b**) Results of the flavor addition experiment.

In general, a single aroma attribute was influenced by multiple flavor compounds. Floral notes were primarily shaped by esters, alcohols, and aromatic compounds; sweet notes by esters, aromatics, lactones, and aldehydes; bready notes by alcohols, lactones, and aldehydes; and fruity notes by esters and alcohols. Previous studies have reported that fruity characteristics in beer are associated with high ester and relatively low alcohol concentrations [50]. 3-Methylbutanal, ethyl acetate, and benzeneacetaldehyde have been identified as aroma-active compounds in brewing barley [43], and 2,5-dimethyl-4-hydroxy-2H-furan-3-one has been repeatedly confirmed as aroma-active in caramel malt beer and wheat beer [18,20]. Collectively, the 20 flavor compounds were verified as key differential flavor compounds contributing to the aroma expression of different lager beer brands.

However, it should be noted that although the base matrix used in the addition experiment was a real beer (Yanjing Qing Shuang Beer), matrix effects may still influence the volatility, solubility, and perceptual intensity of the added compounds. In addition, the perception of aroma may also be modulated by cross-modal interactions, where taste attributes like bitterness or sweetness can influence how aromas are perceived. Although our study focused primarily on aroma-active volatiles, future investigations should incorporate more integrated designs to explore these multidimensional sensory interactions and their influence on flavor perception.

4. Conclusions

In this study, multiple sample pretreatment techniques were combined with advanced analytical instrumentation to comprehensively characterize the volatile compound profiles of four commercial lager beers. By integrating GC-MS, GC×GC-TOF-MS, and GC-O-MS with OAV/TAV calculation, multivariate statistical modeling, and sensory validation, we identified twenty differential volatile compounds as key contributors to brand-specific aroma expression. These compounds, predominantly aromatic compounds and acids, were found to shape typical sensory notes such as fruity, floral, caramel, and roasted characteristics through synergistic interactions. The integrated chemical-sensory approach adopted here offers a practical framework for exploring aroma complexity in fermented beverages and supports the development of flavor-targeted strategies in beer production. Despite these contributions, several limitations should be considered when interpreting the findings. The limited sample set, while representative of mainstream lager products in the Chinese market, may not capture the full diversity of lager styles across broader geographic or stylistic categories. Additionally, although storage conditions were controlled to minimize compound degradation, some volatile compounds remain highly sensitive to oxidation and evaporation, potentially influencing results. The detection of ultra-trace or unstable compounds also presents analytical challenges, even when employing advanced platforms. Building on these insights, future research should aim to address these limitations while deepening the understanding of aroma mechanisms. In particular, investigating the perceptual interactions between sub-threshold and supra-threshold aroma compounds may help clarify the sensory differences observed between recombination models and original beers.

Author Contributions: Y.C.: Conceptualization, Methodology, Software, Validation, Formal analysis, Investigation, Writing—original draft, Visualization. H.H.: Methodology, Formal analysis, Investigation, Data curation, Writing—original draft. R.Y.: Methodology, Validation, Formal analysis, Investigation, Writing—original draft. X.H.: Investigation, Data curation. L.G.: Investigation, Resources. Y.S.: Investigation. D.Z.: Supervision, Project administration, Conceptualization, Writing—review & editing. J.S.: Software, Visualization. J.L.: Resources. M.H.: Supervision. B.S.: Supervision, Resources. All authors have read and agreed to the published version of the manuscript.

Funding: This research was funded by the National Natural Science Foundation of China (Grant No. 32322068), the National Key Research and Development Program of China (Grant

No. 2022YFD2101205), and the Beijing Elite Scientist Sponsorship Program of BAST (Grant No. BYESA.2023055).

Institutional Review Board Statement: The study was conducted according to the guidelines of the Declaration of Helsinki and approved by the Scientific Research Ethics Committee of Beijing Business and Technology University (Approval No. 148 was granted on 12 July 2024).

Informed Consent Statement: Informed consent was obtained from all subjects involved in the study.

Data Availability Statement: Data will be made available on request.

Conflicts of Interest: Author R.Y., X.H., L.G. and Y.S. was employed by the Technology Center of Beijing Yanjing Beer Co., Ltd. The remaining authors declare that the research was conducted in the absence of any commercial or financial relationships that could be construed as a potential conflict of interest.

Abbreviations

The following abbreviations are used in this manuscript:

LLE	Liquid–liquid extraction
HS-SPME	Headspace solid-phase microextraction
SAFE	Solvent-assisted flavor evaporation
GC-MS	Gas chromatography–mass spectrometry
GC×GC-TOF MS	Comprehensive two-dimensional gas chromatography–time-of-flight mass spectrometry
GC-O-MS	Gas chromatography–olfactometry–mass spectrometry
OAV	Odor activity value
TAV	Taste activity value
PLS-DA	Partial least squares discriminant analysis
VIP	Variable importance in projection
YJ	U8, Beijing Yanjing Brewery Co., Ltd.
QD	Classic, Tsingtao Brewery Group Co., Ltd.
HR	Brave the World, China Resources Beer (Holdings) Co., Ltd.
BW	Ice Beer, Budweiser Asia Pacific Holdings Ltd.

Appendix A

Table A1. Brand, manufacturer, original wort concentration, and ingredients of lager beer samples used in this study.

Code	Product Name	Manufacturer	Original Wort Concentration	Ingredients
YJ	U8	Beijing Yanjing Brewery Co., Ltd.	8 °P	Water, malt, rice, hops
QD	Classic	Tsingtao Brewery Group Co., Ltd.	8 °P	Water, malt, rice, hops
HR	Brave the World	China Resources Beer (Holdings) Co., Ltd.	8 °P	Water, malt, brewing syrup, hops
BW	Ice Beer	Budweiser Asia Pacific Holdings Ltd.	8 °P	Water, malt, rice, hop extract, yeast
–	Qing Shuang Beer	Beijing Yanjing Brewery Co., Ltd.	10 °P	Water, malt, rice, hops

Table A2. Quantitative calibration curves of volatile compounds.

No.	Compound Name	CAS	Quantifier Ion	Calibration Curve				
				n	Slope	Intercept	R^2	Range (mg/L)
1	Isoamyl acetate	123-92-2	43	9	0.00005	−15.2830	0.9972	2.34–1200.00
2	Ethyl hexanoate	123-66-0	88	8	0.000003	−0.9841	0.9993	6.25–800.00
3	Ethyl propanoate	105-37-3	29	7	0.0000005	1.2961	0.9998	0.31–160.00
4	Hexyl butanoate	2639-63-6	43	9	0.000003	3.6897	0.9974	1.25–320.00
5	Methyl decanoate	110-42-9	74	10	0.000003	0.8804	0.9990	0.78–400.00
6	Ethyl octanoate	106-32-1	88	7	0.0000002	−0.4058	0.9976	0.43–27.50
7	Ethyl decanoate	110-38-3	88	8	0.0000004	−0.1858	0.9997	0.16–40.00
8	Isoamyl butyrate	106-27-4	71	7	0.000004	−3.6818	0.9855	3.13–200.00
9	Ethyl trans-2-decenoate	7367-88-6	55	11	0.0000005	0.4049	0.9996	0.16–160.00
10	Octyl acetate	112-14-1	43	9	0.0000007	−0.3902	0.9998	0.39–100.00
11	Ethyl stearate	111-61-5	88	9	0.0000004	−1.2460	0.9994	0.39–100.00
12	Ethyl isovalerate	108-64-5	88	6	0.000001	−0.6628	0.9988	0.39–50.00
13	Ethyl myristate	124-06-1	88	7	0.0000004	−0.1408	0.9999	0.39–25.00
14	Ethyl lactate	97-64-3	45	7	0.000002	−0.6235	0.9977	0.78–50.00
15	Ethyl acetate	141-78-6	43	7	0.000003	−1.2344	0.9993	12.5–800.00
16	Ethyl heptanoate	106-30-9	88	8	0.0000008	−0.1803	0.9992	0.16–20.00
17	Hexyl acetate	142-92-7	43	8	0.000003	1.0401	0.9955	1.25–160.00
18	Diethyl succinate	123-25-1	101	10	0.0000009	0.1174	0.9995	0.31–160.00
19	Butyl acetate	123-86-4	43	9	0.000002	0.6073	0.9928	0.08–20.00
20	Ethyl 3-hydrobutyrate	5405-41-4	43	7	0.000002	0.0074	0.9997	0.02–1.25
21	Ethyl nonanoate	123-29-5	88	8	0.0000007	0.2045	0.9993	0.31–40.00
22	Ethyl hydrogen succinate	1070-34-4	101	6	0.000008	−1.0704	0.9992	10.00–320.00
23	Ethyl valerate	539-82-2	29	8	0.000002	0.3861	0.9909	0.31–40.00
24	Methyl 2-octynate	111-12-6	95	9	0.000003	−0.5746	0.9981	0.78–200.00
25	(−)-Ethyl L-lactate	687-47-8	45	8	0.000003	−1.9181	0.9973	0.78–100.00
26	2-Hydroxyethyl acetate	542-59-6	43	8	0.000002	0.1359	0.9926	0.16–20.00
27	Propyl acetate	109-60-4	43	8	0.000003	−1.9656	0.9971	0.16–20.00
28	2,3-Dihydroxypropyl acetate	106-61-6	43	9	0.000003	−1.7321	0.9967	0.16–40.00
29	Methyl propionate	554-12-1	29	9	0.000002	0.2601	0.9901	0.16–40.00
30	Isopropyl formate	625-55-8	45	8	0.000002	0.3989	0.9995	1.25–160.00
31	Ethyl dodecanoate	106-33-2	88	8	0.000002	0.6648	0.9987	0.16–20.00
32	Ethyl 3-hexenoate	2396-83-0	29	8	0.000002	1.7706	0.9918	0.31–40.00
33	Ethyl butyrylacetate	3249-68-1	71	8	0.000003	0.7792	0.9963	0.16–40.00
34	Ethyl 3-methylvalerate	5870-68-8	88	8	0.000001	−0.4345	0.9988	0.16–20.00
35	Ethyl undecanoate	627-90-7	88	8	0.000001	−1.6635	0.9984	0.16–20.00
36	(+)-Diethyl L-tartrate	87-91-2	104	8	0.000002	1.1348	0.9984	0.16–20.00
37	2,3-Butaneiol	513-85-9	45	9	0.00003	16.4440	0.9951	4.69–1200.00
38	3-Methyl-1-butanol	123-51-3	55	7	0.000006	−32.0320	0.9990	25.00–1600.00
39	1,2,3-Propanetriol	56-81-5	61	7	0.000004	124.5400	0.9992	125.00–8000.00
40	2-Methyl-1-propanol	78-83-1	43	9	0.00001	−6.9598	0.9996	4.69–1200.00
41	Diisobutylcarbinol	108-82-7	69	8	0.0000007	0.2155	0.9941	0.39–50.00
42	1-Butanol	71-36-3	56	8	0.000005	−0.6615	0.9998	1.56–200.00
43	1-Octanol	111-87-5	56	7	0.0000008	−0.1317	0.9995	0.31–20.00
44	1-Pentanol	71-41-0	42	10	0.000001	−0.4668	0.9991	0.31–320.00
45	3-Methyl-3-buten-1-ol	763-32-6	41	9	0.000006	0.0446	0.9966	0.04–10.00
46	α-Terpineol	98-55-5	59	6	0.0000007	0.0775	0.9993	0.16–5.00
47	2-Ethyl-1-hexanol	104-76-7	57	8	0.0000009	−0.6655	0.998	0.31–40.00
48	4-Methyl-1-pentanol	626-89-1	56	8	0.000003	0.7926	0.996	0.31–80.00
49	1,2-Propylene glycol	57-55-6	45	6	0.000005	1.6696	0.9993	1.25–40.00
50	2-Hexyl-1-decanol	2425-77-6	57	8	0.0000009	−0.6035	0.961	0.31–40.00
51	1-Hexanol	111-27-3	56	7	0.000004	−0.3672	0.9996	1.56–100.00
52	Linalool	78-70-6	71	8	0.000005	−0.5625	0.9998	0.78–100.00

Table A2. *Cont.*

No.	Compound Name	CAS	Quantifier Ion	Calibration Curve				
				n	Slope	Intercept	R^2	Range (mg/L)
53	1-Decanol	112-30-1	70	8	0.000005	−0.5974	0.9992	0.78–100.00
54	Diethylene glycol monoethyl ether	111-90-0	45	8	0.000005	−1.2538	0.9999	1.56–200.00
55	(−)-Isolongifolol	1139-17-9	109	7	0.000004	−0.0935	0.9997	1.56–100.00
56	Phytol	150-86-7	71	7	0.000004	0.1171	0.9996	0.39–25.00
57	β-Eudesmol	473-15-4	59	8	0.000001	0.0652	0.9982	3.13–200.00
58	Guaiol	489-86-1	161	9	0.000002	−0.3251	0.9997	0.78–200.00
59	2,6-Dimethyl-5,7-octadien-2-ol	5986-38-9	93	7	0.000001	0.0317	0.9964	1.56–100.00
60	Phenethyl alcohol	60-12-8	91	9	0.000007	−97.3390	0.9851	7.81–4000.00
61	2-Phenylethyl acetate	103-45-7	104	10	0.000003	−8.9800	0.9958	0.78–800.00
62	Phenol	108-95-2	94	10	0.000001	−4.5197	0.9993	1.17–600.00
63	Benzeneacetaldehyde	122-78-1	91	7	0.00001	0.5234	0.9916	1.25–80.00
64	Benzyl alcohol	100-51-6	79	7	0.0000009	0.0445	0.9999	0.16–10.00
65	Ethyl benzoate	93-89-0	105	7	0.000002	−0.0393	0.9997	0.63–40.00
66	Benzaldehyde	100-52-7	77	6	0.000003	0.0024	0.9904	1.25–40.00
67	2,4-Di-tert-butylphenol	96-76-4	191	8	0.000001	2.3582	0.9989	1.56–200.00
68	2-Methoxy-4-vinylphenol	7786-61-0	135	7	0.000002	5.609	0.9955	3.13–200.00
69	2,6-Di-tert-butyl-4-methylphenol	128-37-0	205	9	0.0000004	0.4619	0.9998	2.50–640.00
70	Benzoic acid	65-85-0	105	6	0.000003	6.6738	0.9964	12.5–400.00
71	p-Hydroxyphenylethanol	501-94-0	107	9	0.000001	2.0534	0.9989	0.78–200.00
72	Benzeneacetic acid	103-82-2	91	6	0.000003	4.3926	0.9943	6.25–200.00
73	Resorcinol	108-46-3	110	6	0.000002	1.6271	0.9992	1.56–50.00
74	2,5-Dimethylphenol	95-87-4	122	7	0.000001	1.6717	0.9967	0.78–50.00
75	α-Methylstyrene	98-83-9	118	6	0.000003	0.3579	0.9924	1.25–40.00
76	1-(2-Hydroxy-5-methylphenyl)ethanone	1450-72-2	135	8	0.000002	0.1579	0.9973	0.08–10.00
77	(R)-(+)-1-Phenylethanol	1517-69-7	107	8	0.000005	0.2135	0.9957	0.08–10.00
78	Toluene	108-88-3	91	6	0.000004	−1.9747	0.9986	7.81–250.00
79	Octanoic acid	124-07-2	60	8	0.000005	45.9690	0.9888	6.25–1600.00
80	Hexanoic acid	142-62-1	60	8	0.000008	−2.3383	0.9990	4.69–600.00
81	Acetic acid	64-19-7	43	6	0.00001	1.6743	0.9987	12.5–800.00
82	3-Methylbutanoic acid	503-74-2	60	8	0.000007	−0.1555	0.9967	3.13–400.00
83	Decanoic acid	334-48-5	60	6	0.000003	11.6970	0.9989	12.5–400.00
84	Dodecanoic acid	143-07-7	60	9	0.000004	3.1751	0.9996	3.13–800.00
85	Elaidic acid	112-79-8	55	8	0.000003	20.8040	0.9958	3.13–800.00
86	DL-3-Methylvaleric acid	105-43-1	60	8	0.000001	1.7304	0.9997	1.56–200.00
87	Heptanoic acid	111-14-8	60	9	0.000002	3.7580	0.9988	1.56–400.00
88	Tridecanoic acid	638-53-9	73	6	0.000001	1.8894	0.9915	0.78–50.00
89	2-Methylvaleric acid	594-61-6	59	6	0.000001	1.1722	0.9987	1.56–50.00
90	Pentanoic acid	109-52-4	60	7	0.000004	5.7311	0.9998	10.00–640.00
91	Nonanoic acid	112-05-0	60	8	0.0000002	0.4131	0.9962	0.31–40.00
92	Palmitic acid	57-10-3	43	6	0.000001	10.45	0.9993	12.5–400.00
93	trans-3-Hexenoic acid	4219-24-3	41	6	0.00001	6.6252	0.9978	0.78–25.00
94	4-Methyl-2-pentenoic acid	10321-71-8	41	8	0.000001	1.5656	0.9991	0.39–50.00
95	Hendecanoic acid	112-37-8	60	7	0.000002	1.1722	0.9987	0.39–25.00
96	Crotonic acid	3724-65-0	86	7	0.000002	−1.0557	0.9953	0.39–25.00
97	2-Methyl-2-pentenoic acid	3142-72-1	41	7	0.000006	−2.8264	0.9958	4.69–300.00
98	Furfuryl alcohol	98-00-0	98	6	0.000007	1.2221	0.9956	1.56–100.00
99	2-Furancarboxylic acid	88-14-2	112	6	0.000004	1.7403	0.9987	5.00–160.00
100	2-Butylfuran	4466-24-4	81	6	0.000004	1.6517	0.9948	1.25–80.00
101	Furfural	98-01-1	96	6	0.000002	2.345	0.9974	3.13–100.00
102	2-Acetyl furan	1192-62-7	95	11	0.000005	0.6997	0.9985	0.08–80.00
103	Methyl 2-furoate	611-13-2	95	7	0.000003	0.9577	0.9986	1.25–80.00

Table A2. *Cont.*

No.	Compound Name	CAS	Quantifier Ion	Calibration Curve				
				n	Slope	Intercept	R^2	Range (mg/L)
104	5-Hydroxymethyl-2-furaldehyde	67-47-0	97	9	0.000005	−7.9761	0.9971	4.68–1200.00
105	2,5-Dimethyl-4-hydroxy-2H-furan-3-one	3658-77-3	43	7	0.000006	3.1029	0.9981	1.56–100.00
106	2(5H)-Furanone	497-23-4	55	8	0.000008	−0.334	0.9933	1.56–200.00
107	Furfuryl sulfide	13678-67-6	81	7	0.000002	−1.394	0.9958	3.13–200.00
108	2,2′-Difurfuryl ether	4437-22-3	81	8	0.000003	−1.8112	0.9959	1.56–200.00
109	(±)-3-Hydroxy-4-butanolide	5469-16-9	44	7	0.00001	19.2420	0.9969	1.17–1200.00
110	γ-Decanolactone	706-14-9	85	7	0.0000006	−0.1815	0.9998	0.39–25.00
111	γ-Butyrolactone	96-48-0	42	10	0.00001	−7.8209	0.998	1.56–800.00
112	4-Nonanolide	104-61-0	85	6	0.000003	0.167	0.9991	0.78–50.00
113	γ-Hexanolactone	695-06-7	85	8	0.000001	0.0428	0.9999	0.08–10.00
114	γ-Octalactone	104-50-7	85	6	0.000004	−0.6705	0.9959	1.25–40.00
115	δ-Valerolactone	542-28-9	42	8	0.000001	0.1065	0.9992	0.08–10.00
116	γ-Valerolactone	108-29-2	56	10	0.000005	0.7945	0.9985	0.16–80.00
117	Costunolide	553-21-9	81	8	0.0000007	−0.4606	0.9992	0.39–50.00
118	5-Hydroxy-4-pentanolide	32780-06-6	85	6	0.000004	−0.3032	0.9977	2.50–80.00
119	2-Hydroxypyridine	142-08-5	95	7	0.000002	0.6471	0.9958	0.31–20.00
120	(Z)-9-Octadecenamide	301-02-0	59	6	0.0000007	0.0624	0.9963	2.50–80.00
121	2-Acetyl pyrrole	1072-83-9	94	7	0.000002	0.5324	0.9922	0.31–20.00
122	N-Butyl-acetamide	1119-49-9	30	8	0.000004	0.6875	0.9995	0.16–20.00
123	2,6-Di-tert-butylpyridine	585-48-8	176	9	0.000001	0.4103	0.994	0.16–40.00
124	5-Methyl-1H-pyrrole-2-carbaldehyde	1192-79-6	108	8	0.0000003	0.1641	0.9996	0.08–10.00
125	6-(Ethoxycarbonyl)nicotinic acid	17874-78-1	123	7	0.000001	−1.0354	0.9992	1.25–160.00
126	Benzylamine	100-46-9	106	7	0.000002	0.195	0.9981	0.63–40.00
127	Diethylamine	109-89-7	58	8	0.000003	0.2945	0.9963	0.08–10.00
128	3-Methylthiopropanol	505-10-2	106	10	0.000006	−1.3947	0.9995	1.56–800.00
129	Thiophene	110-02-1	84	9	0.0000005	−1.7580	0.9902	0.31–160.00
130	Methyl mercaptan	74-93-1	47	9	0.000006	−0.711	0.9982	1.56–100.00
131	Dimethyl Sulfoxide	67-68-5	63	8	0.00002	7.776	0.9962	3.13–400.00
132	Dimethyl sulfone	67-71-0	79	8	0.000007	0.5096	0.9975	0.31–40.00
133	Thioacetic acid	507-09-5	43	7	0.00002	9.9358	0.9964	3.13–200.00
134	Tetrahydrothiophene	110-01-0	60	7	0.00001	6.1179	0.995	1.56–100.00
135	2-Acetyl-2-thiazoline	29926-41-8	43	7	0.00002	−0.398	0.9984	6.25–400.00
136	4-Methyl-5-acetyl thiazole	38205-55-9	126	7	0.00003	0.7128	0.9961	1.56–100.00
137	(E)-2-Nonenal	18829-56-6	43	7	0.000001	0.4996	0.9996	1.56–100.00
138	Isovaleraldehyde	590-86-3	44	9	0.000001	−1.3097	0.9990	1.56–400.00
139	Acetaldehyde	75-07-0	29	8	0.000002	0.1996	0.9996	1.56–50.00
140	Hexadecanal	629-80-1	82	7	0.000001	0.2471	0.9991	0.78–50.00
141	4-Hydroxy-2-butanone	590–90-9	43	6	0.000002	3.5000	0.9997	5.00–160.00
142	(Z)-β-Ionone	79-77–6	177	8	0.000002	2.9139	0.9992	1.56–200.00
143	3-Hydroxy-2-butanone	513-86–0	45	8	0.000002	1.3398	0.9987	0.63–160.00
144	Cholestane	481-21-0	217	8	0.000003	1.1282	0.9989	3.13–400.00
145	1-Heptene	592-76-7	56	7	0.00003	−10.3550	0.9955	0.39–50.00
146	1-Undecene	821-95-4	43	9	0.0000008	−0.5146	0.9998	0.16–80.00
147	2-Methyl-2-butene	513-35-9	55	7	0.000002	1.0146	0.9972	0.78–50.00
148	Myrcene	123-35-3	41	7	0.000002	1.0361	0.9986	0.78–50.00
149	Diisopropyl ether	108-20-3	45	7	0.000002	1.8727	0.9972	0.78–50.00
150	3-Methyl-1-butene	563-45-1	55	7	0.000003	0.0584	0.9993	0.78–50.00

Table A3. Identification of volatile compounds in different brands of lager beer.

No.	Compound Name	CAS	RI		Identification Method	Sample Preparation	Presence in Samples			
			DB-WAX	DB-FFAP			YJ	QD	HR	BW
					Alcohols (98)					
1	2-Propen-1-ol	107-18-6	1016		MS, RI	LLE-SAFE	√	√	√	√
2	1-Methoxy-2-propanol	107-98-2	1028		MS, RI	LLE-SAFE	√	√	√	√
3	1-Butanol	71-36-3	1044		MS, RI, S	LLE-SAFE	√	√	√	√
4	3-Penten-2-ol	1569-50-2	1070		MS, RI	LLE-SAFE	√	√	√	√
5	(±)-2-Methyl-1-butanol	137-32-6	1104	1145	MS, RI, S	LLE-SAFE, SPME	√	√	√	√
6	(S)-(−)-2-Methyl-1-butanol	1565-80-6	1106	1141	MS, RI	LLE-SAFE, SPME	√	√	√	√
7	3-Methyl-1-butanol	123-51-3	1107	1131	MS, RI, aroma, S	LLE-SAFE, SPME	√	√	√	√
8	3-Butyn-2-ol	2028-63-9	1111		MS, RI	LLE-SAFE	√			
9	3-Methyl-3-buten-1-ol	763-32-6	1147		MS, RI, S	LLE-SAFE	√	√	√	√
10	1-Pentanol	71-41-0	1149		MS, RI, S	LLE-SAFE	√	√	√	√
11	2-Cyclopropylethanol	2566-44-1	1200		MS, RI	LLE-SAFE	√	√	√	√
12	4-Penten-1-ol	821-09-0	1200		MS, RI	LLE-SAFE	√	√	√	√
13	4-Methyl-1-pentanol	626-89-1	1213	1205	MS, RI, S	LLE-SAFE, SPME	√			√
14	2-Methyl-2-buten-1-ol	4675-87-0	1219		MS, RI	LLE-SAFE			√	
15	3-Methyl-2-buten-1-ol	556-82-1	1219		MS, RI	LLE-SAFE	√	√	√	√
16	2-Pentyn-1-ol	6261-22-9	1235		MS, RI	LLE-SAFE		√		
17	Cyclobut-1-enylmethanol	89182-08-1	1235		MS, RI	LLE-SAFE	√	√	√	√
18	1,4-Pentadien-3-ol	922-65-6	1235		MS, RI	LLE-SAFE		√		
19	2-Methoxyethanol	109-86-4	1236		MS, RI	LLE-SAFE			√	√
20	1-Hexanol	111-27-3	1252	1227	MS, RI, S	LLE-SAFE, SPME	√	√	√	√
21	4-Methyl-3-penten-1-ol	763-89-3	1285		MS, RI	LLE-SAFE				√
22	Propargyl alcohol	107-19-7	1294		MS, RI	LLE-SAFE				√
23	1-Heptanol	111-70-6	1352		MS, RI, S	LLE-SAFE	√			
24	(2S)-2-Oxiranylmethanol	60456-23-7	1356		MS, RI	LLE-SAFE	√		√	
25	2-Ethyl-1-hexanol	104-76-7	1387	1311	MS, RI, S	LLE-SAFE, SPME				√
26	2-Methylbutane-2,3-diol	5396-58-7	1411		MS, RI	LLE-SAFE			√	√
27	(R)-(−)-2-Hexanol	26549-24-6	1418		MS, RI	LLE-SAFE	√			
28	(R)-2-Octanol	5978-70-1	1418		MS, RI	LLE-SAFE	√			
29	(2R,3R)-(−)-2,3-Butanediol	513-85-9	1434	1541	MS, RI, aroma, S	LLE-SAFE, SPME	√	√	√	√
30	(S,S)-(+)-1,3-Butaneiol	19132-06-0	1435		MS, RI	LLE-SAFE	√	√		√
31	Linalool	78-70-6	1443	1332	MS, RI	LLE-SAFE, SPME	√	√	√	
32	1-Octanol	111-87-5	1456	1348	MS, RI, S	LLE-SAFE, SPME	√	√	√	√
33	2-(2-Methoxyethoxy)ethanol	111-77-3	1480	1955	MS, RI	LLE-SAFE, SPME				√
34	(S)-(+)-1,2-Propanediol	4254-15-3	1484		MS, RI	LLE-SAFE	√	√	√	√
35	1,2-Propylene glycol	57-55-6	1484	1592	MS, RI, aroma, S	LLE-SAFE	√	√	√	√
36	3-Ethoxy-1-propanol	111-35-3	1507		MS, RI	LLE-SAFE	√		√	√
37	Ethylene glycol	107-21-1	1516	1627	MS, RI	LLE-SAFE	√	√	√	√
38	Cyclopropanemethanol	2516-33-8	1545		MS, RI	LLE-SAFE	√	√	√	√
39	Cyclobutanol	2919-23-5	1545		MS, RI	LLE-SAFE	√			√
40	1-Methoxy-2-butanol	53778-73-7	1550		MS, RI	LLE-SAFE	√	√	√	√
41	1,2-Butanediol	584-03-2	1550		MS, RI	LLE-SAFE		√		
42	α-Terpineol	98-55-5	1593	1386	MS, RI, S	LLE-SAFE, SPME	√	√	√	

Table A3. *Cont.*

No.	Compound Name	CAS	RI		Identification Method	Sample Preparation	Presence in Samples			
			DB-WAX	DB-FFAP			YJ	QD	HR	BW
					Alcohols (98)					
43	4,5-Octanediol	22607-10-9	1598		MS, RI	LLE-SAFE			√	
44	2-Nonanol	628-99-9	1618		MS, RI	LLE-SAFE	√			
45	1,3-Butaneiol	107-88-0	1634		MS, RI	LLE-SAFE		√	√	√
46	2-Methyl-3-hexanol	617-29-8	1639		MS, RI	LLE-SAFE			√	
47	1-Decanol	112-30-1	1659	1420	MS, RI	LLE-SAFE, SPME		√	√	√
48	1-Nonanol	143-08-8	1659		MS, RI, S	LLE-SAFE	√	√		√
49	5-Methyl-1-hepten-4-ol	99328-46-8	1676		MS, RI	LLE-SAFE		√		
50	2-(2-Butoxyethoxy)ethanol	112-34-5	1688		MS, RI	LLE-SAFE		√		
51	2,2-Dimethyl-1,3-propanediol	126-30-7	1697		MS, RI	LLE-SAFE	√			
52	1,1-Oxydi-2-propanol	110-98-5	1726	2389	MS, RI	LLE-SAFE, SPME		√	√	√
53	2-(2-Hydroxypropoxy)-1-propanol	106-62-7	1777		MS, RI	LLE-SAFE		√		
54	Diethylene glycol	111-46-6	1865		MS, RI	LLE-SAFE	√	√	√	√
55	1-Nonene-4-ol	35192-73-5	1886		MS, RI	LLE-SAFE	√	√	√	√
56	1,2-Heptanediol	3710-31-4	1886		MS, RI	LLE-SAFE	√		√	√
57	1,6-Heptadien-4-ol	2883-45-6	1978		MS, RI	LLE-SAFE	√	√		√
58	1-Buten-3-ol	598-32-3	1997		MS, RI	LLE-SAFE	√		√	
59	2-Methyl-1-penten-3-ol	2088/7/5	2012		MS, RI	LLE-SAFE		√		
60	2-Hexen-4-ol	4798-58-7	2012		MS, RI	LLE-SAFE				√
61	1,2,3-Propanetriol	56-81-5	2197	2323	MS, RI, S	LLE-SAFE	√	√	√	√
62	Triethylene glycol	112-27-6	2216	1942	MS, RI	LLE-SAFE, SPME	√	√	√	√
63	2-Methyl-2-propanol	75-65-0	2219		MS, RI, S	LLE-SAFE			√	
64	2E,6E-Farnesol	106-28-5	2249		MS, RI, S	LLE-SAFE		√	√	
65	Farnesol	4602-84-0	2249		MS, RI	LLE-SAFE		√		
66	2,2-Dimethyl-5-hexen-3-ol	19550-89-1	2261		MS, RI	LLE-SAFE			√	
67	3-Decyn-2-ol	69668-93-5	2469		MS, RI	LLE-SAFE				√
68	2,3-Epoxy-1-propanol	57044-25-4	2476		MS, RI	LLE-SAFE	√		√	√
69	1-Dodecanol	112-53-8	2481		MS, RI	LLE-SAFE				√
70	3-Methyl-2-hexanol	2313-65-7	2503		MS, RI	LLE-SAFE	√			
71	2-(Vinyloxy)ethanol	764-48-7	2503	1685	MS, RI	LLE-SAFE, SPME	√	√	√	√
72	2-Butene-1,4-diol	110-64-5	2561		MS, RI	LLE-SAFE				√
73	Isopropyl alcohol	67-63-0	2596		MS, RI, S	LLE-SAFE				√
74	Di(ethylene glycol) vinyl ether	929-37-3	2600		MS, RI	LLE-SAFE	√			√
75	(R)-(−)-1,2-Propanediol	4254-14-2	2816		MS, RI	LLE-SAFE	√		√	
76	4-Penten-2-ol	625-31-0	2946		MS, RI	LLE-SAFE				√
77	2-Eyhoxyethanol	110-80-5	3099		MS, RI	LLE-SAFE			√	√
78	Glycidol	556-52-5	3220		MS, RI	LLE-SAFE	√	√	√	√
79	2-Methyl-1-propanol	78-83-1	996	682	MS, RI, S	LLE-SAFE, SPME	√	√	√	√
80	4-Methyl-2-pentanol	108-11-2		2241	MS, RI	SPME	√	√		
81	Diisobutylcarbinol	108-82-7		1215	MS, RI, S	SPME	√		√	√
82	2,5-Dimethyl-2,5-hexanediol	110-03-2		1269	MS, RI	SPME				√
83	(+)-β-Citronellol	1117-61-9		1340	MS, RI	SPME			√	
84	Diethylene glycol monoethyl ether	111-90-0		2248	MS, RI	SPME	√	√	√	√
85	(−)-Isolongifolol	1139-17-9		2421	MS, RI	LLE-SAFE		√		√

Table A3. *Cont.*

No.	Compound Name	CAS	RI		Identification Method	Sample Preparation	Presence in Samples			
			DB-WAX	DB-FFAP			YJ	QD	HR	BW
					Alcohols (98)					
86	Phytol	150-86-7		1061	MS, RI	SPME	√	√	√	
87	2-Methyl-3-heptanol	18720-62-2		1217	MS, RI	SPME		√	√	√
88	4-Methyl-4-nonanol	23418-38-4		2402	MS, RI	SPME	√			√
89	2-Hexyl-1-decanol	2425-77-6		2377	MS, RI, aroma, S	LLE-SAFE	√		√	
90	β-Eudesmol	473-15-4			MS, S	LLE-SAFE	√	√	√	√
91	Pentaethylene glycol	4792-15-8		2006	MS, RI	SPME	√	√	√	√
92	Guaiol	489-86-1		2203	MS, RI, S	SPME		√	√	√
93	Octaethylene glycol	5117-19-1		1986	MS, RI	SPME	√	√	√	√
94	2,2,4-Trimethyl-3-pentanol	5162-48-1		1261	MS, RI	SPME		√		√
95	Heptaethylene glycol	5617-32-3		2082	MS, RI	SPME	√	√	√	√
96	1-Methylcyclohexanol	590-67-0		1050	MS, RI	SPME	√		√	√
97	2,6-Dimethyl-5,7-octadien-2-ol	5986-38-9		1387	MS, RI	SPME	√		√	
98	5-Nonanol	623-93-8		1273	MS, RI	SPME			√	
					Nitrogen-containing compounds (91)					
1	Triethylamine	121-44-8	1110		MS, RI	LLE-SAFE		√		
2	N,N,O-Triacetylhydroxylamine	17720-63-7	1112		MS, RI	LLE-SAFE		√	√	√
3	2-Methylpyrazine	109-08-0	1162		MS, RI, S	LLE-SAFE	√		√	√
4	N,N-Dimethylformamide	1968-12-2	1223		MS, RI	LLE-SAFE	√	√	√	√
5	2-Oxopropanamide	631-66-3	1531		MS, RI	LLE-SAFE		√		√
6	N-Methylacetamide	79-16-3	1533		MS, RI	LLE-SAFE				√
7	N-Ethylacetamide	625-50-3	1533		MS, RI	LLE-SAFE	√	√	√	√
8	N-Acetyglycinamide	2620-63-5	1610		MS, RI	LLE-SAFE			√	
9	2,3-Butanedione monoxime	57-71-6	1627		MS, RI	LLE-SAFE	√		√	
10	Acetamide	60-35-5	1656		MS, RI	LLE-SAFE	√		√	√
11	Formamide	1975/12/7	1675		MS, RI	LLE-SAFE	√	√	√	√
12	3-(Ethoxycarbonyl)pyridine	614-18-6	1706		MS, RI	LLE-SAFE	√	√	√	√
13	N-Methylsuccinimide	1121-07-9	1793		MS, RI	LLE-SAFE	√		√	√
14	2-Pyridinecarbaldehyde oxime	873-69-8	1806		MS, RI	LLE-SAFE			√	
15	3-Methylbutyramide	541-46-8	1811		MS, RI	LLE-SAFE	√			√
16	2-Acetyl pyrrole	1072-83-9	1862	1978	MS, RI, aroma, S	LLE-SAFE	√	√	√	√
17	3-Benzylsydnone	16844-42-1	1862		MS, RI	LLE-SAFE			√	
18	2-Pyrrolecarbaldehyde	1003-29-8	1895		MS, RI	LLE-SAFE	√	√	√	√
19	2-Pyrrolidinone	616-45-5	1928		MS, RI	LLE-SAFE	√	√	√	√
20	1-Methylpyrrole-2-carboxaldehyde	1192-58-1	1989		MS, RI	LLE-SAFE	√	√	√	√
21	Butanamide	541-35-5	2000		MS, RI	LLE-SAFE	√	√	√	√
22	Hexanamide	628-02-4	2000		MS, RI	LLE-SAFE	√		√	√
23	5-Aminopentanamide	13023-70-6	2021		MS, RI	LLE-SAFE			√	
24	2-Piperidinone	675-20-7	2021		MS, RI	LLE-SAFE				√
25	N-Acetylglycine ethyl ester	1906-82-7	2044		MS, RI	LLE-SAFE	√	√	√	√
26	ε-Caprolactam	105-60-2	2074		MS, RI	LLE-SAFE	√	√	√	√
27	3,5-Dihydroxy-6-methyl-2,3-dihydro-4H-pyran-4-one	28564-83-2	2157		MS, RI	LLE-SAFE	√	√	√	√
28	Ethosuximide	77-67-8	2252		MS, RI	LLE-SAFE	√	√	√	√

Table A3. *Cont.*

No.	Compound Name	CAS	RI		Identification Method	Sample Preparation	Presence in Samples			
			DB-WAX	DB-FFAP			YJ	QD	HR	BW
					Nitrogen-containing compounds (91)					
29	Glutarimide	1121-89-7	2264		MS, RI	LLE-SAFE	√		√	√
30	N,N,3,5-Tetramethylaniline	4913-13-7	2269		MS, RI	LLE-SAFE	√			
31	N-Acetylethanolamine	142-26-7	2277		MS, RI	LLE-SAFE		√	√	
32	Indole	120-72-9	2329		MS, RI	LLE-SAFE	√	√	√	√
33	5H-cyclopenta[b]pyridine	270-91-7	2329		MS, RI	LLE-SAFE	√	√	√	
34	Succinimide	123-56-8	2355		MS, RI	LLE-SAFE				√
35	N,S-Diacetylcysteamine	1420-88-8	2411		MS, RI	LLE-SAFE	√	√	√	
36	N-(2-Phenylethyl)acetamide	877-95-2	2473		MS, RI	LLE-SAFE		√		
37	1-Methyl-1H-tetrazole	16681-77-9	2475		MS, RI	LLE-SAFE				√
38	4-Amino-1-butanol	13325-10-5	2479		MS, RI	LLE-SAFE	√			
39	DL-Pyroglutamic acid	149-87-1	2497		MS, RI	LLE-SAFE		√		
40	Ethyl 5-oxo-L-prolinate	66183-71-9	2497		MS, RI	LLE-SAFE	√	√	√	√
41	L-Pyroglutamicacid	98-79-3	2500		MS, RI	LLE-SAFE	√			
42	Benzamide	55-21-0	2575		MS, RI	LLE-SAFE		√		√
43	Phenylacetamide	103-81-1	2607		MS, RI	LLE-SAFE			√	
44	Valeramide	626-97-1	2654		MS, RI	LLE-SAFE		√	√	√
45	Enanthamide	628-62-6	2657		MS, RI	LLE-SAFE	√			
46	Octanamide	629-01-6	2657		MS, RI	LLE-SAFE	√	√	√	√
47	Pent-4-enylamine	22537-07-1	2705		MS, RI	LLE-SAFE		√		
48	Cyclobutylamine	2516-34-9	2762		MS, RI	LLE-SAFE	√		√	√
49	3-Indoleethanol	526-55-6	2767		MS, RI	LLE-SAFE		√		
50	(2-Hydroxyethyl)hydrazine	109-84-2	2811		MS, RI	LLE-SAFE		√		
51	Dodecanamide	1120-16-7	2883		MS, RI	LLE-SAFE		√		√
52	(Z)-9-Octadecenamide	301-02-0	2887	2432	MS, RI, aroma, S	LLE-SAFE	√	√	√	√
53	2-Propoxyethylamine	42185-03-5	2937		MS, RI	LLE-SAFE			√	
54	2-Methoxyethylamine	109-85-3	2963		MS, RI	LLE-SAFE			√	√
55	2-Ethoxyethylamine	110-76-9	2968		MS, RI	LLE-SAFE				√
56	Nonanamide	1120-07-6	3105		MS, RI	LLE-SAFE	√	√	√	√
57	1,2-Propanediamine	78-90-0	3147		MS, RI	LLE-SAFE			√	√
58	N-Methylisobutylamine	625-43-4	3222		MS, RI	LLE-SAFE			√	
59	N-Methyltyramine	370-98-9	884		MS, RI	LLE-SAFE		√		√
60	4-Hydroxypyrazole	4843-98-5	924		MS, RI	LLE-SAFE	√			
61	4H-1,2,4-Triazol-4-amine	584-13-4	925		MS, RI	LLE-SAFE		√		
62	Benzylamine	100-46-9		1188	MS, RI	SPME	√			√
63	2,4,6-Triamino-5-nitrosopyrimidine	1006-23-1			MS	LLE-SAFE		√		
64	1,3,5-Trimethylpyrazole	1072-91-9		2157	MS, RI	LLE-SAFE		√	√	
65	Diethylamine	109-89-7		597	MS, RI	SPME	√			√
66	N-Butyl-acetamide	1119-49-9		1118	MS, RI, aroma, S	LLE-SAFE, SPME		√	√	√
67	cis-13-Docosenoamide	112-84-5			MS	LLE-SAFE			√	√
68	5-Methyl-1H-pyrrole-2-carbaldehyde	1192-79-6		2120	MS, RI, aroma, S	LLE-SAFE	√			√
69	Octadecanamide	124-26-5			MS	LLE-SAFE		√	√	
70	2-Hydroxypyridine	142-08-5		1468	MS, RI, aroma, S	LLE-SAFE			√	√
71	6-(Ethoxycarbonyl) nicotinic acid	17874-78-1			MS, aroma, S	LLE-SAFE			√	√

Table A3. *Cont.*

No.	Compound Name	CAS	RI		Identification Method	Sample Preparation	Presence in Samples			
			DB-WAX	DB-FFAP			YJ	QD	HR	BW
					Nitrogen-containing compounds (91)					
72	Diethyl iminodiacetate	19617-44-8		2035	MS, RI	SPME	√	√	√	√
73	N-Ethylisopropylamine	19961-27-4		1270	MS, RI	SPME		√	√	√
74	2-Hydroxy-Propanamide	2043-43-8		667	MS, RI	SPME			√	√
75	5,6,7,8-Tetrahydro-1-naphthylamine	2217-41-6		2039	MS, RI	SPME		√		
76	4-Hydroxyindole	2380-94-1		2284	MS, RI	SPME			√	
77	5-Amino-1-pentanol	2508-29-4		1043	MS, RI	SPME			√	
78	Pyrazole	288-13-1		2243	MS, RI	LLE-SAFE	√			
79	4-Hydroxy-6-methylpyrimidine	3524-87-6		2172	MS, RI	LLE-SAFE			√	
80	2-Amino-1,3,4-thiadiazole	4005-51-0		1294	MS, RI	SPME	√			
81	N-Ethylmaleamic acid	4166-67-0		2233	MS, RI	SPME	√	√	√	√
82	N-Ethyl-pentanamide	54007-33-9		1267	MS, RI	SPME		√	√	√
83	Isobutyramide	563-83-7		590	MS, RI	SPME	√	√		
84	2,6-Di-tert-butylpyridine	585-48-8		2457	MS, RI, aroma, S	LLE-SAFE	√	√		√
85	Ethylhydrazine	624-80-6		1710	MS, RI	SPME			√	
86	Imidazole-4-acetic acid	645-65-8		1185	MS, RI	SPME	√	√		
87	3-Hydroxypiperidine	6859-99-0		1194	MS, RI	SPME		√		
88	N,N-Dimethylthioformamide	758-16-7		1786	MS, RI	SPME	√	√	√	√
89	N,N-Dimethylpropanamide	758-96-3		664	MS, RI	SPME			√	√
90	Ethyl 3-aminopropanoate	924-73-2		1269	MS, RI	SPME		√		
91	2-Ethyl-4-methylimidazole	931-36-2			MS	LLE-SAFE	√	√		
					Esters (86)					
1	Isoamyl acetate	123-92-2	1024	1014	MS, RI, aroma, S	LLE-SAFE, SPME	√	√	√	√
2	2-Methylbutyl acetate	624-41-9	1024		MS, RI	LLE-SAFE	√		√	
3	Pentyl acetate	628-63-7	1024		MS, RI, S	LLE-SAFE		√		√
4	Ethyl valerate	539-82-2	1038	1433	MS, RI, S	LLE-SAFE	√	√	√	√
5	Ethyl hexanoate	123-66-0	1135	1157	MS, RI, aroma, S	LLE-SAFE, SPME	√	√	√	√
6	Ethyl Pyruvate	617-35-6	1164		MS, RI	LLE-SAFE	√	√	√	√
7	Hexyl acetate	142-92-7	1171	1183	MS, RI, S	LLE-SAFE, SPME	√	√	√	√
8	Allyl butanoate	2051-78-7	1175		MS, RI	LLE-SAFE	√	√	√	√
9	Ethyl heptanoate	106-30-9	1232	1214	MS, RI, S	LLE-SAFE, SPME	√	√	√	√
10	(−)-Ethyl L-lactate	687-47-8	1238		MS, RI	LLE-SAFE	√	√	√	√
11	Ethyl lactate	97-64-3	1238		MS, RI, S	LLE-SAFE	√	√	√	√
12	Hexyl formate	629-33-4	1250		MS, RI, S	LLE-SAFE				√
13	2-Propenoic acid ethenyl ester	2177-18-6	1294		MS, RI	LLE-SAFE	√	√		√
14	Methyl acrylate	96-33-3	1294		MS, RI	LLE-SAFE			√	√
15	Ethyl octanoate	106-32-1	1332	1303	MS, RI, S	LLE-SAFE, SPME	√	√	√	√
16	Heptyl formate	112-23-2	1352		MS, RI	LLE-SAFE	√			
17	3-Methoxybutyl acetate	4435-53-4	1411		MS, RI	LLE-SAFE		√		
18	Ethyl 2-hydroxyisobutyrate	80-55-7	1411		MS, RI	LLE-SAFE		√	√	

Table A3. *Cont.*

No.	Compound Name	CAS	RI		Identification Method	Sample Preparation	Presence in Samples			
			DB-WAX	DB-FFAP			YJ	QD	HR	BW
					Esters (86)					
19	Ethyl 3-hydrobutyrate	5405-41-4	1411	1876	MS, RI, S	LLE-SAFE, SPME			√	√
20	Octyl formate	112-32-3	1454		MS, RI	LLE-SAFE		√	√	
21	2-Hydroxypropyl acetate	627-69-0	1467		MS, RI	LLE-SAFE	√			
22	Ethyl levulinate	539-88-8	1500		MS, RI	LLE-SAFE			√	
23	2-Hydroxyethyl formate	628-35-3	1514		MS, RI	LLE-SAFE	√	√	√	√
24	2-Hydroxyethyl acetate	542-59-6	1528		MS, RI	LLE-SAFE	√	√	√	√
25	Ethyl decanoate	110-38-3	1535	1377	MS, RI, S	LLE-SAFE, SPME	√		√	√
26	Diethyl succinate	123-25-1	1570		MS, RI, S	LLE-SAFE	√	√	√	√
27	Dimethyl glutarate	1119-40-0	1593		MS, RI	LLE-SAFE	√	√		
28	Isopropyl isobutyrate	617-50-5	1600		MS, RI	LLE-SAFE			√	
29	Propyl acetate	109-60-4	1630		MS, RI, S	LLE-SAFE	√	√		
30	1,3-Diacetoxy-propane	628-66-0	1632		MS, RI	LLE-SAFE	√	√	√	√
31	Neryl formate	2142-94-1	1744		MS, RI	LLE-SAFE	√			
32	1,1-Ethanediol diacetate	542-10-9	1749		MS, RI	LLE-SAFE			√	√
33	Butyl butyrate	109-21-7	1760		MS, RI	LLE-SAFE		√		
34	Butyl 2-methyl propanoate	97-87-0	1760		MS, RI, S	LLE-SAFE		√		
35	Pentyl 2-methylprop-2-enoate	2849-98-1	1936		MS, RI	LLE-SAFE				√
36	Allyl propionate	2408-20-0	2012		MS, RI	LLE-SAFE			√	
37	Vinyl butyrate	123-20-6	2012		MS, RI	LLE-SAFE		√		
38	Allyl isobutyrate	15727-77-2	2015		MS, RI	LLE-SAFE	√		√	
39	Ethyl cinnamate	103-36-6	2019		MS, RI	LLE-SAFE				√
40	Vinyl acetate	108-05-4	2038		MS, RI	LLE-SAFE	√			
41	Methyl acetate	79-20-9	2102		MS, RI, S	LLE-SAFE	√			
42	Methyl tridecanoate	1731-88-0	2112		MS, RI	LLE-SAFE		√		
43	Glycidyl acrylate	106-90-1	2139		MS, RI	LLE-SAFE			√	√
44	2,3-Dihydroxypropyl acetate	106-61-6	2173		MS, RI	LLE-SAFE	√	√	√	√
45	Ethyl cyclohexanepropionate	10094-36-7	2233		MS, RI	LLE-SAFE	√	√	√	√
46	Ethyl nonanoate	123-29-5	2233	1285	MS, RI, S	LLE-SAFE, SPME	√	√	√	√
47	Allyl propyl ether	1471-03-0	2589		MS, RI	LLE-SAFE	√			
48	2-Oxooctadecanoic acid methyl ester	2380-18-9	2607		MS, RI	LLE-SAFE	√			
49	L-Lactide	4511-42-6	2630		MS, RI	LLE-SAFE	√			
50	Ethenyl formate	692-45-5	2716		MS, RI	LLE-SAFE		√	√	
51	Methyl propionate	554-12-1	2729		MS, RI, S	LLE-SAFE, SPME	√	√		
52	Butyl lactate	138-22-7	2751		MS, RI, S	LLE-SAFE			√	√
53	Lactic acid methyl ester	547-64-8	2811		MS, RI	LLE-SAFE			√	
54	Isopropyl formate	625-55-8	2939		MS, RI	LLE-SAFE	√		√	
55	DL-Lactide	95-96-5	3127		MS, RI	LLE-SAFE			√	√
56	Ethyl acetate	141-78-6	913	606	MS, RI, S	LLE-SAFE, SPME	√	√	√	√
57	Isobutyl acetate	110-19-0	990		MS, RI, S	LLE-SAFE	√			
58	Butyl acetate	123-86-4	990		MS, RI, S	LLE-SAFE			√	√
59	2,2-Dimethoxypropionic acid methyl ester	10076-48-9		2237	MS, RI	SPME	√		√	

Table A3. *Cont.*

No.	Compound Name	CAS	RI		Identification Method	Sample Preparation	Presence in Samples			
			DB-WAX	DB-FFAP			YJ	QD	HR	BW
				Esters (86)						
60	sec-Butyl Crotonate	10371-45-6		1304	MS, RI	SPME	√	√		
61	Ethyl propanoate	105-37-3		2101	MS, RI, aroma, S	LLE-SAFE	√	√	√	√
62	Isoamyl butyrate	106-27-4		1102	MS, RI, S	SPME	√			
63	Ethyl dodecanoate	106-33-2		2256	MS, RI	LLE-SAFE	√		√	
64	Ethyl hydrogen succinate	1070-34-4		2388	MS, RI, aroma, S	LLE-SAFE	√	√	√	√
65	Ethyl isovalerate	108-64-5		1302	MS, RI, S	SPME		√		
66	Methyl decanoate	110-42-9		2215	MS, RI, aroma, S	LLE-SAFE	√	√	√	√
67	Methyl 2-octynate	111-12-6		2415	MS, RI, aroma, S	LLE-SAFE			√	√
68	Ethyl Stearate	111-61-5		1301	MS, RI, S	SPME	√	√	√	√
69	Octyl Acetate	112-14-1		1298	MS, RI, S	SPME	√	√		
70	Ethyl myristate	124-06-1		1382	MS, RI, S	SPME	√	√	√	√
71	Ccrotonic acid isopropyl ester	18060-77-0		1263	MS, RI	SPME	√	√		√
72	Ethyl nonadecanoate	18281-04-4		1299	MS, RI	SPME	√			√
73	Methyl (Z)-3,7-dimethylocta-2,6-dienoate	1862-61-9		1394	MS, RI	SPME	√			
74	Ethyl 3-hexenoate	2396-83-0		1206	MS, RI, S	SPME	√	√		√
75	2-Ethylhexyl Butyrate	25415-84-3		1320	MS, RI	SPME		√		
76	Hexyl butanoate	2639-63-6		2144	MS, RI, aroma, S	LLE-SAFE	√	√	√	√
77	Ethyl butyrylacetate	3249-68-1		2297	MS, RI	SPME	√	√	√	
78	Heptadecanyl margarate	36617-50-2		1422	MS, RI	SPME		√		√
79	Dimethyl dl-malate	38115-87-6		1197	MS, RI	SPME		√	√	
80	Methyl 4-methoxyacetoacetate	41051-15-4		2275	MS, RI	SPME	√			
81	Ethyl 3-methylvalerate	5870-68-8		1299	MS, RI	SPME	√			
82	Ethyl undecanoate	627-90-7		1271	MS, RI	SPME	√		√	
83	Dodecyl isobutyrate	6624-71-1		2332	MS, RI	SPME		√	√	
84	Ethyl trans-2-decenoate	7367-88-6		1194	MS, RI, S	SPME			√	
85	Isobutyric acid 2-ethyl-3-hydroxyhexyl ester	74367-31-0		677	MS, RI	SPME	√			
86	(+)-Diethyl L-tartrate	87-91-2		1526	MS, RI	SPME			√	
				Alkanes (57)						
1	1,1-Dimethyl cyclopropane	1630-94-0	886		MS, RI	LLE-SAFE	√	√	√	√
2	s-Trioxane	110-88-3	1063		MS, RI	LLE-SAFE	√	√	√	√
3	Nonane	111-84-2	1105		MS, RI	LLE-SAFE			√	
4	2,4-Dimethyldecane	2801-84-5	1105		MS, RI	LLE-SAFE			√	
5	n-Hendecane	1120-21-4	1105		MS, RI	LLE-SAFE			√	
6	2,3-Dimethylbutane	79-29-8	1111		MS, RI	LLE-SAFE	√			
7	Decane	124-18-5	1201		MS, RI	LLE-SAFE			√	√
8	3,7-Dimethyldecane	17312-54-8	1201		MS, RI	LLE-SAFE		√		
9	2-Methylnonane	871-83-0	1201		MS, RI	LLE-SAFE				√
10	Tridecane	629-50-5	1203		MS, RI	LLE-SAFE		√	√	√
11	Propyl cyclopropane	2415-72-7	1250		MS, RI	LLE-SAFE			√	
12	Cyclododecane	294-62-2	1659		MS, RI	LLE-SAFE	√			
13	2,3-Dimethyloxirane	3266-23-7	1713		MS, RI	LLE-SAFE				√
14	1,4- Diacetoxybutane	628-67-1	1769		MS, RI	LLE-SAFE		√		
15	trans-1,2-Dimethylcyclopropane	2402/6/4	2039		MS, RI	LLE-SAFE		√		

Table A3. *Cont.*

No.	Compound Name	CAS	RI		Identification Method	Sample Preparation	Presence in Samples			
			DB-WAX	DB-FFAP			YJ	QD	HR	BW
				Alkanes (57)						
16	1,2-Epoxyhexane	1436-34-6	2155		MS, RI	LLE-SAFE			√	√
17	Methylcyclobutane	598-61-8	2264		MS, RI	LLE-SAFE	√		√	
18	6-Ethyl-2-methyldecane	62108-21-8	2401		MS, RI	LLE-SAFE	√			
19	2,7-Dimethyloctane	1072-16-8	2491		MS, RI	LLE-SAFE		√		
20	Dimethylmethane	74-98-6	2514		MS, RI	LLE-SAFE			√	√
21	2,6,10-Trimethyldodecane	3891-98-3	2709		MS, RI	LLE-SAFE		√		
22	Hexadecane	544-76-3	2805		MS, RI	LLE-SAFE	√	√	√	√
23	2-Methylpropane	75-28-5	2996		MS, RI	LLE-SAFE	√		√	
24	Butane	106-97-8	3044		MS, RI	LLE-SAFE	√	√		
25	1,3,6-Trioxocane	1779-19-7	3054		MS, RI	LLE-SAFE				√
26	Pentane	109-66-0	881		MS, RI	LLE-SAFE	√			
27	Bicyclo[2,1,0]pentane	185-94-4	889		MS, RI	LLE-SAFE	√	√	√	√
28	Ethylene oxide	75-21-8	893		MS, RI	LLE-SAFE	√		√	
29	Isobutylene oxide	558-30-5	910		MS, RI	LLE-SAFE	√	√	√	√
30	Cyclopropane	75-19-4	998		MS, RI	LLE-SAFE	√			√
31	1,3-Dimethoxybutane	10143-66-5		2290	MS, RI	SPME	√			
32	Acetaldehyde dipropyl acetal	105-82-8		2254	MS, RI	SPME		√	√	√
33	Methylcyclohexane	108-87-2			MS	LLE-SAFE	√	√	√	√
34	Tetratriacontane	14167-59-0			MS, aroma, S	LLE-SAFE	√	√		
35	Cycloheptane	291-64-5		1237	MS, RI	SPME	√			
36	Cyclooctane	292-64-8		1415	MS, RI	SPME	√			
37	1,2,3,4-Tetramethoxybutane	3011-85-6		2305	MS, RI	SPME	√	√	√	
38	1,1,3-Trimethylcyclohexane	3073-66-3			MS	LLE-SAFE			√	√
39	1,2-Dicyclohexylethane	3321-50-4			MS	LLE-SAFE		√	√	√
40	2,2-Dimethoxybutane	3453-99-4		2017	MS, RI	SPME			√	
41	Cholestane	481-21-0			MS, aroma, S	LLE-SAFE	√	√	√	√
42	11-Decyl-docosane	55401-55-3			MS	LLE-SAFE		√		
43	1-(1-ethoxyethoxy)-Butane	57006-87-8		671	MS, RI	SPME		√	√	
44	2,4-Dimethylhexane	589-43-5		1303	MS, RI	LLE-SAFE			√	
45	Heptacosane	593-49-7		2304	MS, RI	LLE-SAFE	√		√	√
46	1-Ethyl-2-propylcyclohexane	62238-33-9			MS	LLE-SAFE			√	
47	n-Pentadecane	629-62-9			MS	LLE-SAFE	√		√	√
48	n-Heneicosane	629-94-7			MS	LLE-SAFE			√	
49	n-Pentacosane	629-99-2			MS	LLE-SAFE		√		
50	Hexacosane	630-01-3			MS, aroma, S	LLE-SAFE	√		√	√
51	n-Octacosane	630-02-4			MS	LLE-SAFE	√	√	√	√
52	n-Nonacosane	630-03-5			MS	LLE-SAFE		√	√	√
53	Hentriacontane	630-04-6		2406	MS, RI	LLE-SAFE	√	√	√	√
54	n-Triacontane	638-68-6			MS	LLE-SAFE		√	√	√
55	Tetracosane	646-31-1			MS	LLE-SAFE	√	√		√
56	1,3,3-Trimethoxybutane	6607-66-5		2367	MS, RI	SPME	√		√	
57	Tetratetracontane	7098-22-8			MS, aroma, S	LLE-SAFE		√		√

Table A3. *Cont.*

No.	Compound Name	CAS	RI		Identification Method	Sample Preparation	Presence in Samples			
			DB-WAX	DB-FFAP			YJ	QD	HR	BW
					Furans (42)					
1	2-Methyltetrahydrofuran-3-one	3188-00-9	1160		MS, RI	LLE-SAFE	√	√	√	√
2	2,2,5,5-Tetramethyltetra hydrofuran	15045-43-9	1307		MS, RI	LLE-SAFE			√	
3	Furfural	1998/1/1	1354	1303	MS, RI	LLE-SAFE, SPME	√	√	√	√
4	2-Acetyl furan	1192-62-7	1396		MS, RI, S	LLE-SAFE	√	√	√	√
5	5-Methyl-2-furaldehyde	620-02-0	1462		MS, RI, S	LLE-SAFE			√	
6	2-Propionylfuran	3194-15-8	1465		MS, RI	LLE-SAFE			√	
7	Furfuryl alcohol	98-00-0	1555	1375	MS, RI, aroma, S	LLE-SAFE, SPME	√	√	√	√
8	Tetrahydrofuran-2-ylmethylacetat	637-64-9	1566		MS, RI	LLE-SAFE		√		
9	2,2-Di(2-tetrahydrofuryl)propane	89686-69-1	1604		MS, RI	LLE-SAFE		√		
10	3-Methyl-2(5H)-furanone	22122-36-7	1605		MS, RI	LLE-SAFE	√	√	√	√
11	2(5H)-Furanone	497-23-4	1639		MS, RI	LLE-SAFE	√	√	√	√
12	2,5-Dimethyl-4-hydroxy-2H-furan-3-one	3658-77-3	1749	1865	MS, RI, aroma, S	LLE-SAFE	√	√	√	√
13	2-(1-Oxo-2-hydroxyethyl)furan	17678-19-2	1892		MS, RI	LLE-SAFE	√	√	√	√
14	5-Acetyltetrahydrofuran-2-one	29393-32-6	1945		MS, RI	LLE-SAFE	√	√	√	√
15	4-Hydroxy-5-methyl-3-furanone	19322-27-1	2009		MS, RI	LLE-SAFE		√	√	√
16	2H-Pyran-2,6(3H)-dione	5926-95-4	2009		MS, RI	LLE-SAFE			√	
17	2-Furaldehyde diethyl acetal	13529-27-6	2012		MS, RI	LLE-SAFE	√			
18	4-Methoxy-5H-furan-2-one	69556-70-3	2056		MS, RI	LLE-SAFE	√			
19	3-Furanmethanol	4412-91-3	2085		MS, RI	LLE-SAFE	√			
20	Ethyl 5-oxooxolane-2-carboxylate	1126-51-8	2116		MS, RI	LLE-SAFE	√	√	√	
21	Methyl 5-oxotetrahydrofuran-2-carboxylate	3885-29-8	2116		MS, RI	LLE-SAFE	√			
22	Tetrahydrofurfruyl alcohol	97-99-4	2155		MS, RI, S	LLE-SAFE			√	√
23	2-Furanmethanamine	617-89-0	2170		MS, RI	LLE-SAFE	√	√	√	√
24	2-Methyl-4H,5H-furo[3,2-c]pyridin-4-one	26956-44-5	2269		MS, RI	LLE-SAFE	√		√	√
25	5-Hydroxymethyl-2-furaldehyde	67-47-0	2387		MS, RI, aroma, S	LLE-SAFE	√	√	√	√
26	5-(Hydroxymethyl)dihydro-2(3H)-furanone	10374-51-3	2390		MS, RI	LLE-SAFE				√
27	5-(1-Piperidyl)furan-2-carbaldehyde	22868-60-6	2433		MS, RI	LLE-SAFE		√		

Table A3. *Cont.*

No.	Compound Name	CAS	RI		Identification Method	Sample Preparation	Presence in Samples			
			DB-WAX	DB-FFAP			YJ	QD	HR	BW
					Furans (42)					
28	5-(Hydroxymethyl)furfuryl alcohol	1883-75-6	2469		MS, RI	LLE-SAFE	√	√	√	√
29	3-Furaldehyde	498-60-2	2514		MS, RI	LLE-SAFE	√		√	√
30	2,3-Dihydrofuran	1191-99-7		1116	MS, RI	SPME			√	
31	Furfuryl sulfide	13678-67-6			MS	LLE-SAFE		√		
32	4,6-Dimethoxy-2,3-dihydrobenzofuran-3-one	4225-35-8		2389	MS, RI	LLE-SAFE		√		
33	2,2′-Difurfuryl ether	4437-22-3		1190	MS, RI	SPME		√	√	√
34	2-Butylfuran	4466-24-4		1186	MS, RI, S	SPME			√	
35	Phthalan	496-14-0		1371	MS, RI	SPME			√	
36	2,3-Dihydrobenzofuran	496-16-2		2402	MS, RI	LLE-SAFE		√		
37	Methyl 2-furoate	611-13-2		2021	MS, RI, aroma, S	LLE-SAFE	√	√	√	√
38	2,5-Furandicarboxaldehyde	823-82-5		1999	MS, RI	LLE-SAFE	√	√	√	√
39	2-Furancarboxylic acid	88-14-2		2249	MS, RI, aroma, S	LLE-SAFE	√	√		√
40	3-Methylfuran	930-27-8		1206	MS, RI	SPME	√	√		
41	5-Methoxy-2,3-dihydrobenzofuran-3-acetic acid	93198-71-1			MS	LLE-SAFE			√	
42	2-Methyltetrahydrofuran	96-47-9		690	MS, RI	SPME		√		
					Aromatic compounds (41)					
1	Styrene	100-42-5	1152		MS, RI	LLE-SAFE		√	√	√
2	Benzocyclobutene	694-87-1	1152		MS, RI	LLE-SAFE		√		
3	Benzaldehyde	100-52-7	1411		MS, RI, S	LLE-SAFE			√	
4	Benzeneacetaldehyde	122-78-1	1531		MS, RI, S	LLE-SAFE	√	√	√	√
5	Ethyl benzoate	93-89-0	1558		MS, RI, S	LLE-SAFE	√			
6	2-Phenylethyl acetate	103-45-7	1706	1444	MS, RI, aroma, S	LLE-SAFE, SPME	√	√	√	√
7	Benzyl alcohol	100-51-6	1767		MS, RI, S	LLE-SAFE	√	√	√	√
8	Phenethyl alcohol	1960/12/8	1801	1471	MS, RI, aroma, S	LLE-SAFE, SPME	√	√	√	√
9	Toluene	108-88-3	1803		MS, RI	LLE-SAFE	√	√	√	√
10	2,6-Di-tert-butyl-4-methylphenol	128-37-0	1807		MS, RI, S	LLE-SAFE	√	√	√	√
11	DL-β-Ethylphenethyl alcohol	2035-94-1	1876		MS, RI	LLE-SAFE	√			
12	Phenol	108-95-2	1894	2009	MS, RI, S	LLE-SAFE	√	√	√	√
13	3-Phenoxypropionic acid	7170-38-9	1964		MS, RI	LLE-SAFE	√			
14	2-Methoxy-4-vinylphenol	7786-61-0	2083	1647	MS, RI, aroma, S	LLE-SAFE, SPME	√	√	√	√
15	3-Hydroxy-4-phenylbutane-2-one	5355-63-5	2146		MS, RI	LLE-SAFE	√	√	√	√
16	Ethyl 2-hydroxy-3-phenylpropanoate	15399-05-0	2164		MS, RI	LLE-SAFE	√	√	√	√
17	1,3-Dioxolane,2-(1-phenylethyl)	4362-22-5	2165		MS, RI	LLE-SAFE	√		√	
18	2,4-Di-tert-butylphenol	96-76-4	2207	2309	MS, RI, aroma, S	LLE-SAFE	√	√	√	√
19	1-Phenyl-2-propanone	103-79-7	2219		MS, RI	LLE-SAFE			√	√
20	4-Vinylphenol	2628-17-3	2281		MS, RI	LLE-SAFE	√	√	√	√

Table A3. *Cont.*

No.	Compound Name	CAS	RI		Identification Method	Sample Preparation	Presence in Samples			
			DB-WAX	DB-FFAP			YJ	QD	HR	BW
					Aromatic compounds (41)					
21	1,3-Diphenylpropan-2-ol	5381-92-0	2400		MS, RI	LLE-SAFE	√	√	√	√
22	3-Hydroxy-3-phenylbutan-2-one	3155/1/9	2410		MS, RI	LLE-SAFE		√	√	√
23	α-Methylstyrene	98-83-9	2679		MS, RI	LLE-SAFE	√	√	√	√
24	4-n-Propylphenol	645-56-7	2703		MS, RI, S	LLE-SAFE				√
25	4-(2-Acetoxy-ethyl)phenol	58556-55-1	2821		MS, RI	LLE-SAFE	√	√	√	√
26	p-Hydroxybenzaldehyde	123-08-0	2836		MS, RI, S	LLE-SAFE			√	
27	4-Methoxyresorcinol	6100-60-3	2846		MS, RI	LLE-SAFE		√	√	√
28	2-Methoxyhydroquinone	824-46-4	2846		MS, RI, S	LLE-SAFE		√	√	√
29	4-Hydroxyphenylethanol	501-94-0	2893		MS, RI, aroma, S	LLE-SAFE	√	√	√	√
30	Benzeneacetic acid	103-82-2			MS, aroma, S	LLE-SAFE	√	√	√	√
31	Resorcinol	108-46-3		2084	MS, RI, aroma, S	LLE-SAFE				√
32	1-(2-Hydroxy-5-methylphenyl)ethanone	1450-72-2		1647	MS, RI	SPME		√		√
33	(R)-(+)-1-Phenylethanol	1517-69-7		1220	MS, RI	SPME	√	√		√
34	4-Phenylbutanal	18328-11-5		1428	MS, RI	SPME		√		√
35	4-Methoxyphenoxyacetic acid	1877-75-4			MS	LLE-SAFE	√		√	√
36	4-Hydroxyphenoxyacetic acid	1878-84-8			MS	LLE-SAFE			√	
37	3,5-Dimethoxyphenol	500-99-2			MS, S	LLE-SAFE		√		
38	2,3,5,6-Tetramethyl-pheno	527-35-5		1645	MS, RI, S	SPME	√		√	
39	2,5-Di-tert-butylphenol	5875-45-6		1701	MS, RI	SPME	√	√	√	√
40	Benzoic acid	65-85-0		2449	MS, RI, aroma, S	LLE-SAFE	√	√	√	√
41	2,5-Dimethylphenol	95-87-4		2196	MS, RI, aroma, S	LLE-SAFE			√	
					Ketones (37)					
1	3-Penten-2-one	3102-33-8	1026		MS, RI	LLE-SAFE		√		
2	3-Penten-2-one	625-33-2	1026		MS, RI	LLE-SAFE		√	√	
3	Cyclopentanone	120-92-3	1082		MS, RI	LLE-SAFE	√			√
4	2,2,5-Trimethylhexane-3,4-dione	20633-03-8	1105		MS, RI	LLE-SAFE				√
5	3-Hydroxy-2-butanone	513-86-0	1179	1277	MS, RI, S	LLE-SAFE	√	√	√	√
6	Hydroxyacetone	116-09-6	1191		MS, RI	LLE-SAFE	√	√	√	√
7	2-Cyclopenten-1-one	930-30-3	1248		MS, RI	LLE-SAFE	√	√	√	√
8	2-Hydroxy-3-pentanone	5704-20-1	1250		MS, RI	LLE-SAFE		√	√	
9	4-Hydroxy-4-methyl-2-pentanone	123-42-2	1254		MS, RI	LLE-SAFE	√	√	√	√
10	4-Hydroxy-3-hexanone	4984-85-4	1302		MS, RI	LLE-SAFE			√	
11	4-Hydroxy-2-pentanone	4161-60-8	1350		MS, RI	LLE-SAFE		√	√	√
12	2-Butanone	78-93-3	1359		MS, RI	LLE-SAFE		√	√	
13	2,5-Hexanedione	110-13-4	1394		MS, RI	LLE-SAFE		√		√

Table A3. *Cont.*

No.	Compound Name	CAS	RI		Identification Method	Sample Preparation	Presence in Samples			
			DB-WAX	DB-FFAP			YJ	QD	HR	BW
					Ketones (37)					
14	4-Hydroxy-2-butanone	590-90-9	1427	1737	MS, RI, aroma, S	LLE-SAFE	√	√	√	√
15	3-Hydroxy-3-methyl-2-butanone	115-22-0	1451		MS, RI	LLE-SAFE			√	√
16	Isophorone	78-59-1	1483		MS, RI	LLE-SAFE	√	√	√	√
17	3-Methylcyclopentane-1,2-dione	765-70-8	1726		MS, RI	LLE-SAFE	√		√	√
18	3,4-Dihydroxy-2-butanone	57011-15-1	1819		MS, RI	LLE-SAFE	√		√	√
19	1,3-Dioxolan-2-one	96-49-1	1827		MS, RI	LLE-SAFE	√		√	
20	1-Hydroxy-2-pentanone	64502-89-2	1978		MS, RI	LLE-SAFE			√	
21	4-Methyl-2,3-pentanedione	7493-58-5	2003		MS, RI	LLE-SAFE	√			
22	2-Ethyl-cyclopentanone	4971-18-0	2009		MS, RI	LLE-SAFE	√			
23	2,3-Butanedione	431-03-8	2038		MS, RI, S	LLE-SAFE			√	
24	4-Acetoxy-2-butanone	10150-87-5	2424		MS, RI	LLE-SAFE	√	√	√	√
25	4-Hydroxy-β-damascone	102488-09-5	2425		MS, RI	LLE-SAFE		√	√	√
26	4-(Hydroxymethyl)-1,3-dioxolan-2-one	931-40-8	2716		MS, RI	LLE-SAFE	√		√	
27	Acetone	67-64-1	917		MS, RI	LLE-SAFE	√	√	√	√
28	2,3-Pentanedione	600-14-6	982		MS, RI	LLE-SAFE			√	√
29	2,2,6-Trimethylcyclohexanone	2408-37-9			MS	LLE-SAFE	√			√
30	2-Ethyl-3-methoxy-2-cyclopentenone	25112-86-1			MS	LLE-SAFE				√
31	3-Methyl-4-nonanone	35778-39-3		681	MS, RI	SPME	√		√	
32	3,4,5,6-Tetrahydropseudoionone	4433-36-7			MS	LLE-SAFE			√	
33	5-Methyl-3-heptanone	541-85-5		2215	MS, RI	SPME		√		
34	4-Octanone	589-63-9		1150	MS, RI	SPME	√	√	√	√
35	3-Methyl-cyclohexanone	591-24-2		1188	MS, RI	SPME	√			
36	(Z)-β-Ionone	79-77-6			MS, aroma, S	LLE-SAFE		√		√
37	Verbenone	80-57-9		1645	MS, RI	SPME			√	
					Acids (33)					
1	2-Methylvaleric acid	594-61-6	1411		MS, RI, S	LLE-SAFE	√	√	√	√
2	Acetic acid	64-19-7	1473	1296	MS, RI, aroma, S	LLE-SAFE, SPME	√	√	√	√
3	4-Methyl-3-pentenoic acid	504-85-8	1478		MS, RI	LLE-SAFE	√	√	√	√
4	3-Hydroxypropionic acid	503-66-2	1489		MS, RI	LLE-SAFE			√	
5	Malonic acid	141-82-2	1715		MS, RI	LLE-SAFE			√	
6	Butanoic acid	107-92-6	1718		MS, RI	LLE-SAFE		√		
7	Hexanoic acid	142-62-1	1824	1441	MS, RI, aroma, S	LLE-SAFE, SPME	√	√	√	√
8	4-Methylvaleric acid	646-07-1	1832		MS, RI	LLE-SAFE				√
9	Pentanoic acid	109-52-4	1870		MS, RI, S	LLE-SAFE	√	√	√	√
10	4-Methylpent-4-enoic acid	1001-75-8	2006		MS, RI	LLE-SAFE			√	
11	Octanoic acid	124-07-2	2006	1544	MS, RI, aroma, S	LLE-SAFE, SPME	√	√	√	√

Table A3. *Cont.*

No.	Compound Name	CAS	RI		Identification Method	Sample Preparation	Presence in Samples			
			DB-WAX	DB-FFAP			YJ	QD	HR	BW
					Acids (33)					
12	2-Methyl-2-pentenoic acid	3142-72-1	2011	1199	MS, RI, S	LLE-SAFE, SPME	√	√	√	√
13	3-Methylbutanoic acid	503-74-2	2062	1379	MS, RI, aroma, S	LLE-SAFE, SPME	√	√	√	√
14	2-Propynyl acetate	627-09-8	2112		MS, RI	LLE-SAFE	√	√		√
15	2-Oxopropionic acid	127-17-3	2229		MS, RI	LLE-SAFE	√	√	√	√
16	Decanoic acid	334-48-5	2322	1684	MS, RI, aroma, S	LLE-SAFE, SPME	√	√	√	√
17	Nonanoic acid	112-05-0	2342		MS, RI, S	LLE-SAFE				√
18	L-Lactic acid	79-33-4	2947		MS, RI	LLE-SAFE		√		
19	4-Methyl-2-pentenoic acid	10321-71-8		1955	MS, RI	LLE-SAFE			√	√
20	DL-3-Methylvaleric acid	105-43-1		1373	MS, RI, S	SPME		√		
21	Heptanoic acid	111-14-8		1619	MS, RI, S	SPME	√		√	√
22	Hendecanoic acid	112-37-8		1492	MS, RI	SPME	√		√	√
23	Elaidic acid	112-79-8			MS, aroma, S	LLE-SAFE	√	√		√
24	3-Ethylheptanoic acid	14272-47-0		1629	MS, RI	SPME	√	√	√	
25	Dodecanoic acid	143-07-7		2486	MS, RI, aroma, S	LLE-SAFE	√	√	√	√
26	2-(2-Methoxyethoxy)acetic acid	16024-56-9		2311	MS, RI	SPME	√			
27	4-Methoxybutyric acid	29006-02-8		2321	MS, RI	SPME	√		√	√
28	Crotonic acid	3724-65-0		2395	MS, RI	LLE-SAFE		√		
29	trans-3-Hexenoic acid	4219-24-3		2128	MS, RI, aroma, S	LLE-SAFE	√	√	√	√
30	3-Ethoxypropionic acid	4324-38-3		1859	MS, RI	SPME	√			√
31	Palmitic acid	1957/10/3			MS, aroma, S	LLE-SAFE	√	√	√	√
32	Tridecanoic acid	638-53-9		1620	MS, RI, S	SPME	√	√	√	√
33	Citric acid	77-92-9		1730	MS, RI	SPME				√
					Sulfur-containing compounds (27)					
1	Thiazole	288-47-1	1145		MS, RI	LLE-SAFE	√			
2	Acetyl Sulfide	3232-39-1	1164		MS, RI	LLE-SAFE		√	√	√
3	2-(Methylthio)ethanol	5271-38-5	1422		MS, RI, S	LLE-SAFE	√	√	√	√
4	Dimethyl sulfoxide	67-68-5	1467		MS, RI, S	LLE-SAFE	√	√	√	√
5	3-(Methylthio)-1-propanol	505-10-2	1610	1714	MS, RI, aroma, S	LLE-SAFE, SPME	√	√	√	√
6	Thioacetic acid	507-09-5	1630		MS, RI, S	LLE-SAFE	√			√
7	S-Ethyl ethanethioate	625-60-5	1704		MS, RI, S	LLE-SAFE	√			
8	Dimethyl sulfone	67-71-0	1785		MS, RI, S	LLE-SAFE	√	√	√	√
9	4-methyl-5-hydroxyethyl thiazole	137-00-8	2197		MS, RI	LLE-SAFE	√	√		√
10	Methyl p-tolyl sulfone	3185-99-7	2504		MS, RI	LLE-SAFE				√
11	Methyl mercaptan	74-93-1	893		MS, RI, S	LLE-SAFE	√	√	√	√
12	Tetrahydrothiophene	110-01-0		1679	MS, RI	SPME	√	√		
13	Thiophene	110-02-1		1031	MS, RI, aroma, S	LLE-SAFE, SPME	√	√	√	√
14	2,3-Dihydrothiophene	1120-59-8		2395	MS, RI	LLE-SAFE		√		
15	2-Thiopheneacetic acid	1918-77-0		1187	MS, RI	SPME		√	√	√
16	(Butylthio)acetic acid	20600-61-7		1989	MS, RI	SPME		√		
17	[(2-Methylpropyl)thio]acetic acid	20600-62-8		2282	MS, RI	SPME	√			

Table A3. *Cont.*

No.	Compound Name	CAS	RI		Identification Method	Sample Preparation	Presence in Samples			
			DB-WAX	DB-FFAP			YJ	QD	HR	BW
					Sulfur-containing compounds (27)					
18	3-(n-Butylsulphanyl)propionic acid	22002-73-9		2383	MS, RI	SPME		√		
19	2-Pyrrolidinethione	2295-35-4		1219	MS, RI	SPME			√	√
20	Isothiazole	288-16-4		652	MS, RI	LLE-SAFE			√	√
21	2-Acetyl-2-thiazoline	29926-41-8		1631	MS, RI	SPME		√		
22	4-Methyl-5-acetyl thiazole	38205-55-9		1349	MS, RI	SPME				√
23	Thiazolidine-4-carboxylic acid	444-27-9		2219	MS, RI	SPME	√	√	√	
24	Thiazolidine	504-78-9		1893	MS, RI	SPME				√
25	Diethyl sulfite	623-81-4		2166	MS, RI	SPME	√	√		√
26	5-Methylthio-1,3,4-thiadiazole-2-thiol	6264-40-0		2158	MS, RI	SPME				√
27	Divinyl sulfide	627-51-0		2399	MS, RI	LLE-SAFE			√	
					Lactones (24)					
1	α-Methyl-γ-butyrolactone	1679-47-6	1476		MS, RI	LLE-SAFE	√	√	√	√
2	4,4-Dimethylbut-2-en-4-olide	20019-64-1	1496		MS, RI	LLE-SAFE	√	√	√	√
3	γ-Valerolactone	108-29-2	1496		MS, RI, S	LLE-SAFE	√	√	√	√
4	3-Methyl-4-butanolide	1679-49-8	1500		MS, RI	LLE-SAFE	√	√	√	√
5	γ-Butyrolactone	96-48-0	1512		MS, RI, S	LLE-SAFE	√	√	√	√
6	γ-Hexanolactone	695-06-7	1589		MS, RI, S	LLE-SAFE	√	√	√	√
7	δ-Hexanolide	823-22-3	1679		MS, RI, S	LLE-SAFE	√	√	√	√
8	δ-Valerolactone	542-28-9	1688		MS, RI, S	LLE-SAFE	√	√	√	√
9	3-Methyl-2-buten-4-olide	6124-79-4	1769	1903	MS, RI	LLE-SAFE	√	√	√	√
10	γ-Octalactone	104-50-7	1803		MS, RI, S	LLE-SAFE	√	√	√	√
11	3-Methyl-2-penten-5-olide	2381-87-5	1903		MS, RI	LLE-SAFE	√	√	√	√
12	4-Nonanolide	104-61-0	1915		MS, RI, S	LLE-SAFE	√	√	√	√
13	L-(+)-Pantolactone	5405-40-3	1917		MS, RI	LLE-SAFE	√	√		√
14	D-(−)-Pantolactone	599-04-2	1917		MS, RI	LLE-SAFE	√	√	√	√
15	DL-Pantoyl Lacyone	79-50-5	1917		MS, RI	LLE-SAFE		√		
16	2-Hydroxy-γ-butyrolactone	19444-84-9	2053		MS, RI	LLE-SAFE	√	√	√	√
17	Dihydroactinidiolide	15356-74-8	2224		MS, RI, S	LLE-SAFE	√	√	√	√
18	(R)-Dihydro-actinidiolide	17092-92-1	2224		MS, RI	LLE-SAFE				√
19	5-Hydroxy-4-pentanolide	32780-06-6	2364		MS, RI	LLE-SAFE	√	√	√	√
20	DL-Mevalonolactone	674-26-0	2428		MS, RI	LLE-SAFE	√	√	√	√
21	(±)-3-Hydroxy-4-butanolide	5469-16-9	2479		MS, RI, aroma, S	LLE-SAFE	√	√	√	√
22	β-Butyrolactone	3068-88-0	2531		MS, RI	LLE-SAFE	√			
23	Costunolide	553-21-9			MS, aroma, S	LLE-SAFE		√	√	
24	γ-Decanolactone	706-14-9		2040	MS, RI, aroma, S	LLE-SAFE	√	√	√	√
					Aldehydes (19)					
1	3-Methyl-2-butenal	107-86-8	1096		MS, RI	LLE-SAFE	√	√	√	
2	Nonanal	124-19-6	1289		MS, RI, S	LLE-SAFE		√	√	
3	1,3,5,7-Tetroxane	293-30-1	1418		MS, RI	LLE-SAFE	√	√	√	√
4	Methyl glyoxal	78-98-8	1458		MS, RI	LLE-SAFE	√	√	√	√

Table A3. *Cont.*

No.	Compound Name	CAS	RI		Identification Method	Sample Preparation	Presence in Samples			
			DB-WAX	DB-FFAP			YJ	QD	HR	BW
					Aldehydes (19)					
5	Glutaraldehyde	111-30-8	1545	2353	MS, RI	LLE-SAFE, SPME		√	√	√
6	(Z)-2-Methyl-2-butenal	1115-11-3	1636		MS, RI	LLE-SAFE				√
7	Methacrolein	78-85-3	1686		MS, RI	LLE-SAFE	√	√	√	√
8	2-Ethyl-4-pentenal	5204-80-8	2038		MS, RI	LLE-SAFE	√			
9	Methoxy acetaldehyde	10312-83-1	2216		MS, RI	LLE-SAFE	√		√	√
10	cis-6-Nonenal	2277-19-2	2517		MS, RI	LLE-SAFE				√
11	Glyoxylic acid	298-12-4	2643		MS, RI	LLE-SAFE		√		
12	2,2-Dimethylocta-3,4-dienal	590-71-6	2796		MS, RI	LLE-SAFE				√
13	3-Hydroxybutyraldehyde	107-89-1	2929		MS, RI	LLE-SAFE	√	√	√	√
14	Acetaldehyde	75-07-0	890		MS, RI, S	LLE-SAFE	√	√	√	√
15	Hexanal	66-25-1	993		MS, RI	LLE-SAFE		√	√	
16	trans-2-Nonenal	18829-56-6		1414	MS, RI, S	SPME	√	√		
17	Isovaleraldehyde	590-86-3		2047	MS, RI, S	SPME	√			
18	(E,E)-2,4-Nonadienal	5910-87-2		1123	MS, RI	SPME	√			√
19	Hexadecanal	629-80-1			MS	LLE-SAFE	√		√	
					Acetals (2)					
1	2-Benzyl-1,3-dioxolane	101-49-5	2165		MS, RI	LLE-SAFE	√		√	
2	Tetraethylene glycol	112-60-7	2597	2144	MS, RI	LLE-SAFE, SPME	√	√	√	√
					Others (37)					
1	Myrcene	123-35-3	1066	1056	MS, RI, S	LLE-SAFE, SPME	√		√	√
2	Dimethyl ether	115-10-6	1110		MS, RI	LLE-SAFE			√	√
3	Acetic anhydride	108-24-7	1134		MS, RI	LLE-SAFE	√	√		√
4	1,3,5,7-Cyclooctatetraene	629-20-9	1152		MS, RI	LLE-SAFE				√
5	3,5-Dimethylhex-1-ene	7423-69-0	1659		MS, RI	LLE-SAFE			√	
6	Ethoxyacetylene	927-80-0	1676		MS, RI	LLE-SAFE		√		
7	1,5-Heptadien-3-yne	3511-27-1	1806		MS, RI	LLE-SAFE	√	√	√	
8	Isobutyl anhydride	97-72-3	2012		MS, RI	LLE-SAFE		√	√	
9	2-Methyl-2-butene	513-35-9	2039		MS, RI, S	LLE-SAFE	√	√	√	√
10	3-Methylene-nonane	51655-64-2	2039		MS, RI	LLE-SAFE	√			
11	Valeric anhydride	2082-59-9	2116		MS, RI	LLE-SAFE				√
12	2-Methylsuccinic anhydride	4100-80-5	2264		MS, RI	LLE-SAFE	√	√	√	√
13	1-Docosene	1599-67-3	2481		MS, RI	LLE-SAFE				√
14	1-Hexadecene	629-73-2	2481		MS, RI	LLE-SAFE				√
15	1,4-Dioxane	123-91-1	2713		MS, RI	LLE-SAFE		√		
16	Cyclopentene	142-29-0	889		MS, RI	LLE-SAFE				√
17	Propene	115-07-1	908		MS, RI	LLE-SAFE	√	√	√	√
18	1,3-Butadiyne	460-12-8	918		MS, RI	LLE-SAFE				√
19	1-Buten-3-yne	689-97-4	921		MS, RI	LLE-SAFE		√		
20	1-Nonyne	3452/9/3		1115	MS, RI	SPME				√
21	cis-2-Octene	7642/4/8		1292	MS, RI	SPME	√	√		√
22	Diisopropyl ether	108-20-3		2325	MS, RI	SPME	√		√	√
23	2-Pentene	109-68-2		606	MS, RI, aroma, S	LLE-SAFE		√	√	
24	3-Ethyl-3-hexene	16789-51-8		1282	MS, RI	SPME				√
25	β-Pinene	18172-67-3		1040	MS, RI, S	SPME	√	√	√	
26	2-Methyl-2-hexene	2738-19-4		1412	MS, RI	SPME				√
27	(E)-2-Hexene	4050-45-7		1175	MS, RI	SPME			√	
28	Dodecyl ether	4542-57-8			MS	LLE-SAFE	√		√	√
29	3-Methyl-1-butene	563-45-1		605	MS, RI	LLE-SAFE		√	√	√
30	1,2-Butadiene	590-19-2		613	MS, RI	LLE-SAFE				√

Table A3. *Cont.*

No.	Compound Name	CAS	RI		Identification Method	Sample Preparation	Presence in Samples			
			DB-WAX	DB-FFAP			YJ	QD	HR	BW
				Others (37)						
31	1-Heptene	592-76-7		1228	MS, RI, S	SPME	√	√	√	√
32	1-Octadecyne	629-89-0			MS	LLE-SAFE	√		√	√
33	1,1-Diethoxy-3,7-dimethylocta-2,6-diene	7492-66-2		1216	MS, RI	SPME	√	√		
34	2-Methyl-1-pentene	763-29-1		1050	MS, RI	SPME	√	√		√
35	2-Methyl-1,3-butadiene	78-79-5		605	MS, RI	LLE-SAFE	√			
36	1-Undecene	821-95-4		1349	MS, RI, S	SPME	√	√	√	√
37	Vinyl isopropyl ether	926-65-8		1044	MS, RI	SPME		√	√	

Note: √ indicates the presence of the compound in the corresponding brand.

Table A4. GC-O-MS sniffing results of volatile compounds in different brands of lager beer.

No.	Compound Name	CAS	Sniffing Description	YJ	BW	HR	QD
1	4-Vinylguaiacol	7786-61-0	Coffee bean, nut shell, sour	4	3	1.5	3
2	γ-Decalactone	706-14-9	Sweet, floral, gardenia, creamy	4	4.5	4	4
3	Phenylacetic acid	103-82-2	Floral, rose, sweet, grassy	3.5	4	2.5	2
4	Isovaleric acid	503-74-2	Sour, durian-like	3.5	3	3.5	2.5
5	2-Phenylethyl acetate	103-45-7	Sweet, floral, fruity	3	2.5	3.5	1
6	Acetic acid	64-19-7	Sour, muddy	3	2.5	4	3
7	Octanoic acid	124-07-2	Grassy, vegetal	3	2.5	2.5	2
8	Hexyl butyrate	2639-63-6	Sweet, floral, honey-like	2.5	2	2	1.5
9	6-Methyl-5-hepten-2-one	3658-77-3	Caramel, sweet	2.5	3	2.5	2
10	Phenylethanol	1960/12/8	Rose-like, sweet	2.5	3.5	3.5	2.5
11	Pineapple alcohol	505-10-2	Sour, muddy	2.5	2.5	3	3
12	2,3-Butanediol	513-85-9	Roasted, dark wheat	2	1	-	-
13	Hexanoic acid	142-62-1	Lemon-like, sour, bitter	2	2	2.5	0.5
14	Decanoic acid	334-48-5	Sour, hoppy, grassy	2	1.5	1.5	0.5
15	2-Acetylpyrrole	1072-83-9	Malty, sweet, caramel	1.5	2.5	1.5	1
16	Furoic acid	88-14-2	Rooty, wheaty	1.5	2	-	1.5
17	4-Hydroxyphenylethanol	501-94-0	Floral, sweet, fruity	1.5	2	3	1
18	Ethyl propionate	105-37-3	Floral, fruity, strawberry-like	1	2	1.5	1
19	Hexacosane	630-01-3	Floral, honey-like	1	2	0.5	-
20	Resorcinol	108-46-3	Burnt, sweet	-	2	-	-
21	trans-Oleic acid	112-79-8	Dark wheat	-	2	-	2
22	5-Methylpyrrole-2-carboxaldehyde	1192-79-6	Rooty	1.5	1.5	-	-
23	trans-3-Hexenoic acid	4219-24-3	Floral, sweet, burnt	1.5	1.5	1	-
24	Isoamyl alcohol	123-51-3	Nut shell, roasted	1	1.5	2	1
25	Furfuryl alcohol	98-00-0	Sour, putrid	1	1.5	0.5	-
26	Palmitic acid	1957/10/3	Dark wheat	1	1.5	-	-
27	(±)-3-Hydroxy-4-butyrolactone	5469-16-9	Floral, woody	1	1.5	1	1.5
28	Monoethyl succinate	1070-34-4	Malty	-	1.5	-	-
29	2,4-Di-tert-butylphenol	96-76-4	Roasted, nut shell, yeasty	1	1	1	1.5
30	Ethyl hexanoate	123-66-0	Sweet, fruity, floral	0.5	1	1.5	1.5
31	4-Hydroxy-2-butanone	590-90-9	Floral, oily, sweet	0.5	1	2	0.5
32	Methyl octanoate	111-12-6	Dusty, moldy, bitter	-	1	1	-
33	6-(Ethoxycarbonyl)nicotinic acid	17874-78-1	Smoky	-	1	-	-
34	(Z)-β-Ionone	79-77-6	Floral, sweet	-	1	-	0.5
35	Cholestane	481-21-0	Roasted, dark wheat	1	0.5	-	-
36	1,2-Propanediol	57-55-6	Nut shell	-	0.5	-	-
37	Isoamyl acetate	123-92-2	Floral	-	0.5	-	-
38	Tetratetracontane	7098-22-8	Nut shell	-	0.5	-	-

Table A4. *Cont.*

No.	Compound Name	CAS	Sniffing Description	YJ	BW	HR	QD
39	Methyl decanoate	110-42-9	Apple-like, sweet, floral	1.5	-	-	1
40	(Z)-9-Octadecenamide	301-02-0	Sweet, yeasty	1	-	-	1
41	2,6-Di-tert-butylpyridine	585-48-8	Ashy	1	-	-	-
42	5-Hydroxymethylfurfural	67-47-0	Yeasty	1	-	-	-
43	Benzoic acid	65-85-0	Ashy	1	-	-	-
44	Lauric acid	143-07-7	Fruity	1	-	-	-
45	2-Hexyl-1-decanol	2425-77-6	Floral	0.5	-	0.5	-
46	Thiophene	110-02-1	Garlic, oily	-	-	2.5	-
47	2-Hydroxypyridine	142-08-5	Hoppy, bitter	-	-	2	-
48	2-Pentene	109-68-2	Burnt, plastic-like	-	-	2	-
49	2,5-Dimethylphenol	95-87-4	Nut shell	-	-	1	-
50	Methyl furoate	611-13-2	Nut shell	-	-	0.5	-
51	N-Butylacetamide	1119-49-9	Sweet	-	-	-	1
52	Tetratriacontane	14167-59-0	Sweet	-	-	-	2
53	Costunolide	553-21-9	Floral	-	-	-	0.5

Table A5. Odor and taste activity values (OAV and TAV) of flavor compounds in different lager beer samples.

No.	Compound Name	Odor Threshold (μg/L)	OAV				Taste Threshold (μg/L)	TAV			
			YJ	QD	HR	BW		YJ	QD	HR	BW
1	Isoamyl acetate	0.13	2,046,526	1,217,009	4,338,735	2,821,490	2.63	102,326	60,850	216,937	141,074
2	Ethyl hexanoate	4.35	8113	6941	4690	10,366	4.35	8113	6941	4690	10,366
3	Ethyl propanoate	8.88	4468	2403	6090	5094	8.88	4468	2403	6090	5094
4	Hexyl butanoate	172.75	1354	718	1797	1547	—	—	—	—	—
5	Methyl decanoate	3.75	19,448	16,822	29,701	45,970	871.00	84	72	128	198
6	Ethyl octanoate	16.73	105	30	79	97	0.09	20,170	5840	15,231	18,693
7	Ethyl decanoate	4.31	249	—	320	634	17.24	62	—	80	158
8	Isoamyl butyrate	12.93	3658	—	—	—	—	—	—	—	—
9	Ethyl trans-2-decenoate	10,000.00	—	—	<1	—	—	—	—	—	—
10	Octyl acetate	0.04	99	22	—	—	182.28	22	5	—	—
11	Ethyl stearate	0.53	26	23	12	27	—	—	—	—	—
12	Ethyl isovalerate	0.10	—	31,502	—	—	0.17	—	17,326	—	—
13	Ethyl myristate	3440.00	1	<1	<1	1	—	—	—	—	—
14	Ethyl lactate	51,550.00	<1	<1	<1	<1	257,750.00	<1	<1	<1	<1
15	Ethyl acetate	50.00	11,099	8987	10,306	7351	6765.00	82	66	76	54
16	Ethyl heptanoate	1.65	350	409	254	623	147.90	4	5	3	7
17	Hexyl acetate	20.00	286	392	574	551	34.80	164	225	330	317
18	Diethyl succinate	104,700.00	<1	<1	<1	<1	1,094,115.00	<1	<1	<1	<1
19	Butyl acetate	51.04	—	—	13	14	88.00	—	—	8	8
20	Ethyl 3-hydrobutyrate	1000.00	—	—	<1	<1	—	—	—	—	—
21	Ethyl nonanoate	326.48	7	2	9	16	1039.20	2	1	3	5
22	Ethyl hydrogen succinate	1,141,000.00	<1	<1	<1	<1	1,369,200.00	<1	<1	<1	<1
23	Ethyl valerate	5.08	774	679	596	623	787.50	5	4	4	4
24	Methyl 2-octynate	23.00	—	—	721	575	—	—	—	—	—
25	(−)-Ethyl L-lactate	—	—	—	—	—	—	—	—	—	—
26	2-Hydroxyethyl acetate	—	—	—	—	—	—	—	—	—	—
27	Propyl acetate	1776.00	<1	<1	—	—	710.40	1	<1	—	—
28	2,3-Dihydroxypropyl acetate	—	—	—	—	—	1,616,040.00	<1	<1	<1	<1
29	Methyl propionate	4209.00	—	<1	—	—	53.07	—	73	—	—
30	Isopropyl formate	—	—	—	—	—	—	—	—	—	—
31	Ethyl dodecanoate	5091.70	1	—	<1	—	284.79	24	—	17	—
32	Ethyl 3-hexenoate	10,000.00	3	—	<1	<1	—	—	—	—	—
33	Ethyl butyrylacetate	—	—	—	—	—	—	—	—	—	—
34	Ethyl 3-methylvalerate	—	—	—	—	—	—	—	—	—	—
35	Ethyl undecanoate	—	—	—	—	—	859.00	56	—	3	—
36	(+)-Diethyl L-tartrate	—	—	—	—	—	—	—	—	—	—
37	2,3-Butaneiol	100,200.00	2	<1	4	5	50,100.00	5	1	8	11
38	3-Methyl-1-butanol	792.82	710	531	1045	913	202.25	2785	2082	4098	3579
39	1,2,3-Propanetriol	25,000,000.00	<1	<1	<1	<1	6,562,500.00	<1	<1	<1	<1
40	2-Methyl-1-propanol	11.00	14,796	12,246	15,732	6183	8.83	18,426	15,251	19,592	7700
41	Diisobutylcarbinol	1051.70	—	—	3	2	—	—	—	—	—
42	1-Butanol	3483.00	3	<1	<1	<1	162,000.00	<1	<1	<1	<1
43	1-Octanol	104.04	4	5	11	8	44.66	10	11	27	18
44	1-Pentanol	121.81	2030	1596	2460	2104	64,880.00	4	3	5	4
45	3-Methyl-3-buten-1-ol	466.70	<1	<1	<1	<1	—	—	—	—	—

Table A5. *Cont.*

No.	Compound Name	Odor Threshold (μg/L)	OAV				Taste Threshold (μg/L)	TAV			
			YJ	QD	HR	BW		YJ	QD	HR	BW
46	α-Terpineol	1116.00	<1	<1	<1	—	279.00	2	2	1	—
47	2-Ethyl-1-hexanol	21,227.00	—	—	—	<1	—	—	—	—	—
48	4-Methyl-1-pentanol	673.22	1	—	—	99	—	—	—	—	—
49	1,2-Propylene glycol	352,240.00	<1	<1	<1	<1	1,450,400.00	<1	<1	<1	<1
50	2-Hexyl-1-decanol	—	—	—	—	—	—	—	—	—	—
51	1-Hexanol	318.27	10	24	13	10	162.80	20	47	26	20
52	Linalool	941.34	71	6	3	—	23.49	2854	242	114	—
53	1-Decanol	642.48	—	16	16	—	19.07	—	548	536	—
54	Diethylene glycol monoethyl ether	—	—	—	—	—	47,952.00	<1	<1	<1	<1
55	(−)-Isolongifolol	—	—	—	—	—	—	—	—	—	—
56	Phytol	—	—	—	—	—	—	—	—	—	—
57	β-Eudesmol	—	—	—	—	—	—	—	—	—	—
58	Guaiol	—	—	—	—	—	—	—	—	—	—
59	2,6-Dimethyl-5,7-octadien-2-ol	—	—	—	—	—	—	—	—	—	—
60	Phenethyl alcohol	397.80	5968	3462	8289	4426	50,100.00	5	1	8	11
61	2-Phenylethyl acetate	257.58	100	16	231	72	102,000.00	23	14	32	17
62	Phenol	59,000.00	<1	<1	<1	<1	20.64	1248	205	2877	894
63	Benzeneacetaldehyde	6.80	4206	5867	990	633	5890.50	<1	<1	1	1
64	Benzyl alcohol	2660.80	<1	<1	<1	<1	9.71	2944	4107	693	443
65	Ethyl benzoate	58.06	615	—	—	—	5747.50	<1	<1	<1	<1
66	Benzaldehyde	783.93	—	—	2	—	313,500.00	<1	—	—	—
67	2,4-Di-tert-butylphenol	443.50	18	157	73	88	313.20	—	—	5	—
68	2-Methoxy-4-vinylphenol	20.69	1128	1171	1740	1290	—	—	—	—	—
69	2,6-Di-tert-butyl-4-methylphenol	1048.00	500	274	572	327	21.78	1072	1113	1653	1226
70	Benzoic acid	1080.00	102	126	133	82	—	—	—	—	—
71	p-Hydroxy phenylethanol	—	—	—	—	—	313,200.00	<1	<1	<1	<1
72	Benzeneacetic acid	12,972.00	8	6	6	7	—	—	—	—	—
73	Resorcinol	7620.00	—	—	—	<1	108.10	936	696	684	846
74	2,5-Dimethylphenol	388.40	—	—	6	—	93,980.00	—	—	—	<1
75	α-Methylstyrene	—	—	—	—	—	485.50	—	—	5	—
76	1-(2-Hydroxy-5-methylphenyl) ethanone	—	—	—	—	—	—	—	—	—	—
77	(R)-(+)-1-Phenylethanol	—	—	—	—	—	—	—	—	—	—
78	Toluene	—	—	—	—	—	—	—	—	—	—
79	Octanoic acid	2730.00	151	101	210	190	4550.00	91	60	126	114
80	Hexanoic acid	0.60	258,687	198,095	474,974	419,423	0.56	279,058	213,694	512,378	452,452
81	Acetic acid	23,078.00	<1	<1	<1	<1	74,479.00	<1	<1	<1	<1
82	3-Methylbutanoic acid	1110.00	17	27	31	23	462.50	40	64	75	54
83	Decanoic acid	8930.00	8	9	14	22	4554.30	16	18	27	42
84	Dodecanoic acid	10,000.00	9	6	15	12	529.80	172	121	277	221
85	Elaidic acid	—	—	—	—	—	—	—	—	—	—
86	DL-3-Methylvaleric acid	42.78	—	183	—	—	9.30	—	843	—	—
87	Heptanoic acid	587.52	11	—	11	9	2111.40	3	—	3	3
88	Tridecanoic acid	9582.00	<1	<1	<1	<1	—	—	—	—	—
89	2-Methylvaleric acid	—	—	—	—	—	11,868,480.00	<1	<1	<1	<1
90	Pentanoic acid	15,963.00	13	7	20	20	469.50	426	247	682	684
91	Nonanoic acid	4167.60	—	—	—	<1	1359.00	—	—	—	<1
92	Palmitic acid	8520.00	5	28	7	11	—	—	—	—	—
93	trans-3-Hexenoic acid	—	—	—	—	—	—	—	—	—	—
94	4-Methyl-2-pentenoic acid	—	—	—	—	—	—	—	—	—	—
95	Hendecanoic acid	8900.00	<1	—	<1	<1	890.00	5	—	3	2
96	Crotonic acid	—	—	—	—	—	—	—	—	—	—
97	2-Methyl-2-pentenoic acid	—	—	—	—	—	—	—	—	—	—
98	Furfuryl alcohol	5108.10	3	2	5	4	1135.00	14	9	24	18
99	2-Furancarboxylic acid	—	—	—	—	—	23,832.00	<1	<1	—	<1
100	2-Butylfuran	4.43	—	—	708	—	—	—	—	—	—
101	Furfural	3480.00	<1	1	2	2	9280.00	<1	<1	<1	<1
102	2-Acetyl furan	16,498.00	<1	<1	<1	<1	87,840.00	<1	<1	<1	<1
103	Methyl2-furoate	—	—	—	—	—	—	—	—	—	—
104	5-Hydroxymethyl-2-furaldehyde	1,243,000.00	<1	<1	<1	<1	1,243,000.00	<1	<1	<1	<1
105	2,5-Dimethyl-4-hydroxy-2H-furan-3-one	167.84	37	245	37	48	10.49	592	3926	600	772
106	2(5H)-Furanone	—	—	—	—	—	—	—	—	—	—
107	Furfuryl sulfide	—	—	—	—	—	—	—	—	—	—
108	2,2′-Difurfuryl ether	—	—	—	—	—	—	—	—	—	—
109	(±)-3-Hydroxy-4-butanolide	—	—	—	—	—	—	—	—	—	—

Table A5. *Cont.*

No.	Compound Name	Odor Threshold (μg/L)	OAV				Taste Threshold (μg/L)	TAV			
			YJ	QD	HR	BW		YJ	QD	HR	BW
110	γ-Decanolactone	2.46	1192	1474	2091	3559	379.20	8	10	14	23
111	γ-Butyrolactone	1120.00	5	6	20	22	11,200.00	<1	<1	2	2
112	4-Nonanolide	26.35	265	164	272	389	976.00	7	4	7	11
113	γ-Hexanolactone	12,525.00	<1	<1	<1	<1	13,026.00	<1	<1	<1	<1
114	γ-Octalactone	17.56	480	271	509	659	93.20	90	51	96	124
115	δ-Valerolactone	—	—	—	—	—	1,105,000.00	<1	<1	<1	<1
116	γ-Valerolactone	10,000.00	<1	<1	<1	<1	105,000.00	<1	<1	<1	<1
117	Costunolide	—	—	—	—	—	—	—	—	—	—
118	5-Hydroxy-4-pentanolide	—	—	—	—	—	—	—	—	—	—
119	2-Hydroxypyridine	—	—	—	—	—	—	—	—	—	—
120	(Z)-9-Octadecenamide	—	—	—	—	—	—	—	—	—	—
121	2-Acetyl pyrrole	—	—	—	—	—	111,430.00	<1	<1	<1	<1
122	N-Butyl-acetamide	—	—	—	—	—	—	—	—	—	—
123	2,6-Di-tert-butylpyridine	—	—	—	—	—	—	—	—	—	—
124	5-Methyl-1H-pyrrole-2-carbaldehyde	—	—	—	—	—	—	—	—	—	—
125	6-(Ethoxycarbonyl) nicotinic acid	—	—	—	—	—	—	—	—	—	—
126	Benzylamine	2,943,000.00	<1	—	—	<1	209,934.00	<1	<1	<1	<1
127	Diethylamine	14,989.00	<1	—	—	<1	7070.00	<1	<1	<1	<1
128	3-Methylthio propanol	71.07	349	345	563	383	2060.00	12	12	19	13
129	Thiophene	88,284.00	1	1	1	1	8.41	12,028	15,518	13,595	15,080
130	Methyl mercaptan	0.17	6794	1432	6750	9059	1.73	679	143	675	906
131	Dimethyl Sulfoxide	—	—	—	—	—	—	—	—	—	—
132	Dimethyl sulfone	—	—	—	—	—	—	—	—	—	—
133	Thioacetic acid	100.00	183	—	—	105	—	—	—	—	—
134	Tetrahydrothio phene	—	—	—	—	—	—	—	—	—	—
135	2-Acetyl-2-thiazoline	—	—	—	—	—	1.17	—	70,957	—	—
136	4-Methyl-5-acetyl thiazole	—	—	—	—	—	—	—	—	—	—
137	(E)-2-Nonenal	0.16	149,938	41,011	—	—	0.21	113,953	31,168	—	—
138	Isovaleraldehyde	0.95	8845	—	—	—	36.39	231	—	—	—
139	Acetaldehyde	49.46	53	33	17	15	7850.00	<1	<1	<1	<1
140	Hexadecanal	—	—	—	—	—	—	—	—	—	—
141	4-Hydroxy-2-butanone	—	—	—	—	—	—	—	—	—	—
142	(Z)-β-Ionone	0.01	—	14,243,050	—	12,784,795	—	—	—	—	—
143	3-Hydroxy-2-butanone	14.18	5325	4822	2838	5525	17,221.00	4	4	2	5
144	Cholestane	—	—	—	—	—	—	—	—	—	—
145	1-Heptene	1045.50	478	441	578	489	—	—	—	—	—
146	1-Undecene	—	—	—	—	—	—	—	—	—	—
147	2-Methyl-2-butene	—	—	—	—	—	—	—	—	—	—
148	Myrcene	3.88	1083	—	962	—	13.13	320	—	284	—
149	Diisopropyl ether	—	—	—	—	—	—	—	—	—	—
150	3-Methyl-1-butene	—	—	—	—	—	—	—	—	—	—

References

1. Kaczyński, P.; Iwaniuk, P.; Hrynko, I.; Łuniewski, S.; Łozowicka, B. The effect of the multi-stage process of wheat beer brewing on the behavior of pesticides according to their physicochemical properties. *Food Control* **2024**, *160*, 110356. [CrossRef]
2. Biazon, C.L.; Brambilla, R.; Rigacci, A.; Pizzolato, T.M.; dos Santos, J.H.Z. Combining silica-based adsorbents and SPME fibers in the extraction of the volatiles of beer: An exploratory study. *Anal. Bioanal. Chem.* **2009**, *394*, 549–556. [CrossRef] [PubMed]
3. Stewart, G.G. The Production of Secondary Metabolites with Flavour Potential during Brewing and Distilling Wort Fermentations. *Fermentation* **2017**, *3*, 63. [CrossRef]
4. Holt, S.; Mukherjee, V.; Lievens, B.; Verstrepen, K.J.; Thevelein, J.M. Bioflavoring by non-conventional yeasts in sequential beer fermentations. *Food Microbiol.* **2018**, *72*, 55–66. [CrossRef]
5. Stefanuto, P.-H.; Perrault, K.A.; Dubois, L.M.; L'Homme, B.; Allen, C.; Loughnane, C.; Ochiai, N.; Focant, J.-F. Advanced method optimization for volatile aroma profiling of beer using two-dimensional gas chromatography time-of-flight mass spectrometry. *J. Chromatogr. A* **2017**, *1507*, 45–52. [CrossRef]
6. Toh, D.W.K.; Chua, J.Y.; Liu, S.Q. Impact of simultaneous fermentation with Saccharomyces cerevisiae and Torulaspora delbrueckii on volatile and non-volatile constituents in beer. *LWT* **2018**, *91*, 26–33. [CrossRef]
7. Lodolo, E.J.; Kock, J.L.F.; Axcell, B.C.; Brooks, M. The yeast Saccharomyces cerevisiae– the main character in beer brewing. *FEMS Yeast Res.* **2008**, *8*, 1018–1036. [CrossRef]

8. Lehnhardt, F.; Becker, T.; Gastl, M. Flavor stability assessment of lager beer: What we can learn by comparing established methods. *Eur. Food Res. Technol.* **2020**, *246*, 1105–1118. [CrossRef]
9. Richter, T.M.; Eyres, G.T.; Silcock, P.; Bremer, P.J. Comparison of four extraction methods for analysis of volatile hop-derived aroma compounds in beer. *J. Sep. Sci.* **2017**, *40*, 4366–4376. [CrossRef] [PubMed]
10. Andres-Iglesias, C.; Montero, O.; Sancho, D.; Blanco, C.A. New trends in beer flavour compound analysis. *J. Sci. Food Agric.* **2015**, *95*, 1571–1576. [CrossRef]
11. Vieira, A.C.; Pereira, A.C.; Marques, J.C.; Reis, M.S. Multi-target optimization of solid phase microextraction to analyse key flavour compounds in wort and beer. *Food Chem.* **2020**, *317*, 126466. [CrossRef]
12. Bettenhausen, H.M.; Benson, A.; Fisk, S.; Herb, D.; Hernandez, J.; Lim, J.; Queisser, S.H.; Shellhammer, T.H.; Vega, V.; Yao, L.; et al. Variation in Sensory Attributes and Volatile Compounds in Beers Brewed from Genetically Distinct Malts: An Integrated Sensory and Non-Targeted Metabolomics Approach. *J. Am. Soc. Brew. Chem.* **2020**, *78*, 136–152. [CrossRef]
13. Bertrand, E.; Meyer, X.-M.; Machado-Maturana, E.; Berdague, J.-L.; Kondjoyan, A. Modelling the Maillard reaction during the cooking of a model cheese. *Food Chem.* **2015**, *184*, 229–237. [CrossRef]
14. Nan, F.; Li, X.; Feng, J.; Lv, J.; Liu, Q.; Liu, X.; Liu, Y.; Zhang, R.; Bai, B.; Xie, S. Production, characterization and antioxidant analysis on the Undaria-based alcoholic beverages using response surface method and HS-SPME-GC × GC-TOF-MS. *Food Chem. X* **2025**, *27*, 102428. [CrossRef]
15. Yu, M.; Yang, P.; Song, H.; Guan, X. Research progress in comprehensive two-dimensional gas chromatography-mass spectrometry and its combination with olfactometry systems in the flavor analysis field. *J. Food Compos. Anal.* **2022**, *114*, 104790. [CrossRef]
16. Grosch, W. Evaluation of the key odorants of foods by dilution experiments, aroma models and omission. *Chem. Senses* **2001**, *26*, 533–545. [CrossRef]
17. Plutowska, B.; Wardencki, W. Application of gas chromatography-olfactometry (GC-O) in analysis and quality assessment of alcoholic beverages—A review. *Food Chem.* **2008**, *107*, 449–463. [CrossRef]
18. Reglitz, K.; Fechir, M.; Mall, V.; Voigt, J.; Steinhaus, M. The impact of caramel and roasted wheat malts on aroma compounds in top-fermented wheat beer. *J. Inst. Brew.* **2022**, *128*, 138–149. [CrossRef]
19. Zhang, Y.; Li, S.; Meng, Q.; Song, H.; Wang, X. Characterization of Key Odor-Active Compounds in Draft Beers for the Chinese Market Using Molecular Sensory Science Approaches. *Molecules* **2024**, *29*, 2537. [CrossRef]
20. Fechir, M.; Reglitz, K.; Mall, V.; Voigt, J.; Steinhaus, M. Molecular Insights into the Contribution of Specialty Barley Malts to the Aroma of Bottom-Fermented Lager Beers. *J. Agric. Food Chem.* **2021**, *69*, 8190–8199. [CrossRef] [PubMed]
21. Yang, Q.; Liang, N.; Chen, S.; Chen, J.; Chen, M.; Tu, J.; Xiang, Z. Unravelling the key flavor components of beer based on a new online recombination olfactometry of mixed targeted compounds. *Food Chem.* **2025**, *479*, 143702. [CrossRef]
22. Chen, Y.; Huang, H.; Yin, R.; Wang, S.; Hong, J.; Wu, Y.; Guo, L.; Song, Y.; Zhao, D.; Sun, J.; et al. Exploration of key flavor quality factors in beer and its distilled spirits based on flavor metabolomics. *Lwt-Food Sci. Technol.* **2025**, *224*, 117832. [CrossRef]
23. D'Auria, M.; Racioppi, R. Volatiles organic compounds in craft beers produced in Basilicata (Southern Italy). *Nat. Product. Res.* **2024**. [CrossRef] [PubMed]
24. Kelly, T.J.; Mannion, D.T.; Oconnor, C.; Kilcawley, K.N. Comparison of head space solid phase micro extraction with conventional and comprehensive gas chromatography mass spectrometry for volatile profiling of Irish whiskey. *Talanta Open* **2024**, *10*, 100346. [CrossRef]
25. Hong, J.; Huang, H.; Zhao, D.; Sun, J.; Huang, M.; Sun, X.; Sun, B. Investigation on the key factors associated with flavor quality in northern strong aroma type of Baijiu by flavor matrix. *Food Chem.* **2023**, *426*, 136576. [CrossRef]
26. Fang, X.; Chen, Y.; Gao, J.; Run, Z.; Chen, H.; Shi, R.; Li, Y.; Zhang, H.; Liu, Y. Application of GC–TOF/MS and GC×GC–TOF/MS to Discriminate Coffee Products in Three States (Bean, Powder, and Brew). *Foods* **2023**, *12*, 3123. [CrossRef] [PubMed]
27. Liu, H.; Sun, B. Effect of Fermentation Processing on the Flavor of Baijiu. *J. Agric. Food Chem.* **2018**, *66*, 5425–5432. [CrossRef]
28. Van Gemert, L. Flavour thresholds. In *Compilations of Flavour Threshold Values in Water and Other Media*, 2nd ed.; Oliemans Punter & Partner: Utrecht, The Netherlands, 2011.
29. Van Gemert, L. Odour thresholds. In *Compilations of Odour Threshold Values in Air, Water and Other Media*; Oliemans, Punter & Partners BV: Zeist, The Netherlands, 2011.
30. Nuzzi, M.; Lo Scalzo, R.; Testoni, A.; Rizzolo, A. Evaluation of Fruit Aroma Quality: Comparison Between Gas Chromatography–Olfactometry (GC–O) and Odour Activity Value (OAV) Aroma Patterns of Strawberries. *Food Anal. Methods* **2008**, *1*, 270–282. [CrossRef]
31. Shang, L.; Liu, C.; Tang, F.; Chen, B.; Liu, L.; Hayashi, K. Machine-Learning-Based Olfactometry: An Auxiliary System for Human Assessors in Olfactory Measurement. *bioRxiv* **2022**. [CrossRef]
32. Chen, Y.; Xie, J.; Yuan, X.; Zhang, C.; Hong, J.; Zhao, Z.; Zhao, D.; Sun, B.; Wang, S.; Sun, J.; et al. Flavoromics-based profiling of flavor compound dynamics across the strong-flavor Baijiu production chain. *J. Food Compos. Anal.* **2025**, *148*, 108132. [CrossRef]

33. Wu, Y.; Chen, H.; Sun, Y.; Huang, H.; Chen, Y.; Hong, J.; Liu, X.; Wei, H.; Tian, W.; Zhao, D.; et al. Integration of Chemometrics and Sensory Metabolomics to Validate Quality Factors of Aged Baijiu (Nianfen Baijiu) with Emphasis on Long-Chain Fatty Acid Ethyl Esters. *Foods* **2023**, *12*, 3087. [CrossRef]
34. Jespersen, L.; Jakobsen, M. Specific spoilage organisms in breweries and laboratory media for their detection. *Int. J. Food Microbiol.* **1996**, *33*, 139–155. [CrossRef]
35. Vanderhaegen, B.; Neven, H.; Coghe, S.; Verstrepen, K.J.; Verachtert, H.; Derdelinckx, G. Evolution of chemical and sensory properties during aging of top-fermented beer. *J. Agric. Food Chem.* **2003**, *51*, 6782–6790. [CrossRef]
36. Blankenship, M.; Grigorova, M.; Katz, D.; Maier, J. Retronasal Odor Perception Requires Taste Cortex, but Orthonasal Does Not. *Curr. Biol.* **2019**, *29*, 62–69. [CrossRef] [PubMed]
37. Ai, Y.; Han, P. Neurocognitive mechanisms of odor-induced taste enhancement: A systematic review. *Int. J. Gastron. Food Sci.* **2022**, *28*, 100535. [CrossRef]
38. Clapperton, J.F. FATTY ACIDS CONTRIBUTING TO CAPRYLIC FLAVOUR IN BEER. THE USE OF PROFILE AND THRESHOLD DATA IN FLAVOUR RESEARCH. *J. Inst. Brew.* **1978**, *84*, 107–112. [CrossRef]
39. Saison, D.; De Schutter, D.P.; Uyttenhove, B.; Delvaux, F.; Delvaux, F.R. Contribution of staling compounds to the aged flavour of lager beer by studying their flavour thresholds. *Food Chem.* **2009**, *114*, 1206–1215. [CrossRef]
40. Gamero, A.; Ferreira, V.; Pretorius, I.S.; Querol, A. Wine, Beer and Cider: Unravelling the Aroma Profile. In *Molecular Mechanisms in Yeast Carbon Metabolism*; Piškur, J., Compagno, C., Eds.; Springer: Berlin/Heidelberg, Germany, 2014; pp. 261–297.
41. Shao, D.; Cheng, W.; Jiang, C.; Pan, T.; Li, N.; Li, M.; Li, R.; Lan, W.; Du, X. Machine-Learning-Assisted Aroma Profile Prediction in Five Different Quality Grades of Nongxiangxing Baijiu Fermented During Summer Using Sensory Evaluation Combined with GC×GC–TOF-MS. *Foods* **2025**, *14*, 1714. [CrossRef]
42. Akarachantachote, N.; Chadcham, S.; Saithanu, K. CUTOFF THRESHOLD OF VARIABLE IMPORTANCE IN PROJECTION FOR VARIABLE SELECTION. *Int. J. Pure Appl. Math.* **2014**, *94*, 307–322. [CrossRef]
43. Dong, L.; Hou, Y.; Li, F.; Piao, Y.; Zhang, X.; Zhang, X.; Li, C.; Zhao, C. Characterization of volatile aroma compounds in different brewing barley cultivars. *J. Sci. Food Agric.* **2015**, *95*, 915–921. [CrossRef]
44. Takoi, K.; Itoga, Y.; Koie, K.; Kosugi, T.; Shimase, M.; Katayama, Y.; Nakayama, Y.; Watari, J. The Contribution of Geraniol Metabolism to the Citrus Flavour of Beer: Synergy of Geraniol and β-Citronellol Under Coexistence with Excess Linalool. *J. Inst. Brew.* **2010**, *116*, 251–260. [CrossRef]
45. Liu, Y.; Qian, X.; Xing, J.; Li, N.; Li, J.; Su, Q.; Chen, Y.; Zhang, B.; Zhu, B. Accurate Determination of 12 Lactones and 11 Volatile Phenols in Nongrape Wines through Headspace-Solid-Phase Microextraction (HS-SPME) Combined with High-Resolution Gas Chromatography-Orbitrap Mass Spectrometry (GC-Orbitrap-MS). *J. Agric. Food Chem.* **2022**, *70*, 1971–1983. [CrossRef]
46. Wanikawa, A.; Hosoi, K.; Kato, T. Conversion of Unsaturated Fatty Acids to Precursors of γ-Lactones by Lactic Acid Bacteria during the Production of Malt Whisky. *J. Am. Soc. Brew. Chem.* **2000**, *58*, 51–56. [CrossRef]
47. Techakriengkrai, I.; Paterson, A.; Piggott, J. Relationships of Sweetness in Lager to Selected Volatile Congeners. *J. Inst. Brew.* **2004**, *110*, 360–366. [CrossRef]
48. Schieberle, P. Primary odorants of pale lager beer. *Z. Lebensm.-Unters. Forsch.* **1991**, *193*, 558–565. [CrossRef]
49. Gonzalez Viejo, C.; Fuentes, S.; Torrico, D.D.; Godbole, A.; Dunshea, F.R. Chemical characterization of aromas in beer and their effect on consumers liking. *Food Chem.* **2019**, *293*, 479–485. [CrossRef] [PubMed]
50. Meier-Dörnberg, T.; Hutzler, M.; Michel, M.; Methner, F.-J.; Jacob, F. The Importance of a Comparative Characterization of Saccharomyces Cerevisiae and Saccharomyces Pastorianus Strains for Brewing. *Fermentation* **2017**, *3*, 41. [CrossRef]

Disclaimer/Publisher's Note: The statements, opinions and data contained in all publications are solely those of the individual author(s) and contributor(s) and not of MDPI and/or the editor(s). MDPI and/or the editor(s) disclaim responsibility for any injury to people or property resulting from any ideas, methods, instructions or products referred to in the content.

foods

MDPI

Review

Ecological Risks in Daqu Storage and Their Impact on Baijiu Flavor: Precision Process Strategies for Damage Mitigation While Preserving Aroma

Dandan Song [1,2], Chunlin Zhang [1,2], Yashuai Wu [3] and Liang Yang [1,2,*]

[1] School of Brewing Engineering, Moutai Institute, Renhuai 564501, China; songdd0330@163.com (D.S.); zcl818075@163.com (C.Z.)
[2] Guizhou Key Laboratory of Microbial Resources Exploration in Fermentation Industry, Kweichow Moutai Group, Zunyi 564501, China
[3] School of Food Science and Engineering, South China University of Technology, Guangzhou 510640, China; wyss995418706@163.com
* Correspondence: moutaiyl0725@163.com

Abstract

Daqu functions as a core saccharifying and fermenting starter in Baijiu production and acts as a complex microecological reactor in open solid-state fermentation. The formation of Baijiu flavor is closely associated with microbial community assembly, enzymatic activities, and metabolic interactions occurring within Daqu. However, the open production environment also exposes the Daqu system to multiple external disturbances that may influence its microecological stability and fermentation performance. This review summarizes recent advances in understanding the microecology of Daqu, focusing on microbial succession, metabolic pathways related to flavor formation, and environmental factors affecting Daqu quality. Particular attention is given to how external disturbances during production and storage may influence microbial communities, enzymatic functions, and aroma compound formation. Based on current knowledge, a conceptual framework linking environmental factors, microbial community dynamics, metabolic activity, and flavor outcomes is proposed. In addition, strategies for maintaining microecological stability and ensuring flavor consistency are discussed, including environmental management, process optimization, physical control technologies, and integrated quality monitoring systems. Emphasis is placed on combining process control with modern analytical approaches such as multi-omics technologies and process analytical technologies (PAT) to improve traceability and precision management during Daqu production. Overall, this review provides a systematic perspective on the relationships among Daqu microecology, process conditions, and flavor formation and highlights future research directions for achieving stable and controllable Baijiu fermentation systems.

Keywords: Daqu microecology; Baijiu fermentation; flavor formation; microbial community; process control

1. Introduction

Baijiu was one of the six major distilled spirits worldwide and was distinguished by a traditional process in which solid raw materials underwent simultaneous saccharification and fermentation [1–4]. In this process, Daqu served as the core saccharifying and fermenting agent, and its quality directly determined brewing success and the flavor profile. Daqu

production relied on open natural fermentation. Long domestication enriched a relatively stable and complex microbiota that provided diverse enzyme systems and flavor precursors and laid the foundation for Baijiu fermentation [5,6]. Studies showed that bacteria, fungi (including molds and yeasts), and actinomycetes commonly coexisted in Daqu and together formed a dynamically balanced microecosystem. This unique microbial ecology endowed Baijiu with complex and diverse flavors and a distinctive aroma spectrum [7,8]. The openness that created flavor diversity also made stability susceptible to external influences. Invasion by exogenous microbes or insects could disrupt the balance. During production and storage, undesirable microbes unavoidably mixed into the system and caused fluctuations in Daqu quality, reduced alcohol yield, and increased costs [9–11].

In recent years, particular attention has been drawn to Daqu-associated pests. During cultivation and storage, Daqu was prone to infestation by various stored product insects, among which *Tribolium castaneum* and the coffee bean weevil were dominant grain pests [12]. These pests multiplied within Daqu and consumed and bored through bricks, which led to the loss of active components. Their activity also altered internal distributions of moisture and nutrients and affected physicochemical properties and enzyme activities. Reports indicated that severe infestation caused marked declines in saccharifying and fermentative power, with quality losses up to 20% to 30%, and serious deterioration of aroma [9]. More concealed interactions likely existed between pests and the Daqu microbiota [9,13,14]. On one hand, pests carried or enriched certain microbes from the environment, and their feeding could alter community structure. On the other hand, symbionts in the insect gut overlapped with fungi in Daqu and suggested a vector role during feeding that influenced microbial distribution within bricks. These findings prompted a reassessment of the ecological role of pests and highlighted a special challenge in maintaining microecological stability and flavor.

To ensure flavor consistency and process controllability, both the complexity and stability of the Daqu microecosystem required attention [15–18]. The internal interactions of the microbiota and their impact on flavor synthesis needed to be resolved with modern microbiome approaches [19,20]. External disturbance by pests also needs effective process control [21]. In traditional practice, functional strains or consortia had been added to adjust the community and enhance enzyme activity and aroma formation. Because of intrinsic complexity, such reinforcement sometimes failed to meet expectations and could cause flavor imbalance or quality decline [22]. Pest management faced a similar dilemma. Heavy reliance on chemical insecticides could damage beneficial microbes and raise residue concerns, while a lack of control allowed pests to impair flavor [23,24]. How to balance microecology, flavor, and process control and achieve precise pest control while maintaining normal fermentation and aroma formation has become an urgent challenge for the industry.

Encouraging progress had been reported. Low-dose electron beam irradiation was explored to disinfect Daqu while essentially preserving the microbiota [12]. At suitable doses, treated Daqu recovered its microecology to untreated levels after months of storage, and key indices such as saccharifying power, liquefying power, and acidity met brewing requirements [25–27]. This suggested a path to control pests without constraining aroma by removing insects with precise measures while protecting aroma formation. Researchers also proposed RNA interference to target pest symbionts for green control [9,28,29]. These directions reflected the integration of ecological mechanisms and process practice. They clarified how infestation affected ecology and offered strategies that maintained disinfestation efficacy and protected flavor.

In summary, Daqu played an irreplaceable role in Baijiu brewing. The impacts of pests on flavor and Daqu quality and the resulting fluctuations and instability urged closer examination of the interaction among microecology, flavor, and control. With advances in

ecological fermentation and community regulation, strengthening research on the Daqu microbiome and developing precise pest control technologies were expected to stabilize flavor and optimize traditional practice. This review aims to summarize recent progress on Daqu microecology, flavor formation, and pest control and to explore the path from ecological mechanisms to process implementation that controls pests without constraining aroma, providing new ideas for quality control in Baijiu brewing.

To improve the transparency and reproducibility of this review, the relevant literature was retrieved primarily from the Web of Science database. The search covered publications indexed from the inception of the database to 28 February 2026. A keyword-based search strategy was adopted, and the search terms were developed on the basis of the title, abstract, and keywords of the present review, including Daqu, Baijiu fermentation, Daqu microecology, flavor formation, microbial community, process control, ecological risks, environmental disturbances, Daqu storage, aroma preservation, damage mitigation, and solid-state fermentation. The retrieved studies were then screened according to their relevance to Daqu microecology, flavor formation, environmental disturbance, storage risk, and process control during Daqu production and storage.

2. Daqu Production Processes and the Microenvironments That Enabled Colonization by Daqu-Associated Pests

2.1. Definition, Classification, and Core Functions of Daqu

Daqu was a solid saccharifying and fermenting agent made mainly from wheat or from wheat with barley or peas. It was obtained through open natural fermentation, and it provided enzymes, starter, and aroma [30,31]. In essence, it was a porous, brick-like microhabitat in which self-heating occurred in the qu room. Microbial metabolism generated biothermal energy and moisture gradients. These forces selected functional consortia with distinct tolerance and metabolic traits. The consortia supplied diverse enzyme systems and flavor precursors for saccharification, seed mash establishment, and main fermentation. Prior studies treated Daqu as a shared ecological reactor in solid-state fermentation. Coupled biothermal flux and humidity with oxygen loss were shown to drive community assembly. This explained the marked differences in communities and metabolic trajectories among sites and seasons [32,33].

Based on the peak temperature reached during making, Daqu was grouped into three types. High-temperature Daqu reached about sixty to seventy degrees Celsius. Medium-temperature Daqu reached about fifty to sixty degrees Celsius. Low-temperature Daqu reached about forty to fifty degrees Celsius [30]. Each range favored different dominant groups and enzyme profiles and thus shaped flavor styles. High-temperature Daqu tended to enrich thermotolerant bacilli and actinomycetes and supported precursors for roasted and sauce-like notes. Medium-temperature Daqu balanced saccharification and ester formation. Low-temperature Daqu retained more yeasts and *Aspergillus* for saccharification and aroma and was linked to softer profiles. Evidence for the temperature ranges and the linkage between flavor and function had recurred across comparative studies and had been verified on multiple Daqu types [34–36].

The high-temperature stage reshaped not only enzyme patterns but also networks of flavor precursors. In sauce-aroma production, high-temperature Daqu often reached about seventy degrees Celsius. The heat reduced the expression of some saccharification enzymes yet raised pathways for the degradation of aromatic compounds and for building roasted precursors. This suggested a tradeoff in which saccharification was reduced while precursors were promoted. Such thresholds explained divergent aroma backbones during later stacked fermentation under different temperature regimes [37]. Daqu was not only a collection of functional microbes. It was also a microecological mosaic molded by the open

environment and grain substrates. The process drew exogenous microbes from air, tools, and raw materials. Temperature and humidity curves and ventilation strategies in the qu room created spatial heterogeneity across positions. A combined passive domestication and active selection produced a mature community and metabolic fingerprint distinct from the initial state [26,38]. This natural selection effect was observable at metagenomic and metabolic phenotypes and was tightly linked to internal and surface gradients [26,38–40].

From the process perspective, four core functions were evident [41,42]. First, enzyme supply. Complex enzyme systems such as amylases, proteases, lipases, and polysaccharide-degrading enzymes provided fermentable substrates and flavor precursors. Second, starter supply. Relay communities of bacteria, yeasts, and filamentous fungi seeded stacked and pit fermentations [43,44]. Third, aroma formation. Heat stress and redox fluctuations in the bricks promoted pyrazines, carbonyls, and many ester precursors. Fourth, regulation. Physical and chemical indices and microbial quality of Daqu shaped community structure during main fermentation and the flavor of the final product. Fluctuations in Daqu quality translated into differences in yield and aroma spectra [45,46].

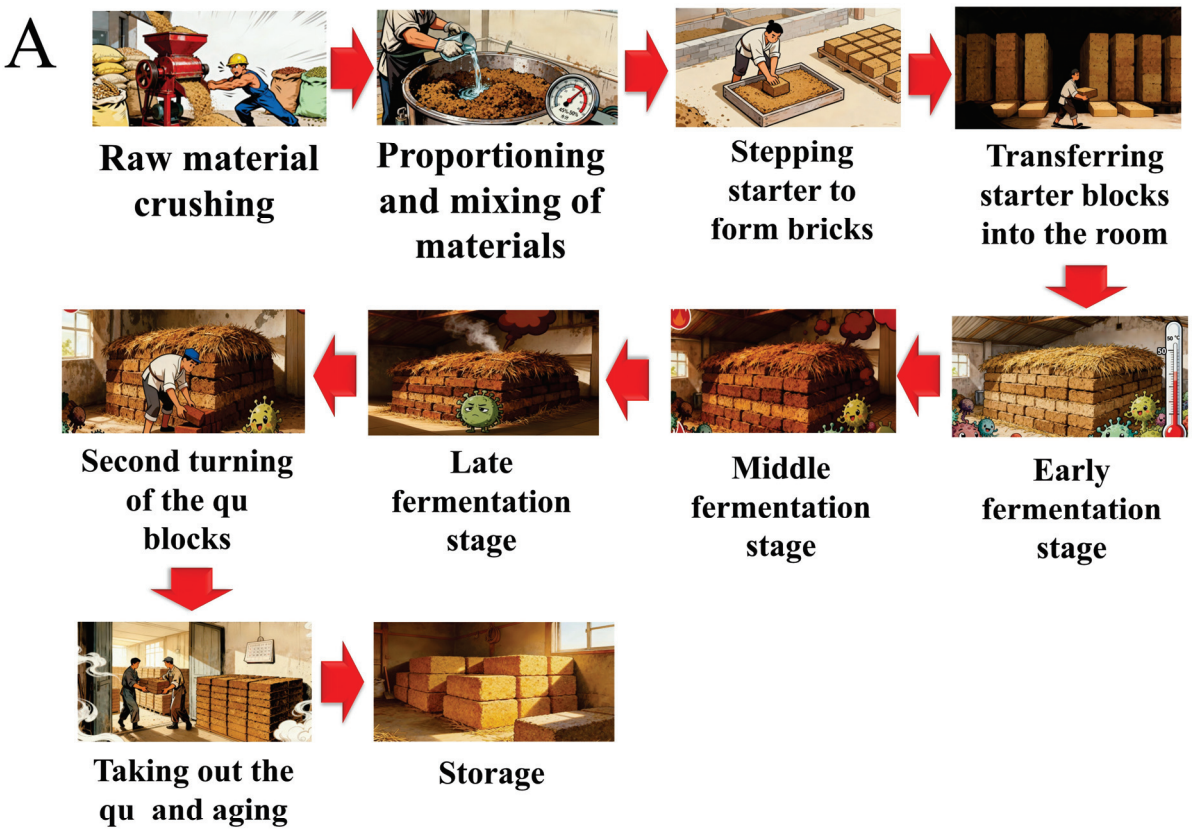
These traits meant that Daqu carried a compound microenvironment of heat, moisture, matrix, and surfaces. This could overlap with the ecological niches of Daqu-associated pests. The insects fed on grain fines and fungal biofilms and preferred high humidity and habitable pores. Production, maturation, and storage offered a continuous environmental gradient. After a phase of lethal heat, cooling created suitable periods. These windows permitted occasional or seasonal colonization.

2.2. Process Flows of Different Daqu Types and Their Microenvironmental Features

A typical flow included raw material selection and milling, moistening and mixing, brick forming and pressing, room entry with stacked fermentation under controlled temperature and humidity, turning with slow cooling, discharge with air-drying, and maturation storage [45,47]. The timeline often spanned several weeks to more than one month. During stacking, the bricks self-heated to a peak plateau. Cooling and ripening then followed. Sites and aroma styles differed in ratios, moisture, stacking modes, and ventilation regimes. Yet the shared physical chain of self-heating, water migration, oxygen diffusion, and surface renewal was consistent. Practice and research showed that this chain governed community succession and built superposed temperature and humidity gradients in both the room and the bricks [6,7,48].

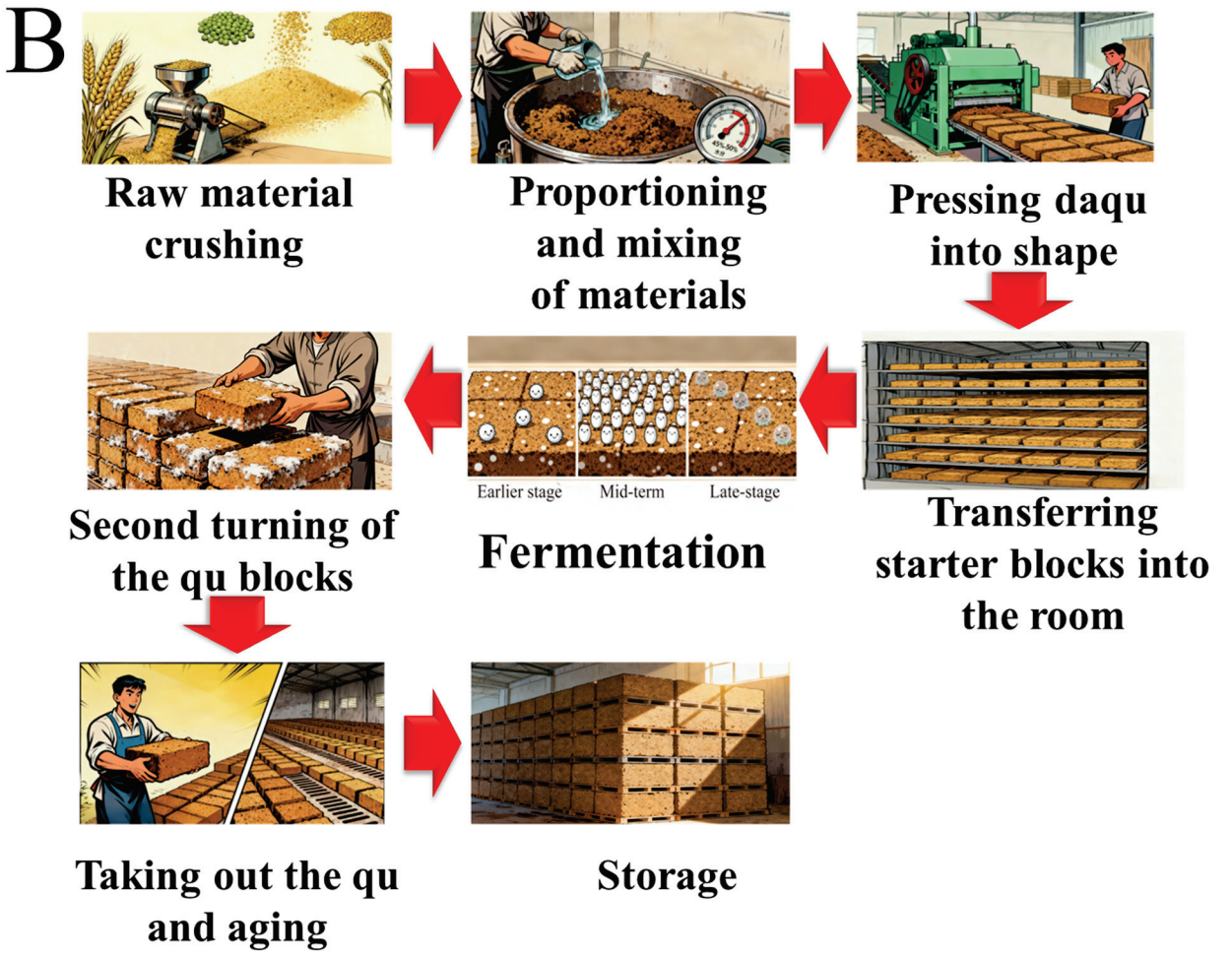
According to Figure 1A and Supplementary Table S1, high-temperature Daqu showed the strongest heat pulse. Continuous monitoring showed that about one week after room entry, the peak reached not less than sixty degrees Celsius and could persist for several days to more than a week. Internal relative humidity stayed high, and oxygen diffusion was restricted. The surface dried and exchanged gases by convection. The depth gradient allowed thermotolerant actinomycetes, *Bacillus*, and thermotolerant fungi to occupy different strata. Marked differences in communities and functional roles arose between the core and the surface. As the temperature fell, water redistributed and moved outward. Surface microbes regained an advantage. Mature Daqu thus displayed spatial heterogeneity [49–51].

https://doi.org/10.3390/foods15071195



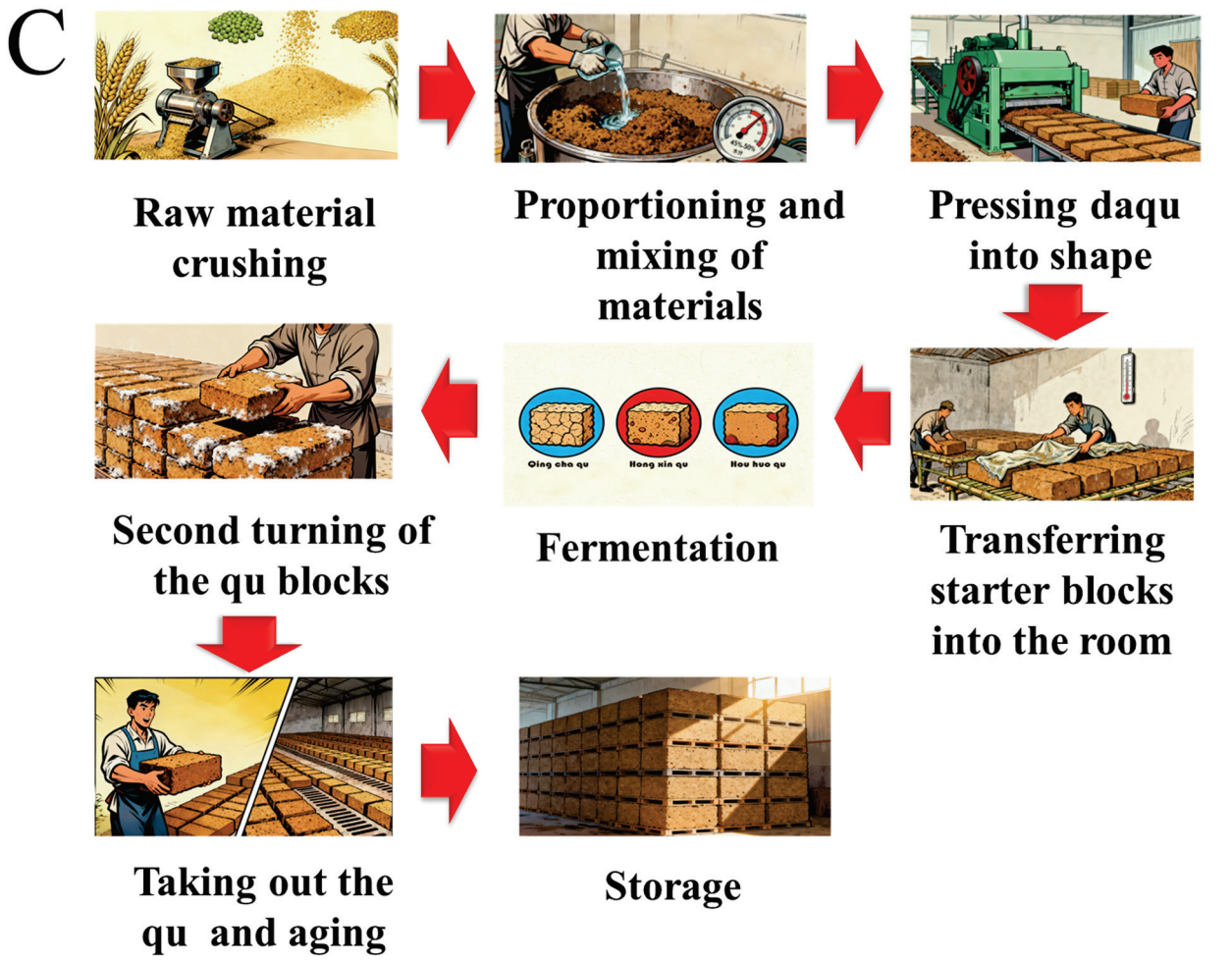
1. **High-temperature stress (>60°C) serves as the core selection pressure;**
2. **The daqu-making room features an open structure with high environmental openness;**
3. **The intensity of volatile signals is strong.**
4. **A large number of pyrazines and furans are generated through Maillard reaction and other processes.**
5. **An insect community dominated by heat-tolerant and aroma-philic species (e.g., *Araecerus fasciculatus*, *Cryptolestes turcicus*) is screened out, with a specialized community structure.**

Figure 1. *Cont.*



1. Medium environmental openness;
2. Medium intensity of volatile signals;
3. Potential highest species diversity;
4. A mixed insect community consisting of widespread species and moderately thermophilic species.

Figure 1. *Cont.*



1. The qu-making room is relatively closed with low environmental openness;
2. Weak intensity of volatile signals;
3. Few insect species;
4. Dominated by conventional stored-grain pests with limited activity.

Figure 1. Production process flowchart of Daqu. (**A**) High-temperature Daqu; (**B**) medium-temperature Daqu; (**C**) low-temperature Daqu.

Medium-temperature Daqu had milder temperature and humidity trajectories yet showed higher sensitivity to environmental management. Room temperature and relative humidity altered the heating rate and drying speed of the bricks and thereby shifted

https://doi.org/10.3390/foods15071195

community composition and interaction networks. Room humidity strongly drove the succession of *Aspergillus*, *Wickerhamomyces*, and several filamentous fungi. Room temperature correlated more directly with the rise and fall of yeasts (Figure 1B, Supplementary Table S1). This indicated that coupling between process and microecology could be tuned by finer ventilation and turning schedules to balance saccharification, fermentation, and ester potential [20,52,53].

Low-temperature Daqu typically peaked at about forty-five to fifty degrees Celsius. Communities retained more *Aspergillus*, mildly thermotolerant fungi, and yeasts, and were often associated with gentle and clean aromas (Figure 1C, Supplementary Table S1). Because heat stress was weaker, enzyme fidelity and diversity in aromatic metabolism reflected a mild balance. Such microenvironments suited production aimed at elegant styles [7,54].

Within the same temperature class, molding and stacking altered porosity and channels for heat and moisture transfer. Mature bricks thus formed micro-landforms at different depths. The result appeared as spatial differences in aroma-active compounds and dominant taxa. Recent multi-batch comparisons showed that coupling among structure, microbes, and flavor explained differences in aroma among workshops in the same plant and among stacks in the same batch. This suggested that structural variables were manageable ecological variables [55–57].

Turning was a key traditional operation and acted as a microenvironment rebalancing step. It broke local overheating and anoxia, rebuilt convection paths and vapor escape, and brought surface-to-core coupling of temperature, humidity, and oxygen back into a controllable zone. In medium-temperature production, small changes in the timing and frequency of turning altered community assembly and metabolic phenotypes in the following days. Mechanistic interpretation had shifted from experience, such as preventing caking, to process optimization based on community dynamics and heat transfer models [58].

Slow air-drying after discharge and maturation were further micro-environment shaping stages that had been undervalued. As free water continued to decline and highly volatile components were removed, aroma stabilized. Off-odors were smoothed. The bricks still underwent slow metabolism and chemical reactions under microaerobic conditions. A more stable base of enzymes and aroma was thus built. This later ripening, together with the earlier heat shock, formed a two-stage setting of Daqu quality over time [6,30].

Viewed through the niche of pests, several windows for colonization were evident [10,59]. The early high-humidity phase after room entry and stacking offered free water and broken particles that supported insect feeding on biofilms and grain fines. The subsequent heat platform imposed lethal stress, especially at the core. During the cooling and drying transition, surfaces and crevices with temperatures around twenty to thirty degrees Celsius and still high humidity became key refuges. During maturation storage, high relative humidity in the warehouse and biofilm on the brick surface promoted expansion of populations in surfaces, pores, and joints. Stored product insects and storage mites were highly sensitive to humidity. Rising critical relative humidity multiplied development and reproduction. Drying or higher vapor pressure deficit shortened survival. Extensive studies on grains and hard cheeses showed that booklice, flour mites, and flour beetles developed rapidly at thirty-two to forty degrees Celsius under high relative humidity, whereas many mobile stages died quickly when humidity fell or when temperature rose to about forty to forty-five degrees Celsius [29]. These rules arose from storage ecology yet were transferable to the grain-based, high-humidity, open-surface conditions of Daqu production, maturation, and storage and should be included in integrated control of production and warehousing [59]. Furthermore, microenvironments under different temperature classes determined spatial patterns of potential harm. In high-temperature Daqu, the core during

the peak was almost uninhabitable. The surface remained warm and moist for a longer time after cooling. If ventilation and drying were insufficient, the surface became the first choice for colonization. In medium- and low-temperature Daqu, the cooling was slower. Suitable windows inside the bricks appeared earlier and lasted longer. Earlier turning, destacking, and moisture control were therefore needed to narrow these windows. Translating these insights into practice meant designing processes that minimized pest niches by coupling trajectories of temperature and humidity, brick structure, and storage climate [32,60].

Airborne microbes inside and outside the qu-room and regional climate also influenced the initial state of microecology through temperature and precipitation and interacted with potential colonization by pests [61,62]. Cross-region comparisons showed that changes in year and climate factors altered the base community during early fermentation and indirectly shifted aroma composition and stability of mature Daqu [63]. This indicated that control of temperature and humidity in the process and drying during storage were not only internal variables. They needed coordination with the seasonal climate at the production site to form an integrated design that linked the qu room, storage, and climate.

3. Operational Definition, Representative Taxa, and Infestation Assessment of Daqu-Associated Pests

In the context of Daqu production and storage, Daqu-associated pests may be operationally defined as stored-product insects that are repeatedly detected in Daqu-making workshops, Daqu storage environments, or closely connected grain-handling spaces, and that are capable of colonizing raw materials, brick surfaces, cracks, dust layers, fines, or fungal biofilms, thereby interfering with physicochemical stability, microbial community assembly, enzymatic functions, or flavor consistency [12,59]. From the perspective of stored-product entomology, these insects can be broadly divided into primary pests, which are able to attack intact kernels or relatively compact substrates, and secondary pests, which preferentially exploit broken kernels, powders, dust, and mold-associated residues [64]. This classification is particularly relevant to the Daqu system because the production process creates a continuum of ecological niches ranging from intact grain particles to cracked surfaces, dust-rich corners, porous brick matrices, and post-cooling moist fissures. Therefore, the insects that deserve primary attention in the Daqu scenario are not all stored-product insects, but rather those species that are repeatedly reported in association with grain-based fermentation environments and that show clear ecological compatibility with the thermal, structural, and nutritional conditions of Daqu production and storage.

Based on the currently available literature and the biological summary compiled in the present revision, the most representative taxa included *Rhyzopertha dominica*, *Sitophilus zeamais*, *Sitophilus oryzae*, *Tribolium castaneum*, *Araecerus fasciculatus*, *Cryptolestes ferrugineus*, *Latheticus oryzae*, and *Cryptolestes turcicus* [59,65]. These species were selected because they collectively covered the major ecological roles that were relevant to the Daqu environment. *R. dominica*, *S. zeamais*, and *S. oryzae* represented internal or primary grain-feeding pests with a strong capacity to invade relatively intact grain-derived substrates [66]. *T. castaneum* represented a typical secondary flour and dust feeder and has already been reported as a major pest infesting sauce-flavor Daqu [67]. *A. fasciculatus* represented a warm- and humid-adapted polyphagous species with a strong affinity for mold-rich and nutrient-diverse substrates. *C. ferrugineus*, *L. oryzae*, and *C. turcicus* represented crack-associated and fines-associated secondary pests that were especially relevant to fragmented materials, dust deposits, and crevice-rich storage microhabitats [68,69] (Table 1). In other words, these taxa did not simply constitute a species list. Rather, they represented a functional pest assemblage that corresponded to the major ecological vulnerability points of the Daqu

system, including intact grain invasion, powder-associated colonization, crack exploitation, and persistence under warm and humid storage conditions [59].

Infestation severity in the Daqu system should not be assessed by insect presence alone. A more useful framework should combine direct entomological indicators, microenvironmental indicators, and process-linked response indicators. Direct entomological indicators may include pheromone or food-bait trap captures, light-trap captures where applicable, direct insect counts from surface and crevice sampling, and detection of frass, exuviae, carcasses, or perforated grain residues [70,71]. Microenvironmental indicators may include dust and fines accumulation, crack width and density, localized moisture retention, relative humidity in stacking zones, and visible fungal film development [12,64]. Process-linked response indicators may include changes in saccharifying activity, liquefying activity, acidification behavior, microbial community deviation, and shifts in key volatile compounds associated with flavor quality [59,65]. In this sense, infestation severity should be understood as a multi-dimensional ecological disturbance state rather than as a simple insect-count variable. This integrated assessment is consistent with stored-product monitoring principles, in which trap data, spatial hotspot analysis, and environmental context are interpreted together rather than independently. It also better fits the Daqu system, where insect activity, microbial succession, and flavor precursor transformation are tightly coupled.

It should also be emphasized that a unified quantitative standard for Daqu infestation severity has not yet been established. For this reason, the present review proposed a practical assessment logic in which pest intensity was characterized by species identity + spatial position + residue signal + process response. Such an approach may help distinguish between low-level incidental occurrence and biologically meaningful infestation. For example, occasional captures of secondary beetles in peripheral corridors may indicate external immigration only, whereas repeated detection of flour-feeding or crack-dwelling species together with increasing dust deposits, fungal films, and physicochemical deviation in bricks may indicate active colonization with real process implications. Accordingly, the present review argued that the operational definition of Daqu-associated pests should be tied not only to taxonomy but also to ecological role, habitat compatibility, and process relevance.

https://doi.org/10.3390/foods15071195

Table 1. Operational summary of representative Daqu-associated pests, their ecological roles, and suggested indicators for infestation assessment.

Species	Major Ecological Role	Typical Niche in the Daqu System	Key Biological Features Relevant to Daqu	Suggested Infestation Indicators	Potential Impact on Fermentation and Flavor	References
Rhyzopertha dominica	Primary/internal feeder	Grain-derived particles, compact substrate zones, inner brick pores or surrounding crevices	Strong boring capacity, broad host range, rapid spread under warm and humid conditions	Adult captures, bored particles, kernel perforation, fine powder generation, and internal damage signs	Structural disruption, increased powdering, altered water activity, potential shift in microbial assembly	[72,73]
Sitophilus zeamais	Primary/internal feeder	Moist grain-rich areas, early-stage bricks, storage-linked grain interfaces	Flight-capable, concealed larval development, strong performance in warm and humid conditions	Trap captures near intake and storage, perforated kernels, emergence holes, and localized grain residues	Hidden damage to substrate integrity, rapid colonization, and possible reduction in process stability	[74–76]
Sitophilus oryzae	Primary/internal feeder	Humid southern or coastal production environments, early-stage bricks with grain residues	Internal feeding life cycle, relatively high fecundity, strong compatibility with moist grain-derived substrates	Surface and cross-section inspection, emergence holes, frass particles, and trap captures	Changes in pore structure and gas diffusion, altered release of enzymatic and aroma precursors	[77,78]
Tribolium castaneum	Secondary flour and dust feeder	Brick surface cracks, dust-rich corners, equipment bases, powder deposits	Polyphagous, rapid development, high fecundity, strong migration ability, strong adaptation to fines and flour	Pheromone trap captures, dust-associated counts, frass and exuviae residues, and repeated captures in surface hotspots	Surface nutrient disturbance, biofilm restructuring, contamination risk, possible off-odor contribution	[67,79,80]
Araecerus fasciculatus	Warm-humid polyphagous secondary pest	Mold-rich surfaces, wet cracks, stack edges, poorly ventilated corners	Broad host range, strong association with humid and fungus-rich substrates, good dispersal ability	Trap captures in warm-humid zones, detection in mold-associated substrates, and residue accumulation	Damage to brick surface structure, enhancement of fungal–insect interaction, instability of aroma development	[81–83]
Cryptolestes ferrugineus	Secondary crack and fines feeder	Broken particles, fines, dusty fissures, edge zones with moisture retention	Rapid life cycle, strong response to temperature and humidity gradients, high mobility in fragmented substrates	Trap captures in warm stack edges, counts in dust layers, and frass and exuviae in cracks	Expansion from edge to interior, increased dust and fragmentation, indirect disturbance of microecology	[69,84,85]

https://doi.org/10.3390/foods1

Table 1. *Cont.*

Species	Major Ecological Role	Typical Niche in the Daqu System	Key Biological Features Relevant to Daqu	Suggested Infestation Indicators	Potential Impact on Fermentation and Flavor	References
Latheticus oryzae	Secondary fissure and powder-associated feeder	Warm storage crevices, dusty corners, fragmented grain or flour residues	Multiple generations, preference for warm and humid conditions, strong crack-associated survival	Direct counts in crevices, dust accumulation index, repeated captures in poorly cleaned zones	Persistent hidden infestation, increased powder load, possible fungal co-amplification	[59,86]
Cryptolestes turcicus	Secondary humid fines-associated feeder	Warm and humid cracks, broken grain interfaces, powder-rich storage microhabitats	Moisture-dependent development, rapid spread in humid conditions, strong crevice affinity	Trap captures in humid storage zones, counts in crack-associated fines, and residue build-up	Enhanced risk under wet storage, persistent low-visibility colonization, disturbance to microenvironmental stability	[87–89]

https://doi.org/10.3390/foods1

4. Daqu Production and Microecology

Daqu is not merely a fermentation starter but also a structured biological carrier in which matrix architecture, porosity, moisture migration, aeration, temperature gradients, and microbial succession jointly determine saccharification, liquefaction, esterification, and subsequent flavor formation [6,39,42]. In this system, the physical brick structure and the microecological environment are tightly coupled. Stable internal channels for ventilation and drying support enzyme initiation, surface-to-core differentiation, and orderly community assembly, whereas disruption of these features may alter both fermentation performance and flavor development.

Accordingly, pest occurrence in Daqu production should not be interpreted only as a sanitation problem. More importantly, it should be regarded as a disturbance factor capable of interfering with the structural and ecological basis on which Daqu functionality depends. In other words, pests may influence the carrier that supports early microbial colonization, enzymatic onset, and precursor release, rather than causing superficial material loss alone [32]. This conceptual starting point is essential for understanding why relatively low-density infestations may still produce disproportionate quality consequences in Daqu and in downstream Baijiu fermentation.

5. Sources of Ecological Disturbances

To avoid overstating conclusions, this section explicitly distinguishes direct evidence from Daqu/Baijiu systems, indirect evidence from stored-grain and food-storage studies, and conceptual hypotheses that remain to be validated. As shown in Figure 2, pest-associated ecological disturbance can therefore be discussed at three levels, namely direct interference with the Daqu matrix, indirect microecological risks inferred from related postharvest systems, and possible downstream consequences for flavor formation.

5.1. Direct Evidence from Daqu/Baijiu Systems and Current Boundaries

Direct evidence specific to Daqu/Baijiu does not yet demonstrate a fixed causal chain from pest occurrence to a defined flavor defect. What is directly established is that Daqu is an open, non-sterile solid-state starter whose quality depends on stable community assembly, enzyme activity, and the physicochemical environment of the brick [63,90–92]. Studies on Daqu microbiology and flavor have further shown that changes in community structure are closely associated with enzyme expression and with the formation of volatile compounds, indicating that disturbance of the solid carrier can have process-level consequences [6,39,42,93].

Accordingly, visible infestation in bricks, fines, stack gaps, or storage areas should first be interpreted as a direct event of physical contamination and process interference. In stored-grain systems, insect damage has been associated with more broken kernels, altered local humidity, and conditions favorable to mold development [94]. For Daqu, the concern is amplified because microbial colonization, heat and mass transfer, and enzyme initiation rely on the structural integrity of a porous solid matrix. Pest feeding, movement, and aggregation may enlarge fissures, increase loose particles, and weaken the carrier that supports early saccharification and fermentation rather than causing merely superficial damage [95]. Once the matrix is destabilized, local ventilation, aeration, and moisture migration can be altered, and the conditions required for timely enzyme initiation may be weakened or delayed [91]. Even so, quantitative thresholds linking infestation density to losses in Daqu functionality or to specific liquor flavor deviations remain insufficiently established [91,96,97].

https://doi.org/10.3390/foods15071195

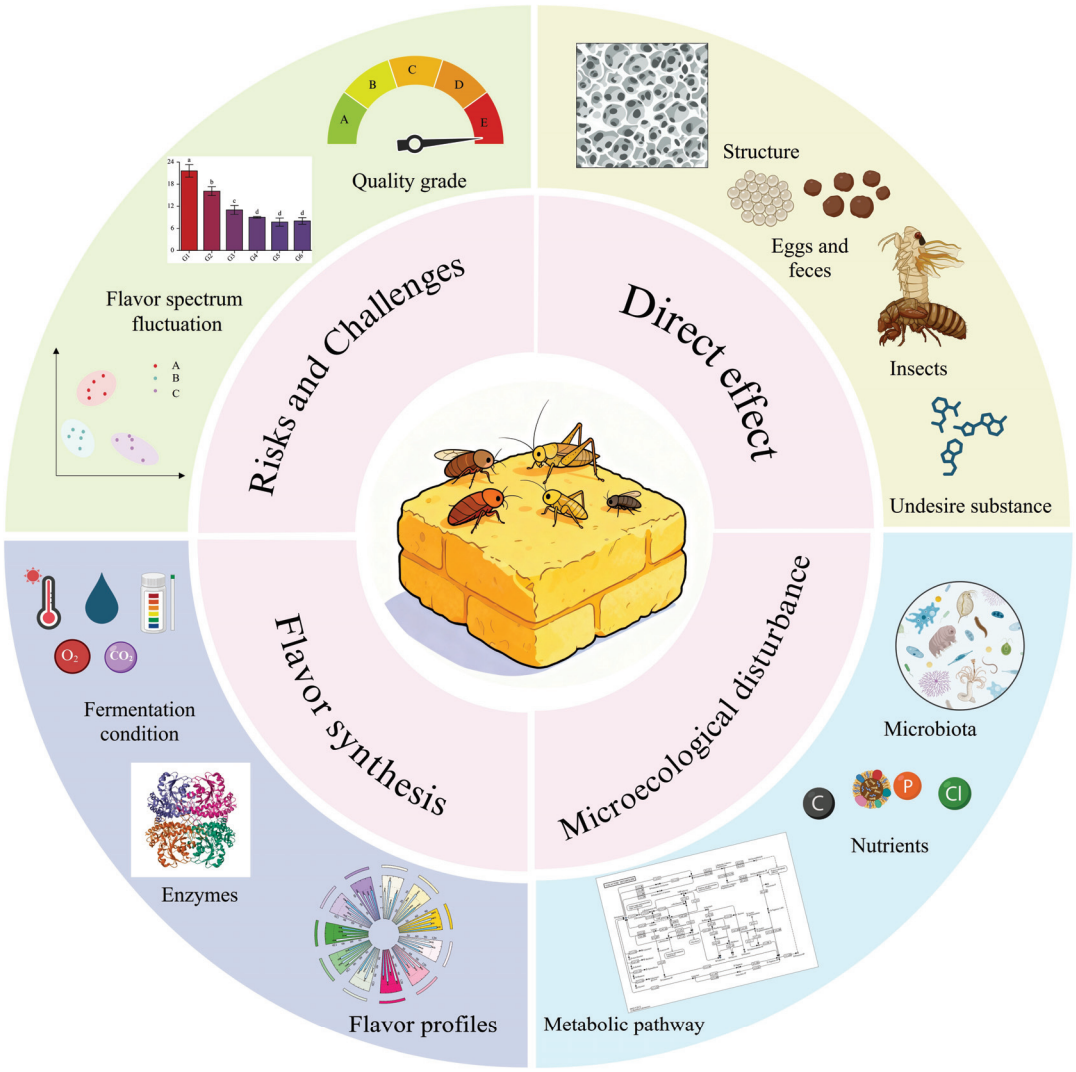


Figure 2. Impact of Daqu-associated pests on the microecology and production of Daqu. Insect feeding, oviposition, feces, exuviae, and other residues can damage the Daqu structure and introduce contamination, thereby disturbing microbiota, nutrient availability, and metabolic pathways. These changes may further affect fermentation conditions, enzyme performance, and flavor profiles, ultimately leading to flavor fluctuation, unstable quality grading, and broader production challenges. Overall, the figure illustrates a directional pathway from insect-induced structural disturbance to microecological imbalance and product-quality variation.

5.2. Indirect Evidence from Stored Grain and Food Storage Systems

Stronger statements regarding hygiene risk, allergen exposure, microbial vectoring, and odor disturbance are presently supported mainly by indirect evidence from stored grain, flour, and food-processing environments rather than by dedicated Daqu studies. In infested grain systems, higher loads of insect fragments, frass, uric acid, and associated microbial contamination have been reported [95,98]. Food and occupational studies likewise show that insect-derived materials, including fragments and dried fecal matter, can contribute to allergic or respiratory reactions, which supports their relevance to sanitation management and worker exposure in enclosed production spaces [58,59,65].

Indirect evidence also supports the possibility that pests can transport microorganisms and intensify local contamination pressure. Studies in stored products report that insects may carry fungal spores, bacterial consortia, or mycelial fragments, including taxa such as *Aspergillus*, *Fusarium*, and *Penicillium* [99]. As insects move across surfaces, dust, and damaged particles, introduced microorganisms can accumulate in cracks and settled micro-

zones, creating joint insect–microbe patches that favor localized ecological change [99–103]. In parallel, stored-product systems have shown that insect infestation may co-occur with higher mycotoxin risk under favorable microclimatic conditions [104,105]. These observations are informative for Daqu risk assessment, but they should be interpreted as analogical support rather than as direct evidence that the same processes occur to the same extent in Baijiu starters.

Evidence for odor alteration is also largely indirect. In grain and flour systems, infestation has been associated with shifts in lipids, proteins, enzyme activities, and volatile profiles, indicating that insect activity can influence aroma-related chemistry [63,90,106]. On this basis, insect secretions, metabolic wastes, frass odors, and decaying remains should be regarded as plausible sources of odor interference in Daqu. However, whether such inputs measurably alter the baseline aroma of Daqu or the final flavor profile of Baijiu still requires direct experimental verification.

5.3. Mechanisms of Insect–Microbe–Substrate Interactions

Given the current evidence base, the three-pathway framework discussed below should be regarded as a conceptual hypothesis for future validation rather than as an established causal model. Its scientific rationale is nonetheless grounded in two well-supported premises. Daqu quality depends on microbial succession within an open solid-state system [63,90–92], and microbial community structure is closely linked to enzyme activity and flavor generation [6,39,42,93,107,108].

The first proposed pathway is microbial introduction and redistribution. If pests enter during shaping, stacking, turning, room exit, or storage, they may carry exogenous microorganisms into fissures, margins, and dust-rich sites, thereby perturbing the initial microbiome and its subsequent assembly sequence [99]. The second pathway is substrate perturbation. Frass, exuviae, carcasses, fragments, and damaged grain particles can act as localized nutrient pulses. In stored-product ecology, insect residues and necromass are known to reshape carbon and nitrogen flows and to influence microbial substrate utilization [102,109,110]. A related, but still unverified, extension in Daqu is that gut-associated microorganisms or insect-transformed excreta may further modify local substrate chemistry and microbial interactions [110–112]. The third pathway is microenvironmental remodeling. Pest activity may enlarge cracks, redistribute fines, and alter local retention of moisture and air exchange, thereby changing pH, water activity, oxygen diffusion, and interfacial contact between substrate particles and microbial films [111,112].

If these three processes operate together, they could plausibly change the timing and proportion of metabolite formation by functional consortia, leading to shifts in esters, alcohols, acids, pyrazines, carbonyls, and related compounds [109,113,114]. At present, however, it is more rigorous to state that pest disturbance may increase the probability of pathway deviation and flavor imbalance than to claim direct formation of any specific off-note compound. Even parallels from other fermented foods, such as mite-associated flavor alteration reported in cheese, should therefore be cited only as conceptual analogies rather than as evidence for Daqu itself [115,116]. Accordingly, possible deviations in esters, aldehydes, pyrazines, amino acid derivatives, or sulfur-containing compounds should be discussed as hypothesis-driven targets for verification, not as already demonstrated outcomes in Daqu [60,63,90,117,118].

5.4. Impacts on Fermentation Performance and Flavor

From an industrial perspective, the most defensible conclusion at present is that pest occurrence in Daqu production should be treated as a combined sanitation, process-stability, and quality-risk signal. Indirect evidence from stored-food systems supports

concern over impurity accumulation and consumer or hygiene risk [94,119], volatile-profile disturbance and batch instability [95,120], and measurable economic loss under inadequate control [95,121]. For Baijiu production, such risks are more likely to appear first as weakened process robustness and greater batch-to-batch variability than as a single uniform defect aroma [41].

Accordingly, pest management should be integrated into quality assurance rather than handled only as routine housekeeping. Preventive control should emphasize raw-material hygiene, ventilation, dust control, residue removal, and crack management. When infestations are detected, intervention should be followed by verification at the levels of Daqu quality, microbial status, and early precursor or volatile signals. At the same time, an important caveat must remain explicit throughout the manuscript. Most current evidence still derives from grain storage, packaged foods, and general postharvest ecology rather than from the solid-state Daqu system, whose high-temperature, porous, and enzyme-coupled characteristics may alter routes of spread and impact [14,59,122]. Future research should therefore move from analogy to validation by quantifying the relationships among colonization density, residue burden, enzyme capacity, community succession, and flavor deviation under actual Daqu production conditions.

6. Control Strategies and Process Management

6.1. Environmental and Process Prevention

The topic was framed within a modern IPM perspective, and a low-infestation baseline was treated as the primary goal [123,124]. The first step was to build a suppressive environment for the koji rooms and bricks rather than to rely on reactive measures after outbreaks [123,124]. In solid-state Daqu production, prevention included clean raw and auxiliary materials, ventilation and drying in the koji room, sealing and zoned sanitation, and optimized material turnover. Only the combination of these actions established an effective barrier [123,124].

At the source, grain materials such as wheat, barley, or legumes that carried eggs or residues already acted as a seed bank for pests. Studies in grain science showed that cleaning, sieving, removal of defective kernels, and dust separation reduced early infestation rates by stored-product insects [125]. The same logic applied to Daqu. Removal of impurities and dust before moistening, followed by timely drying, lowered the chance that sources were carried into the koji room and colonized the bricks at the formation stage. After arrival, raw materials were processed without long storage. Prolonged holding increased small humidity and temperature drifts, dust accumulation, and the probability of immigration. Ventilation, humidity, and temperature control, and effective sealing of the qu-room were critical [126]. Proper ventilation allowed rapid moisture loss and cooling in early stacking. Prolonged warm and wet pockets created ideal sites for colonization and spread. Surveys in stored-product systems showed that poorly ventilated corners, wall gaps, and hidden crevices formed aggregation hot spots [99,121,127]. If stacking created heat retention or slow rewetting, preferred niches could form on brick surfaces and edges. Whole-room ventilation, tiered turning, and gap sealing were recommended to avoid leak points and dust traps.

Zoned sanitation was also essential. Qu-rooms were divided into clean areas, operation areas, and stacking areas. Equipment, corridors, and tools were dedicated or cleaned on a routine schedule [128,129]. Dust, fines, and spills were primary early aggregation points. Research showed a strong positive association between dust load and initial colonization [121,125]. After each turning step, accumulated dust and fines were removed. Brick stacks were kept away from walls and corridors, excessive stack height was avoided, bottom ventilation was maintained, and floors were kept clean. Material turnover was

https://doi.org/10.3390/foods15071195

optimized as well. Long residence of incoming grain, extended stacking time, and improper post-room aging created retention nodes. These nodes often coincided with humidity rebound, dust buildup, and attractive conditions for pests. Work in storage and processing plants indicated that higher movement frequency and timely turning reduced outbreak risk [99,127,130]. Time limits were defined for each node from intake to Daqu making to exit from the room, with records for traceability. After exit, bricks entered storage or transfer quickly rather than remaining in warm rooms where hidden explosions could start.

A critical view was necessary when translating storage practices to Daqu. Stacks in qu-rooms were irregular, with fast humidity and temperature dynamics and complex structures [10]. Static storage benchmarks such as moisture below thirteen percent or temperatures below fifteen degrees Celsius were not directly applicable [131,132]. Community activity and enzyme dynamics were high. These features favored flavor but also supported rapid pest growth. Preventive control, therefore, required dynamic adaptation rather than static thresholds. Trade-offs were common. Faster drying or earlier turning could protect against pests but might compromise sensitive aroma notes. Preventive design was tuned under flavor constraints rather than as a stand-alone hygiene task [133–135].

In summary, environmental and process prevention held strategic value for the aim of controlling pests without loss of aroma. Clean inputs, ventilated and dry rooms, zoned sanitation, and controlled turnover built a low-risk baseline. These steps protected enzyme potential, microbial stability, and flavor consistency at the same time. Mastery of dynamic control of gradients of temperature and humidity, cleaning frequency for dust and fines, ventilation efficiency, turning cadence, and turnover time embeds prevention within the production system rather than as an afterthought.

6.2. Physical and Thermal Treatments

Physical tools such as heat, low temperature, or modified atmospheres and inert powders provided gentle choices [41]. These tools minimized chemical residues and protected the flavor-relevant microecology, yet they still faced constraints from brick tolerance, enzyme sensitivity, and stability of flavor precursors [136].

Heat treatment has wide use in stored-product IPM. In practice, facilities were heated to fifty to sixty degrees Celsius and held for hours to ensure lethality across life stages. Reports showed that six to twenty-four hours in the range of fifty to sixty degrees Celsius controlled most stored-product insects [59,121]. In Daqu, this step could be placed near the brick exit or during handling to create a clean window before spreading. Care was needed. Enzyme systems, key precursors, and microbial activity could be temperature sensitive. Heat applied during enzyme initiation or early community assembly might suppress activity and weaken flavor development [121,127,137,138]. Parameters were therefore optimized for temperature and time to achieve lethality with minimal impact.

Low temperature and modified atmospheres offered another path. Reduction in temperature, oxygen depletion, or elevation of carbon dioxide suppressed pest metabolism [139]. Studies reported that more than sixty percent carbon dioxide at thirty degrees Celsius achieved complete adult mortality of several species within four days [140]. Such green methods were attractive due to low residue. In Daqu, bricks could be held under cool or modified atmospheres after exit and before storage to target eggs or larvae. The challenge lay in the brick as a porous body. Water content, pore structure, and gas diffusion complicated the maintenance of target atmospheres and the protection of enzyme and microbial functions. Gas-tight structures, monitoring, and careful matching to process windows were required [141–144]. Costs, sealing, and integration with turning and ventilation were also addressed.

https://doi.org/10.3390/foods15071195

Inert powders such as diatomaceous earth and zeolitic materials acted as physical barriers. Work showed that some powders at a dose of 0.5 g per square meter caused full adult mortality of three key stored-product species within seven days [145]. The action depended on abrasion of the cuticular wax layer and rapid desiccation rather than toxicity. In Daqu, powders were applied to walls, floors, ducts, and crevices to block ingress. High humidity and heavy dust loads in koji rooms could coat or deactivate powders and reduce efficacy. Mixing into bricks was avoided because pore structures and surface dust content might be altered, and indirect effects on flavor could follow. Doses and locations were chosen with ventilation, cleaning, and turning schedules in mind [72,142].

Operational guidance followed from the goal of control of pests without loss of aroma. First, physical tools were applied before full activation of enzyme systems and before extensive microbial assembly [128]. Second, parameters for temperature, atmosphere, and powders were set by brick tolerance. Pilot tests measured effects on amylase and protease activity, microbial communities, and precursor release before plant-wide adoption. Third, measures were integrated with monitoring, sanitation, ventilation, and turning, not used in isolation. For example, turning was paired with powder sweeping on paths and with a short period of cool or high carbon dioxide holding. Fourth, physical options were prioritized ahead of chemical measures to preserve flexibility for emergency use [121,136,138,140–142].

Daqu bricks expanded and contracted with heat and cold, breathed through complex pores, and carried sensitive enzymes. Simple transfer of grain-storage recipes ignored the balance between flavor generation, microbial stability, and the process path of temperature and humidity. Heat left no chemical residue, yet could alter moisture and deactivate enzymes. Low temperature or modified atmospheres were gentle but required sound containment and monitoring to avoid retardation of fermentation onset [146]. Plant trials and risk assessments were therefore essential before scale-up.

In conclusion, physical and thermal tools formed the preferred non-chemical options. Heat offered rapid action. Cool or modified atmospheres offered gentle suppression. Inert powders built peripheral barriers. Successful use depended on process matching. Protection of brick tolerance, microecology, and the flavor pathway was treated as the central constraint.

6.3. Irradiation and Electron Beam Technology

Electron beam irradiation was evaluated as a non-thermal option. It delivered a short processing time, high efficacy, and controllable parameters. It still required careful alignment with brick tolerance, flavor sensitivity, and plant logistics. Electron beams, as ionizing radiation, break nucleic acids of pests or microbes. In grain and feed studies, doses near two to five kGy reduced molds, yeasts, and aerobic bacteria with limited impact on nutrition and sensory quality [147,148]. For stored-product pests, the electron beam offered very short exposures, little residue, and no heating. These features positioned the tool as a green option [149,150].

Several advantages were noted for Daqu. Processing time was brief. Thermal disturbance was minimal. Dose, speed, and penetration were adjustable. These traits allowed a node such as brick exit to be coupled to an irradiation pass and then to storage. Yet key questions remained. Brick tolerance had to be proven. Daqu production involved self-heating, active microbial assembly, enzyme initiation, and aroma precursor formation. If irradiation were applied during early biochemical windows, enzyme activation, community assembly, or precursor release might be altered. A dose of three kGy produced little sensory change in some feed models, but those matrices differed from porous and enzyme-rich bricks. Pilot verification of dose against flavor was required to define the

https://doi.org/10.3390/foods15071195

minimum effective level, the best timing, and the envelope of effects on key activities and metabolites [151].

Process matching was another challenge. Equipment layouts, penetration through stacked bricks, avoidance of shadowing, immediate transfer to storage, and prevention of re-infestation had to be engineered. Safety, dosimetry, and certification systems were established for plant use. Capital costs and retrofits were justified by risk reduction and quality benefits. Public sources on full-scale use in solid-state starter bricks were still limited, which motivated staged trials. Small sets of bricks were treated at one, three, and five kGy, followed by enzyme assays, precursor release tests, microbial profiling, and final fermentation outcomes.

From a flavor-risk view, the electron beam was gentle but not zero-impact. Some food systems showed small shifts in volatile profiles, oxidation reactions, or color after irradiation [12]. In Daqu, attention focused on the initiation of enzymatic activity, the release of aroma precursors, and the synthesis of aroma compounds. Slight overdoses might suppress sensitive microbes or enzymes and shift esters, aldehydes, pyrazines, and related targets [123]. The tool was therefore embedded within a flavor-risk framework.

Implementation advice followed. The electron beam was positioned as a preferred non-thermal physical option that preceded chemical measures. Design considered process compatibility, flavor sensitivity, operating cost, layout, dose response, and feedback. Pilot verification established dose bands such as two, three, and five kGy and documented effects on enzyme and aroma metrics. Process nodes were synchronized. For example, bricks passed through the beam after exit and before storage, with checks of humidity, microbes, and key precursors. Monitoring confirmed freedom from survivors and compliance of enzyme and aroma metrics [123,147–149].

Overall, electron beam irradiation showed promise but required careful alignment with the process. It was accepted as gentle and efficient. It still demanded dose-flavor validation, integration with handling, and continuous monitoring before it could serve the aim of control of pests without loss of aroma.

6.4. Biological Control and Ecological Modulation

Entomopathogenic fungi such as *Beauveria bassiana* and *Metarhizium anisopliae* have accumulated evidence in stored-product systems. These fungi attached to the cuticle, penetrated, proliferated, and released toxins. Trials reported that at 1×10^8 conidia per milliliter, mortality of *Sitophilus oryzae* approached ninety percent at twenty degrees Celsius within seven days when *Metarhizium* or *Isaria* strains were used [124,152–154]. Such data supported the concept that early deployment in Daqu could depress populations to low baselines. Advantages included low environmental residue and acceptable safety profiles, which fit IPM. Compatibility with the brick microecology remained a key concern [153,155]. The qu-room was hot and humid with complex aeration. Microbial assembly and enzyme activation were rapid. Poor timing or excessive doses could suppress beneficial fungi, yeasts, or actinomycetes and alter amylase, protease, and esterase trajectories. The efficacy of many strains also depended on temperature, humidity, and substrate. Higher temperatures sometimes reduced performance [154,156,157]. Windows for use were chosen before widespread use and during favorable microclimates.

Parasitoids and plant-derived agents added options. *Anisopteromalus calandrae* parasitized larvae or pupae of grain pests and reduced adult emergence in storage systems [158,159]. Plant-based products showed low toxicity, small residues, and potential compatibility with sensitive microecologies, although evidence in storage insects was still developing. Layering these tools created multi-point suppression. Pathogenic fungi re-

duced adults and larvae. Parasitoids suppressed the next generation. Plant agents protected entry routes and contact surfaces [160].

Operational guidance emphasized staged use. Fungi were applied near intake or early stacking as a base barrier in low-density conditions. Parasitoids or plant agents were placed at vents, wall gaps, and dust-prone corners to weaken ingress. Monitoring tracked mycosis rates, parasitism, and efficacy of plant agents together with community metrics in bricks such as diversity, counts of functional groups, enzyme onset, and aroma outcomes [161,162]. If fungal or plant tools depressed pests but altered enzyme or aroma metrics, timing or dose was adjusted, or gentler strains or formulations were selected. Practical challenges persisted. Performance depended on microclimate, substrate, and density. Costs, stability, and ease of use needed improvement for large plants. Biological tools were slower to act than heat or chemicals, which tested the cadence of production [163–165].

In sum, biological control and ecological modulation were integrated with environmental prevention to deliver multi-point suppression. Compatibility with the microecology, enzyme initiation, and aroma formation was verified before scale-up. Future work focused on coupled measurements of pest density, functional microbes, enzyme activity, and aroma compounds inside the bricks to convert the concept of control of pests without loss of aroma into an operational biotechnological program [124,147,154,155,163–165].

6.5. Boundaries for Chemical Control

Chemical tools were treated as last-resort options in koji and fermentation systems and not as defaults [166,167]. Daqu environments were hot and porous with active microecology. Fumigants, residual sprays, and protectants posed risks to communities, enzyme onset, and aroma formation. Health and environmental concerns were well documented in storage and processing contexts. Phosphine and other fumigants created acute and chronic risks when combined with enclosed spaces, poor aeration, heat, and dust [59,168,169]. Broader reviews described persistence, bioaccumulation, resistance, and impacts on soil, water, plants, and human health [170]. In Daqu, such effects translated into trade-offs. A short-term knockdown could leave residues or depress the activity of fungi, yeasts, or actinomycetes. This depression could reduce the formation of esters, aldehydes, alcohols, and related aroma compounds. Chemical actions also required shutdowns for ventilation and sanitation and disrupted production rhythm.

Within the framework of control of pests without loss of aroma, strict boundaries were set. Non-chemical options were prioritized. Chemical use was limited to emergencies in which other options failed and risk had escalated, and only under quantified and traceable conditions [162]. The scope of use excluded critical windows such as enzyme onset and early community assembly. Small-scale verification preceded plant use. Post-use cleaning and verification included residue tests, monitoring of microbial recovery, and ventilation to restore conditions. Records linked chemical use to flavor and batch outcomes to enable review. Rising resistance to fumigants and protectants, costs, and consumer concern about residues and sustainability further narrowed long-term suitability [133,171–173]. Hidden costs included flavor imbalance and loss of product consistency [121,157].

Therefore, chemical control occupied a tightly bound position. It was not routine. It was used only when non-chemical routes were ineffective and after evaluation of risks to microecology and flavor.

6.6. Closed Loop of Monitoring, Intervention, and Verification

Modern practice favored a closed loop. Monitoring captured signals, interventions were triggered by thresholds, and verification measured outcomes. In solid-state Daqu production, this loop extended from pests to microecology, metabolism, and flavor [174,175].

Monitoring used pheromone traps, light traps, and quantitative sampling to obtain high-frequency spatial data. Visual checks alone were insufficient. Devices and cards were placed at key positions, and counts were recorded with time and location. Such tools mapped hot spots and movement in storage systems [161,174]. Data were linked to process variables. Examples included stack residence time, number of turns, surface temperature, humidity of bricks, and dust accumulation. Trends were reviewed on a routine schedule. If capture counts rose above predefined bands or if aggregation persisted, the system moved to intervention. Threshold-based control replaced ad hoc reactions [176–178].

Triggers were clear and tiered. When counts exceeded baselines by a set percentage or when hot spots persisted, the least intensive tool was used first. Turning, gap cleaning, and targeted trapping were preferred. If signals continued to rise, physical heat or low-dose measures were applied. Actions were traceable and recorded. Advanced setups linked interventions to process analytics and PAT platforms for synchronization [104,175,178].

Verification closed the loop. HACCP identified critical points such as brick exit, early storage, and early turning, and defined monitoring and documentation [179]. PAT tools followed microbial indicators, key aroma compounds, and timing of enzyme onset to quantify the effects of interventions [104,180]. If pests declined while flavor or enzyme metrics shifted, the plan was adjusted. If pests persisted, thresholds and tools were recalibrated.

Embedding the loop within the quality system moved pest control from a stand-alone task to an integrated assurance function. Plants adapt in real time while preserving the flavor pathway. Evidence in storage and food processing was stronger than in solid-state starters, so plants calibrated thresholds and indicators with internal data and trials. The direction was clear. Only through a monitored trigger and verification loop could control of pests without loss of aroma be delivered with consistency.

7. Process, Practice, and Enterprise Application for Control of Pests Without Loss of Aroma

Before implementation at the plant scale, a baseline diagnosis was required. This step served as the entry point of pest management and turned the risks across pests, microbes, and aromas into measurable items. Enterprises first mapped risks across Daqu rooms, warehouses, and packaging areas. The map specified how each space (raw material receiving, stacking in the Daqu room, post-room storage, and packaging corridors) aligned with points of pest ingress, microbially sensitive zones, and aroma-critical nodes. For example, traps were placed at the receiving end. Higher trap counts were often recorded along wall cracks and dust accumulations near the Daqu room. Stored-product monitoring recommended at least biweekly quantitative sampling of insects or trap counts to obtain a time-series trend. Next, indicators including trap counts, dust accumulation rate, crack growth, moisture readings, and ventilation temperature–humidity differentials were associated with microbial parameters and key aroma compounds (for example, ethyl acetate, phenylacetaldehyde, and 2,5-dimethylpyrazine) as critical quality attributes. Community assembly shifts were tracked by the proportions of yeasts, filamentous fungi, and actinomycetes at Daqu release as CQAs [46,181–183]. Historical data and field surveys then supported threshold setting. Examples included a trap count that exceeded the baseline mean by 1.5 times on two consecutive checks or a crack width above 3 mm with dust thickness above 2 mm. With this baseline, decisions moved from experience to data. A risk model that coupled pest, microbe, and aroma guided later interventions and verification.

The second step was minimal intervention. After diagnosis, when pest or risk indicators reached set thresholds, environmental and physical measures were prioritized over chemical or high-intensity actions. For instance, when edge traps around a fresh batch showed a twofold rise over baseline, the plant initiated restacking, sealing of edges, dust

https://doi.org/10.3390/foods15071195

removal, and stronger ventilation, along with inert powders or physical traps at cracks. If two subsequent checks still showed elevated counts, gentle options such as e-beam or mild heat were considered. Chemical treatment remained the final resort. This sequence minimized disturbance to the Daqu microbiome and aroma formation. Teams recorded timing, method, cost, and initial effects to enable later optimization. The QbD and PAT principle of minimum effective intervention was followed. During environmental optimization, ventilation and humidity changes, dust reduction, and moisture decline were monitored to ensure that actions targeted pest suppression rather than surface housekeeping only [184].

The third step was evidence closure. After interventions, verification confirmed control efficacy and integrated the results into quality assurance. HACCP and QbD PAT served as the reference framework [185]. Key control points were defined at re-stacking in the Daqu room, post-room stacking, and pest monitoring. Each batch recorded trap counts, crack depth, dust mass, stack temperature–humidity differentials, and airflow, with alert thresholds. After release or storage entry, samples were tested for microbial communities by 16S and ITS sequencing to obtain yeast or mold proportions, for key volatiles such as ethyl acetate and phenylacetaldehyde, and for sensory outcomes. Online and offline PAT tools, such as near-infrared, e-nose, and real-time volatile monitoring, created a data stream to connect process shifts with microbial and metabolic responses [186,187]. If verification showed pest control but a deviating volatile profile or delayed enzyme activation, the model parameters and trigger thresholds were adjusted, or protective measures for the microbiome were revised. This formed a closed loop from diagnosis to intervention to verification and ensured low pest risk, together with aroma consistency and fermentation performance.

In enterprise deployment, the three steps were executed through an information backbone, decision rules, and an operations team. In practice, a monitoring platform was established with traps, regular sampling, dust and fines measurement, temperature–humidity sensors, and crack imaging tools. Computer vision models such as yo-LO SG Insects were used for assisted recognition [188]. Monitoring data were linked to the process system with dashboards, early-warning thresholds, and named owners. When a trigger was reached, production, quality, and safety units acted together. The execution team performed restacking, cleaning, ventilation, and sealing while keeping gentle options such as e-beam as reserves. During verification, online volatile monitoring, periodic microbiome analysis, and sensory sampling were integrated into batch reports and fed back into the quality system. Several challenges were recognized. Baseline diagnosis required early investment. Many plants lacked online sensors, trap networks, or PAT infrastructure [174,177,189]. The promise of control without loss of aroma set a high bar for consistency. Without sound verification and feedback, plants could achieve low pest counts yet still face aroma drift. A phased pilot on one line or one room for three to six months was therefore recommended before scale-up. Overall, the three-step pathway provided a system framework that joined pest monitoring, trigger-based intervention, and aroma assurance. Through risk mapping, minimum interventions, and HACCP plus QbD PAT verification, enterprises built a closed loop from pest surveillance to aroma quality.

8. Prospects and Conclusions

8.1. Future Research Directions

Current evidence supports treating insects in Daqu production as a potential source of ecological disturbance rather than as a confirmed direct cause of specific flavor defects. Because Daqu production depends on natural inoculation, open fermentation, and microbiota-driven enzyme and flavor formation, future work should focus on whether insect occurrence measurably alters microbial succession, key enzyme activities, and early flavor precursors under actual Daqu conditions [6,30]. Multi-omics approaches, including

16S/ITS sequencing, metagenomics, metatranscriptomics, metabolomics, and volatile profiling, may provide a practical route for testing these links in a quantitative manner [190].

8.2. A Conceptual Framework Requiring Validation

At present, the proposed insect-mediated effects should be regarded as a conceptual framework for future validation rather than as an established mechanism. Three pathways remain especially worthy of investigation: microbial vectoring by insect bodies or residues, local substrate perturbation caused by frass, exuviae, and necromass, and gut-mediated biotransformation of returned particles [41]. These routes are biologically plausible and are broadly consistent with indirect evidence from stored-product systems, where insect infestation has been associated with volatile changes and quality deterioration (Figure 3). However, whether these pathways occur in Daqu and whether they are sufficient to alter Baijiu flavor remains to be demonstrated experimentally.

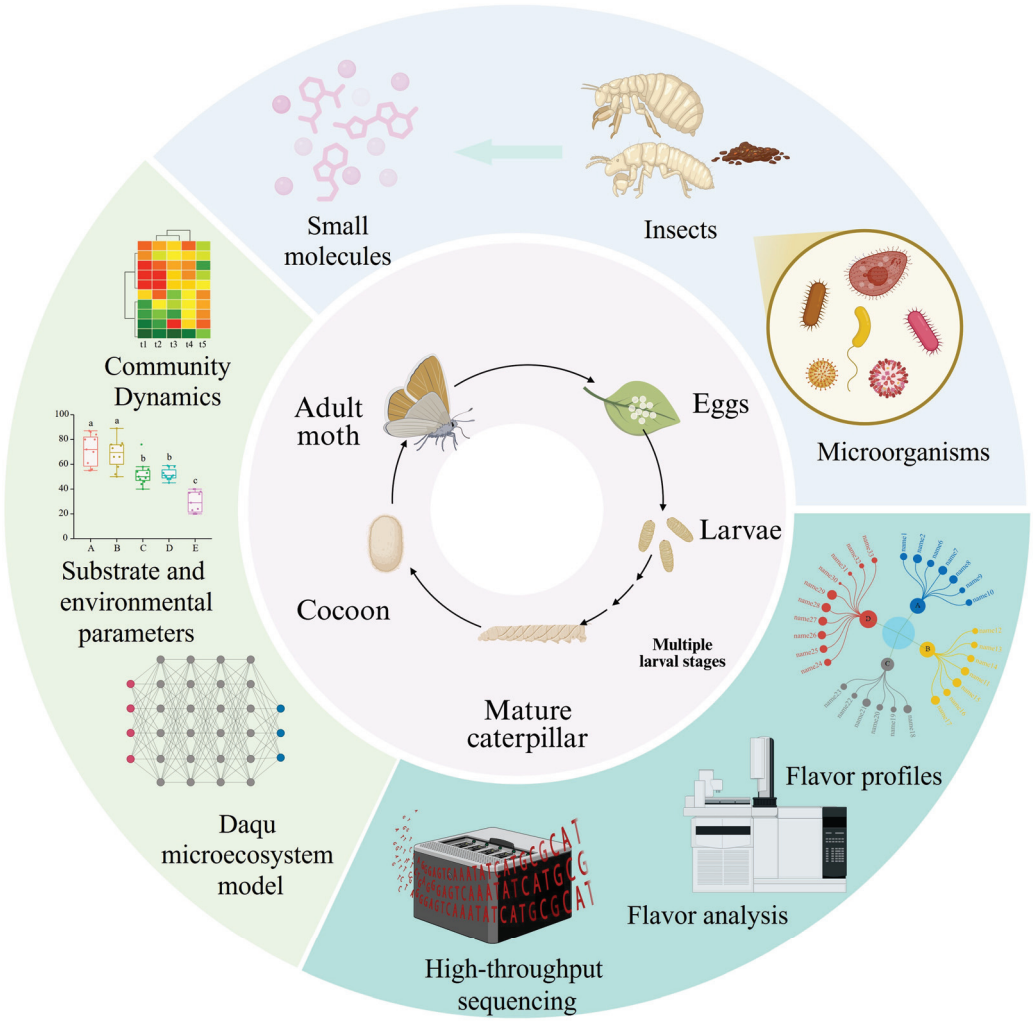


Figure 3. Cross-domain coupling among Daqu-associated pests, microorganisms, and flavor. The central circle represents the continuous pest life cycle, indicating that all developmental stages may act as recurrent disturbance sources during Daqu production and storage. The upper-right sector shows insect–microbe–metabolite interactions, highlighting pests as both substrate consumers and potential vectors or modifiers of microbial communities. The lower-right sector indicates that such disturbances may alter flavor profiles and can be monitored by high-throughput sequencing and flavor analysis. The left sector represents the system-level feedback layer linking community dynamics, environmental factors, and the Daqu microecosystem model. Overall, the figure illustrates a directional pathway from pest persistence to microbial and metabolic perturbation, flavor variation, and mechanistic interpretation for process control.

https://doi.org/10.3390/foods15071195

9. Limitations

This review has several limitations. First, direct evidence from Daqu and Baijiu systems remains limited, and many mechanistic interpretations are inferred from stored grain, food storage ecology, or general pest-management literature. Second, the specific features of Daqu, including open fermentation, high-temperature phases, porous solid matrices, and complex microbial succession, mean that findings from other systems cannot be transferred directly. Third, the proposed three-pathway hypothesis should be understood as a research framework rather than a confirmed causal model. Accordingly, the present article is best interpreted as a synthesis of direct evidence, indirect evidence, and conceptual hypotheses with different levels of certainty.

10. Conclusions

As summarized in Table 2, Daqu-associated insects should be regarded as a potential ecological disturbance factor relevant to process stability rather than as a minor sanitation issue alone. Current Daqu research clearly supports that Daqu is an open, microbially driven fermentation starter and that microbial succession is closely linked to enzyme activity and flavor formation. However, most insect-related mechanisms in Daqu are still not directly validated, and the proposed three-pathway framework should therefore be treated as a conceptual model for future testing rather than as an established causal mechanism. From a practical perspective, insect management should be integrated into quality assurance through prevention, monitoring, threshold-based intervention, and post-control verification so that pest control supports flavor stability without causing unnecessary interference with Daqu microecology.

https://doi.org/10.3390/foods15071195

Table 2. Integrated summary of evidence levels, proposed mechanisms, control implications, and research priorities for Daqu-associated insects in Baijiu production.

Domain	Core Point	Direct Evidence from Daqu/Baijiu Systems	Indirect Evidence or Conceptual Inference from Related Systems	Potential Impact on Daqu and Baijiu Quality	Control or Monitoring Implication	Research Priority
Insect occurrence and process relevance	Insects should be treated as process-relevant ecological disturbance factors rather than as marginal sanitation issues only	Surveys, workshop observations, and process-based discussions in the reviewed manuscript indicate that insects can occur during brick making, stacking, fermentation, storage, and workshop management	Related stored-product studies show that infestation is common in solid food matrices and can affect quality, storage stability, and processing performance	Increased process instability, higher risk of local contamination, and greater uncertainty in flavor consistency	Include insect occurrence in the routine process risk assessment rather than limiting it to sanitation inspection	Establish plant-specific occurrence maps by stage, location, and season
Structural disturbance of the Daqu matrix	Feeding, crawling, and residue accumulation may alter fissures, porosity, dust distribution, and local moisture migration	Daqu studies support the importance of matrix integrity, porosity, temperature, humidity, and microbial colonization for proper community assembly and enzyme formation	Stored-grain studies indicate that insect damage increases broken material, local humidity variation, and structural deterioration	Disturbance of the physical carrier that supports microbial colonization, heat and mass transfer, and enzyme initiation	Monitor crack ratio, dust deposition, edge damage, and local moisture retention in infested zones	Quantify links between infestation intensity and changes in Daqu physicochemical structure
Hygiene, impurity, and allergen burden	Fragments, exuviae, carcasses, and feces may increase impurity load and sanitation pressure	Direct Daqu-specific quantification remains limited	Food-processing and stored-product studies show associations with insect fragments, fecal material, microbial burden, and occupational exposure risks	Lower hygienic quality, possible increase in biological load, higher plant sanitation, and audit risk	Add impurity-related indicators and residue checks into workshop hygiene control	Define acceptable residue thresholds for Daqu production scenarios
Microbial vectoring pathway	Insects may carry exogenous or environmental microbes into bricks, fissures, and stack gaps	Daqu research clearly shows that microbial succession is central to enzyme activity and flavor formation, but direct demonstration of insect-mediated inoculation in Daqu is still lacking	Stored-product studies indicate that insects can carry fungal spores, bacterial cells, and mycelial fragments and redistribute them in food environments	Altered initial seeding pattern, shifted succession order, and possible disturbance of dominant functional guilds	Extend pest monitoring from counts alone to possible microbial carriage risk	Characterize insect-surface microbiota and compare it with the early-stage Daqu community assembly

https://doi.org/10.3390/foods1

Table 2. *Cont.*

Domain	Core Point	Direct Evidence from Daqu/Baijiu Systems	Indirect Evidence or Conceptual Inference from Related Systems	Potential Impact on Daqu and Baijiu Quality	Control or Monitoring Implication	Research Priority
Substrate pulse or necromass pathway	Bodies, exuviae, feces, and damaged particles may create localized nutrient pulses rich in nitrogen, chitin, and lipid residues	Daqu systems support the general importance of substrate state and microbial metabolism, but direct validation of insect-derived nutrient pulses is insufficient	Stored-product ecology suggests that residues and necromass can reshape local nutrient flow and microbial utilization	Selective enrichment or suppression of functional microbes, altered carbon and nitrogen flow, and biased precursor formation	Strengthen crack cleaning, dust removal, and residue management as part of quality control	Measure local chemistry, particle size, nitrogen distribution, and microbial response in residue-rich microzones
Gut-mediated biotransformation pathway	Insects may preprocess substrate particles through gut microbes and digestive enzymes and return transformed particles to the brick	No direct Daqu-specific proof has yet been established	Biologically plausible from insect digestive ecology and gut-microbe studies in grain-feeding insects	Changed accessible substrate spectrum, altered selective pressure, and modified timing of precursor release	Regarding insects, not only as removable contaminants but also as potential agents of substrate pre-transformation	Analyze insect feces chemistry, gut microbiota, and subsequent effects on Daqu enzyme activity and flavor precursors
Microenvironmental remodeling	Insect activity may jointly reshape pH, water activity, oxygen diffusion, fines concentration, and biofilm–substrate interfaces	Daqu's research strongly supports the importance of environmental parameters for microbial stabilization and flavor-related metabolism	Related systems suggest that infestation can induce local hotspots, moisture accumulation, and altered VOC behavior	Shifts in micro-zonal metabolism, community balance, and enzyme onset timing	Combine insect monitoring with local environmental sensing rather than using insect counts alone	Build coupled models linking insect activity, microenvironmental change, and community drift
Flavor-pathway deviation	Insect disturbance may ultimately affect ester, alcohol, aldehyde, pyrazine, sulfur, and other flavor-related pathways	Daqu and Baijiu studies support the link between microbiota, enzyme activity, and flavor compound formation	Infested flour and cereal studies report detectable VOC differences after infestation, supporting the plausibility of flavor-level effects	Flavor imbalance, weakened style typicality, batch variation, or latent aroma drift	Use early flavor precursors and volatile profiling as verification tools in addition to pest inspection	Verify whether specific volatile shifts can be reproducibly linked to insect density or residue load under Daqu conditions
Integrated pest management	Pest control should prioritize prevention, monitoring, and staged intervention rather than relying on chemicals alone	This aligns with the process-control logic proposed in the manuscript	IPM literature consistently defines prevention, monitoring, and corrective action as the basis of stored-product pest management	Better protection of process stability while minimizing unintended interference with microbiota and aroma formation	Prioritize source reduction, environmental management, physical or thermal suppression, and carefully bounded chemical use	Develop Daqu-adapted IPM criteria balancing pest suppression and flavor preservation

https://doi.org/10.3390/foods1

Table 2. *Cont.*

Domain	Core Point	Direct Evidence from Daqu/Baijiu Systems	Indirect Evidence or Conceptual Inference from Related Systems	Potential Impact on Daqu and Baijiu Quality	Control or Monitoring Implication	Research Priority
Monitoring–intervention–verification loop	Effective control requires a closed loop from detection to threshold-based action and post-control verification	Strongly consistent with the logic of HACCP, PAT, and quality-by-design style process management proposed in the manuscript	Stored-product IPM also emphasizes monitoring and action thresholds for corrective measures	Improves within-batch and between-batch consistency and converts pest control into a measurable quality-management process	Track insects, residues, cracks, dust, community indicators, enzyme activities, and key volatiles in one loop	Define data-driven thresholds for action and feedback adjustment
Digitalization and industrial deployment	Future implementation should move toward enterprise-level digital warning and rapid response platforms	Direct evidence is still emerging	Current literature supports increasing use of sensing, VOC monitoring, and intelligent management in fermentation and grain systems	Faster warning, more precise intervention, and stronger traceability of quality variation	Integrate trap data, environmental sensing, microbiome indicators, and aroma signals into linked dashboards	Build cross-plant models and validate the transferability of thresholds and early-warning indicators
Evidence boundaries and limitations	The current knowledge base mixes direct evidence, indirect evidence, and conceptual hypotheses	Direct Daqu/Baijiu evidence is strongest for the role of microbiota, process environment, and flavor formation	Many insect-specific mechanisms still rely on analogy from stored grain and food-storage ecology	Risk of overstatement if all mechanisms are treated as already proven in Daqu	Conclusions and management recommendations should be expressed with evidence boundaries should be made explicit	Move from conceptual plausibility to causal validation under real Daqu production conditions

https://doi.org/10.3390/foods1

Supplementary Materials: The following supporting information can be downloaded at: https://www.mdpi.com/article/10.3390/foods15071195/s1, Table S1: Characteristics of the microenvironment in Daqu. References [10,11,30,35,41,53,55] are cited in the supplementary materials.

Author Contributions: Conceptualization, D.S. and L.Y.; methodology, D.S., C.Z. and Y.W.; software, Y.W.; validation, D.S. and Y.W.; formal analysis, D.S., C.Z. and Y.W.; investigation, D.S., C.Z. and Y.W.; resources, D.S. and L.Y.; data curation, C.Z. and D.S.; writing—original draft preparation, D.S. and C.Z.; writing—review and editing, D.S., C.Z., Y.W. and L.Y.; visualization, Y.W. and C.Z.; supervision, L.Y.; project administration, D.S. and L.Y.; funding acquisition, D.S. and L.Y. All authors have read and agreed to the published version of the manuscript.

Funding: This work was financially supported by the National Natural Science Foundation of China (NSFC 32460269); Guizhou Provincial Basic Research Program (Natural Science) (No. QianKeHeJiChu-ZD [2025]018); Guizhou Key Laboratory of Microbial Resources Exploration in Fermentation industry (Qiankehe Platform Talent–ZDSYS [2023] 007); The Science and Technology Innovation Team of Moutai Institute (MTXYTD202501); Research Foundation for Scientific Scholars of Moutai Institute (mygccrc [2022]013, mygccrc [2022]026); Moutai Institute & Guangdong Li'er'an Chemical Industry Group Co., Ltd. (XYNJ20240104); and Baijiu Industry-Related Scientific Research Projects by the Education Development Foundation of Moutai Institute (BJXG2025-003).

Institutional Review Board Statement: Not applicable.

Informed Consent Statement: Not applicable.

Data Availability Statement: No new data were created or analyzed in this study. Data sharing is not applicable to this article.

Conflicts of Interest: Author Dandan Song was employed by Kweichow Moutai Group. She mainly participated in Conceptualization, Investigation, Resources, Data curation, Writing—original draft preparation, Writing—review & editing, Project administration, and Funding acquisition. Author Liang Yang was employed by Kweichow Moutai Group. He mainly participated in Conceptualization, Resources, Writing—review & editing, Supervision, Project administration, and Funding acquisition. Author Chunlin Zhang was employed by Kweichow Moutai Group. He mainly participated in Investigation, Data curation, Writing—original draft preparation, Writing—review & editing, and Visualization. The remaining authors declare that the research was conducted in the absence of any commercial or financial relationships that could be construed as a potential conflict of interest. The authors declare that this study received funding from Kweichow Moutai Group. The funder contributed to covering part of the article processing charge. The funder was not involved in the study design, collection, analysis, interpretation of data, the writing of this article, or the decision to submit it for publication.

References

1. Zhang, G.; Xiao, P.; Yuan, M.; Li, Y.; Xu, Y.; Li, H.; Sun, J.; Sun, B. Roles of sulfur-containing compounds in fermented beverages with 2-furfurylthiol as a case example. *Front. Nutr.* **2023**, *10*, 1196816. [CrossRef]
2. Xu, Y.; Zhao, J.; Liu, X.; Zhang, C.; Zhao, Z.; Li, X.; Sun, B. Flavor mystery of Chinese traditional fermented baijiu: The great contribution of ester compounds. *Food Chem.* **2022**, *369*, 130920. [CrossRef] [PubMed]
3. Miao, Z.; Hao, H.; Yan, R.; Wang, X.; Wang, B.; Sun, J.; Li, Z.; Zhang, Y.; Sun, B. Individualization of Chinese alcoholic beverages: Feasibility towards a regulation of organic acids. *LWT-Food Sci. Technol.* **2022**, *172*, 114168. [CrossRef]
4. Wu, Y.; Hou, Y.; Chen, H.; Wang, J.; Zhang, C.; Zhao, Z.; Ao, R.; Huang, H.; Hong, J.; Zhao, D.; et al. "Key Factor" for Baijiu Quality: Research Progress on Acid Substances in Baijiu. *Foods* **2022**, *11*, 2959. [CrossRef] [PubMed]
5. Yang, L.; Li, S.; Liu, Z.; Ma, J.; Wang, X.; Zhong, Y.; Wang, Y.; Guo, J.; Zhang, C. Construction of microecological discrimination models for high-temperature Daqu from different regions. *Food Chem. X* **2026**, *34*, 103699. [CrossRef]
6. Tang, J.; Wei, J.; Yang, Y.; Ge, X.; Zuo, Q.; Zhao, C.; Huang, Y. Spatio-temporal scales of the Chinese Daqu microbiome: Heterogeneity, niche differentiation, and assembly mechanisms. *Trends Food Sci. Technol.* **2025**, *156*, 104832. [CrossRef]
7. Kang, J.; Xue, Y.; Chen, X.; Han, B.Z. Integrated multi-omics approaches to understand microbiome assembly in Jiuqu, a mixed-culture starter. *Compr. Rev. Food. Sci. Food Saf.* **2022**, *21*, 4076–4107. [CrossRef]

8. Yang, L.; Fan, W.; Xu, Y. Chameleon-like microbes promote microecological differentiation of Daqu. *Food Microbiol.* **2023**, *109*, 104144. [CrossRef]
9. Lü, J.; Xu, S.; Teng, C.; Huang, R.; Xiong, G.; Cheng, Q. Comparative analysis of gut symbionts in *Tribolium castaneum* (Coleoptera: Tenebrionidae) and their dietary substrate, sauce-flavored Daqu. *Front. Insect Sci.* **2025**, *5*, 1614310. [CrossRef]
10. Yang, L.; Fan, W.; Xu, Y. Effects of storage period and season on the microecological characteristics of Jiangxiangxing high-temperature Daqu. *Food Res. Int.* **2024**, *196*, 115034. [CrossRef]
11. Yang, L.; Fan, W.; Xu, Y. Qu-omics elucidates the formation and spatio-temporal differentiation mechanism underlying the microecology of high temperature Daqu. *Food Chem.* **2024**, *438*, 137988. [CrossRef] [PubMed]
12. Zeng, Y.; Qiu, Y.; Wang, Y.; Zhang, X.; Wang, D.; Chen, X.; Gao, P.; Du, L.; Xie, F.; Wang, J. Effects of γ-ray irradiation on insect pests, physicochemical properties, and microbial community of strong-flavor Daqu during maturation. *Appl. Radiat. Isot.* **2025**, *220*, 111780. [CrossRef] [PubMed]
13. Yang, S.; Mei, X.D.; Zhang, X.F.; Li, Y.F.; She, D.; Zhang, T.; Ning, J. Attraction of Coffee Bean Weevil, *Araecerus fasciculatus*, to Volatiles from the Industrial Yeast *Kluyveromyces lactis*. *J. Chem. Ecol.* **2017**, *43*, 180–187. [CrossRef] [PubMed]
14. Zhang, X.; Huang, R.; Chen, Y.; Li, W.; Zhang, X.; Yang, J.; Lv, J. Complete mitochondrial genome of *Tribolium castaneum* (Coleoptera: Tenebrionidae) reared on sauce-flavor Daqu. *Front. Insect Sci.* **2025**, *5*, 1621855. [CrossRef]
15. Li, H.; Liu, S.; Liu, Y.; Hui, M.; Pan, C. Functional microorganisms in Baijiu Daqu: Research progress and fortification strategy for application. *Front. Microbiol.* **2023**, *14*, 1119675. [CrossRef]
16. Yang, Y.; Zou, Y.; Zeng, K.; Chen, D.; Li, Z.; Guo, H.; Huang, D.; Wang, X.; Luo, H. Effect of Bacillus subtilis fortified inoculation on the microbial communities in different niches of Daqu. *J. Biosci. Bioeng.* **2022**, *134*, 407–415. [CrossRef]
17. Fan, G.; Fu, Z.; Teng, C.; Wu, Q.; Liu, P.; Yang, R.; Minhazul, K.A.H.M.; Li, X. Comprehensive analysis of different grades of roasted-sesame-like flavored Daqu. *Int. J. Food Prop.* **2019**, *22*, 1205–1222. [CrossRef]
18. Zhao, J.; Yang, Y.; Chen, L.; Zheng, J.; Lv, X.; Li, D.; Fang, Z.; Shen, C.; Mallawaarachchi, V.; Lin, Y.; et al. Quantitative metaproteomics reveals composition and metabolism characteristics of microbial communities in Chinese liquor fermentation starters. *Front. Microbiol.* **2023**, *13*, 1098268. [CrossRef]
19. Cai, W.; Xue, Y.A.; Wang, Y.; Wang, W.; Shu, N.; Zhao, H.; Tang, F.; Yang, X.; Guo, Z.; Shan, C. The Fungal Communities and Flavor Profiles in Different Types of High-Temperature Daqu as Revealed by High-Throughput Sequencing and Electronic Senses. *Front. Microbiol.* **2021**, *12*, 784651. [CrossRef]
20. Mu, Y.; Yao, S.; Huang, Y.; Zhu, Z.; Li, D.; Song, Y.; Liu, Z.; Zhang, C.; Yu, S. Unveiling the metabolic heterogeneity and formation mechanism in Chinese typical Daqu based on Qu-omics. *Food Res. Int.* **2025**, *202*, 115735. [CrossRef]
21. Yuan, H.; Zheng, J.; Ding, L.; Wang, H.; Jiang, Q.; Zhang, C.; Xie, T.; Nan, G.; Li, L.; Lou, K. Temperature-Driven Divergence in Microbial Consortia and Physicochemical Functionality: A Comparative Study of High- and Medium-Temperature Daqu. *Microorganisms* **2025**, *13*, 1312. [CrossRef] [PubMed]
22. Wang, Y.; Xue, J.; Qiu, Y.; Zhang, X.; Wang, D.; Chen, X.; Gao, P.; Du, L.; Xie, F.; Xia, X.; et al. Effect of irradiation insecticidal technology on microbiome, physicochemical properties of strong-flavor Baijiu Daqu. *World J. Microbiol. Biotechnol.* **2025**, *41*, 279. [CrossRef] [PubMed]
23. Shanqimuge; Tang, P.; Qiao, M.; Wang, F.; Guo, Y.; Wang, L.; Bi, R.; Hao, S.; Kang, X.; Qin, L.; et al. Unveiling the Metabolic Function of Three Types of High-Temperature Daqu During Baijiu Fermentation. *J. Food Biochem.* **2025**, *2025*, 6762405. [CrossRef]
24. Wang, Y.; Yun, J.; Zhou, M.; Wang, Z.; Li, D.; Jia, X.; Gao, Q.; Chen, X.; Xie, G.; Wu, H.; et al. Exploration and application of Saccharomyces cerevisiae NJ002 to improve the fermentative capacity of medium-high temperature Daqu. *Bioresour. Technol. Rep.* **2023**, *23*, 101571. [CrossRef]
25. Cao, R.; Zhou, Q.; Ma, Y.; Yan, X.; Li, A.; Du, H.; Xu, Y. Multimodal integration: Mechanisms of temperature dynamics and quality formation critical period in Daqu. *Food Res. Int.* **2025**, *221*, 117622. [CrossRef]
26. Huang, P.; Jin, Y.; Liu, M.; Peng, L.; Yang, G.; Luo, Z.; Jiang, D.; Zhao, J.; Zhou, R.; Wu, C. Exploring the Successions in Microbial Community and Flavor of Daqu during Fermentation Produced by Different Pressing Patterns. *Foods* **2023**, *12*, 2603. [CrossRef]
27. Yang, H.; Xia, H.; Liu, S.; Chen, S.; Li, L.; Liao, X.; Fei, L.; Xie, L.; Tian, J.; Hu, X. A study on time-series prediction and analysis of acidity of Daqu based on multivariate data fusion and KNN-Attention-LSTM-XGBoost modeling. *Bioprocess Biosyst. Eng.* **2025**, *48*, 1451–1465. [CrossRef]
28. Bharathi, V.S.K.; Jian, F.; Jayas, D.S. Biology, Ecology, and Behavior of Rusty Grain Beetle (*Cryptolestes ferrugineus* (Stephens)). *Insects* **2023**, *14*, 590. [CrossRef]
29. Campbell, J.F. *Stored-Product Psocid Behavior and Its Implications for Pest Monitoring Programs*; CABI: Wallingford, UK, 2023; Volume 5, pp. 65–93. [CrossRef]
30. Shen, S.; Hu, B.; Zheng, J.; Xing, S.; Shi, G.; Zhang, B.; Lin, L.; Zhang, C. Unraveling flavor formation in Jiuqu: Source pathways, influencing factors, and regulatory strategies. *Food Chem. X* **2025**, *31*, 103009. [CrossRef]
31. Ali, A.; Li, W.; Chen, X.; Patil, P.J.; Li, H.; Zhang, Y.; Li, X. Interdisciplinary omics of Daqu and Baijiu: A bibliometric analysis (2011–2025). *Food Biosci.* **2025**, *71*, 107372. [CrossRef]

32. Deng, J.; Zheng, J.; Li, X.; Huang, D.; Ye, G.; Luo, H. Characterization of Qu-aroma of medium–high temperature Daqu from different production areas using sensory evaluation, E-nose, and GC–MS/O analysis. *Bioresour. Bioprocess.* **2025**, *12*, 16–40.
33. Lei, Y.; Cai, W.; Wang, Y.; Wang, B.; Liu, M.; Shan, C.; Guo, Z. Elucidating the physicochemical parameters, bacterial community structure, and correlation characteristics of medium-high temperature Daqu. *Food Biosci.* **2024**, *58*, 103679. [CrossRef]
34. Chen, C.; Ni, D.; Yang, Y.; Tian, J.; Yang, F.; Ye, X. Characterizing the microbial community constructure and the metabolites among different colour Moutai Daqu. *Food Chem. X* **2025**, *26*, 102223. [CrossRef] [PubMed]
35. Du, H.; Wang, X.; Zhang, Y.; Xu, Y. Exploring the impacts of raw materials and environments on the microbiota in Chinese Daqu starter. *Int. J. Food Microbiol.* **2019**, *297*, 32–40. [CrossRef] [PubMed]
36. Liu, P.; Zhang, L.; Du, X.; Zhao, J.; Gao, G.; Zhang, X. Dynamic Analysis of Physicochemical and Biochemical Indices and Microbial Communities of Light-Flavor Daqu during Storage. *J. Am. Soc. Brew. Chem.* **2019**, *77*, 287–294. [CrossRef]
37. Yi, Z.; Jin, Y.; Xiao, Y.; Chen, L.; Tan, L.; Du, A.; He, K.; Liu, D.; Luo, H.; Fang, Y.; et al. Unraveling the Contribution of High Temperature Stage to Jiang-Flavor Daqu, a Liquor Starter for Production of Chinese Jiang-Flavor Baijiu, With Special Reference to Metatranscriptomics. *Front. Microbiol.* **2019**, *10*, 472. [CrossRef]
38. Zhang, Y.; Xu, C.; Xing, G.; Yan, Z.; Chen, Y. Evaluation of microbial communities of Chinese Feng-flavor Daqu with effects of environmental factors using traceability analysis. *Sci. Rep.* **2023**, *13*, 7657. [CrossRef]
39. Tang, P.; Wang, L.; Zhao, Q.; Lu, J.; Qiao, M.; Li, C.; Xiao, D.; Guo, X. Characterization of key aroma compounds and relationship between aroma compounds and sensory attributes in different quality of high temperature Daqu. *LWT-Food Sci. Technol.* **2024**, *194*, 115801.
40. He, G.; Dong, Y.; Huang, J.; Wang, X.; Zhang, S.; Wu, C.; Jin, Y.; Zhou, R. Alteration of microbial community for improving flavor character of Daqu by inoculation with *Bacillus velezensis* and *Bacillus subtilis*. *LWT* **2019**, *111*, 1–8. [CrossRef]
41. Luo, Y.; Wu, L.; Wu, M.; Liao, H.; Yao, Y.; Luo, Y.; Ji, W.; Gao, L.; Wang, Z.; Xia, X. Intelligent Manufacturing Challenges and Directions of the Baijiu Starter Culture-Daqu Industry: Microbiome and Engineering Perspectives. *Trends Food Sci. Technol.* **2024**, *153*, 104724. [CrossRef]
42. Tang, P.; Li, Q.; Li, C.; Xiao, D.; Wang, X.; Guo, X. Analysis and formation mechanism of Key aroma compounds with ammonia-like off-flavors in Jiang-flavored high-temperature daqu: Substances composition and main microorganisms. *Food Biosci.* **2025**, *73*, 107656. [CrossRef]
43. Wang, Z.; Chen, L.; Yang, F.; Wang, X.; Hu, Y.; Wang, T.; Lu, X.; Lu, J.; Hu, C.; Tu, H.; et al. High-sensitivity profiling of dipeptides in sauce-flavor Baijiu Daqu by chemical derivatization and ultrahigh-performance liquid chromatography coupled with high-resolution mass spectrometry. *Food Chem. X* **2024**, *21*, 101097. [CrossRef] [PubMed]
44. Wu, M.; Luo, Y.; Yao, Y.; Ji, W.; Xia, X. Multidimensional analysis of wheat original crucial endogenous enzymes driving microbial communities metabolism during high-temperature Daqu fermentation. *Int. J. Food Microbiol.* **2024**, *413*, 110589. [CrossRef] [PubMed]
45. Han, P.J.; Luo, L.J.; Han, Y.; Song, L.; Zhen, P.; Han, D.Y.; Wei, Y.H.; Zhou, X.; Wen, Z.; Qiu, J.Z.; et al. Microbial Community Affects Daqu Quality and the Production of Ethanol and Flavor Compounds in Baijiu Fermentation. *Foods* **2023**, *12*, 2936. [CrossRef]
46. Tu, W.; Cao, X.; Cheng, J.; Li, L.; Zhang, T.; Wu, Q.; Xiang, P.; Shen, C.; Li, Q. Chinese Baijiu: The Perfect Works of Microorganisms. *Front. Microbiol.* **2022**, *13*, 919044. [CrossRef]
47. Fan, G.; Fu, Z.; Teng, C.; Liu, P.; Wu, Q.; Rahman, M.; Li, X. Effects of aging on the quality of roasted sesame-like flavor Daqu. *BMC Microbiol.* **2020**, *20*, 67. [CrossRef]
48. Shi, W.; Chai, L.J.; Fang, G.Y.; Mei, J.L.; Lu, Z.M.; Zhang, X.J.; Xiao, C.; Wang, S.T.; Shen, C.H.; Shi, J.S.; et al. Spatial heterogeneity of the microbiome and metabolome profiles of high-temperature Daqu in the same workshop. *Food Res. Int.* **2022**, *156*, 111298. [CrossRef]
49. Zhang, Y.; Shen, Y.; Niu, J.; Ding, F.; Ren, Y.; Chen, X.; Han, B.Z. Bacteria-induced amino acid metabolism involved in appearance characteristics of high-temperature Daqu. *J. Sci. Food. Agric.* **2023**, *103*, 243–254. [CrossRef]
50. Lei, Z.; Zhang, Z.; Huang, J.; Tang, Q.; Zhou, R. Revealing the synergistic effects of Qupi-shaping pattern and spatial variation on high-temperature Daqu attributes. *LWT-Food Sci. Technol.* **2025**, *215*, 117194. [CrossRef]
51. Mu, Y.; Liu, L.; He, J.; Zhang, H.; Yu, S.; Zhu, Z.; Huang, Y.; Mou, M.; Zhang, C. Investigating the variations in microbiome and volatilome characteristics of sauce-flavor Muqu across different grades and production rounds. *Food Chem.* **2025**, *492*, 145394. [CrossRef]
52. Cui, M.; Cai, W.; Yu, P.; Chen, W.; Shan, C.; Zhuang, G.; Wang, Y. Characterization and Correlation Analysis of Bacterial Composition and Physicochemical Quality in High- and Medium-Temperature Daqu from China's Binzhou Region. *Curr. Microbiol.* **2025**, *82*, 72. [CrossRef] [PubMed]
53. Huang, X.; Li, R.; Xu, J.; Kang, J.; Chen, X.; Han, B.; Xue, Y. Integrated multi-omics uncover viruses, active fermenting microbes and their metabolic profiles in the Daqu microbiome. *Food Res. Int.* **2025**, *208*, 116061. [CrossRef] [PubMed]
54. Liu, H.; Sun, B. Effect of Fermentation Processing on the Flavor of Baijiu. *J. Agric. Food. Chem.* **2018**, *66*, 5425–5432. [CrossRef] [PubMed]

55. Hou, Q.; Wang, Y.; Cai, W.; Ni, H.; Zhao, H.; Zhang, Z.; Liu, Z.; Liu, J.; Zhong, J.A.; Guo, Z. Metagenomic and physicochemical analyses reveal microbial community and functional differences between three types of low-temperature Daqu. *Food Res. Int.* **2022**, *156*, 111167. [CrossRef]
56. Hu, Y.; Huang, X.; Yang, B.; Zhang, X.; Han, Y.; Chen, X.X.; Han, B.Z. Contrasting the microbial community and metabolic profile of three types of light-flavor Daqu. *Food Biosci.* **2021**, *44*, 101395. [CrossRef]
57. Zong, E.; Bo, T.; Dang, L.; Zhang, J.; Li, H.; Lv, N.; He, Y.; Bai, B.; Zhang, J.; Fan, S. Different functions can be provided by low temperature Daqu with different appearance features due to variations in the microbial community structure during fermentation. *LWT* **2024**, *193*, 115763. [CrossRef]
58. Wen, Z.; Wei, Y.H.; Han, D.Y.; Song, L.; Zhu, H.Y.; Guo, L.C.; Chen, S.X.; Lin, B.; He, C.J.; Guo, Z.X.; et al. Deciphering the role of traditional flipping crafts in medium-temperature Daqu fermentation: Microbial succession and metabolic phenotypes. *Curr. Res. Food Sci.* **2025**, *10*, 101063. [CrossRef]
59. Huang, Y.; Zhang, S.; Huang, Z.; Li, S. Research Progress on the Hazards of Daqu Pests in the wine-brewing Daqu and Their Control Methods. *Fujian Agric. For. Technol.* **2024**, *55*, 29–34. [CrossRef]
60. Chen, Y.; Li, K.; Liu, T.; Li, R.; Fu, G.; Wan, Y.; Zheng, F. Analysis of Difference in Microbial Community and Physicochemical Indices Between Surface and Central Parts of Chinese Special-Flavor Baijiu Daqu. *Front. Microbiol.* **2021**, *11*, 592421. [CrossRef]
61. Xu, Y.; Qiao, X.; He, L.; Wan, W.; Xu, Z.; Shu, X.; Yang, C.; Tang, Y. Airborne microbes in five important regions of Chinese traditional distilled liquor (Baijiu) brewing: Regional and seasonal variations. *Front. Microbiol.* **2023**, *14*, 1324722. [CrossRef]
62. Zhou, J.; Li, X.; Li, S.; Ding, H.; Lang, Y.; Xu, P.; Wang, C.; Wu, Y.; Liu, X.; Qiu, S. Airborne microorganisms and key environmental factors shaping their community patterns in the core production area of the Maotai-flavor Baijiu. *Sci. Total Environ.* **2023**, *912*, 169010. [CrossRef] [PubMed]
63. Guan, T.; Wei, X.; Qiu, X.; Liu, Y.; Yu, J.; Hou, R.; Liu, M.; Mao, Y.; Liu, Q.; Tian, L.; et al. Precipitation and temperature drive microbial community changes affecting flavor quality of Nongxiangxing Daqu. *Food Chem. X* **2024**, *24*, 102063. [CrossRef] [PubMed]
64. Mbata, G.N.; Danso, J.K.; Holton, R.L. Peanut Aflatoxin: Impact of Postharvest Insect Infestation and Storage Systems. *Insects* **2024**, *15*, 836. [CrossRef] [PubMed]
65. Jianli, Z.; Jianfeng, H.; Guohua, Y.; Ping, H. Research progress in outbreak characteristics and control methods of Jiuqu insects. *Chin. Brew.* **2019**, *38*, 7–11. [CrossRef]
66. Boopathy, H.; Bharathi, V.S.K.; Jayas, D.S.; Jian, F. Three-dimensional movement and distribution of *Tribolium castaneum* (Coleoptera: Tenebrionidae) and *Cryptolestes ferrugineus* (Coleoptera: Laemophloeidae) in stored wheat at different temperatures and at different times. *Environ. Entomol.* **2025**, *54*, 15–26. [CrossRef]
67. Jagadiswaran, B.; Jayas, D.S.; Jian, F. Population dynamics of *Tribolium castaneum* (Coleoptera: Tenebrionidae) in wheat and in wheat mixed with cracked wheat held in different types of containers. *J. Econ. Entomol.* **2024**, *117*, 323–332. [CrossRef]
68. Anukiruthika, T.; Jayas, D.S.; Jian, F. Synergistic and antagonistic effects of temperature and moisture differences on movement and distribution of *Cryptolestes ferrugineus* (Coleoptera: Laemophloeidae) adults in horizontal columns of wheat. *J. Econ. Entomol.* **2024**, *117*, 333–347. [CrossRef]
69. Jian, F. The Innate Rates of Increase in Two Common Stored Grain Insects under Different Grain Storage Conditions and Times. *Insects* **2024**, *15*, 441. [CrossRef]
70. Cui, K.; He, L.; Cui, G.; Zhang, T.; Chen, Y.; Zhang, T.; Mu, W.; Liu, F. Biological Activity of trans-2-Hexenal Against the Storage Insect Pest *Tribolium castaneum* (Coleoptera: Tenebrionidae) and Mycotoxigenic Storage Fungi. *J. Econ. Entomol.* **2021**, *114*, 979–987. [CrossRef]
71. Channale, S.M.; Bhide, A.J.; Yadav, Y.; Kashyap, G.; Pawar, P.K.; Maheshwari, V.L.; Ramasamy, S.; Giri, A.P. Characterization of two coleopteran α-amylases and molecular insights into their differential inhibition by synthetic α-amylase inhibitor, acarbose. *Insect Biochem. Mol. Biol.* **2016**, *74*, 1–11. [CrossRef]
72. Yu, L.; Cao, X.L.; Zheng, W.; Li, J.; Xie, F.Y.; Zheng, X.L. Aggregation pheromones of Bostrichidae: A review. *J. Stored Prod. Res.* **2025**, *114*, 102767. [CrossRef]
73. Bian, Q.; Ambrose, R.P.K.; Subramanyam, B. Effects of insect-infested kernels on bulk flow properties of wheat. *J. Stored Prod. Res.* **2015**, *63*, 51–56. [CrossRef]
74. Broadhead, G.T.; Liu, H.; Sumrall, G.L.; Block, A.K.; Hunter, C.T.; Beck, J.J. Volatile Byproducts of Carotenoid Degradation as Biomarkers of Maize Infestation by the Maize Weevil (*Sitophilus zeamais*) (Motsch.). *J. Agric. Food. Chem.* **2025**, *73*, 1835–1843. [CrossRef] [PubMed]
75. Abedi, Z.; Razmjou, J.; Rafiee Dastjerdi, H.; Ebadollahi, A. Physical and biochemical characteristics of cereal grains affect population growth parameters of *Sitophilus oryzae* (L.) (Coleoptera: Curculionidae). *J. Stored Prod. Res.* **2024**, *109*, 102459. [CrossRef]
76. Quellhorst, H.E.; Kim, T.N.; Zhu, K.Y.; Morrison, W.R. Short-term spatial dispersion patterns between the larger grain borer and the maize weevil in grain columns. *Environ. Entomol.* **2024**, *53*, 127–142. [CrossRef]

77. Arya, P.S.; Srivastava, C.; Rajna, S.; Ranjith, H.V.; Subramanian, S. Physicochemical grain properties of wheat cultivars and insect biology drive resistance to *Sitophilus oryzae* L. *Sci. Rep.* **2025**, *15*, 35308–35312. [CrossRef]
78. Zhang, Q.; Lu, J.; Ahmed, Z.; Jiang, S.; Xu, B. Effect of temperature and relative humidity on the development of *Oryzaephilus surinamensis* L. (coleoptera: Silvanidae) reared on dried noodles. *J. Stored Prod. Res.* **2025**, *111*, 102541. [CrossRef]
79. Zhang, J.; Gao, S.; Faidah, A.N.; Wagan, S.; Mo, J.; Qi, Q.; Sun, L.; Cao, C. Effects of modified atmospheres, temperature and humidity on the growth and development of *Tribolium castaneum* (Herbst) (Coleoptera: Tenebrionidae) in feihe infant milk powder. *J. Stored Prod. Res.* **2024**, *108*, 102378. [CrossRef]
80. Tripathi, R.; Jayas, D.S.; Jian, F.; Hervet, V.A.D. Population dynamics of red flour beetle (*Tribolium castaneum* (Herbst)) under different temperatures and patch sizes. *J. Stored Prod. Res.* **2021**, *94*, 101865. [CrossRef]
81. Jian, L.; Yang, Y.; Xie, S.; Lou, Y.; Chen, L.; Dai, F.; Agrafioti, P.; Cao, Y.; Athanassiou, C.G.; Li, C. Life Table Parameters and Digestive Enzyme Activity of *Araecerus fasciculatus* (Coleoptera: Anthribidae) Feeding on Different Stored Products. *Insects* **2025**, *16*, 428. [CrossRef]
82. Olubunmi, A.F.; Zhang, Y.; Mohany, M.; Al-Rejaie, S.S. Insect pests of dried yam (*Dioscorea* sp.) chips and the perception of processors and marketers on their control. *J. Stored Prod. Res.* **2024**, *109*, 102429. [CrossRef]
83. Zeng, G.; Xie, S.; Jian, L.; Agrafioti, P.; Wu, K.; Athanassiou, C.G.; Cao, Y. Behavioral responses of *Araecerus fasciculatus* (Coleoptera: Anthribidae) to volatiles of selected stored Chinese medicinal plant products. *J. Econ. Entomol.* **2024**, *117*, 2669–2677. [CrossRef]
84. Zhang, C.; Wang, H.; Zhuang, G.; Zheng, H.; Zhang, X. Comparative transcriptome analysis of *Callosobruchus chinensis* (L.) (Coleoptera: Chrysomelidae-Bruchinae) after heat and cold stress exposure. *J. Therm. Biol.* **2023**, *112*, 103479. [CrossRef] [PubMed]
85. Anukiruthika, T.; Jayas, D.S.; Jian, F. Response of *Cryptolestes ferrugineus* (Coleoptera: Laemophloeidae) adults to small temperature (0–6 °C) and moisture (1%) differences in wheat. *Environ. Entomol.* **2023**, *52*, 814–823. [CrossRef] [PubMed]
86. Athanassiou, C.G.; Paly Vos, N.E.; Eliopoulos, P.A.; Papadoulis, G.T. Distribution and migration of insects and mites in flat storage containing wheat. *Phytoparasitica* **2001**, *29*, 379–392. [CrossRef]
87. Wang, D.; Zeng, F.; Xiao, Z.; Bai, C.; Zhao, C.; Cao, X.; Jian, F. Full mortality time prediction on eggs of S- and R-strains of Cryptolestes turcicus Grouville based on adult immobilization observed by video camera imaging in phosphine fumigation. *J. Stored Prod. Res.* **2025**, *111*, 102512. [CrossRef]
88. Chen, L.; Yan, H.; Di, S.; Guo, C.; Zhang, H.; Zhang, S.; Gold, A.; Wang, Y.; Hu, M.; Wu, D.; et al. Mapping pesticide-induced metabolic alterations in human gut bacteria. *Nat. Commun.* **2025**, *16*, 4355. [CrossRef]
89. Zhang, Y.; Liu, H.; Jing, H. Community differences and potential function along the particle size spectrum of microbes in the twilight zone. *Microbiome* **2025**, *13*, 121. [CrossRef]
90. Ying, H.; Yang, J.; Yu, L.; Wei, J.; Sheng, Q.; Yuan, Y.; Yue, T. Metagenomics and GC-IMSanalyses reveal microbial community differences and flavor characteristics among three types of Feng flavor Daqu. *Food Res. Int.* **2025**, *221*, 117551. [CrossRef]
91. Li, W.; Han, M.; Zhang, H.; Zhang, Q.; Lang, Y.; Hu, S.; Li, X.; Sun, B. Exploring the differences in sauce-flavour Daqu from different regions and its contribution to Baijiu brewing based on microbial communities and flavours. *Int. J. Food Sci. Technol.* **2024**, *59*, 7357–7371. [CrossRef]
92. Cao, L.; Sun, H.; Wang, Y.; Wei, Z.; Zhang, J.; Wang, Y.; Yan, J.; Zhu, Y.; Cheng, N.; He, S.; et al. Comparative analysis of metagenomics between high- and medium-temperature daqu, and microbial succession in Jiang-Nong Jianxiang Baijiu fermentation. *BMC Genom.* **2025**, *26*, 852. [CrossRef]
93. Gao, Y.; Qiao, L.; Wang, J.; Zhang, H.; Huang, C.; Feng, S.; Li, H.; Zhang, N.; Zheng, F.; Huang, M. Aroma comparison of Qingke baijiu and other light-aroma baijiu produced with Daqu using molecular sensory science. *J. Food Compos. Anal.* **2025**, *147*, 107997. [CrossRef]
94. Wu, Y.; Yin, R.; Guo, L.; Song, Y.; He, X.; Huang, M.; Ren, Y.; Zhong, X.; Zhao, D.; Li, J.; et al. The Identification and Analysis of Novel Umami Peptides in Lager Beer and Their Multidimensional Effects on the Sensory Attributes of the Beer Body. *Foods* **2025**, *14*, 2743. [CrossRef] [PubMed]
95. Stathas, I.G.; Sakellaridis, A.C.; Papadelli, M.; Kapolos, J.; Papadimitriou, K.; Stathas, G.J. The Effects of Insect Infestation on Stored Agricultural Products and the Quality of Food. *Foods* **2023**, *12*, 2046. [CrossRef] [PubMed]
96. Li, Z.; Yan, X.; Zou, S.; Ji, C.; Dong, L.; Zhang, S.; Liang, H.; Lin, X. Analysis of Fungal Diversity, Physicochemical Properties and Volatile Organic Compounds of Strong-Flavor Daqu from Seven Different Areas. *Foods* **2024**, *13*, 1263. [CrossRef]
97. Zuo, Q.; Huang, Y.; Guo, M. Evaluation of bacterial diversity during fermentation process: A comparison between handmade and machine-made high-temperature Daqu of Maotai-flavor liquor. *Ann. Microbiol.* **2020**, *70*, 57. [CrossRef]
98. Stejskal, V.; Vendl, T.; Li, Z.; Aulicky, R. Efficacy of visual evaluation of insect-damaged kernels of malting barley by *Sitophilus granarius* from various observation perspectives. *J. Stored Prod. Res.* **2020**, *89*, 101711. [CrossRef]
99. Jian, F. Influences of Stored Product Insect Movements on Integrated Pest Management Decisions. *Insects* **2019**, *10*, 100. [CrossRef]
100. Kumari, R.; Jayachandran, L.E.; Ghosh, A.K. Investigation of diversity and dominance of fungal biota in stored wheat grains from governmental warehouses in West Bengal, India. *J. Sci. Food Agric.* **2019**, *99*, 3490–3500. [CrossRef]

101. Sevim, A.; Sevim, E.; Demirci, M.; Sandallı, C. The internal bacterial diversity of stored product pests. *Ann. Microbiol.* **2016**, *66*, 749–764. [CrossRef]
102. Solanki, M.K.; Abdelfattah, A.; Britzi, M.; Zakin, V.; Wisniewski, M.; Droby, S.; Sionov, E. Shifts in the Composition of the Microbiota of Stored Wheat Grains in Response to Fumigation. *Front. Microbiol.* **2019**, *10*, 1098. [CrossRef] [PubMed]
103. Xue, D.; Chen, T.; Li, Q.; Yang, Y.; Wu, Y. Microbiota composition of allopatric laboratory and wild populations of *Rhyzopertha dominica*. *J. Stored Prod. Res.* **2023**, *104*, 102202. [CrossRef]
104. Hurley, T.M.; Sun, H. Softening Shock and Awe Pest Management in Corn and Soybean Production with IPM Principles. *J. Integr. Pest Manag.* **2019**, *10*, 7. [CrossRef]
105. Khan, A.A. Insect as major carrier of aflatoxins and mycotoxin in foods: A review. *J. Entomol. Zool. Stud.* **2024**, *12*, 46–53. [CrossRef]
106. Cai, W.; Wang, Y.; Ni, H.; Liu, Z.; Liu, J.; Zhong, J.A.; Hou, Q.; Shan, C.; Yang, X.; Guo, Z. Diversity of microbiota, microbial functions, and flavor in different types of low-temperature Daqu. *Food Res. Int.* **2021**, *150*, 110734. [CrossRef]
107. Hou, Q.; Wang, Y.; Qu, D.; Zhao, H.; Tian, L.; Zhou, J.; Liu, J.; Guo, Z. Microbial communities, functional, and flavor differences among three different-colored high-temperature Daqu: A comprehensive metagenomic, physicochemical, and electronic sensory analysis. *Food Res. Int.* **2024**, *184*, 114257. [CrossRef]
108. Yuan, M.; Lu, T.; Zhang, H.; Wang, J.; Cui, M.; Zhao, W.; Wu, Y.; Ren, X.; Yao, P.; Zhang, X. Verification of the esters-producing properties of *Thermoascus aurantiacus* QH-1 derived from low-temperature Daqu by multiomics. *Food Microbiol.* **2026**, *134*, 104946. [CrossRef]
109. Shen, T.; Wu, Q.; Tan, Y.; Ju, X.; Han, G. Diet-induced gut microbiota shifts in grasshoppers: Ecological implications for management and adaptation under varying grazing intensities. *Pest Manag. Sci.* **2025**, *81*, 6128–6138. [CrossRef]
110. van de Zande, E.M.; Wantulla, M.; van Loon, J.J.A.; Dicke, M. Soil amendment with insect frass and exuviae affects rhizosphere bacterial community, shoot growth and carbon/nitrogen ratio of a brassicaceous plant. *Plant Soil.* **2024**, *495*, 631–648. [CrossRef]
111. Senthilkumar, T.; Jayas, D.S.; White, N.D.G.; Freund, M.S.; Shafai, C.; Thomson, D.J. Characterization of volatile organic compounds released by granivorous insects in stored wheat. *J. Stored Prod. Res.* **2012**, *48*, 91–96. [CrossRef]
112. Liu, X.; Jiang, H.; Xu, H.; Shang, S.; Wang, D.; Bai, Y.; Zeng, F. Volatile Organic Compounds as Early Detection Indicators of Wheat Infected by *Sitophilus oryzae*. *Foods* **2024**, *13*, 3390. [CrossRef]
113. Li, J.; Liu, Y.; Zhang, M.; Xu, H.; Ning, K.; Wang, B.; Chen, M. Melatonin increases growth and salt tolerance of Limonium bicolor by improving photosynthetic and antioxidant capacity. *BMC Plant Biol.* **2022**, *22*, 16. [CrossRef] [PubMed]
114. Zhang, Y.; Zhang, S.; Xu, L. The pivotal roles of gut microbiota in insect plant interactions for sustainable pest management. *npj Biofilms Microbomes* **2023**, *9*, 12–66. [CrossRef] [PubMed]
115. Brueckner, A.; Heethoff, M. Scent of a mite: Origin and chemical characterization of the lemon-like flavor of mite-ripened cheeses. *Exp. Appl. Acarol.* **2016**, *69*, 249–261. [CrossRef] [PubMed]
116. Shimizu, N.; OConnor, B.M.; Hiruta, S.F.; Hagino, W.; Shimano, S. Mite secretions from three traditional mite-ripened cheese types: Are ripened French cheeses flavored by the mites (Acari: Astigmata)? *Exp. Appl. Acarol.* **2022**, *87*, 309–323. [CrossRef]
117. Wu, Y.; Huang, M.; Zhao, D.; Xie, J.; Chen, Y.; Sun, J.; Huang, M.; Sun, B. Molecular information and sensomics based identification of bitter peptides in lager beer and their multidimensional sensory impacts on beer body. *Food Biosci.* **2026**, *76*, 108200. [CrossRef]
118. Ali, A.; Wu, Y.; Li, W.; Chen, X.; Patil, P.J.; Han, M.; Shah, H.; Zhao, L.; Li, X. Biotechnological approaches for targeted strain screening and enhancement of Daqu for quality baijiu production. *Food Biosci.* **2024**, *61*, 104885. [CrossRef]
119. Korunic, Z. Allergenic components of stored agro products. *Arh. Hig. Rada Toksikol.* **2001**, *52*, 43–48.
120. Cai, L.; Macfadyen, S.; Hua, B.; Zhang, H.; Xu, W.; Ren, Y. Identification of Biomarker Volatile Organic Compounds Released by Three Stored-Grain Insect Pests in Wheat. *Molecules* **2022**, *27*, 1963. [CrossRef]
121. Guru, P.N.; Mridula, D.; Dukare, A.S.; Ghodki, B.M.; Paschapur, A.U.; Samal, I.; Nikhil Raj, M.; Padala, V.K.; Rajashekhar, M.; Subbanna, A.R.N.S. A comprehensive review on advances in storage pest management: Current scenario and future prospects. *Front. Sustain. Food Syst.* **2022**, *6*, 993341. [CrossRef]
122. Zhi, Y.; Wu, Q.; Du, H.; Xu, Y. Biocontrol of geosmin-producing *Streptomyces* spp. by two Bacillus strains from Chinese liquor. *Int. J. Food Microbiol.* **2016**, *231*, 1–9. [CrossRef]
123. Li, C.; Zhang, R.; Sogore, T.; Feng, J.; Liao, X.; Wang, X.; Zhang, Z.; Ding, T. Electron beam irradiation in food processing: Current applications and strategies for commercial scale implementation. *Sustain. Food Technol.* **2025**, *3*, 875–893. [CrossRef]
124. Ak, K. Efficacy of entomopathogenic fungi against the stored-grain pests, *Sitophilus granarius* L. and *S. oryzae* L. (Coleoptera: Curculionidae). *Egypt. J. Biol. Pest Control* **2019**, *29*, 12. [CrossRef]
125. Kalpna; Hajam, Y.A.; Kumar, R. Management of stored grain pest with special reference to *Callosobruchus maculatus*, a major pest of cowpea: A review. *Heliyon* **2022**, *8*, e08703. [CrossRef] [PubMed]
126. Pan, F.; Qiu, S.; Lv, Y.; Li, D. Exploring the controllability of the Baijiu fermentation process with microbiota orientation. *Food Res. Int.* **2023**, *173*, 113249. [CrossRef]

127. Gerken, A.R.; Morrison, W.R. Farm2Fork through the lens of community ecology: Concepts and applications in postharvest storage. *Front. Sustain. Food Syst.* **2023**, *7*, 1137683. [CrossRef]
128. Wu, Q.; Zhu, Y.; Fang, C.; Wijffels, R.H.; Xu, Y. Can we control microbiota in spontaneous food fermentation?—Chinese liquor as a case example. *Trends Food Sci. Technol.* **2021**, *110*, 321–331. [CrossRef]
129. Xu, Y.; Sun, B.; Fan, G.; Teng, C.; Xiong, K.; Zhu, Y.; Li, J.; Li, X. The brewing process and microbial diversity of strong flavour Chinese spirits: A review. *J. Inst. Brew.* **2017**, *123*, 5–12. [CrossRef]
130. Zhou, W.; Arcot, Y.; Medina, R.F.; Bernal, J.; Cisneros-Zevallos, L.; Akbulut, M.E.S. Integrated Pest Management: An Update on the Sustainability Approach to Crop Protection. *ACS Omega* **2024**, *9*, 41130–41147. [CrossRef]
131. Dong, W.W.; Yu, X.; Wang, L.Y.; Zou, M.L.; Ma, J.Y.; Liu, J.; Feng, Y.L.; Zhao, S.M.; Yang, Q.; Hu, Y.L.; et al. Unveiling the microbiota of sauce-flavor Daqu and its relationships with flavors and color during maturation. *Front. Microbiol.* **2024**, *15*, 1345772. [CrossRef]
132. Niu, J.; Li, W.; Du, B.; Wu, Y.; Lang, Y.; Sun, B.; Sun, W.; Li, X. Temporal heterogeneity of microbial communities and flavor metabolism during storage of high-temperature Daqu. *Food Chem.* **2025**, *464*, 141577. [CrossRef]
133. Anukiruthika, T.; Jayas, D.S. Chemical cues in grain storage: A review on semiochemical types, pest behavior, and control strategies. *J. Stored Prod. Res.* **2025**, *113*, 102674. [CrossRef]
134. Macfadyen, S.; Vajargah, M.M.; Umina, P.; Hoffmann, A.; Nash, M.; Holloway, J.; Severtson, D.; Hill, M.; Van Helden, M.; Barton, M. Identifying critical research gaps that limit control options for invertebrate pests in Australian grain production systems. *Austral Entomol.* **2019**, *58*, 9–26. [CrossRef]
135. Plarre, R. More than a pest management tool-45 years of practical experience with insect pheromones in stored-product and material protection. *J. Plant Dis. Prot.* **2013**, *120*, 145–152. [CrossRef]
136. Quan, Y.; Wu, K. Managing Practical Resistance of Lepidopteran Pests to Bt Cotton in China. *Insects* **2023**, *14*, 179. [CrossRef]
137. Arthur, F.H. Residual efficacy of deltamethrin as assessed by rapidity of knockdown of *Tribolium castaneum* on a treated surface: Temperature and seasonal effects in field and laboratory settings. *J. Stored Prod. Res.* **2018**, *76*, 151–160. [CrossRef]
138. Tilley, D.R.; Casada, M.E.; Arthur, F.H. Heat treatment for disinfestation of empty grain storage bins. *J. Stored Prod. Res.* **2007**, *43*, 221–228. [CrossRef]
139. Ali, A.; Wu, Y.; Li, W.; Duan, Z.; Zhang, R.; Liu, J.; Patil, P.J.; Shah, H.; Li, X. Insight into microorganisms and flavor substances in traditional Chinese fermented food starter: Daqu. *Process Biochem.* **2024**, *146*, 433–450. [CrossRef]
140. Lin, J.; Yan, X.; Zhou, Y.; Zhu, G.; Ariyo, O.S.; Wang, S.; Chen, J.; Zhu, Y.; Wang, C.; Li, D.; et al. Modified atmosphere and ozone treatment technologies in stored grain pest control: Mechanism, applications and challenges. *Agric. Prod. Process. Storage* **2025**, *1*, 16. [CrossRef]
141. Barzman, M.; Bàrberi, P.; Birch, A.N.E.; Boonekamp, P.; Dachbrodt-Saaydeh, S.; Graf, B.; Hommel, B.; Jensen, J.E.; Kiss, J.; Kudsk, P.; et al. Eight principles of integrated pest management. *Agron. Sustain. Dev.* **2015**, *35*, 1199–1215. [CrossRef]
142. Ekström, G.; Ekbom, B. Pest Control in Agro-ecosystems: An Ecological Approach. *Crit. Rev. Plant Sci.* **2011**, *30*, 74–94. [CrossRef]
143. Magan, N.; Aldred, D. Post-harvest control strategies: Minimizing mycotoxins in the food chain. *Int. J. Food Microbiol.* **2007**, *119*, 131–139. [CrossRef] [PubMed]
144. Meissle, M.; Mouron, P.; Musa, T.; Bigler, F.; Pons, X.; Vasileiadis, V.P.; Otto, S.; Antichi, D.; Kiss, J.; Pálinkás, Z.; et al. Pests, pesticide use and alternative options in European maize production: Current status and future prospects. *J. Appl. Entomol.* **2010**, *134*, 357–375. [CrossRef]
145. Baliota, G.V.; Athanassiou, C.G. Evaluation of Inert Dusts on Surface Applications and Factors That Maximize Their Insecticidal Efficacy. *Appl. Sci.* **2023**, *13*, 2767. [CrossRef]
146. de Sousa, I.S.G.A.; Oliveira, J.; Mexia, A.N.O.; Barros, G.A.; Almeida, C.; Brazinha, C.; Vega, A.; Brites, C. Advances in Environmentally Friendly Techniques and Circular Economy Approaches for Insect Infestation Management in Stored Rice Grains. *Foods* **2023**, *12*, 511. [CrossRef]
147. Ameer, A.; Seleshe, S.; Kang, S.N. Effect of Various Doses of Electron Beam Irradiation Treatment on the Quality Characteristics of Vacuum-Packed Dry Fermented Sausage during Refrigerated Storage. *Prev. Nutr. Food Sci.* **2022**, *27*, 323–334. [CrossRef]
148. Uazhanova, R.; Ametova, M.; Nabiyeva, Z.; Danko, I.; Kurtibayeva, G.; Tyutebayeva, K.; Khamit, A.; Myrzamet, D.; Sogut, E.; Toishimanov, M. Improving Grain Safety Using Radiation Dose Technologies. *Agriculture* **2025**, *15*, 1669. [CrossRef]
149. de Oliveira, P.C.A.S.; de Souza Coelho, C.C.A.; Campos, R.D.S.; Freitas-Silva, O.; Júnior, M.F. Effects of electron-beam (E-beam) irradiation on the postharvest quality of 'golden' papayas. *Food Phys.* **2025**, *2*, 100054. [CrossRef]
150. Mshelia, R.D.Z.R.A.; Dibal, N.I.; Chiroma, S.M. Food irradiation: An effective but under-utilized technique for food preservations. *J. Food Sci. Technol.* **2022**, *60*, 2517–2525. [CrossRef]
151. Orynbekov, D.; Kalibekkyzy, Z.; Nurgazezova, A.; Nurymkhan, G.; Smolnikova, F.; Kakimov, M.; Rskeldiyev, B.; Baimaganbetova, G.; Baikadamova, A.; Abdullina, E. Investigation of the Effects of Electron Beam Irradiation on the Functional Properties and Stability of Various Feed Products During Storage. *Appl. Sci.* **2025**, *15*, 9855. [CrossRef]

152. Hansen, L.S.R.; Steenberg, T. Combining larval parasitoids and an entomopathogenic fungus for biological control of *Sitophilus granarius* (Coleoptera: Curculionidae) in stored grain. *Biol. Control* **2007**, *40*, 237–242. [CrossRef]
153. Wakil, W.; Kavallieratos, N.G.; Eleftheriadou, N.; Yaseen, T.; Rasool, K.G.; Husain, M.; Aldawood, A.S. Natural Warriors against Stored-Grain Pests: The Joint Action of Beauveria bassiana and *Steinernema carpocapsae*. *J. Fungi* **2023**, *9*, 835. [CrossRef] [PubMed]
154. Wakil, W.; Kavallieratos, N.G.; Ghazanfar, M.U.; Usman, M.; Habib, A.; El-Shafie, H.A.F. Efficacy of different entomopathogenic fungal isolates against four key stored-grain beetle species. *J. Stored Prod. Res.* **2021**, *93*, 101845. [CrossRef]
155. Irsad; Shahid, M.; Haq, E.; Mohamed, A.; Rizvi, P.Q.; Kolanthasamy, E. Entomopathogen-based biopesticides: Insights into unraveling their potential in insect pest management. *Front. Microbiol.* **2023**, *14*, 1208237. [CrossRef]
156. Batta, Y.A. Recent advances in formulation and application of entomopathogenic fungi for biocontrol of stored-grain insects. *Biocontrol Sci. Technol.* **2016**, *26*, 1171–1183. [CrossRef]
157. Batta, Y.A.; Kavallieratos, N.G. The use of entomopathogenic fungi for the control of stored-grain insects. *Int. J. Pest Manag.* **2017**, *64*, 77–87. [CrossRef]
158. Guo, Y.; Lü, J.; Bai, C.; Guo, C.; Huang, Y. Influence of temperature and exposure time of cold storage on the fitness of *Anisopteromalus calandrae* (Howard) (Hymenoptera: Pteromalidae). *J. Stored Prod. Res.* **2023**, *104*, 102184. [CrossRef]
159. Azam, S.M.; Faizan, M.; Ahmad, N.; Shah, S.; Farooq, M.; Sagheer, M. Biological Control Potential of *Anisopteromalus calandrae* against *Callosobruchus maculates* in Brown Lentils under Controlled Environmental Conditions. *Egypt. J. Vet. Sci.* **2023**, *54*, 275–279. [CrossRef]
160. Karanastasi, E.; Kavallieratos, N.G.; Boukouvala, M.C.; Christodoulopoulou, A.D.; Papadopoulou, A.A. Effect of three entomopathogenic nematode species to *Trogoderma granarium* Everts (Coleoptera: Dermestidae) larvae on stored-wheat. *J. Stored Prod. Res.* **2020**, *88*, 101641. [CrossRef]
161. Campbell, J.F.; Mullen, M.A.; Dowdy, A.K. Monitoring stored-product pests in food processing plants with pheromone trapping, contour mapping, and mark-recapture. *J. Econ. Entomol.* **2002**, *95*, 1089–1101. [CrossRef]
162. Harush, A.; Quinn, E.; Trostanetsky, A.; Rapaport, A.; Kostyukovsky, M.; Gottlieb, D. Integrated Pest Management for Stored Grain: Potential Natural Biological Control by a Parasitoid Wasp Community. *Insects* **2021**, *12*, 1038. [CrossRef]
163. Fleurat-Lessard, F. Integrated management of the risks of stored grain spoilage by seedborne fungi and contamination by storage mould mycotoxins—An update. *J. Stored Prod. Res.* **2017**, *71*, 22–40. [CrossRef]
164. Pattanaik, K.P.; Jena, S.; Mahanty, A.; Gadratagi, B.G.; Patil, N.; Pandi, G.G.P.; Golive, P.; Mohapatra, S.D.; Adak, T. Exploitation of volatile organic compounds for rice field insect-pest management: Current status and future prospects. *Physiol. Plant.* **2025**, *177*, e70240. [CrossRef] [PubMed]
165. Thia, J.A.; Hoffmann, A.A.; Umina, P.A. Empowering Australian insecticide resistance research with genetic information: The road ahead. *Austral Entomol.* **2020**, *60*, 147–162. [CrossRef]
166. Maiga, I.H.; Lecoq, M.; Kooyman, C. Ecology and management of the *Senegalese grasshopper Oedaleus senegalensis* (Krauss 1877) (Orthoptera: Acrididae) in West Africa: Review and prospects. *Ann. Soc. Entomol. Fr.* **2013**, *44*, 271–288. [CrossRef]
167. Togola, A.; Beyene, Y.; Bocco, R.; Tepa-Yotto, G.; Gowda, M.; Too, A.; Boddupalli, P. Fall armyworm (*Spodoptera frugiperda*) in Africa: Insights into biology, ecology and impact on staple crops, food systems and management approaches. *Front. Agron.* **2025**, *7*, 1538198. [CrossRef]
168. Gerken, A.R.; Campbell, J.F. Spatial and Temporal Variation in Stored-Product Insect Pest Distributions and Implications for Pest Management in Processing and Storage Facilities. *Ann. Entomol. Soc. Am.* **2022**, *115*, 239–252. [CrossRef]
169. Anukiruthika, T.; Jian, F.; Jayas, D.S. Movement and behavioral response of stored product insects under stored grain environments—A review. *J. Stored Prod. Res.* **2021**, *90*, 101752. [CrossRef]
170. Pathak, V.M.; Verma, V.K.; Rawat, B.S.; Kaur, B.; Babu, N.; Sharma, A.; Dewali, S.; Yadav, M.; Kumari, R.; Singh, S.; et al. Current status of pesticide effects on environment, human health and it's eco-friendly management as bioremediation: A comprehensive review. *Front. Microbiol.* **2022**, *13*, 962619. [CrossRef]
171. Ye, F.; Wang, S.; Zheng, H. Engineering insect–microbe symbiosis: Synthetic microbial communities for sustainable insect management. *Trends Parasitol.* **2025**, *41*, 613–616. [CrossRef]
172. Chidemo, S.C.; Musundire, R.; Mashavakure, N. Higher dosage of phosphine is required to control resistant strains of pests in outdoor grain storage systems: Evidence from Zimbabwe. *J. Stored Prod. Res.* **2023**, *100*, 102046. [CrossRef]
173. Nayak, M.K.; Daglish, G.J.; Phillips, T.W.; Ebert, P.R. Resistance to the Fumigant Phosphine and Its Management in Insect Pests of Stored Products: A Global Perspective. *Annu. Rev. Entomol.* **2020**, *65*, 333–350. [CrossRef] [PubMed]
174. Giles, K.L.; McCornack, B.P.; Royer, T.A.; Elliott, N.C. Incorporating biological control into IPM decision making. *Curr. Opin. Insect Sci.* **2017**, *20*, 84–89. [CrossRef] [PubMed]
175. Karthikeyan, K.; Jacob, S.; Beevi, P.; Purushothaman, S.M. Evaluation of different integrated pest management modules for the management of major pests of rice (*Oryza sativa*). *Indian J. Agric. Sci.* **2010**, *80*, 59–62.

176. Babendreier, D.; Hou, M.; Tang, R.; Zhang, F.; Vongsabouth, T.; Win, K.K.; Kang, M.; Peng, H.; Song, K.; Annamalai, S.; et al. Biological Control of Lepidopteran Pests in Rice: A Multi-Nation Case Study From Asia. *J. Integr. Pest Manag.* **2020**, *11*, 5. [CrossRef]
177. Ribeiro, L.P.; Ansante, T.F.; Niculau, E.S.; Pavarini, R.; Silva, M.F.G.F.; Seffrin, R.C.; Vendramim, J.D. *Pimenta pseudocaryophyllus* Derivatives: Extraction Methods and Bioactivity Against *Sitophilus zeamais* Motschulsky (Coleoptera: Curculionidae). *Neotrop. Entomol.* **2015**, *44*, 634–642. [CrossRef]
178. Tratwal, A.; Jakubowska, M.; Pietrusińska-Radzio, A. Decision Support Systems in Integrated Pest and Disease Management: Innovative Elements in Sustainable Agriculture. *Sustainability* **2025**, *17*, 8111. [CrossRef]
179. Ropkins, K.; Beck, A.J. Using HACCP to control organic chemical hazards in food wholesale, distribution, storage and retail. *Trends Food Sci. Technol.* **2003**, *14*, 374–389. [CrossRef]
180. Hilgendorf, K.; Wang, Y.; Miller, M.J.; Jin, Y.S. Precision fermentation for improving the quality, flavor, safety, and sustainability of foods. *Curr. Opin. Biotechnol.* **2024**, *86*, 103084. [CrossRef]
181. Dong, H.; Li, Y.; Lai, X.; Hao, M.; Sun, L.; Li, Q.; Chen, R.; Li, Q.; Sun, S.; Wang, B.; et al. Effects of fermentation duration on the flavour quality of large leaf black tea based on metabolomics. *Food Chem.* **2024**, *444*, 138680. [CrossRef]
182. Hu, Y.; Zhang, L.; Wen, R.; Chen, Q.; Kong, B. Role of lactic acid bacteria in flavor development in traditional Chinese fermented foods: A review. *Crit. Rev. Food. Sci. Nutr.* **2020**, *62*, 2741–2755. [CrossRef] [PubMed]
183. Jin, G.; Zhu, Y.; Xu, Y. Mystery behind Chinese liquor fermentation. *Trends Food Sci. Technol.* **2017**, *63*, 18–28. [CrossRef]
184. Wu, H.; Khan, M.A. Quality-by-Design (QbD): An Integrated Process Analytical Technology (PAT) Approach for Real-Time Monitoring and Mapping the State of a Pharmaceutical Coprecipitation Process. *J. Pharm. Sci.* **2010**, *99*, 1516–1534. [CrossRef] [PubMed]
185. Ropkins, K.; Beck, A.J. Controlling organic chemical hazards in food manufacturing: A hazard analysis critical control points (HACCP) approach. *Food/Nahrung* **2002**, *46*, 258–269. [CrossRef]
186. Bhardwaj, N.; Kumar, B.; Agrawal, K.; Verma, P. Current perspective on production and applications of microbial cellulases: A review. *Bioresour. Bioprocess.* **2021**, *8*, 95. [CrossRef]
187. Rathore, A.S.; Mishra, S.; Nikita, S.; Priyanka, P. Bioprocess Control: Current Progress and Future Perspectives. *Life* **2021**, *11*, 557. [CrossRef]
188. Zhu, X.; Li, D.; Zheng, Y.; Ma, Y.; Yan, X.; Zhou, Q.; Wang, Q.; Zheng, Y. A YOLO-Based Model for Detecting Stored-Grain Insects on Surface of Grain Bulks. *Insects* **2025**, *16*, 210. [CrossRef]
189. Trivedi, T.P.; Ahuja, D.B. Integrated pest management: Approaches and implementation. *Indian J. Agric. Sci.* **2011**, *81*, 981–993.
190. Li, Y.; He, W.; Liu, S.; Hu, X.; He, Y.; Song, X.; Yin, J.; Nie, S.; Xie, M. Innovative omics strategies in fermented fruits and vegetables: Unveiling nutritional profiles, microbial diversity, and future prospects. *Compr. Rev. Food. Sci. Food Saf.* **2024**, *23*, e70030. [CrossRef]

Disclaimer/Publisher's Note: The statements, opinions and data contained in all publications are solely those of the individual author(s) and contributor(s) and not of MDPI and/or the editor(s). MDPI and/or the editor(s) disclaim responsibility for any injury to people or property resulting from any ideas, methods, instructions or products referred to in the content.

foods

MDPI

Review

From Artisan Experience to Scientific Elucidation: Preparation Processes, Microbial Diversity, and Food Applications of Chinese Traditional Fermentation Starters (Qu)

Dandan Song [1], Xian Zhong [1], Yashuai Wu [2], Jiaqi Guo [3], Lulu Song [1] and Liang Yang [1,*]

[1] School of Brewing Engineering, Moutai Institute, Renhuai 564501, China; songdd0330@163.com (D.S.); zhongxian2025@163.com (X.Z.); songlulu@mtxy.edu.cn (L.S.)
[2] School of Food Science and Engineering, South China University of Technology, Guangzhou 510640, China; wyss995418706@163.com
[3] China Food Flavor and Nutrition Health Innovation Center, Beijing Technology and Business University, Beijing 100048, China; guojiaq7@163.com
* Correspondence: moutaiyl0725@163.com; Tel.: +86-18786819825

Abstract

Background: Qu was the core starter of traditional Chinese fermentation and had long relied on artisan experience, which led to limited batch stability and standardization. This review organized the preparation processes, microbial diversity, and application patterns of qu in foods from experience to science perspective. Methods: This work summarized typical process parameters for daqu, xiaoqu, hongqu, wheat bran or jiangqu, douchi qu, and qu for mold curd blocks used for furu. Parameters covered raw material moisture, bed thickness, aeration or turning, drying, final moisture, and classification by peak temperature. Multi-omics evidence was used to analyze the coupling of temperature regime, community assembly, and functional differentiation. Indicators for pigment or enzyme production efficiency and safety control such as citrinin in hongqu were included. Results: Daqu showed low, medium, and high temperature regimes. Thermal history governed differences in communities and enzyme profiles and determined downstream fermentation fitness. Xiaoqu rapidly established a three-stage symbiotic network of *Rhizopus*, *Saccharomyces*, and lactic acid bacteria, which supported integrated saccharification and alcohol fermentation. Hongqu centered on *Monascus* and achieved coordinated pigment and aroma formation with toxin risk control through programmed control of temperature, humidity, and final moisture. Wheat bran or jiangqu served as an enzyme production engine for salt-tolerant fermentation, and the combined effects of heat and humidity during the qu period, aeration, and bed loading determined hydrolysis efficiency in salt. Douchi and furu mold curd blocks used thin-layer cultivation and near-saturated humidity to achieve stable mold growth and reproducible interfacial moisture. Conclusions: Parameterizing and online monitoring of key variables in qu making built a process fingerprint with peak temperature, heating rate, and moisture rebound curve at its core. Standardization and functional customization guided by temperature regime, community, and function were the key path for the transition of qu from workshop practice to industry and from experience to science. This approach provided replicable solutions for flavor consistency and safety in alcoholic beverages, sauces, vinegars, and soybean products.

Keywords: traditional fermentation qu; qu making processes; microbial diversity; temperature regime driven; food applications and safety

1. Introduction

Qu was defined as a functional fermentation starter that was produced in cereal or bran substrates by mixed microorganisms including filamentous fungi, yeasts, and bacteria under solid-state conditions. Its core role was to supply both the microbial consortium that carried out fermentation and aroma formation and the enzyme system responsible for saccharification, proteolysis, and lipolysis. It therefore occupied a central position in the solid-state fermentation system in China [1]. Historical and archeological evidence indicated a long continuity of qu-centered solid-state fermentation technologies in East Asia. At the Shangshan site in Zhejiang, pottery residues revealed plant- and fungus-based brewing with rice as the main substrate and microorganisms typical of qu such as Monacus and yeasts. The chronology reached about ten thousand years before present, which suggested that cereal fermentation initiated by qu had long served as a key node in regional technological traditions and food culture structures [2–4].

Within a modern fermentation science framework, qu was redefined as an engineered natural bioreactor. Under solid-state conditions with controlled moisture and convective heat transfer, community assembly and succession created multi-enzyme networks for substrate conversion. These networks supplied fermentable sugars, amino acids, and fatty acids from macromolecular substrates and drove the production of ethanol and flavor compounds [5–7]. Major Chinese fermented categories including Baijiu, Huangjiu, vinegar, soy sauce, soybean pastes, and soy-based products all built the first principles of flavor and structure from qu as the starting point [8]. Reviews from flavor chemistry and microbial ecology jointly argued that qu served as the vehicle for optimal microbial collaboration in traditional fermented foods such as Baijiu. Its enzyme profiles and metabolic routes determined sensory trajectories and quality stability in both alcoholic and non-alcoholic products [9–13]. Traditional workshops had long relied on artisanal know-how to adjust qu making such as particle size of raw materials, water addition, stacking thickness, turning points, and aeration. Under open natural inoculation, batch variability and regional effects were pronounced, which hindered consistent outputs across workshops, seasons, and sites [2,10,14,15]. Over roughly the past decade [3,11,15,16], research on qu moved from experience to measurable and model-based fermentation engineering. Heat and mass transfer in SSF acted as the nexus for advances in raw material pretreatment, online process profiling, data-driven modeling, and equipment upgrades such as intelligent qu rooms with closed-loop control of temperature, humidity, and airflow. This engineering perspective provided the methodological basis for the modern redefinition of qu [17–20]. At the frontier of microbiology [21], qu was not a static set of strains but a self-organized microecology driven by temperature trajectories, moisture, and oxygen transfer [9,10,12,13,22,23]. Multi-omics studies demonstrated thermal stratification in high, medium, and low temperature types and spatiotemporal heterogeneity during preparation and storage. Core functional guilds and metabolic routes diverged accordingly [24]. Paradigms such as qu omics connected assembly rules and metabolic phenotypes with process variables, which supplied a coherent chain of evidence for functional customization, standard evaluation, and quality traceability of qu [2,3,25–29].

Against this background, this review aimed to address three focused research questions. The first concerned process engineering. Raw material types such as wheat, barley, pea, rice or rice flour, and bran, together with forming and drying methods, moisture and aeration settings, and stacking thickness, jointly shaped the pore structure and the regimes of heat and mass transfer in qu, which defined enzyme profiles and subsequent fermentation kinetics. The second concerned community ecology. Thermal types and environmental factors drove assembly and functional divergence of mixed microbial communities, which mapped through enzyme substrate microbe coupling to flavor chemistry routes. The third

concerned food applications and quality and safety. The functional positions of different qu in alcoholic beverages, sauces, vinegars, and soy-based products, together with key control points QCP and risk factors such as *Monascus*-related mycotoxin citrinin and biogenic amines, formed a closed loop from identification to intervention. Based on these three questions, this review integrated the four dimensions of process, microecology, flavor, and quality into a testable research framework intended to support the transition from artisanal practice to industrialization and intelligent manufacturing. At the academic level, this work juxtaposed SSF engineering with community ecology and flavor omics to rebuild the evidence chain from variables and mechanisms to phenotypes and to provide material for causal models linking qu functions, fermentation performance, and product flavor. At the industrial level, this work focused on implementable parameters and indicator systems such as moisture and aeration-linked temperature trajectories, enzyme intensities, yields of flavor precursors, and sensory readouts for standardized qu making, cross-site consistency, and development of greener products with reduced salt and sugar.

To ensure traceable scope and evidence, databases included Web of Science Core Collection, Scopus, PubMed, and Google Scholar for historical and technological sources. The time window covered 2000 to October 2025. English peer-reviewed papers and authoritative reviews were prioritized. The keyword strategy combined subject headings and free terms. The terms included Jiuqu, Qu starter, Daqu, Xiaoqu, Hongqu, *Monascus* or koji Chinese, soy sauce koji, rice wine starter, together with microbiome, metagenomics, process or engineering, and solid-state fermentation. Chinese terms were used in parallel for cross-checking of history and terminology. Title and abstract relevance guided the first screening. Inclusion in the second screening required explicit process parameters, community data, or flavor or safety indicators. Duplicates were removed before thematic synthesis. To avoid narratives without data, verifiable parameters or quantitative ranges were reported at key assertions. Objects, methods, and sources of uncertainty were specified when cross-study comparisons were made.

2. Process Engineering of Qu Making

2.1. Daqu from Temperature Regime to Finished Starter Process Engineering

Daqu preparation was viewed as an open solid-state fermentation chain that linked raw materials, forming, heap cultivation, drying with maturation, and storage. The core control variables were not isolated recipes (Figure 1A). They were boundaries of heat and mass transfer defined by brick geometry and stacking and the coupled temperature–moisture trajectory that evolved on these boundaries. The traditional low, medium, and high temperature types defined by the maximum core temperature were more than quality labels. They corresponded to distinct thermal histories and moisture paths, which determined enzyme retention, precursor formation, and the kinetic fitness of downstream fermentation [30]. Within this framework, selecting a temperature type amounted to a combined setting of target heat flux, evaporation flux, and oxygen transfer capacity. The engineering meaning exceeded the fine-tuning of any single parameter.

During heap cultivation, the rise, hold, and fall of temperature were dominated by biological heat. Ventilation and surface evaporation shaped the peak and its decline. Rather than listing exact times, emphasis was placed on coordinated scheduling of turning, aeration, and humidification and its role in within-batch consistency [31]. Turning reshaped vertical gradients of heat and moisture, synchronized drying and maturation among positions, and reduced early enzyme inactivation caused by local overheating or over drying. Programmed control of airflow and moisture stabilized peak level and rewetting rhythm within a given temperature window, which provided a reproducible thermal background for target enzyme profiles and flavor precursors [31]. Recent mappings of

spatiotemporal profiles showed that the middle layer often carried higher moisture and gentler fluctuations. This heterogeneity arose from mismatches among stacking density, porosity, and duct layout. It was more effective to co-optimize heap geometry and air paths at the design stage to smooth potential gradients in advance, so that top, middle, and bottom layers experienced similar drying and maturation, which reduced batch and layer variation at the source [32]. Under the same formula, stacking geometry and airflow organization often became the watershed for obtaining good qu because they changed effective heat exchange area and gas–solid contact, and in turn reshaped temperature–moisture trajectories and metabolic flux.

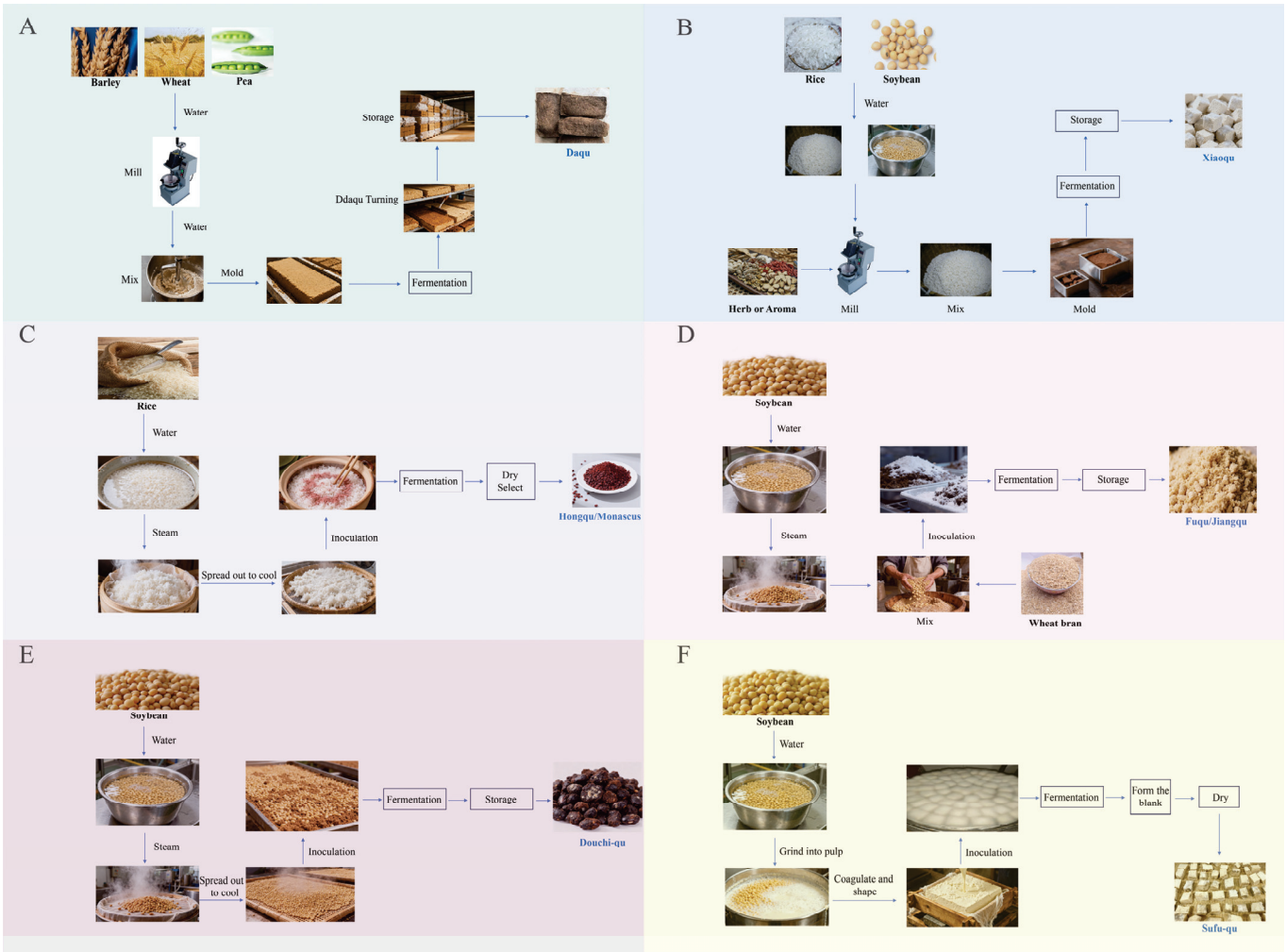


Figure 1. Schematic of qu-making processes and process engineering. Panels (**A**–**F**) were daqu, xiaoqu, hongqu (*Monascus*), fuqu/jiangqu, and sufu-qu.

Initial moisture and forming parameters showed threshold effects on early heating and structural stability [30]. Excessive moisture suppressed early heating and increased collapse and sticking. Insufficient moisture led to weak heating and early enzyme deactivation. It was more meaningful to discuss these variables within the feasible region defined by achievable temperature type and controllable peak shape rather than fixating on a single value. Brick size and density determined conductive paths and flow resistance. Standardized geometry provided reproducible heating and drying under similar climates. Pursuit of higher peak temperature or a richer volatile profile required a new balance between stacking density and ventilation intensity to avoid overfiring or overdrying that harmed enzymes and precursors [30]. Cross-workshop harmonization should not rely on

a universal moisture or brick-weight threshold. Combinations of heap form, ventilation, and humidification were back-calculated from the target temperature type and ambient climate [4,33,34].

Online monitoring and closed-loop control were necessary to make the temperature–moisture trajectory explicit and parameterized [35]. Drying and maturation inherited water and heat management from the heap stage. The task was to obtain mechanical and transfer stability suitable for storage and dosing without sacrificing enzymatic activity. Rather than emphasizing a single terminal moisture or a fixed drying temperature, attention was paid to the coupling among drying rate, stress release of the body, and storage time. Rapid water loss caused structural stress and surface densification, which impaired later water uptake, disintegration, and uniform dosing. Slow drying increased self-heating and secondary rewetting risk. Plants therefore used airflow organization, tiered relocation, and split sampling to align drying rate and storage duration with the post-treatment window of the selected temperature type, which promoted within-batch uniformity and cross-batch comparability [10,36].

In sum, finished quality was governed by the four-factor coupling of temperature type, heap form, ventilation, and moisture, while external climate expanded or narrowed the feasible region by altering dissipation and evaporation boundaries [37]. Cross-season and cross-site consistency depended on reconstructing boundary conditions and process curves according to climate rather than locking a fixed recipe so that target peak temperature, heating slope, and rewetting window remained reproducible and comparable [37]. This path agreed with recent studies linking temperature and precipitation to differences in community assembly and metabolism of daqu, which suggested a stable mapping between engineering variables and microbial ecology that supported process design and quality prediction.

2.2. Xiaoqu Engineering Control of the Rice Based Dual Fermentation Platform

The engineering essence of xiaoqu was framed as a continuous chain that used rice or rice flour as the carrier and linked forming, short incubation, mild drying, and stable storage to build a solid inoculum with long shelf life and controllable dosing (Figure 1B). Unlike daqu that relied on thick heaps and metabolic heat, the thermal and moisture trajectory of xiaoqu was governed by room boundaries. Key variables concentrated on dough moisture, piece size, and the coupling of ventilation with dehumidification. These parameters determined the early exothermic curve, the retention of the enzyme profile, and the handover efficiency of the dual fermentation in which saccharification preceded alcohol formation [30]. During the forming and incubation of the front half, moisture and shaping were more critical than any single operating detail. Higher dough moisture created a continuous aqueous phase and cohesive structure, which supported early heat release and stable mass transfer. Miniaturized pieces lowered internal thermal resistance so the rise and fall of product temperature could be finely controlled by room temperature, humidity, and air exchange. Their coupling set the starting activity, within-batch consistency, and the repeatability of the drying endpoint. Modern descriptions therefore emphasized inoculation with standardized mother powder and consistency management of forming so that the short thermal history of heat up, hold, and cool down remained reproducible [38].

During incubation, thin spreading with medium temperature and high humidity served as the dominant strategy to obtain a stable thermal history. Thin layers reduced vertical gradients, medium temperature limited early enzyme deactivation, and high humidity prevented a dry crust while supporting continuous mycelial expansion. Rather than listing exact set points, control prioritized their relative weights. When air exchange was insufficient, thinning the layer and staged ventilation were used to dissipate heat

accumulation. When surface water loss increased, gentle humidification and covering were used to maintain the interfacial water film and avoid an irreversible barrier layer. This combination enabled xiaoqu to develop a reproducible short thermal history within days and to deposit a stable enzyme profile, which preserved process flexibility for storage and dosing [39–42]. Related studies on xiaoqu in rice wine and regional Baijiu likewise indicated that coordinated optimization of room temperature, humidity, and ventilation determined the predictability of aroma and ethanol formation paths. In drying and curing, the focus lay in balancing activity retention, storage safety, and mechanical stability rather than chasing a single endpoint. Mild hot air or natural ventilation aimed to yield low moisture, structural stability, and easy disintegration and rehydration at dosing. Subsequent room temperature dark storage was used to release stress and stabilize physicochemical and sensory precursors. Although final moisture thresholds were often used as a general safety line, the engineering emphasis rested on the coupling among drying rate, internal structure, and activity decay. Overfast drying caused surface densification and hindered internal migration, whereas overslow drying raised the risks of rewetting and contamination. Joint release that considered final moisture, block strength, and disintegration was preferable to any single indicator [43–46]. Systematic reviews of rice wine processing likewise highlighted that the advantages of xiaoqu in storage stability and downstream consistency arose from parameterized management at the drying endpoint and during curing rather than from a fixed operating number.

As the interface of the rice-based dual fermentation, xiaoqu also paced dosing. Instead of enumerating numerical ratios or temperatures, two matches were stressed. The substrate temperature before dosing needed to return to a medium range to reduce thermal stress and protect the enzyme system. The dosing ratio needed to align with the degree of cooking and bed thickness so that the kinetics of saccharification in the front half and alcohol formation in the back half remained matched, and phase mismatch in sugar to alcohol conversion was avoided. This coordination of temperature, dose, and loading was key to strong initiation, steady conversion, and predictable flavor, and it matched the engineering features of short room temperature incubation and mild drying in xiaoqu to form a continuous and controllable chain from inoculation to main fermentation [42,45].

For quality control and standardization, window type indicators were preferred over rigid single points at process endpoints. An upper window of qu acidity was used to judge whether moisture loss and acid accumulation during incubation were acceptable, and it was combined with final moisture, block strength, and disintegration for release. On the equipment side, fixed diameter and weight molds, zoned ventilation, and online temperature humidity monitoring reduced within-batch thermal and moisture gradients and improved consistency across seasons and facilities [42,47].

2.3. Hongqu (Hongqu/Monascus) Dual-Objective Engineering for Pigment and Aroma Production with Toxin Control

Hongqu was prepared on steamed rice as a solid-state koji. The process was framed as a compromise that maximized color and aroma while minimizing the risk of CIT within coupled boundaries of moisture, temperature, oxygen supply, and heat dissipation. Rather than listing fixed settings, these variables were treated as factors of one objective function (Figure 1C). Initial moisture and ambient relative humidity defined resistance to heat and mass transfer and also governed oxygen diffusion. The temperature program and aeration reshaped the profile of metabolic heat and the window for pigment synthesis. Practice indicated that a variable temperature profile with moderate moisture increased product activity and suppressed toxin accumulation. The reproducibility of the thermal and moisture trajectory was more critical than a single set point. A representative study achieved "not detected" CIT by staged temperature control with moderate moisture, which exempli-

fied optimization through process windows instead of point parameters [48]. Within this framework, excessive moisture caused agglomeration, reduced effective surface area, and hindered oxygen diffusion, which depressed coloration and created abnormal hot spots. Insufficient moisture limited metabolism and pigment formation. The temperature zone also showed an optimum band. Early overheating raised self-heating risk and induced by-metabolism, whereas overcooling delayed growth and synthesis. Programmed staging with gentle drying stabilized the metabolic route [49].

Equipment and bed design were aligned to uniform oxygen delivery with controlled heat removal and dehumidification. Compared with thin bamboo trays, perforated beds and rotary or recirculating-air devices shortened the initial lag and smoothed interlayer gradients. Batches then reached more consistent color and activity. These systems shaped the metabolic thermal history through bed homogenization and programmable temperature–humidity curves, which reduced intervention while stabilizing output [50]. Regardless of carrier or duct layout, the core objective was to reduce spatial stratification that produced hot interiors and cool exteriors and to hold parameter fluctuations within the target window so that process consistency yielded quality consistency.

Quality and compliance were integrated into one control loop. In Europe, products based on red yeast rice were controlled at a maximum level of 100 μg/kg for CIT, and market surveys reported exceedances. Production therefore linked parameterized pretreatment, bed heat–moisture management, programmed cooling, early mild drying, and endpoint release testing as one strategy. Source suppression was implemented in parallel with terminal quantification by HPLC or LC–MS/MS, which avoided reliance on a single end step [51]. Drying and deactivation were managed under a triple objective of stability, safety, and functional retention. Mild hot air and timely deactivation preserved pigments and functional components and enabled low-moisture storage. Source control along the chain was more feasible and cost-effective than post-process removal [52].

2.4. Fuqu/Jiangqu the Enzyme Engine for Salt-Tolerant Fermentation

Fuqu/Jiangqu used a composite matrix of wheat flour or bran with soybean or defatted soybean meal. The engineering aim was to build an enzyme engine that still worked efficiently during subsequent high-salt fermentation. The matrix ratio determined porosity and apparent moisture. It reshaped heat and mass transfer boundaries and the aw window during the koji stage (Figure 1D). Under the same temperature, humidity, and aeration, a bean-rich formula, a bean–wheat parity formula, and a bran-as-skeleton formula were not equivalent in enzyme profiles or salt-stage hydrolysis efficiency. These differences amplified regional process variations in flavor and in the release rate of amino nitrogen [53]. In this framework, the primary role of thermal treatment was not edibility. It lowered contaminant loads and stabilized microstructure, which provided an adherent, oxygen-permeable, and moisture-drainable base for *Aspergillus*. Thus, raw material histology and room climate acted as coupled variables that jointly determined enzyme trajectories rather than independent factors [53].

Inoculation and bed loading were treated as decisive parameters. Compared with dry sprinkling, liquid starters with metered spraying or rolling coatings improved spatial uniformity and synchrony of awakening. Bed positions then approached a shared thermal and moisture history, which reduced turning burden and early enzyme decline. Liquid inoculation validated gains in structure, pH, and key hydrolase activities and supported advantages of optimized bean to wheat ratios at the enzyme output, providing a reference for cost reduction and efficiency improvement on the raw material side of fuqu [54,55]. From bed geometry to oxygen supply paths, flat thin beds, multi-layer conveyors, and perforated rotary beds shared one goal. They maintained boundaries that allowed heat

removal, moisture discharge, and uniform oxygen supply at the bed scale. Thickness switching and zoned ventilation functioned as process tools to offset metabolic heat peaks and local hypoxia. Their performance finally appeared in color, odor, and enzyme protein stability within the same batch [55–57].

Control of temperature, humidity, and aeration shifted from set points to trajectories. Static settings of a single temperature or relative humidity could not satisfy germination, hyphal spread, and secretion phases at once. A dynamic coupling of temperature control, moisture retention, oxygen supply, and heat removal used time-segmented turning and aeration to manage heat peaks and to dissolve interlayer gradients. This supported spatially uniform maturation and temporally stable enzyme production. The direct benefit was stable salt-stage hydrolysis and predictable flavor precursors without extra enzyme addition [56,57]. Release criteria at the end of koji making were also shifted. Empirical judgments based on color and hand feel were weakened. Structural integrity, moisture, and functional enzyme activities formed composite thresholds for release as auditable and reproducible control points [58].

The final test occurred after salting. High salt marsh or low-salt solid systems inhibited *Aspergillus* growth, yet the extracellular enzymes formed and anchored in the solid phase during the koji stage carried the main hydrolytic task. Each upstream adjustment of moisture, heap geometry, aeration, and turning was magnified through a chain of porosity, heat generation, enzyme profile, and salt-stage stability. It then appeared as differences in the formation rates of soluble amino nitrogen and reducing sugars and in flavor layering of moromi. Treating formulation, bed loading, oxygen supply, and heat removal as an integrated process design rather than a disconnected checklist was the key path by which fuqu/jiangqu moved from artisanal experience to industrial consistency [53–58].

2.5. Douchi-Qu: Process Branches of Multi-Type Starters

The qu making for douchi was the first half of a two-stage process. The goal was not a fixed set of optimal parameters. The goal was to build a stable and scalable starter on cooked soybean or black soybean surfaces. This starter provided a reproducible enzymatic base and a physical interface for later salting and maturation. From a process view, preprocessing, inoculation, and qu formation formed a continuum of heat and mass transfer with community assembly (Figure 1E). Raw material cooking set pore structure and bound water. Cooling and inoculation set initial colonization and contamination risk. Bed arrangement and room climate set the coupling efficiency of metabolic heat release and transfer paths. It was more useful to identify sensitive variables, their interactions, and the trade-offs across process branches than to list formulas, times, and thicknesses [59].

Moisture, aeration, and bed thickness acted as the main coupled factors during qu formation. Excess kernel moisture weakened oxygen diffusion and enlarged heat accumulation. Insufficient moisture limited hyphal front advance and extracellular enzyme secretion. Poor aeration caused an inner hot and outer cool gradient. Excess aeration caused dry crust and local desiccation. A very thick bed increased vertical thermal resistance. A thin bed improved heat removal and vapor migration but required stricter control of airflow uniformity and floor space. Practice showed that better outcomes were achieved by moderate moisture with directed aeration and a medium bed to balance the heat and moisture field. This setting supported continuous oxic metabolism and avoided overlapping of peak temperature and rewetting risk in space. Window ranges rather than point values reduced batch and seasonal effects and eased scale transfer [59].

Three main process branches were present. Their differences lay in rhythm, boundary conditions, and endpoint control. The *Aspergillus*-led route used a fast rhythm and higher process controllability. Stable room temperature and humidity with uniform spreading

rapidly built hyphal networks and multi-enzyme systems. It supported clear release criteria and smooth transfer to salting. The cycle was short and scalable, but it relied more on uniform cooling and inoculation [60]. The *Mucor* or *Rhizopus* route emphasized thin layers and zoned aeration to relieve interlayer heat build-up and to keep controllable water gradients. The cultivation period was longer and often used mild washing and pre-drying to stabilize the qu–salt interface moisture. It gave typical texture shaping and flavor precursors and was more sensitive to airflow organization and final drying strategy [61]. The bacteria-led or bottled solid route changed container scale and thermal resistance to gain a more uniform heat and moisture field with lower contamination risk. It suited standardized and clean production. It needed container geometry and loading design to compensate for the loss of environmental diversity seen in open beds. It improved uniformity while weakening environmental selection pressure [62]. Comparative studies showed repeatable differences in time constants. *Aspergillus* and *Rhizopus* routes ran on tighter rhythms. *Mucor* routes required a longer enzyme-building stage. This pattern supported planning and equipment use without fixing a single duration [63]. Temperature trajectories described engineering quality better than single points. Many flows used a moderate initial rise, a stable platform, then a slow decline to match hyphal expansion and extracellular enzyme peaks. Control focused on the rate of rise and platform stability to avoid core overheating and on a gentle final decline to promote water redistribution and reduce crusting. The *Aspergillus* route favored a stable platform for sustained secretion. The *Mucor* or *Rhizopus* route was more sensitive to the heating gradient and airflow direction. Bottled processes relied on both environment and container control to achieve equivalent management. Trajectory design was prioritized over absolute values [59–62].

Release endpoints and interface moisture set salt diffusion rate and osmotic shock in the salting stage. Overwet endpoints caused local dilution and osmotic oscillation at the start of brining. Overdry endpoints inhibited brine penetration and affected precursor migration and conversion. Each route used short pre-drying, warm water washing, or natural re-softening. The aim was not a single moisture number. The aim was to place qu moisture and surface state within a reproducible interface range. Stable salt diffusion, proteolysis, and flavor release kinetics were then obtained. This approach emphasized endpoint ranges. It allowed predictable maturation under different seasons and equipment conditions [60,61].

In sum, process design for multi-type douchi starters began from variable sensitivity and coupling. A ternary set of moisture, aeration, and thickness shaped a controllable heat and moisture field. Temperature trajectories rather than point values aligned hyphal expansion and enzyme profiles. Endpoint ranges rather than a single moisture value secured seamless handover to salting. Within this frame, different branches balanced cycle time, uniformity, and flavor potential [59–63].

2.6. Sufu Qu Preconditioning Engineering for Cheese Like Texture

Sufu-qu functioned as the key transition from a tofu matrix to a controllable mold curd and established a stable entry point for the enzyme–texture interface required by salting and ripening. The aim of the pretreatment was to tune substrate moisture, pore structure, and initial microbial load to support surface growth of molds while keeping internal integrity (Figure 1F). Common coagulants such as bittern or gypsum with moderate pressing created a balance between high moisture and connected pores, which afforded adhesion and spreading of the mycelial layer and penetration of extracellular enzymes. Standardized heat treatment and inoculation reduced interference from undesirable microbes and improved within-batch consistency. These factors jointly determined the uniformity of mold coverage and the reproducibility of the enzyme system during the qu-making stage [64,65].

Room cultivation was governed by coupled optimization of temperature, humidity, and time. Moderate temperature and near-saturation humidity provided a permissive range for white-mold sufu to grow and secrete enzymes, yet strains responded differently within this range. Lower temperature with a moderate cultivation period favored a continuous, compact mycelial layer and balanced surface water loss with internal migration. Higher temperature or shorter cultivation can raise single-enzyme activities but tended to cause surface crusting or internal heat build-up, which enlarged within-batch variation. Evidence indicated that the preferred window was defined by stable output of combined protease, lipase, and amylase rather than a peak of one enzyme, which protected mold quality and the stability of later texture formation [66].

Tray geometry and airflow organization determined spatial uniformity of oxygen supply and heat release. Thin-layer loading, spaced stacking, and zoned supply–return air managed evaporative cooling and removal of metabolic heat at the bed scale and reduced thermal stratification and end cracking. Matching inoculation with loading strategies shortened awakening heterogeneity and cut the need for frequent turning. Process monitoring of gap size and face velocity helped maintain similar thermal–moisture trajectories across batch sizes and equipment and achieved spatial consistency of thermal history in the same chamber [67–69].

Release criteria and interface moisture were anchored to whether salting could proceed stably while preserving texture–flavor synergy. Fingerprint-style indices were preferred over a single endpoint. Coverage and continuity of the mold layer, stable ranges of moisture and soluble solids, and mechanical integrity with predictable salt uptake served as the basis for release. For products requiring a denser surface and a finer cheese-like mouthfeel, a lower temperature with a modestly extended cultivation was used while maintaining high humidity and avoiding excessive convection to keep interface continuity. In summary, a method chain that linked tofu substrates of fixed size and loading, a short moderate-temperature high-humidity window, harmonized tray airflow, and release standards centered on functional enzyme spectra, and texture intake was adopted. This approach enabled reproducible sufu molds in non-aseptic and scaled environments and provided a benchmarked pretreatment interface for subsequent salting and flavor maturation [65,70].

3. Microbial Diversity and Community Ecology

3.1. Daqu Communities, Temperature-Regime Driven Assembly, and Functional Differentiation

Daqu was an open solid-state composite inoculum. Community assembly was strongly driven by the temperature regime, defined by the highest temperature reached during making. By peak temperature it was grouped as low temperature at about 40–50 °C, medium temperature at about 50–60 °C, and high temperature at about 60–70 °C. This stratification matched distinct thermal histories during making and systematic differences in community composition and functional outputs. A representative study on strong-aroma daqu tracked the full course from making to storage, defined these temperature zones, and compared co-evolution of community structure and physicochemical indices [71].

The primary driver role of temperature appeared in quantitative shifts in alpha and beta diversity and in replacement and enrichment of core taxa. For medium-temperature daqu (MT-Daqu), mature inner and outer layers reached 625–773 and 597–632 OTUs, respectively, by 16S or ITS sequencing, showing a spatial heterogeneity with higher richness at the center. At the genus level, *Bacillus* dominated bacteria, with 47.02% relative abundance in the inner layer versus 21.07% in the outer layer, while *Saccharopolyspora* reached 6.11% in the outer layer versus 0.79% in the inner layer. Counts of aerobes and yeasts dipped when the temperature rose to about 60 °C on day 17, then recovered during storage and

stabilized after three months. This indicated coupling between the heat peak, slow cooling, and maturation and the restructuring of the community [71].

High-temperature daqu (HT-Daqu) under stronger heat stress showed a dual dominance by thermotolerant bacteria and fungi. A regional comparison across four HT-Daqu samples from core producing areas in northern Guizhou and adjacent Sichuan and Chongqing found *Desmospora* sp. 8437 as a consistent dominant taxon at 3.6–7.3% by metagenomics. *Bacillaceae* correlated positively with differences in saccharifying and proteolytic power and with pyrazine levels. *Kroppenstedtia* associated with variations in aldehydes and ketones, revealing redundancy and division of labor among functional cores under similar thermal histories. This work also noted production peaks up to 60–75 °C in HT-Daqu, supporting the chain of high temperature, thermotolerant communities, and strong pyrazine- and protein-cleaving capacity [72]. At finer time scales, heat pulses promoted a phylum-level shift toward Firmicutes. Parallel monitoring of sauce-aroma HT-Daqu made by hand or machine showed that, over 40 days, Firmicutes rose from 43.15% and 27.16% to 93.10% and 97.88%. Proteobacteria fell from 41.13% and 54.26% to 6.53% and 1.50%. At the genus level, Lentibacillus rose to 72.19% and 40.16% by day 40. This showed that spore-forming, salt- and heat-tolerant bacilli gained overwhelming advantages in the high-temperature window. The differences indicated that even with different forming methods the thermal history remained the first cause deciding the core taxa [73].

In contrast, low-temperature daqu (LT-Daqu) showed a yeast–lactic acid bacterium cohabiting signature in the initial community. In a multi-omics study of light-aroma systems, mature daqu contained Ascomycota at about 39%. At the genus or species level, *Pichia* at 33.2% and *Lactobacillus* at 17.4% were dominant. At the start, *Pichia* and *Lactobacillus* were 24.0% and 20.7%. Yeasts then declined while lactic acid bacteria increased as fermentation progressed. This reflected a mild thermal history with rising acid stress and takeover by LAB. The pattern matched the lower peak temperature of LT-Daqu and explained a gentle co-platform for saccharification and acid production [74].

Different temperatures changed what was present and what each group did. In MT-Daqu, the dominant filamentous fungi split by position. *Aspergillus* and *Rhizopus* were enriched inside. *Thermomyces*, *Thermoascus*, and *Rhizomucor* were enriched at the surface. On the bacterial side, *Bacillus* dominated inside and *Saccharopolyspora* at the surface. This pointed to inner-layer priming of starch and protein hydrolysis, surface-layer dominance in thermotolerant enzymes, lipolysis, and conversion of volatile precursors. In HT-Daqu with color types, bacterial alpha diversity by Chao and Shannon showed a dip followed by a rise in maturity, and dominant genera differed among colors. Black qu was dominated by *Kroppenstedtia*, which rose to 68.20% on day 30 then fell to 3.11% on day 180. Yellow qu favored *Virgibacillus*. White qu kept *Bacillus* above 80% and maintained higher fermentative activity. Fungi were commonly centered on *Thermoascus*. These results showed that heat history and acidity reshaped the functional core by selection pressures and that new steady states formed during maturation and storage [30,71].

Taken together, temperature regime, community assembly, and functional differentiation followed three representative ecological routes. First, LT-Daqu formed a mild community at lower peaks with yeast and LAB synergy that supported early coupling of saccharification and acid production. Second, MT-Daqu formed an inner–outer division of labor under moderate peaks and higher inner alpha diversity, with *Bacillus* plus filamentous fungi such as *Aspergillus* or *Rhizopus* inside versus *Thermomyces* or *Thermoascus* at the surface. Third, HT-Daqu under high heat pulses and extended holds selected thermotolerant core bacteria such as *Bacillaceae*, *Kroppenstedtia*, and *Desmospora*, which coexisted with thermotolerant fungi such as *Thermoascus*. Community function shifted toward efficient cleavage of proteins and polysaccharides and formation of nitrogen-heterocycle flavor

precursors. Multi-source sequencing and metagenomic quantification including relative abundance, OTU or ASV counts, alpha diversity indices, and time–space comparisons supported these conclusions and reflected a temperature-history-centered ecological rule in Chinese solid-state fermentation.

3.2. Xiaoqu Communities, a Rhizopus–Saccharomyces–Lactic Acid Bacterium Symbiotic Network

Compared with daqu, rice-based xiaoqu showed fewer core genera with more pronounced dominance. This allowed rapid formation of a functional network based on molds, yeasts, and LAB early in fermentation. A comparison of Cantonese fire-aroma or chi-aroma and rice-aroma systems reported fewer species in xiaoqu than in daqu. *Rhizopus*, *Saccharomyces* and related yeasts, and LAB still supported integrated saccharification and alcohol fermentation. This indicated a small but efficient configuration as the ecological background [75].

In rice-aroma baijiu, the fungal side showed dual dominance of molds and yeasts. At the genus level, *Saccharomyces* reached 7.06–83.50% and *Rhizopus* 15.21–90.89%. In xiaoqu itself, *Saccharomyces* once reached 88.41%. After inoculation, *Rhizopus* rose rapidly from 15.21% and peaked at 90.89% on day 10. This formed a relay with molds driving saccharification and yeasts producing alcohol. On the bacterial side, LAB dominated. Across xiaoqu, saccharification, and fermentation, *Lactobacillus* reached 62.88–99.23% and reached 99.23% at the end. In xiaoqu itself, the top four bacteria were *Weissella* at 59.53%, *Pediococcus* at 29.18%, *Acetobacter* at 3.65%, and *Lactobacillus* at 1.35%. This showed an assembly that opened with *Weissella* and *Pediococcus* in the starter and then shifted to *Lactobacillus* after vatting [76]. Multi-omics work also revealed the source and assembly logic. In a rice-aroma system, xiaoqu held 383 bacterial species yet shared only 48 with day-0 mash and only 10 with the end of fermentation. In contrast, xiaoqu held only five fungal species. Xiaoqu therefore provided the core framework with *Rhizopus* and *Saccharomyces*, while many bacteria entered later from raw materials and the environment and were reshaped under acid stress as LAB rose. Dominance was highly concentrated. During rice-aroma fermentation, the top five bacterial genera, *Lactobacillus*, *Weissella*, *Pediococcus*, *Lactococcus*, and *Acetobacter*, exceeded 97%, giving the community a strong acidifying tendency [76].

Cross-system evidence reinforced a three-stage symbiosis of *Rhizopus* first, yeast takeover, and LAB steady state. In parallel monitoring of hongqu rice wine and xiaoqu rice wine, *Rhizopus* in xiaoqu reached 32.14% in the starter, jumped to 80.69% on day 2, and stabilized near 50% mid-fermentation. This matched the rising trend of *Rhizopus* in rice-aroma baijiu and pointed to a shared path of rice substrate, mold saccharification, and acid-mediated competition. Late dominance by *Lactobacillus* near 99% coincided with accumulation of ethyl lactate. In rice-aroma systems, ethyl lactate often exceeded ethyl acetate, and 2-phenylethanol could reach more than ten times the sum of those two. This reflected coupling between lactic acid, ethanol, and ethyl lactate driven by LAB and yeasts [76,77].

From a coupling view, metabolism in xiaoqu communities focused on energy and structural substrates. An integrated metagenome and metabolome study of traditional Guizhou xiaoqu showed that metabolic functions accounted for 58.16% of microbial genes, followed by genetic information processing at 12.57% and organismal systems at 8.29%. Carbohydrate metabolism, cofactors and vitamins, and amino acid metabolism were the most enriched pathways. This matched the division of labor in which *Rhizopus* supplied sugars, yeasts produced alcohol, and LAB shaped an acid environment and drove ester precursors. *Rhizopus*–*Saccharomyces*–LAB was thus not a simple inoculation trio. In a rice-based solid environment, it formed a self-organized network through substrate release,

control of pH and redox, and selection pressures. Core quantitative features including genus-level abundance ranges, assembly overlap, and functional enrichment showed consistency across independent lines of study [78].

3.3. Hongqu Communities, Monascus-Centered Secondary-Metabolism Ecology

Rice-based hongqu, also known as red koji or red yeast rice, was a fungal-led and multi-domain solid micro-ecosystem centered on *Monascus*. *Monascus* led early fungal establishment at the community level and determined pigment, lovastatin, and mycotoxin potential such as citrinin through multiple biosynthetic gene clusters. In practical dynamics, *Monascus* often dominated at the start after inoculation. *Saccharomyces* then became dominant after day 3. *Aspergillus* could also co-dominate with yeasts in some systems and in comparisons of xiaoqu rice wines and hongqu or huangjiu. This *Monascus*-first and yeast-takeover trajectory was repeatedly observed in metagenomic studies of hongqu rice wine [79,80].

Joint metagenomic and metabolomic analyses depicted *Monascus*-driven coupling. In a comparison of high- and low-biogenic-amine systems for hongqu rice wine, *Monascus*, *Saccharomyces*, and *Aspergillus* were the three core fungal genera. In high-amine systems, *Monascus* dominated early and *Saccharomyces* became absolutely dominant after day 3. In low-amine systems, *Aspergillus* plus *Saccharomyces* co-dominated and *Monascus* declined. Species–metabolite networks showed significant associations between dominant fungi and volatiles or amines derived from amino acid metabolism. This suggested that *Monascus* shaped the substrate framework and pH or redox through pigments, organic acids, and polyketides in the early stage, which created conditions for later takeover by yeasts and LAB [79].

Community and metabolism also differed by regional hongqu types. In two widely used types, Gutian qu and Wuyi qu, *Monascus* species dominated in the former. The two types showed distinct pathway enrichments for fungal communities and flavor formation during fermentation, indicating that the *Monascus*-centered niche varied in strength and direction among types. These differences were also reflected in enrichment of downstream metabolic routes such as amino-acid-derived volatiles and in abundance networks of key enzyme genes [81].

Monascus secondary-metabolism ecology was not single-track. Potential for monacolin K varied greatly among species and strains. An industrial M. pilosus reached 9.5 mg/g MK under optimized solid-state conditions with no CIT detected, while some *M. purpureus* lacked MK loci. In co-culture with yeasts or LAB, reports noted pigment up-regulation with toxin down-regulation or broader profile shifts. This indicated a self-organized system modulated by interaction signals such as fatty acids and pH. Cross-level indicators including gene cluster length and composition, gene counts, time nodes, and product concentrations supported this picture. Through its BGC architecture and expression program, *Monascus* set energy and carbon flows in hongqu communities and guided time-scale rearrangement and stabilization across sugar, amino acid, and polyketide networks.

3.4. Fuqu and Jiangqu Communities, a Relay Between Koji-Stage Molds and Salt-Stage Moromi Bacteria

Fuqu or jiangqu systems showed a two-stage ecological relay. The first stage was the koji period on bran–soy or wheat substrates. The second stage was the high-salt dilute moromi. In the solid and oxygen-rich koji stage, filamentous fungi and facultative salt-tolerant bacteria expanded rapidly and assembled a high-throughput hydrolytic enzyme pool. After transfer into moromi at 18–22% NaCl, the hypertonic, low-oxygen liquid selected salt-tolerant LAB and halophilic yeasts. Diversity converged over time on a few core groups. The ecological task shifted from enzymatic breakdown to salt-phase

conversion. Under typical practice, the koji stage lasts about 26 h to 7 days. Moromi at 18–22% NaCl lasted about 3–6 months [56,57]. During koji, the relative abundance of molds rose together with some early colonizing bacteria. In samples from industrial high-salt diluted soy sauce, *Aspergillus* and *Weissella* rose from 0.98% and 0.31% to 38.45% and 30.41% within 0–48 h. Amino acids and volatile precursors accumulated markedly, providing substrates and exogenous enzymes for moromi. The study also noted that a solid, well-ventilated, and high-humidity room near 95% supported coexistence of fungi and facultative salt-tolerant LAB, which anticipated the later salt-stage relay [56].

After mixing koji with brine, salinity and oxygen transfer became decisive filters. In a metagenomic comparison of Japanese-style and Cantonese-style moromi, Tetragenococcus rose from 0.02% to 59.2% between days 7 and 120 in the Japanese style. In the Cantonese style at 120 days, Tetragenococcus and Staphylococcus reached 36.7% and 29.7%. Koji-borne fungi rapidly moved to the margins in moromi. *Aspergillus* averaged up to 18.2% early in the Japanese style or 10.93% in the Cantonese style but fell to 0.65% or less by the end. At the family or phylum level, Aspergillaceae signals dropped from 33.0% and 17.5% to 0.13% and 0.67%, while the whole community shifted toward bacteria. Bacterial sequences rose from 59.3% to 98.5% in the Japanese style. These data pointed to high salt suppressing continued growth of koji-borne molds and opening niches for salt-tolerant LAB and cocci that drove late acidification and nitrogen- and carbon-backbone conversions [82]. The physiology behind this relay matched salt-tolerance limits. Tetragenococcus halophilus grew at up to about 20% NaCl and showed an optimal zone often at 5–10% yet retained activity at higher salinities, which matched 18–22% NaCl in moromi and gave it a competitive advantage to control organic acid and amino acid routes [83,84]. The osmophilic and halotolerant yeast *Zygosaccharomyces rouxii* also adapted at 18% NaCl and contributed to flavor metabolism. Transcriptomic and lipidomic data showed higher unsaturated fatty acids under salt and formation of key flavor precursors such as 3-methyl-1-butanol and 2-phenylethanol [85–88]. Dominant taxa in moromi were not fixed. They were coupled with temperature and aeration strategies. With the same koji, Japanese-style practice near 25 °C with some stirring favored Tetragenococcus and *Weissella*. Cantonese-style practice at 18–22 °C with little stirring often favored Staphylococcus and higher *Bacillus* signals. This temperature–oxygen coupling explained metabolic and flavor differences among process families at the same salinity and again verified the general relay from enzyme supply during koji to salt-phase metabolism during moromi [82].

3.5. Douchi-Qu Communities, Typified Assembly

Douchi fermentation followed three stages with an initial starter, a natural microbial pool, and salt-driven post-ripening. Community assembly showed distinct typification. By dominant microbes, it was grouped as *Aspergillus*-type, *Mucor* or *Rhizopus*-type, and bacterial-type, with some sources listing non-inoculated and bacteria-led products as the bacterial type. This classification matched the types of starters and environmental exposure and determined dominant phyla and metabolic potential downstream. Recent work found that industrial and household samples contained all three lineages, with *Aspergillus*-type and bacterial-type being the most frequent. These two showed different emphases in aroma and amino-acid-release routes. In two traditional bacterial-type douchi from Gansu, 16S and ITS data showed *Bacillus*, *Ignatzschineria*, *Proteus*, and *Providencia* as dominant bacteria. *Pichia*, *Candida*, and *Rhodosporidium* were dominant fungi. This indicated that without a mold starter, bacteria and yeasts could still build a backbone network for fermentation and flavor [89].

In *Aspergillus*-type douchi, community succession showed a reproducible turn from molds to yeasts or bacteria. High-throughput tracking of Yangjiang samples showed that

molds accounted for about 70% of the fungi during early koji making. Yeasts then rose rapidly in later fermentation and reached about 90%. The two then approached balance at the end. This indicated niche replacement within fungi and staged differences in substrate use [90]. At finer time scales, the koji stage was dominated by Staphylococcus and *Weissella*. Later, *Bacillus*, *Corynebacterium*, and *Acinetobacter* rose. *Weissella* rose from 34.05% to 48.79% on days 1–3 then fell to 2.6% and rose again to 15%. This reflected short-cycle fluctuations under salt penetration and substrate shifts. At the phylum level, bacteria were dominated by Firmicutes, Actinobacteria, and Proteobacteria. Fungi were dominated by Ascomycota and Zygomycota [91–93]. These results indicated that the starter not only supplied early enzymes but also built a micro-ecological base through a mold-dominant window for later salt- and acid-tolerant members to take over. Compared with *Aspergillus*-type, *Mucor* or *Rhizopus*-type samples showed different dominant mold sets and co-occurrence networks during the koji stage. A comparison of the two types reported that *Aspergillus*, *Candida*, Meyerozyma, and Lecanicillium shared dominant fungal genera in more than half the samples during koji. Relative abundance and interaction strength differed systematically between types. Although that work focused on taste indices, its community-level results provided direct evidence for typified assembly [94]. Bacterial-type douchi was seen as a no-mold or bacteria-led model. Across regions, Firmicutes dominated. *Bacillus* was often the dominant genus. *Candida*, *Millerozyma*, and *Lichtheimia* co-appeared in some samples, indicating a bacteria-led sample with yeast-supported symbiosis [95,96]. In summary, *Aspergillus*-type douchi formed a stepwise replacement of molds, yeasts, and bacteria during making and fermentation, *Mucor* or *Rhizopus*-type differed in the mold set during koji with resulting differences in taste precursors, and bacterial-type used *Bacillus* and related Gram-positive rods as the backbone with osmotolerant yeasts to deepen flavor during post-ripening.

3.6. Sufu Pehtze Communities, Mold–Bacterium Synergy for Texture and Flavor

Sufu production started from molded tofu, or pehtze. It was a filamentous fungus-led system that formed early interactions with bacteria. Sequencing across stages showed that the pehtze fungus community was built around the inoculated mold and held absolute dominance. In mixed black- and yellow-soy sufu, *Rhizopus* reached 77.96% and 93.35% relative abundance at the pehtze and salted-pehtze nodes. At the phylum level, *Mucoromycota* was enriched during pre-fermentation, while Ascomycota and Basidiomycota were enriched during later stages. Bacteria kept high alpha diversity throughout. This indicated that while molds controlled structure during pehtze, a bacterial baseline already existed and influenced later flavor and texture. In the mid to late post-fermentation, bacterial communities converged toward Enterococcus, Enterobacter, and in some cases *Bacillus*. This showed a path of early mold dominance followed by bacterial convergence [97].

From a community–function view, extracellular hydrolases formed during pehtze set the substrate supply for later softening and flavor precursors and shaped niches for companion bacteria. In full-factor tests at 25–35 °C and 73–97% RH over 12–60 h, *Rhizopus* oligosporus reached growth and enzyme activities comparable to *Actinomucor* elegans at temperatures of about 10 °C higher. This suggested ecological substitution potential in hot seasons. These quantitative results across temperature, humidity, time, and enzyme output explained why *Actinomucor* commonly laid the fine basis for cheese-like texture and why introducing *Rhizopus* under hot conditions still maintained protein and oligosaccharide cleavage and supplied amino acids and fermentable sugars for later bacterial metabolism [98].

Bacteria were not absent during pehtze. They acted as molded collaborators. Classic surveys of commercial sufu showed LAB at 10^5–10^7 CFU/g in white sufu, indicating

that salt- and acid-tolerant bacteria gradually took over parts of acidification, amino acid decarboxylation or conversion, and ester-precursor supply across pehtze, salting, and ripening. In line with this, community comparisons of commercial red and white sufu found significant differences in relative abundance of Firmicutes and Proteobacteria at $p < 0.01$ and significant genus-level differences for *Lactococcus* and Tetragenococcus between products at $p < 0.01$. This revealed directions of bacterial convergence under high salt and suggested that amino acid and organic-acid spectra formed by molds during pehtze exerted feed-forward effects on bacterial assembly in different product lines [99,100].

Core pehtze fungi had been delineated for sources and key members. Identification of commercial starter molds from factories in provinces of China and in Vietnam showed *Actinomucor repens*, *A. taiwanensis*, *Mucor circinelloides*, *M. hiemalis*, *M. racemosus*, and *Rhizopus microsporus* var. microsporus as a stable starter pool. Phylogeny showed *Mucor* and *Actinomucor* as closer and *Rhizopus* as more distant. The cross-regional stability of this pool explained the commonality of similar appearance and texture at the pehtze stage, while later bacterial differences by region appeared more in salting and ripening stages through metabolic and flavor divergence [101].

Overall, the sufu pehtze ecology followed three elements. Molds laid the base. Core filamentous fungi such as *Actinomucor*, *Mucor*, and *Rhizopus* released high-throughput proteases and glycosidases within 24–60 h and supplied utilizable nitrogen and oligosaccharides. Bacteria were pre-loaded. They remained at low abundance and high diversity early, then converged under high-salt and low-oxygen selection toward LAB and *Bacillus* and took over. Co-formation of flavor and texture followed. Enzyme flux and substrate spectra during pehtze set the material landscape for later acidification and esterification and drove the depth of cheese-like texture and flavor. This self-organized mold–bacterium synergy was indicated by stage-wise relative abundance values such as *Rhizopus* at 77.96–93.35% [97].

As shown in Table 1 and Figure 2, the community structures of the various starter cultures were shaped by environmental filtering dominated by heat history, substrate, and salinity, and were coupled to flavor formation and quality stability through a spatiotemporal relay of enzyme production and conversion. In summary, the temperature type of daqu acted as the primary constraint on assembly and functional differentiation. High-temperature daqu enriched Firmicutes and thermotolerant fungi under heat pulses and drove protein and polysaccharide cleavage and pyrazine-related metabolism, whereas low-temperature daqu favored a mild platform of yeasts and lactic acid bacteria, reflecting an ecology guided by thermal history. Xiaoqu formed a compact triad composed of *Rhizopus*, *Saccharomyces*, and lactic acid bacteria that rapidly completed the relay from saccharification to ethanol production and acidification. Hongqu was centered on *Monascus*, which regulated pigment and polyketide networks through secondary-metabolism gene clusters and interacted with yeasts over time. The soy sauce system exhibited a two-stage relay in which the koji stage supplied enzymes and the moromi stage selected salt-tolerant metabolism, with Tetragenococcus and *Zygosaccharomyces* gaining ecological advantage under high salt to drive acidification and the formation of key flavor precursors. Douchi and sufu showed, respectively, typified assembly and a cooperative path in which molds laid the foundation and bacteria followed, thereby completing a continuous ecological design from the initial starter to late maturation.

Table 1. Summary overview of microbial diversity and community ecology.

System	Ecological Driver and Key Boundaries	Dominant/Core Taxa (Genus Level)	Functional Orientation and Representative Metabolism	Typical Spatiotemporal Features
Daqu—low temperature	Lower temperature regime; mild heat stress; acidity gradually increased	*Pichia*, *Lactobacillus*, etc.	Saccharification and acid production proceeded in parallel, forming a gentle metabolic base	Early yeast dominance followed by LAB takeover; smooth succession
Daqu—medium temperature	Moderate peak temperature; spatial structure with a "more enriched center layer"	*Bacillus* (higher in the inner layer), *Saccharopolyspora* (higher in the outer layer); filamentous fungi *Aspergillus*, *Rhizopus*, *Thermomyces*, *Thermoascus* co-occurred with layer preferences	Inner layer favored primary hydrolysis of glyco-/proteinaceous substrates; surface favored thermotolerant enzymes and lipolysis jointly drove flavor precursor conversion	Community reassembly coupled to "heat peak–slow cooling–maturation"; stabilization during storage
Daqu—high temperature	Strong selection by high-temperature pulses and extended holding	*Bacillaceae*, *Kroppenstedtia*, *Desmospora* with thermotolerant fungi (e.g., *Thermoascus*); *Lentibacillus* dominated in the high-temperature window	Efficient cleavage of proteins/polysaccharides and generation of nitrogen-containing flavor precursors; pyrazine-related pathways active	α-diversity decreased then increased; functional core reshaped; Firmicutes proportion markedly increased
Xiaoqu community	Rice-based solid state with few core genera and concentrated dominance	*Rhizopus*, *Saccharomyces*, *Lactobacillus* (with *Weissella*/*Pediococcus* at the start)	Mold-led saccharification, yeast-driven alcohol fermentation; LAB established an acidic environment and coupled to ethyl lactate formation	Three-stage symbiosis: "*Rhizopus* first—yeast takeover—LAB steady state"; xiaoqu provided the core backbone while the environment supplied additional bacteria
Red koji community	*Monascus*-led and biosynthetic gene clusters (BGCs) steered metabolism; pigment/lovastatin outputs balanced against CIT risk	*Monascus*, *Saccharomyces* (with *Aspergillus* in some systems)	Pigment and polyketide synthesis; subsequent yeast and LAB co-modulated flavor; CIT was modulated by strain and interactions	Succession of "Monascus leading—yeast takeover"; pathway enrichment differed across starters
Wheat-bran/soy-sauce koji community	Two-stage ecological relay: solid-state, oxygen-rich koji → high-salt, low-oxygen moromi	Koji stage: *Aspergillus* with early colonizing bacteria; moromi stage: *Tetragenococcus*, *Staphylococcus*, *Zygosaccharomyces* rouxii and other halotolerant members	Front end built an extracellular enzyme library and depolymerized substrates; back end completed acidification and N/C-skeleton transformations at 18–22% NaCl	Fungal signals decayed rapidly in moromi; bacterial diversity converged over time; temperature–oxygen strategy shaped dominant genera

Table 1. *Cont.*

System	Ecological Driver and Key Boundaries	Dominant/Core Taxa (Genus Level)	Functional Orientation and Representative Metabolism	Typical Spatiotemporal Features
Douchi-qu community	Typified assembly across "starter—natural microbial pool—salt infiltration and ripening"	*Aspergillus*-type, *Mucor*/*Rhizopus*-type, and *bacterial*-type; *Bacillus* dominated in the bacterial type	*Aspergillus*-type relied on mold leadership with subsequent yeast/bacterial relay; bacterial type depended on a *Bacillus* backbone with osmotic-tolerant yeasts to deepen flavor	Stepwise succession; systematic differences in co-occurrence networks and metabolic emphases
Sufu mold-curd community	Short-course, high-humidity molding; mold–bacterium synergy for texture	Core molds: *Actinomucor*, *Mucor*, *Rhizopus*; later convergence of LAB and Enterococcus	High-throughput extracellular hydrolases during molding shaped "cheese-like" texture and precursor supply; during salting/ripening, bacteria took over flavor formation	Molds built the base; bacteria took over under high osmotic/low-oxygen conditions; the starter mold pool was stable across regions

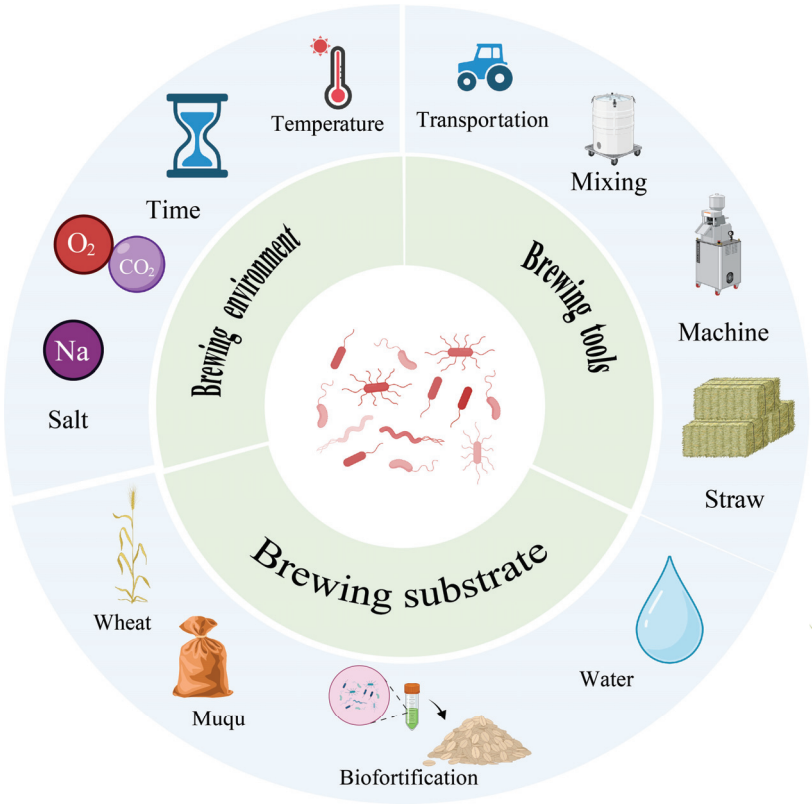


Figure 2. Linkage between engineering factors and microbial functions.

4. Food Application Spectrum Centered on Qu

4.1. Daqu as a General Engine for Distilled Spirits and Grain Vinegars

4.1.1. Coupling Between Baijiu Aroma Style and the Daqu Temperature Regime

As shown in Figure 3, in sauce-aroma baijiu production, high-temperature daqu with peak making temperatures of 60–65 °C provided thermotolerant enzyme systems and, through piling and airing before cellaring, promoted Maillard reactions and pyrazine

formation. This formed the base notes of sauce, roasted, and toasted characters. The process used stronger daqu dosing. A daqu to raw material ratio near 1:1 was reported as an industry trait. This helped maintain high enzyme activity and precursor supply across multiple fermentation rounds.

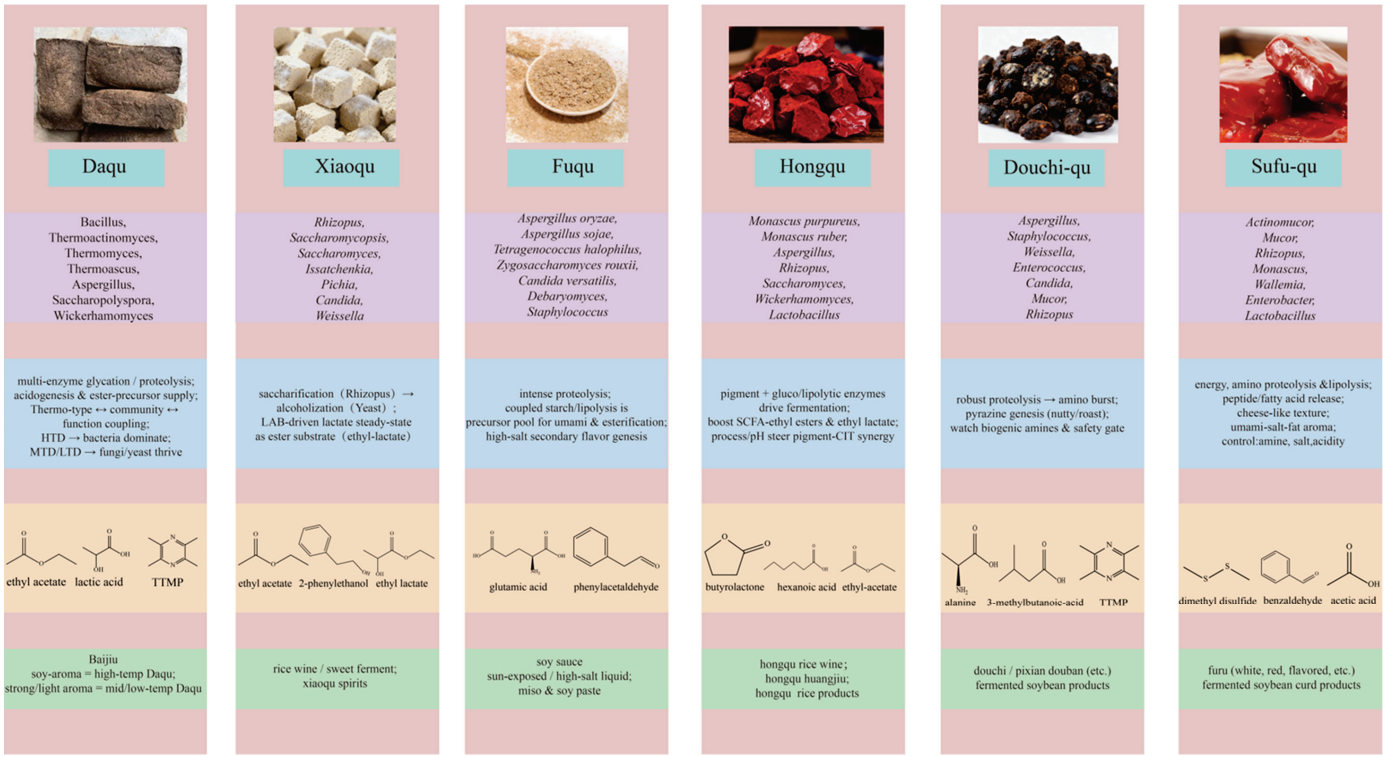


Figure 3. Schematic of the food application spectrum centered on qu.

During piling, the heap temperature rose to 48–55 °C before cellaring. Each round in-cellar lasted about 30 days. The full cycle often reached seven rounds. This reflected high daqu use, high temperature, and many rounds. The link between high-temperature daqu and directed pyrazine formation was quantified. By contrast, strong-aroma practice relied on medium-temperature daqu. The pit–mash system targeted high ethyl acetate and ethyl hexanoate. Recent work optimized parameters from the perspective of high ethyl hexanoate production and verified coupling with daqu dose and piling strategy. Medium-temperature daqu often acted with functional strains in solid-state systems; for example, yeasts selected for high ethyl hexanoate. Light-aroma practice relied more on the saccharification–alcohol fermentation efficiency of low- or medium-temperature daqu and on clean flavor output. Dependence on long pit aging was lower. The process emphasized stable saccharifying power and neutral or acidic protease activity of the qu [102]. Notably, different "color qu" inside high-temperature daqu, namely white, yellow, and black, showed measurable differences in saccharifying enzymes and neutral proteases. White qu was higher. This suggested that blending by inner-type and ratio allowed fine-tuning of flavor and buffering of quality variation during base spirit design [103–111]. These parameterized data connected temperature regime, daqu dose, heap temperature, number of rounds, and key flavor compounds to executable operating windows.

4.1.2. Daqu in Traditional Grain Vinegars

In grain vinegar exemplified by Shanxi aged vinegar and Zhenjiang aromatic vinegar, daqu based on barley or pea, also called vinegar qu or wheat qu, first drove starch saccharification and alcohol formation, and then the process entered solid-state acetification.

In the Shanxi aged vinegar specification, total acid stayed at or above 6 g/100 mL over years. This reflected efficient docking across qu, alcohol, and vinegar stages. In comparison with Zhenjiang aromatic vinegar, a dry-gelatinization route reached 16.2% v/v ethanol within five days versus six days and 13.9% by a traditional route. During acetification, total acid reached 7.178% w/v and 7.092% w/v at 18–20 days. This showed that higher upstream saccharification and alcohol conversion translated to stronger acid formation later. Other work found total acid commonly at 3.5–8.0 g/100 mL in grain vinegars. Acetic and lactic acids usually exceed 80% of total organic acids. Their ratio tracked the saccharified products such as glucose and dextrins and the ethanol formation rate during alcohol fermentation. Industry studies on community–process coupling in Zhenjiang aromatic vinegar across seasons and with qu addition or inoculation strategies confirmed that daqu quality and dosing altered the initial alcohol level and the slope of acid rise. They also changed the accumulation rates of key precursors such as acetoin and diacetyl. This set the final landscape of free amino acids and organic acids [112–114]. In short, the three-stage chain centered on qu in grain vinegar could be tuned directly and quantitatively to target acid and flavor by choosing the qu type, dosing, pretreatment, and inoculation strategy.

4.2. Xiaoqu in Southern Rice-Based Beverages and Local Baijiu

4.2.1. Household and Workshop Systems Such as Rice Wine, Sweet Rice Wine, and Black Glutinous Rice Wine

In rice-based beverages centered on xiaoqu, process control did not target high alcohol. It targeted a balance of high sugars, low alcohol, and soft acidity. This matched high saccharifying activity, mild ethanol formation, and moderate acidification supplied by xiaoqu. In sweet rice wine, recent evaluations showed low alcohol across treatments when traditional sweet xiaoqu was used. All groups stayed below 2.0% vol. This matched low conversion by xiaoqu yeasts and a preference to retain sugars, which suited sweet and glutinous products used in desserts or warm drinks [115]. Time–temperature windows were compressed into short dual-fermentation periods of 24–48 h. A representative study tracked 0, 24, 36, and 43 h and observed a steady fall of soluble sugars with rising total acid and slow alcohol accumulation. This verified the cooperative path of *Rhizopus*-led saccharification, *Saccharomyces* alcohol formation, and LAB mild acidification. The design met household or workshop needs for fast turnaround and reduced contamination risks from long cycles [116]. Formulation and substrate adjustments also worked. Adding pretreated rice bran by extrusion to sweet rice wine increased soluble solids and antioxidant indices without changing the low-alcohol trait, which stayed below 2% vol. This provided a handle to enrich flavor and nutrition for low-strength sweet profiles [115].

On the supply side of xiaoqu function, key hydrolases from *Rhizopus* in traditional rice wine starters differed by orders of magnitude among regions. This set sugar release rates and controllability of final sweetness in short fermentations. In a survey of 29 regions, 78 *Rhizopus arrhizus* isolates from rice wine qu showed acidic protease at 280–1023 U/g, amylase at 557–1681 U/g, and esterase at 370–2949 U/g. The wide span indicated that selecting qu and process in combination could set saccharification strength and esterification potential with precision. These data supported style settings from home or workshop to small industry [117]. In black glutinous rice wine, xiaoqu from Sichuan, Jiangxi, and Hubei used on the same substrate yielded 61 volatile compounds in total, with 16 at OAV > 0.1. Functional differences among regional xiaoqu shifted the relative contributions of ethyl acetate, ethyl lactate, and 2-phenylethanol. This produced clear sensory divergence under the same recipe and different qu, which supported regional product development and mapping of standardized flavor spaces [118]. In sum, the engineering value of xiaoqu in rice beverages lay in stable output of sweet, low-alcohol, and clean aromas through three-way coupling of short temperature control often near 28–30 °C, adjustable enzyme

activity by qu selection, and material pretreatment by steaming, extrusion, or gelatinization. Quantified enzyme and schedule parameters supported scale-up [42,115].

4.2.2. Xiaoqu Baijiu and Regional Styles

Solid-state making of xiaoqu baijiu, represented by rice-aroma baijiu, followed xiaoqu use, semi-solid fermentation, and solid distillation. Key flavor groups including higher alcohols and esters such as ethyl acetate and ethyl lactate were highly sensitive to the source and properties of xiaoqu. In a production description for a rice-aroma line, xiaoqu supplied starch hydrolysis and primary precursors early. A semi-solid fermentation of about 13 days completed alcohol formation before distillation. The coupling between temperature and total acid acted as the main external drivers for shifts in communities and metabolic flux. In plant samples, *Lactobacillus* reached 62.88–99.23% at the end of fermentation. *Saccharomyces* and *Rhizopus* on the fungal side ranged 7.06–83.50% and 15.21–90.89%. These showed significant positive associations with ethyl acetate, ethyl lactate, and total acid in redundancy analyses, which supported engineering control of flavor by process variables [76]. Choice of xiaoqu for style targets also pulled a higher alcohol to ester balance. A comparison of six commercial xiaoqu showed ethyl acetate and ethyl lactate rising rapidly early, leveling later, and jumping after distillation. Redundancy analysis indicated strong association between *Saccharomyces* from qu and the formation of these two esters and higher alcohols. This showed a direct effect of qu diversity on final distributions via the qu–yeast–ester synthase path and guided selection for routes that targeted low higher alcohols and high esters [119].

Quantitative flavor profiles from cross-category and within-style statistics placed xiaoqu systems at high ester and moderate higher alcohol levels. A systematic evaluation of rice-aroma baijiu reported a typical ratio of total acid to total ester to total alcohol near 1:1.2:1.5. Lactic and acetic acids exceeded 90% of total acids. Esters were led by ethyl lactate, followed by ethyl acetate. 2-Phenylethanol was among the highest of the four main baijiu styles. These ratios guided cut points during distillation and blending [2,120]. Raw materials and process also pulled targets. In black rice wine, regional xiaoqu with the same substrate delivered reproducible differences in 16 OAV > 0.1 markers by intensity and profile. Moving this qu effect into rice-aroma baijiu pilots allowed a higher ethyl acetate to ethyl lactate ratio to improve freshness and top-note lift [118,121]. Combining qu addition, mash moisture, and time was used to constrain total higher alcohols into a sensory-friendly zone. Composite qu and redesigned fermentation windows kept total higher alcohols at several hundred mg/L and raised ethyl esters. This achieved refined and elegant regional expressions such as Lingnan rice-aroma without sacrificing body [119,122]. In general, regional style in xiaoqu baijiu depended not only on materials and distillation or blending but also on engineered coupling of qu diversity, process variables, and distillation cuts. Parameter windows centered on the ratio of ethyl acetate to ethyl lactate and thresholds for higher alcohols used qu choice, temperature and acid control, and water management as core levers.

4.3. Hongqu, a Combined Platform for Pigment and Aroma

4.3.1. Hongqu Rice Wine and Hongqu Huangjiu

In hongqu rice wine and hongqu huangjiu, hongqu performed saccharification and pigment formation and linked positively with ester generation. In a recent pilot model that used pure cultures together with hongqu, co-fermentation by *Monascus purpureus* and *Saccharomyces cerevisiae* yielded 29 volatiles. Esters dominated with ten species, and ethyl acetate was the leading ester. With 25% Trichosanthes fruit pulp added as a flavor and enzymatic co-substrate, ethyl acetate still dominated. Ethyl lactate, methyl heptanoate,

and lactones appeared. Ethyl lactate made up 12% of total esters. For higher alcohols, 3-methyl-1-butanol and 2-phenylethanol reached 36.08 μg/mL and 8.71 μg/mL by SPME–GC–MS at room sampling. This showed that under parallel saccharification and alcohol fermentation with hongqu, esters and alcohols could be raised by formulation without sacrificing cleanliness or color stability. The work also summarized 81 and 102 total volatiles in traditional reports, suggesting that mixed-culture fermentations had richer spaces than pure cultures. This matched process reliance on qu complexity. These data provided anchors for co-optimizing process strengthening such as co-fermenting materials or adding flavor substrates and flavor targets such as high ester ratios [123].

Beyond flavor, pigment production and enzyme flux could be tuned quantitatively by formulation and process. Response surface optimization for *M. purpureus* G11 in liquid culture on a mix of rice flour, peptone, copper ions, and vitamin B1 gave a theoretical pigment yield of 113.77 U/mL and a saccharification-related SP activity of 362.91 U/mL. This supported industrial stability of color and precursors by linking functional seed culture and qu rooms. Although obtained in liquid, the directions of effects across carbon, nitrogen, trace elements, and cofactors informed solid-state scale-up and guided pretreatment and moisture management of qu bricks [124].

4.3.2. Hongqu Vinegar and Hongqu Sufu

In hongqu vinegar, hongqu first completed saccharification and alcohol formation; then, the mash entered acetification. Metabolic studies of traditional practice resolved 60 volatiles, 23 amino acids, and seven organic acids across the process. Acetic acid, lactic acid, and esters of these acids accumulated in the middle and late stages and set total acid and aroma structure. This three-stage interface gave process rationale for using hongqu on the raw material side [125].

In sufu, hongqu rice and pigments raised color directly and altered organic acid spectra and flavor composition. A multi-site survey of commercial red sufu and white sufu showed lactic acid as the main acid. Lactic acid was 1.969 ± 0.300 g/kg in red sufu and 2.790 ± 0.612 g/kg in white sufu. Acetic acid was 0.715 ± 0.102 g/kg and 0.855 ± 0.090 g/kg. Citric acid was 0.805 ± 0.050 g/kg and 0.679 ± 0.153 g/kg. This suggested that hongqu contributed not only color but also shifts in organic acids and volatiles via substrate and osmotic effects, which shaped final flavor [99].

4.4. Fuqu or Jiangqu as the Salt-Tolerant Core for Soy Sauce and Soybean Pastes

4.4.1. Soy Sauce Koji with *Aspergillus oryzae* or *A. sojae*

In the soy sauce process, mature koji was combined with brine to form moromi. Salinity fell in the high-salt liquid fermentation zone to ensure safety and allow long maturation. Salt levels of about 18–23% *w*/*v* NaCl were reported. Maturation ranged from months to at least four years according to process and product positioning. Neutral and acidic proteases, glutaminase, α-amylase, and glycosidases produced during koji still supplied substrates under high salt and low water activity. This drives amino nitrogen and key flavor-threshold compounds during aging. Under the JAS grading for soy sauce nitrogen at the linked site, grades centered on total nitrogen and amino nitrogen. This supported the industrial practice of securing nitrogen indices by ensuring enzyme output during koji. Process trials showed that moromi temperature and intermittent aeration changed alcohol and acid metabolism. In a comparison between 25, 35, and 45 °C, the higher temperature at 45 °C accelerated changes in aging indices but lowered ethanol and did not change total nitrogen significantly. This suggested that temperature and aeration should be balanced to maintain flavor and stability in high salt. Traditional sun fermentation used outdoor insolation and stirring to promote mass transfer and redox

reactions. Modern work still treated natural sun fermentation as a basis for traditional premium flavor [53,126–128]. These windows of temperature, salt, and time gave an operable interface from koji to moromi. Producers therefore optimized enzyme output upstream with the end in mind to meet amino nitrogen and characteristic aroma grades later.

4.4.2. Doubanjiang, Huangdoujiang, and Tianmianjiang

In high-salt solid or semi-solid pastes, fuqu served as an enzyme engine that set nitrogen release and flavor potential. The Codex regional standard set floors for amino nitrogen and total nitrogen in fermented soybean pastes. For pure soybean pastes, amino nitrogen had to be at least 0.30% w/w and total nitrogen at least 1.6% w/w. For soybean plus cereals, amino nitrogen had to be at least 0.12% w/w. These indices correlated with proteolysis intensity during koji. Producers therefore raised effective neutral and acidic proteases by managing moisture, layer thickness, and turning to improve amino nitrogen and stabilize free amino acid release [129].

In industrial Sichuan-style douban, a closed gradient steady thermal field over 90 days detected 75 volatiles, compared with 67 in constant temperature and 68 in traditional outdoor processes. The closed system showed more esters and alcohols. This suggested that engineered gradients and ventilative stirring improved accessibility and mass transfer for ester precursors and thus improved layering of paste and ester notes. Work on salt reduction or replacement showed that under controlled risk and stable operation, low-salt options could somewhat raise amino nitrogen or adjust volatiles but required stronger enzyme output and tighter monitoring during koji. Mechanistic work also showed continued peptide degradation and amino acid accumulation during the high-osmotic moromi stage of douban. This indicated a relay of extracellular proteases from koji into the salt-tolerant stage and formed the key link from qu to amino nitrogen to volatiles [129].

4.5. Douchi-Qu, Community Differences, and Quality Indicators in Aspergillus-Type, Mucor or Rhizopus-Type, and Bacterial-Type Douchi

In industrial contexts, the qu type set community assembly and the output profile of flavor in douchi. Horizontal comparisons of commercial products found both shared volatile foundations and type-specific fingerprints. In a comparison across mold-type douchi, the three types shared 26 volatiles. Unique compounds also appeared, with nine in *Aspergillus*-type, seven in *Mucor*-type, and nine in *Rhizopus*-type. *Aspergillus*-type had higher free amino acids and umami notes with $p < 0.01$. This suggested a process-amplifiable coupling between qu, community, and flavor [130].

For *Aspergillus*-type, the route included making the starter or bricks, post-ripening, and drying. Community succession and aroma formation showed stage windows. Tracking through the process found molds near 70% in early making. Yeasts rose later and approached 90%. The two then balanced near the end. Across five steps, 83 volatiles were identified, including 20 alcohols, 12 aldehydes, eight ketones, 15 esters, and eight aromatics. The profile shifted from bean-derived alcohols and aldehydes such as 1-hexanol, 1-octen-3-ol, and nonanal to phenolics and ketones that raised paste, smoky, and nutty notes. This mold-to-yeast relay gave clear handles for control [90].

Mucor or *Rhizopus*-type emphasized a composite base of yogurt-like acid, caramel, and smoke. In Yongchuan *Mucor*-type douchi, GC–O, AEDA, and OAV identified 49 odor-active compounds, with 22 at high FD 8–2048. Acetic acid at 535.58 μg/g and maltol at 153.23 μg/g led by amount. Dimethyl trisulfide at OAV 8818 and 2-methoxyphenol at OAV 1317 contributed strongly to aroma. This combination of organic acids, sulfur compounds, and phenolics set the key dimensions that separated *Mucor*-type from *Aspergillus*-type by e-nose and sensory [131]. For *Rhizopus*-type, evidence showed shifts toward caramelized

ketones, sesquiterpenes, and some pyrazines. In a comparison of pure and mixed cultures, 5% *Rhizopus arrhizus* at 30 °C in solid state for eight days formed different key volatiles such as 2,3-butanedione, dihydro-3-methyl-2(3H)-furanone, and α-pinene. Co-fermentation with *Aspergillus* or *Bacillus* broadened ester and ketone coverage. This suggested potential to expand aroma by strain–process synergy in short-cycle and strong-modification settings [132].

Bacterial-type led by *Bacillus* showed industrial readability in communities and safety–quality indices. In "water douchi" under room temperature natural fermentation, total bacteria averaged 1.6×10^6 CFU/g, LAB 5.9×10^4 CFU/g, and fungi 7.6×10^3 CFU/g. Amino nitrogen reached 2.08 g/kg, titratable acid 3.44 g/kg, and reducing sugars 25.78 g/kg. Polyamines were detected such as putrescine at 131.3 mg/kg, cadaverine at 83.4 mg/kg, and tryptamine at 61.5 mg/kg. These gave thresholds and alerts for raw materials and salt–temperature–aeration strategies. Two traditional bacterial-type douchi from Longnan and Qingyang differed. Forty-eight and forty-one volatiles were detected. ROAV-selected key odorants formed different sets by region. *Carnobacterium*, *Ignatzschineria*, and *Bacillus* dominated. This supported the view that bacterial-type formed a savory and salty base with ester and acid extension [89].

In summary, *Aspergillus*-type suited staged temperature and humidity control to yield a rich profile with yeast-led post-ripening and amplified phenolics and ketones. *Mucor* or *Rhizopus*-type anchored yogurt-like acid, smoke, and caramel clusters and suited short cycles or seasonal windows to raise key OAV compounds. Bacterial-type featured high amino nitrogen and clear microbial and physicochemical thresholds that enabled data-driven control and safety evaluation. Industrial choice among the three should integrate target flavor indices such as OAV > 10 sulfur or phenolics and ester or pyrazine coverage, community stability, and quality and safety indices including amino nitrogen, acidity, and amines.

4.6. Sufu-Qu, the Cheese-like Path of Molded Tofu

In modern sufu production, sufu-qu pre-digested tofu blocks during a short solid-state stage. This supplied soluble nitrogen, fermentable and esterifiable substrates, and texture softening for long maturation in salty alcoholic brine. For hot seasons, different rooms, and flavor targets, the pehtze stage used division of labor among qu sources to control enzyme windows. With *Actinomucor* elegans, peak protease of 108 U/g, lipase of 172 U/g, and glutaminase of 176 U/g were reached at 25 °C, 95–97% RH, and 48 h. To raise saccharification and oligosaccharide removal, α-amylase of 279 U/g and α-galactosidase of 227 U/g were reached at 30 °C and 95–97% RH at 48 h and 60 h. When ambient temperature rose to 30–35 °C in summer, *Rhizopus oligosporus* served as a thermotolerant alternative. At 35 °C and 95–97% RH, peak protease and lipase reached 104 U/g and 187 U/g at 48 h. At 36 h, α-amylase and glutaminase reached 288 U/g and 187 U/g. α-Galactosidase reached 226 U/g at 30 °C and 36 h. These quantified enzyme–time–temperature–humidity coordinates supported room settings and seasonal switching and linked enzyme output at the qu stage to later flavor formation [98].

After pehtze, maturation proceeded in brine with salt, alcohol, and spices. Extracellular and some intracellular enzymes from pehtze continued to act under high salt and low water activity. Emulsification, protein breakdown, and small flavor precursors proceeded. In 23 commercial sufu, NaCl ranged 6.2–14.8% *w*/*w* and ethanol 0.5–6.3% *w*/*w*. Free amino nitrogen and reducing sugars such as glucose at 0–6.2% and fructose at 0–4.8% varied. These endpoint ranges across brands confirmed the need to convert insoluble macromolecules into soluble nitrogen and esterification substrates during pehtze.

They also set benchmarks for maturity criteria before brining, such as lower moisture and elasticity and higher soluble nitrogen [100].

In the process chain, sufu-qu also standardized interfaces between product categories and styles. Commercial practice cut tofu is cultivated for two to seven days at 12–30 °C to form pehtze covered evenly by hyphae. Maturation then occurred in salty alcoholic brine for months. Starter identification across *Actinomucor*, *Mucor*, and *Rhizopus* showed industrial strains of *Actinomucor repens* or *A. taiwanensis*, *Mucor circinelloides* or *M. hiemalis* or *M. racemosus*, and *Rhizopus microsporus*. The clades were clear and matched process tolerance and enzyme spectra. This chain of cultivation schedules, brine maturation, and starter phylogeny supported reproducible standards for raw material acceptance, qu selection, and environmental tolerance at the pehtze stage [101].

Viewed from the product end, the levels of volatiles and soluble nitrogen after maturation were largely set by enzyme flux and structural remodeling during pehtze. In a model with black and yellow soybeans at 1:1, after 60 days in brine, 79 volatiles were resolved including 31 esters and nine alcohols. Seventeen free amino acids were detected. Coupled SPME–GC/MS and sequencing proved that protein and lipid cleavage during pehtze provided the base for later ester formation and umami amino acids [97]. Producers could therefore scale the three segments of pehtze parameters, brine formulation, and aging time to quantitative targets for ester fractions and amino nitrogen thresholds.

In sum, sufu-qu process engineering was summarized as maximizing target enzyme systems and texture modification in a short solid-state period and transferring that potential smoothly into long maturation in high-salt alcoholic brine. Producers could switch seasonally between *Actinomucor* and *Rhizopus* according to ambient temperature and flavor targets, lock in 25, 30, or 35 °C at 95–97% RH for 36–60 h as optimal enzyme windows, and back-calculate pehtze maturity and brining timing from endpoint ranges such as 6.2–14.8% NaCl and 0.5–6.3% ethanol. This achieved stable cheese-like texture and layered flavor output.

5. Cross-Scale Coupling Between Functional Enzyme Spectra and Flavor Formation

5.1. A Synergistic Network of Saccharification, Alcohol Fermentation, Proteolysis, and Lipolysis with Flavor Routes

Flavor in Chinese qu-based fermentations was produced by a synergistic enzyme network. In solid-state systems, starches, proteins, and lipids were hydrolyzed to small molecules by microbial enzymes. These intermediates were converted through central metabolism and released complex flavor compounds. Carbohydrates were first saccharified to provide sugars and energy. Amylases hydrolyzed starch to fermentable sugars. Yeasts converted sugars through glycolysis and the TCA cycle to pyruvate and ethanol. Acetyl CoA served as a key precursor for ester synthesis. In the presence of yeast ethanol, esterases generated ethyl acetate and related aromatic esters. In strong-aroma baijiu, ethyl hexanoate formed from hexanoic acid and ethanol through enzymatic esterification [133,134]. During fermentation, saccharification and alcohol formation proceeded in parallel. Molds supplied sugars and yeasts produced alcohol. Their products entered subsequent reactions. LAB converted glucose to lactic acid. Lactic acid then esterified with yeast ethanol to form ethyl lactate and increased body. Measurements showed that fortified qu enhanced cooperative ester formation by LAB and yeasts, and one trial group reached 128.01 mg/L ethyl lactate [135–137].

Proteins were hydrolyzed by proteases to amino acids and peptides. These provided nitrogen for yeasts and LAB and also acted as taste components and volatile precursors. Glutamate contributed umami flavors. Branched chain amino acids entered the Ehrlich

route and yielded higher alcohols such as isoamyl alcohol. Protease activity shaped the types and levels of alcohols and organic acids and thus the amounts and ratios of esters, which shifted flavor trajectories. In high-temperature qu, abundant protein breakdown products reacted with sugars under suitable heat and moisture through Maillard chemistry to produce nitrogen heterocycles such as pyrazines and gave nutty roasted notes. Tetramethylpyrazine was a typical Maillard product that imparted roasted and nutty characters in sauce-aroma qu. Lipids were hydrolyzed by lipases to glycerol and free fatty acids. These lipolysis products served as energy sources and also contributed flavor. Short-chain fatty acids such as acetic, butyric, and hexanoic acids were important to qu aroma. Hexanoic acid carried sharp acidic notes. Free fatty acids esterified with alcohols under esterases to raise aromatic intensity with fruity and floral notes. Adding exogenous lipase to the system significantly promoted esterification and increased flavor ester concentrations in baijiu by up to thirty-one-fold.

Microbial roles were divided in traditional qu mashes. Bacilli with strong enzyme production secreted amylases, proteases, and lipases to hydrolyze substrates and supplied sugars, amino acids, and fatty acids as precursors. They also produced acids and aroma directly. *Bacillus* licheniformis in solid-state fermentation generated aromatic compounds, C4 short-chain compounds, pyrazines, and volatile organic acids. *Aspergillus* strains in qu produced broad spectrum hydrolases, saccharified starch, hydrolyzed proteins, and transformed polyphenols. When *Bacillus* and *Aspergillus* co-fermented, complementary enzymes accelerated aroma metabolism and increased phenols, aldehydes, and other complex volatiles. Cascades also linked metabolites together. LAB produced lactic acid that yeasts esterified to ethyl lactate and softened body. Balanced LAB with hexanoic acid producers favored hexanoate accumulation, which then combined with ethanol to form ethyl hexanoate with a clean and rich bouquet.

In sum, saccharification, alcohol formation, proteolysis, and lipolysis in qu formed an interwoven network. Degradation products served as substrates for the next group of microbes and were converted stepwise to higher alcohols such as 1 butanol and isoamyl alcohol with green apple or fruity hints, to organic acids such as acetic and butyric acids that gave acidity and irritation when excessive, and to esters such as ethyl acetate and ethyl hexanoate that provided floral, honeyed, and fruity notes. Minor nitrogen volatiles such as ammonia, pyrazines, and indole contributed distinctive fermented aromas and built layered sensory quality.

5.2. Enzyme–Substrate–Microbe Interactions from Substrate Specificity to Molecular Origins of Aroma and Taste

Substrate composition selected colonizing microbes and enzyme expression and set molecular starting points and routes for flavor. In starch-led systems such as grain-based daqu or hongqu, starch-rich substrates favored amylase-producing molds such as *Aspergillus* and *Rhizopus*. Rapid saccharification supplied sugars. Osmotolerant yeasts such as *Saccharomyces* and film-forming yeasts grew well and converted sugars to ethanol and organic acids. Enzymes then transformed these intermediates to diverse volatiles. This substrate bias produced aroma spectra dominated by alcohols and esters. High ethanol and various organic acids formed ethyl acetate, ethyl lactate, ethyl hexanoate, and related esters under esterases and gave rich fruity and full-bodied profiles. In medium-temperature daqu made from starchy materials, 328 volatile compounds were detected, whereas only 140 were detected in low-temperature qu. This showed that starch-rich environments with suitable microbial synergy produced richer flavor components [138–141]. Hongqu rice wine used glutinous rice and followed the same starch-led logic. Its profile featured mellow, smooth, and sweet traits that matched alcohols and esters formed from fully fermented saccharification products [142]. Traditional hongqu huangjiu contained more than one

hundred volatiles, with reports up to 102 compounds that included higher alcohols such as isoamyl alcohol and 2 phenylethanol, esters such as ethyl acetate and ethyl phenylacetate, and minor aldehydes and ketones. These built the characteristic aroma and lingering sweetness of hongqu wines [143].

Protein- and lipid-led fermentations such as sufu followed different flavor routes. Starch in fermented tofu was minimal. Molds expressed proteases and lipases rather than amylases. Filamentous fungi such as *Mucor* and *Aspergillus* grew on tofu and secreted proteases with high activity. *Mucor* proteases exceeded those in other fermentations and hydrolyzed soybean proteins to small peptides and amino acids. Strains also produced lipases that released abundant fatty acids [144]. Under these substrates, microbes including later brine bacteria used amino acids and fatty acids for metabolism and generated nitrogen- and oxygen-containing flavor compounds. Proteases from molds and bacteria released amino acids that supplied sour, sweet, bitter, salty, and umami tastes and acted as precursors. Through deamination, transamination, and chain cleavage, different amino acids yielded aldehydes, ketones, alcohols, and organic acids. Together with lipid products, they formed the composite aroma of sufu. Accumulation of alanine and other amino acids brought slight sweetness. Long maturation increased ester formation and added fruity notes. In deeply fermented products such as stinky tofu, this appeared as a sweet and mellow trait. Roles were divided among microbes. Leuconostoc like cocci and members of Clostridiaceae contributed short-chain acids and esters. Enterobacteriaceae and Enterococcus promoted flavor amino acids and reducing sugars. LAB and molds produced and accumulated lipases that catalyzed lipid hydrolysis and released fatty acids. During ripening, these fatty acids esterified with alcohols present in brine and produced esters such as ethyl hexanoate that gave buttery richness. Salt and huangjiu added to the brine also affected enzyme–substrate action. High salt suppressed microbial activity and reduced amino acid formation, which lowered alcohols, ketones, and phenolics. Moderate addition of rice wine or distilled spirits introduced yeasts for minor alcohol fermentation and supplied alcohol for esterification to raise aroma complexity.

Thus, substrate composition drove microbial ecology and enzyme expression. Starch-rich qu favored saccharification and alcohol routes and produced vinous and fruity notes. Protein- and lipid-rich qu favored proteolysis and lipolysis and produced umami notes from amino acids, special odors from ammonia and amines, and buttery notes from lipid oxidation products. Multi-omics work confirmed that functional communities in different qu adjusted enzyme spectra to substrates. Integrated meta-omics and transcriptomics revealed substrate-specific expression of key enzymes and activation of metabolic pathways. Yi et al. [24] reported up to 11 aromatic compound pathways activated in HT-Daqu to break down and use complex aromatic precursors. Kang et al. [145] resolved assembly mechanisms in jiuqu communities and clarified functional partitioning and enzymatic cooperation among populations under different raw materials. In sum, enzyme–substrate–microbe interactions set the molecular origins of flavor. Substrate types and ratios shaped microbial ecology and functional enzymes. These governed formation and conversion of flavor precursors. Elucidating this cross-scale linkage supported targeted control of qu enzyme composition and fermentation strategies to optimize flavor quality in traditional fermented foods.

6. Quality and Safety from Risk Identification to Process Control

6.1. Monascus Related Citrinin Risk

As shown in Figure 4, *Monascus* in red koji fermentations could co-produce the mycotoxin citrinin (CIT), which is cytotoxic to kidney and liver cells [146]. CIT occurrence has been widely reported worldwide, and limits have been strictly managed. Japan set a

limit of no more than 0.2 mg/kg for *Monascus* fermented products as early as 1999 [147]. For detection, HPLC was routinely used to quantify CIT with high accuracy. LC–MS/MS offered higher sensitivity and improved confirmation. Several rapid screens supported source control. On coconut milk agar under UV, *Monascus* that produced CIT showed fluorescence, which allowed removal of toxigenic strains at the seed stage.

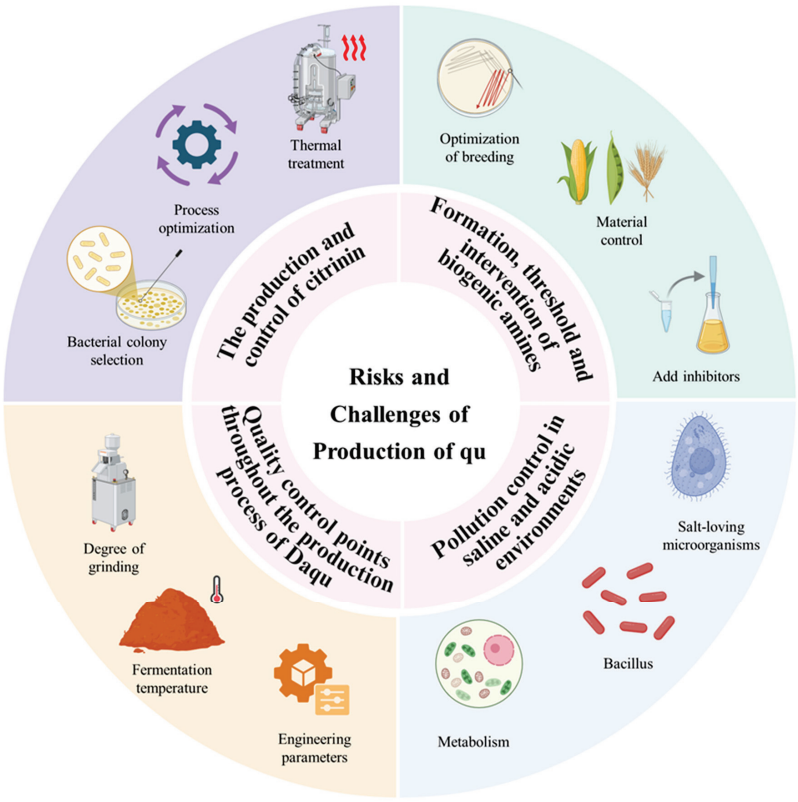


Figure 4. Risk identification and process control for qu.

CIT reduction strategies span strain selection, process optimization, and end treatment. Selecting low-producing or nonproducing *Monascus* strains was fundamental. Strains of the same species differed by several-fold. In angkak, the JK2 strain yielded 1.10 ± 0.021 μg/g CIT while the control FNCC 6008 reached 3.01 ± 0.072 μg/g, which significantly lowered toxin output. Genetic screening of pksCT or ctnA also identified weak producers [148]. Process optimization further suppressed CIT. Controlling fermentation near 28 °C minimized CIT, since *M. purpureus* produced the most CIT at about 35 °C in solid state or 32 °C in liquid and dropped at 28 °C [149]. Adjusting pH helped. The scheme started at pH 5.5 and raised to pH 8.5 at the end gave high pigment with lower CIT. Nutrient design also intervened in CIT biosynthesis. In liquid culture, adding the flavonoid genistein at 2 g/L lowered CIT by about 80%. La^{3+} addition promoted pigment while suppressing CIT. Prompt product separation and limiting late-stage degradation reduced accumulation [149]. Post treatments removed residual toxin. Although CIT was heat resistant, heating at 140–160 °C decomposed about 20% and converted a fraction to a non-cytotoxic H_2 isomer. Physical adsorption and biological detox were combined in some studies. Magnetic nanoparticles adsorbed about 70% of CIT, while heat-inactivated yeast cells (121 °C) reached up to 98% removal [149].

In sum, combining strain control at the source, process regulation during fermentation, and terminal inactivation effectively lowered CIT risk in *Monascus*-fermented foods and realized a full chain path from risk identification to process control.

6.2. Formation, Thresholds, and Intervention for Biogenic Amines Such as Histamine and Tyramine

In protein-rich fermented foods, microbial decarboxylation of amino acids generates biogenic amines (BA) such as histamine and tyramine. Excess intake causes safety problems, including histamine poisoning from scombroid fish and hypertensive crises from tyramine, the "cheese effect" [150]. Food histamine at about 100 mg/kg was considered toxic for some consumers. Tyramine posed risk at 100–800 mg/kg. Phenethylamine showed a lower threshold near 30 mg/kg. Several jurisdictions set limits. In fish and fish products, common limits for histamine were 50–100 mg/kg. Some countries advised $\leq$200 mg/kg tyramine for high-risk cheeses. Although BA levels in most fermented foods stayed safe, some traditional products showed exceedance. In several Asian fermented soy foods, maximum histamine reached 2–27 times the suggested toxic dose. Tyramine and phenethylamine in some soy pastes also exceeded safe doses. Modern fermentation targeted BA risk through integrated controls from raw materials to strains and process [151–157].

Strain choice was critical. Producers with strong decarboxylase activity were avoided, and selected starters were used. In fermented soy foods, introducing nonproducing or BA-degrading strains reduced BA at the source. Inoculating *Bacillus subtilis*, *Bacillus licheniformis*, or *Pediococcus pentosaceus* in soy paste or douchi lowered histamine and tyramine in finished products. Selected LAB starters in meats and cheeses similarly suppressed spoilage producers and limited BA [151,154,156]. Raw material and storage control reduced free amino acid precursors and the load of BA producers. Materials were kept fresh and cold. Components rich in free amino acids were moderated. Low-temperature storage suppressed spoilage growth. For histamine-prone marine fish, rapid chilling was essential. At 5 °C for 10 d, histamine in mackerel stayed below about 50–70 mg/kg [158]. In warm conditions, histamine rose within hours and exceeded toxic thresholds [159]. Pre-fermentation handling such as chilling and permitted preservatives thus lowered the baseline for BA formation. Additives that selectively inhibited producers or enzymes also helped. Small doses of food grade agents or plant extracts reduced decarboxylase activity or growth. In a high-tyramine Korean doenjang model, adding 0.5% glycine, 0.1% sodium benzoate, or 0.1% potassium sorbate at fermentation start significantly lowered final tyramine versus control. Glycine cut tyramine by about 76.1%, and benzoate or sorbate lowered it by about 50% [150]. Nicotinic acid completely blocked tyramine in that model but was not practical at high levels [150]. Polyphenol-rich extracts also reduced BA. Rose polyphenols and spice extracts from cinnamon, star anise, or clove reduced histamine and tyramine in several fermented foods [159,160].

By using low BA starters, controlling raw materials, and applying selective inhibitors, BA contents were kept within safe thresholds. The chain ran from risk identification in high protein or high free amino acid contexts to process control by antimicrobial or anti-enzyme measures.

6.3. Contamination Control in Salt and Acid Tolerant Environments the Double-Edged Roles of Halophiles and Bacillus

Many traditional fermentations proceeded under high salt or low pH to suppress general contaminants. Halophiles and acid-tolerant *Bacillus* often survived and acted as a double-edged group. They could be beneficial fermenters or persistent contaminants. In high salt, extreme halophilic archaea posed typical hazards. Halobacterium grew well at above 20% salt and caused pink discoloration on salted fish or meats due to carotenoid pigments. This "pink spoilage" served as a visible indicator of halophile contamination. By contrast, some halo-tolerant species were used as functional fermenters. Tetragenococcus tolerated 15–20% salt and was applied in fish sauce and soy sauce to acidify and protect flavor under high salt [161–168]. Risk management balanced these

roles. First, salt sources and purity were controlled. Solar salt could carry spores or cells of halophiles, so refining and sterilization received attention. High-purity refined salt reduced exogenous halophiles [169]. Second, process conditions favored beneficial groups. In early soy sauce moromi, halo-tolerant yeasts and LAB produced alcohol and acids quickly and suppressed spoilers. Overaeration or overheating was avoided to prevent blooms of halophiles. Color and viscosity were checked. Abnormal pink spots or slime signaled possible halophile contamination and triggered corrective actions such as removing surface layers or raising salt, though quality had already been affected [170–172].

Bacillus also played key roles in salt- and acid-tolerant systems. In many fermented soy or grain foods, *Bacillus* such as B. subtilis acted as beneficial groups. They produced proteases and exopolymers and improved flavor and functions, as in natto and douchi. Yet risk species existing in the family. B. cereus and B. thuringiensis were reported in traditional soy pastes and douchi and produced heat-stable toxins such as the emetic cereulide. Food poisoning risk rose when B. cereus exceeded about 10^5 CFU/g [173]. Salt or acid did not fully suppress spores. B. coagulans grew near pH 4 and caused flat sour spoilage in acidic canned foods, with large economic losses [174]. Thus, *Bacillus* had to be used while guarded.

Process control introduced beneficial competitors and tightened hygiene. Inoculating dominant *Bacillus* suppressed harmful species. In low-salt cooked fermented doubanjiang, adding beneficial B. licheniformis antagonized B. cereus that had been deliberately introduced. Initial counts of 3–4 log CFU/g dropped to undetectable levels after fermentation while product quality improved and BA remained low. This showed strong antagonism in practice. Routine microbiological monitoring and sanitation were reinforced. Batches with B. cereus above limits were discarded or reprocessed. Environments were cleaned and disinfected to prevent spore buildup. In late high-salt stages or during drying, moderate heat steps such as brief dry heat at about 80 °C were considered to kill vegetative cells. Spores remained dormant under low moisture and did not grow in finished products [16,173,175–177].

In summary, halophiles and *Bacillus* were leveraged for their tolerance, while salt, temperature, pH, and hygiene were precisely controlled to prevent shifts from symbiosis to spoilage or pathogenicity. Problems were anticipated by risk identification and solved by process control.

6.4. From Experience to Standards Quality Control Points Across Raw Materials, Qu, Fermentation, and Finished Products

Traditional fermented foods had relied on experience and manual skills. Modern industry practices introduced quality control points and standardized each stage, from raw materials to qu or starters, fermentation, and finished products [15,178].

Raw material control was the start. All inputs were tested for safety and quality and pretreated when needed. For fermented vegetables and pickles, vegetables were fresh and free of pesticide residues and pathogens and were washed with clean water. In commercial production, food grade sanitation was advised, such as soaking in chlorinated water at about 100 ppm free chlorine followed by rinsing. Some studies advised a second rinse at 50 mg/L after salting to further reduce residual contaminants. These steps replaced or quantified traditional sun drying or repeated washing and were formalized as SOP. For grains, moldy kernels were removed and aflatoxins were tested to prevent hazards from entering the system (https://www.gov.mb.ca/agriculture/food-safety/education-resources/pubs/fermented-veg.pdf, accessed on 17 October 2025).

Control of qu or starter assured purity and stable function. Natural inoculation or back slopping carried risk of drift. Standardized qu or pure starters were adopted, and QCP were set in qu making. In soy sauce koji, substrate sterilization, inoculum size,

and temperature and humidity were controlled. Finished koji were tested for enzyme activity and microbial load such as total molds and coliforms. Only qualified lots entered fermentation. In red koji rice, quick screens removed toxigenic strains. Coconut agar with UV retained only non-fluorescent isolates for qu, which prevented CIT producers from entering production [149].

Fermentation control was central. Environmental conditions and in-process indices were given limits and monitored in real time. In fermented vegetables, pH drops indicated safety. For kimchi, experience said that room temperature fermentation for days gave sourness. Modern work set clear CCP. At 18–22 °C, pH had to fall to 4.6 or below within 48 h to suppress pathogens. If pH did not reach 4.6 by day 3, the batch was deemed failed and unsafe and had to be discarded. A schedule also specified targets for slow low-temperature fermentation (https://www.gov.mb.ca/agriculture/food-safety/education-resources/pubs/fermented-veg.pdf, accessed on 17 October 2025). In soy sauce, salinity, moisture, and amino nitrogen were monitored against standards. About 18% salt prevented nonhalophiles, and salt was adjusted if it fell. Modern tools such as online sensors and IoT upgraded experience to data-driven control [15,178]. Continuous pH and temperature logging with cloud alarms enabled early correction and kept conditions within standard ranges. This replaced purely sensory judgment.

Finished product control closed the loop. Products were released only after meeting safety indices in sensory, physico-chemical, and microbiological tests. For raw ready-to-eat ferments, pH had to stay in the safe range and maturation time had to ensure die-off of residual pathogens. In Korea, raw kimchi with pH < 4.2 was advised to be held under refrigeration for at least two weeks so acid-tolerant pathogens such as some E. coli O_{157}:H_7 declined to safe levels before sale [179]. Red koji products were tested for functional components such as monacolin K and for CIT against regulations. Dried fermented soy foods were tested for water activity and for toxins and BA. Products carried traceable batch records and standards.

6.5. Embedding the Qu to Fermentation Process Within HACCP and Regulatory Frameworks

To place the main risks such as *Monascus*-related citrinin, biogenic amines, and contamination under high salt or low pH within an auditable safety system, the stages from raw and auxiliary materials through qu making, primary fermentation, and storage or release were mapped to a food safety management framework centered on HACCP and aligned with current regulations and standards. At the operational level, the Codex General Principles of Food Hygiene and its seven HACCP principles served as the backbone to establish hazard analysis, critical control points, and verification with records, while the management system requirements of ISO 22000 [180] were used to formalize procedures. For markets in the European Union or those adopting EU standards, chemical hazards such as citrinin in red yeast rice raw materials and finished-product release limits were aligned. For the United States, consistency mapping was made to hazard analysis and preventive controls under FSMA in 21 CFR Part 117 (https://en.wikipedia.org/wiki/ISO_22000?utm_source; http://data.europa.eu/eli/reg/2004/852/oj; https://ecfr.io/Title-21/Part-117, accessed on 16 October 2025).

For concrete points of risk and control, three complementary paths were distinguished. First, prerequisite programs at the source focused on gatekeeping for raw materials and strains, including screening *Monascus* strains for toxigenic potential and baseline control of freshness and contaminant load, and key parameters such as moisture, salinity, pH, and thermo-humidity trajectories were managed as operational PRPs. Second, CCPs were set at a small number of nodes with decisive impact on safety outcomes, including time control before acidity or salinity reached safety thresholds and conformity checks for heat treatment

or inactivation. Third, verification and release required terminal indicators and sampling frequencies that were benchmarked to regulations; for example, the EU maximum level for citrinin in food supplements based on rice fermented with *Monascus purpureus*, and internal control lines and retain-sample retesting were set accordingly. These practices converted chemical and microbiological risks into a tabulated system of parameters, limits, and evidence (https://eur-lex.europa.eu/legal-content/EN-CS/TXT/?from=en&uri=CELEX:32023R0915&utm_source, accessed on 16 October 2025).

The interface with regulations and systems balanced regional differences with audit friendliness. Within the EU, food business operators established procedures based on HACCP under Regulation (EC) No 852/2004 and maintained hazard analyses and records appropriate to product and process. In the United States, the emphasis lay on preventive controls rather than universal mandatory industry HACCP, and firms documented, monitored, and corrected process, allergen, and sanitation preventive controls under 21 CFR Part 117. For multi-market operations, ISO 22000 functioned as a unifying management skeleton that aligned the technical core of Codex HACCP with organizational requirements for documented systems, internal audits, and management review, which reduced duplication in multi-pronged compliance (http://data.europa.eu/eli/reg/2004/852/oj; https://ecfr.io/Title-21/Part-117, accessed on 16 October 2025).

In sum, a matrix linking hazards, parameters, and evidence was applied across the entire process. High-priority risks including citrinin, biogenic amines, and halotolerant or spore-forming contaminants were tied to strain and raw-material admission as PRPs, to process windows as OPRPs or CCPs, and to terminal verification as release indicators and regulatory limits. Monitoring, corrective actions, verification, and recordkeeping were fixed stepwise into traceable forms and audit evidence. This path remained consistent with Codex HACCP principles and interfaced smoothly with EU 852/2004, US 21 CFR Part 117 and ISO 22000, converting risk identification into an integrated compliance solution across processes and markets.

Overall, quantitative control points across raw materials, qu, fermentation, and finished products, together with modern monitoring and automation, upgraded traditional fermentation from experience to scientific standards. Safety and consistency were improved, and a full process loop from risk identification to process control was achieved.

7. Conclusions and Prospects

7.1. Limitations and Knowledge Gaps

7.1.1. Lack of Standardization in Metagenomic and Metabolomic Protocols

Metagenomic and metabolomic workflows still lack unified standards and a minimum information set for solid-state fermentation scenarios. Generic frameworks such as MIxS and STORMS did provide metadata and reporting elements, yet no reusable industry checklist had formed for key dimensions such as daqu source, heap temperature history, moisture trajectory, and sampling layers, which limited cross-study reproducibility and model transfer. On the metabolomics side, the MSI system and later reporting norms existed, but the suitability of identification confidence and cross-platform calibration remained insufficient in high-salt and high-viscosity matrices, which broke the evidence chain for data sharing and pooled analysis. Process variables and multi-omics metadata needed to be listed as required items in parallel.

7.1.2. Poor Linkage Between Enzyme Activity and Sensory Outcomes

The quantitative linkage between enzyme activity and sensory evaluation remains weak. Existing work often used correlation networks or data fusion to depict associations between metabolites and sensory scores, which could suggest pathways and candidate

molecules, but could not infer effect sizes in oral perception from the strength of extracellular enzyme profiles during the koji stage because of matrix effects, interactions, and supra-threshold integration. The lack of a causality-centered loop that linked enzyme profiles, key flavor factors, and sensory contribution hindered generalizable predictive models. Subsequent studies should place standardized sensory protocols and repeatable chemical quantitation in one design and replace post hoc correlations with prospective designs and intervention trials.

7.1.3. Limited Modeling of Thermohydrometric Dynamics in Solid-State Fermentations

Dynamic models of temperature and humidity in solid-state fermentation still did not capture spatiotemporal gradients at the bed scale. Predictions built only on initial concentrations and temperature curves were unreliable in traditional food systems, and seasonal or process fluctuations enlarged errors. Existing heat and mass transfer models were often built under idealized beds and limited sensing, which failed to cover nonuniform aeration, local rewetting, and self-heating peak shifts in real koji rooms. Observable modeling for actual equipment was needed, with online sensing and identifiable parameters and with water activity and gas–solid coupling included as state variables, so that consistency control across seasons and sites could be supported.

7.2. Integration of Traditional Wisdom and Modern Biomanufacturing

7.2.1. From Natural Inoculation to Targeted Functional Seed Qu: Isolation, Recombination, and Solid-State Scale-Up of Core Microbes

To meet scale and consistency, natural fall-inoculation with experiential screening moved toward functional seed qu guided by target flavor. Core microbes with key metabolic routes were isolated from mature qu or fermentation matrices. Their aroma-forming, enzyme-producing, or stress-tolerant traits were clarified. Simplified or synthetic consortia were then recombined into solid media so that saccharification, acid or alcohol formation, and esterification were co-designed, tunable, and scalable within a single seed qu. This idea was extended to integrated design across seed qu, fermented grain, and pit mud. Multi-omics with metabolic-flux quantification verified causal links between blend ratios and outcomes, enabling reproducible modules for goals such as raising esters, lowering lactic acid, enhancing umami flavors, or suppressing off-notes.

7.2.2. Smart Qu Making: Digital Monitoring and Closed-Loop Control of Temperature, Humidity, Airflow, and Biogenic Heat

Solid-state qu making featured tightly coupled heat release, heat transfer, and mass transfer. Peak internal temperatures reached about 55–62 °C with relative humidity near 90 percent. If ventilation and humidification or heat removal were not synchronized, vertical gradients in temperature and moisture increased, causing local inactivation or contamination windows. Online sensing and closed-loop control of temperature, humidity, and O_2/CO_2 were therefore required in industrial rooms. Layered sensors across the qu bed were combined with forced air and variable-frequency fans to predictably reduce thermal gradients as airflow increased. Exhaust humidity and dew-point monitoring allowed inference of bed moisture to guide misting. Digital-twin and physics-data fusion models indicated that solid-state fermentation, including koji for soy sauce, already supported triple loops of online sensing, cloud models, and local execution for quality consistency. Evaluations of packed-bed fermenters emphasized that forced aeration played dual roles in oxygen supply and heat removal, which governed the coupling of peak temperature and moisture. Thermal imaging or fiber thermometry, exhaust spectra, and pressure-drop monitoring formed a multi-dimensional data stack that upgraded operation from experiential inspection to early anomaly detection, prediction, and correction.

7.2.3. Low-Salt or Low-Sugar and Health-Oriented Products: Technical Challenges and Flavor-Compensation Strategies

Consumer demand for salt reduction and metabolic health requires new balances between lower NaCl, flavor retention, and safety. In soy sauce and related systems, benchmark salt levels were often 18–20 percent w/v, while WHO suggested daily salt intake at or below 5 g. Process options included staged salting, late salt addition, and partial replacement with KCl or potassium lactate, supported by flavor compensation. Model-food studies showed that an 18 percent sodium reduction in soups did not reduce liking, indicating that umami and aroma synergy could help maintain acceptance. KCl-based blends that claimed no added sodium increased stated acceptance. For qu-based products, a branch worth exploration enriched GABA or raised polyphenols or small peptides to offset the loss of savory flavors and body under salt reduction. Online phase plots combining texture, volatile profiles, and amino nitrogen guided tri-objective compromises among low salt, flavor, and safety. Coupling with smart qu rooms allowed co-monitoring of lactic acid and amine risks and microbial load to curb over-acidification and rises in biogenic amines during salt reduction.

7.2.4. Balancing Regional Flavor and Geographical Indications

Future work would couple geographical indications with process fingerprints to balance shared identity and local character. At the shared level, internationally recognized GI frameworks would lock raw materials, processes, and environmental boundaries. Zhenjiang Xiang Cu obtained EU PGI registration in 2012 and specified brewing materials and geographic scope. Shaoxing Jiu entered the China–EU mutual recognition list, which provided a legal basis for cross-border compliance and name protection (https://eur-lex.europa.eu/legal-content/EN/TXT/HTML/?uri=CELEX%3A52020PC0214&utm_source, accessed on 16 October 2025).

At the individual level, quantifiable phenotypes from qu, substrates, and microenvironments outline flavor maps. For example, Pixian Douban in China specified sources of inputs and the spatiotemporal rhythm of sun exposure and turning, setting verifiable thresholds for sun fermentation and qu-driven aroma building. Technical specifications appeared as machine-readable metadata, which reduced drift between name and flavor. A two-layer assessment followed. GI constrained geography and inputs, while process fingerprints described flavor character through thermal trajectories in qu rooms, moisture and ventilation curves, and key physicochemical indices. This enabled benchmarking in global trade while preserving differentiated regional expression.

7.2.5. Evidence Linking Qu, Foods, and Health

Health functions driven by qu needed an evidence chain from molecular mechanisms to models to human data. Future work would combine human trials with real-world evidence in foods. With explicit labels of starter type, dose, matrix, and population subtypes, interventions on lipids, blood pressure, and sensory acceptance would be deposited in open platforms to build reusable, multi-layer evidence networks that support regulatory compliance and clinical translation.

7.2.6. Open Data and Standardization: Reproducible Qu Evaluation and Cross-Process Benchmarking

As shown in Figure 5, upgrading craftsman experience to computable processes required open data and standardization in concert. On standards, the Regional Standard for Fermented Soybean Paste set quantitative thresholds for quality factors; for example, total nitrogen at or above 1.6 percent for soybean pastes, amino nitrogen at or above 0.3 percent, and moisture at or below 60 percent. These brought key physicochemical indices from

starter to final product into unified methods under CXS 234, together with additive and contaminant limits and labeling rules, to form comparable evaluation frameworks across companies and regions (https://www.fao.org/fao-who-codexalimentarius/sh-proxy/fr/?lnk=1&url=https%253A%252F%252Fworkspace.fao.org%252Fsites%252Fcodex%252FStandards%252FCXS+298R-2009%252FCXS_298Re.pdf, accessed on 16 October 2025). On open data, microbial and metabolite platforms already supported FAIR practices [181,182]. Qiita enabled cross-study reanalysis and rapid meta-analysis. GNPS/ReDU and the unified cross-repository identifiers connected MetaboLights, Metabolomics Workbench, and GNPS/MassIVE for reuse of untargeted data, which informed cross-project benchmarking of qu, volatiles or peptides, and flavor. A minimum information set was therefore proposed. It recorded qu room temperature, humidity, airflow, filling and ventilation parameters, and unified fields for α-amylase and protease activities, amino nitrogen, and key volatile panels. Raw sequence and spectral files were archived, and reanalysis scripts were released together. Regional process differences were then translated into comparable process fingerprints, enabling reproducible benchmarking of starters across companies, processes, and regions.

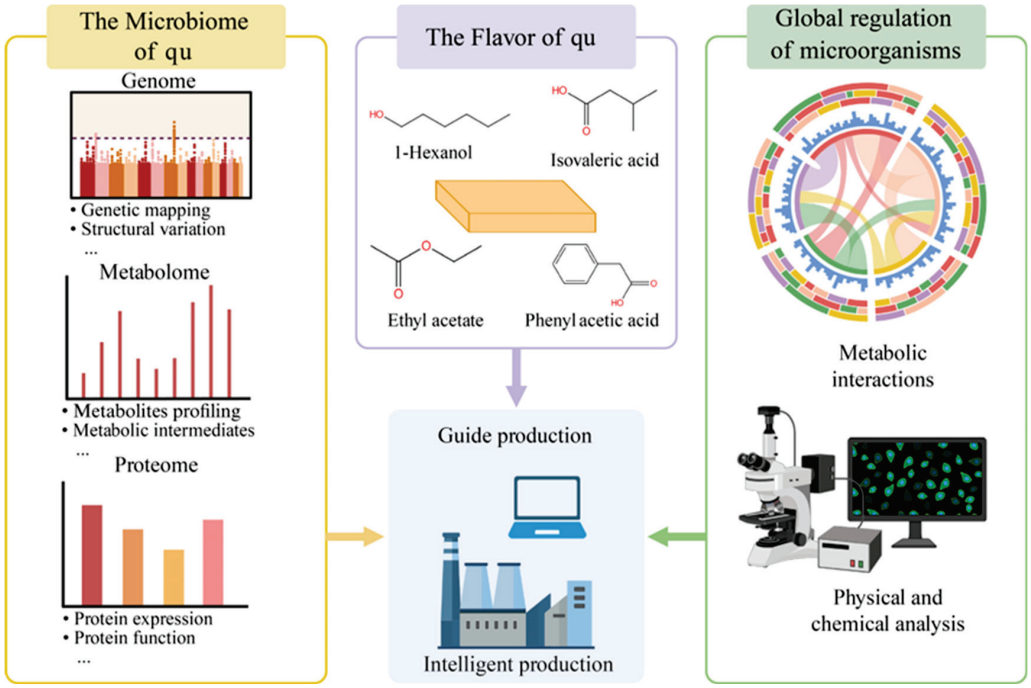


Figure 5. Schematic of the modernization outlook for qu.

7.3. Conclusions

This review restated the contemporary role of starter koji from three dimensions: process, community, and quality and safety. The key boundary conditions of solid-state starter making were summarized as moisture, oxygen supply, ventilation and heat removal, and thermal history trajectory. A reproducible process fingerprint was built for benchmarking across processes and seasons. Evidence showed that temperature type was the primary driver of daqu assembly and functional differentiation. Replacement of related phyla and genera and their metabolic directions occurred alongside heat peaks, gradual cooling, and maturation. In the soy sauce system, the salt-tolerant relay between the koji stage and the moromi stage, together with the adaptation of lactic acid bacteria and halotolerant yeasts under high salt, provided a model of cross-stage coordination between enzyme supply and salt-tolerant conversion. In the Hongqu scenario, CIT risk control and regulatory limits

further indicated that quality and safety had become constraints embedded in process design. These points supported a modern redefinition of starter koji as a natural bioreactor.

Traditional experience was therefore replaced and elevated by two paths. The first was process parameterization. Online visualization and limit management brought peak temperature, heating rate, bed pressure drop, and water activity into process control points. Within the HACCP framework of fermented foods, acidification, salinity, and time–concentration trajectories of key hazards were turned into release thresholds. The second was microbiome-guided design. Metagenomic and metabolomic analyses informed the assembly of starter consortia and the optimization of symbiosis around functional cores and interaction networks, which balanced flavor and safety. The coupling of these paths constituted a shift from workshop craft to engineering and from experience to reproducible manufacturing.

Future work was suggested in three actionable directions. First, cross-platform standards for omics and process data should be formed to support long-term accumulation on community assembly rules and functional cores. Second, a closed evidence loop from enzyme profiles to material flux and to sensory and consumer responses should be established to move metrics from physicochemical endpoints to explainable sensory causality. Third, dynamic models of solid-state fermentation that couple heat and mass transfer with metabolic flux should be developed and linked with online sensing and digital twins to predict and correct batch variation. These efforts would align reproducible thermal and moisture trajectories, designable community structures, and verifiable quality and safety into a unified engineering language and would accelerate the transition of Chinese fermented foods toward standardization and high consistency.

Author Contributions: Conceptualization, D.S. and L.Y.; methodology, X.Z., Y.W. and J.G.; software, Y.W., J.G. and L.S.; validation, Y.W. and X.Z.; formal analysis, Y.W. and L.Y.; investigation, J.G. and L.S.; resources, D.S., X.Z., Y.W., J.G., L.S. and L.Y.; data curation, D.S., X.Z. and L.S.; writing—original draft preparation, Y.W. and L.Y.; writing—review and editing, Y.W., J.G., L.S. and L.Y.; visualization, X.Z. and L.S.; supervision, L.Y. and D.S. All authors have read and agreed to the published version of the manuscript.

Funding: This work was financially supported by the Guizhou Provincial Basic Research Program (Natural Science) [2025]018); Moutai Institute & Guizhou Guiding distillery cooperation research and development project (XYNJ20240374, XYNJ20250032); Research on the Microbial Community Structure of Sauce-Flavor Baijiu Daqu and Its Impact on Flavor Formation (mygccrc [2022]013); The Zunyi Technology and Big Data Bureau-Moutai institute; Joint Science and Technology Research and Development Project (grant number Zun-Shi-Ke-He HZ zi [2023]110); Moutai Institute & Guangdong Li'ran Chemical Group Co., Ltd. Cooperation Research and Development Project (XYNJ20240104); and Zunyi City Science and Technology Plan Project: [Contract No.: Zun Shi Ke He HZ Zi (2023) 112].

Institutional Review Board Statement: Not applicable.

Informed Consent Statement: Not applicable.

Data Availability Statement: The original contributions presented in the study are included in the article, further inquiries can be directed to the corresponding author.

Conflicts of Interest: The authors declare that they have no known competing financial interests or personal relationships that could have appeared to influence the work reported in this paper.

Abbreviations

AEDA	Aroma extract dilution analysis
aw	Water activity
BA	Biogenic amines
BGC(s)	Biosynthetic gene cluster(s)
CCP(s)	Critical control point(s)
CFU	Colony-forming unit (e.g., CFU/g)
CFR	Code of Federal Regulations (e.g., 21 CFR Part 117)
CIT	Citrinin (mycotoxin)
EC	European Communities/Commission (e.g., Regulation (EC) No 852/2004)
e-nose	Electronic nose
EU	European Union
FD (factor)	Flavor dilution (factor)
FSMA	Food Safety Modernization Act
GABA	γ-Aminobutyric acid
GC–O	Gas chromatography–olfactometry
GI	Geographical indication(s)
HACCP	Hazard analysis and critical control point(s)
HPLC	High-performance liquid chromatography
HT-Daqu	High-temperature daqu
IoT	Internet of Things
ISO 22000	Food safety management standard by the International Organization for Standardization
KCl	Potassium chloride
LC–MS/MS	Liquid chromatography–tandem mass spectrometry
LT-Daqu	Low-temperature daqu
LAB	Lactic acid bacteria
MK	Monacolin K
MT-Daqu	Medium-temperature daqu
NaCl	Sodium chloride
O_2/CO_2	Oxygen/carbon dioxide
OAV	Odor activity value
PGI	Protected geographical indication
PRP(s)	Prerequisite program(s) (ISO 22000 context)
QCP(s)	Quality control point(s)
RH	Relative humidity
ROAV	Relative odor activity value
SOP	Standard operating procedure(s)
SP (activity)	Saccharifying power (enzyme activity)
SPME–GC–MS	Solid-phase microextraction gas chromatography–mass spectrometry
UV	Ultraviolet
WHO	World Health Organization
w/*v*	Weight/volume
v/*v*	Volume/volume

References

1. Wu, Y.; Yin, R.; Guo, L.; Song, Y.; He, X.; Huang, M.; Ren, Y.; Zhong, X.; Zhao, D.; Li, J.; et al. The Identification and Analysis of Novel Umami Peptides in Lager Beer and Their Multidimensional Effects on the Sensory Attributes of the Beer Body. *Foods* **2025**, *14*, 2743. [CrossRef]
2. Tu, W.; Cao, X.; Cheng, J.; Li, L.; Zhang, T.; Wu, Q.; Xiang, P.; Shen, C.; Li, Q. Chinese Baijiu: The Perfect Works of Microorganisms. *Front. Microbiol.* **2022**, *13*, 919044. [CrossRef]
3. Kang, J.; Huang, X.; Li, R.; Zhang, Y.; Chen, X.; Han, B. Deciphering the core microbes and their interactions in spontaneous Baijiu fermentation: A comprehensive review. *Food Res. Int.* **2024**, *188*, 114497. [CrossRef]

4. Jin, G.; Zhu, Y.; Xu, Y. Mystery behind Chinese liquor fermentation. *Trends Food Sci. Technol.* **2017**, *63*, 18–28. [CrossRef]
5. Liu, L.; Li, Y.; Hou, J. Making beer with malted cereals and qu starter in the Neolithic Yangshao culture, China. *J. Archaeol. Sci. Rep.* **2020**, *29*, 102134. [CrossRef]
6. Liu, L.; Zhang, Y.; Ge, W.; Lin, Z.; Sinnott-Armstrong, N.; Yang, L. Revealing the 2300-Year-Old Fermented Beverage in a Bronze Bottle from Shaanxi, China. *Fermentation* **2024**, *10*, 365. [CrossRef]
7. Liu, L.; Zhang, J.; Li, J.; He, Y.; Gao, Z.; Jiang, L. Identification of 10,000-year- old rice beer at Shangshan in the Lower Yangzi River valley of China. *Proc. Natl. Acad. Sci. USA* **2024**, *121*, e2412274121. [CrossRef]
8. Yang, L.; Fan, W.; Xu, Y. Qu-omics elucidates the formation and spatio-temporal differentiation mechanism underlying the microecology of high temperature Daqu. *Food Chem.* **2024**, *438*, 137988. [CrossRef]
9. Sakandar, H.A.; Hussain, R.; Khan, Q.F.; Zhang, H. Functional microbiota in Chinese traditional Baijiu and Mijiu Qu (starters): A review. *Food Res. Int.* **2020**, *138*, 109830. [CrossRef]
10. Zhang, K.; Li, Q.; Wu, W.; Yang, J.; Zou, W. Wheat Qu and Its Production Technology, Microbiota, Flavor, and Metabolites. *J. Food Sci.* **2019**, *84*, 2373–2386. [CrossRef]
11. Mao, X.; Yue, S.; Xu, D.; Fu, R.; Han, J.; Zhou, H.; Tang, Y. Research Progress on Flavor and Quality of Chinese Rice Wine in the Brewing Process. *ACS Omega* **2023**, *8*, 32311–32330. [CrossRef] [PubMed]
12. Wang, M.; Yang, J.; Zhao, Q.; Zhang, K.; Su, C. Research Progress on Flavor Compounds and Microorganisms of Maotai Flavor Baijiu. *J. Food Sci.* **2019**, *84*, 6–18. [CrossRef]
13. Yang, Y.; Hu, W.; Xia, Y.; Mu, Z.; Tao, L.; Song, X.; Zhang, H.; Ni, B.; Ai, L. Flavor Formation in Chinese Rice Wine (Huangjiu): Impacts of the Flavor-Active Microorganisms, Raw Materials, and Fermentation Technology. *Front. Microbiol.* **2020**, *11*, 580247. [CrossRef] [PubMed]
14. Wang, B.; Wu, Q.; Xu, Y.; Sun, B. Synergistic Effect of Multiple Saccharifying Enzymes on Alcoholic Fermentation for Chinese Baijiu Production. *Appl. Environ. Microbiol.* **2020**, *86*, e00013-20. [CrossRef]
15. Jin, G.; Zhao, Y.; Xin, S.; Li, T.; Xu, Y. Solid-State Fermentation Engineering of Traditional Chinese Fermented Food. *Foods* **2024**, *13*, 3003. [CrossRef] [PubMed]
16. Balasubramanian, R.; Schneider, E.; Gunnigle, E.; Cotter, P.D.; Cryan, J.F. Fermented foods: Harnessing their potential to modulate the microbiota-gut-brain axis for mental health. *Neurosci. Biobehav. Rev.* **2024**, *158*, 105562. [CrossRef]
17. Deng, J.; Zheng, J.; Li, X.; Huang, D.; Ye, G.; Luo, H. Characterization of Qu-aroma of medium-high temperature Daqu from different production areas using sensory evaluation, E-nose, and GC-MS/O analysis. *Bioresour. Bioprocess.* **2025**, *12*, 40. [CrossRef]
18. Lv, X.; Huang, Z.; Zhang, W.; Rao, P.; Ni, L. Identification and characterization of filamentous fungi isolated from fermentation starters for Hong Qu glutinous rice wine brewing. *J. Gen. Appl. Microbiol.* **2012**, *58*, 33–42. [CrossRef]
19. Lin, X.; Ren, X.; Huang, Y.; Liang, Z.; Li, W.; Su, H.; He, Z. Regional characteristics and discrimination of the fermentation starter Hong Qu in traditional rice wine brewing. *Int. J. Food Sci. Technol.* **2021**, *56*, 5664–5673. [CrossRef]
20. Lv, X.; Jia, R.; Li, Y.; Chen, F.; Chen, Z.; Liu, B.; Chen, S.; Rao, P.; Ni, L. Characterization of the dominant bacterial communities of traditional fermentation starters for Hong Qu glutinous rice wine by means of MALDI-TOF mass spectrometry fingerprinting, 16S rRNA gene sequencing and species-specific PCRs. *Food Control* **2016**, *67*, 292–302. [CrossRef]
21. Mu, Y.; Yao, S.; Huang, Y.; Zhu, Z.; Li, D.; Song, Y.; Liu, Z.; Zhang, C.; Yu, S. Unveiling the metabolic heterogeneity and formation mechanism in Chinese typical Daqu based on Qu-omics. *Food Res. Int.* **2025**, *202*, 115735. [CrossRef]
22. Park, K.H.; Liu, Z.; Park, C.; Ni, L. Microbiota associated with the starter cultures and brewing process of traditional Hong Qu glutinous rice wine. *Food Sci. Biotechnol.* **2016**, *25*, 649–658. [CrossRef]
23. Xu, Y.; Wang, D.; Fan, W.L.; Mu, X.Q.; Chen, J. Traditional Chinese Biotechnology. In *Advances in Biochemical Engineering-Biotechnology*; Tsao, G.T., Ouyang, P., Chen, J., Eds.; Springer: Berlin/Heidelberg, Germany, 2010; Volume 122, pp. 189–233. ISBN 978-3-642-14994-8.
24. Yi, Z.; Jin, Y.; Xiao, Y.; Chen, L.; Tan, L.; Du, A.; He, K.; Liu, D.; Luo, H.; Fang, Y.; et al. Unraveling the Contribution of High Temperature Stage to Jiang-Flavor Daqu, a Liquor Starter for Production of Chinese Jiang-Flavor Baijiu, with Special Reference to Metatranscriptomics. *Front. Microbiol.* **2019**, *10*, 472. [CrossRef]
25. Zhang, J.; Hou, Y.; Liu, Q.; Zhang, Y.; Gao, B.; Zou, W.; Zhang, K. Fortified Jiuqu of the Chinese Baijiu: A review on its functional microorganisms, strengthening effects, current challenges, and perspectives. *Food Biosci.* **2023**, *55*, 103045. [CrossRef]
26. Zhang, Y.; Yin, H.; Zhao, T.; Zhan, C.; Wang, A.; Xu, Y.; Chen, M. The volatile flavor and the antioxidant properties of a novel chrysanthemum rice wine during natural aging. *Food Sci. Nutr.* **2023**, *11*, 2382–2392. [CrossRef] [PubMed]
27. Chen, C.; Zheng, Z.; Wang, Y.; Ji, X.; Li, D.; Li, P.; Liu, Y. Function-driven high-throughput screening and isolation of ester-producing strains for glutinous rice wine fermentation. *Food Res. Int.* **2025**, *199*, 115393. [CrossRef]
28. Cui, D.; Wei, Y.; Lin, L.; Chen, S.; Feng, P.; Xiao, D.; Lin, X.; Zhang, C. Increasing Yield of 2,3,5,6-Tetramethylpyrazine in Baijiu Through *Saccharomyces cerevisiae* Metabolic Engineering. *Front. Microbiol.* **2020**, *11*, 596306. [CrossRef]
29. Minhua, L.; Wenhong, Z.; Weidong, B.; Yuanshan, Y.; Chuqiang, L.; Conggui, C.; Yongtao, F. Research progress on the influence of microbial flora of Baijiu Jiuqu on flavor formation. *China Brewing* **2023**, *42*, 22–27.

30. Dong, W.; Yu, X.; Wang, L.; Zou, M.; Ma, J.; Liu, J.; Feng, Y.; Zhao, S.; Yang, Q.; Hu, Y.; et al. Unveiling the microbiota of sauce-flavor Daqu and its relationships with flavors and color during maturation. *Front. Microbiol.* **2024**, *15*, 1345772. [CrossRef]
31. Zhu, C.; Cheng, Y.; Zuo, Q.; Huang, Y.; Wang, L. Exploring the impacts of traditional crafts on microbial community succession in Jiang-flavored Daqu. *Food Res. Int.* **2022**, *158*, 111568. [CrossRef]
32. Wei, Y.; Wen, Z.; Yao, S.; Cheng, P.; Huang, W.; Jiang, L.L.; Bai, M.; Han, D.; Song, L.; Zhu, H.; et al. Tempo-spatial dynamics of physicochemical properties and microbial communities in high-temperature Daqu during the fermentation process. *Food Chem. X* **2025**, *29*, 102815. [CrossRef] [PubMed]
33. Tang, Q.; He, G.; Huang, J.; Wu, C.; Jin, Y.; Zhou, R. Characterizing Relationship of Microbial Diversity and Metabolite in Sichuan Xiaoqu. *Front. Microbiol.* **2019**, *10*, 696. [CrossRef] [PubMed]
34. Xu, Y.; Wu, M.; Niu, J.; Lin, M.; Zhu, H.; Wang, K.; Li, X.; Sun, B. Characteristics and Correlation of the Microbial Communities and Flavor Compounds during the First Three Rounds of Fermentation in Chinese Sauce-Flavor Baijiu. *Foods* **2023**, *12*, 207. [CrossRef] [PubMed]
35. Wen, Z.; Wei, Y.; Han, D.; Song, L.; Zhu, H.; Guo, L.; Chen, S.; Lin, B.; He, C.; Guo, Z.; et al. Deciphering the role of traditional flipping crafts in medium-temperature Daqu fermentation: Microbial succession and metabolic phenotypes. *Curr. Res. Food Sci.* **2025**, *10*, 101063. [CrossRef]
36. Xu, J.; Wu, H.; Wang, Z.; Zheng, F.; Lu, X.; Li, Z.; Ren, Q. Microbial dynamics and metabolite changes in Chinese Rice Wine fermentation from sorghum with different tannin content. *Sci. Rep.* **2018**, *8*, 4639. [CrossRef]
37. Guan, T.; Wei, X.; Qiu, X.; Liu, Y.; Yu, J.; Hou, R.; Liu, M.; Mao, Y.; Liu, Q.; Tian, L.; et al. Precipitation and temperature drive microbial community changes affecting flavor quality of Nongxiangxing Daqu. *Food Chem. X* **2024**, *24*, 102063. [CrossRef]
38. Xiao, R.; Chen, S.; Wang, X.; Chen, K.; Hu, J.; Wei, K.; Ning, Y.; Xiong, T.; Lu, F. Microbial community starters affect the profiles of volatile compounds in traditional Chinese Xiaoqu rice wine: Assement via high-throughput sequencing and gas chromatography-ion mobility spectrometry. *LWT-Food Sci. Technol.* **2022**, *170*, 114000. [CrossRef]
39. Wang, S. An Archaeological Perspective of Alcoholic Beverages in the Song Dynasty (960–1279). *Archaeologies-J. World Archaeol. Congr.* **2022**, *18*, 436–467. [CrossRef]
40. Sun, H.; Liu, S.; Mao, J.; Yu, Z.; Lin, Z.; Mao, J. New insights into the impacts of huangjiu compontents on intoxication. *Food Chem.* **2020**, *317*, 126420. [CrossRef]
41. Liu, Q. Determination of inorganic selenium species in commercial wine collected from the Beijing region, China. *Chem. Speciat. Bioavailab.* **2010**, *22*, 81–85. [CrossRef]
42. Peng, B.; Huang, H.; Xu, J.; Xin, Y.; Hu, L.; Wen, L.; Li, L.; Chen, J.; Han, Y.; Li, C. Rice Wine Fermentation: Unveiling Key Factors Shaping Quality, Flavor, and Technological Evolution. *Foods* **2025**, *14*, 2544. [CrossRef]
43. Geng, J.; Li, D.; He, S.; Min, C.; Long, J.; Yang, S. The influence of cardamine hupingshanensis on the microbial community structure of jiuqu and the variation of flavor during the fermentation process of selenium-rich Chinese huangjiu. *Int. J. Gastron. Food Sci.* **2024**, *36*, 100947. [CrossRef]
44. Wang, Z.; Wang, C.; Shen, C.; Wang, S.; Mao, J.; Li, Z.; Ganzle, M.; Mao, J. Microbiota stratification and succession of amylase-producing *Bacillus* in traditional Chinese Jiuqu (fermentation starters). *J. Sci. Food. Agric.* **2020**, *100*, 3544–3553. [CrossRef]
45. Geng, J.; He, S.; Zhang, S.; Tian, H.; Jin, W. Impact of Incorporating Shiitake Mushrooms (*Lentinula edodes*) on Microbial Community and Flavor Volatiles in Traditional Jiuqu. *Foods* **2024**, *13*, 1019. [CrossRef]
46. Li, M.; Zhao, X.; Liu, L.; Huang, Y.; Wang, J.; Zhang, J.; Liu, J. Screening of aroma-producing yeasts and their effects on the flavor characteristics of millet Huangjiu (Chinese rice wine). *Food Biosci.* **2025**, *65*, 105992. [CrossRef]
47. Guan, T.; Yin, X.; Jiang, Y.; Li, Y.; Rao, Y.; Shao, J.; Liu, Y.; Tian, L.; Mao, Y.; Wang, X. Study on the preparation of compound mold enhanced Xiaoqu and its effect on the yield and flavor of Qingxiangxing baijiu. *Food Chem. X* **2025**, *29*, 102721. [CrossRef] [PubMed]
48. Yuan, X.; Gao, S.; Tan, Y.; Cao, J.; Yang, S.; Zheng, B. Production of red yeast rice rich in monacolin K by variable temperature solid fermentation of *Monascus purpureus*. *RSC Adv.* **2023**, *13*, 27303–27308. [CrossRef]
49. Yanli, F.; Xiang, Y. Perspectives on Functional Red Mold Rice: Functional Ingredients, Production, and Application. *Front. Microbiol.* **2020**, *11*, 606959. [CrossRef]
50. Chiu, C.; Ni, K.; Guu, Y.; Pan, T. Production of red mold rice using a modified Nagata type koji maker. *Appl. Microbiol. Biotechnol.* **2006**, *73*, 297–304. [CrossRef] [PubMed]
51. Righetti, L.; Dall'Asta, C.; Bruni, R. Risk Assessment of RYR Food Supplements: Perception vs. Reality. *Front. Nutr.* **2021**, *8*, 792529. [CrossRef]
52. Subsaendee, T.; Kitpreechavanich, V.; Yongsmith, B. Growth, Glucoamylase, Pigments and Monacolin K Production on Rice Solid Culture in Flask and Koji Chamber Using *Monascus* sp. KB9. *Chiang Mai J. Sci.* **2014**, *41*, 1044–1057.
53. Devanthi, P.V.P.; Gkatzionis, K. Soy sauce fermentation: Microorganisms, aroma formation, and process modification. *Food Res. Int.* **2019**, *120*, 364–374. [CrossRef]

54. Choi, J.; Kwon, T.; Park, Y.; Kim, A.Y. Characteristics of Koji Using Liquid Starter for Soy Sauce Production. *Fermentation* **2023**, *9*, 979. [CrossRef]
55. Diez-Simon, C.; Eichelsheim, C.; Mumm, R.; Hall, R.D. Chemical and Sensory Characteristics of Soy Sauce: A Review. *J. Agric. Food. Chem.* **2020**, *68*, 11612–11630. [CrossRef]
56. Tan, G.; Hu, M.; Li, X.; Li, X.; Pan, Z.; Li, M.; Li, L.; Wang, Y.; Zheng, Z. Microbial Community and Metabolite Dynamics During Soy Sauce Koji Making. *Front. Microbiol.* **2022**, *13*, 841529. [CrossRef]
57. Zhang, L.; Xiong, S.; Du, T.; Xiao, M.; Peng, Z.; Xie, M.; Guan, Q.; Xiong, T. Effects of microbial succession on the dynamics of flavor metabolites and physicochemical properties during soy sauce koji making. *Food Biosci.* **2023**, *53*, 102636. [CrossRef]
58. He, X.; Gong, Q.; Li, Z. Composition for Brewing Soy Sauce and Method for Producing Soy Sauce Koji. CN201410123898.1, 30 September 2015.
59. He, G.; Chen, H.; Liu, T.; Yang, H. A Process for Fermenting and Producing Douchi. CN106235021A, 8 November 2019.
60. Wang, F. A Production Process for *Aspergillus oryzae*-Based Douchi. CN101485426B, 31 August 2011.
61. Jiang, L.; Liao, L.; Nie, Q. A Rapid Fermentation Method for Liuyang Douchi Using Pure Starter Cultures via Controlled-Process. CN103932077B, 8 April 2015.
62. Zhang, P.; Lai, T.; Chen, F.; Xie, N. A Process for Producing Douchi Through Edible Mushroom Fermentation. CN103053952A, 24 April 2013.
63. Li, A.; Yang, G.; Wang, Z.; Liao, S.; Du, M.; Song, J.; Kan, J. Comparative evaluation of commercial Douchi by different molds: Biogenic amines, non-volatile and volatile compounds. *Food Sci. Hum. Wellness* **2024**, *13*, 434–443. [CrossRef]
64. Xi, X.; Ke, J.; Ma, Y.; Liu, X.; Gu, X.; Wang, Y. Physiochemical and taste characteristics of traditional Chinese fermented food sufu. *J. Food Process Preserv.* **2022**, *46*, e16845. [CrossRef]
65. Han, B.Z.; Sesenna, B.; Beumer, R.R.; Nout, M. Behaviour of *Staphylococcus aureus* during sufu production at laboratory scale. *Food Control* **2005**, *16*, 243–247. [CrossRef]
66. Chou, C.; Ho, F.; Tsai, C. Effects of Temperature and Relative Humidity on the Growth of and Enzyme Production by *Actinomucor taiwanensis* during Sufu Pehtze Preparation. *Appl. Environ. Microbiol.* **1988**, *54*, 688–692. [CrossRef]
67. Zhao, L.; Liu, Y.; Xu, Q.; Yu, Y.; Zheng, G.; Wang, Y.; Zhang, Q.; Xu, X.; Zhang, N.; Chu, J.; et al. Microbial Community Succession and Its Correlation with Quality Characteristics during Gray Sufu Fermentation. *Foods* **2023**, *12*, 2767. [CrossRef]
68. Chen, Z.; Chen, C.; Yang, R.; Jin, H.; Liu, B.; Wang, Z.; Tan, Y.; Xue, Q.; Hu, Y. The formation mechanism of sufu gels fermented by mucor racemosus during pre-fermentation. *LWT-Food Sci. Technol.* **2024**, *203*, 116309. [CrossRef]
69. Kanlayakrit, W.; Phromsak, K. Novel conditions for tofu and pehtze preparation to overcome bacterial contamination in pehtze. *Int. Food Res. J.* **2014**, *21*, 335–342.
70. Phuc, T.M.; Quan, T.H.; Nhung, D.T.T.; Lien, D.T.P.; Toan, H.T. Effects of Incubation Conditions on the Nutrient Composition and Antioxidative Activity of Fermented Tofu Supplemented with Purple Sweet Potato by *Actinomucor Elegans*. *Acta Sci. Pol. Technol. Aliment.* **2024**, *23*, 513–524. [CrossRef]
71. Hou, X.; Hui, M.; Sun, Z.; Li, X.; Shi, X.; Xiao, R.; Wang, J.; Pan, C.; Li, R. Comparative analysis of the microbiotas and physicochemical properties inside and outside medium-temperature Daqu during the fermentation and storage. *Front. Microbiol.* **2022**, *13*, 934696. [CrossRef]
72. Yan, C.; Huang, Z.; Tu, R.; Zhang, L.; Wu, C.; Wang, S.; Huang, P.; Zeng, Y.; Shi, B. Revealing the Differences in Microbial Community and Quality of High-Temperature Daqu in the Southern Sichuan-Northern Guizhou Region. *Foods.* **2025**, *14*, 570. [CrossRef]
73. Zuo, Q.; Huang, Y.; Guo, M. Evaluation of bacterial diversity during fermentation process: A comparison between handmade and machine-made high-temperature Daqu of Maotai-flavor liquor. *Ann. Microbiol.* **2020**, *70*, 57. [CrossRef]
74. Xue, T.; Zhang, J.; Wang, T.; Bai, B.; Hou, Z.; Cheng, J.; Bo, T.; Fan, S. Reveal the microbial communities and functional prediction during the fermentation of Fen-flavor Baijiu via metagenome combining amplicon sequencing. *Ann. Microbiol.* **2023**, *73*, 16. [CrossRef]
75. Liang, J.; Deng, L.; Li, Z.; Fei, Y.; Bai, W.; Zhao, W.; He, S.; Cao, R. Metagenomic analysis of core differential microbes between traditional starter and Round-Koji-mechanical starter of Chi-flavor Baijiu. *Front. Microbiol.* **2024**, *15*, 1390899. [CrossRef]
76. Hu, Y.; Lei, X.; Zhang, X.; Guan, T.; Wang, L.; Zhang, Z.; Yu, X.; Tu, J.; Peng, N.; Liang, Y.; et al. Characteristics of the Microbial Community in the Production of Chinese Rice-Flavor Baijiu and Comparisons with the Microflora of Other Flavors of Baijiu. *Front. Microbiol.* **2021**, *12*, 673670. [CrossRef]
77. Yan, Y.; Liang, Z.; Huo, Y.; Wu, Q.; Ni, L.; Lv, X. A Comparative Study of Microbial Communities, Biogenic Amines, and Volatile Profiles in the Brewing Process of Rice Wines with Hongqu and Xiaoqu as Fermentation Starters. *Foods* **2024**, *13*, 2452. [CrossRef] [PubMed]
78. Zhao, C.; Su, W.; Mu, Y.; Mu, Y.; Jiang, L. Integrative Metagenomics-Metabolomics for Analyzing the Relationship Between Microorganisms and Non-volatile Profiles of Traditional Xiaoqu. *Front. Microbiol.* **2021**, *11*, 617030. [CrossRef]

79. Yang, Z.; Li, W.; Yuan, Y.; Liang, Z.; Yan, Y.; Chen, Y.; Ni, L.; Lv, X. Metagenomic Insights into the Regulatory Effects of Microbial Community on the Formation of Biogenic Amines and Volatile Flavor Components during the Brewing of Hongqu Rice Wine. *Foods* **2023**, *12*, 3075. [CrossRef] [PubMed]
80. Yang, Y.; Liu, B.; Du, X.; Li, P.; Liang, B.; Cheng, X.; Du, L.; Huang, D.; Wang, L.; Wang, S. Complete genome sequence and transcriptomics analyses reveal pigment biosynthesis and regulatory mechanisms in an industrial strain, *Monascus purpureus* YY-1. *Sci. Rep.* **2015**, *5*, 8331. [CrossRef] [PubMed]
81. Liang, Z.; Chen, S.; Wang, H.; Wu, Q.; Guo, W.; Ni, L.; Lv, X. Metagenomic and Metabolomic Profiling Reveals the Differences of Flavor Quality between Hongqu Rice Wines Fermented with Gutian Qu and Wuyi Qu. *Foods* **2024**, *13*, 3114. [CrossRef]
82. Tan, G.; Wang, Y.; Hu, M.; Li, X.; Li, X.; Pan, Z.; Li, M.; Li, L.; Zheng, Z. Comparative evaluation of the microbial diversity and metabolite profiles of Japanese-style and Cantonese-style soy sauce fermentation. *Front. Microbiol.* **2022**, *13*, 976206. [CrossRef]
83. Pei, R.; Lv, G.; Guo, B.; Li, Y.; Ai, M.; He, B.; Wan, R. Physiological and transcriptomic analyses revealed the change of main flavor substance of *Zygosaccharomyces* rouxii under salt treatment. *Front. Nutr.* **2022**, *9*, 990380. [CrossRef]
84. Link, T.; Vogel, R.F.; Ehrmann, M.A. The diversity among the species Tetragenococcus halophilus including new isolates from a lupine seed fermentation. *BMC Microbiol.* **2021**, *21*, 320. [CrossRef]
85. Zheng, S.; Zhang, Z.; Zhao, X.; Li, W.; Hou, L. A Method of Reducing Salt Content in Fermented Soy Sauce Improves Its Flavor and Quality. *Foods* **2024**, *13*, 971. [CrossRef]
86. Ruan, L.; Ju, Y.; Zhan, C.; Hou, L. Improved umami flavor of soy sauce by adding enzymatic hydrolysate of low-value fish in the natural brewing process. *LWT-Food Sci. Technol.* **2022**, *155*, 112911. [CrossRef]
87. Lijun, B.; Yuwei, W.; Qingsong, L.; Ziyao, L.; Haiyu, F.; Bohua, W.; Jing, Y.; Xiaoming, L.; Xuewei, J. Brewing-related genes annotation of *Bacillus* velezensis CS1.10S isolated from traditional moromi and its effects on promoting soy sauce fermentation. *Food Biosci.* **2023**, *56*, 103267.
88. Lin, X.; Tang, Y.; Hu, Y.; Lu, Y.; Sun, Q.; Lv, Y.; Zhang, Q.; Wu, C.; Zhu, M.; He, Q.; et al. Sodium Reduction in Traditional Fermented Foods: Challenges, Strategies, and Perspectives. *J. Agric. Food. Chem.* **2021**, *69*, 8065–8080. [CrossRef]
89. Qiao, H.; Li, Y.; Cui, F.; Zhang, W.; Zhang, Z.; Li, H. Nutrition, Flavor, and Microbial Communities of Two Traditional Bacterial Douchi from Gansu, China. *Foods* **2024**, *13*, 3519. [CrossRef]
90. Zhao, H.; Xu, J.; Wang, R.; Liu, X.; Peng, X.; Guo, S. Succession and Diversity of Microbial Flora during the Fermentation of Douchi and Their Effects on the Formation of Characteristic Aroma. *Foods* **2023**, *12*, 329. [CrossRef]
91. Zhang, P.; Li, H.; Zhao, W.; Xiong, K.; Wen, H.; Yang, H.; Wang, X. Dynamic analysis of physicochemical characteristics and microbial communities of *Aspergillus*-type douchi during fermentation. *Food Res. Int.* **2022**, *153*, 110932. [CrossRef] [PubMed]
92. Yang, L.; Yang, H.; Tu, Z.; Wang, X. High-Throughput Sequencing of Microbial Community Diversity and Dynamics during Douchi Fermentation. *PLoS ONE* **2016**, *11*, e0168166. [CrossRef]
93. Luo, A.; Liu, T.; Shi, S.; Liu, X.; Shi, X.; Hu, B. Characterization of Microbial Community and Flavor Compounds in Traditional Fermented Douchi Using HTS and HS-SPME-GC-MS. *Food Sci. Nutr.* **2025**, *13*, e4660. [CrossRef] [PubMed]
94. He, B.; Li, H.; Hu, Z.; Zhang, Y.; Sun, M.; Qiu, S.; Zeng, B. Difference in microbial community and taste compounds between *Mucor*-type and *Aspergillus*-type Douchi during koji-making. *Food Res. Int.* **2019**, *121*, 136–143. [CrossRef]
95. Li, L.; Ruan, L.; Ji, A.; Wen, Z.; Chen, S.; Wang, L.; Wei, X. Biogenic amines analysis and microbial contribution in traditional fermented food of Douchi. *Sci. Rep.* **2018**, *8*, 12567. [CrossRef]
96. Fong, F.L.Y.; Lam, K.Y.; Lau, C.S.; Ho, K.H.; Kan, Y.H.; Poon, M.Y.; El-Nezami, H.; Sze, E.T.P. Reduction in biogenic amines in douchi fermented by probiotic bacteria. *PLoS ONE* **2020**, *15*, e0230916. [CrossRef]
97. Yao, D.; Xu, L.; Wu, M.; Wang, X.; Wang, K.; Li, Z.; Zhang, D. Microbial Community Succession and Metabolite Changes During Fermentation of BS Sufu, the Fermented Black Soybean Curd by *Rhizopus microsporus*, *Rhizopus oryzae*, and *Actinomucor elegans*. *Front. Microbiol.* **2021**, *12*, 665826. [CrossRef]
98. Han, B.Z.; Ma, Y.; Rombouts, F.M.; Nout, M. Effects of temperature and relative humidity on growth and enzyme production by *Actinomucor elegans* and *Rhizopus oligosporus* during sufu pehtze preparation. *Food Chem.* **2003**, *81*, 27–34. [CrossRef]
99. Tan, G.; Hu, M.; Li, X.; Pan, Z.; Li, M.; Li, L.; Yang, M. High-Throughput Sequencing and Metabolomics Reveal Differences in Bacterial Diversity and Metabolites Between Red and White Sufu. *Front. Microbiol.* **2020**, *11*, 758. [CrossRef]
100. Han, B.Z.; Beumer, R.R.; Rombouts, F.M.; Nout, M. Microbiological safety and quality of commercial sufu—A Chinese fermented soybean food. *Food Control* **2001**, *12*, 541–547. [CrossRef]
101. Han, B.Z.; Kuijpers, A.; Thanh, N.V.; Nout, M. Mucoraceous moulds involved in the commercial fermentation of Sufu Pehtze. *Antonie. Van. Leeuwenhoek.* **2004**, *85*, 253–257. [CrossRef] [PubMed]
102. Wu, Y.; Hou, Y.; Chen, H.; Wang, J.; Zhang, C.; Zhao, Z.; Ao, R.; Huang, H.; Hong, J.; Zhao, D.; et al. "Key Factor" for Baijiu Quality: Research Progress on Acid Substances in Baijiu. *Foods* **2022**, *11*, 2959. [CrossRef] [PubMed]
103. Niu, J.; Yang, S.; Shen, Y.; Cheng, W.; Li, H.; Sun, J.; Huang, M.; Sun, B. What Are the Main Factors That Affect the Flavor of Sauce-Aroma Baijiu. *Foods* **2022**, *11*, 3534. [CrossRef] [PubMed]

104. Yang, L.; Fan, W.; Xu, Y. GC × GC-TOF/MS and UPLC-Q-TOF/MS based untargeted metabolomics coupled with physicochemical properties to reveal the characteristics of different type daqus for making soy sauce aroma and flavor type baijiu. *LWT-Food Sci. Technol.* **2021**, *146*, 111416. [CrossRef]
105. Tang, Q.; Zhang, Y.; Huang, J.; Zhou, R. Synthetic and natural microbial communities in high-temperature Daqu production: Insights into metabolic pathways and volatile organic compounds. *Food Res. Int.* **2025**, *219*, 116962. [CrossRef]
106. Wu, J.; Chen, R.; Li, X.; Fu, Z.; Xian, C.; Zhao, W.; Zhao, C.; Wu, X. Comprehensive identification of key compounds in different quality grades of soy sauce-aroma type baijiu by HS-SPME-GC-MS coupled with electronic nose. *Front. Nutr.* **2023**, *10*, 1132527. [CrossRef]
107. Xiang, D.; Li, P.; Gong, R.; Sun, Y.; Chen, X.; Wei, H.; Xu, Y. Quantification and Distribution of Thiols in Fermented Grains of Sauce-Aroma Baijiu Production Process. *Foods* **2023**, *12*, 2658. [CrossRef] [PubMed]
108. Yan, Y.; Chen, S.; He, Y.; Nie, Y.; Xu, Y. Quantitation of pyrazines in Baijiu and during production process by a rapid and sensitive direct injection UPLC-MS/MS approach. *LWT-Food Sci. Technol.* **2020**, *128*, 109371. [CrossRef]
109. Wang, J.; Liu, Z.; Wang, X.; Zhu, J.; Xu, J.; Zhang, R.; Cai, F.; Zhu, Z.; Cao, J.; Yu, Q. Optimizing Baijiu fermentation with high-yield ethyl caproate-producing *Candida parapsilosis* strain. *LWT-Food Sci. Technol.* **2024**, *203*, 116347. [CrossRef]
110. Zhang, P.; Liu, Y.; Li, H.; Hui, M.; Pan, C. Strategies and Challenges of Microbiota Regulation in Baijiu Brewing. *Foods* **2024**, *13*, 1954. [CrossRef] [PubMed]
111. Que, P.; Yao, S.; Hu, J.; Hu, F.; Wang, D.; Huang, W. Associations of microbial communities with metabolites and enzyme activities in different colors of high-temperature Daqu. *World J. Microbiol. Biotechnol.* **2025**, *41*, 324. [CrossRef] [PubMed]
112. Nie, Z.; Zheng, Y.; Xie, S.; Zhang, X.; Song, J.; Xia, M.; Wang, M. Unraveling the correlation between microbiota succession and metabolite changes in traditional Shanxi aged vinegar. *Sci. Rep.* **2017**, *7*, 9240. [CrossRef]
113. Wang, K.; Shi, Y.; Feng, J.; Zhao, Y.; Zhu, H.; Chen, D.; Gong, X.; Fang, M.; Yu, Y. Investigation of Zhenjiang Aromatic Vinegar Production Using a Novel Dry Gelatinization Process. *Foods* **2024**, *13*, 1071. [CrossRef]
114. Ye, X.; Yu, Y.; Liu, J.; Zhu, Y.; Yu, Z.; Liu, P.; Wang, Y.; Wang, K. Inoculation strategies affect the physicochemical properties and flavor of Zhenjiang aromatic vinegar. *Front. Microbiol.* **2023**, *14*, 1126238. [CrossRef]
115. Li, W.; Han, T.; Wen, Y.; Zhang, H.; Li, D. Preparation of Rice Bran-Enriched Sweet Rice Wine and Its Quality Improvement Through Extrusion. *Foods* **2025**, *14*, 1582. [CrossRef]
116. Tian, P.; Wan, J.; Yin, T.; Liu, L.; Ren, H.; Cai, H.; Liu, X.; Zhang, H. Acidity, sugar, and alcohol contents during the fermentation of Osmanthus-flavored sweet rice wine and microbial community dynamics. *PeerJ.* **2025**, *13*, e18826. [CrossRef]
117. Wan, B.; Tian, T.; Xiong, Y.; Wang, S.; Luo, X.; Liao, W.; Liu, P.; Miao, L.; Gao, R. Isolation and Evaluation of *Rhizopus arrhizus* Strains from Traditional Rice Wine Starters (Jiuqu): Enzyme Activities, Antioxidant Capacity, and Flavour Compounds. *Foods* **2025**, *14*, 312. [CrossRef]
118. Tang, A.; Peng, B. Diversifying the Flavor of Black Rice Wines through Three Different Regional Xiaoqus in China and Unraveling Their Core Functional Microorganisms. *Foods* **2023**, *12*, 3576. [CrossRef] [PubMed]
119. Yu, X.; Huang, T.; Huang, Z.; Wu, Z.; Che, J.; Qin, F.; Zhang, W. Effects of six commercially available koji (Chinese Xiaoqu) on the production of ethyl acetate, ethyl lactate, and higher alcohols in Chinese Baijiu (distilled spirit) brewing. *Heliyon* **2023**, *9*, e17739. [CrossRef]
120. Yin, X.; Yoshizaki, Y.; Kurazono, S.; Sugimachi, M.; Takeuchi, H.; Han, X.; Okutsu, K.; Futagami, T.; Tamaki, H.; Takamine, K. Characterization of Flavor Compounds in Rice-flavor baijiu, a Traditional Chinese Distilled Liquor, Compared with Japanese Distilled Liquors, awamori and kome-shochu. *Food Sci. Technol. Res.* **2020**, *26*, 411–422. [CrossRef]
121. Wang, H.; Sun, C.; Yang, S.; Ruan, Y.; Lyu, L.; Guo, X.; Wu, X.; Chen, Y. Exploring the impact of initial moisture content on microbial community and flavor generation in Xiaoqu baijiu fermentation. *Food Chem. X* **2023**, *20*, 100981. [CrossRef]
122. Zhao, Z.; Sugimachi, M.; Yoshizaki, Y.; Yin, X.; Han, X.; Okutsu, K.; Futagami, T.; Tamaki, H.; Takamine, K. Correlation between key aroma and manufacturing processes of rice-flavor baijiu and awamori, Chinese and Japanese traditional liquors. *Food Biosci.* **2021**, *44*, 101375. [CrossRef]
123. Dong, H.; Liu, S.; Cai, G.; Yang, H. Improving the Quality and Flavor of *Monascus* Rice Wine Brewed by Pure Culture Using the Addition of Trichosanthis Fructus. *Fermentation* **2024**, *10*, 192. [CrossRef]
124. Huang, Y.; Chen, J.; Chen, Q.; Yang, C. Effects of Main Nutrient Sources on Improving *Monascus* Pigments and Saccharifying Power of *Monascus purpureus* in Submerged Fermentation. *Fermentation* **2023**, *9*, 696. [CrossRef]
125. Jiang, Y.; Lv, X.; Zhang, C.; Zheng, Y.; Zheng, B.; Duan, X.; Tian, Y. Microbial dynamics and flavor formation during the traditional brewing of *Monascus vinegar*. *Food Res. Int.* **2019**, *125*, 108531. [CrossRef] [PubMed]
126. Wu, T.Y.; Kan, M.S.; Siow, L.F.; Palniandy, L.K. Effect of temperature on moromi fermentation of soy sauce with intermittent aeration. *Afr. J. Biotechnol.* **2010**, *9*, 702–706. [CrossRef]
127. Zhou, W.; Sun-Waterhouse, D.; Xiong, J.; Cui, C.; Wang, W.; Dong, K. Desired soy sauce characteristics and autolysis of *Aspergillus oryzae* induced by low temperature conditions during initial moromi fermentation. *J. Food Sci. Technol.-Mysore* **2019**, *56*, 2888–2898. [CrossRef] [PubMed]

128. Jiang, X.; Xu, Y.; Ye, J.; Yang, Z.; Huang, S.; Liu, Y.; Zhou, S. Isolation, identification and application on soy sauce fermentation flavor bacteria of CS1.03. *J. Food Sci. Technol.-Mysore* **2019**, *56*, 2016–2026. [CrossRef]
129. Ding, W.; Liu, Y.; Zhao, X.; Peng, C.; Ye, X.; Che, Z.; Liu, Y.; Liu, P.; Lin, H.; Huang, J.; et al. Characterization of volatile compounds of Pixian Douban fermented in closed system of gradient steady-state temperature field. *Food Sci. Nutr.* **2021**, *9*, 2862–2876. [CrossRef]
130. Guo, Q.; Zhao, J.; Peng, J.; Huang, Y.; Yang, W. Unraveling the correlation between physicochemical properties, volatile flavor compounds, and microbial communities during the fermentation of *Aspergillus*-type douchi. *Curr. Res. Food Sci.* **2025**, *11*, 101192. [CrossRef]
131. Wang, S.; Chang, Y.; Liu, B.; Chen, H.; Sun, B.; Zhang, N. Characterization of the Key Aroma-Active Compounds in Yongchuan Douchi (Fermented Soybean) by Application of the Sensomics Approach. *Molecules* **2021**, *26*, 3048. [CrossRef]
132. Sui, L.; Wang, S.; Wang, X.; Su, L.; Xu, H.; Xu, W.; Chen, L.; Li, H. Analysis of Different Strains Fermented Douchi by GCxGC-TOFMS and UPLC-Q-TOFMS Omics Analysis. *Foods* **2024**, *13*, 3521. [CrossRef]
133. Zelong, Z.; Tianyi, L.; Kaiping, H.; Min, Z.; Xiaoxue, C.; Yansong, X.; Beizhong, H.; Diqiang, W.; Jun, L. Microbial enzymes: The bridge between Daquflavor and microbial communities. *Food Innov. Adv.* **2024**, *3*, 426–437.
134. Zhou, J.; Li, X.; Li, S.; Ding, H.; Lang, Y.; Xu, P.; Wang, C.; Wu, Y.; Liu, X.; Qiu, S. Airborne microorganisms and key environmental factors shaping their community patterns in the core production area of the Maotai-flavor Baijiu. *Sci. Total Environ.* **2024**, *912*, 169010. [CrossRef] [PubMed]
135. He, G.; Huang, J.; Zhou, R.; Wu, C.; Jin, Y. Effect of Fortified Daqu on the Microbial Community and Flavor in Chinese Strong-Flavor Liquor Brewing Process. *Front. Microbiol.* **2019**, *10*, 56. [CrossRef] [PubMed]
136. Mu, Y.; Huang, J.; Zhou, R.; Mao, F.; Pan, Q.; Chen, S.; Lu, Z.; Du, L.; Xie, F. Exploring the response patterns of strong-flavor baijiu brewing microecosystem to fortified Daqu under different pit ages. *Food Res. Int.* **2022**, *155*, 111062. [CrossRef] [PubMed]
137. He, G.; Huang, J.; Wu, C.; Jin, Y.; Zhou, R. Bioturbation effect of fortified Daqu on microbial community and flavor metabolite in Chinese strong-flavor liquor brewing microecosystem. *Food Res. Int.* **2020**, *129*, 108851. [CrossRef]
138. Chenxi, Z.; Fuping, Z.; Hehe, L.; Jihong, W.; Mingquan, H.; Baoguo, S. Research progress on flavor compounds of Baijiu Daqu. *China Brewing.* **2019**, *38*, 6–12.
139. Qin, D.; Shen, Y.; Yang, S.; Zhang, G.; Wang, D.; Li, H.; Sun, J. Whether the Research on Ethanol-Water Microstructure in Traditional Baijiu Should Be Strengthened? *Molecules* **2022**, *27*, 8290. [CrossRef]
140. Sun, J.; Wang, Z.; Sun, B. Low Quantity but Critical Contribution to Flavor: Review of The Current Understanding of Volatile Sulfur-containing Compounds in Baijiu. *J. Food Compos. Anal.* **2021**, *103*, 104079. [CrossRef]
141. Wang, J.; Chen, H.; Wu, Y.; Zhao, D. Uncover the flavor code of strong-aroma baijiu: Research progress on the revelation of aroma compounds in strong-aroma baijiu by means of modern separation technology and molecular sensory evaluation. *J. Food Compos. Anal.* **2022**, *109*, 104499. [CrossRef]
142. Chen, G.; Yuan, Y.; Tang, S.; Yang, Z.; Wu, Q.; Liang, Z.; Chen, S.; Li, W.; Lv, X.; Ni, L. Comparative analysis of microbial communities and volatile flavor components in the brewing of Hongqu rice wines fermented with different starters. *Curr. Res. Food Sci.* **2023**, *7*, 100628. [CrossRef]
143. Yuan, Y.; Yang, Z.; Liang, Z.; Wu, Q.; Yan, Y.; Chen, S.; Li, X.; Ai, L.; Ni, L.; Lv, X. The regulatory effects of microbial community on the formation of higher alcohols and volatile flavor components in Hongqu rice wine brewing. *Food Biosci.* **2023**, *56*, 103142. [CrossRef]
144. Xu, Y.; Zhao, J.; Liu, X.; Zhang, C.; Zhao, Z.; Li, X.; Sun, B. Flavor mystery of Chinese traditional fermented baijiu: The great contribution of ester compounds. *Food Chem.* **2022**, *369*, 130920. [CrossRef]
145. Kang, J.; Xue, Y.; Chen, X.; Han, B. Integrated multi-omics approaches to understand microbiome assembly in Jiuqu, a mixed-culture starter. *Compr. Rev. Food. Sci. Food Saf.* **2022**, *21*, 4076–4107. [CrossRef]
146. Mou, L.; Pan, R.; Jiang, W.; Zhang, W.; Xin, F.; Jiang, Y.; Jiang, M. Strategies on improvement of pigment formation and reduction of citrinin in *Monascus* fermentation. *Biofuels Bioprod. Biorefining* **2023**, *17*, 261–272. [CrossRef]
147. Zhang, C.; Sun, Q.; Yang, L.; Ablimit, A.; Dong, H.; Wang, H.; Wang, C.; Wang, C. Mutation Breeding of *Monascus* to Produce a High Yield of Orange Pigment and Low Citrinin Content Using the ARTP Method. *J. Fungi* **2024**, *10*, 553. [CrossRef]
148. Li, Z.; Liu, Y.; Li, Y.; Lin, F.; Wu, L. Screening and identification of *Monascus* strains with high-yield monacolin K and undetectable citrinin by integration of HPLC analysis and *pksCT* and *ctnA* genes amplification. *J. Appl. Microbiol.* **2020**, *129*, 1410–1418. [CrossRef]
149. Farawahida, A.H.; Palmer, J.; Flint, S. *Monascus* spp. and citrinin: Identification, selection of *Monascus* spp. isolates, occurrence, detection and reduction of citrinin during the fermentation of red fermented rice. *Int. J. Food Microbiol.* **2022**, *379*, 109829. [CrossRef] [PubMed]
150. Kim, D.; Jin, Y.H.; Mah, J. Biogenic amine reduction by food additives in Cheonggukjang, a Korean fermented soybean paste, fermented with tyramine-producing heterogeneous bacterial species. *Heliyon* **2024**, *10*, e26135. [CrossRef] [PubMed]

151. Turna, N.S.; Chung, R.; Mcintyre, L. A review of biogenic amines in fermented foods: Occurrence and health effects. *Heliyon* **2024**, *10*, e24501. [CrossRef]
152. Kalac, P. Health effects and occurrence of dietary polyamines: A review for the period 2005–mid 2013. *Food Chem.* **2014**, *161*, 27–39. [CrossRef]
153. Wust, N.; Rauscher-Gabernig, E.; Steinwider, J.; Bauer, F.; Paulsen, P. Risk assessment of dietary exposure to tryptamine for the Austrian population. *Food Addit. Contam. Part A-Chem.* **2017**, *34*, 404–420. [CrossRef]
154. Yilmaz, C.; Gokmen, V. Neuroactive compounds in foods: Occurrence, mechanism and potential health effects. *Food Res. Int.* **2020**, *128*, 108744. [CrossRef]
155. Hemme, D.; Foucaud-Scheunemann, C. *Leuconostoc*, characteristics, use in dairy technology and prospects in functional foods. *Int. Dairy J.* **2004**, *14*, 467–494. [CrossRef]
156. Xie, Y.; Geng, Y.; Yao, J.; Ji, J.; Chen, F.; Xiao, J.; Hu, X.; Ma, L. N-nitrosamines in processed meats: Exposure, formation and mitigation strategies. *J. Agric. Food Res.* **2023**, *13*, 100645. [CrossRef]
157. Kalac, P.; Krausová, P. A review of dietary polyamines: Formation, implications for growth and health and occurrence in foods. *Food Chem.* **2005**, *90*, 219–230. [CrossRef]
158. Trevisani, M.; Cevoli, C.; Ragni, L.; Cecchini, M.; Berardinelli, A. Effect of Non-thermal Atmospheric Plasma on Viability and Histamine-Producing Activity of Psychotrophic Bacteria in Mackerel Fillets. *Front. Microbiol.* **2021**, *12*, 653597. [CrossRef]
159. Margareta, G.; Nakamura, A.; Nimura, K.; Yamazaki, M.; Oshima, I.; Kuda, T.; Takahashi, H. Investigation of bacterial community and histamine production in fresh mackerel at low temperature storage. *PLoS ONE* **2025**, *20*, e0331331. [CrossRef]
160. Swider, O.; Roszko, M.L.; Wojcicki, M. The inhibitory effects of plant additives on biogenic amine formation in fermented foods—A review. *Crit. Rev. Food. Sci. Nutr.* **2024**, *64*, 12935–12960. [CrossRef]
161. Kuda, T.; Mihara, T.; Yano, T. Detection of histamine and histamine-related bacteria in fish-nukazuke, a salted and fermented fish with rice-bran, by simple colorimetric microplate assay. *Food Control* **2007**, *18*, 677–681. [CrossRef]
162. Ventosa, A.; Nieto, J.J. Biotechnological applications and potentialities of halophilic microorganisms. *World J. Microbiol. Biotechnol.* **1995**, *11*, 85–94. [CrossRef] [PubMed]
163. Ardakani, M.R.; Poshtkouhian, A.; Amoozegar, M.A.; Zolgharnein, H. Isolation of Moderately Halophilic *Pseudoalteromonas* Producing Extracellular Hydrolytic Enzymes from Persian Gulf. *Indian J. Microbiol.* **2012**, *52*, 94–98. [CrossRef]
164. Gu, J.; Dong, X.; Zhou, Y.; Zhao, Y.; Du, Q.; Chen, J.; Mao, X.; Wang, F.; Tu, B. Analysis of Halophilic Phenotypic Variation and Cytotoxicity of Vibrio parahaemolyticus from Different Sources. *Pathogens* **2025**, *14*, 182. [CrossRef] [PubMed]
165. Klein, J.; Schwarz, T.; Lentzen, G. Ectoine as a natural component of food: Detection in red smear cheeses. *J. Dairy. Res.* **2007**, *74*, 446–451. [CrossRef]
166. Caglayan, P.; Birbir, M.; Sanchez-Porro, C.; Ventosa, A. Detection of industrially potential enzymes of moderately halophilic bacteria on salted goat skins. *Turk. J. Biochem.* **2018**, *43*, 312–322. [CrossRef]
167. Graü, C.; Elguezabal, L.; Vallenilla, O.; Zerpa, A. Evaluation of halophile microbial flora spoiling dry-salted fish processed in Sucre state. *Rev. Cient.-Fac. Cienc. Vet.* **2003**, *13*, 319–325.
168. Delgado-Garcia, M.; Flores-Gallegos, A.C.; Kirchmayr, M.; Rodriguez, J.A.; Mateos-Diaz, J.C.; Aguilar, C.N.; Muller, M.; Camacho-Ruiz, R.M. Bioprospection of proteases from *Halobacillus andaensis* for bioactive peptide production from fish muscle protein. *Electron. J. Biotechnol.* **2019**, *39*, 52–60. [CrossRef]
169. Satari, L.; Guillen, A.; Latorre-Perez, A.; Porcar, M. Beyond Archaea: The Table Salt Bacteriome. *Front. Microbiol.* **2021**, *12*, 714110. [CrossRef]
170. Jing, Y.; Xi-hong, Y.; Chen, L.; Dong-xing, Y.; Wan-cui, X. Research progress on the effects of halophilic microorganisms on the flavor of fermented seafood condiments. *Food Mach.* **2020**, *36*, 203–234.
171. Kivisto, A.T.; Karp, M.T. *Halophilic anaerobic* fermentative bacteria. *J. Biotechnol.* **2011**, *152*, 114–124. [CrossRef] [PubMed]
172. Chen, J.; Qiao, D.; Yuan, T.; Feng, Y.; Zhang, P.; Wang, X.; Zhang, L. Biotechnological production of ectoine: Current status and prospects. *Folia. Microbiol.* **2024**, *69*, 247–258. [CrossRef]
173. Gopikrishna, T.; Suresh Kumar, H.K.; Perumal, K.; Elangovan, E. Impact of *Bacillus* in fermented soybean foods on human health. *Ann. Microbiol.* **2021**, *71*, 30. [CrossRef]
174. Icer, M.A.; Ozbay, S.; Agagunduz, D.; Kelle, B.; Bartkiene, E.; Rocha, J.M.F.; Ozogul, F. The Impacts of Acidophilic Lactic Acid Bacteria on Food and Human Health: A Review of the Current Knowledge. *Foods* **2023**, *12*, 2965. [CrossRef] [PubMed]
175. Francesco, B.; Frederic, L. Review: Bacterially produced vitamin K2 and its potential to generate health benefits in humans. *Trends Food Sci. Technol.* **2024**, *147*, 104461. [CrossRef]
176. Nagarajan, M.; Rajasekaran, B.; Venkatachalam, K. Microbial metabolites in fermented food products and their potential benefits. *Int. Food Res. J.* **2022**, *29*, 466–486. [CrossRef]
177. Li, K.J.; Brouwer-Brolsma, E.M.; Burton-Pimentel, K.J.; Vergeres, G.; Feskens, E.J.M. A systematic review to identify biomarkers of intake for fermented food products. *Genes Nutr.* **2021**, *16*, 5. [CrossRef] [PubMed]

178. Yee, C.S.; Zahia-Azizan, N.A.; Abd Rahim, M.H.; Zaini, N.A.M.; Raja-Razali, R.B.; Ushidee-Radzi, M.A.; Ilham, Z.; Wan-Mohtar, W.A.A.Q. Smart Fermentation Technologies: Microbial Process Control in Traditional Fermented Foods. *Fermentation* **2025**, *11*, 323. [CrossRef]
179. Twaruzek, M.; Altyn, I.; Kosicki, R. Dietary Supplements Based on Red Yeast Rice-A Source of Citrinin? *Toxins* **2021**, *13*, 497. [CrossRef]
180. *ISO 22000:2018*; Food Safety Management Systems—Requirements for Any Organization in the Food Chain. International Organization for Standardization: Geneva, Switzerland, 2018.
181. Gonzalez, A.; Navas-Molina, J.A.; Kosciolek, T.; McDonald, D.; Vazquez-Baeza, Y.; Ackermann, G.; DeReus, J.; Janssen, S.; Swafford, A.D.; Orchanian, S.B.; et al. Qiita: Rapid, web-enabled microbiome meta-analysis. *Nat. Methods* **2018**, *15*, 796. [CrossRef] [PubMed]
182. Jarmusch, A.K.; Wang, M.; Aceves, C.M.; Advani, R.S.; Aguirre, S.; Aksenov, A.A.; Aleti, G.; Aron, A.T.; Bauermeister, A.; Bolleddu, S.; et al. ReDU: A framework to find and reanalyze public mass spectrometry data. *Nat. Methods* **2020**, *17*, 901. [CrossRef] [PubMed]

Disclaimer/Publisher's Note: The statements, opinions and data contained in all publications are solely those of the individual author(s) and contributor(s) and not of MDPI and/or the editor(s). MDPI and/or the editor(s) disclaim responsibility for any injury to people or property resulting from any ideas, methods, instructions or products referred to in the content.

MDPI AG
Grosspeteranlage 5
4052 Basel
Switzerland
Tel.: +41 61 683 77 34

Foods Editorial Office
E-mail: foods@mdpi.com
www.mdpi.com/journal/foods



Disclaimer/Publisher's Note: The title and front matter of this reprint are at the discretion of the Guest Editors. The publisher is not responsible for their content or any associated concerns. The statements, opinions and data contained in all individual articles are solely those of the individual Editors and contributors and not of MDPI. MDPI disclaims responsibility for any injury to people or property resulting from any ideas, methods, instructions or products referred to in the content.





Academic Open
Access Publishing

mdpi.com

ISBN 978-3-7258-9052-1